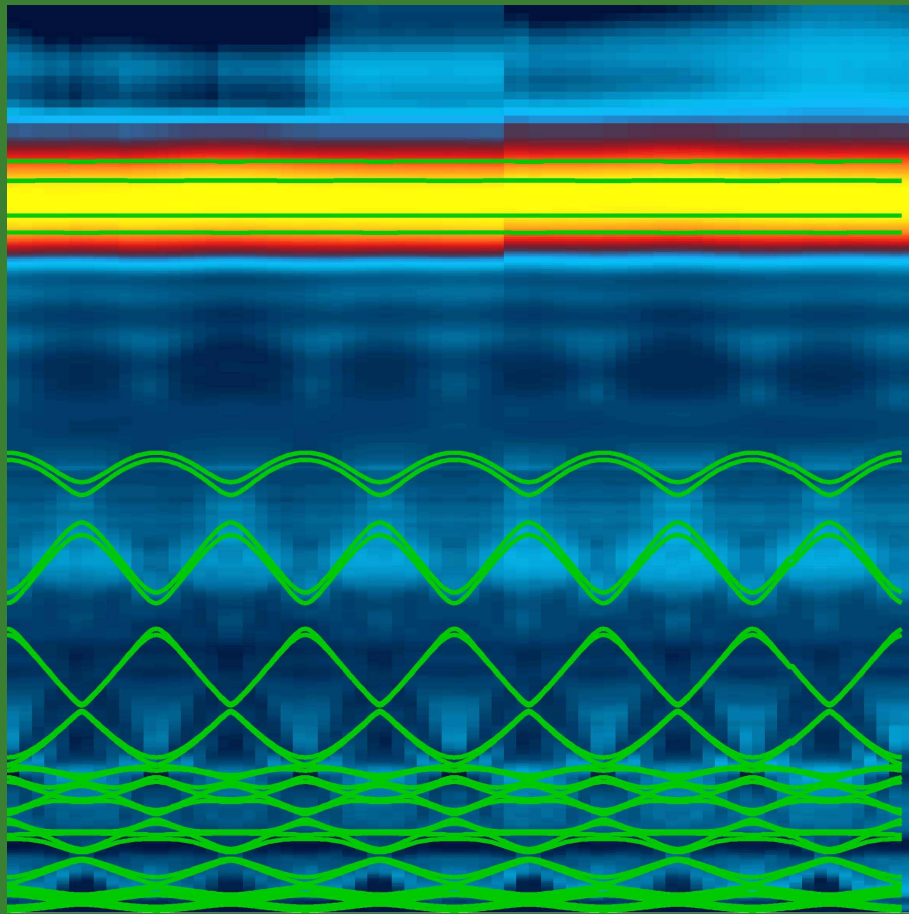


UNIVERSITÄT LEIPZIG

REPORT
Institute für Physik
The Physics Institutes

2009



The Physics Institutes of Universität Leipzig, Report 2009
M. Grundmann (Ed.)

Technical Editor: Anja Heck

This work is subject to copyright. All rights are reserved.
© Universität Leipzig 2010

Printed in Germany by
MERKUR Druck und Kopierzentrum GmbH, Leipzig

online available at
http://www.uni-leipzig.de/~exph2/report_2009.pdf

Front cover

The front cover image shows reflection spectra of a colloidal photonic crystal (460 nm polystyrene beads) at fixed angle of incidence with changing azimuthal angle around the 111 surface normal. The lines represent the calculated photonic band structure of the crystal. (For more details see page 39.)

Inside back covers

Poster of MECO34 conference, part of our 600 year celebration.

Back covers

Cover of issue 247(6) of Physica Status Solidi(b) with the scientific report of Forschergruppe 522 as special section.

**Institut für Experimentelle Physik I
Institut für Experimentelle Physik II
Institut für Theoretische Physik**

**Fakultät für
Physik und Geowissenschaften**

Universität Leipzig

**Institute for Experimental Physics I
Institute for Experimental Physics II
Institute for Theoretical Physics**

Faculty of Physics and Earth Sciences

Universität Leipzig

Report 2009

Addresses

Institute for Experimental Physics I

Linnéstraße 5

D-04103 Leipzig, Germany

Phone: +49 341 97-32551

Fax: +49 341 97-32599

WWW: http://www.uni-leipzig.de/~gasse/nysid_a/inst/exp_1.htm

Mailing

address: Postfach 10 09 20, D-04009 Leipzig, Germany

Institute for Experimental Physics II

Linnéstraße 5

D-04103 Leipzig, Germany

Phone: +49 341 97-32650

Fax: +49 341 97-32668

WWW: <http://www.uni-leipzig.de/~exph2>

Mailing

address: Postfach 10 09 20, D-04009 Leipzig, Germany

Institute for Theoretical Physics

Vor dem Hospitaltore 1

D-04103 Leipzig, Germany

Phone: +49 341 97-32420

Fax: +49 341 97-32548

WWW: <http://www.physik.uni-leipzig.de>

Mailing

address: Postfach 10 09 20, D-04009 Leipzig, Germany

Preface

This 2009 Report of the Physics Institutes of the Universität Leipzig presents to you an overview of our research in numerous projects, enjoyably conducted with colleagues and partners worldwide. We are grateful to our guests for enriching our academic year with their contributions in the colloquium and within the work groups.

Our scientific success encompasses the fully automatic characterization of the elasticity of individual cells using an optical stretcher with integrated microfluidic chip and computer-controlled pump system in the Institute for Experimental Physics I. Primary breast cells could be distinguished from primary breast cancer cells; the latter are more deformable by the light beam. This result is currently transferred to other types of cancer in clinical studies. Among the results of the Institute for Experimental Physics II are the identification of defects as source of ferromagnetism in undoped and transition metal doped oxide thin films. Also fully transparent metal-semiconductor thin film field-effect transistors were achieved. This work stands in the great tradition of three physicists from Leipzig: Ferdinand Braun who discovered rectification in metal-semiconductor contacts (1874), Karl Bädeker who reported the first transparent conductive oxide (1907) and Julius E. Lilienfeld who holds the first patents for field-effect transistors (1920s). The Institute for Theoretical Physics is connected with the IMPRS (International Max Planck Research School) *Mathematics in the Sciences* and several Top-Level Research Areas within Universität Leipzig.

Our activities are only possible due to the generous support from various funding agencies which is individually acknowledged. Special mentioning deserves the start of the ESF-Nachwuchsforschergruppe (Young Scientists Research Group) *Multiscale Functional Structures*, coordinated by Dr. Holger von Wenckstern. The involved doctoral candidates study in the graduate school Leipzig School of Natural Sciences – Building with Molecules and Nano-objects (BuildMoNa). The project also strengthens our cooperation with the Leibniz-Institute for Surface Modification, Leipzig (IOM) and industrial partners.

Leipzig,
June 2010

M. Grundmann
J. A. Käs
R. Verch
Directors

Contents

1	Structure and Staff of the Institutes	21
1.1	Institute for Experimental Physics I	21
1.1.1	Office of the Director	21
1.1.2	Molecular Nano-Photonics, Molekulare Nanophotonik [MON]	21
1.1.3	Molecular Physics, Molekülphysik [MOP]	21
1.1.4	Physics of Interfaces, Grenzflächenphysik [GFP]	22
1.1.5	Soft Matter Physics, Physik der weichen Materie [PWM]	23
1.2	Institute for Experimental Physics II	24
1.2.1	Office of the Director	24
1.2.2	Magnetic Resonance of Complex Quantum Solids, Magnetische Resonanz Komplexer Quantenfestkörper [MQF]	25
1.2.3	Nuclear Solid State Physics, Nukleare Festkörperphysik [NFP]	25
1.2.4	Semiconductor Physics, Halbleiterphysik [HLP]	26
1.2.5	Solid State Optics and Acoustics, Festkörperoptik und -akustik [FKO]	28
1.2.6	Superconductivity and Magnetism, Supraleitung und Magnetismus [SUM]	29
1.3	Institute for Theoretical Physics	29
1.3.1	Office of the Director	29
1.3.2	Computational Quantum Field Theory, Computerorientierte Quantenfeldtheorie [CQT]	29
1.3.3	Molecular Dynamics / Computer Simulation, Moleküldynamik / Computersimulation [MDC]	30
1.3.4	Quantum Field Theory and Gravity, Quantenfeldtheorie und Gravitation [QFG]	31
1.3.5	Theory of Condensed Matter, Theorie der kondensierten Materie [TKM]	31
1.3.6	Theory of Elementary Particles, Theorie der Elementarteilchen [TET]	32

I	Institute for Experimental Physics I	33
2	Molecular Nano-Photonics	35
2.1	Introduction	35
2.2	Photothermal Correlation Spectroscopy	36
2.3	Orientation and Rotational Diffusion of Gold Nanorods	37
2.4	Photonic Crystals	38
2.5	Electrochemical Manipulation of the Emission of Quantum Dots	40
2.6	Single Molecule Diffusion Anisotropy in Liquid Crystals	41
2.7	Single Molecule Nanorheology in Polymer Melts	42
2.8	Funding	43
2.9	Organizational Duties	43
2.10	External Cooperations	44
2.11	Publications	44
2.12	Graduations	46
2.13	Guests	47
3	Molecular Physics	49
3.1	Introduction	49
3.2	Interfacial interactions and their impact on the glassy dynamics of thin layers of atactic poly(methyl methacrylate)	49
3.3	Molecular weight dependence of the glassy dynamics of thin polystyrene layers	50
3.4	Real and apparent changes in the glassy dynamics of thin polymer layers - theoretical considerations	51
3.5	Impact of a novel preparation method on the glassy dynamics of thin polymer layers studied by means of Dielectric Spectroscopy	52
3.6	Signatures in charge transport and glassy dynamics of molecular liquids	54
3.7	Rotational and translational diffusion in ionic liquids	55
3.8	Charge transport and dipolar relaxations in hyperbranched polymers .	55
3.9	Characteristic hopping lengths and molecular volumes of ionic liquids	57
3.10	Charge transport and diffusion of ionic liquids in nanoporous silica membranes	58
3.11	Charge transport and dipolar relaxations in Imidazolium-based Ionic Liquids	59
3.12	Hierarchies in the structural organization of spider silk- A quantitative combined model	60
3.13	Spider silk: A soft solid with a unidirectional phononic band gap	62
3.14	Electromechanical properties of smectic C* liquid crystal elastomers under shear	63
3.15	Infrared transition moment orientational analysis (IR-TMOA)	64
3.16	A novel position determination technique for polystyrene and silica colloids using video microscopy	65
3.17	Forces of Interaction between Poly(2-vinylpyridine) Brushes As Measured by Optical Tweezers	65
3.18	Interaction forces between a single pair of blank Silica surfaces as measured by Optical Tweezers	66

3.19	Electrokinetics and Charge Inversion as studied by Single Colloid Electrophoresis (SCE)	68
3.20	Microscopic fluctuations and the emergence of irreversibility: Investigating stochastic thermodynamics	69
3.21	Funding	71
3.22	Organizational Duties	71
3.23	External Cooperations	71
3.24	Publications	73
3.25	Graduations	74
3.26	Guests	74
4	Physics of Interfaces	75
4.1	Introduction	75
4.2	Investigating Surface Barriers and Sorbate-Induced Transition Effects of Silicalite-1 by Means of Interference Microscopy	76
4.3	Characterizing Molecular Transport in Nanopores	77
4.4	Transport through Zeolitic Imidazolate Frameworks: From Molecular Diffusion to Membrane Permeation	78
4.5	Correlating the Results of Different Techniques of Diffusion Measurement in Nanoporous Glasses	79
4.6	Ordered Mesoporous Solids as Model Substances for Liquid Adsorption	80
4.7	Design of Liquid/Solid Adsorption Isotherms by Energy Distribution Functions	81
4.8	NMR Relaxometry Study of Pore Water in Hydrating Cements with Addition of Modified Superabsorbent Polymers	82
4.9	Fundamental Host-Guest Interactions in Porous Metal Organic Frameworks	83
4.10	¹³ C PFG NMR Diffusion Studies in Metall Organic Frameworks	84
4.11	Multidimensional NMR Diffusion Studies in NaX	85
4.12	Permanent Magnet Arrangements for Low-Field NMR	86
4.13	Network Effects within Independent Pores	87
4.14	Dynamics of Molecules Confined to Structured Nano-Channels	89
4.15	Disorder Effects during Freezing in Linear Pores	90
4.16	Funding	91
4.17	Organizational Duties	93
4.18	External Cooperations	94
4.19	Publications	96
4.20	Graduations	101
4.21	Guests	102
5	Soft Matter Physics	103
5.1	Introduction	103
5.2	Feeling for Cells with Light: Illuminating the Role of Biomechanics for Cancer Metastasis	104
5.3	Origin and Spatial Distribution of Forces in Motile Cells	107
5.4	Mechanosensitive Behavior of Neuronal Growth Cones	108

5.5	Structural Investigation on the Absorption of the MARCKS Peptide on Anionic Lipid Monolayers	109
5.6	Mechanical properties of transiently crosslinked F-actin bundles	111
5.7	Funding	113
5.8	Organizational Duties	114
5.9	External Cooperations	114
5.10	Publications	115
5.11	Graduations	117
5.12	Guests	118
5.13	Awards	118
II	Institute for Experimental Physics II	119
6	Magnetic Resonance of Complex Quantum Solids	121
6.1	Introduction	121
6.2	Evidence for two electronic components in high-temperature superconductivity from NMR for a TwoComponent Model	121
6.3	Spatial Inhomogeneities in Single-Crystal HgBa ₂ CuO _{4+δ} from ⁶³ Cu NMR Spin and Quadrupole Shifts	122
6.4	High sensitivity nuclear magnetic resonance probe for anvil cell pressure experiments	122
6.5	Spin-Coupling and Hyperfine Interaction of the Nitrogen Donors in 6H-SiC	123
6.6	Size effects of aromatic substitution in the <i>ortho</i> position on the photodimerization kinetics of <i>α-trans</i> cinnamic acid derivatives. A solid-state NMR study	123
6.7	Solid-state NMR investigations of Cu ₃ (BTC) ₂ and MIL-53 metal-organic frameworks (MOFs)	124
6.8	The influence of domains on tetrahedrally coordinated Cr ⁵⁺ in ferroelectric BaTiO ₃ : an electron paramagnetic resonance study	125
6.9	Funding	125
6.10	Organizational Duties	126
6.11	External Cooperations	127
6.12	Publications	128
6.13	Graduations	131
6.14	Guests	132
7	Nuclear Solid State Physics	135
7.1	Introduction	135
7.2	Trace element mapping in Parkinsonian brain by quantitative ion beam microscopy	136
7.3	Combined STIM- and PIXE-Tomography	137
7.4	Characterization and elemental analysis of nano- and microdimensional structures using PIXE and RBS	138

7.5	Spatially resolved characterisation of electronic properties of solar cells using the IBICC technique	138
7.6	Defect production by single ions traversing multigraphene	139
7.7	Micro-fluidic target chamber machined by proton beam writing for the in-situ analysis of gas absorption in synthetic crystals	141
7.8	Creation of 3D microsculptures in PMMA by multiple angle proton irradiation	142
7.9	Proton beam writing on different types of semiconductor systems	142
7.10	Neuronal Networks on structured Petri-dishes	143
7.11	Low dose targeted cell bombardment with counted ions at LIPSION	144
7.12	Study of ZnO-thin film scintillators for use as an ion transmission detector	145
7.13	Study of the nuclear reaction $^{11}\text{B}(p, \alpha)^8\text{Be}$	146
7.14	Characterization of TiO_2 nanomaterials by TDPAC	146
7.15	Funding	147
7.16	Organizational Duties	148
7.17	External Cooperations	149
7.18	Publications	150
7.19	Graduations	154
7.20	Guests	154
8	Semiconductor Physics	155
8.1	Introduction	155
8.2	ZnO-based metal-semiconductor field-effect transistors on glass substrates	155
8.3	High-gain integrated inverters based on ZnO MESFET technology	157
8.4	Transparent rectifying contacts and their application in transparent electronics	159
8.5	Growth and transport properties of ZnO- and ZnO:P-microwires	160
8.6	Resistivity control in ZnO nanowires by Al doping	161
8.7	Donor-acceptor pair recombination in non-stoichiometric ZnO thin films	163
8.8	Lineshape theory of photoluminescence from semiconductor alloys	165
8.9	Identification of a donor related recombination channel in ZnO thin films	167
8.10	Temperature-dependent properties of nearly ideal ZnO Schottky diodes	168
8.11	Dielectric passivation of ZnO-based Schottky Diodes	169
8.12	Investigation of structural and electronic properties of $\text{Mg}_x\text{Zn}_{1-x}\text{O}$ thin films	171
8.13	Defects in nitrogen-implanted ZnO thin film	173
8.14	Space-charge regions in ZnO-based metal-semiconductor-metal photodetectors	175
8.15	Space-charge regions in ZnO-based Schottky diodes and metal-semiconductor field-effect transistors	176
8.16	Correlation of pre-breakdown sites and bulk defects in multicrystalline silicon solar cells	178
8.17	Influence of the incorporation of sodium on electrical properties of flexible $\text{Cu}(\text{In},\text{Ga})\text{Se}_2$ solar cells	180
8.18	Polarization behaviour of the exciton-polariton emission in ZnO-based microresonators	181

8.19	Growth of ZnO-cavities for planar microresonators	183
8.20	2D and 3D confined ZnO-nanopillar resonators	184
8.21	Growth and characterization of MgZnO nanowires	185
8.22	Trap saturation in ZnO microwires observed by time-resolved photoluminescence	186
8.23	Lattice constants of PLD-grown $Mg_xZn_{1-x}O$ thin films	187
8.24	Refractive index tensor of ZnO bulk and microwire single crystals	189
8.25	Low-temperature dielectric tensor of a -plane $Mg_xZn_{1-x}O$ thin films	190
8.26	Observation of the quantum confined Stark effect in ZnO/MgZnO quantum wells	191
8.27	Dielectric function of BaTiO ₃ thin films in IR and VUV range	192
8.28	Phonon modes of BaTiO ₃ thin films	193
8.29	Optical properties of BaTiO ₃ /ZnO heterostructures under the effect of an electric bias	195
8.30	Teaching	196
8.30.1	Mathematical pendulum with finite amplitude	196
8.30.2	Collapse of the Tacoma Narrows bridge	196
8.30.3	Explaining the Rubens flame tube	196
8.31	Funding	197
8.32	Organizational Duties	199
8.33	External Cooperations	200
8.34	Publications	201
8.35	Graduations	208
8.36	Guests	211
9	Solid State Optics and Acoustics	213
9.1	Introduction	213
9.2	Cartilage tissue engineering by collagen scaffold associated mesenchymal stem cells in a novel bioreactor	214
9.2.1	Objectives	214
9.2.2	Material and Methods	214
9.2.3	Results and Conclusions	215
9.3	Non invasive high resolution acoustic monitoring of mesenchymal stem cells	217
9.4	Ultra-high resolution thin film delineation using reflection phase-sensitive acoustic microscopy	218
9.5	Characterization of elastomers with transverse sonic waves	221
9.6	High speed ultrasonic monitoring of joint kinematics of athletes trained for high performance sport	225
9.6.1	Introduction	225
9.6.2	Methods and results	225
9.7	Stress detection with guided acoustic ultrasonic waves by non-linear elastic and geometric effects	228
9.7.1	Introduction	228
9.7.2	Stress dependence of the time-of-flight of transversal and longitudinal polarized acoustic waves in strings and rods	229

9.7.3	Experimental results	232
9.7.4	Conclusions	233
9.8	Surface acoustic wave generation and detection by Coulomb excitation	233
9.9	Funding	236
9.10	Organizational Duties	237
9.11	External Cooperations	237
9.12	Publications	238
9.13	Graduations	239
9.14	Guests	240
10	Superconductivity and Magnetism	241
10.1	Introduction	241
10.2	Defect-induced magnetic order in pure ZnO films	241
10.3	Ferroelectric switching in multiferroic magnetite thin films	242
10.4	Magneto- and electroresistance of La _{0.7} Ca _{0.3} MnO ₃ /Nb:SrTiO ₃ junctions	243
10.5	Funding	244
10.6	Organizational Duties	245
10.7	External Cooperations	245
10.8	Publications	246
10.9	Graduations	248
10.10	Guests	248
III	Institute for Theoretical Physics	251
11	Computational Quantum Field Theory	253
11.1	Introduction	253
11.2	Edwards-Anderson Ising Spin Glass Model	255
11.3	Stretching Polymers in Crowded Environments	256
11.4	Worm Algorithm Applied to Critical Loop Gases	257
11.5	Partially Asymmetric Exclusion Processes	259
11.6	Pair-Factorized Steady States in Stochastic Mass-Transport Models	260
11.7	Ground-States and Thermodynamics of Tubelike Flexible Polymers	262
11.8	Dominance of Finite-Size Effects in Nucleation Processes	263
11.9	Microcanonical Analysis of Macromolecule Aggregation	265
11.10	Microcanonical Analyses of Polymer Adsorption Transitions	266
11.11	Peptide Adhesion to Semiconductor Substrates: Simulations and Experiments	268
11.12	Free-Energy Barrier at Droplet Condensation	270
11.13	Quantum Critical Points for Mixed Heisenberg Spin Chains	271
11.14	Critical Behaviour of Quantum Compass and Plaquette Orbital Models	272
11.15	Universal Amplitude Ratios for the Potts Model	275
11.16	Parallel Tempering Cluster Algorithm	276

11.17	Error Estimation and Reduction with Cross Correlations	277
11.18	Funding	278
11.19	Organizational Duties	280
11.20	External Cooperations	282
11.21	Publications	284
11.22	Graduations	292
11.23	Guests	292
12	Molecular Dynamics / Computer Simulation	295
12.1	Introduction	295
12.2	Analytical Treatment and Computer Simulations of the influence of the crystal surface on the exchange of guest molecules between zeolite nanocrystals and the surrounding gas phase	296
12.3	Diffusion and Rotation of Water in the Zeolite Chabazite	296
12.4	How Do Guest Molecules Enter Zeolite Pores? Quantum Chemical Calculations and Classical MD Simulations	297
12.5	Investigation of the rotation and diffusion of pentane in the zeolite ZK5	297
12.6	Diffusion of Guest Molecules in Metal Organic Frameworks	298
12.7	Phase equilibria and critical behaviour of molecular fluids in bulk systems and under geometrical restrictions	299
12.8	Simulation of fluid phase equilibria in very narrow slit-like pores: Transition range to two dimensions	300
12.9	Funding	301
12.10	Organizational Duties	302
12.11	External Cooperations	302
12.12	Publications	303
12.13	Graduations	304
12.14	Guests	304
13	Quantum Field Theory and Gravity	305
13.1	Geometry Dependence of the Casimir Force	305
13.2	Casimir effect and real media	305
13.3	Structure of the gauge orbit space and study of gauge theoretical models	308
13.4	Quantum field theory on non-commutative geometries, quantum field theory and cosmology, generally covariant quantum field theory	309
13.5	Funding	310
13.6	Organizational Duties	311
13.7	External Cooperations	312
13.8	Publications	313
13.9	Graduations	316
13.10	Guests	317
14	Theory of Condensed Matter	319
14.1	Introduction	319
14.2	Stochastic Phenomena in Systems with Many Degrees of Freedom	320
14.3	Mathematical Modeling of the Immune System	321

14.4	Tube Width Fluctuations in F-Actin solutions	322
14.5	The conformations of a stiff polymer in random media	324
14.6	Glassy dynamics in pectin networks	324
14.7	Force transmission through the cytoskeleton	325
14.8	Inelastic mechanics of sticky biopolymer networks	326
14.9	Hot Brownian Motion	326
14.10	Funding	327
14.11	Organizational Duties	327
14.12	External Cooperations	328
14.13	Publications	329
14.14	Graduations	332
14.15	Awards	333
14.16	Guests	333
Author Index		335

1

Structure and Staff of the Institutes

1.1 Institute for Experimental Physics I

1.1.1 Office of the Director

Prof. Dr. Josef A. Käs (director)

Prof. Dr. Frank Cichos (vice director)

1.1.2 Molecular Nano-Photonics, Molekulare Nanophotonik [MON]

Prof. Dr. Frank Cichos

Secretary

Christine Adolph

Technical staff

Dipl.-Phys. Uwe Weber

PhD candidates

Subhasis Adhikari, M.Sc.

Dipl.-Phys. Nicole Amecke

Dipl.-Phys. Nils Neubauer

Dipl.-Phys. Martin Pumpa

Dipl.-Phys. Romy Radünz

Markus Selmke

Dipl.-Phys. Rebecca Wagner

Students

Marco Braun

Leander Fiedler

Georg Kropat

1.1.3 Molecular Physics, Molekülphysik [MOP]

Prof. Dr. F. Kremer

Secretary

Karin Girke
Ines Grünwald

Technical staff

Tech. Hartmut Domröse
Dipl.-Ing. Jörg Reinmuth
Dipl.-Phys. Viktor Skokov

Academic staff

Dr. Mahdy Elmahdy
Dr. Periklis Papadopoulos

PhD candidates

Dipl.-Chem. Roxana Ene
Dipl.-Phys. Christof Gutsche
Ciprian Ghiorghita Iacob, M.Sc.
Dipl.-Phys. Kati Kegler
Emmanuel U. Mapesa, M.Sc.
Joshua Rume Sangoro, M.Sc.
Ilya Semenov, M.Sc.
Dipl.-Phys. Gunter Stober
Carolin Wagner

Students

Wilhelm Kossack
Christina Krause
Martin Treß
Olaf Ueberschär

**1.1.4 Physics of Interfaces,
Grenzflächenphysik [GFP]**

Prof. Dr. Jörg Kärger
Dr. habil. Frank Stallmach (since April 2009)

Secretary

Katrin Kunze

Technical staff

Dipl.-Phys. Cordula Bärbel Krause
Lutz Moschkowitz
Stefan Schlayer

Academic staff

Dr. Ziad Adem
Dr. Christian Chmelik
Dr. Muslim Dvoyashkin
Prof. Dr. Dieter Freude
Dr. Karen Friedemann

Dr. Petrik Galvosas
Dr. habil. Grit Kalies
Prof. Dr. Jörg Kärger
Dr. Sergej Naumov
Dr. habil. Frank Stallmach
Dr. Rustem Valiullin

PhD candidates

Dipl.-Phys. Tomas Binder
Dipl.-Phys. Wadinga Fomba
Dipl.-Chem. Filipe Furtado
Dipl.-Phys. Marcel Gratz
Dipl.-Phys. Lars Heinke
Dipl.-Phys. Florian Hibbe
Dipl.-Phys. Carsten Horch
Dipl.-Phys. Aleksey Khokhlov
Dipl.-Math. Daria Kondrashova
Dipl.-Geol. Ivonne Mitreiter
Dipl.-Phys. Anne-Kristin Pusch
Dipl.-Phys. Ekaterina Romanova
Dipl.-Phys. Oraphan Saengsawang
Dipl.-Phys. Tobias Titze
Dipl.-Phys. Markus Wehring
Dipl.-Phys. Philipp Zeigermann

Students

Ramona Y.G. Baum
Steffen Beckert
Stefan Hertel
Kathleen Kirchner
Tom Kirchner

1.1.5 Soft Matter Physics, Physik der weichen Materie [PWM]

Prof. Dr. Josef A. Käs

Secretary

Claudia Honisch

Technical staff

Dipl. Ing. Undine Dietrich
Dipl.-Phys. Bernd Kohlstrunk
Ing. Elke Westphal

Academic staff

Dr. Claus Fütterer
Dr. Carsten Selle
Dr. Mareike Zink

PhD candidates

Dipl.-Phys. Claudia Brunner
Susanne Ebert, M. Sc.
Anatol Fritsch, M. Sc.
Thomas Fuhs, M. Sc.
Brian Gentry, M. Sc.
Markus Gyger, M. Sc.
Dipl.-Phys. Florian Huber
Dipl.-Phys. Tobias Kießling
Dipl.-Phys. Melanie Knorr
Daniel Koch, M. Sc.
Dipl.-Phys. Karla Müller
Kenechukwu David Nnetu, M. Sc.
Dipl.-Phys. Philipp Rauch
Dipl.-Phys. Florian Rückerl
David Smith, M.Sc.
Dipl.-Phys. Roland Stange
Dipl.-Phys. Dan Strehle
Dipl.-Phys. Carsten Stüber
Björn Stuhmann, M.Sc.
Dipl.-Phys. Franziska Wetzel
Dipl.-Phys. Lydia Woiterski

Students

Sebastian Ehrig
Chris Händel
Tina Händler
Paul Heine
Lukas Hilde
Kathleen Kirchner
Tom Kirchner
Fabian Klüpfel
Frank Kupfer
Steve Pawlizak
Jörg Schnauß
Carsten Schuldt
Sebastian Schmidt
Matthias Steinbeck
Johannes Stelzer
Carsten Vogt

1.2 Institute for Experimental Physics II**1.2.1 Office of the Director**

Prof. Dr. Marius Grundmann (director)
Prof. Dr. Tilman Butz (vice director)

1.2.2 Magnetic Resonance of Complex Quantum Solids, Magnetische Resonanz Komplexer Quantenfestkörper [MQF]

Prof. Dr. Jürgen Haase

Secretary

Sophie Jung

Technical staff

Konrad Eisinger

Dipl.-Ing. Joachim Hoentsch

Dipl.-Phys. Gert Klotzsche

Dipl.-Ing. Kathrin Koch

Academic staff

PD Dr. Marko Bertmer

Prof. Dr. Andreas Pöppel

Dr. Damian Rybicki

PhD candidates

Dipl.-Phys. Ingo Hilschenz

Dipl.-Phys. Benno Meier

Dipl.-Phys. Thomas Meißner

Dipl.-Phys. Gregor Thörmer

Dipl.-Phys. Alexander Jäger

Dipl.-Chem. Bettina Jee

M. sc. Farhana Gul-E-Noor

M. sc. Michael Jurkutat

M. sc. Dimo Ivanov

Dipl.-Phys. Pavel Sedykh

Students

Daniel Blaschke

Nataliya Georgieva

Juliane Höhne

Anusree Viswanath Kuttatheyil

Marc Lux

1.2.3 Nuclear Solid State Physics, Nukleare Festkörperphysik [NFP]

Prof. Dr. Tilman Butz

Technical staff

Carsten Pahnke

Dipl.-Ing. Joachim Starke

Academic staff

Dr. Frank Menzel
Dr. Tilo Reinert
Dr. Daniel Spemann
Dr. Jürgen Vogt

PhD candidates

Dipl.-Phys. Tobias Andrea
Nirav Barapatre, M.Sc.
Dipl.-Phys. René Feder
Dipl.-Biol. Anja Fiedler
Dipl.-Phys. Steffen Jankuhn
Dipl.-Phys. (Med.-Phys.) Torsten Koal
Dipl.-Phys. Christoph Meinecke
Dipl.-Phys. Martin Rothermel

Students

Alexander Arndt
Arjen de Hoon
Alexander Malwin Jakob
Wolfgang Larisch
Niklas Liebing
Dirk Mehlhorn
Tilman Piffel
Marko Röder
Uwe Scholz
Ronja Thies
Ronald Werner

**1.2.4 Semiconductor Physics,
Halbleiterphysik [HLP]**

Prof. Dr. Marius Grundmann

Secretary

Anja Heck

SANDiE Network Office/BuildMoNa Office

Dr. Alexander Weber (Officer)
Birgit Wendisch (Secretary)

Technical staff

Dipl.-Phys. Gabriele Benndorf
Dipl.-Ing. Gisela Biehne
Monika Hahn
Dipl.-Ing. Holger Hochmuth
Dipl.-Phys. Jörg Lenzner
Gabriele Ramm
Roswitha Riedel

Academic staff

Dr. Karsten Goede
PD Dr. Michael Lorenz
PD Dr. Rainer Pickenhain
Prof. Dr. Bernd Rheinländer (retired)
Dr. Rüdiger Schmidt-Grund
Dr. Alexander Weber
Dr. Holger von Wenckstern

PhD candidates

Dipl.-Phys. Tammo Böntgen
Dipl.-Phys. Kerstin Brachwitz
Dipl.-Phys. Matthias Brandt
Dipl.-Phys. Christian Czekalla
Dipl.-Phys. Christof Peter Dietrich
Dipl.-Phys. Martin Ellguth
Dipl.-Phys. Heiko Frenzel
Dipl.-Phys. Helena Hilmer
Dipl.-Phys. Philipp Kühne
Dipl.-Phys. Alexander Lajn
Dipl.-Phys. Martin Lange
Dipl.-Phys. Michael Lorenz
Dipl.-Phys. Alexander Müller
Dipl.-Phys. Matthias Schmidt
Dipl.-Phys. Stefan Schöche
Dipl.-Phys. Marko Stölzel
Dipl.-Phys. Chris Sturm
Dipl.-Phys. Gregor Zimmermann
Dipl.-Phys. Jan Zippel
Dipl.-Phys. Zhang Zhipeng

Students

Uta Allenstein
Ronny Bakowskie
Lucie Behnke
Michael Bonholzer
Martin Glaser
Christof Grüner
Lars Heerklotz
Robert Heinhold
Fabian Klüpfel
Oliver Kramer
Christian Kranert
Andreas Kraus
Johannes Kupper
Thomas Lüder
Annekatriin Meißner

Stefan Müller
Friedrich Leonhard Schein
Florian Schmidt
David Schumacher
Peter Schwinkendorf
Dieter Stender
Nuchjarim Yensuong

1.2.5 Solid State Optics and Acoustics, Festkörperoptik und -akustik [FKO]

Prof. Dr. Wolfgang Grill

Secretary

Mrs. Annette Käthner

Technical staff

PTA Hans-Joachim vom Hofe
Dipl.-Ing. (FH) Frank Peinemann
Dipl.-Ing. (FH) Ulrike Teschner
Dipl.-Phys. Horst Voigt

Academic staff

Dr. Mieczyslaw Pluta
Dr. Gerhard Birkelbach Trevor Byrnes, MBA
Omar Torres, B.A.

Doctoral students

Amro Abdelrahman, M.Sc.
Esam Eldin Ahmed Mohamed, M.Sc.
Umar Amjad, M.Sc.
Dipl.-Phys. Erik von der Burg
Dipl.-Phys. Moritz von Buttlar
Albert Kamanyi, M.Sc.
Zakir Hossain Muhammad, M.Sc.
Khurram Shahzad Tarar, M.Sc.

Students

Dipl.-Phys. Katrin Hahn (2009)
Angeline Kasina, M. Sc. (2009)
The Gia Tang, M. Sc. (2009)
Jonas Buchmann
Thomas Megel

1.2.6 Superconductivity and Magnetism, Supraleitung und Magnetismus [SUM]

Prof. Dr. Pablo Esquinazi

Technical staff

Dr. Winfried Böhlmann
Klaus Grünwald
Dipl.-Krist. Annette Setzer
Monika Steinhardt

Academic staff

Dr. José Barzola-Quiquia
Dr. German Brideaux
Dr. Roland Höhne
Dr. Detlef Spoddig
PD Dr. Michael Ziese

PhD candidates

Ana Ballestar, M.Sc.
Srujana Dusari, M.Sc.
Xiasong Jiang, M.Eng.
Muhammad Khalid, M.Sc.

Students

Francis Bern
Daniel Blaschke
Andreas John
Nico Klingner
Axel Molle
Thomas Scheike
Ralf Wunderlich

1.3 Institute for Theoretical Physics

1.3.1 Office of the Director

Prof. Dr. Rainer Verch (director)
Prof. Dr. Klaus Kroy (vice director)

Secretary

Susan Hussack
Gabriele Menge
Lea Voigt

1.3.2 Computational Quantum Field Theory, Computerorientierte Quantenfeldtheorie [CQT]

Prof. Dr. Wolfhard Janke

Academic staff

PD Dr. Michael Bachmann
Dr. Elmar Bittner
Dr. Adriaan M.J. Schakel
Dr. Bartłomiej Waclaw

PhD candidates

Dipl.-Phys. Mathias Aust
Dipl.-Phys. Rainer Bischof
Dipl.-Phys. Mario Collura (jointly with Nancy Université)
Dipl.-Phys. Monika Möddel
Dipl.-Phys. Andreas Nußbaumer
Dipl.-Phys. Stefan Schnabel
Dipl.-Phys. Sebastian Schöbl
Dipl.-Phys. Thomas Vogel
Sandro Wenzel, M.Sc.
Dipl.-Phys. Micha Wiedenmann

Students

Niklas Fricke
Jonathan Groß
Steffen Karalus
Martin Marenz
Hannes Nagel
Johannes Zierenberg

**1.3.3 Molecular Dynamics / Computer Simulation,
Moleküldynamik / Computersimulation [MDC]**

PD Dr. Horst-Ludger Vörtler (Speaker)
PD Dr. Siegfried Fritzsche

Academic staff

Prof. Dr. L. Ping
Dr. O. Saengsawang
Dr. T. Nanok

PhD candidates

Dipl.-Phys. M. Knauth
K. Seehamart, M.Sc.
R. Channajaree, M.Sc.
Somphob Thompho, M.Sc.

Students

K. Richter
L. Hertäg
S. Kalisch
D. Plotzki

1.3.4 Quantum Field Theory and Gravity, Quantenfeldtheorie und Gravitation [QFG]

Prof. Dr. Gerd Rudolph
Prof. Dr. Rainer Verch

Academic staff

PD Dr. Michael Bordag
Dr. Pjotr Marecki
Dr. Matthias Schmidt

Retired

Prof. em. Bodo Geyer
Prof. em. Armin Uhlmann

PhD candidates

Zhirayr Avetisyan, M.Sc.
Dipl.-Phys. Marcus Borris
Dipl.-Phys. Benjamin Eltzner
Dipl.-Phys. Alexander Hertsch
Dipl.-Phys. Thomas Ludwig
Dipl.-Phys. Jan Schlemmer
Dipl.-Phys. Jan Zschoche

Students

Andreas Degner
Erik Fuchs
Florian Fürstenberg
Michael Gransee
Martin Hofmann
André Jäschke
Alexander Knospe
Falk Lindner
Michael Schellenberger Costa
Juliane Stanja
Martin Teuchler
Almut Tröller
Konrad Zimmermann

1.3.5 Theory of Condensed Matter, Theorie der kondensierten Materie [TKM]

Prof. Dr. Ulrich Behn (Speaker)
Prof. Dr. Klaus Kroy
Prof. Dr. Dieter Ihle (retired)
Prof. Dr. Adolf Kühnel (retired)

Academic staff

Dipl.-Phys. Daniel Rings
Dr. Dipanjan Chakraborty

PhD candidates

Dipl.-Phys. Jens Glaser
Dipl.-Phys. Marcel Hennes
Dipl.-Phys. Holger Schmidtchen
Dipl.-Phys. Sebastian Sturm
Dipl.-Phys. Lars Wolff

Students

Frank Anselmi
Jakob Bullerjahn
Marc Höll
Andrea Kramer
Andreas Kühn
Norma Kühn
Damaris Kröber
Marc Lämmel
Heinz Seder
Benjamin Werner
Sven Willner

**1.3.6 Theory of Elementary Particles,
Theorie der Elementarteilchen [TET]**

Prof. Dr. Klaus Sibold

Academic staff

Dr. Burkhard Eden
PD Dr. Roland Kirschner
PD Dr. Holger Perlt
PD Dr. Arwed Schiller
Dr. Mathieu Segond

I

Institute for Experimental Physics I

2

Molecular Nano-Photonics

2.1 Introduction

The challenge of experimental physics on the nanoscale is to access local phenomena, that occur for example at interfaces, at specific molecular sites or at certain places within nano-structured materials. These local phenomena may control molecular dynamics, drive self-organization, cause charge separation or alter light propagation. Their importance extends to almost every field involved in future nanotechnology. The research of the molecular nano-photonics group thus aims at the development and application of optical techniques to access nanoscale (dynamical) processes in various fields such as chemical physics, biology or semiconductor physics. The understanding of these dynamical processes shall ultimately lead to a control over single molecules and other nano-objects by applying heat, flow, shear forces, electric fields or current.

The main experimental tool within our research is optical single molecule detection by ultra-sensitive microscopic techniques including time-resolved confocal microscopy, wide-field fluorescence or photothermal microscopy. Single molecules or semiconductor quantum dots provide the ideal local probes to access nanoscale physical properties inside materials while keeping the information on the heterogeneity of the system. Using these techniques recent projects focused on the

- Photothermal detection of single gold nanoparticles and nanorods
- Heat Transfer on the Nanoscale
- Nanometric distance measurements with single gold nanoparticle pairs
- Electrochemical manipulation of the emission of colloidal semiconductor nanocrystals
- Defocused imaging of single emitters in photonic crystals
- Single molecule diffusion in ultrathin confined liquid films, polymers and liquid crystals

During the year 2009 the Molecular Nanophotonics Group has established new experimental facilities including

- a confocal laser scanning optical microscope for single molecule detection at low temperatures
- a second sample scanning photothermal microscope for photothermal correlation spectroscopy
- fluorescence wide field microscope for high speed single molecule detection
- spatial modulation spectroscopy microscope for absorption cross-section measurements on single nanoparticles

The group has contributed in 2009 significant work to the DFG research unit 877 "From Local Constraints to Macroscopic Transport". Especially first collaborations with the group of Prof. Dr. Klaus Kroy (University Leipzig) and Dr. Michael Mertig (TU Dresden) have been very fruitful. Collaborative measurements with the groups of Prof. Friedrich Kremer and Prof. Markus Grundmann have been carried out.

Frank Cichos

2.2 Photothermal Correlation Spectroscopy

R. Schachoff, M. Selmke, M. Braun, F. Cichos, D. Rings*, K. Kroy[†],

*Institute of Theoretical Physics

[†]Institute of Theoretical Physics

Single molecule detection is a powerful technique to study dynamical processes in complex materials at the limit of analytical chemistry namely focusing on just one single molecule. It is, however, always restricted to fluorescent probes such as organic dye molecules or quantum dots. Within this project, we develop the technique of photothermal correlation spectroscopy [1] to trace the dynamics of single non-fluorescent nano-objects such as gold nanoparticles and nanorods in liquids and biomaterials.

Photothermal correlation spectroscopy (PhoCS) is based on the absorption of light and therefore free of photochemical processes such as photo-blinking or photobleaching. The release of the absorbed photon energy creates a local temperature gradient around the absorbing nano-object. The temperature gradient modifies the local refractive index which is used to detect single particles optically even though the scattering cross section is far below the single particle detection limit.

In our PhoCS approach, the absorbing nanoparticles are freely diffusing in water causing a photothermal signal burst at each passage through the microscopy focus. The length of these bursts provide information on the diffusion constant of these particles. During the last year, we have developed a burst length analysis for PhoCS. The burst length analysis measures directly the statistics of particle transit times. The transit time distributions (Figure 2.1) reveals a power law distribution which is cut-off by an exponential function. The decay time of this exponential function provides the diffusion time through the focal volume. Using this technique as well as the standard autocorrelation analysis, we have studied the diffusion of heated fold nanoparticles in water

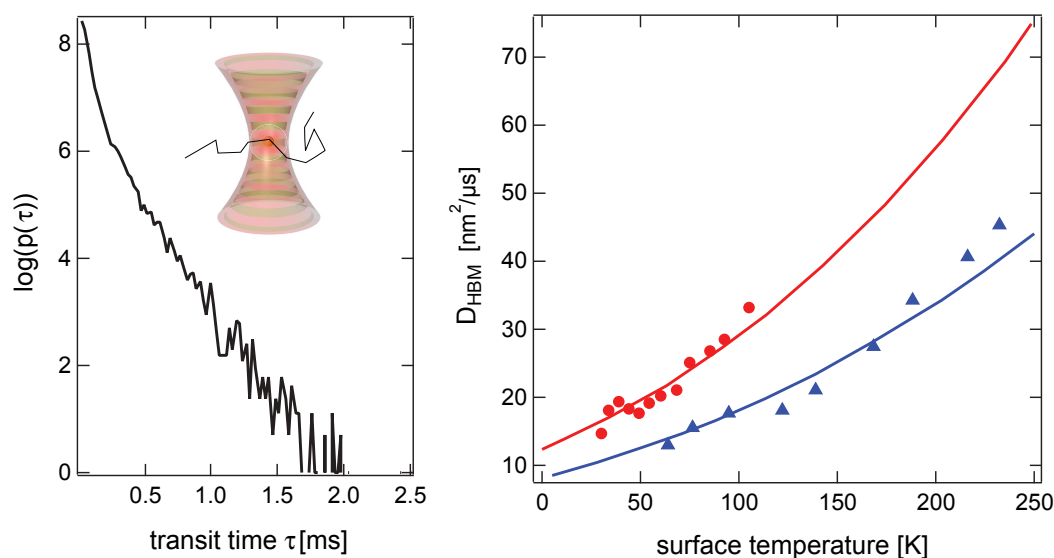


Figure 2.1: *Left:* Transit time probability density distribution of 60 nm gold nanoparticles in water as determined from photothermal correlation spectroscopy measurements. The inset shows a sketch of the technique using a modulated green (532 nm) heating laser and a red (645 nm) probe laser. *Right:* Calculated effective diffusion coefficients according to the theory (solid lines, blue: 60 nm gold nanoparticles, red: 40 nm gold nanoparticles) as a function of the particle surface temperature. The symbols represent the experimental data obtained from the burst width analysis in our photothermal measurements.

to evaluate the influence of the reduced hydrodynamic friction as well as the increased thermal fluctuations around heated particles.

This non-equilibrium Brownian motion is called Hot Brownian Motion (HBM) and can be well described by a new generalized Stokes-Einstein relation [2] as developed in collaboration with the group of Prof. Klaus Kroy (University Leipzig). A comparison of the obtained results are shown in Figure 2.1 and provide the basis for a future application of this technique as a replacement of fluorescence correlation spectroscopy.

[1] R. Radünz, D. Rings, K. Kroy, F. Cichos, *J. Phys. Chem. A* **113**, 1674 (2009).

[2] arXiv:1003.4596, submitted (2010), arxiv.org/abs/1003.4596

2.3 Orientation and Rotational Diffusion of Gold Nanorods

M. Selmke, M. Braun, A. Bregulla, F. Cichos

Rotational motion of single dye molecules is typically detected by polarization resolved emission microscopy, since the emission dipole of a dye molecule is rigidly linked to its structure. When utilizing photothermal detection as a tool to track non-fluorescent objects such as gold-nanoparticles, other properties have to be used to study rotational motion in soft matter. Here we employ the photothermal detection technique (see 2.2)

to detect gold nanorods as small as a few nm and to reveal their orientation when combined with a polarized excitation. Advantageous properties such as almost unlimited photo-stability and bio-inertness make it a promising tool for in-vitro applications.

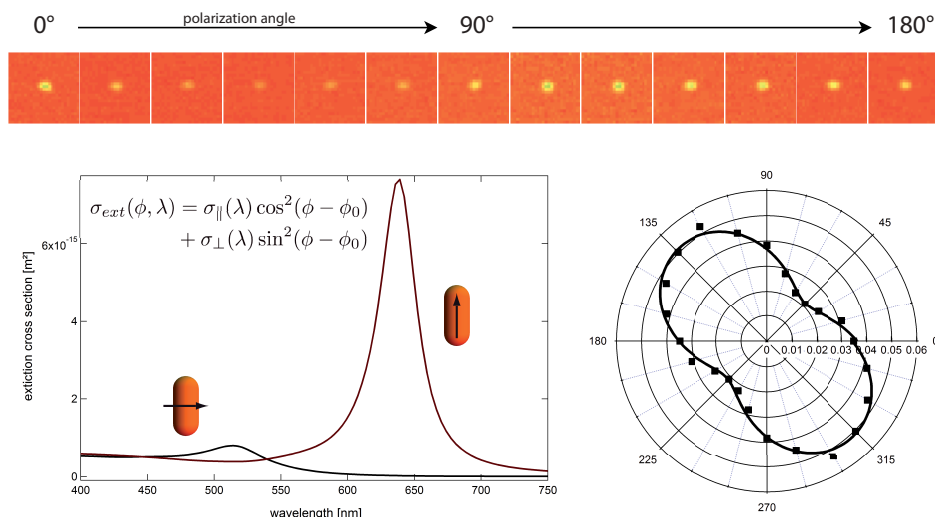


Figure 2.2: *Left:* Extinction cross section of gold nanorods (25 nm axial diameter and 60 nm length) for the light polarized parallel and perpendicular to the long axis of the rod. All intermediate polarizations are given by the superposition of these (formula). *Top & Right:* Rotating the polarizer by steps of 15° results in a modulation of the photothermal signal (photothermal images on top) and provides the rod orientation (polar diagram on the right).

Gold nanorods exhibit transverse and longitudinal surface plasmon resonances (SPR) that correspond to electron oscillations perpendicular and parallel to the rod length direction, respectively. One therefore has a polarization dependent extinction cross section (see Fig. 2.2). This gives us the opportunity to study the orientation of nanorods for instance immobilized on a glass substrate in the photothermal microscope. By rotating the polarization of the heating laser, one switches between parallel and perpendicular absorption, i.e. the photothermal signal which is a measure for the heat released by the nanorod to its surrounding thus is modulated.

Our current work is concentrated on the effect of rotational diffusion of single freely rotating gold nanorods in viscous melts on photothermal signal as detected by PhoCS. These studies should deliver new informations on the local environment of the nanorods in addition to PhoCS with gold nanospheres.

2.4 Photonic Crystals

R. Wagner, G. Kropat, F. Cichos

Photonic crystals (PCs) are materials with periodically varying refractive index. Scattering of light on this material leads to the formation of a photonic band structure, similar to the electronic band structure in semiconductors. This band structure modifies the propagation of light in the material. Since the variation of the refractive index

is depending on the position and the direction in the material, this is also true for the optical properties of a PC. We are investigating this properties using different spatial and angle resolved methods.

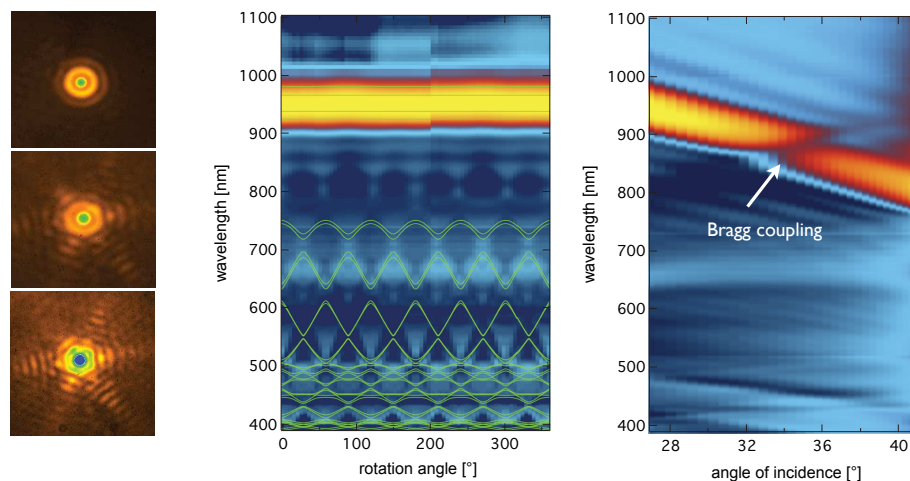


Figure 2.3: *Left:* Defocused images of a Nile red doped polystyrene bead in a 460 nm polystyrene colloidal photonic crystal. The images clearly show radial symmetry. *Middle:* Reflectivity of a 460 nm PC at an angle of incidence of 27° as a function of wavelength and the rotational angle in the sample plane (around the 111 direction). A six-fold symmetry can be observed, which is the result of the twinning structure of the photonic crystal. *Right:* Reflectivity of a 460 nm PC as a function of wavelength and the angle of incidence. A minimum in the reflectivity is observed for an incidence angle of 35° due to a coupling of Bragg reflections from different lattice plane families.

The PCs under investigation are 3D fcc crystals made by vertical deposition of polystyrene spheres. A small number of these beads contains fluorophores and can be used as local probes for the investigation of the PC. By varying the diameter of the polystyrene beads, different spectral regions of the band structure can be probed. The fluorescent beads are investigated by wide field microscopy in a defocused imaging mode. This results in spatially extended diffraction patterns which contain information about the anisotropic propagation of light in the PC. While the patterns show radial symmetry for smaller bead diameters, where emission of the fluorophores occurs in the region of the band gap, a three(six) fold symmetry is observed for larger beads (Fig. 2.3, left). This can be explained by Bragg reflections on different lattice plane families. Thus defocused imaging of emitters inside the PC provides a new method to reveal angle resolved light propagation with a single image. As our method uses internal emitters, we are further not restricted to optical modes which couple from the outside to the photonic crystal. To support the newly developed method we have carried out angle resolved reflection measurements in cooperation with the semiconductor physics group of Prof. Grundmann. For light with a frequency in the photonic band gap, the Bragg condition is fulfilled and light is reflected. For certain angles of incidence, however, the reflectivity is decreased to about half of the usual value (Fig. 2.3, right). This occurs, if the Bragg condition is fulfilled also for other lattice plane families. In this case part of the light is reflected into another direction and is therefore not detected. This effect takes place for certain combinations of angle of incidence and turning angle due to the symmetry of the crystal.

2.5 Electrochemical Manipulation of the Emission of Quantum Dots

A. Heber, N. Amecke, F. Cichos

Quantum Dots and dye molecules show an intermittent emission on timescales ranging from microseconds up several minutes. Such extremely long periods without any emission are still a mystery. They are thought to be related to photo induced charging processes. A charge, presumably an electron is ejected from excited state of an emitter by a tunneling process to the surrounding environment, which is often an unordered polymers or glass. Due to the rugged energy landscape in amorphous environments, the "on-off" blinking in quantum dots follows a robust power law statistics, which makes the characterization of the physical processes behind the blinking very difficult. In addition intensity fluctuations in so-called gray levels are observed, that correlate

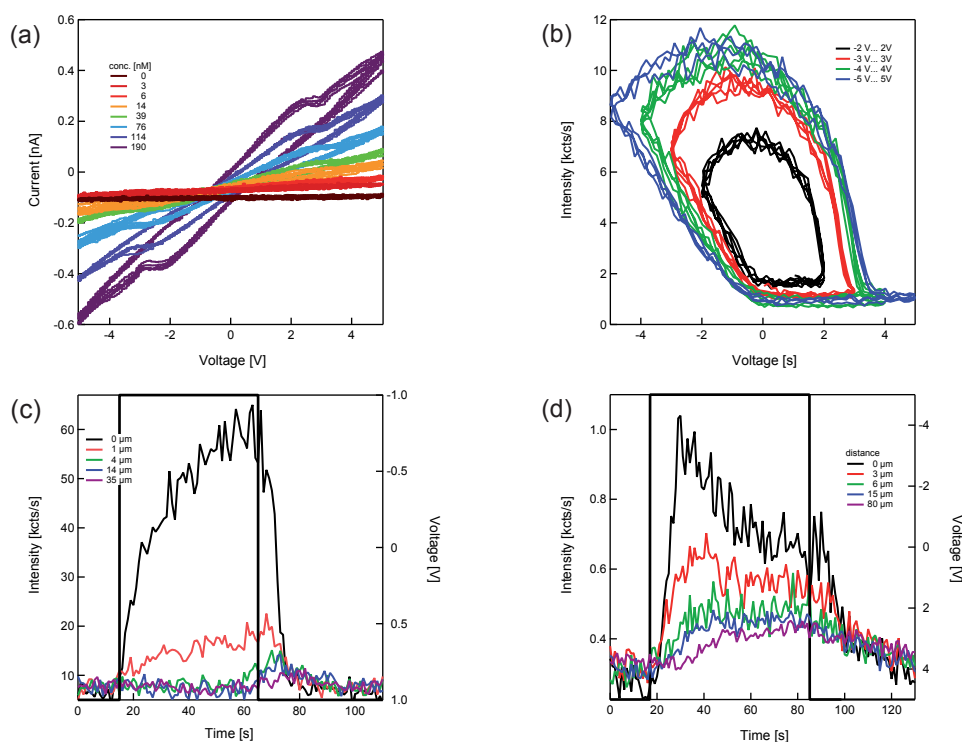


Figure 2.4: (a) Current-voltage diagrams for a suspension of CdSe/ZnS core shell quantum dots in toluene. (b) Emission intensity at the negative electrode during a voltage cycle of different voltage amplitude. Emission intensity of quantum dots at variable distance from the negative electrode for 1 V (c) and (d) 5 V.

proportionally with the measured lifetime. These levels are explained by fluctuating charge carriers at the quantum dot surface or close environment leading to an additional non-radiative decay channel comparable to the intrinsic radiative decay. Our studies are aimed at the direct correlation of a quantum dot charged state (especially its manipulation) and its fluorescence in solution to develop models for quantum dot emission intermittency and to eventually control it for applications. For this purpose we investigate the motion and fluorescence of quantum dots in solution in electric

fields. At low applied voltages (Fig. 2.4 (c)) we find a directed motion of quantum dots to the cathode, thus showing their net positive charge. Here especially the absence of particles with negative charge, is surprising. At higher voltages (Fig. 2.4 (d)) fluorescence at the cathode first rises but then falls, which we explain with the charging of quantum dot cores in analogy to blinking off-periods. Additional measurements of the current-voltage characteristics show redox-peaks which may be attributed to quantum dot charging potentials.

Thus our present experiments demonstrate the feasibility of optical detection and electrochemical manipulation of the charge state of colloidal quantum dots. Our future efforts will extend these measurements to single quantum dots to clarify the physical origin of quantum dot blinking.

2.6 Single Molecule Diffusion Anisotropy in Liquid Crystals

M. Pampa, F. Cichos

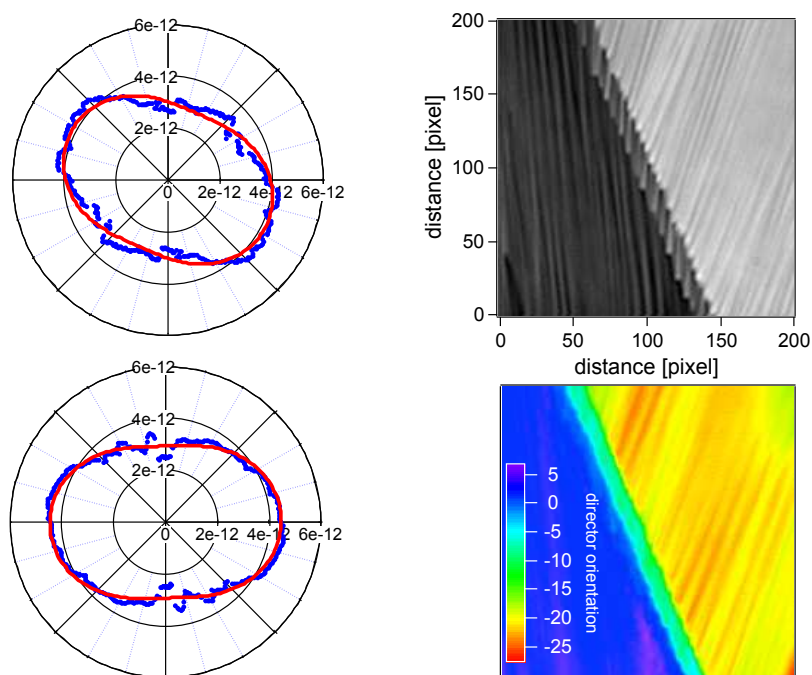


Figure 2.5: *Left top:* Angular dependence of the single molecule (dye: PDI) diffusion coefficient in the liquid crystal 8CB at room temperature as determined from the bright region of the top right image. *Left bottom:* Angular dependence of the single molecule (dye: PDI) diffusion coefficient in the liquid crystal 8CB at room temperature as determined from the dark region of the top right image. *Right top:* Polarization contrast image of the liquid crystal structure at crossed polarizers. *Right bottom:* Calculated director orientation of the liquid crystal in the different domains as obtained from a polarization image series.

In addition to the importance in display technology, liquid crystals appear in many applications in industry and research. From simple temperature sensors to their use in

tunable photonic crystals and a variety of optical components, wherever they are in use, their unique correlation between structure and dynamics is of importance. To obtain information about this behavior on the scale of nanometers, we dope the liquid crystal with single fluorescent molecules (PDI). The dye adopts the dynamical properties of the surrounding LC-Matrix and therefore serve as probes for spatially changing order and mobility. Our single molecule tracking experiments reveal the validity of this assumption. To compare the mobility of single tracer molecules with the actual structure in our sample cell, we make use of polarization contrast microscopy. Figure 2.5 shows recent results in a sample cell of the smectic A liquid crystal 8CB. A clear correlation between structure and dynamics of the probe-molecules can be seen, since the direction of fast diffusion points along the preferred orientation of the LC molecules in the two shown regions of the sample. Calculations from polarization contrast measurements clearly confirm this and thus allow for the first time a direct access to local structure-dynamics correlation at different location inside the liquid-crystalline domains. Future studies will involve temperature dependent measurements and more detailed studies at domain boundaries.

2.7 Single Molecule Nanorheology in Polymer Melts

M. Selmke, S. Adhikari, F. Cichos

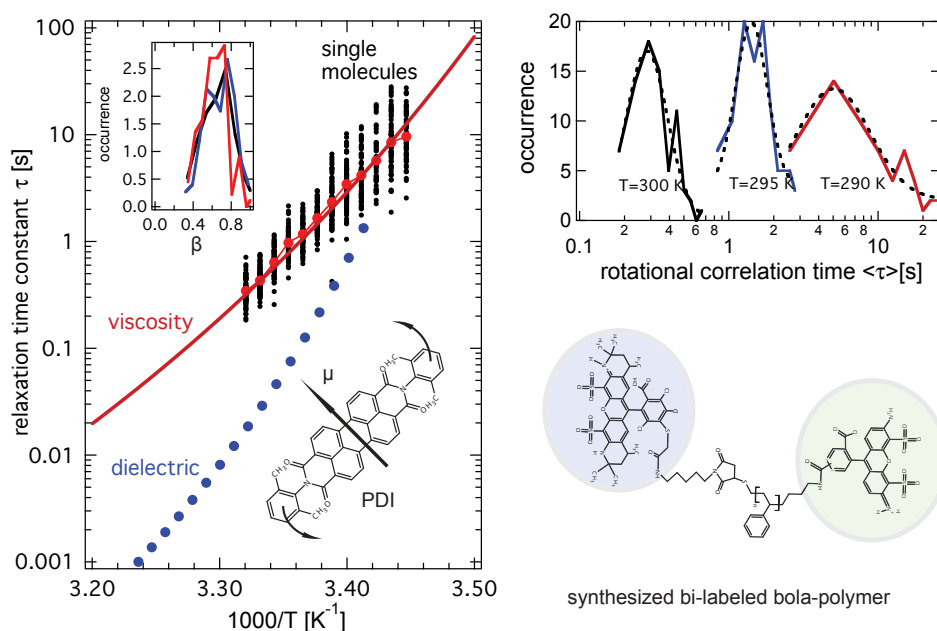


Figure 2.6: *Left:* Single molecule rotational diffusion times (black dots) of PDI (see structure inset) in polymethylacrylate as a function of the inverse temperature. The data is compared to shear viscosity measurements (red line) and dielectric spectroscopy data obtained for the same sample. The inset shows the stretching exponent β used in the stretched exponential function to fit the rotational correlation function. *Top right:* Distribution of rotational correlation times from single molecule trajectories at different sample temperature. *Bottom right:* Synthesized bi-labeled polystyrene molecule for energy transfer based distance fluctuation measurements.

The optical detection of single molecules (SMs) and the analysis of their rotational dynamics embedded in complex media such as glass-forming entangled polymer networks (studied so far: PMA poly(methyl acrylate), PVAc (poly(vinyl acetate))) revealed a surprising behavior of these nm-sized objects: They behave just like the fluctuation dissipation theorem and macroscopic hydrodynamics of spheres would predict, i.e. their reorientation fluctuations follow the macroscopic bulk viscosity η/T in value (applying the Debye-Stokes-Einstein (DSER) relation for rotational diffusion) and temperature dependence. While their rotational correlation times appear distributed and only a stretched exponential can describe the decay of orientation-correlation, a fluctuating environment model accurately recovers all statistical details of the extensive ensembles of single molecules which were studied for several temperatures, dyes and polymers. The application of a hydrodynamic framework to single molecules renders the development of a new form of what is known as micro-rheology promising: nano-rheology would utilize the distance-dependent interaction (FRET) of two fluorescent dyes separated by designed synthesis of a bola-like polymer-dual-dye-labeled molecule. The theory for two-point micro-rheology was therefore extended to the near-field.

2.8 Funding

Light Emission of Single Emitters in 3-dimensional Photonic Crystals

Frank Cichos

CI 33/5-2

Ortsaufgelöste Detektion von Struktur und Dynamik in nematischen Phasen biaxialer Moleküle

Frank Cichos

CI 33/6-1

FG 877: Constrained Single Molecule Dynamics in Glassy Polymer Systems

Frank Cichos

CI 33/7-1

BuildMONA, ESF-NFG: Funktionale multiskalige Strukturen

2.9 Organizational Duties

Frank Cichos

- Speaker DFG Research Unit 877 "From Local Constraint to Macroscopic Transport"
- Vorsitzender Eignungsfeststellungskommission Fakultät für Physik und Geowissenschaften
- stellv. Vorsitzender Promotionsausschuss
- Mitglied Prüfungsausschuss
- Mitglied Studienkommission
- Referee: Phys. Rev. B, Phys. Rev. Lett., Nature, Chem. Phys. Lett., Appl. Phys. Lett., ACS Petroleum Research Fund

2.10 External Cooperations

Academic

- TU Dresden
Prof. Dr. Michael Mertig
- University Konstanz
Regine von Klitzing
- TU Chemnitz
Prof. Dr. Christian von Borczyskowski
- TU Chemnitz
Dr. Harald Graaf
- Universität Mainz
Prof. Dr. T. Basché

2.11 Publications

Journals

Hot Brownian Particles and Photothermal Correlation Spectroscopy, R. Radünz, D. Rings, K. Kroy, F. Cichos, *J. Phys. Chem. A* 113, (2009), 1674.

Nanoscale Distance Fluctuations probed by Photothermal Correlation Spectroscopy, M. Wähnert, R. Radünz, F. Cichos, *Proc. SPIE* (2009) 71850(V).

FRET and ligand related NON-FRET processes in single quantum dot-perylene bisimide assemblies, D. Kowerko, J. Schuster, N. Amecke, M. Abdel-Mottaleb, R. Dobrawa, F. Würthner, C. von Borczyskowski, *PCCP* 12, (2009) Volume: 12, 4112-4123.

Identification of Different Donor-Acceptor Structures via Förster Resonance Energy Transfer (FRET) in Quantum-Dot-Perylene Bisimide Assemblies, D. Kowerko, S. Krause, N. Amecke, M. Abdel-Mottaleb, J. Schuster, C. von Borczyskowski, *Int. J. Mol. Sci.* 10, (2009), 5239-5256.

Electron tunneling effects and non-resonant photoluminescent quenching of semiconductor nanocrystals CdSe/ZnS and CdSe by porphyrin molecules in combined complexes, E. I. Zenkevich, T. Blaudeck, F. Cichos, C. von Borczyskowski *Theo. Exp. Chem.* 45(1) (2009) 17-26.

in press

Measuring Flow Profiles and Slip by Single Molecule Tracking Experiments, A. Schob, M. Pampa, M. Selmke, F. Cichos, *J. Phys. Chem. A* (in press).

Single Molecule Diffusion at Step Edges, A. Schob, F. Cichos, *Chem. Phys. Lett.* (in press).

Talks

Fluctuations in Nanosystems, TU Chemnitz, 2009, invited

Photothermal Detection and Photothermal Correlation Spectroscopy, Nanobiophysics, Antigua, 2009

Photothermal Correlation Spectroscopy, SPIE Spring Meeting, San Jose, 2009

Photothermal Correlation Spectroscopy, DPG Spring Meeting, Hamburg, March 2009, invited

Diffusion on Chemically Patterned Substrates and Diffusion of Hot Brownian Particles, DPG Spring Meeting, Dresden, March 2009, invited

Application of Photothermal Correlation Spectroscopy to the Study of Hot Brownian Motion, Verhandlungen der DPG, IV 44, 5 (2009) 100.

Analyzing Anisotropic Light Propagation by Defocused Imaging of Single Emitters, Verhandlungen der DPG, IV 44, 5 (2009) 114.

Distance Measurements by Photothermal Detection of Coupled Gold Nanoparticles, Graduate School BuildMoNa, Doctoral Workshop, Neukirchen/Pleiße, October 2009.

Single Molecule Dynamics in Polymers - Comparison to Dielectric and Mechanical Measurements, SFG 877 Symposium, Eibenstock, 11.03. – 13.03.2009

Polymers / Nanorheology, Orientation Tracking through Pattern Recognition, SFG 877 Meeting, Leipzig, 03.12.2009

Distance Measurements by Photothermal Detection of Coupled Gold Nanoparticles, Graduate School BuildMoNa, Doctoral Workshop, Neukirchen/Pleisse, 08.10. - 09.10.2009

Posters

Nano two-point Microrheology: Structure and Dynamics of Polymer-melts near T_g , Selmke, M., Adhikari, S. and Cichos, F., Verhandlungen der DPG, IV 44, 5 (2009) 82

Heterogeneous Dynamics of Polymer PMA Close to Glass Transition Temperature, Adhikari, S., Selmke, M. and Cichos, F., Verhandlungen der DPG, IV 44, 5 (2009) 96

Study of Glassy Dynamics of Polymer PMA by Single Molecule Detection Technique, Adhikari, S., Selmke, M. and Cichos, F., German-Indian Symposium "Frontiers of Chemistry", Leipzig, 16.09. – 19.09.2009

Investigations to the Influences of Charges on the Fluorescence of Single CdSe/ZnS Quantum Dots Dependent on Crystal Size, Amecke-Mönnighoff, N. and Cichos, F., Verhandlungen der DPG, IV 44, 5 (2009) 73

Optically Detected Cyclic Voltammetry on Single Semiconductor Quantum Dots, Amecke-Mönnighoff, N., Topalov, A. and Cichos, F., Bunsentagung, (2009) 95

Optically Detected Cyclic Voltammetry on Single Semiconductor Quantum Dots, Topalov, A., Amecke-Mönnighoff, N. and Cichos, F., Verhandlungen der DPG, IV 44, 5 (2009) 84

Modifying Single Particle Diffusion by Chemical Surface Patterning, Pumpa, M. and Cichos, F., Verhandlungen der DPG, IV 44, 5 (2009) 112

Application of Photothermal Correlation Spectroscopy to the Study of Hot Brownian Motion, Radünz, R., Rings, D., Kroy, K. and Cichos, F., Verhandlungen der DPG, IV 44, 5 (2009) 100

Thermal Trapping of Single Molecules in Liquids, Radünz, R., Cichos, F. and Würger, A., Verhandlungen der DPG, IV 44, 5 (2009) 86

Controlled Optical Heating of Single Metal Nanoparticles in an Optical Trap, Nedev, S., Radünz, R. and Cichos, F., Verhandlungen der DPG, IV 44, 5 (2009) 119

Photothermal Fluctuation Spectroscopy on Gold Nanoparticle Dimers, Wähnert, M., Neubauer, N., Radünz, R. and Cichos, F., Verhandlungen der DPG, IV 44, 5 (2009) 86 - 87

Photothermal Imaging of Gold Particles in Living Cells, Neubauer, N., Stüber, C., Käs, J. and Cichos, F., Verhandlungen der DPG, IV 44, 5 (2009) 88

Photothermal Fluctuation Spectroscopy on Gold Nanoparticle Dimers, Neubauer, N., Wähnert, M., Radünz, R. and Cichos, F., Graduate School BuildMoNa, 2nd Scientific Symposium, Leipzig, 02.04. – 03.04.2009

Analyzing Anisotropic Light Propagation by Defocused Imaging of Single Emitters, Wagner, R. and Cichos, F., Verhandlungen der DPG, IV 44, 5 (2009) 98

2.12 Graduations

Diploma

- Georg Kropat
Mehrfach-Bragg-Beugung in photonischen Kristallen
in progress
- Marco Braun
Local Temperature Measurements of Nanostructures Using Optical Methods
in progress

Master

- Angel Topalov
Optically Detected Cyclic Voltammetry on Single Semiconductor Quantum Dots
May 2009
- Zachar Krumer
Investigation of Fluorescence Intermittence in Semiconductor Nanocrystals
July 2009

- Spas Nedev
Controlled Optical Heating of Single Metal Nanoparticles in an Optical Trap
October 2009

Bachelor

- Christian Blume *Diffusion Einzelner Partikel auf Chemisch Strukturierten Oberflächen*
September 2009
- Leander Fiedler *Manipulation of the Diffusion of Nanoparticles by Thermal Fields*
September 2009

2.13 Guests

- Alois Würger
Université Bordeaux I, Frankreich
25.5.-30.5.2009
- Jörg Wrachtrup
Universität Stuttgart
28.4.2009

3

Molecular Physics

3.1 Introduction

Significant progress was made in all the traditional fields of research of our group including Broadband Dielectric Spectroscopy (BDS), time-resolved, polarized FTIR-Spectroscopy and experiments with Optical Tweezers. For "Ionic Liquids", the interplay between glassy dynamics and charge transport was unravelled and traced back to the laws of Brownian fluctuations as discovered by Einstein and Smoluchowski in 1905. Based on this, Joshua Rume Sangoro found a way to extract diffusion coefficients in a broad temperature and frequency range from dielectric measurements. This opens for BDS a completely new field of applications. Furthermore, the approach using nano-structured electrodes was successfully employed to study the molecular dynamics in nm thin polymer layers. With time-resolved polarized FTIR-Spectroscopy, details of the structural levels of organization of spider silk were explored. Especially, the phenomenon of super-contraction could be understood on a molecular level. Optical tweezers proved to be a versatile tool in Nano-(Bio)-Physics. Pioneering experiments on the interaction between polymer-grafted colloids and Single-Colloid-Electrophoresis could be carried out, to name a few.

Friedrich Kremer

3.2 Interfacial interactions and their impact on the glassy dynamics of thin layers of atactic poly(methyl methacrylate)

M. Tress, E.U. Mapesa, A. Serghei*, F. Kremer

*Polymer Science and Engineering, University of Massachusetts, Amherst

Broadband Dielectric Spectroscopy (BDS) and spectroscopic vis-Ellipsometry are combined to study the glassy dynamics of thin (≥ 10 nm) layers of atactic poly(methyl methacrylate) (PMMA) prepared under identical conditions. In order to unravel a possible effect of the underlying substrate the interfacial interactions are systematically modified ranging from strong attractive interactions for covalently bonded PMMA

brushes with high grafting density and for native silicon oxide (Si/SiO_x) to weak and strong repulsive interactions as realized by Au coated and HMDS treated Si/SiO_x surfaces, respectively. Down to the thinnest analyzed PMMA films and independently from the applied substrate both methods deliver - within the experimental accuracy (± 0.5 K for BDS and ± 2 K for Ellipsometry) a coinciding result. The glassy dynamics are not altered due to the geometrical confinement in these thin polymer layers (Fig. 3.1)

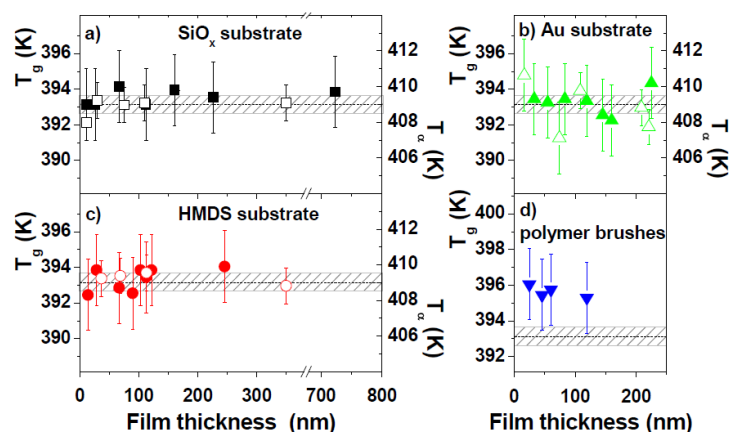


Figure 3.1: Glass transition temperature T_g measured by ellipsometry (filled symbols) and characteristic temperature T_α measured by BDS (open symbols) plotted versus film thickness. The measurements were carried out on different substrates having hydrophilic (a, Si/SiO_x) to hydrophobic (b, gold coating; c, silanized with HMDS) surfaces. Additionally, covalently bonded PMMA brushes on Si/SiO_x with strong attractive interfacial interactions were studied. As guidance for the eyes the calorimetrically determined T_g is shown as dashed line (an experimental error of ± 0.5 K was plotted for comparison).

[1] Erber, M.; Tress, M.; Mapesa, E.; Serghei, A.; Eichhorn, K.-J.; Voit, B. & Kremer, F. in preparation

3.3 Molecular weight dependence of the glassy dynamics of thin polystyrene layers

E.U. Mapesa, M. Tress, A. Serghei*, F. Kremer

*Polymer Science and Engineering, University of Massachusetts, Amherst

The glassy dynamics of ultra-thin (≥ 5 nm) layers of polystyrene (PS) is studied by means of Broadband Dielectric Spectroscopy (BDS) and vis-Ellipsometry under identical and well controlled conditions for a wide range of molecular weights (58.9 kg/mol - 8090 kg/mol). This revisits a controversial discussion raised 15 years ago by Keddy and Jones, who found pronounced changes of the glass transition temperature T_g in thin PS layers in their ellipsometric studies. Since that time numerous investigations focussed on this effect which is supposed to be caused by geometrical confinement.

Instead of unravelling its origin the results are contradictory as some studies do not observe confinement effects at all while others do definitely and even the used method seemed to affect the particular finding. Knowing about the strong impact of the sample preparation the present investigation emphasizes the identical preparation procedures in both applied methods and the coincidence of the results. Furthermore no confinement effects, namely no shift of the T_g , no change of the mean relaxation time and no broadening of the relaxation time distribution was found. Additionally the glassy dynamics is hardly affected by the molecular weight. The characteristic temperature of the α relaxation T_α of all molecular weights under study lies within a range of 4 K while the experimental error is as big as ± 2 K (Fig. 3.2).

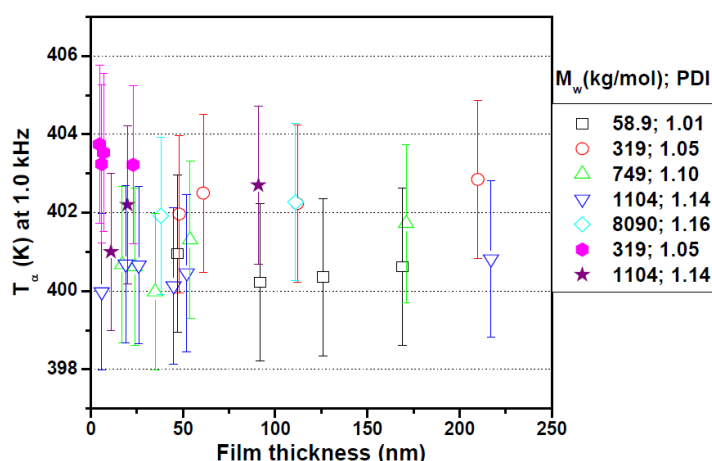


Figure 3.2: Thickness dependence of T_α at 1 kHz for different molecular weights of polystyrene as indicated. Empty symbols stand for measurements prepared with evaporated electrodes while filled symbols indicate the application of nanostructured electrodes. Within the limits of experimental uncertainty, down to 4.8 nm, dielectric relaxation dynamics are independent of both film thickness and molecular weight.

[1] Mapesa, E. U., M. Erber, M. Tress, A. Serghei, K.-J. Eichhorn, B. Voit and F. Kremer, in preparation

3.4 Real and apparent changes in the glassy dynamics of thin polymer layers - theoretical considerations

M. Tress, A. Serghei*, F. Kremer

*Polymer Science and Engineering, University of Massachusetts, Amherst

Manifold methods like Ellipsometry, Calorimetry and BDS were applied to unravel the mechanisms of confinement-effects in thin polymer layers. These effects are supposed to rise due to the changes of the polymer glassy dynamics in the nanometric vicinity of confining interfaces. However, beyond factors that can lead to real changes in the polymer dynamics, in the case of BDS measurements there are passive effects which can mimic confinement effects. To which extent this passive effect contributes to observed

changes of the dynamics depends strongly on parameters describing the heterogeneity of the system. A fairly simple model allows to calculate (equ. 1 and 2 for evaporated and nanostructured electrodes, respectively) some of these dependencies analytically while further investigation requires numerical analysis.

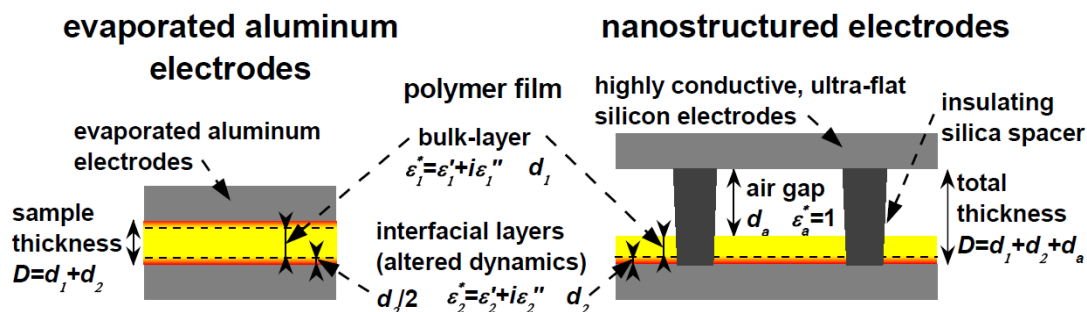


Figure 3.3: Sketch of the proposed layer model of a polymer film in two accessible sample arrangements.

[1] A. Serghei, A., M. Tress and F. Kremer, J. Chem. Phys. 131, 154904 (2009)

3.5 Impact of a novel preparation method on the glassy dynamics of thin polymer layers studied by means of Dielectric Spectroscopy

E.U. Mapesa, M. Tress, A. Serghei*, F. Kremer

*Polymer Science and Engineering, University of Massachusetts, Amherst

The impact of a recently developed preparation method on the measured glassy dynamics of thin polymer layers by means of BDS is investigated for different materials and compared to the results obtained with a common sample preparation. The new sample arrangement employs highly conductive ultra-flat silicon wafers as electrodes whereof one acts as support of the polymer layer while the other one is covered with silica nanostructures as spacers. The latter caps the polymer layer and acts as counter electrode, thus evaporation (like in common sample arrangement) is avoided and an additional air gap is created. The glassy dynamics of thin layers of PS (≥ 5 nm) were studied in both sample geometries. No shift of the mean relaxation time is observed in both geometries. However, using the conventionally evaporated electrodes leads to an increased broadening of the relaxation time distribution with decreasing layer thickness. Similar measurements were carried out on PVAc layers of constant thickness which were spin-coated onto silica layers of different thicknesses. These systems model the simplest case of altered dynamics in an interfacial layer, namely a $\text{O}^{\text{dead}}\text{O}$ layer ($\epsilon'' = \text{const.}$). In the samples prepared with evaporated electrodes a broadening is observed which depends on the ratio of the thicknesses of both layers while samples prepared with nanostructured electrodes do not show a broadening in the same range of thickness ratios.

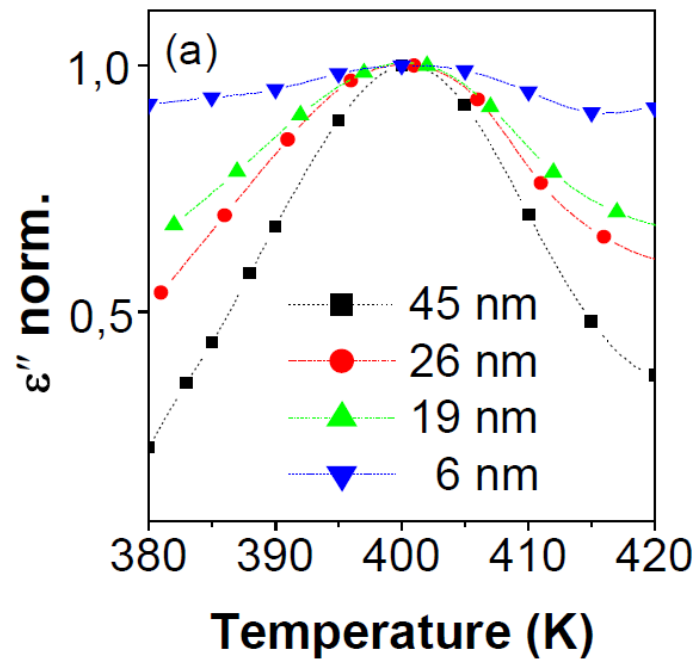


Figure 3.4: Normalized dielectric loss of thin PS layers prepared with evaporated (a) and nanostructured (b) electrodes at 0.8 kHz and 1 kHz, respectively.

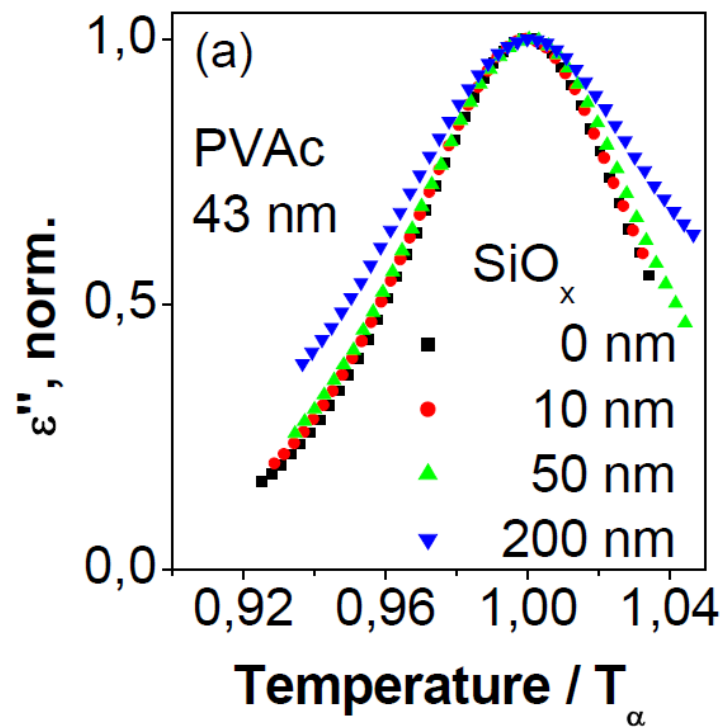


Figure 3.5: Normalized dielectric loss of PVAc layers on silica layers (thicknesses varied as indicated) prepared with evaporated (a) and nanostructured (b) electrodes at 123.9 kHz.

[1] Tress, M., E. U. Mapesa, A. Serghei, and F. Kremer, in preparation

3.6 Signatures in charge transport and glassy dynamics of molecular liquids

T. Schubert, J.R. Sangoro, C. Iacob, F. Kremer

Charge transport and glassy dynamics in a variety of amorphous materials are investigated by Broadband Dielectric Spectroscopy (BDS) [1]. Despite the apparently similar Vogel - Fulcher - Tammann - type thermal activation of the characteristic quantities (structural α -relaxation rate, diffusion rate and dc conductivity [Fig. 3.6 a]) significant differences are revealed by applying a model free derivative technique [1, 2] [Fig. 3.6 b]. A detailed analysis of the dielectric strength and its temperature dependence shows distinct characteristics caused by the differences in the type of molecular interactions involved in the materials studied.

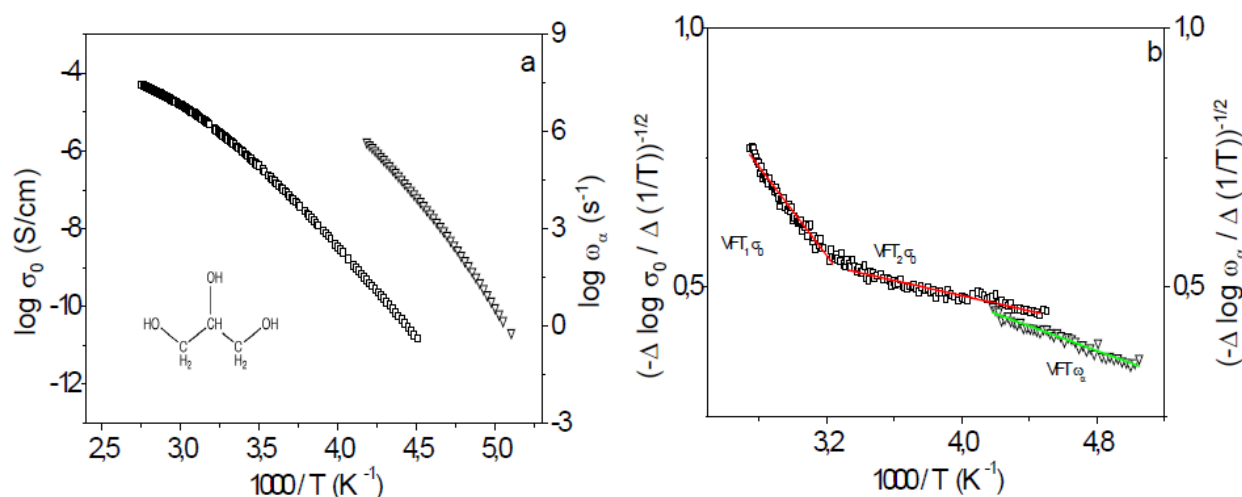


Figure 3.6: (a) Temperature dependence of the dc conductivity as well as the activation plot of the structural α -relaxation for Glycerol. Inset: structural formula for Glycerol. (b) Experimentally determined difference quotients of the dc conductivity ($(-\Delta(\log(\sigma_0))/\Delta(1/T))^{-1/2}$ vs $1000/T$; two VFT-fits are applied) and the structural α -relaxation ($(-\Delta(\log(\omega_\alpha))/\Delta(1/T))^{-1/2}$ vs $1000/T$ with one VFT-fit).

- [1] F. Kremer, A. Schönhal (Eds.) Broadband Dielectric Spectroscopy (Springer, Berlin, 2003)
- [2] F. Stickel et al. :Dynamics of glass-forming liquids. I : Temperature-derivative analysis of dielectric data, J. Chem. Phys. 102, 6251-6257 (1995)

3.7 Rotational and translational diffusion in ionic liquids

J.R. Sangoro, C. Iacob, F. Kremer

Charge transport and glassy dynamics of a variety of glass-forming ionic liquids (ILs) are investigated in a wide frequency and temperature range by means of Broadband Dielectric Spectroscopy (BDS), Pulsed Field Gradient Nuclear Magnetic Resonance (PFG NMR), AC Calorimetry, Differential Scanning Calorimetry and Rheology. The dielectric spectra are dominated – on the low-frequency side – by electrode polarization effects while, for higher frequencies, charge transport in a disordered matrix is the underlying physical mechanism. While the absolute values of dc conductivity and the characteristic charge transport rate vary over more than 11 decades with temperature, pressure and upon systematic structural variation of the ILs, a universal plot of the transport parameters is obtained (Fig. 1 (a)). This is discussed within the framework of the concept of dynamic glass transition driven hopping traced back to Einstein, Einstein-Smoluchowski, and Maxwell relations. A novel approach is applied to extract diffusion coefficients from BDS spectra in quantitative agreement with PFG NMR values but in a much broader range. It becomes possible to extract from the dielectric spectra separately the number density and the mobilities of the charge carriers and the type of their thermal activation (Fig. 1 (b)). It is shown that the observed Vogel-Fulcher-Tammann (VFT) dependence of the dc conductivity can be traced back to a similar temperature dependence of the mobility while for the number density an Arrhenius-type thermal activation is found.

- [1] Broadband Dielectric Spectroscopy, edited by F. Kremer and A. Schönhal, Springer (2003); J. R. Sangoro, A. Serghei, S. Naumov, P. Galvosas, J. Kärger, C. Wespe, F. Bordusa, and F. Kremer, *Phys. Rev. E* 77, 051202 (2008); J. R. Sangoro et al, *J. Chem. Phys.* 128, 214509 (2008) ; J. R. Sangoro, C. Iacob, A. Serghei, C. Friedrich, F. Kremer, *Phys. Chem. Chem. Phys.* 11, 913 (2009). J. R. Sangoro et al., (2010), under preparation.

3.8 Charge transport and dipolar relaxations in hyper-branched polymers

J.R. Sangoro, G. Turky, F. Kremer

Broadband Dielectric Spectroscopy, Pulsed Field Gradient Nuclear Magnetic Resonance (PFG NMR) and differential scanning calorimetry are combined to study charge transport and dipolar relaxations in novel hyper-branched polyamide amines (1-3). The dielectric spectra is dominated by conductivity contributions at higher temperatures (masking out the structural α -relaxation process)- whereas two secondary dipolar relaxation processes are observed at lower temperatures for the two samples investigated (Fig. 3.8). Based on Einstein and Einstein-Smoluchowski relations the diffusion coefficient is extracted from the dielectric spectra - in quantitative agreement with independent PFG NMR measurements. It exhibits a Vogel-Fulcher-Tammann-temperature dependence, while the effective number density of the charge carriers varies only

- [1] Broadband Dielectric Spectroscopy, edited by F. Kremer and A. Schönhal, Springer (2003).
- [2] Sangoro, J. R., Turkey, G., Abdel-Rehim, M., Naumov, S., Ghoneim, A., Kärger, J., and Kremer, F. (2009). *Macromolecules*, 42(5) 1648-1651.
- [3] Turkey, G., Sangoro, J. R., Abdel-Rehim, M., and Kremer, F. (2010). *J. Polym. Sci. B: Polym. Phys.*, in press

3.9 Characteristic hopping lengths and molecular volumes of ionic liquids

J.R. Sangoro, C. Iacob, F. Kremer

Translational diffusion in bis(trifluoromethylsulfonyl)imide-based glass-forming ionic liquids (ILs) is investigated in a wide frequency and temperature range by means of Broadband Dielectric Spectroscopy (BDS), and Pulsed Field Gradient Nuclear Magnetic Resonance (PFG NMR) [1-3] as shown in Fig. 3.9. It is experimentally shown that in the time-scale characterising the cross-over from sub-diffusive to diffusive ion dynamics, the hopping lengths are of the order of molecular diameters determined from quantum-chemical calculations [3]. This provides a direct means - via Einstein-Smoluchowski relation - to determine diffusion coefficient by BDS over more than 8 decades unambiguously and in quantitative agreement with PFG NMR measurements. Unprecedented possibilities in the study of charge transport and dynamic glass transition are thus opened.

- [1] Broadband Dielectric Spectroscopy, edited by F. Kremer and A. Schönhal, Springer (2003).
- [2] J. R. Sangoro, A. Serghei, S. Naumov, P. Galvosas, J. Kärger, C. Wespe, F. Bordusa, and F. Kremer, *Phys. Rev. E* 77, 051202 (2008); J. R. Sangoro et al, *J. Chem. Phys.* 128, 214509 (2008) ; J. R. Sangoro, C. Iacob, A. Serghei, C. Friedrich, F. Kremer, *Phys. Chem. Chem. Phys.* 11, 913 (2009).
- [3] J. R. Sangoro et al, (2010) Under preparation; J. R. Sangoro (2010), Doctoral dissertation, submitted.

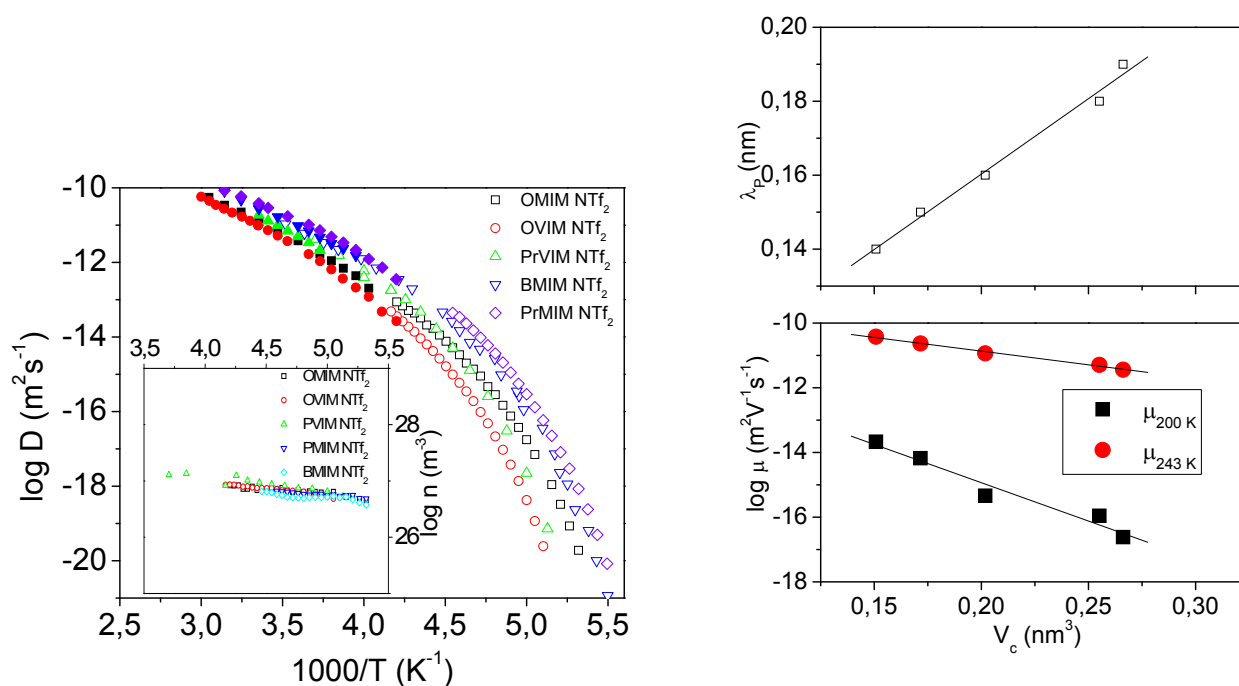


Figure 3.9: (a) Diffusion coefficients determined from broadband dielectric spectra (open symbols) upon applying the Einstein-Smoluchowski equation for a series of ionic liquids based on bis(trifluoromethylsulfonyl)imide anion as well as the diffusion coefficient measured by PFG NMR (filled symbols) versus inverse temperature. Inset: the effective number density of charge carriers as a function of inverse temperature. (b) The experimentally obtained hopping lengths (upon combining PFG NMR and BDS) versus the sum of molecular volumes of anions and cations obtained from quantum chemical calculations for the different ionic liquids based on the same bis(trifluoromethylsulfonyl)imide anion. The calculations are carried out in the temperature ranges spanned by both techniques. The mobility at two selected temperatures are also compared to the computed volumes.

3.10 Charge transport and diffusion of ionic liquids in nanoporous silica membranes

C. Iacob, J.R. Sangoro, F. Kremer

Charge transport in 1-hexyl-3-methylimidazolium hexafluorophosphate ionic liquid in oxidized nanoporous silicon membranes – prepared by electrochemical etching of (100) p-type silicon- is investigated in a wide frequency and temperature range by a combination of Broadband Dielectric Spectroscopy (BDS) and Pulsed Field Gradient Nuclear Magnetic Resonance (PFG NMR). By applying the Einstein-Smoluchowski relation to the dielectric spectra, diffusion coefficient is obtained in quantitative agreement with independent PFG NMR measurements (Fig. 3.10). More than 10-fold systematic decrease in the diffusion coefficient from the bulk value is observed in silica nanopores. This is explained within the framework of a model taking into account a decreased mobility at the interface of the pore and the nanoporous membrane due to the ability of the hydrogen-bonded ionic liquid to attach to SiO₂ surfaces. By that, it becomes possible to

probe the size of the adsorption layer and its temperature dependence. This has direct technological implications to the use of ionic liquids in fuel cells and nanobatteries.

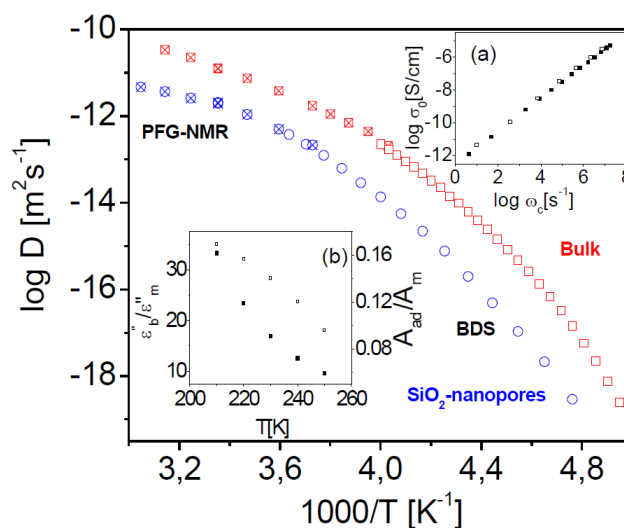


Figure 3.10: Diffusion coefficient determined by applying the Einstein-Smoluchowski equation to the dielectric spectra of HMIM PF6 (in bulk and nanopores denoted by empty squares and circles respectively) and measured by PFG NMR (in bulk and nanopores represented by crossed squares and circles respectively) versus inverse temperature. Inset: (a) dc-conductivity σ_0 versus the characteristic rate of charge transport ω_c (in bulk and nanopores represented by square filled symbols and empty square symbols respectively), (b) Temperature dependence of the ratio of the dielectric loss in bulk to the total dielectric loss in nanopores (full squares). The ratio of the surface area of the adsorption layer to the total area of the pores as a function of temperature are also given as shown (A_{ad}/A_m) (empty squares). This plot illustrates the origin of the deviation of the measured dc conductivity (and consequently diffusion coefficient) in nanopores from the bulk values.

- [1] Arndt, M., R. Stannarius, W. Gorbatschow, F. Kremer, Phys. Rev. E 54, 5377-5390 (1996)
- [2] C. Iacob, J. R. Sangoro, S. Naumov, R. Valiullin, J. Kärger and F. Kremer, Submitted to Phys.Chem.Chem.Phys.,(2010)

3.11 Charge transport and dipolar relaxations in Imidazolium-based Ionic Liquids

C. Krause, J.R. Sangoro, C. Iacob, F. Kremer

Charge transport and dipolar relaxations in a series of imidazolium-based ionic liquids are studied by means of broadband dielectric spectroscopy. Despite the shift of more than 5 decades in the dielectric spectra upon systematic variation of the anion, scaling with respect to the dc conductivities and the characteristic rates yields a collapsing plot. The dielectric spectra are described at higher frequencies in terms of dipolar relaxations whereas hopping conduction in a random spatially varying energy landscape is

quantitatively shown to dominate the spectra at lower frequencies. The α -relaxations observed for both the precursor and the ionic liquids are assigned to librational motion of the imidazolium ring. The corresponding dielectric strength exhibits a strong dependence on the anion [1].

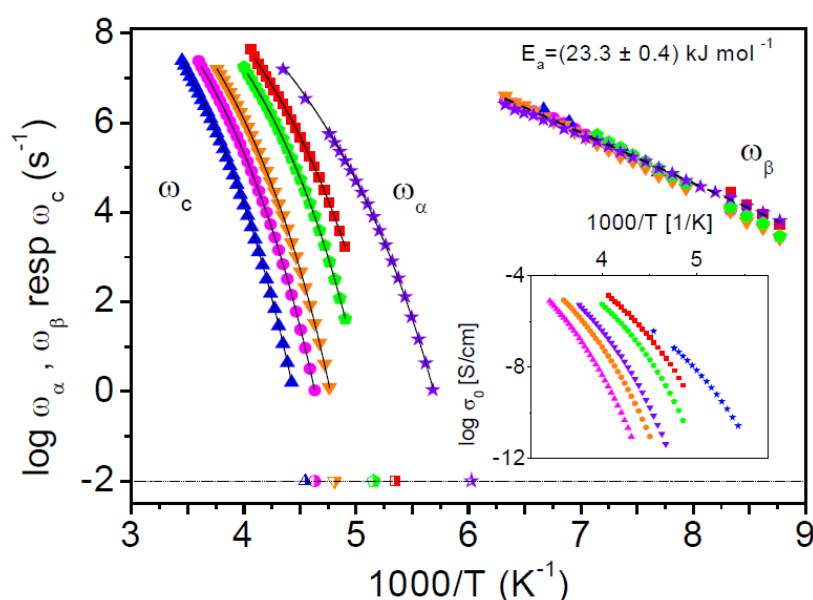


Figure 3.11: Temperature dependence of the structural α -relaxation rates of 1-hexyl-2-methylimidazole and the characteristic rates of charge transport as well as α -relaxations for the different ionic liquids. Inset: dc conductivity σ_0 as functions of inverse temperature ([HMIM][BF₄] (open squares), $T_g = 187$ K; [HMIM][Br] (open circles), $T_g = 216$ K; [HMIM][Cl] (open triangles), $T_g = 220$ K; [HMIM][I] (inverted open triangles), $T_g = 208$ K; [HMIM][PF₆] (open pentagons), $T_g = 194$ K; 1-hexyl-2-methylimidazole (open stars), $T_g = 166$ K). The error bars are smaller than the size of the symbols, if not specified otherwise. The experimentally determined values of calorimetric glass transition temperature T_g indicated by open symbols with vertical line.

[1] Krause, C., Sangoro, J.R., Iacob, C., Kremer, F. J. Phys. Chem. B, 114, 382D386 (2010)

3.12 Hierarchies in the structural organization of spider silk- A quantitative combined model

R. Ene, P. Papadopoulos, F. Kremer

Combined time-resolved mechanical and polarized Fourier-transform infrared measurements allow us to determine the interconnection of the nanocrystal and amorphous phases in major ampullate spider silk in the native and supercontracted states [1]. Crystal stress can be measured from the frequency shift of main-chain vibrations (Fig. 1a) [2]. In native silk the crystal stress is proportional to the external stress, regardless of strain, suggesting that a serial arrangement between the crystalline and amorphous phase dominates the nanostructure. However, supercontracted silk shows a different

behavior. At low strain, before being stretched to a threshold of ~ 0.2 GPa, the ratio of crystal to external stress is higher. At higher strain is irreversibly reduced to a value similar to native. These observations suggest that a hydrogen-bonded network is formed in the amorphous phase, due to release of pre-stress and hydrophobic effects. A three-component combined model of crystals in serial arrangement with amorphous chains and a fraction of chains bypassing them can describe all states of spider silk, assuming hydrogen bonding of worm-like chains at low pre-strain (Fig 1a)-inset) [3]. The understanding of the role of water in the formation of the hydrogen-bonded network in the supercontracted state is essential in the effort of relating the mechanical properties to the nanostructure. For this reason, water permeability of dragline silk is studied by measuring changes in amide deuteration (Fig.1b) [4]. The results show that the chemical exchange of amide hydrogen occurs in a large fraction of amino acids, including β -sheeted alanine residues, suggesting that also the crystalline regions are accessible to water. It is noteworthy that hydrogen at highly oriented moieties are most easily exchanged.

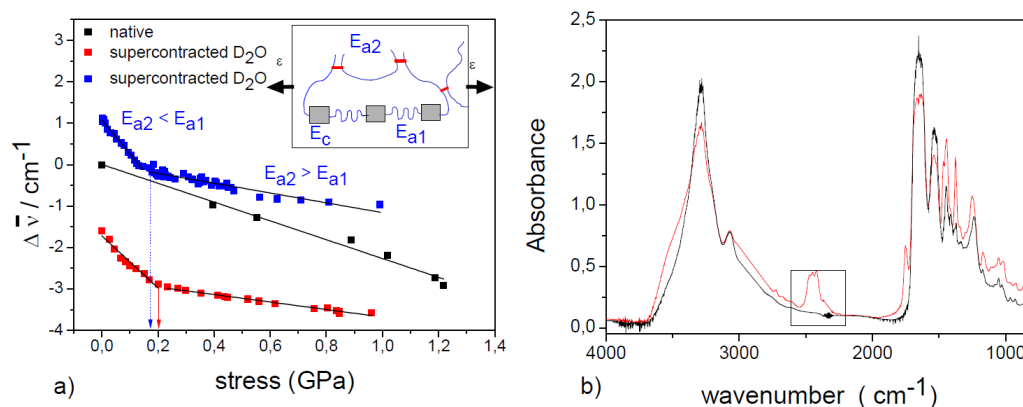


Figure 3.12: Crystal stress as a function of external stress. Inlet-combined structural model of organization in native and supercontracted spider silk. b) IR absorption spectrum of major ampullate silk from *Nephila edulis* in native state (black curve) and supercontracted state (D₂O-red curve). The spectral region between 2750 and 2250 cm^{-1} contains the ND bands resulted from the exchange of hydrogen with deuterium.

- [1] P. Papadopoulos, R. Ene, I. Weidner, F. Kremer *Macromol. Rapid Commun* 30, 851 (2009).
- [2] P. Papadopoulos, J. Sölter, F. Kremer; *Eur. Phys. J. E: Soft Matter* 24, 193 (2007)
- [3] R. Ene, P. Papadopoulos, F. Kremer, *Soft Matter* 5, 4568-4574 (2009)
- [4] R. Ene, P. Papadopoulos, F. Kremer (in preparation)

3.13 Spider silk: A soft solid with a unidirectional phononic band gap

P. Papadopoulos, F. Kremer

The superior properties of spider dragline silk, compared to synthetic polymers with similar chemical structure, such as polyamides, are due to the hierarchical nanostructure that is created in the spinning duct. Here we employ spontaneous Brillouin light scattering (BLS), a unique non-destructive and non-contact optical technique to probe propagation of thermally excited acoustic waves (phonons) at hypersonic frequencies (and hence wavelengths at the sub-micrometer length scale) in microstructures along different symmetry directions [1]. An unsuspected unidirectional phononic band gap is observed along the fiber axis (Fig. 1). At low wavevector values the dispersion diagram shows an acoustic behavior. The difference between the parallel and perpendicular directions is due to the high orientation of the protein along the fiber axis. At higher wavevector q in the parallel direction a stop band is observed, for the first time in biological structures [2]. Unlike periodic structures, such as colloidal crystals, it is not a Bragg-type band gap, since the nanocrystals do not form a periodic superstructure. In order to investigate possible relations between the supramolecular structure and the observed unidirectional gap, we study fibers with decreased or increased pre-strain, created by supercontracting or stretching, respectively. The reduced pre-strain increases the contrast between nanocrystals and the interconnecting amorphous chains and, therefore, between domains of higher and lower crystallinity. Stretching has the opposite effect, increasing mechanical anisotropy.

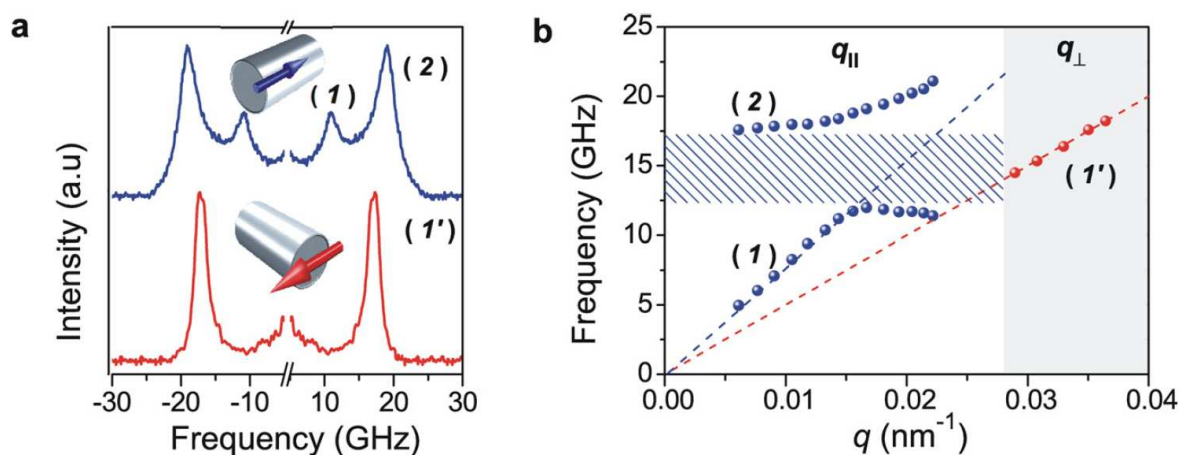


Figure 3.13: BLS spectra and experimental dispersion diagram of the native spider dragline silk along two symmetry directions. (a) BLS spectra at $q_{//}=0.0167 \text{ nm}^{-1}$ (in blue) with two peaks (1 and 2) along the fiber and at $q_{\perp}=0.0365 \text{ nm}^{-1}$ (in red) with one peak (1') normal to the fiber axis. (b) Dispersion relations for modes (1) and (2) (?) and mode (1') (?) representing elastic wave propagation parallel and normal to the fiber, respectively. The two dashed lines indicate the effective medium sound velocities in the two directions whereas the hatched area denotes the unidirectional stop band.

- [1] N. Gomopoulos, W. Cheng, M. Efremov, P.F. Nealey, G. Fytas (2009) *Macromolecules* 42:7164
 [2] N. Gomopoulos, P.Papadopoulos, F.Kremer, G.Fytas; submitted to PNAS (2010)

3.14 Electromechanical properties of smectic C* liquid crystal elastomers under shear

P. Papadopoulos, F. Kremer

Liquid crystal elastomers combine the electrical and optical anisotropy of liquid crystals with the mechanical properties of polymer networks. In smectic C systems, doping with chiral mesogen induces the formation of domains with permanent electric dipole moment. During the simultaneous crosslinking and orientation of the mesogen in a uniaxial mechanical field a polydomain morphology is obtained, where the piezoelectric effects are averaged out. Shear breaks the symmetry and induces the formation of monodomain structure (Fig. 1a) [1]. The piezoelectric coefficient reaches its maximum at a certain shear angle that corresponds to the completion of polydomain to monodomain transformation (Fig. 1b). The complex coefficient shows a strong dependence on temperature, especially near the smectic to isotropic transition (Fig. 2), but also on the static mechanical stress and frequency [2].

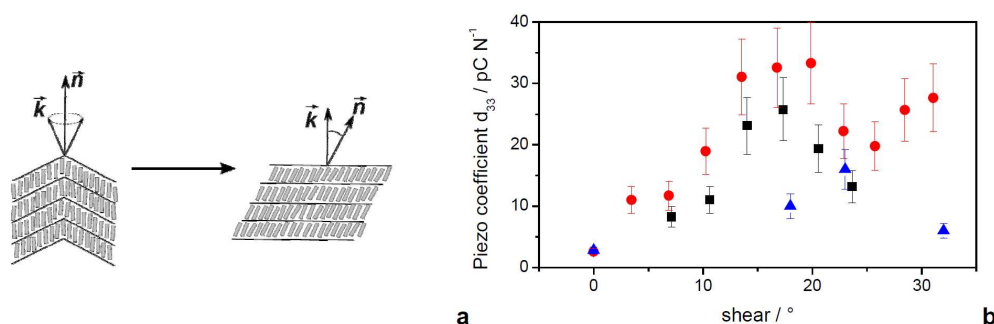


Figure 3.14: Shear dependence of the piezoelectric coefficient. (a) The polydomain morphology is converted to monodomain after shearing. (b) In all three independent measurements (three different samples) a clear maximum around 15-20deg is observed coinciding with the completion of polydomain to monodomain morphology conversion [1]. The measurements were carried out at 40 deg C, 100 Hz, static strain of 0.04 and static stress=0.5 MPa.

- [1] P. Heinze, H. Finkelmann; *Macromolecules* (2010)
 [2] P. Papadopoulos, P. Heinze, H. Finkelmann, F. Kremer; in preparation.

3.15 Infrared transition moment orientational analysis (IR-TMOA)

W. Kossack, P. Papadopoulos, F. Kremer

A novel spectroscopic method is developed for unravelling the mean orientation and molecular order parameter in any IR-transparent or translucent material. Combining the variation of inclination and polarization of the incoming electromagnetic wave the electric field can be chosen nearly arbitrarily. Taking advantage of the specificity of the IR spectral range, the directional dependence of the absorption coefficient provides detailed information concerning the directional distributions of the molecular moieties of the sample under study [1]. Furthermore a theory was developed, that takes into account the special properties of polymer films in the near infrared region and corrects for scattering and reflection [2]. Based on numerical solutions of Maxwell's equations the (three-dimensional) complex refractive index tensor can be determined for non-scattering samples [3].

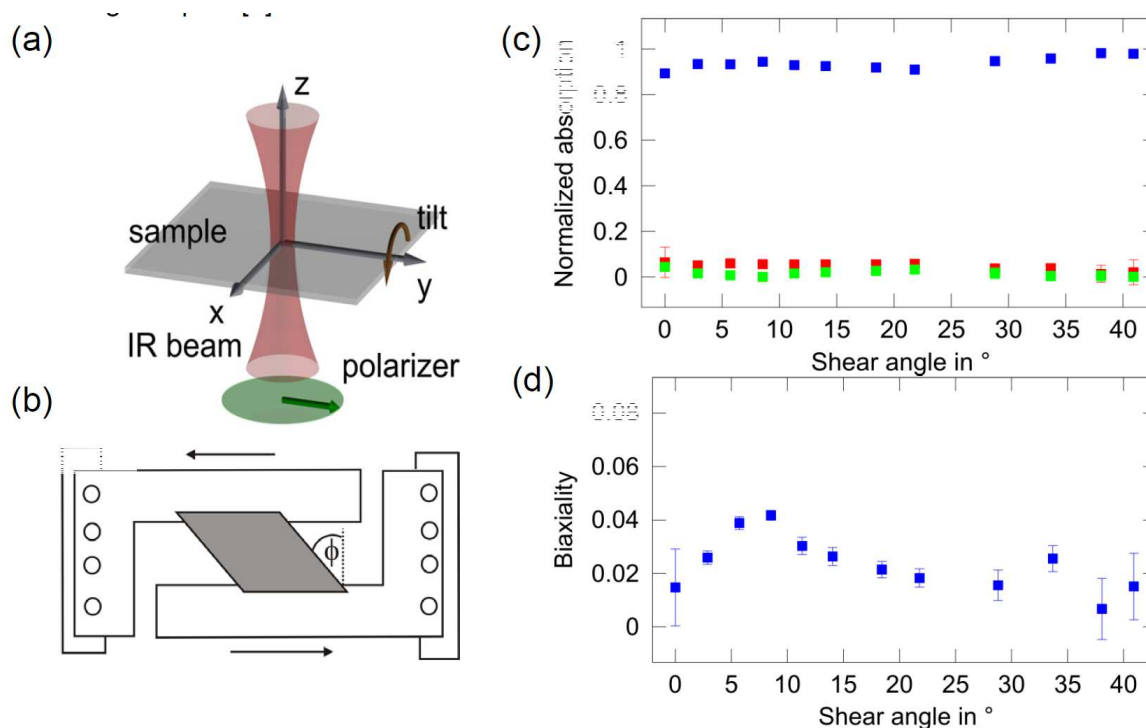


Figure 3.15: (a) Measurement principle used for the IR-TMOA technique. The electric field vector of the IR beam (green) can be rotated with a polariser, while the sample can be tilted. This way the electric field can have any direction. (b) Geometry of the shear measurement with definition of the shear angle ϕ ; The sample is indicated as the grey rhombus. (c) and (d) Application of IR-TMOA to a smectic liquid crystalline elastomer, (c) Normalized absorption coefficients are shown for three perpendicular directions. Since they are proportional to the quadratic averaged probabilities to find a molecule in that direction, it can be seen, that the sample is nearly uniaxial at the beginning but evolves with shear to a biaxial configuration before it returns to uniaxiality. The corresponding biaxiality parameter, which records the difference of the two minor absorption axes, is shown in (d).

- [1] Skupin, Dissertation (2001)
- [2] Kossack, P. Papadopoulos, F. Kremer in preparation (2010)
- [3] Yeh: Optical Waves in Layered Media (1948)

3.16 A novel position determination technique for polystyrene and silica colloids using video microscopy

C. Gutsche, O. Ueberschär, M.M. Elmahdy, G. Dominguez-Espinosa, F. Kremer

Common position detection methods in video microscopy typically produce significant artefacts when two or more colloids under observation are in close proximity to each other. In the paper [1] we present a new technique (Fig. 3.16) which is not subject to such artefacts up to a spatial resolution of ± 2 nm, the latter being the experimental uncertainty and thus lower limit of the used optical tweezers setup.

- [1] C. Gutsche, O. Ueberschär, M.M. Elmahdy, G. Dominguez-Espinosa and F. Kremer submitted to Rev. Sci. Instrum.

3.17 Forces of Interaction between Poly(2-vinylpyridine) Brushes As Measured by Optical Tweezers

M.M. Elmahdy, A. Synytska, A. Drechsler, C. Gutsche, P. Uhlmann, M. Stamm, F. Kremer

Forces of interaction within single pairs of poly(2-vinylpyridine) (P2VP) grafted colloids have been measured by optical tweezers (OT) with an extraordinary resolution of ± 0.5 pN [1]. Parameters to be varied are the concentration and type of salt (KCl, CaCl₂, and LaCl₃) of the surrounding medium as well as its pH. The observed force-distance relation is quantitatively described by the Jusufi model [2] for spherical polyelectrolyte brushes which takes into account the entropic effect of the counterions and enables one to estimate the ionic concentration inside the brush. The transition from an osmotic to the salted brush regime is analysed in detail. For the scaling of the brush height a power law is found having an exponent of 0.24 ± 0.01 which ranges between the values expected for spherical and planar brushes. At pH 4 a strong transition from a brush to a pancake conformation takes place.

- [1] M.M. Elmahdy, A. Synytska, A. Drechsler, C. Gutsche, P. Uhlmann, M. Stamm, F. Kremer *Macromolecules* 42, 9096 (2009).
- [2] A. Jusufi, C.N. Likos, M. Ballauff *Colloid Polym Sci.* 282, 910 (2004).

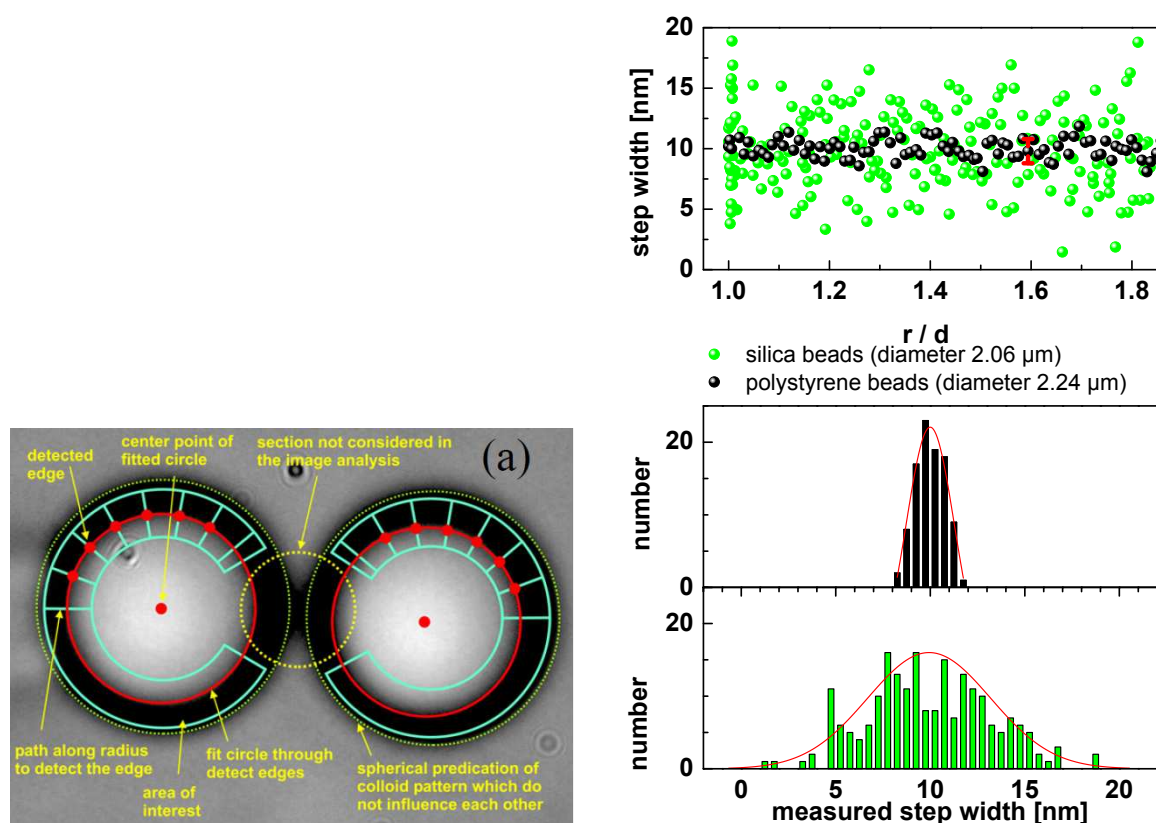


Figure 3.16: (a) Example of an obtained video image of polystyrene beads in the described experimental situation. The left-hand colloid is held by the tip of a micropipette whereas the right-hand one is trapped by the photonic potential. The effects of the superposition of the corresponding diffraction patterns as the cause for the deformation of the outer dark diffuse ring are apparent for distance-diameter ratios of $r/d < 1.4$. The yellow dotted circle indicates the area of deformation while the green small dotted circles adumbrate the (hypothetical) spherical diffraction patterns of the single colloids. The cyan and red lines illustrate the fitting framework for the position detection. (b) (top) Obtained step width of the colloid fixed to the pipette which was moved by the piezo stage in 10 nm steps versus the distance between the two colloids. The step width was measured by means of the discussed edge detection algorithm. The black spheres represent a measurement on polystyrene beads with a diameter of 2.24 μm whereas the green spheres correspond to an experiment with silica beads having a diameter of 2.04 μm . The red error bar indicates the position uncertainty of the piezo stage. (bottom) Distribution of the measured step widths. The upper histogram shows the distribution for polystyrene beads (black bars) while the lower histogram was obtained for silica beads (green bars). The red lines indicate the respective Gauss fits.

3.18 Interaction forces between a single pair of blank Si-lica surfaces as measured by Optical Tweezers

T. Stangner, M.M. Elmahdy, C. Gutsche, F. Kremer

Optical Tweezers are an excellent tool to investigate the interaction force between a single pair of spherical blank SiO₂ colloids (diameter $4.85 \pm 0.05 \mu\text{m}$) with an extraordinary resolution of ± 0.5 pN. The concentration dependence was recorded

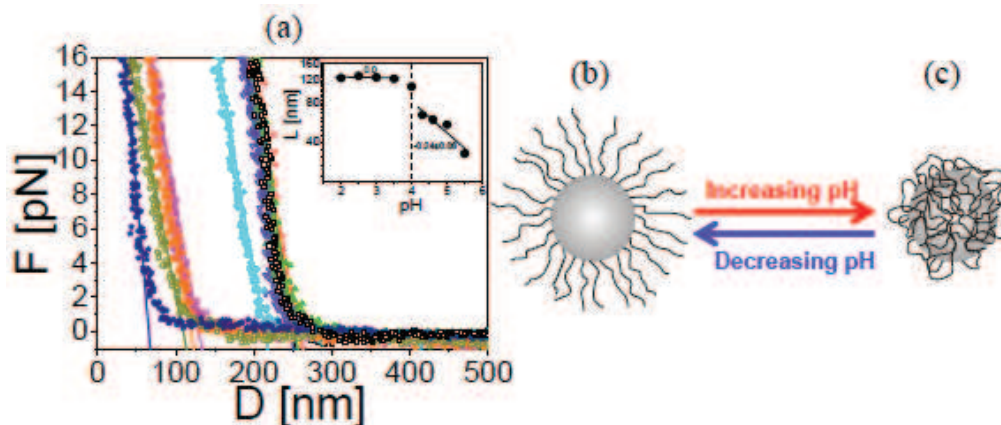


Figure 3.17: (a) Forces vs. separation D as measured for a single pair of P2VP-grafted colloids in media of varying pH: 2 (full squares), 2.5 (full circles), 3 (full up-triangles), 3.5 (full down-triangles), 4 (full diamond), 4.3 (full left-triangles), 4.6 (full right-triangles), 5 (full hexagon) and 5.5 (full stars) at 10^{-3} M KCl. To ensure full reproducibility of the exchange of the medium the sample cell was flushed again with 10^{-3} M at pH 2 (open squares) at the end of a measurement cycle. The solid lines represent the fits to the experimental data with Jusufi model. Inset: brush height L vs. pH at 10^{-3} M KCl obtained from analyzing the data using Jusufi model (full circles). The line of slope 0.24 indicates theoretical scaling law predictions for comparison. Right: Schematic illustration of the P2VP conformations with increasing and decreasing pH values. (b) At pH < 4 the P2VP chains are stretched away from the surface forming a brush-like conformation. (c) At pH > 4 the P2VP segments adsorb strongly to the underlying surface in a ‘pancake’-like conformation.

under different conditions e.g. varying salt concentration and valency (see Figure 1). The data are well described by Derjaguin-Landau-Verwey-Overbeek (DLVO) theory [3]. The main results are: i) the potential becomes steep with increasing the salt concentration (fig. (a)), ii) the effective surface charge decreases with increasing valency (inset) and iii) the interaction length λ decreases with increasing salt concentration and increasing valency (fig. (b))

- [1] M.M. Elmahdy, A. Drechsler, C. Gutsche, A. Synytska, P. Uhlmann, F. Kremer, M. Stamm, *Langmuir* 25, 12894 (2009)
- [2] C. Gutsche, U.F. Keyser, K. Kegler, F. Kremer, *Physical Review E* 76, 031403 (2007)
- [3] B.V. Derjaguin, L. Landau, *Acta Physicochim. URSS* 14, 633 (1941)

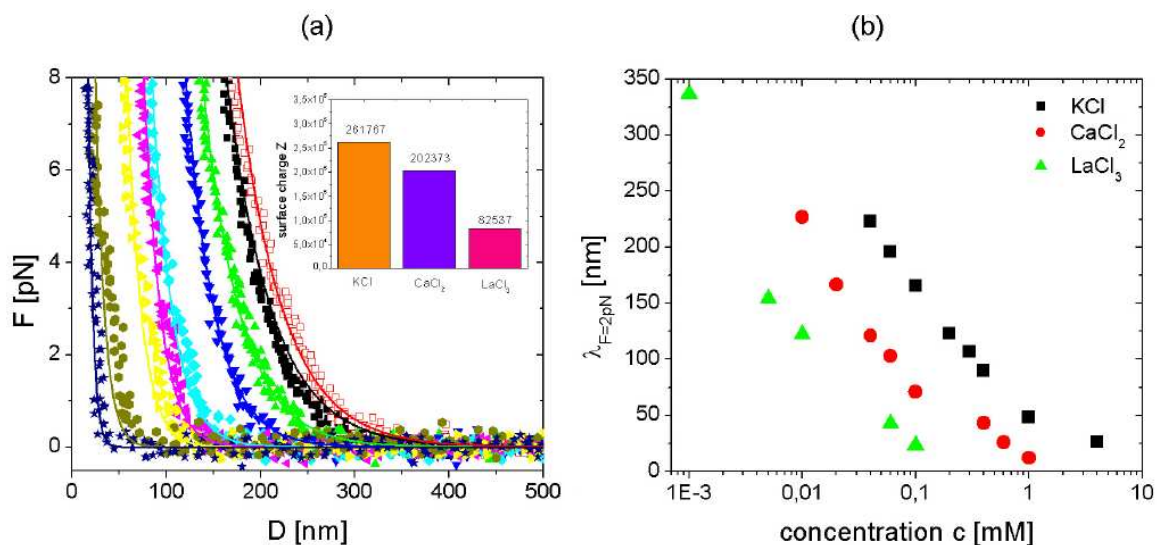


Figure 3.18: (a) Force vs. surface - to - surface distance D for a single pair of blank SiO₂ colloids (diameter $\sim 4.85 \pm 0.05 \mu\text{m}$) in aqueous solution of varying KCl concentration: 4×10^{-5} M (black squares), 6×10^{-5} M (green up-triangles), 10^{-4} M (blue down-triangles), 2×10^{-4} M (cyan diamonds), 3×10^{-4} M (magenta left-triangles), 4×10^{-4} M (yellow right-triangles), 10^{-3} M (dark yellow diamonds), 4×10^{-3} M (navy blue stars). At the end of this circle the cell was flushed again with $c = 4 \times 10^{-5}$ M (open red squares) to ensure the full reproducibility of the medium exchange. The dataset was fitted by DLVO theory [3]. Inset: Valency dependence of the effective surface charge as obtained from the fits. The surface charge decreases with increasing valency (orange bar: KCl, violet bar: CaCl₂, pink bar: LaCl₃). (b) The interaction length λ at a certain force of 2 pN in dependence of salt concentration and valency (black squares: KCl, red circles: CaCl₂, green up-triangles: LaCl₃).

3.19 Electrokinetics and Charge Inversion as studied by Single Colloid Electrophoresis (SCE)

I. Semenov, G. Stober, P. Papadopoulos, F. Kremer

Single Colloid Electrophoresis (SCE) [1] is employed to measure in a specifically designed microfluidic cell the electrophoretic mobility of a single particle and the electroosmotic mobility of a surrounding liquid using the identical colloid. Charge inversion in dependence on concentration and valency is observed and is proved to be fully reversible. In aqueous solution, electrostatic interactions play an important role for various properties of charged systems. The determination and prediction of the surface charge density of the particle's surface are thus of prime importance. This requires an accurate model for the electric double layer at the solid/liquid interface. The standard electrokinetic model [2,3], especially based on its mean field approximation, where the ions are treated as charged hard spheres and the solvent as a dielectric continuum is often used to describe these systems. However, this theory is not accurate in strongly coupled systems. That is, for systems containing multivalent ions, high ionic concentration and/or strong surface charge. A phenomenon known as charge inversion may be seen in electrokinetic measurements such as electrophoresis in presence of multivalent ions, where the sign of the electrokinetic potential appears to be opposite to the

expected one. The interpretation of such a result is still controversial. Often it is explained by specific chemical adsorption of multivalent counter-ions [4]. However, the pure electrostatic interactions, i.e. the ion-ion correlations, can cause charge inversion by the strong accumulation of counter-ions in contact with a charged surface [5]. In the present experimental study the complex electrophoretic response of a single colloid in monovalent (KCl), divalent (CaCl₂) and trivalent (LaCl₃) aqueous solutions is measured. Electrophoretic mobility of a single particle vs. ionic strength and ion valency are obtained.

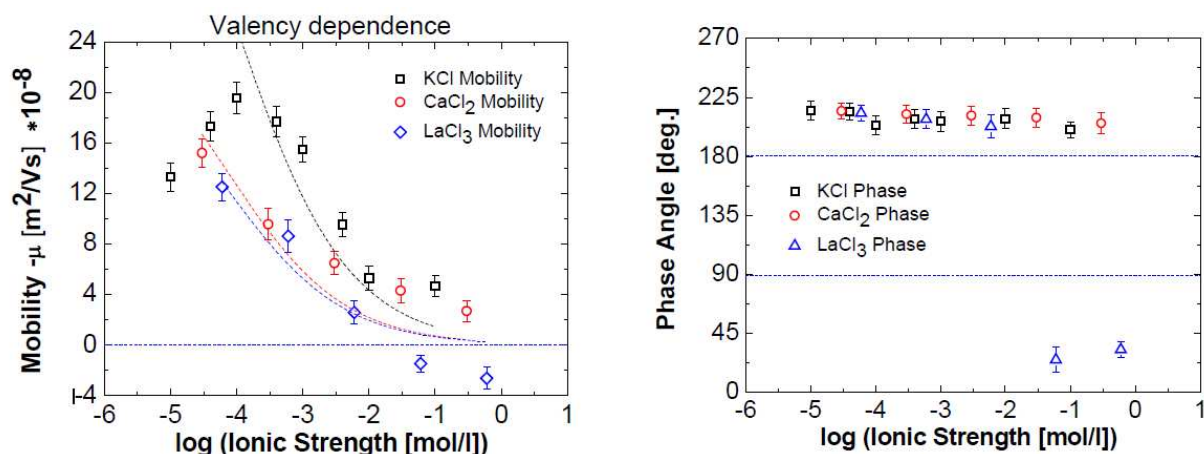


Figure 3.19: Electrophoretic mobility and Phase vs. ionic strength as indicated respectively for the identical negatively charged PS colloid (diameter: 2.23 μm), within a channel of length $l = 8$ mm. Laser power 0.2 W. The lines represent the Standard Electrokinetic Model (dashed line represent predictions for monovalent ions, solid line for divalent ions and dotted line for trivalent ions).

- [1] I. Semenov, O. Otto, G. Stober, P. Papadopoulos, U. F. Keyser and F. Kremer. *J. of Col. and Int. Sci.*, 337 (2009) 260-264
- [2] R. J. Hunter. *Zeta Potential in Colloid Science*. Academic Press, London, 1981.
- [3] J. Lyklema, *Fundamentals of Interfaces and Colloid Science*, vol. II, Academic Press, New York 1995
- [4] Johannes Lyklema. *Col. and Sci. A: Physicochem. Eng. Aspects.*, 291 (2006) 3-12
- [5] J. Lyklema. *Adv. in Col. and Int. Sci.*, 147-148 (2009) 205-213

3.20 Microscopic fluctuations and the emergence of irreversibility: Investigating stochastic thermodynamics

O. Ueberschär, F. Kremer

Since spring of 2008 we have been working on the experimental verification and application of several universal theorems of stochastic thermodynamics by means of optical tweezers. One of the major objectives of this new branch of modern thermodynamics is to find a consistent linkage between a macroscopic description and approaches at

the nano- and micrometre scale. For this purpose, well-known macroscopic quantities such as work, heat and entropy have to be generalized in such a way that their definitions prove reasonable, consistent and eventually useful even for single microparticles, e.g. micrometre-sized colloids. As a result, the corresponding, usually distinct levels of microscopic and macroscopic description of irreversible processes are finally unified. Starting from the widely accepted formal framework established by U. Seifert and others [7, 8], we follow and extend the experimental approaches of G. M. Wang et al. first published in 2002 [4-6]. In this way, we experimentally demonstrate the validity of several so-called fluctuation theorems for special non-equilibrium states of optically trapped colloids. In general, these fluctuation theorems form rigorous quantitative rules describing the emergence and quantitative evolution of irreversibility from a microscopic point of view. In detail, our measurements confirm the theoretical prediction that the microscopic total system entropy intriguingly may decrease on sufficiently short time scales. Our pertinent results in this context exceed the scope of Wang et al. 2002-2005 [4-6]. For instance, we have been able to verify the so-called detailed transient fluctuation theorem (TFT) and the universal integral fluctuation theorem (UIFT) as well as the integral fluctuation theorem (IFT) for a reproducible transient non-equilibrium state of a single colloid system.

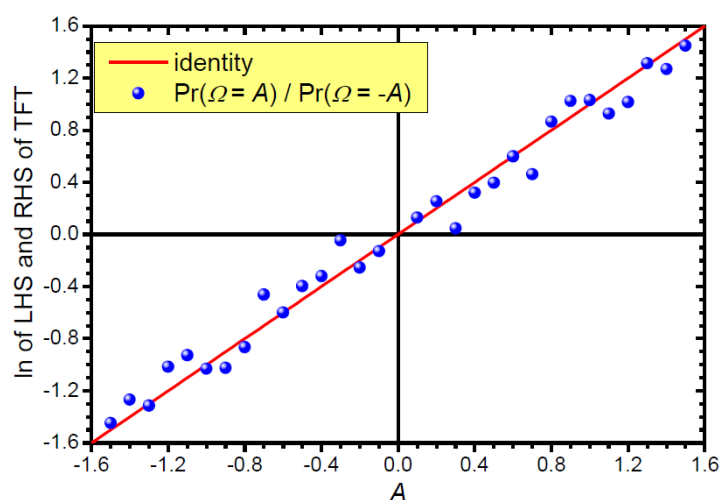


Figure 3.20: Experimental verification of the TFT. The graph shows the comparison of the left-hand side (LHS,) and the right-hand side (RHS, red line) of the TFT, i.e. for 6 000 single trajectories were measured in a reproducible transient non-equilibrium state for an identical colloid.

- [1] O. Ueberschär, C. Gutsche, F. Kremer, J. Phys. D: Appl. Phys, submitted (2009)
- [2] D. J. Evans et al., Phys. Rev. Lett. 71, 2401 (1993)
- [3] C. Jarzynski, Phys. Rev. Lett. 78, 2690 (1997)
- [4] G. M. Wang et al., Phys. Rev. Lett. 89, 050601 (2002)
- [5] D. M. Carberry et al., Phys. Rev. Lett. 92, 14, 140601 (2004)
- [6] G. M. Wang et al., Phys. Rev. E 71, 046142 (2005)
- [7] U. Seifert, Phys. Rev. Lett. 95, 040602 (2005)
- [8] U. Seifert, Eur. Phys. J. B (2008)

3.21 Funding

DFG-Teilprojekt "Nano- und Mikrofluidik: Von der molekularen Bewegung zur kontinuierlichen Strömung" SPP 1164 DFG-Schwerpunktprogramm 1164

Prof. Dr. F. Kremer

KR 1138/14-3 (2006-2010)

DFG-Projekt "Physicochemical characterisation of ionic liquids-mediated peptide acylation reactions" SPP 1191

Prof. Dr. F. Kremer

KR 1138/18-1 (2008-2010)

DFG-Projekt "In-situ Untersuchung der Wechselwirkungskräfte an Polyelektrolytbürsten"

Prof. Dr. F. Kremer

KR 1138/20-1 (2006-2009)

FOR877, DFG-Projekt: "From local constraints to macroscopic transport: Dynamics of DNA under tension and confinement"

Prof. Dr. F. Kremer and Prof. Dr. K. Kroy

KR 1138/21-1 (2007-2010)

SPP "Polymer-Festkörper-Kontakte: Grenzflächen und Interphasen" DFG-Teilprojekt "Interfacial dynamic of polymers in interaction with solid substrates" DFG-Projekt "In-situ Untersuchung der Wechselwirkungskräfte an Polyelektrolytbürsten"

Prof. Dr. F. Kremer

KR 1138/23-1 (2008–2011)

Prof. Dr. F. Kremer is Principal Investigator and Lecturer in the International Research Training Group "Diffusion in Porous Materials" headed by Prof. Dr. J. Kärger and Prof. Dr. F. Kapteijn.

Prof. Dr. F. Kremer

3.22 Organizational Duties

Prof. Dr. F. Kremer

- Project Reviewer: Deutsche Forschungsgemeinschaft (DFG)
- Editor: J. Coll. Polym. Sci.
- Member of Editorial Board: Macromol. Rapid Commun., Macromol. Chem. Phys., Polym. Adv. Technol.

3.23 External Cooperations

Academic

- Max-Planck-Institute for Microstructure, Halle, Germany
M. Alexe, F. Bordusa
- Leibniz-Institut für Oberflächenmodifizierung, Leipzig, Germany
D. Hirsch
- University of California, Santa Barbara, USA
Y.W. Kim
- Universität Konstanz, Germany
M. Krüger
- Universität Düsseldorf, Germany
C.N. Likos
- Lund University, Sweden
P.Linse
- Technische Universität München, Germany
V. Lobaskin, R. Netz
- Technische Universität Dresden, Germany
M. Mertig
- Universität Stuttgart, Germany
J. Harting, M. Rauscher
- Institute of Entomology, Ceske Budejovice, Czech Republic
A. Sponner
- Leibniz-Institut für Polymerforschung, Dresden, Germany
A. Drechsler, M. Stamm, A. Synytska, P. Uhlmann
- Brown University, Providence, USA 10
D. Stein
- University of Cambridge, UK
U. F. Keyser
- Universität Bayreuth, Germany
W. Zimmermann
- Universität Regensburg, Germany
R. Buchner
- Universität Potsdam, Germany
V. Strehmel
- University of California, Santa Barbara, USA
J. Israelachvili
- University of Princeton, USA
R. Prud'homme

Industry

- Novocontrol GmbH, Hundsangen, Germany

- Clariant Produkte (Deutschland) GmbH, Frankfurt am Main, Germany
- Comtech GmbH, München, Germany
- inotec FEG mbH, Markkleeberg, Germany

3.24 Publications

Journals

Papadopoulos, P., J. Sölter and F. Kremer: *Hierarchies in the structural organization of spider silk - a quantitative model*, Colloid and Polymer Science 287, Issue2, 231-236 (2009)

Sangoro, J. R., C. Iacob, A. Serghei, C. Friedrich and F. Kremer: *Universal scaling of charge transport in glass-forming ionic liquids*, Phys. Chem. Chem. Phys. 11, 913-916 (2009)

Sangoro, J. R., G. Turkey, M. Abdel Rehim, S. Naumov, A. Ghoneim, J. Kärger and F. Kremer: *Charge transport and dipolar relaxation in hyper-branched polyamide amines*. *Macromolecules*, Macromolecules 42 (5), 1648-1651 (2009)

Serghei, A., M. Tress and F. Kremer: *The glass transition of thin polymer films in relation to the interfacial dynamics*, J. Chem. Phys. 131 154904 (2009)

Min, Y., M. Akbulut, J.R. Sangoro, F. Kremer, R.K. Prud'homme, J. Israelachvili: *Measurement of forces between room temperature ionic liquids between mica surfaces*, J. of Physical Chemistry C 113, (37) pp.16445-16449 (2009)

Papadopoulos, P., R. Ene, I. Weidner, F. Kremer: *Similarities in the structural organization of major and minor ampullate spider silk*, Macromol. Rapid. Commun.30, 851-857 (2009)

Semenov, I., O. Otto, G. Stober, P.Papadopoulos, U.F. Keyser, and F. Kremer: *Single colloid electrophoresis*, J. Colloid Interf. Sci. 337, 260-264 (2009)

Serghei, A., M. Tress, J. R. Sangoro and F. Kremer: *Electrode polarization and charge transport at solid interfaces*, Phys. Rev. B 80 184301 (2009)

Ene, R. P. Papadopoulos, F. Kremer: *Combined structural model of spider dragline silk*, Soft Matter, 5, 4568-4574 (2009)

Serghei, A., M. Tress and F. Kremer: *The glass transition of thin polymer films in relation to interfacial dynamics*, J. Chem. Phys. 131,154904 (2009)

Kim, Y.W., V. Lobaskin, C. Gutsche, F. Kremer, P. Pincus, R.R. Netz: *Nonlinear response of grafted semiflexible polymers in shear flow*, Macromolecules, 42, 3650-3655 (2009)

Kipnusu, W.K., G. Katana, C.M. Migwi, I.V.S. Rathore, J.R. Sangoro, J. Tsuwi, A. Serghei, F. Kremer: *Molecular dynamics characterization of nandi flame seed cuticle biomaterials*, J. Polym. Mater, 26, 129 (2009)

Papadopoulos, P.; J. Sölter, F. Kremer: *Structural levels of organization in spider silk - a combined mechanical and infrared spectroscopic study*, *Soft Matter* (2009) DOI: 10.1039/b911159j.

Elmahdy, M.M., A. Drechsler, C. Gutsche, A. Synytska, P. Uhlmann, F. Kremer, M. Stamm: *Forces between blank surfaces as measured by the colloidal probe technique and by optical tweezers - a comparison*, *Langmuir* (2009) ASAP, DOI: 10.1021/la90180a.

Elmahdy, M.M., A. Synytska, A. Drechsler, C. Gutsche, P. Uhlmann, M. Stamm, F. Kremer: *The forces of interaction between poly(2-vinylpyridine) brushes as measured by optical tweezers*, *Macromolecules* (2009) ASAP, DOI: 10.1021/ma901567d.

Krause, C., J.R. Sangoro, C. Iacob and F. Kremer: *Secondary relaxations in imidazolium-based ionic liquids*, *J. Phys. Chem. B*, 114, 382-386 (2010)

in press

Kremer, F., A. Serghei, J.R. Sangoro, M. Tress and E. U. Mapesa, "Broadband dielectric spectroscopy in nano-(bio)-physics." *IEEE Transactions on Dielectrics and Electrical Insulation*, in press (2010)

3.25 Graduations

Doctorate

- Dipl. -Phys. Gunter Stober
Astrophysical Studies on Meteors using an All-Sky Meteor Radar - SKiYMET
June 2009

Diploma

- Wilhelm Kossack
Struktur-Eigenschaftsbeziehungen in Flüssigkristallinen Elastomeren
September 2009
- Olaf Ueberschär
Quantitative Untersuchungen zu Fluktuation, Dissipation und Irreversibilität anhand einzelner optisch gefangener Kolloide
June 2009

3.26 Guests

- Prof. Gamal Turkey
NRC, Cairo, Egypt
June -September 2009

4

Physics of Interfaces

4.1 Introduction

The year 2009 was a year of change in the academic staff and leadership of the group of Interface Physics. Our former students Konstanin Ulrich, Lars Heinke, Aleksey Khokhlov and Ekatarina Romanova, who successfully defended their Ph.D theses, left our group and continued their careers with attractive positions outside the University of Leipzig. In April, PD Dr. Frank Stallmach assumed the duties as interim group leader. Prof. Jörg Kärger retired from his duties at our university and Prof. Petrik Galvosas moved to a permanent position at the School of Chemical and Physical Sciences of the Victoria University of Wellington (New Zealand). Both scientists remain involved in the activities of the group by continuing their on-going projects, supervising the Ph.D students under their tutelage and, last but not least, by organizing the *10th Bologna meeting on Magnetic Resonance in Porous media* (MRPM 10), which will be hosted by our faculty in September 2010.

Besides these changes in the academic staff, the excellent funding situation through national and international collaborative research projects as well as individual grants by public foundations and industry partners allowed us to maintain and even improve our internationally recognized expertise in studying transport and interaction of molecules under the influence of internal interfaces of nano-structured materials. As Heisenberg fellows, Grit Kalies and Rustem Valiullin were successfully integrated in our group. They worked in their own research fields extending in this way our traditional NMR and optical microscopy tools to state-of-the-art adsorption techniques, synthesis of mesoporous materials with controlled pore structures and new theoretical approaches to analyse hysteresis phenomena in porous materials.

The following abstracts highlight in a more detailed way our research activities in 2009. They show how we developed our experimental methods and how we successfully applied them to study microporous metal-organic frameworks and zeolites, new types of mesoporous glasses and silica as well as disordered porous materials such as natural sediments and hydrating cements. We hope that you will find them as interesting as we do and would like to encourage you to contact us, if you have further questions.

Jörg Kärger and Frank Stallmach

4.2 Investigating Surface Barriers and Sorbate-Induced Transition Effects of Silicalite-1 by Means of Interference Microscopy

T. Binder, F. Hibbe, C. Chmelik, W. Schmidt*, J. Kärger

*Max-Planck-Institut für Kohlenforschung, Mülheim a.d. Ruhr, Germany

For studying the uptake and release of guest molecules into Zeolites or Metal-Organic Frameworks (MOFs), the combination of IR- and Interference Microscopy (IFM) proved to yield deep insights into single crystal sorption behaviour as well as characteristics of surface barriers. The present work focuses on Silicalite-1 (MFI-type framework) and the effects of surface modification and sorbate-induced transitions. The evaluation of surface permeabilities especially benefits from the unique ability of the IFM technique, to record spatially and time resolved intra-crystalline concentration profiles.

Complementing older IR and IFM studies [1, 2], recent results of TMCS modified Silicalite-1 show a much stronger influence of residual water on the surface permeability during isobutane adsorption and therefore on the kinetics of this process compared to unmodified crystals.

Furthermore, a quite challenging transition effect induced by a certain loading of benzene or p-xylene in Silicalite-1 is under investigation. In this case for the first time in IFM studies the change of a crystal's optical density has been found to be no longer proportional to the intra-crystalline concentration of guest molecules. This may indicate a transition of framework symmetry as well as in the orientation of the adsorbed molecules within the channels.

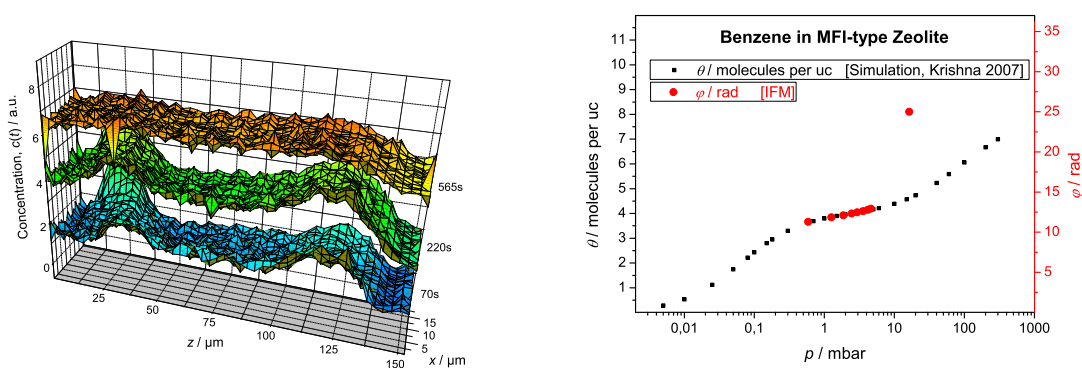


Figure 4.1: 2D concentration profiles of isobutane in surface-modified Silicalite-1 (*left*). Isotherm of Benzene in Silicalite-1, comparison of simulation and experiment (*right*). IFM value at 16 mbar shows the sorbate-induced transition effect.

[1] C. Chmelik et. al.: Chem. Mater. **19**, 6012 (2007)

[2] D. Tzoulaki et. al.: Micropor. Mesopor. Mater. **110**, 72 (2008)

4.3 Characterizing Molecular Transport in Nanopores

C. Chmelik, H. Bux*, J. Caro*, L. Heinke, F. Hibbe, J. Kärger

*Leibniz Universität Hannover

Zeolitic imidazolate frameworks (ZIFs) exhibit a high thermal and chemical stability and belong to the most promising candidates for new technical applications among the group of metal-organic frameworks (MOFs; a new class of nanoporous materials). Diffusion is among the key properties which may decide about the use in mass separation or catalysis.

We investigated adsorption and diffusion of methanol, ethanol, and ethane in large crystals of ZIF-8 using IR microscopy [1]. The results reveal features of mass transfer (Fig. 4.2) which, though suggested by first-principles considerations, have never before been confirmed experimentally to a similar extent: (i) self- and transport diffusivities merge for vanishing concentration, (ii) with increasing concentrations, they may easily transferred into each other via the adsorption isotherms, which includes (iii) the option of self-diffusivities exceeding the transport diffusivities (i.e. *fluxes are accelerated rather than slowed down by counter fluxes!*). This can be rationalized by considering the strong inter-molecular interaction and the dominating role of inter-cage hopping in mass transfer [1].

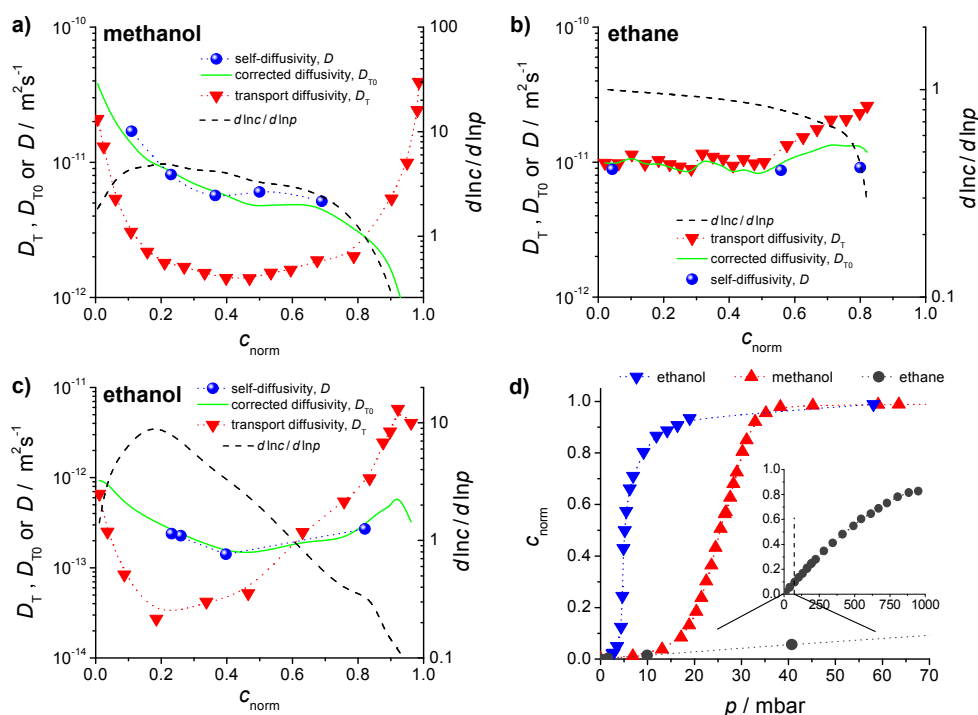


Figure 4.2: Methanol, Ethane and Ethanol in ZIF-8 at 298 K. Loading dependence of transport (D_T), corrected (D_{T0}) and self-diffusivity (D) of (a) methanol, (b) ethane and (c) ethanol. The inverse thermodynamic factor $d \ln c / d \ln p$ (obtained from (d)) is also shown. (d) Adsorption isotherms: The isotherms of methanol and ethanol exhibit a pronounced S-shape (type III or V isotherm), whereas the isotherm of ethane follows the common type I trend [1].

[1] C. Chmelik et al.: Phys. Rev. Lett. **104**, 085902 (2010)

4.4 Transport through Zeolitic Imidazolate Frameworks: From Molecular Diffusion to Membrane Permeation

C. Chmelik, H. Bux*, J. Caro*, S. Fritzsche, L. Hertäg, R. Krishna[†], J. Kärger

*Leibniz Universität Hannover

[†]University of Amsterdam, The Netherlands

Recently, several patents were issued involving ZIFs (e.g. [1]) and permeation results on the first gas-separating ZIF-membrane (ZIF-8) have been published [2]. For understanding, predicting and optimizing such separation processes knowledge on the adsorption and diffusion mechanisms of the guest molecules is essential.

IR microscopy (IRM) was applied to study the adsorption (Fig. 4.3a) and diffusion (Fig. 4.3b) of CO₂ and CH₄ and their mixtures in giant ZIF-8 crystals (up to 300 μm) aimed to provide some insight in the separation potential of this system. The results were compared with molecular simulations and data from membrane permeation and found to be in consistent agreement.

We note that the (single component) diffusivity of CH₄ increases much steeper with loading than for CO₂. Except from very low loadings the diffusivity of CH₄ is substantially higher than for CO₂. In accordance with the common experience in mixture diffusion we found that the more mobile component (CH₄) is slowed down much more severely than the mobility of the tardier component (CO₂) is increased. Finally we could demonstrate that the permeation selectivity of a membrane may be estimated by multiplying the adsorption and diffusion selectivities. The selectivity depends notably on the applied pressure and has to be carefully chosen to optimize the membrane performance.

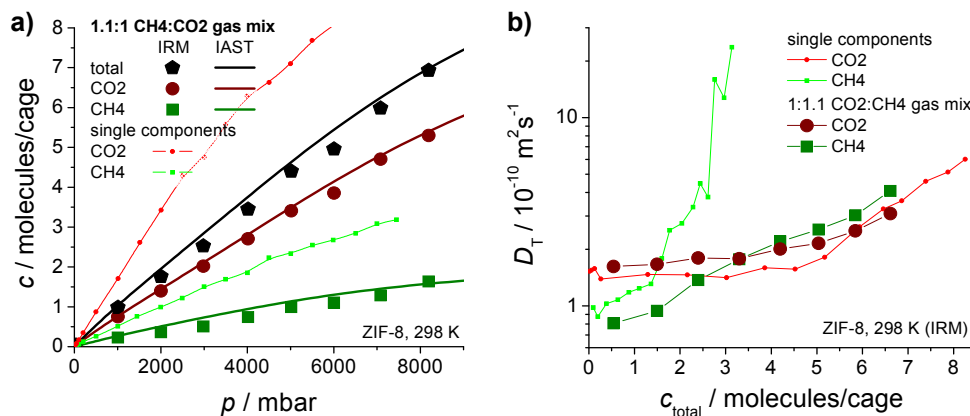


Figure 4.3: (a) Adsorption isotherms of CO₂ and CH₄ which have been calibrated using CMBC data. The IRM mixture isotherms show a good agreement with the prediction from single component data using IAST. (b) Loading dependence of the CO₂ and CH₄ diffusivity. The (single component) diffusivity of CH₄ increases much steeper than for CO₂. While we note for CO₂ only a mild increase of the diffusivity in presence of CH₄, the CH₄ diffusivity, in turn, is reduced dramatically in presence of CO₂.

[1] S.C. Reyes et. al.: United States (2009) patent appl. no. 20090216059

[2] H. Bux et. al.: J. Am. Chem. Soc. **131**, 16000 (2009)

4.5 Correlating the Results of Different Techniques of Diffusion Measurement in Nanoporous Glasses

T. Titze, C. Chmelik, D. Enke*, P. Galvosas, O. Gobin[†], A. Jentys[†], H. Jobic[‡], J. Kärger, C.B. Krause, J. Kullmann*, J. Lercher[†], S. Naumov

*Leipzig University, Institute of Technical Chemistry, Germany

[†]Technical University Munich, Technical Chemistry 2, Germany

[‡]Institute de Recherches sur la Catalyse, Villeurbanne, France

With the application of pulsed field gradient (PFG) NMR to diffusion studies in zeolites the outcome of the different techniques of diffusion measurement to nanoporous materials is well-known to be far from uniform [1]. Usually the measured diffusivities decreased with increasing diffusion path lengths considered in the experiment, as a consequence of the increasing necessity to overcome higher resistances [2]. By choosing porous glass with mean pore diameters of typically 1.3 nm and 2 nm as a host system [3] we disposed of a system which was assumed to represent an essentially homogeneous nanoporous body with no additional internal transport resistances.

Microscopic diffusion measurements have been performed by quasi-elastic neutron scattering (QENS), and by PFG NMR [4]. The *macroscopic* diffusion data have been deduced from both frequency response (FR) and gravimetric measurements and from IR micro-imaging (IRM) operating in the integral mode [5]. The obtained results are shown in figure 4.4. In consideration of the different observed diffusion path lengths (QENS: 4 nm, NMR: 0.5–10 μm) all experimental diffusivity data are found to be mutually compatible.

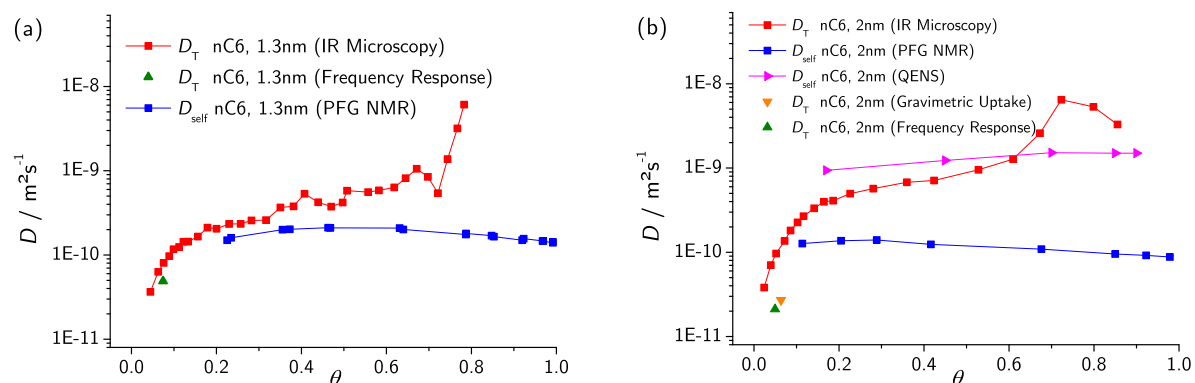


Figure 4.4: Diffusivities of n-hexane measured by different methods in (a) 1.3 nm and (b) 2 nm samples

- [1] J. Kärger and D. M. Ruthven: *Diffusion in zeolites and other microporous solids*, 1st Ed. (Wiley Interscience, New York 1992)
- [2] S. Vasenkov and J. Kärger: *Micropor. Mesopor. Mater.* **55**, 139 (2002)
- [3] D. Enke et. al.: *Micropor. Mesopor. Mater.* **60**, 19 (2003)
- [4] J. Kärger: *Diffusion Measurements by NMR Techniques*, in *Adsorption and Diffusion*, 1st Ed., ed. by H.G. Karge, J. Weitkamp, (Springer, Berlin 2008) p 85

- [5] J. Kärger: *Application of IR Spectroscopy, IR Microscopy, and Optical Interference Microscopy to Diffusion in Zeolites*, in *Adsorption and Diffusion*, 1st Ed., ed. by H.G. Karge, J. Weitkamp, (Springer, Berlin 2008) p 135

4.6 Ordered Mesoporous Solids as Model Substances for Liquid Adsorption

G. Kalies, R. Rockmann*, D. Tuma†, J. Gapke

*DBI Gas- und Umwelttechnik GmbH, Leipzig

†BAM Federal Institute of Materials Research and Testing, Berlin

Ordered pore systems have often been used to verify and improve thermodynamic models for the characterization of porous solids by inert gas adsorption isotherms [1]. In our study, liquid-phase adsorption isotherms on well-characterized ordered structures and their analysis lie in the focus of interest. Even if the extraction of geometric and energetic heterogeneity parameters from liquid-phase adsorption isotherms is more complicated than from single gas isotherms, as a) the excess character of adsorption cannot be neglected and b) binary adsorption is the basic information, i.e., surface effects are overlaid by the liquid mixture effects, identical solid information is however given in liquid-phase isotherms [2].

Different ordered mesoporous solids were applied in liquid-phase adsorption. By means of the analysis of experimental data of binary liquid model mixtures, a general way is outlined how to obtain essential and trustworthy solid information from liquid-phase adsorption. Regarding the liquid/vapor equilibrium as a *mirror* of liquid-liquid interaction (Fig. 4.5), it should be possible to combine experimental information from both liquid/vapor and adsorption excess measurements in a suitable way.

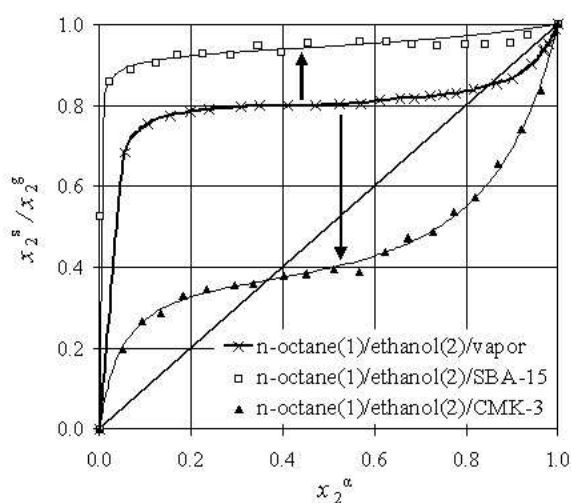


Figure 4.5: Separation diagrams for n-octane(1)/ethanol(2) on SBA-15 and CMK-3 and liquid/vapor equilibrium diagram for n-octane(1)/ethanol(2).

- [1] M. Thommes et al.: *Langmuir* **22**, 756 (2006)
[2] G. Kalies et al.: *J. Coll. Interface Sci.* **331**, 329 (2009)

4.7 Design of Liquid/Solid Adsorption Isotherms by Energy Distribution Functions

G. Kalies, P. Bräuer, M.v. Szombathely

In recent years, significant progress has been achieved in determining porosity, pore size distributions and other textural parameters of porous solids from adsorption isotherms [1]. The calculation of relevant energetic information from gas or liquid adsorption isotherms on porous solids and the design of surface chemistry is a challenging research field, but still remains a problem.

In the case of low-temperature pure gas adsorption, many attempts have been made to calculate relevant energy distributions, and even commercial software tools are available. Compared with gas adsorption, liquid adsorption measurements are rather seldom used to characterize porous solids. Since from liquid phase only competitive adsorption can be studied, energy distribution functions at the liquid/solid interface are quite complex. However, as each method looks with its own eyes, liquid adsorption can provide additional or confirming energetic information [2].

In this study, adsorption excess isotherms of binary liquid mixtures obtained from synthetic adsorption energy distribution functions are investigated (Fig. 4.6). The distribution functions are varied systematically. In this way, the sensitivity or the lack of sensitivity of liquid-phase adsorption isotherms over the whole concentration range for changes in energy distribution functions becomes evident. The question is answered to what extent it makes sense to use liquid adsorption measurements for obtaining relevant information on solid's energetic heterogeneity.

- [1] P. Llewellyn, J. Rouquérol, N. Seaton, eds., *Characterization of Porous Solids VII: Proceedings of the 7th International Symposium on the Characterization of Porous Solids (Cops-VII)*, Elsevier, Amsterdam, 2006
[2] R. Rockmann et al.: *Adsorption* **13**, 515 (2007)

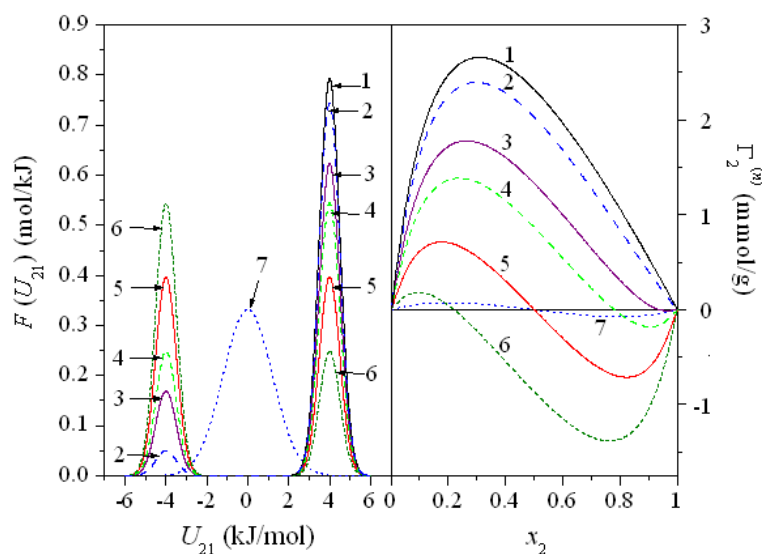


Figure 4.6: Gaussian peak energy distributions $F(U_{12})$ in the interval $-6 \text{ kJ/mol} \leq U_{12} \leq 6 \text{ kJ/mol}$ and corresponding inverted U- and S-shape $\Gamma_2^{(n)}$ isotherms.

4.8 NMR Relaxometry Study of Pore Water in Hydrating Cements with Addition of Modified Superabsorbent Polymers

K. Friedemann, F. Stallmach, C. Horch, N. Nestle*, G. Herth[†]

*BASF SE Ludwigshafen, GKP/P, G201, Ludwigshafen

[†]BASF Construction Chemicals GmbH, GKI/A, Trostberg

In the DFG project "Water balance in high-performance concrete during internal curing with innovative additives", the migration of water from materials added for internal curing into the hydrating cement matrix is investigated by non-destructive low-field NMR relaxometry. After our NMR approach proved to be very useful to characterize the water retardation properties of lightweight expanded glass aggregates [1] and of hydrogels of different polysaccharides [2], we focussed on modified acrylic-acid-based superabsorbent polymers (modSAP), which were introduced recently into this field of materials research by BASF.

The water balance between different modSAP and a hydrating Portland cement matrix was investigated by NMR [3]. Figure 4.7(a) shows the observed time dependent changes in the T_2 relaxation time distributions of water in these materials. The two peaks correspond to the physically bound water in the hydrating cement (left peak) and gel-like water in the modSAP (right peak). The significant shift of the cement peak reflects the compaction of pore space due to the formation of hydration products. Figure 4.7(b) summarizes the time-dependent content of total water in the sample and of the fraction of water retarded in the modSAP. The release of the water from the modSAP starts with the onset of the hydration reaction and is completed after about 20 hours. The

water uptake of the superabsorber inside the cement matrix can be calculated from these non-destructive NMR studies. It amounts to about 20 times of the dry weight of the modSAP [3].

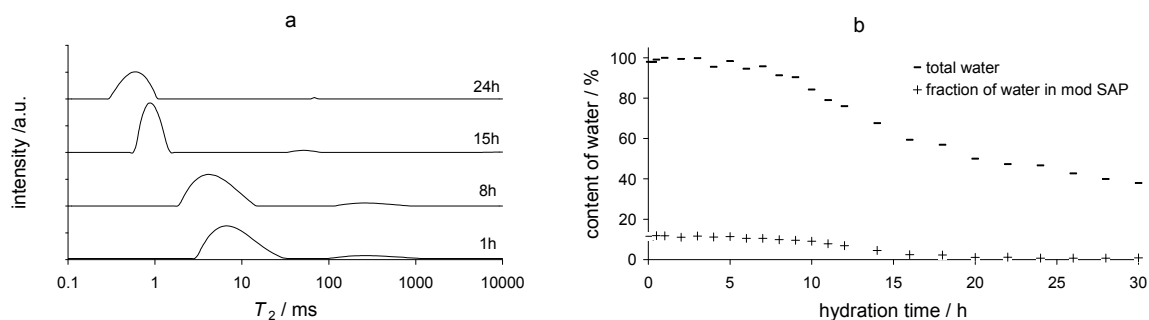


Figure 4.7: (a) Relaxation time distributions of physically bound water in hydrating cement (left peaks) and of water inside the modSAP observed at 1, 8, 15 and 24 h [1]. (b) Total content of water in the sample and of the fraction of water in the modSAP in dependence of hydration time.

- [1] K. Friedemann et al.: *Mater. Struct.* **41**, 1647 (2008)
 [2] K. Friedemann et al.: *Cement Concrete Comp.* **31**, 244 (2009)
 [3] N. Nestle et al.: *Micropor. Mesopor. Mat.* **125**, 51 (2009)

4.9 Fundamental Host-Guest Interactions in Porous Metal Organic Frameworks

M. Wehring, S. Amirjalayer*, S. Hertel, M. Gratz, R. Schmid*, F. Stallmach

*Faculty of Chemistry and Biochemistry, Ruhr-University Bochum

Porous metal-organic frameworks (MOF, [1]) are able to adsorb and transport small guest molecules in the internal void space of their crystalline host structure. Knowledge on how guest molecules interact and move within the host lattice is of fundamental interest with many implications for potential applications of MOFs, e.g., in separation processes and catalysis. In this study, we develop experimental pulsed field gradient (PFG) NMR methods [2] and computer simulation techniques for the investigation of the self-diffusion of hydrocarbons adsorbed in various metal-organic frameworks.

PFG NMR measurements of benzene self-diffusion in MOF-5 showed two phases with different mobilities [1]. Further investigation of the host-guest system with DR-COSY and MAS NMR indicated that the faster component of the diffusion coefficient can be assigned to self-diffusion inside the intact MOF-5 lattice. The activation energy of self-diffusion estimated from temperature dependent PFG NMR measurements is 16 kJ/mol and agrees reasonably well with the value obtained by MD simulations (13.4 kJ/mol, [4]). The experimental self-diffusion coefficients at low loadings agree with the data obtained by MD simulations (see Fig. 4.8) and are consistent with our own earlier studies [3]. However, for loadings above 10 benzene molecules per unit cell, the experimental data show a pronounced drop in the diffusivities, while the MD simulations

predict a opposite loading dependence with a maximum of the diffusivities at about 25 benzene molecules per unit cell. Our current hypothesis for the clarification of this striking difference between experimental and theoretical diffusion data is a clustering of benzene molecules in the MOF-5 as consequence of their intermolecular interactions, which are not yet taken into account in the MD simulations.

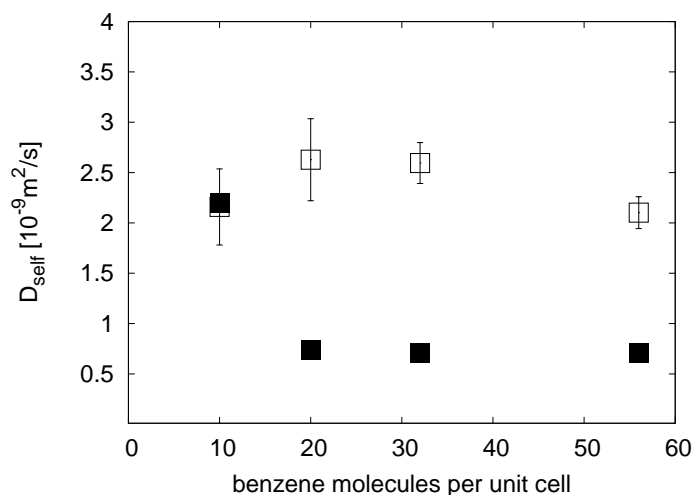


Figure 4.8: Self-diffusion coefficients of benzene molecules inside MOF-5 obtained by PFG NMR measurements (■) and by MD simulations (□) at 298 K for various loadings.

- [1] W. Eddaoudi et al.: *Science* **295**, 469 (2002)
- [2] F. Stallmach, P. Galvosas: *Ann. R. NMR S.* **61**, 51 (2007)
- [3] F. Stallmach et al.: *Angew. Chem. Int. Edit.* **45**, 2123 (2006)
- [4] S. Amirjalayer et al.: *Angew. Chem. Int. Edit.* **46**, 463 (2006)

4.10 ¹³C PFG NMR Diffusion Studies in Metall Organic Frameworks

A.-K. Pusch, St. Schlayer, F. Stallmach, B. Biniwale*, H. Jobic[†], D. Theodorou[‡]

*National Environmental Engineering Research Institute, India

[†]CNRS- Université de Lyon, France

[‡]National Institute University of Athens, Greece

In the EU-India collaborative project *Advanced Materials as CO₂ Removers* (AMCOS) experimental and computational studies of carbon dioxide thermodynamics and diffusion in nanoporous materials are performed. The objective is to characterize new materials like metal-organic framework (MOF) and polymers with respect to their suitability to remove CO₂ from flue gases.

While ¹H NMR diffusion studies with adsorbed hydrocarbons are routinely performed in our lab [1], the application of this method for carbon dioxide has to be

established first. This requires to extend the pulsed field gradient (PFG) NMR methodology to a nonhydrogen ^{13}C containing adsorbate and includes the design of a new NMR probe in order to improve the usually small signal-to-noise ratios in ^{13}C NMR studies (see Figure 4.9).

First NMR experiments were performed using $^{13}\text{CO}_2$ (99 % enriched) adsorbed in a commercial CuBTC MOF sample [2]. The longitudinal relaxation time T_1 , the transverse relaxation time T_2 and the self-diffusion coefficient D were determined in a temperature range of $173\text{ K} \leq T \leq 373\text{ K}$. T_1 times are in the range of 70 to 160 ms and decrease with decreasing temperature. T_2 is found to be much smaller but higher than about 10 ms at all temperatures. The self-diffusion coefficients for CO_2 in CuBTC were found to be in the range of 3.0×10^{-10} to $4.5 \times 10^{-9}\text{ m}^2/\text{s}$.

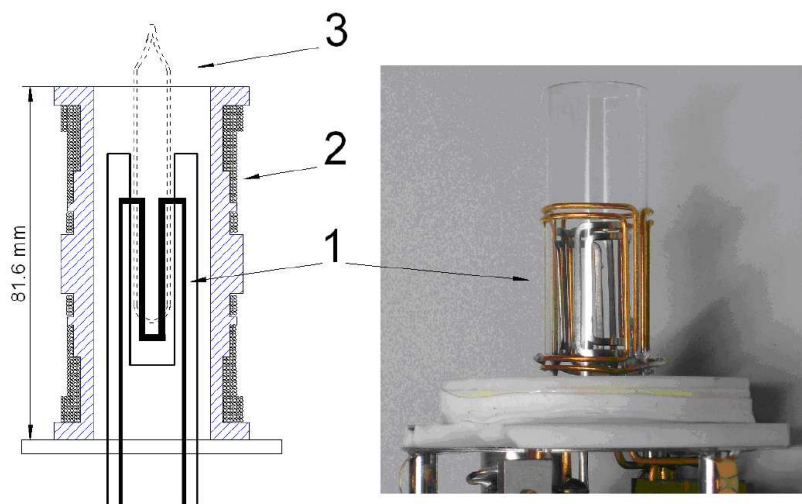


Figure 4.9: Drawing of a new gradient coil designed to upgrade a double resonance NMR probe for ^{13}C NMR diffusion studies. NMR probe (*right*) showing the rf coils (1), the designed gradient coil support (2) and the position of the NMR sample tube (3).

[1] F. Stallmach, P. Galvosas: *Ann. R. NMR S.* **61**, 51 (2007)

[2] S. Chui et al.: *Science* **283**, 1148 (1999)

4.11 Multidimensional NMR Diffusion Studies in NaX

M. Gratz, M. Wehring, S. Schlayer, P. Galvosas, F. Stallmach

The diffusional behavior of selected hydrocarbons adsorbed in NaX zeolites was investigated with pulsed magnetic field gradient (PFG) NMR methods in two different ways. First, the exchange time τ_{exch} of *n*-pentane between the interior and the exterior of the zeolite crystals was determined by two-dimensional diffusion exchange spectroscopy (DEXSY) [1]. The results were compared to the mean life time τ_{intra} as obtained by the fast NMR tracer desorption method [2, see [3] for details].

Second, the diffusion of a propylene-propane mixture adsorbed in the zeolite was studied by Fourier transform PFG NMR, thus employing the chemical shift of the

individual organic constituents as a second dimension for a selective evaluation of the PFG NMR signal decays and the subsequent extraction of corresponding diffusion coefficients.

Modifications of the underlying NMR pulse sequences for the application of ultra-high pulsed magnetic field gradients of up to $\pm 35 \text{ Tm}^{-1}$ in microporous materials were necessary. They included the introduction of read gradients as well as special procedures for gradient matching [3].

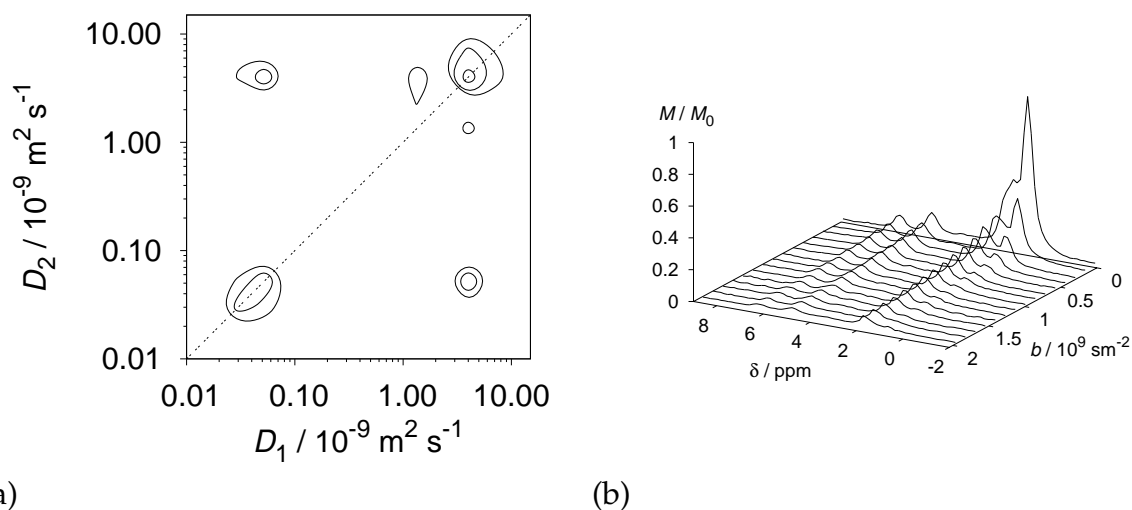


Figure 4.10: (a) DEXSY map of *n*-pentane in NaX. Peaks on the diagonal correspond to molecules that do not change sites during τ_m , whereas the side peaks are assigned to molecules that enter and leave the crystal during τ_m , respectively. (b) FT PFG NMR spectrum of propylene-propane mixture adsorbed in NaX. The rightmost peak is assigned to propane with high mobility, whereas propylene, giving the rest of the peaks, diffuses one order of magnitude slower.

- [1] P. T. Callaghan et al.: Magn. Reson. Imaging **21**, 243 (2003)
- [2] J. Kärger: AIChE J. **28**, 417 (1982)
- [3] M. Gratz et al.: Micropor. Mesopor. Mat. **125**, 30 (2009)

4.12 Permanent Magnet Arrangements for Low-Field NMR

C. Horch, S. Schlayer, F. Stallmach

Nuclear magnetic resonance (NMR) studies with fluids contained in the void space of porous materials such as natural sediments and concretes are a modern non-destructive method in porosimetry (see e.g. [1] or [2]). For such studies we developed two low-cost NMR magnets, which utilize NdFeB permanent magnets as source for the required magnetic flux [3]. A parallel arrangement and circular arrangement of the permanent magnets were designed and their field characteristics were predicted using finite element simulation in COMSOL Multiphysics.

In the parallel arrangement shaped iron plates were placed in front and back of each NdFeB magnet block to control the magnetic flux density (Fig. 4.11, left). Further improvement of the field homogeneity was achieved by adding shim magnets, which

are composed of 2×20 small NdFeB cubes ($2 \times 2 \times 2 \text{ mm}^3$) enframed with small iron bars at their pole faces. The calculated magnetic flux density ($B_0 = 115 \text{ mT}$) and the residual field inhomogeneity ($\frac{\delta B}{B_0} = 2.6 \times 10^{-4}$) agree well with the values measured for the constructed magnet [3].

The circular arrangement consists of two magnet stars each consisting of 16 NdFeB permanent magnet bars ($10 \times 10 \times 40 \text{ mm}^3$) attached to an inner iron ring yoke (Fig. 4.11, right). Both magnet stars are magnetically connected with each other at the opposite poles via 16 small bar-like iron yokes. In a simplified 2D model the homogeneity was optimized using COMSOL Multiphysics. A 3D model delivered the precise dimensions and yielded the correct field strength.

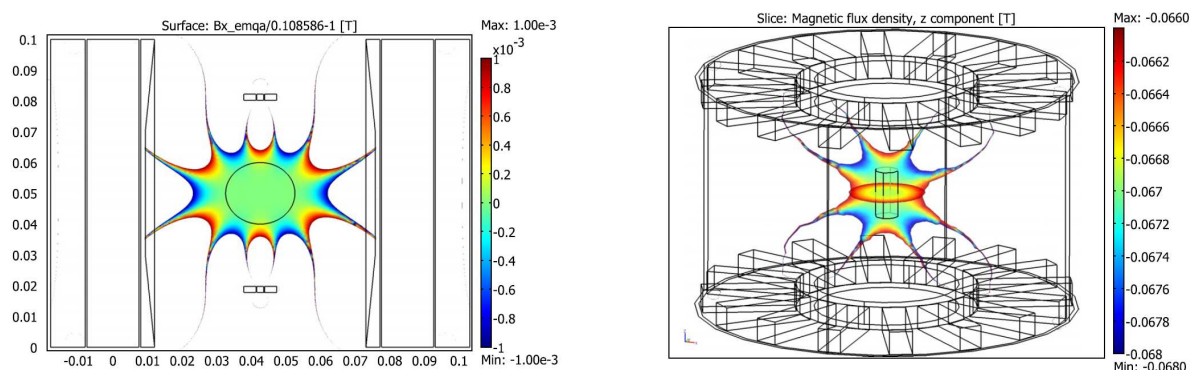


Figure 4.11: Calculated magnetic flux densities in the parallel (*left*) and in the circular (*right*) arrangement of NdFeB permanent magnets for low-field NMR. The sample positions are indicated in the center of both figures.

- [1] W. Schönfelder et al.: J. Appl. Geophys. **65**, 21 (2008)
- [2] K. Friedemann et al.: Cement Concrete Comp. **31**, 244 (2009)
- [3] C. Horch et al.: Proceedings COMSOL Conference 2009, Milan, Italy. see: <http://cds.comsol.com/access/dl/papers/6717/Horch.pdf>

4.13 Network Effects within Independent Pores

S. Naumov, J. Kärger, R. Valiullin

The reduced dimensionality of nanocrystalline Si results in its very interesting properties with a wealth of potential applications. Electrochemical etching of bulk Si provides an extremely simple approach to form porous silicon (PSi), a monolithic film material containing linear non-intersecting pores.

Among the various features, brought about by the procedure of PSi nanostructuring, it is in particular the intrinsic mesoscale disorder that plays a crucial role in determining the material properties. This circumstance induced a huge amount of scientific investigation dealing with the structural and textural characteristics of the PSi in the last two decades.

Among the puzzling phenomena observed in PSi, an asymmetric sorption hysteresis is observed (Fig. 4.12) with is a typical feature of interconnected, disordered materials.

Closing the end of idealized smooth-walled independent pores is expected to eliminate hysteresis since the pore end promotes condensation. In the case of PSi, one observes the same sorption behavior for a pore with both ends open as compared to a pore with one end close [1].

To clarify the issues emerging from previous work, we have performed a series of investigations including sorption and diffusion experiments, accompanied by the calculations by means of the mean field theory (MFT) of a lattice gas to quantify the effect of disorder on the scale of the intrapore fluid.

Our experiments and theoretical calculations have identified the effects of quenched disorder in the channel pores of PSi as the directing feature for adsorption hysteresis [2]. Importantly, our calculations suggest that this disorder has to be relatively pronounced, exceeding disorder on an atomistic level. Thus, the channel pores of PSi turn out to exhibit all effects more commonly associated with three-dimensional disordered networks. In addition, however, their simple geometry makes them an ideal model system for experimental observation and theoretical analysis.

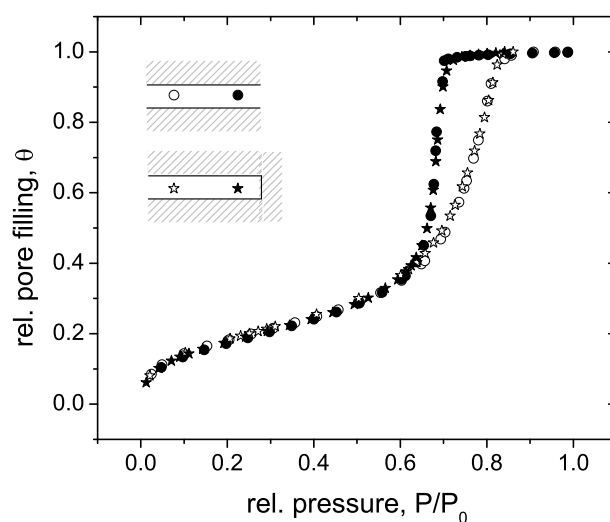


Figure 4.12: Adsorption (*empty symbols*) and desorption (*black symbols*) isotherms of N_2 in PSi material at 77 K. *Circles*: channels open at both ends, *stars*: channels closed at one end.

[1] S. Naumov et al.: Phys. Rev. E **78**, 060601 (2008)

[2] S. Naumov et al.: Phys. Rev. E **80**, 031607 (2009)

4.14 Dynamics of Molecules Confined to Structured Nano-Channels

M. Dvoyashkin, J. Kärger, R. Valiullin

Molecular dynamics under confinement is a broad field of extensive scientific research. Besides fundamental interest, the understanding of the very intrinsic mechanisms of dynamics altered by confinement has an immense impact on application-oriented sciences. Having a possibility of handling and preparation of mesoporous materials with well-defined structural properties, one may comprehensively study structure-related aspects of the molecular propagation in spatially modulated pores by following the diffusion process therein using the pulsed field gradient NMR technique [1].

In the present work, we have used porous silicon as a host material with variable structure. Two of them have only linear pores with mean channel diameters of 5.6 nm (PS6) and 9.2 nm (PS9). Two other samples (PS-M1 and PS-M2) were fabricated to have modulated pore structure consisting of consequently connected pore segments with different pore sites (see Fig. 4.13). The diffusivities of cyclohexane along the channels have been measured using PFG NMR [1]. In the two samples PS6 and PS9, the diffusion propagator is found to be Gaussian with diffusivities $\approx 2.5 \times 10^{-10} \text{ m}^2\text{s}^{-1}$ and $\approx 7 \times 10^{-10} \text{ m}^2\text{s}^{-1}$, respectively. With these diffusivities and observation times used from 4–300 ms, the molecules cover distances from about 1–10 μm .

For the pores with modulated structure, consisting of alternating pore segments with different pore diameters of 5.6 nm and 9.2 nm, the measured diffusivities have also been found almost independent on the diffusion time, with average values of $3.8 \times 10^{-10} \text{ m}^2\text{s}^{-1}$ and $3.2 \times 10^{-10} \text{ m}^2\text{s}^{-1}$ for the samples PS-M1 and PS-M2, respectively. Note that the diffusion length probed by the molecules ($\approx 1–2 \mu\text{m}$) was comparable to the lengths of the segments at the shortest times studied ($\approx 4 \text{ ms}$). For the longest diffusion time studied the molecular displacements were of the order of 20 μm . Thus, the resulting measured diffusivities should bear *information* about both types of the channel sections explored. For further analysis of the diffusion process in them, two analytical models have been considered: (i) model of serial connection of transport resistances [2], which can be analytically solved considering 1st Fick's law applied to the pore geometries depicted in Fig. 4.13, and (ii) model of *parallel* connection of transport resistances [3]. The experimentally effective diffusivities in modulated pores were found to lie in between the predictions of the considered models. This result provides a good basis for further improvement of the theoretical models, where including of the additional factors, e.g. hydrodynamic effect and effects of restricted diffusion, might lead to more precise assessment of the effective diffusivities of molecules in inhomogeneous confined spaces.

[1] M. Dvoyashkin et al.: J. Chem. Phys. **129**, 154702 (2008)

[2] A. Herrmann et al.: Appl. Phys. A-Mater. **72**, 197 (2001)

[3] J. Kärger et al.: Adv. Magn. Reson. **12**, 2 (1988)

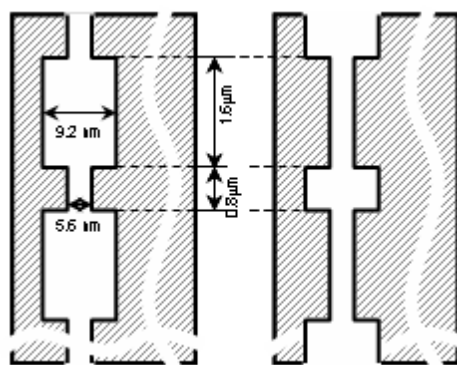


Figure 4.13: Schematic structure of two porous silicon samples PS-M1 (*left*) and PS-M2 (*right*) with modulated pore geometry.

4.15 Disorder Effects during Freezing in Linear Pores

D. Kondrashova, R. Valiullin

Recent progress in the synthesis of nanoporous materials with controlled structural properties made it possible to address various phenomena occurring in mesoscale molecular systems. Among them, different aspects of fluid phase transitions could now be related to the structural properties of mesoporous matrices. In this work, we take advantage of the option to prepare mesoporous silicon with linear, tailor-made pores and thus to study the process of freezing of a fluid under well-defined conditions of confinement [1]. Because of similar physics, better understanding of melting and freezing processes in mesoporous matrices may yield deeper insight into fundamentals of adsorption processes in mesopores and provide an additional, complementary method of structural characterization. In an ideal cylindrical pore one expects a reduction of the freezing temperature in proportion to the pore size, similarly to a reduction of the evaporation pressure. In the material under study, however, freezing starts already before the transition temperature corresponding to the average pore size is reached [1]. This is referred to the fact that the pores possess a certain degree of disorder, namely pore size distribution along the pore axis [2]. The kinetics of this process is found to be very slow and to depend on temperature (Fig. 4.14). At sufficiently high temperatures, the kinetics can be, at long times, approximated by a power-law dependency t^a , with a temperature- and pore size-dependent exponent $a < 1$. To explain such a behavior, we suggest a simple thermodynamical model taking account of mesoscale disorder in porous silicon [3]. The latter inherently results from the preparation procedure. Due to this disorder, it may appear that freezing of a pore section filled with the liquid and adjacent to the frozen part of the pore, may result in a reduction or in an increase of the overall free-energy of the system. Thus, under certain conditions, the solid front propagation may require activated overcoming of the barriers in the free energy. Depending on temperature, average pore size and pore size distribution, which determine the magnitudes of the barrier heights and their distribution, the times required to freeze or melt the individual pore segments can be very broadly distributed. Hence, depending on temperature, the propagation of the solid-liquid interface in such a pore, which generally may be described by a trap-model with a random distribution of the transition rates [3], may exhibit a very rich behavior. We address this issue by means of Monte Carlo

simulations based upon the suggested model. The results obtained strongly suggest that the freezing kinetics is very sensitive to strength of the disorder and their analysis may provide a very accurate information on structural properties on the mesoscale.

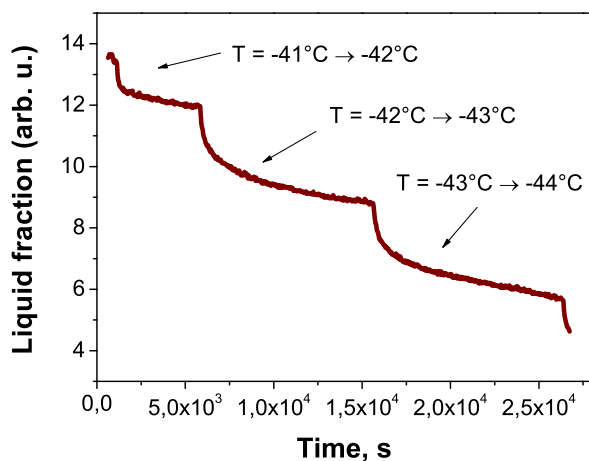


Figure 4.14: Kinetics of the freezing process of nitrobenzene confined in porous silicon with linear pores measured using nuclear magnetic resonance spectroscopy upon a stepwise change of temperature as indicated in the figure.

- [1] M. Dvoyashkin et al.: J. Chem. Phys. **129**, 154702 (2008)
- [2] S. Naumov et al.: Phys. Rev. E **78**, 060601 (2008)
- [3] D. Kondrashova, C. Reichenbach, R. Valiullin: *Probing pore connectivity in random porous materials by scanning freezing and melting experiments*, Langmuir, DOI: 10.1021/la904062h (in press)

4.16 Funding

Studying Zeolitic Diffusion by Interference and IR Microscopy.

Prof. Dr. J. Kärger, Dr. C. Chmelik

DFG-Projekt KA 953/18-3, International Research Group "Diffusion in Zeolites"

Bestimmung mikroskopischer Kenngrößen der Molekültranslation in Schüttungen nanoporöser Partikel mittels PFG NMR und Monte-Carlo-Simulation.

Prof. Dr. J. Kärger, Dr. R. Valiullin

DFG-Projekt KA 953/19-2

Confinement Effects on Diffusion and Reaction in Zeolites, Studied by Dynamic MC Simulations, PFG NMR and Interference/IR Microscopy.

Prof. Dr. J. Kärger

im DFG-Projekt GRK 1056/1, International Research Training Group "Diffusion in Porous Materials"

PFG NMR studies of zeolitic diffusion.

Prof. Dr. P. Galvosas, Prof. Dr. J. Kärger

DGF-Projekt GA 1291/1-2

PFG NMR investigations on formulated catalysts; Bestimmung von Diffusionskoeffizienten an Katalysatoren.

Dr. F. Stallmach

BASF AG

Fourier-Transform-PFG-NMR mit starken Feldgradientenimpulsen zur selektiven Selbstdiffusionsmessung.

Prof. Dr. J. Kärger, Dr. F. Stallmach

DFG-Projekt KA 953/16-1

Innovative Zugabestoffe für die Innere Nachbehandlung von Hochleistungsbeton unter Berücksichtigung der räumlichen und zeitlichen Wasserbilanz.

Prof. Dr. J. Kärger, Dr. F. Stallmach

DFG-Projekt KA 953/22-2

Messung intrakristalliner Diffusions-Reaktions-Profile in Zeolithen mittels IR-Imaging.

Dr. C. Chmelik, Prof. Dr. J. Kärger

DFG-Projekt KA 953/20-1

Messung von Phasenübergängen in mesoskopisch beschränkten Systemen: kombinierter Einsatz von NMR und Molekulardynamik.

Prof. Dr. J. Kärger, Dr. R. Valiullin

DFG-Projekt KA 953/21-1

PFG NMR Untersuchung der Transporteigenschaften von Fluiden in Mesoporen in der Nähe des kritischen Punktes

Prof. Dr. J. Kärger, Dr. R. Valiullin

DFG-Projekt KA 953/25-1

Particle Dynamics in Nano-Structured Channels

Prof. J. Kärger, Dr. R. Valiullin, Prof. W. Janke

DFG-Projekt KA 953/27-1

Transport in microporous MOFs: From molecular diffusion to membrane permeation

Dr. C. Chmelik, Prof. Dr. J. Kärger

DFG-Projekt KA 953/29-1, SPP 1362 MOFs

NMR-Untersuchungen und theoretische Ansätze zur Korrelation des Diffusionsverhaltens in komplementären Porenräumen

Prof. Dr. J. Kärger, Dr. R. Valiullin, Prof. Dr. A. Bunde

DFG-Projekt KA 953/30-1

Thermodynamik und Vorausberechnung der Adsorption von Mischungen

Dr. G. Kalies

DFG-Projekte KA 1560/4-1

Texturelle Charakterisierung von Sandsteinen (Bohrkernen) und kontaminierten Aktivkohlen

Dr. G. Kalies

Gaz de France

Advanced Materials as CO₂ Removers: A Computational Study of CO₂ Sorption Thermodynamics and Kinetics

Dr. F. Stallmach

EU project CP-FP 233502 AMCOS

Fundamental Host-Guest Interactions in Porous Metal Organic Frameworks. A Combined Experimental and Theoretical Approach.

Dr. F. Stallmach

DFG-Projekt STA 648/1-1

4.17 Organizational Duties

Christian Chmelik

- Membership in Editorial Board: Diffusion Fundamentals
- Conference chairman: Diffusion Fundamentals III (Athen, Greece 2009)
- Referee: J. Phys. Chem., Micropor. Mesopor. Mat.

Petrik Galvosas

- Referee: Magnetic Resonance Imaging, Journal of Magnetic Resonance, Concepts in Magnetic Resonance

Grit Kalies

- Referee: J. Phys. Chem., Micropor. Mesopor. Mater., Appl. Surface Sci., Adsorption, J. Coll. Interface Sci.

Jörg Kärger

- Membership in the Programme Committee "Magnetic Resonance in Porous Media" (Leipzig 2010), "Fundamentals of Adsorption" (Kyoto, Japan 2010), "International Zeolite Conference" (Sorento, Italy 2010), "Diffusion Fundamentals III" (Athens, Greece 2009), in the permanent DECHEMA committees Zeolites and Adsorption and in the Board of Directors of the Magnetic Resonance Centre (MRZ) of Leipzig University
- Membership in Editorial Boards: Diffusion Fundamentals (Online Journal, Editor)
- Referee: Nature, Phys. Rev., Phys. Rev. Lett., Angew. Chem., Europhys. Lett., J. Chem. Phys., J. Phys. Chem., Langmuir, Micropor. Mesopor. Mat., Phys. Chem. Chem. Phys., J. Magn. Res.
- Project Reviewer: Deutsche Forschungsgemeinschaft, National Science Foundation (USA)

Frank Stallmach

- Faculty board member
- Referee: Micropor. Mesopor. Mat., Angewandte Chemie, J. Am. Chem. Soc., J. Magn. Res., J. Phys. Chem.
- Project Reviewer: Deutsche Forschungsgemeinschaft
- managing guest editor of the special issue *Diffusion in Micropores* of Micropor. Mesopor. Mat.

Rustem Valiullin

- Membership in Scientific Advisory Committee "Bologna MRPM Conference (Ampere Event)"
- Referee: J. Phys. Chem., Phys. Rev., Adsorption, Micropor. Mesopor. Mat.

4.18 External Cooperations

Academic

- Delft University, Inst.Chem. Tech., Delft, The Netherlands
Prof. Kapteijn
- Institut de Recherches sur la Catalyse, CNRS, Villeurbanne, France
Dr. Jobic
- GeoForschungsZentrum Potsdam (GFZ), Potsdam
H.-M. Schulz
- Helmholtz Zentrum für Umweltforschung UFZ Halle-Leipzig GmbH, Leipzig
S. Oswald
- Max Planck Institut für Kohlenforschung, Mülheim
Dr. Schmidt, Prof. Schüth
- Russian Acad. Sci., Boreskov Inst. Catalysis, Siberian Branch, Novosibirsk, Russia
Dr. Stepanov
- TU München, Lehrstuhl Technische Chemie 2
Prof. Lercher, Dr. Jentys
- University Medical Center Hamburg-Eppendorf, Hamburg, Germany
Dr. M. Koch
- Università di Sassari, Dipartimento Chimica, Sassari, Italy
Prof. Demontis, Prof. Suffritti
- Universiät Eindhoven, Schuit Institute, Eindhoven, The Netherlands
Prof. van Santen
- Universität Erlangen Nürnberg, Dept. Chem. Engin., Erlangen
Prof. Emig, Prof. Schwieger
- Universität Hannover, Dept. Phys. Chem., Hannover
Prof. Caro, Prof. Heitjans
- Universität Leipzig, Institut für Analytische Chemie, Leipzig
Prof. Berger
- Universität Leipzig, Institut für Technische Chemie, Leipzig
Prof. Einicke, Prof. Gläser, Prof. Enke
- Universität Leipzig, Institut für Anorganische Chemie, Leipzig
Prof. Krautscheid
- Universität Leipzig, Institut für Medizinische Physik und Biophysik, Leipzig
Prof. Huster

- TU Dresden, Inst. Biophysik, Dresden
Prof. Brunner
- Universität Stuttgart, Institut für Technische Chemie, Stuttgart
Prof. Klemm, Prof. Hunger, Prof. Weitkamp
- University Athens, Dept Chem. Engn., Athens, Greece
Prof. Theodorou
- University of Amsterdam, Faculty of Science, The Netherlands
Prof. Krishna
- University of Maine, Dept. Chem. Eng., USA
Prof. Ruthven
- Cleveland University, Chem. and Biomed. Eng., USA
Prof. Shah
- University of Edinburgh, UK
Prof. Brandani
- Victoria University of Wellington, MacDiarmid Institute for Advanced Materials and Nanotechnology, School of Chemical and Physical Sciences, New Zealand
Prof. Galvosas, Prof. Callaghan
- LMU München, Dept. Chemistry and Biochemistry
Prof. Bräuchle, Dr. C. Jung
- University of Massachusetts, Dept. of Chemical Engineering, Amherst, USA
Prof. P.A. Monson
- Northwestern University, Dept. of Chem. Eng., Evanston, USA
Prof. Snurr
- Rutgers University, Dept. of Chem. & Chem. Biol., Piscataway, USA
Prof. Li, Prof. Olson
- University of Queensland, Division of Chem. Eng., Brisbane, Australia
Prof. Bhatia
- University of Alicante, Dept. of Inorg. Chem., Alicante, Spain
Prof. Rodríguez-Reinoso
- University of Anwerpen, Dept. of Chem., Wilrijk, Belgium
Prof. Cool, Prof. Vansant
- University of Florida, Dept. of Chem. Eng., Gainesville (FL), USA
Prof. Vasenkov
- Rensselaer Polytechnic Institute, Chem. & Biol. Eng., Troy, USA
Prof. Coppens
- Kent State University Ohio, Department of Chemistry, USA
Prof. Jaroniec
- Marie-Curie-Sklodowska-Universität Lublin, Poland
Prof. Goworek
- DBI Gas- und Umwelttechnik GmbH Leipzig, Germany
Dr. Rockmann

- Institut Madirel Marseille / Université de Provence, France
Dr. Denoyel

Industry

- BASF SE, Ludwigshafen, Germany
Dr. Müller, Dr. Nestle, Dr. Rittig, G. Herth
- DBI Gas- und Umwelttechnik GmbH, Leipzig, Germany
Dr. R. Rockmann
- Grace, Worms, Germany
Dr. McElhiney
- Resonance Instruments Ltd., Witney, UK
J. McKendry
- SINTEF, Oslo, Norway
Prof. Stöcker
- Südchemie, Berlin, Germany
Dr. Tissler, Dr. Tufar, Dr. Lutz
- StatoilHydro, Stavanger, Norway
C. v. d. Zwaag
- Gaz de France, Production and Exploration GmbH Lingen, Germany
Dr.-Ing. W. Kleinitz

4.19 Publications

Journals

- C. Chmelik, L. Heinke, P. Kortunov, J. Li, D. Olson, D. Tzoulaki, J. Weitkamp, J. Kärger: *Ensemble Measurement of Diffusion: Novel Beauty and Evidence*, Chem. Phys. Chem. **10**, 2623 (2009)
- C. Chmelik, L. Heinke, J.M. van Baten, R. Krishna: *Diffusion of n-Butane/iso-Butane Mixtures in Silicalite-1 Investigated Using Infrared (IR) Microscopy*, Micropor. Mesopor. Mat. **125**, 11 (2009)
- C. Chmelik, J. Kärger, M. Wiebcke, J. Caro, J.M. van Baten, R. Krishna: *Adsorption and Diffusion of Alkanes in CuBTC Crystals Investigated Using Infra-Red Microscopy and Molecular Simulations*, Micropor. Mesopor. Mat. **117**, 22 (2009)
- M. Dvoyashkin, A. Khokhlov, S. Naumov, R. Valiullin: *Pulsed Field Gradient NMR Study of Surface Diffusion in Mesoporous Adsorbents*, Micropor. Mesopor. Mat. **125**, 58 (2009)
- K.W. Fomba, P. Galvosas, U. Roland, J. Kärger, F.D. Kopinke: *New Option for Characterizing the Mobility of Organic Compounds in Humic Acids*, Environ. Sci. Technol. **43**, 8264 (2009)

- K. Friedemann, F. Stallmach, J. Kärger: *Carboxylates and Sulfates of Polysaccharides for Controlled Internal Water Release During Cement Hydration*, *Cement Concrete Comp* **31**, 244-249 (2009)
- M. Gratz, M. Wehring, P. Galvosas, F. Stallmach: *Multidimensional NMR Diffusion Studies in Microporous Materials*, *Micropor. Mesopor. Mat.* **125**, 30 (2009)
- L. Heinke, J. Kärger: *Discriminating the Molecular Pathways During Uptake and Release on Nanoporous Host Systems*, *J. Chem. Phys.* **130**, 044707 (2009)
- L. Heinke, D. Tzoulaki, C. Chmelik, F. Hibbe, J.M. van Baten, H. Lim, J. Li, R. Krishna, J. Kärger: *Assessing Guest Diffusivities in Porous Hosts from Transient Concentration Profiles*, *Phys. Rev. Lett.* **102**, 065901 (2009)
- J. Kärger: *Comment on: A.M. Avali et al.: Diffusion and Adsorption Selectivities of Hydrocarbons over FCC Catalysts*, *Chem. Eng. J.* **132**, 67 (2009), *Chem. Eng. J.* **145**, 525 (2009)
- J. Kärger, J. Caro, P. Cool, M.-O. Coppens, D. Jones, F. Kapteijn, F. Rodriguez-Reinoso, M. Stöcker, D. Theodorou, E. F. Vansant, J. Weitkamp: *Benefit of Microscopic Diffusion Measurement for the Characterization of Nanoporous Materials*, *Chem. Eng. Techn.* **32**, 1494 (2009)
- G. Kalies, P. Bräuer, M. Szombathely: *Design of Liquid/Solid Adsorption Isotherms by Energy Distribution Functions*, *J. Coll. Interface Sci.* **331**, 329 (2009)
- M. Krutyeva, F. Grinberg, F. Furtado, P. Galvosas, J. Kärger, A. Silvestre-Albero, A. Sepulveda-Escribano, J. Silvestre-Albero, F. Rodríguez-Reinoso: *Characterization of Carbon Materials with the Help of NMR Methods*, *Micropor. Mesopor. Mat.* **120**, 91 (2009)
- M. Krutyeva, F. Grinberg, J. Kärger, C. Chorro, N. Donzel, D.J. Jones: *Study of the Diffusion of Liquids and their Binary Mixtures in Mesoporous Aluminosilicates under Freezing Conditions*, *Micropor. Mesopor. Mat.* **120**, 104 (2009)
- E.E. Romanova, F. Grinberg, A. Pampel, J. Kärger, D. Freude: *Diffusion studies in confined nematic liquid crystals by MAS PFG NMR*, *J. Magn. Reson.* **196**, 110 (2009)
- E.E. Romanova, F. Scheffler, D. Freude: *Crystallization of zeolite MFI under supergravity, studied in situ by 11B MAS NMR spectroscopy*, *Micropor. Mesopor. Mat.* **126**, 268 (2009)
- S. Naumov, R. Valiullin, J. Kärger, P. A. Monson: *Understanding Adsorption and Desorption Processes in Mesoporous Materials with Independent Disordered Channels*, *Phys. Rev. E* **80**, 031607 (2009)
- D. Tzoulaki, L. Heinke, H. Lim, J. Li, D. Olson, J. Caro, R. Krishna, C. Chmelik, J. Kärger: *Assessing Surface Permeabilities from Transient Guest Profiles in Nanoporous Host Materials*, *Angew. Chem. Int. Ed.* **48**, 3525 (2009)

K. Ulrich, P. Galvosas, J. Kärger, F. Grinberg: *Effects of Self-Assembly on Diffusion Mechanisms of Triblock Copolymers in Aqueous Solution*, *Phys. Rev. Lett.* **102**, 037801 (2009)

K. Ulrich, D. Freude, P. Galvosas, C. Krause, J. Kärger, J. Caro, P. Poladli, H. Papp: *Diffusion of Aromatic Guest Molecules in Zeolite NaX Studied by Pulsed Field Gradient NMR*, *Micropor. Mesopor. Mat.* **120**, 98 (2009)

R. Valiullin, J. Kärger, R. Gläser: *Correlating Phase Behaviour and Diffusion in Mesopores: Perspectives Revealed by Pulsed Field Gradient NMR*, *PCCP* **11**, 2833 (2009)

Books

Z. Adem, T. Titze, C.B. Krause, C. Chmelik, J. Kullmann, D. Enke, P. Galvosas, J. Kärger: *Correlating PFG NMR and IR Diffusion Measurements in Porous Glasses*, in *Diffusion Fundamentals III*, ed. by C. Chmelik, N. Kanellopoulos, J. Kärger, D. Theodorou (Leipziger Universitätsverlag, Leipzig 2009) p 237

C. Chmelik, N. Kanellopoulos, J. Kärger, D. Theodorou : *Diffusion Fundamentals III* (Leipziger Universitätsverlag, Leipzig 2009)

C. Chmelik, L. Heinke, J. Kärger, J.M. van Baten, R. Krishna: *Diffusion of n-Butane/iso-Butane Mixtures in Silicalite-1 Investigated Using Infrared Microscopy*, in *Diffusion Fundamentals III*, ed. by C. Chmelik, N. Kanellopoulos, J. Kärger, D. Theodorou (Leipziger Universitätsverlag, Leipzig 2009) p 247

M. Dvoyashkin, A. Khokhlov, R. Valiullin, J. Kärger, M. Thommes: *Fluid Behavior in Porous Silicon Channels with Complex Pore Structure*, in *Diffusion Fundamentals III*, ed. by C. Chmelik, N. Kanellopoulos, J. Kärger, Doros Theodorou (Leipziger Universitätsverlag, Leipzig 2009) p 469

K. Friedemann, F. Stallmach, J. Kärger: *NMR Relaxometrie und Powers' Modell zur Quantifizierung des Feuchttransportes bei der inneren Nachbehandlung*, in *Proceedings of the 17th ibausil*, ed. by J. Stark, F.A. Finger-Institut für Baustoffkunde. Weimar (2009) vol. I, p 297-302

L. Heinke, D. Tzoulaki, C. Chmelik, F. Hibbe, J. Kärger: *Assessing Details of Molecular Motion in Nanopores by Combining Different Microscopic Techniques*, in *Diffusion Fundamentals III*, ed. by C. Chmelik, N. Kanellopoulos, J. Kärger, D. Theodorou (Leipziger Universitätsverlag, Leipzig 2009) p 257

C. Horch, S. Schlayer, F. Stallmach: *Permanent Magnet Arrangements for Low-Field NMR*, in *Proceedings COMSOL Conference Milan 2009 (online)*, <http://www.comsol.se/academic/papers/6717/> (2009)

D. Kondrashova, A. Khokhlov, R. Valiullin, J. Kärger: *Propagation of Solid-Liquid Interfaces in Disordered Linear Pores*, in *Diffusion Fundamentals III*, ed. by C. Chmelik, N. Kanellopoulos, J. Kärger, Doros Theodorou (Leipziger Universitätsverlag, Leipzig 2009) p 378

P. Zeigermann, M. Dvoyashkin, R. Valiullin, and J. Kärger: *Assessing the Pore Critical Point of the Confined Fluid by Diffusion Measurement*, in *Diffusion Fundamentals III*, ed. by C. Chmelik, N. Kanellopoulos, J. Kärger, Doros Theodorou (Leipziger Universitätsverlag, Leipzig 2009) p 278

in press

M. Dvoyashkin, R. Valiullin, E. Romanova, W. D. Einicke, R. Gläser, J. Kärger: *Diffusion of Cyclohexane in Native and Surface-Modified Mesoporous Glasses*, Appl. Surf. Sci. accepted (2009)

G. Kalies, R. Rockmann, D. Tuma, J. Gapke: *Zum Phänomen der Adsorption*, Appl. Surface Sci. doi: 10.1016/j.apsusc.2009.12.091

S. Arnrich, G. Kalies, P. Bräuer: *On Problems to Compute Adsorption Energy Distributions from Adsorption Isotherms by the Ansatz Method*, Appl. Surface Sci. doi: 10.1016/j.apsusc.2009.12.096

Talks

C. Chmelik, F. Hibbe, D. Tzoulaki, L. Heinke, J. Caro, J. Li, J. Kärger: *Exploring the Nature of Surface Barriers on MOF Zn(tbip) by Applying IR Microscopy in High Temporal and Spatial Resolution*, MOFCAT Workshop 2009 - MOFs on the Road to Application, Oslo, Norway (June 2009)

C. Chmelik, L. Heinke, J. Kärger, W. Schmidt, J.M. van Baten, R. Krishna: *Diffusion of n-Butane/iso-Butane Mixtures in Individual Silicalite-1 Crystals: An IR Microscopy Study*, 21st German Zeolite Conference, Kiel, Germany (March 2009)

M. Dvoyashkin, A. Khokhlov, S. Naumov, R. Valiullin: *Assessing Molecular Transport on Surfaces Using (PFG) NMR*, 7th International Symposium Effects of Surface Heterogeneity in Adsorption and Catalysis on Solids, Kazimiers Dolny, Poland (July, 2009)

C. Horch, S. Schlayer, F. Stallmach: *Permanent Magnet Arrangements for Low-Field NMR*, COMSOL Conference, Milan, Italy (15.10.2009)

S. Naumov, A. Khokhlov, R. Valiullin, J. Kärger, M. Thommes, *Phase Behavior of Fluids in Porous Silicon Materials and their Textural Characterization*, Porous Materials Workshop 2009, Rutgers University, NJ, USA

S. Naumov, R. Valiullin, P. A. Monson, J. Kärger, *Adsorption Hysteresis Phenomena in Mesopores*, EUROMAR 2009, Gothenburg, Sweden

J. Kärger, C. Chmelik: *Nanoporöse Glasformkörper - ein ideales Modellsystem zur Erforschung der Gesetzmäßigkeiten von Stofftransport und Stoffumwandlung in nanoporösen Materialien*, Innovationsforum Nanoporöse Glasformkörper, Leipzig, Germany (November 2009)

J. Kärger: *Diffusion Visualized by Interference and IR Microscopy*, 10th Workshop of the IRTG "Diffusion in Porous Materials", Eindhoven, The Netherlands (November 2009)

J. Kärger, T. Binder, C. Chmelik, L. Heinke, F. Hibbe, T. Titze, D. Tzoulaki: *The Wealth of Information from Transient Guest Profiles*, Diffusion Fundamentals III, Athens, Greece (August 2009)

G. Kalies: *Charakterisierung von porösen Stoffen - ein Überblick über experimentelle Methoden und Modelle zur Datenanalyse*, Institut für Nichtklassische Chemie Universität, Leipzig, Deutschland (Januar 2009)

G. Kalies, R. Rockmann: *Ordered Mesoporous Solids as Model Substances for Adsorption Processes*, Intern. Konferenz ISSHAC-7, Kazimierz Dolny, Polen (Juli 2009)

D. Kondrashova, R. Valiullin: *Freezing Kinetics in Linear Pores with Disorder*, Thermodynamics 2009, Imperial College London, U.K. (September, 2009)

F. Stallmach, C. Horch: *NMR Studies on Gas Shales, Pore Structure and Fluid Saturation Studied by High-Pressure Low-Field ^1H NMR*, Gas Shales in Europe (GASH) Kick off meeting, GFZ Potsdam, Germany (24.09.2009)

R. Valiullin, S. Naumov, J. Kärger, P. A. Monson: *Capillary Condensation and Hysteresis in Porous Silicon: Network Effects within Independent Pores*, DPG Spring Meeting, Dresden, Germany (March 2009)

Posters

S. Arnrich, G. Kalies, P. Bräuer: *Suitable Total Isotherms for Computing Energy Distribution Functions from Liquid/Solid Adsorption by means of Stieltjes Transformation*, Poster, Intern. Konferenz ISSHAC-7, Kazimierz Dolny, Polen (Juli 2009)

C. Chmelik, L. Heinke, J. Kärger, J.M. van Baten, R. Krishna: *Diffusion of n-Butane/iso-Butane Mixtures in Silicalite-1 Investigated Using Infrared Microscopy*, Diffusion Fundamentals III, Athens, Greece (August 2009)

C. Chmelik, L. Heinke, T. Titze, J. Li, D. Olson, J. Caro, J. Kärger: *New Options for Diffusion Studies in Nanoporous Materials Offered by the IR Micro-Imaging Technique*, 21st German Zeolite Conference, Kiel, Germany (March 2009)

L. Heinke, D. Tzoulaki, C. Chmelik, F. Hibbe, J. Kärger: *Assessing Details of Molecular Motion in Nanopores by Combining Different Microscopic Techniques*, Diffusion Fundamentals III, Athens, Greece (August 2009)

F. Hibbe, T. Binder, D. Tzoulaki, J. Kärger: *Applying Interference Microscopy to Study Temperature Effects on Molecular Transport in Nanopores*, Diffusion Fundamentals III, Athens, Greece (August 2009)

D. Kondrashova, A. Khokhlov, R. Valiullin, J. Kärger: *Propagation of Solid-Liquid Interfaces in Disordered Linear Pores*, Diffusion Fundamentals III, Athens, Greece (August, 2009)

T. Titze, Z. Adem, C. Chmelik, C. Krause, J. Kullmann, D. Enke, P. Galvosas, J. Kärger: *Correlating IRM and PFG NMR Diffusion Measurements in Porous Glasses*, Diffusion Fundamentals III, Athens, Greece (August 2009)

M. Wehring, S. Amirjalayer, S. Hertel, M. Gratz, R. Schmid, F. Stallmach: *Fundamental Host-Guest Interactions in Porous Metal Organic Frameworks. A Combined Experimental and Theoretical Approach*, Kick-Off meeting DFG priority program 1362, Dresden, Germany (October 2009)

M. Wehring, S. Hertel, S. Amirjalayer, R. Schmid, F. Stallmach: *Investigation of Diffusion of Aromatic Hydrocarbons Adsorbed in MOF-5 by PFG NMR*, Conference Diffusion Fundamentals 3, Athens, Greece (October 2009)

P. Zeigermann, M. Dvoyashkin, R. Valiullin, W.-D. Einicke, R. Gläser, J. Kärger: *Assessing the Pore Critical Temperature of Confined Fluids by Diffusion Measurements*, Diffusion Fundamentals III, Athens, Greece (Aug. 2009)

4.20 Graduations

Doctorate

- Muslim Dvoyashkin
Molecular Transport of Fluids in Mesopores
20.04.2009
- Lars Heinke
Mass transfer in nanoporous materials: A detailed analysis of transient concentration profiles
06.10.2008
- Aleksey Khokhlov
Nanoporous Silicon: Structural Characterization Using NMR and Applications
20.04.2009
- Sergej Naumov
Hysteresis Phenomena in Mesoporous Materials
20.07.2009
- Ekaterina Romanova
NMR-Untersuchungen an porösen Systemen
05.02.2009

Diploma

- Steffen Beckert
¹H-NMR-Untersuchungen zur Mobilität von Fluiden in Acrylat-Monolithen sowie in MCM-41-Materialien für die Anwendung in Brennstoffzellenmembranen
30.11.2009
- Tomas Binder
Untersuchung des Einflusses der Realstruktur nanoporöser Materialien auf das Diffusionsverhalten von Gastmolekülen mittels Interferenzmikroskopie
31.03.2009
- Tobias Titze
Untersuchung des Stofftransportes in nanoporösen Materialien mittels IR-Microimaging
24.04.2009

4.21 Guests

- Prof. Dr. Randy Snurr
Northwestern University, Dept. of Chem. Eng., Evanston, USA
Leibniz-Professor: April - September 2009
- Prof. Dr. Douglas M. Ruthven
University of Maine, Dept. of Chem. Eng.
March - May 2009
- Pin Domkers
Eindhoven University of Technology, Department of Applied Physics
March - June 2009
- Dr. Anabel Lam Barandela
University of Havana, Cuba
August - October 2009

5

Soft Matter Physics

5.1 Introduction

In his book "What is Life?", Schrödinger recognized the immense challenge to explain biological processes by basic physics and chemistry. Consequentially, traditional medical physics had predominately the role to develop devices for medicine such as sophisticated imaging solutions (X-ray, NMR, multiphoton) or laser scalpels. Commencing with Watson and Crick, science has gained tremendous insight into the molecular basis of biological cells. Over 25 000 genes encode the information of human life, and their subsequent transcription and translation add to the complexity of molecular interactions resulting in an insurmountable combinatorial number of relations. Recent progress in biosciences towards a more quantitative description opens a challenging and new pathway for medical physics to use physics underlying biological processes to directly impact diagnosis and therapy. Despite that this approach is still in its infancy, it may redefine medical physics. This kind of research is based on fundamental biological physics and has in its ideal case applied aspects in medical physics. By identifying cellular subunits acting as independent functional modules this complexity becomes tractable and the fundamental physical principles of these modules can be studied.

A prototypical example for such a module is the intracellular scaffold known as the cytoskeleton. The cytoskeleton is the key structural element in cellular organization and is an indicator of pathological changes in cell function. It is a compound of highly dynamic polymers and molecular motors as active nano-elements inside cells. The cytoskeleton mechanically and chemically senses a cell's environment achieving a high sensitivity by using processes such as stochastic resonance. This active polymeric scaffold generates cellular motion and forces in the tens of nanoNewton sufficiently strong to push rigid AFM cantilevers out of the way. These forces are generated by molecular motor-based nano-muscles and by polymerization through mechanisms similar to Feynman's hypothetical thermal ratchet. A new type of polymer physics describes these active polymer networks since the nano-sized motors overcome the inherently slow, often glass-like Brownian polymer dynamics. This results in novel self-organization of the polymer scaffolds and rapid switching between different ordered states. This organization of the cytoskeleton is tightly controlled in cells. Thus, suspended cells' biomechanical properties are well-defined and distinguish different cellular states and cell types with confidence levels of more than 95% (metastatic from non-metastatic cancer cells, stem cells from differentiated cells in adult tissues, etc.). Since cell elasti-

city depends highly nonlinear on cytoskeletal composition already small changes in a cell's state are measurable by biomechanical changes and recent polymer theories can be used to deduce the cytoskeletal part of a cell's proteomic condition. Recently, the optical stretcher, a photonic device developed in our laboratory, was demonstrated within a clinical study as a highly sensitive non-invasive tool for mechanical classification of cancer cells [1]. The device's versatility was drastically improved by integration of the capability to rotate cells under observation [2]. The cytoskeleton uses up to 30% of cellular ATP, which is a cell's fuel. Optical gradient forces due to cells' dielectric nature can manipulate the cytoskeleton's consequential active and dynamical state. Opto-molecular coupling between laser light and cytoskeletal processes permits optical control of neuronal growth. The specific opto-molecular influence on membrane and cytoskeletal transport is complex. Cells cannot modulate diffusion by the parameters found in the Einstein equation (temperature, viscosity, molecular size).

Consequentially, cells exhibit rich multifaceted intracellular transport including motor-driven motion and anomalous subdiffusion, which can be probed by the use of nanoparticles as tracers. The cytoskeleton as active, soft condensed matter, with structures on nanometer and micron scales representative of individual proteins and cells, calls forth new biological and polymer physics. Our research group's goals center on unraveling this new physics of the cytoskeleton. The current and future research goals are summarized in the following sections.

Josef A. Käs

[1] T. Remmerbach et al.: *Cancer Res.* **69**, 1728 (2009)

[2] M. Kreysing et al.: *Opt. Express* **16**, 16984 (2008)

5.2 Feeling for Cells with Light: Illuminating the Role of Biomechanics for Cancer Metastasis

M. Zink, A. Fritsch, T. Kiessling, D. Nnetu, F. Wetzel, S. Ebert, M. Gyger, R. Stange, J.A. Käs

Light has been used to observe cells since Leeuwenhoek's times; however, we use the forces caused by light described by Maxwell's surface tensor to feel for the cellular cytoskeleton. The cytoskeleton, a compound of highly dynamic polymers and active nano-elements inside biological cells, is responsible for a cell's stability and organization. The Optical Stretcher exploits the nonlinear, thus amplified response of a cell's mechanical strength to small changes between different cytoskeletal proteomic compositions as a high precision cell marker that uniquely characterizes different cell types. During the last month, a computer-controlled system of vacuum pumps was set up to fully automate the experimental procedure which increased the through-put of cells during a measurement by a factor of five.

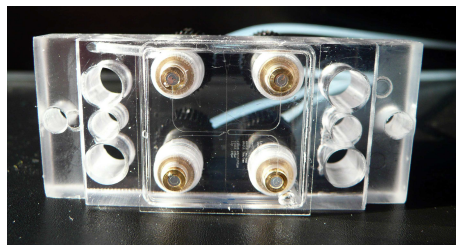


Figure 5.1: The Optical Stretcher is a tool to probe viscoelastic properties of individual cells utilizing the pressure refracted light exerts on a surface. Core piece of the Optical Stretcher is a microfluidic chip.

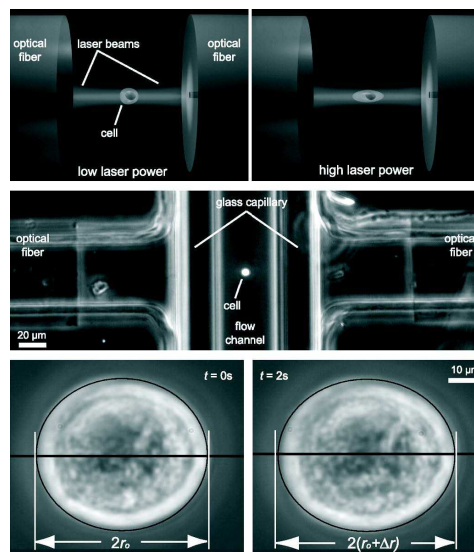


Figure 5.2: During a measurement cells are in suspension in a flow channel. Individual cells are trapped between two counter-propagating divergent laser beams emitted from opposing optical fibers. By increasing the laser power, the surface stress (due to the light pressure) increases and deforms the cell along the laser axis.

Cancer is characterized by uncontrolled growth of the tumor, invasion and, thus, destruction of the surrounding tissue and metastatic behavior. All three properties can directly be derived from cell mechanics employing the Optical Stretcher technology. It turned out that normal and cancerous cells exhibit different elastic properties during optical deformation because the cytoskeleton changes during malignant transformation. Thus, recent experiments show that malignant cells are softer than normal cells [1]. Additional studies proved that cancerous cells proliferate faster than normal cells.

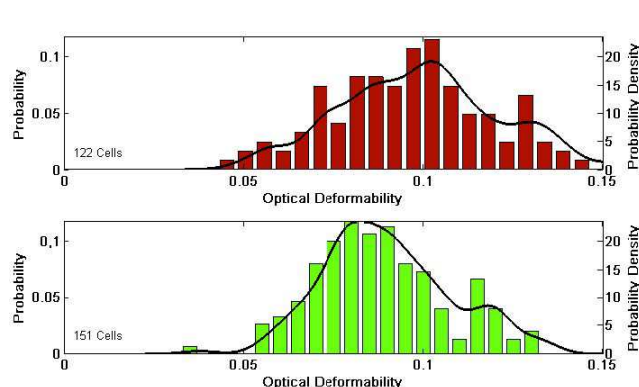


Figure 5.3: Malignant cells (MCF7) are softer than normal cells (MCF10A).

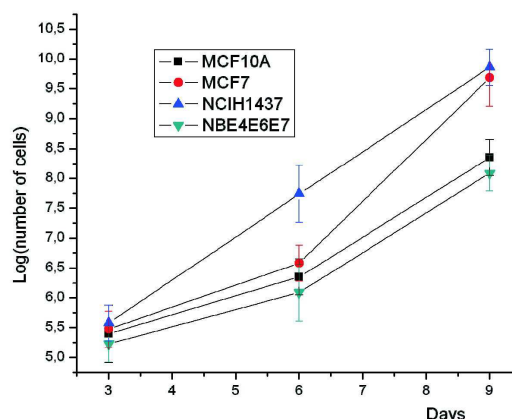


Figure 5.4: Malignant cells (MCF7) proliferate faster than normal cells (MCF10A).

Two clinical studies on the mechanical properties of cancer cells were carried out. First, the Optical Stretcher was used to detect oral cancer by extracting primary cancer

cells with a brush from the patient's mouth which were then taken into culture and subsequently trapped and deformed between two laser beams in the Optical Stretcher[2]. Second, primary breast cell and breast cancer cells were extracted from a patient by biopsy or surgical excision. The tissue was minced, washed, digested in collagenase and DNase and spun down. The isolated tumor cells were taken into culture and subsequently optically deformed. Both studies clearly corroborated the results found from optical deformation of cell lines that malignant cells are softer than normal cells.

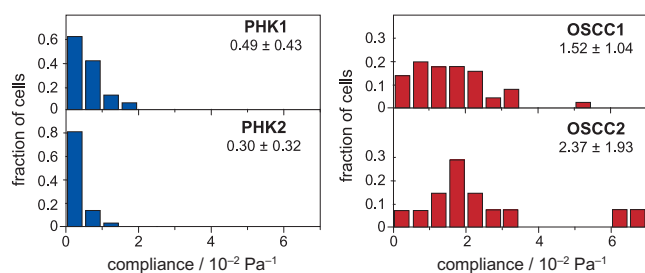


Figure 5.5: The Optical Stretcher was used to detect oral cancer confirming that malignant cells are softer than normal cells. The diagram shows normal samples (primary human keratinocytes, PHK) in comparison to oral squamous cell carcinoma (OSCC) samples [2].

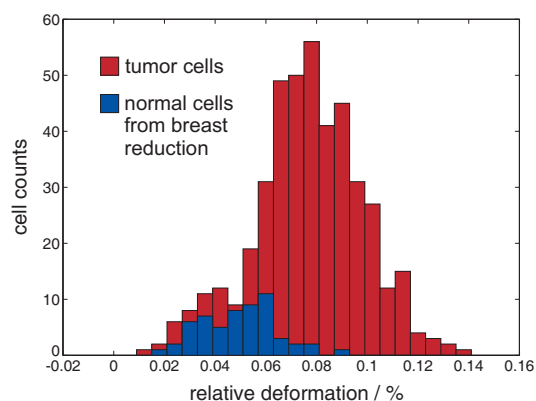


Figure 5.6: The mechanical properties of primary breast cell taken from breast reductions were compared with primary breast cancer cells. It turned out that malignant cells are softer than normal cells.

For the spatial organization of tissue in multicellular organisms the mechanical properties of single cells and their environment are of great importance and influence invasion of the cancerous cells into the surrounding tissue. To investigate possible changes in cells' elasticity due to interactions with the embedding material, the mechanical properties of cell lines that were cultured in plastic petri dishes were compared with freshly extracted primary cells. It turned out that primary cells are stiffer compared to cell lines. Further studies showed that tumor cells grown in suspended spheroids are less deformable than the reference from ordinary monolayer culture.

Additional deformability measurement of non-cancerous MCF10, cancerous MCF7 and metastatic modMCF7 cells showed an increasing softness of metastatic cells in comparison to cancerous and normal cell. Thus, with increasing cancer aggressiveness the cell's compliance increases which can result in a much more precise staging of tumors for diagnosis. Further studies let us suggest that cancer stem cells exhibit an even larger elasticity. Taken together, optical deformability is not solely a promising cell marker in diagnosis. Moreover, it allows the selection of mesenchymal stem cells that are particularly potent in cartilage formation.

[1] C. Brunner et al.: *Soft Matter* **5**, 2171-2178 (2009)

[2] T. Remmerbach et al.: *Cancer Res.* **69**, 1728 (2009)

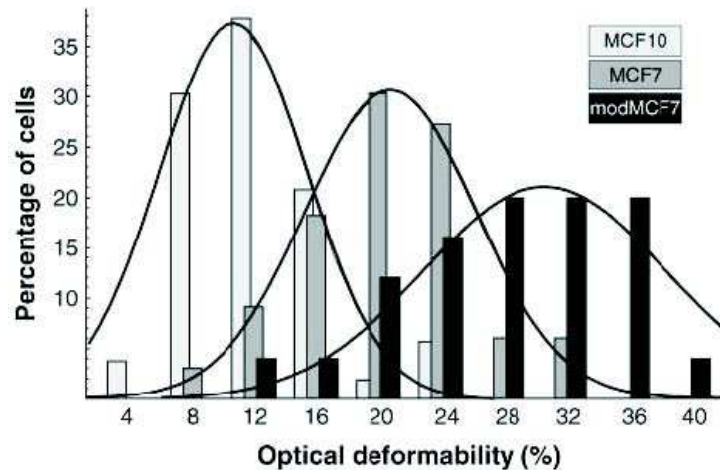


Figure 5.7: Deformability measurement of non-cancerous MCF10, cancerous MCF7 and metastatic modMCF7 cells. Obviously, the modMCF7 are more deformable than MCF7 and MCF10. With increasing cancer aggressiveness the cell's compliance increases.

5.3 Origin and Spatial Distribution of Forces in Motile Cells

C.A. Brunner, M. Gögler, D. Koch,* A. Ehrlicher,[†] T. Fuhs, J.A. Käs

*Georgetown University, USA

[†]Harvard Medical School, USA

A fundamental step in cell migration is the advancement of the cell's leading edge. It is generally accepted that this motion is driven by actin polymerization against the plasma membrane but this has not been directly measured. Here we present precise force measurements using a newly established SFM-technique combined with high resolution imaging and lamellipodium feature tracking analysis. Our SFM-based technique uses the vertical and lateral deflection of a modified cantilever and allows direct measurements of the forces exerted by the cell [1].

A polystyrene bead (blue, Fig. 5.8) glued to a cantilever-tip of an SFM is positioned on the substrate in front of a migrating cell. The cell moves towards the bead, crawls under it, and pushes the cantilever upwards. Alternatively the cell pushes against the bead perpendicular to the cantilever's long axis which leads to a twist of the cantilever and is detected as lateral deflection. Direct measurements of the maximum forces which are generated at the leading edge of the lamellipodium, retrograde forces within the lamellipodium, and the cell body forces are possible. Through selective manipulation of molecular components by addition of different drugs, such as Jasplakinolide, Cytochalasin D, and ML-7 the measured forces and velocity changes can be compared.

This leads to new insights concerning the importance of different force generating processes and reveals actin polymerization as the dominant force generating process at the leading edge. On the other hand myosin does not seem to be responsible for the retrograde flow in the central lamellipodium. We directly measured a force attributed to the retrograde flow within the lamella, which critically demonstrates that the protrusion forces are decoupled from the cell body and are generated exclusively at the leading

edge [2].

To improve the temporal and spatial sensitivity, a combination of the SFM experiment with optical tweezers to stabilize the setup, promises possible measurements of forces on slower and softer cells, like neurons, fibroblast, etc. to complete the phase space of motile cells and to understand the underlying mechanisms nature invented.

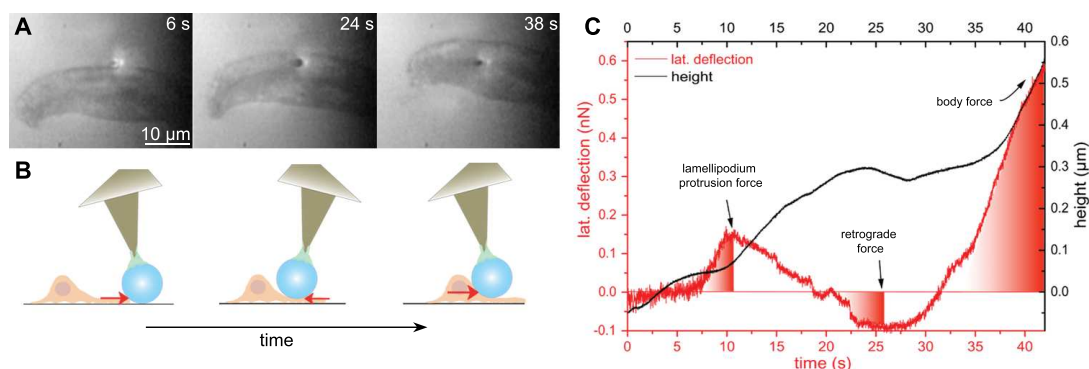


Figure 5.8: SFM-Force measurement of a migrating keratocyte. A: Interference reflection microscopy images: the cell pushes against the cantilevered bead (bright spot) and finally lifts it up. B: Sketch of the experiment, the cell pushes against the cantilever; the lateral deflection corresponds directly to the force. C: Lateral deflection signal (red) reflects the forces the cell exerts in different regions of the cell during the measurement.

- [1] C. A. Brunner, A. Ehrlicher, B. Kohlstrunk, D. Knebel, J. A. Kaes, M. Goegler: *European Biophysical Journal* **35**, 713-719 (2006)
- [2] M. Goegler, C. A. Brunner, A. Ehrlicher, D. Koch, T. Fuhs, C. W. Wolgemuth, J. A. Kaes: *Cell* (under Review)

5.4 Mechanosensitive Behavior of Neuronal Growth Cones

S. Pawlizak, J.A. Käs

Neuronal pathfinding is essential for the development of the central nervous system. Neurons travel through a complex array of tissues, chemical signals and mechanical stimuli to form the connections necessary for life. Therefore growth cones which are highly dynamic and motile structures at the leading edge of neuronal extensions (called axons or neurites) have to interpret the myriad of signals while navigating through the body to finally reach the neurons' target sites. Although it is generally accepted that chemotaxis is the major guidance factor, it seems unlikely that this is the only mechanism directing developmental neurons, especially when considering the length of some pathways.

Recent studies indicate that, in addition to chemical cues, mechanical stimuli also play a non-negligible role for neuronal growth. This process is called mechanotaxis or durotaxis. Unlike most other cell types, neurons show a preference for soft substrates. However, the mechanisms responsible for the neuronal affinity for soft substrates have not yet been identified.

Our *in vitro* studies show that neurons actively palpate their mechanical environment [1]. We observed that growth cones deform substrates with a compliance commensurate to their own. To understand the sensing of stiff substrates, we investigated the precise temporal response of neurons to well-defined mechanical stress. Growth cones were mechanically simulated using a modified scanning force microscope (SFM) probe or a micromanipulator with a narrowed glass pipette tip. When the applied stress exceeded a threshold of approximately 300 Pa, neurons retracted and re-extended their processes, thereby enabling exploration of alternative directions (see Figure 5.9). This threshold corresponds to the maximum substrate stiffness that neurons can visibly deform. An immediate calcium influx through stretch-activated ion channels seems to be correlated with neurite retraction.

Our data illustrate how growing neurons may detect and avoid stiff substrates - as a mechanism involved in axonal branch pruning. Thus, mechanics may act as guidance cue for neuronal growth.

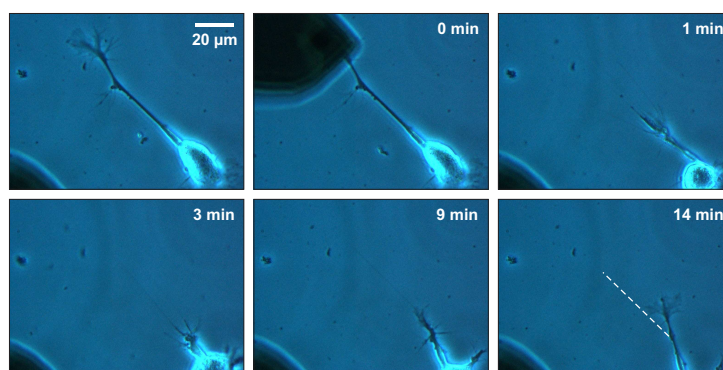


Figure 5.9: Phase contrast images of the stimulated retraction and re-extension of an NG108-15 neurite using a modified SFM cantilever [1].

[1] K. Franze et al.: *Biophys. J.* **97**, 1883-1890 (2009)

5.5 Structural Investigation on the Absorption of the MARCKS Peptide on Anionic Lipid Monolayers

U. Diedrich, P. Krüger*, T. Gutberlet†, J.A. Käs

*Fraunhofer Institute for Non-Destructive Testing, Dresden branch

†Forschungszentrum Jülich GmbH

The presence of charged lipids in the cell membrane constitutes the background for the interaction with numerous membrane proteins. As a result, the valency of the lipids plays an important role concerning their lateral organization in the membrane and therefore the very manner of this interaction. We investigate this aspect in regard to the interaction of two differently charged acidic lipids, the monovalent DPPS and the polyvalent PIP₂, with the highly basic charged effector domain of the MARCKS protein,

observed in monolayer model systems. Film balance, fluorescence microscopy and x-ray reflection/diffraction measurements were used to study the behavior of both lipids, in a mixture with DPPC, for its dependance on the presence of MARCKS (151-175). The obtained results contribute to the comparison of the effects of both differently charged lipids on the monolayer structure.

Both acidic lipids show a complete different behavior in the simple lipid mixture depending on their charge. The polyvalent PIP₂ molecules are arranged in a uniform distribution in the disordered phase of the mixed monolayer. This lateral distribution is presumably caused by the perpendicular orientation of the PI(4,5) group to the membrane interface. The distance of this phosphate group to the level of the phosphodiester groups of the membrane increases with increasing lateral pressure. At a pressure of 30 mN m⁻¹ the PI(4,5) group is 10 Å below the layer of the phosphodiester groups [1]. The behavior of DPPS in the mixture differs from PIP₂. The serine group is completely embedded in the phosphodiester layer. In this way the interaction of the serine groups with the basic residues of MARCKS peptide occurs in the ordered state and hence the lateral PS separation primarily happens in subdomains inside the ordered lipid domains. The large cationic charge of peptide pulls the serine group out of the interface up to 7 Å, which simultaneously leads to an elongation of the phosphodiester groups of the lipid fraction in the direction normal to the surface. The ordered state of the lipid mixture remains undisturbed [2].

The interaction of MARCKS peptide with PIP₂ leads - in contrast to DPPS - to a tilt of the PI(4,5) group in a direction towards the interface, while the position of the phosphodiester group keeps constant. This primary protrusion of the PI(4,5) from the interface promotes the interaction with the charged peptide, which has only an impact on the PI(4,5) without any influence on the surrounding lipid matrix.

Since the PIP₂ molecules are arranged in a uniform distribution in the disordered phase, the PIP₂/peptide complexes exist as well in the disordered phase. The enrichment of MARCKS peptide in the disordered phase potentially facilitates the diffusion of these complexes along the membrane interface. In this manner there is assured a disposability of MARCKS along the interface in comparably small amounts [1].

As it is known, the association of the MARCKS protein with the membrane is a reversible process, which plays a role in the regulation of the PIP₂ availability in the cell membrane. In addition to the two negative charges, the elongation of the PI(4,5) group into the aqueous phase is an important factor for an effective recognition of the lipid by the MARCKS protein at the interface. Due to the enrichment of PIP₂/peptide complexes in the disordered phase, an arbitrary distribution can be assumed to be caused by diffusion and thus the regulating function of the protein occurs along the membrane interface. The association of MARCKS peptide with the serine groups is less pronounced. This interaction occurs only due to the negative charge of the carbonyl group of the serine and is mainly bound to the ordered lipid domains [2].

The lateral arrangement of the anionic lipids within the membrane interface, which depends on their charge values, is an essential parameter in terms of their functionality. The enrichment of PIP₂ in the disordered phase, which on one hand arose from the negative residual charges at the interface and on the other hand from the considerable elongation of the PI(4,5) group into the aqueous phase, promotes the formation of lipid/protein clusters in this phase. This state facilitates the diffusion of these clusters within the cell membrane and gives the reason for the central role of the regulating

function of the protein in interaction with the PIP_2 .

In contrast, the diffusion of DPPS/MARCKS clusters within the membrane interface is clearly constricted due the enrichment of this anionic lipid in the ordered phase. That is already based through the smaller diffusion coefficient of lipids in the ordered phase, compared to the lipids in the disordered phase. Furthermore, the elongation of the phosphodiester groups in the lipid fraction in the direction of the surface normal, induced by the interaction with the MARCKS peptide, leads to a certain thickening of this part of the membrane. Therefore, it would be possible that this kind of interaction plays a role by the formation of the membrane topology.

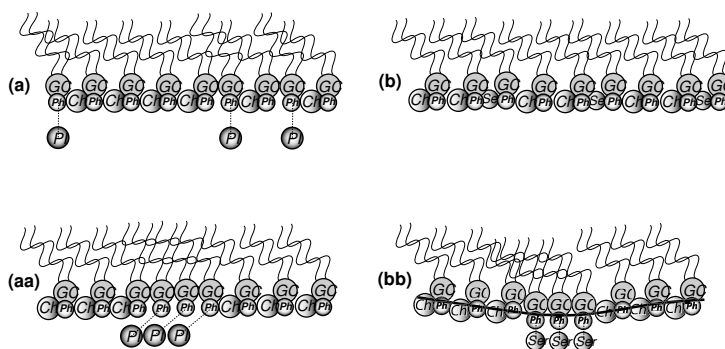


Figure 5.10: Sketch of the structure of the mixed monolayers. (a) DPPC/ PIP_2 , (aa) DPPC/ PIP_2 with MARCKS (151-175) interaction, and (b) DPPC/DPPS, (bb) DPPC/DPPS with MARCKS (151-175) interaction; thereby are GC - glycerol/carbonyl fragment, Ch - choline group, Ph - phosphodiester group, PI - PI(4,5) group of PIP_2 and Ser - serine group of DPPS.

- [1] U. Dietrich et al.: BBA Biomembranes 1788, 1474 (2009)
 [2] U. Dietrich et al.: Langmuir, submitted

5.6 Mechanical properties of transiently crosslinked F-actin bundles

D. Strehle, B. Gentry, J. Schnauss, F. Huber, C. Heussinger*, J. Alvarado[†], E. Frey[‡], M. Bathe[§], J.A. Käs

*Université de Lyon, Univ. Lyon I, Laboratoire de Physique de la Matière Condensée et Nanostructures, CNRS, UMR 5586, 69622 Villeurbanne, France

[†]Biological Soft Matter Group, FOM Institute AMOLF, Science Park 104, 1098 XG Amsterdam, The Netherlands

[‡]Arnold Sommerfeld Center for Theoretical Physics, Ludwig-Maximilians-Universität, Munich

[§]Department of Biological Engineering, MIT, 77 Massachusetts Avenue, Cambridge, MA 02139

Polymeric actin is one major component of the highly dynamic cytoskeleton where it forms dense networks that range structures like the actin cortex just below the outer membrane of suspended cells, the very thin protruding sheets, the lamellipodia, or very compact bundles like stressfibers or filopodia. The mechanical properties of such bundles structures are beginning to be elucidated [1].

We developed a technique to time-dependently probe the mechanical response of dynamically cross-linked actin bundles [2]. This technique uses optical tweezers to manipulate functionalized micro-beads that are attached to the F-actin bundles. We were able to bend bundles several times more than done by thermal fluctuation allowing us to investigate mechanical response to large bending deformations as well as long bending times.

Our studies show that *in vitro* bundles that were reconstituted following the same recipe exhibit tremendous variations in relaxation time following short-time bends. We think that this spread might make a significant contribution to a microscopic explanation of the observed scale-free rheological behavior of cells.

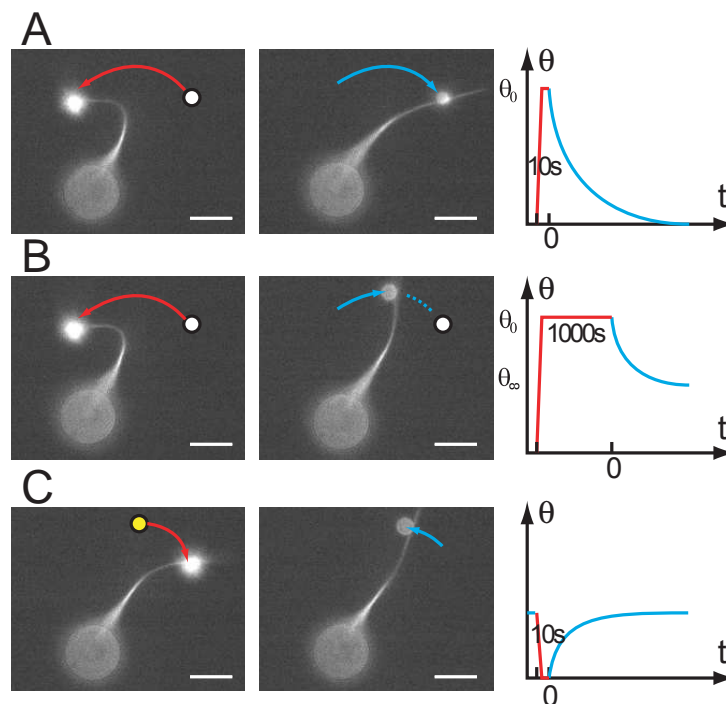


Figure 5.11: Experimental probe of time-dependent F-actin bundle relaxation behavior following large deformations using optical tweezers. (A) Short-hold bend. The F-actin bundle is bent to the bending angle θ_0 by optical tweezers and held there for 10 s (red). Full relaxation occurs in approximately 60 s after the bead's release (cyan). (B) Long hold bend. The same bundle as in A is deformed again to θ_0 but using a 1000s hold (red). Partial return of the bundle to its new resting position θ_∞ occurs in approximately 80 s (cyan). (C) Integrity test bend. The bundle is forcibly returned to its original undeformed position, $\theta = 0$, and held there for 10 s (red). It then returns to its newly acquired resting position (yellow circle) in approximately 140 s (cyan), showing that it is not damaged in the first combination of short and long holding-time bends. Scalebar 5 μm .

Increasing the time of holding bundles in a bent configuration, we could demonstrate that dynamically crosslinked F-actin bundles exhibit an elasto-plastic response. On this time-scale crosslinking proteins such as alpha-actinin are thought to be able to sterically rearrange within the bundle thus stabilizing an energetically more favorable configuration.

Theory suggests that on time-scales in between this purely elastic (after short-hold bends) and elasto-plastic behavior (after long-hold bends), the mechanical properties

of bundles shift from filament to crosslinker dominated [3]. Future work will probe the elastic parameters of actin bundles on different intermediate time scales.

[1] M.M.A.E. Claessens, et. al.: *Nature Matter* **5**, 748-753 (2006)

[2] D. Strehle et. al., in preparation

[3] M. Bathe et. al.: *Biophysical Journal* **94**, 2955-2964 (2008)

5.7 Funding

MS CartPro - Multiparametric Monitoring and Steering of Mesenchymal Stem Cell derived Cartilage Formation in 3D Production Systems

Prof. Dr. J. A. Käs, Dr. J. Guck

Projektbereich 2, BMBF- Project MS CartPro (FKZ: PTJ - BIO/ 31P4282)

Untersuchungen der altersabhängigen Modulation der Elastizität von Hautzellen durch physiologische Stressoren

Prof. Dr. J. A. Käs, F. Wetzel

Beierdorf AG - Forschungsvertrag

Leipziger Schule der Naturwissenschaften - Bauen mit Molekülen und Nano-Objekten

Prof. Dr. E. Hey-Hawkins, Prof. Dr. M. Grundmann and Prof. Dr. J. A. Käs

BuildMoNa - Graduiertenschule

Single Particle and Polymer Tracking in Two-Dimensional Energy-Landscapes

Prof. Dr. J. Kärger, Prof. Dr. F. Cichos and Prof. Dr. J. A. Käs

DFG-Forschergruppe

Optical Stretcher zur hochaufgelösten Darstellung und Analyse von einzelnen Zellen

Prof. Dr. J. A. Käs

Carl-Zeiss MicroImaging GmbH - OSDA - Forschungsvertrag

InterNeuro

Prof. Dr. J. A. Käs and Dr. J. Guck

DFG Graduiertenkolleg (GRK 1097) in Leipzig. Start 04/2005

Von lokaler Beschränkung bis zu makroskopischem Transport

Prof. Dr. F. Cichos, Prof. Dr. J. Käs et al.

DFG-Forschergruppe ("Sächs. Forschergruppe")

Optical Stretcher Methode zur Krebsdiagnose an Biopsien

Prof. Dr. J. Käs

EXPRIMAGE-Forschungsverbund

Inhärente zelluläre, physikalische und Materialeigenschaften zur molekular Marker-freien Isolierung und Charakterisierung seltener Zelltypen

Prof. Dr. J. Käs, Prof. Dr. A. Robitzki et al.

-Theranostik- / SAB-Projekt

Zuverlässige Untersuchung und gezielte Modifikation der mechanischen Eigenschaften retinaler Zellen bei Netzhauterkrankungen und in Glanarben

Prof. Dr. J. Käs, Prof. Dr. A. Reichenbach et al.

Teilprojekt 2 / SAB-Projekt

5.8 Organizational Duties

J. A. Käs

- Advisory committee for soft matter physics, NASA, USA
- Chair, scientific advisory board, Evacyte Inc., USA
- CNRS review committee, Institute Curie, Paris
- Journal review: Nature, Physical Review Letters, Physical Review E, Biophysical Journal, Biophysica and Biochemica Acta, Biochemistry, Proceedings of the National Academy of Science, European Biophysical Journal, Langmuir
- Grant review: National Science Foundation, Div. of Materials Research; National Science Foundation, Div. of Cellular Organization; National Science Foundation, Div. of Computational Biology; National Science Foundation, Div. of Physics, Special Programs; Deutsche Forschungsgemeinschaft, Alexander von Humboldt Foundation, Deutsche Studienstiftung, Centre National de Reserche

5.9 External Cooperations

Academic

- MD Anderson Cancer Center, Houston, Texas
Prof. Dr. Michel Follen
- Center for Nonlinear Dynamics, Austin, Texas
Prof. Dr. Harry Swinney
- University of Texas at Austin
Prof. Dr. Ken Shih
- University of Texas at Austin
Prof. Dr. Mark Raizen
- Institute Curie, Paris
Prof. Dr. Jean-Francois Joanny
- ESPCI, Paris
Prof. Dr. Jacques Prost
- Cea Saclay, France
Prof. Dr. Marie-France Carlier
- Princeton
Prof. Dr. Robert Austin
- University of Saarbruecken
Prof. Dr. Walter Zimmermann

- MPI for Colloids and Interfaces, Potsdam-Golm
Prof. Dr. Reinhardt Lipowsky
- MPI for Complex Systems, Dresden
Prof. Dr. Frank Jülicher

Industry

- Carl Zeiss MicroImaging GmbH, Jena
Dr. Christian Dietrich
- Beiersdorf AG, Hamburg
Dr. Th. Blatt
- Euroderm GmbH, Leipzig
Dr. A. Emmendörffer
- Evotec GmbH, Dresden
Dr. Th. Bauer
- FAUN GmbH, Leipzig
F. Fischer
- GeSim mbH, Dresden
Dr. S. Howitz
- JPK Instruments, Berlin
Dr. Th. Jähnke
- Niendorf & Hamper, Hamburg
Prof. A. Niendorf
- Qiagen GmbH, Hilden
Dr. Th. Singer

5.10 Publications

Journals

K. Franze, J. Gerdelmann, M. Weick, T. Betz, S. Pawlizak, M. Lakadamyali, J. Bayer, K. Rillich, M. Gögler, Y.-B. Lu, A. Reichenbach, P. Janmey, J. Käs: *Neurite Branch Retraction Is Caused by a Threshold-Dependent Mechanical Impact*, *Biophysical Journal* **97**, Issue 7, 1883-1890 (2009)

T. Betz, D. Koch, D. Lim, J. A. Käs: *Stochastic Actin Polymerization and Steady Retrograde Flow Determine Growth Cone Advancement*, *Biophysical Journal* **96**, Issue 12, 5130-5138 (2009)

U. Dietrich, P. Krüger, T. Gutberlet, J. A. Käs: *Interaction of the MARCKS Peptide with PIP2 in Phospholipid Monolayers*, *Biochimica et Biophysica Acta (BBA) - Biomembranes* **1788**, Issue 7, 1474-1481 (2009)

D. Smith, B. Gentry, B. Stuhmann, F. Huber, D. Strehle, C. Brunner, D. Koch, M. Steinbeck, T. Betz, J. A. Käs: *The Cytoskeleton: An Active Polymer-based Scaffold*, *Biophysical Reviews and Letters* **4**, Issues 1-2, 179-208 (2009)

B. Gentry, D. Smith, J. Käs: *Buckling-induced zebra stripe patterns in nematic F-actin*, *Physical Review E* **79**, Issue 3, 031916 (2009)

C. Brunner, A. Niendorf, J. A. Käs: *Passive and active single-cell biomechanics: a new perspective in cancer diagnosis*, *Soft Matter* **5**, 2171-2178 (2009)

T. W. Remmerbach, F. Wottawah, J. Dietrich, B. Lincoln, C. Wittekind, J. Guck: *Oral Cancer Diagnosis by Mechanical Phenotyping*, *Cancer Research* **69**, Issue 5, 1728-1732 (2009)

C. Schulze, K. Müller, J. A. Käs, J. C. Gerdemann: *Compaction of cell shape occurs before decrease of elasticity in CHO-K1 cells treated with actin cytoskeleton disrupting drug cytochalasin D*, *Cell Motility and the Cytoskeleton* **66**, Issue 4, 193-201 (2009)

in press

N. Kikuchi, A. Ehrlicher, D. Koch, J. A. Käs, S. Ramaswamy, M. Rao: *Buckling, stiffening, and negative dissipation in the dynamics of a biopolymer in an active medium*, *PNAS*

Talks

PWM Winter School, Spindler-Mühle, Tschechische Republik, Organizer, February 17-24, 2009

2nd Symposium Sächsische Forschergruppe (DFG: FOR 877), Eibenstock, "Feeling for Cells with Light", March 11-13, 2009

DPG Frühjahrstagung, Dresden, "Soft Brains, Signal Amplification through Noise, and Taking the Bull by its Horns", March 24-25, 2008

Biophysics Symposium on Cell Mechanics and Motility, National Cancer Institute/University of Maryland, USA, "Soft Brains, Signal Amplification through Noise, and Taking the Bull by its Horns", May 5-9, 2009

IZKF-annual conference 2009, Leipzig, "Feeling for Cells with Light", May 15, 2009

World Congress 2009 - Medical Physics and Biomedical Engineering, Cellular Mechanics, September 6-8, 2009

International Bunsen Discussion Meeting 2009, Leipzig, "Biologic Cells, Active Polymeric Machines", September 27-30, 2009

BuildMoNa: Doctoral candidates' workshop, Neukirchen/Pleisse, PI attendance, October 8-9, 2009

Zukunftsworkshop "Zellbasierte Mikrosystemtechnik für die personalisierte Medizin", VDI/VDE Innovation + Technik GmbH, Berlin October 12, 2009

19th Annual Conference on the German Society of Cytometry 2009, Leipzig, New developments in instrumentation October 14-16, 2009

SFB 555 Workshop "Komplexe Nichtlineare Prozesse", HU, Berlin, "Feeling for Cancer with Light", November 27-29, 2009

Patents

Josef Käs, Mark Raizen, Valery Milner, Timo Betz and Allen Ehrlicher: U.S. Patent # 7435568 "Optical Cell Guidance", European and Asian patents are pending

Josef Käs and Jochen Guck: U.S. Patent # 6067859 "Optical Stretcher"

Josef Käs and Jochen Guck: European Patent # 1059871 "Optical Stretcher" for Germany, Great Britain, France, Switzerland, Italy and Spain

Jochen Guck, Josef Käs, Moritz Kreysing: European Patent # 193549811 "Anordnung und Verfahren zur berührungslosen Ausrichtung und Drehung von Partikeln durch anisotrope, elektromagnetische Strahlungsfelder"

5.11 Graduations

Doctorate

- Brian Gentry
F-actin in Parallel Geometries
June 2009
- Björn Stuhrmann
Self-organized active biopolymer networks in migrating living cells
July 2009

Diploma

- Miriam Wähnert
Abstandsmessungen auf der Nanometerskala mit Hilfe von Goldnanopartikelpaaren
May 2009
- Steve Pawlizak
Mechanosensitive behaviour of neuronal growth cones
October 2009
- Frank Kupfer
Inverse durotaxis of neurons
November 2009
- Johannes Stelzer
Cell growth on functionalized lipid bilayers
December 2009

Master

- Moritz Steffler
Interfacing the brain with transparent Semiconductors
June 2009

Bachelor

- Tim Hohmann
Optical surfaceforces acting on dielectric objects
November 2009
- David Zopf
Präparation und Charakterisierung plasmonisch aktiver Dünnschichten auf Nanopartikel-Basis zur Bioanalytik
December 2009

5.12 Guests

- Prof. Dr. Christoph Naumann
Indiana Purdue University, Indianapolis, USA
June 8-July 3, 2009
- Dr. Paul Kriebel
National Cancer Institute, USA
July 12-19, 2009

5.13 Awards

- Prof. Dr. J. Käs
Wolfgang-Paul Prize awarded by the Alexander von Humboldt Foundation
- Prof. Dr. J. Käs
Distinguished Lecturer, SigmaXi Academic Honor Society, USA
- Prof. Dr. J. Käs
Adjunct Professor, Department of Biomedical Engineering, University of Texas at Austin

II

Institute for Experimental Physics II

6

Magnetic Resonance of Complex Quantum Solids

6.1 Introduction

The electronic properties of quantum-solids in which the electrons exhibit strong correlations with each other or with the lattice are particularly rich and will be of special importance in future functional materials. In addition, such solids are challenging for experiment, as well as theory, as the twenty-year history of high-temperature superconductivity shows: we still do not understand the electronic structure of these systems. One particular aspect of strongly correlated electronic materials is their tendency towards nano-scale electronic phase separation. Even in perfect lattices, electronic nanostructures can form. The investigation of such materials requires the use of methods that can give detailed information. Here, magnetic resonance, on nuclei and electrons, is of particular interest as they not only have atomic scale resolution, but also yield bulk information in contrast to surface techniques. As one might expect, the material properties can be quite different from the bulk near the surface.

Jürgen Haase

6.2 Evidence for two electronic components in high-temperature superconductivity from NMR for a TwoComponent Model

J. Haase, C.P. Slichter*, G.V.M. Williams†

*University of Illinois at Urbana-Champaign, Department of Physics, USA

†The MacDiarmid Institute and Industrial Research Limited, New Zealand

A new analysis of ^{63}Cu and ^{17}O NMR shift data on $\text{La}_{1.85}\text{Sr}_{0.15}\text{CuO}_4$ is reported that supports earlier work arguing for a two-component description of $\text{La}_{1.85}\text{Sr}_{0.15}\text{CuO}_4$, but conflicts with the widely held view that the cuprates are a one-component system. The data are analyzed in terms of two components A and B with susceptibilities χ_{AA} , χ_{AB} ($=\chi_{BA}$) and χ_{BB} . We find that above T_c , χ_{AB} and χ_{BB} are independent of temperature and

obtain for the first time the temperature dependence of all three susceptibilities above T_c as well as the complete temperature dependence of $\chi_{AA} + \chi_{AB}$ and $\chi_{AB} + \chi_{BB}$ below T_c .

6.3 Spatial Inhomogeneities in Single-Crystal $\text{HgBa}_2\text{CuO}_{4+\delta}$ from ^{63}Cu NMR Spin and Quadrupole Shifts

D. Rybicki, J. Haase, M. Greven*

*University of Minnesota, Department of Physics, Minneapolis, MN, USA

^{63}Cu Nuclear Magnetic Resonance (NMR) measurements on a single crystal of the single-layer high temperature superconductor $\text{HgBa}_2\text{CuO}_{4+\delta}$ are reported. From the analysis of the quadrupolar satellites and their anisotropic splitting a largely temperature-independent symmetric quadrupole tensor is deduced, despite substantial variation in the electrical field gradients at the ^{63}Cu site. The strongly temperature-dependent magnetic shifts and linewidths of the ^{63}Cu central line for different field orientations also reveal substantial spin shift variations in the material. Linear dependencies on the doping of both, the quadrupole splitting as well as the spin shifts, explain over a large temperature range all the widths with a local doping variation corresponding to $2\delta \approx 0.073$.

6.4 High sensitivity nuclear magnetic resonance probe for anvil cell pressure experiments

J. Haase, S.K. Goh*, T. Meissner, P.L. Alireza†, D. Rybicki

*Cambridge University, Department of Physics, Cavendish Laboratory, Cambridge, UK

†Cambridge University, Department of Physics and Astronomy, University College London, UK

While the highest pressures can be achieved with diamond anvil cells, limited sample size and anvil geometry have hampered their application in nuclear magnetic resonance (NMR) experiments due to weak signal-to-noise. We developed a new probe design that is based on having the resonant radio frequency coil that encloses the sample within the anvil cell inside the gasket hole. This increases the filling factor tremendously and results in greatly enhanced NMR sensitivity. First ^{23}Na and ^{27}Al experiments were done at room temperature at different pressures up to 7 GPa.

6.5 Spin-Coupling and Hyperfine Interaction of the Nitrogen Donors in 6H-SiC

J. Hoentsch, A. Pöpl

The X- and Q-band field-sweep electron spin echo (FS ESE) study of n-type 6H SiC wafers shows besides the well known hyperfine (hf) triplet lines of ^{14}N on two quasi-cubic (N_{c1} , N_{c2}) and hexagonal (N_h) sites additional triplet lines (N_x) of comparatively low intensity with a g-tensor of about the average value of the N_{c2} and N_h spectrum at 4.2 K [1]. The N_x triplet has half of the hf splitting with respect to the nitrogen residing at cubic sites N_{c2} . Pulsed electron nuclear double resonance (ENDOR) measurements (Fig. 6.1) performed on the N_x EPR triplet line demonstrate that there is an efficient spin-coupling between N_h and N_x nitrogen related centers. The N_x triplet lines were attributed to distant donor N_c - N_h pairs between nitrogen atoms residing at quasi-cubic and hexagonal sites having a total electron spin $S = 1$, which were found before in n-type 4H SiC [2]. Based on Q-band FS ESE and X-band pulsed ENDOR measurements the values of the hf interaction for N_{c1} , N_{c2} were reassigned with respect to the assignment accepted hitherto. The super hyperfine (shf) interaction with neighboring atoms of nitrogen on the quasi-cubic lattice sites was studied by FS ESE and pulsed ENDOR. The new shf lines due to ^{29}Si and ^{13}C atoms with large shf interaction which were not observed previously were found in nitrogen FS ESE and ENDOR spectra. One of them, with the largest shf splitting (23.12 MHz), were attributed to the ^{29}Si atoms along the c-axis in nearest-neighbor positions of nitrogen on the quasi-cubic sites which unambiguously confirms that nitrogen substitutes carbon lattice site in 6H SiC.

[1] D. V. Savchenko, E. N. Kalabukhova, V. S. Kiselev, J. Hoentsch, A. Pöpl: phys. stat. sol. (b) **246**, 1908 (2009).

[2] D.V. Savchenko, E.N. Kalabukhova, S.N. Lukin, E.N. Mokhov, J. Hoentsch, A. Pöpl: Physica B **404**, 4753 (2009).

6.6 Size effects of aromatic substitution in the *ortho* position on the photodimerization kinetics of α -trans cinnamic acid derivatives. A solid-state NMR study

I. Fonseca, M. Bertmer

The photoreaction of two α -cinnamic acid derivatives, α -o-methoxy and α -o-ethoxy cinnamic acid, was studied by ^{13}C CPMAS solid-state NMR spectroscopy in order to elucidate effects of aromatic substitution and substituent size on the kinetics of the [2+2] photodimerization. The reactants and products can be clearly differentiated and a detailed spectroscopic characterization was carried out, including 2D PASS spectra, at a low spinning frequency to determine the principal values of the chemical shift tensor. Density functional theory (DFT) calculations of chemical shifts and chemical shift anisotropy tensors were found to be in good agreement with the experimental results and helped in the individual assignments of reactant and photoproduct carbon

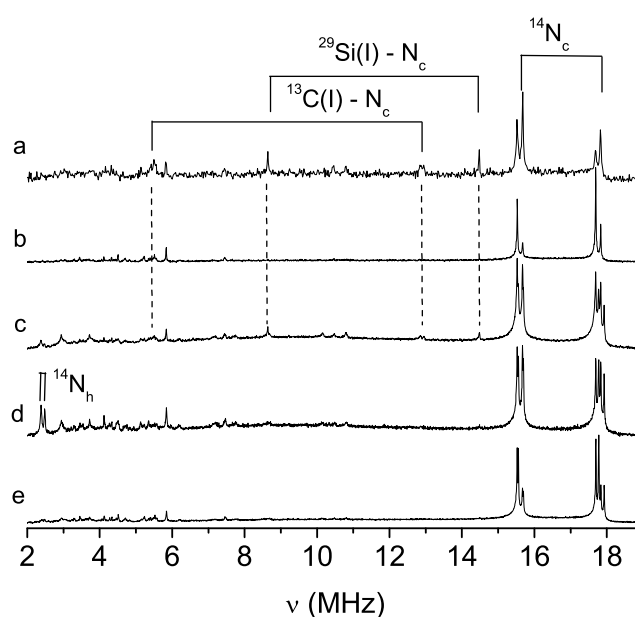


Figure 6.1: X-band pulsed ENDOR spectra in n-type 6H SiC for B||c at T = 6 K. The spectra were recorded at the following ESE observer positions: (a) the outer satellite line of the low field N_{c1} , N_{c2} triplet lines (345.44 mT), (b) low field N_{c1} , N_{c2} triplet lines (346.17 mT), (c) the low field N_x triplet line (346.80 mT), (d) the N_h line (347.10 mT), and (e) the central N_{c1} , N_{c2} triplet lines (347.33 mT).

atoms. The photoreaction kinetics show no systematic variation with substituent size, in that the α -o-methoxy cinnamic acid progresses at a slower rate than unsubstituted α -cinnamic acid, but α -o-ethoxy cinnamic acid at a faster one. Interestingly, the distance between reacting double bonds is not a good indicator of photoreaction rate. The observed trend is in part due to a larger degree of reorientation of the aromatic ring for the o-methoxy cinnamic acid, and a more dominant interaction appears to be the p-orbital overlap between two reacting double bonds in determining the reaction kinetics.

[1] I. Fonseca, S. E. Hayes, M. Bertmer: Phys. Chem. Chem. Phys. **11**, 10211 (2009).

6.7 Solid-state NMR investigations of $\text{Cu}_3(\text{BTC})_2$ and MIL-53 metal-organic frameworks (MOFs)

F. Gul-E-Noor, M. Bertmer

New porous materials made from metal-organic frameworks (MOFs) consisting of metal cations linked together via organic linker molecules have high potential for applications such as catalysis, gas separation, and hydrogen storage. Our focus is on the investigation of the magnetic properties of MOFs mainly dealing with rather well-known candidates, $\text{Cu}_3(\text{BTC})_2$ and MIL-53. $\text{Cu}_3(\text{BTC})_2$ contains antiferromagnetically

coupled copper dimers that give rise to strong hyperfine couplings to the protons which can be used to determine Cu-H distances. Of special importance is the purification of the material which can be clearly documented by solid-state NMR as well as EPR. Despite the magnetic copper, ^1H and ^{13}C NMR spectra can be obtained yielding important information about the local structure.

For MIL-53, mixed-metal materials were prepared containing aluminum and about 1% Cr to enable both NMR and EPR studies. Here, the low- and high-temperature phase can be clearly identified by a large change in the ^{27}Al quadrupole coupling constant, which is sensitive to changes in the local structure. ^1H and ^{13}C NMR spectra are not influenced by the paramagnetic chromium apart from a reduction in spin-lattice relaxation time.

6.8 The influence of domains on tetrahedrally coordinated Cr⁵⁺ in ferroelectric BaTiO₃: an electron paramagnetic resonance study

R. Böttcher, H.T. Langhammer*, T. Müller†

*Physikalisches Institut, Martin-Luther-Universität Halle-Wittenberg

†Chemisches Institut, Martin-Luther-Universität Halle-Wittenberg

Electron paramagnetic resonance (EPR) spectra of quasi-tetrahedrally coordinated Cr⁵⁺ ions (named Cr_{II}⁵⁺ in contrast to the octahedrally coordinated Cr_I⁵⁺) in powdered ceramic samples of BaTiO₃ were investigated in the temperature range 50-220 K at 9.4 and 34.0 GHz (X and Q band). At 50 K, in the ferroelectric low-temperature phase with rhombohedral symmetry, two peaks in the powder spectrum of the 1/2-spin Cr_{II}⁵⁺ centre show a frequency-dependent doublet splitting which is explained assuming the existence of two Cr_{II}⁵⁺ centres with slightly different g tensors. The spontaneous polarization in the ferroelectric domains induces changes in the peak positions in the spectra and generates alignment effects of the off-centred Cr⁵⁺ ions. These effects are caused by the linear coupling of the electric dipole moment, associated with the off-centred Cr⁵⁺ ion within the octahedron of surrounding O²⁻ ions, and the polarization field. At 75 K a dynamic reorientation of the defect ions among the possible positions in the unit cell broadens the powder peaks. Above 150 K only an isotropic single-line spectrum is observed, the line width of which increases with rising temperature.

6.9 Funding

Controlling Mesoscopic Phase Separation

J. Haase

EU-FP6, CoMePhS, NMP4-CT-2005-517039.

Advanced Signal-Processing for Ultra-Fast Magnetic Resonance Spectroscopic Imaging, and Training

J. Haase
EU-CORDIS-FP6, MRTN-CT-2006-035801.

EuroMagNET, JRA NMR

J. Haase
EU, RII3CT-2004-506239.

Magnetic Ground State and Dynamics in High-Temperature Superconductors

J. Haase, O.P. Sushkov, B. Keimer
EU, DP0881336.

Quasi One-Dimensional Ferroelectrics

R. Böttcher, E. Hartmann
DFG BO 1080/8-2 within DFG Forschergruppe FOR 522.

Identification of the paramagnetic centers in nano- and micrometer-sized SiC perspectives for photonic and biotechnology application by pulsed EPR spectroscopy

A. Pöpl
DFG PO 426/6-1.

Characterization of the [2+2] Photodimerization of cinnamic acid and its derivatives with solid-state NMR

M. Bertmer
DFG BE 2434/2-2.

Host - guest interactions and magnetic ordering in MOFs studied by electron and nuclear spin resonance spectroscopy

M. Bertmer
DFG BE 2434/4-1 within SPP 1362.

Fabrication and physical properties of ferroelectrics confined in nanoporous materials

D. Michel, E. V. Charnaya
DFG Mi 390/25-1.

6.10 Organizational Duties

J. Haase

- Direktor des Zentrums für magnetische Resonanz
- Referee: Physical Review

M. Bertmer

- Referee: Angewandte Chemie, Chemistry of Materials, Solid State Nuclear Magnetic Resonance

R.-M- Böttcher

- Referee: Physical Review, Journal of Physics: Condensed Matter, Langmuir, Journal of Magnetic Resonance

A. Pöpl

- Referee: Journal of Magnetic Resonance, Journal of American Chemical Society, Physical Chemistry Chemical Physics, Chemical Physics Letters
- Project Reviewer: German-Israel-Foundation for Scientific Research and Development - GIF

6.11 External Cooperations

Academic

- Laboratoire National des Champs Magnétiques Pulsés Toulouse, France
Prof. Dr. Geert Rikken
- University of Illinois at Urbana-Champaign, Department of Physics, USA
Prof. Dr. Charles P. Slichter
- University of New South Wales Australia, School of Physics, USA
Prof. Dr. Oleg P. Sushkov
- University of Illinois at Urbana-Champaign, Department of Electrical and Computer Engineering, USA
Prof. Dr. Andrew G. Webb
- The MacDiarmid Institute and Industrial Research Limited, New Zealand
Dr. Grant V. M. Williams
- Dresden High Magnetic Field Laboratory, Forschungszentrum Dresden-Rossendorf
Prof. Dr. Joachim Wosnitza
- Washington University, St. Louis, MO, USA, Department of Chemistry
Sophia E. Hayes
- Universität Koblenz-Landau, Koblenz, Abteilung Chemie
Gabriele E. Schaumann
- Martin-Luther-Universität Halle-Wittenberg, Physikalisches Institut
Dr. H. T. Langhammer
- University of Vilnius, Faculty of Physics, Lithuania
Prof. Dr. J. Banyš
- Universität Augsburg, Advanced Materials Science, Institut für Physik
Prof. Dr. M. Hartmann
- Technische Universität München, Anorganisch-chemisches Institut
Prof. Dr. K. Köhler
- NASU, Institute of Semiconductor Physics, Kiev, Ukraine
Prof. Dr. E. N. Kalabukhova
- Université du Maine, Faculté des Sciences, Laboratoire de Physique de l'Etat Condensé, Le Mans, France
Prof. Dr. A. Kassiba

Industry

- NMR-Service, Erfurt
M. Braun
- Bruker BioSpin, Rheinstetten
F. Engelke

6.12 Publications

Journals

I. Fonseca, S. E. Hayes, M. Bertmer: *Size Effects of aromatic substitution in the ortho position on the photodimerization kinetics of -trans cinnamic acid derivatives. A solid-state NMR study*, Phys. Chem. Chem. Phys., **11**, 10211 - 10218 (2009)

A. Pawlik, R. König, G. Scholz, E. Kemnitz, G. Brunklau, M. Bertmer, C. Jäger: *Access to Local Structures of HS-AlF₃ and Its Precursor Determined by High-Resolution Solid-State-NMR*, J. Phys. Chem. C., **113**, 16674 - 16680 (2009)

D. V. Savchenko, E. N. Kalabukhova, S. N. Lukin, E. N. Mokhov, J. Hoentsch, A. Pöpl: *EPR, ESE and pulsed ENDOR study of nitrogen donor pairs on quasi-cubic lattice sites in 6H SiC*, Physica, **404**, 4735 - 4738 (2009)

D. V. Savchenko, A. Pöpl, E. N. Kalabukhova, S. Greulich-Weber, E. Rauls, W. G. Schmidt, U. Gerstmann: *Spin-coupling in Heavily Nitrogen-doped 4H-SiC*, Materials Science Forum **615 - 617**, 343 - 346 (2009)

J. Haase, S. K. Goh, T. Meißner, P. L. Alireza, D. Rybicki: *High sensitivity nuclear magnetic resonance probe for anvil cell pressure experiments*, Review of Scientific Instruments **80**, 073905 (2009)

L. K. Aminov, I. N. Kurkin, R. M. Rakhmatullin, R. Böttcher, A. Pöpl, S. Sen: *EPR of Gd³⁺ Ion in Mixed CeO₂-Y₂O₃ Nanocrystals*, Physics of the Solid State **51**, No. 11 (2009)

D. Rybicki, J. Haase, M. Greven, G. Yu, Y. Li, Y. Cho, X. Zhao: *Spatial Inhomogeneities in Single-Crystal HgBa₂CuO₄ from ⁶³Cu NMR Spin and Quadrupole Shifts*, J. Supercond. Nov. Magn. **22**, 179 - 183 (2009)

R. M. Rakhmatullin, L. K. Aminov, I. N. Kurkin, R. Böttcher, A. Pöpl, H. Avila-Paredes, S. Kim, S. Sen: *Electron paramagnetic resonance linewidth narrowing of Gd³⁺ ions in Y-doped ceria nanocrystals with decreasing crystallite size*, The Journal of chemical Physics **131**, 124515 (2009)

P. Sedykh, D. Michel: *Ferroelectric phase transition in barium titanate nanoparticles*, Physical Review **79**, 134119 (2009)

J. Haase, C. P. Slichter, G. V. M. Williams: *Evidence for two electronic components in high-temperature superconductivity from NMR*, J. Phys. Condens. Matter **210**, 455702 (2009)

D. Schneider, H. Toufar, A. Samoson, D. Freude: ^{17}O DOR and other solid-state NMR studies concerning the basic properties of zeolites LSX, *Solid State Nuclear Magnetic Resonance* **35**, 87 - 92 (2009)

K. Ulrich, D. Freude, P. Galvosas, C. Krause, J. Kärger, J. Caro, P. Poladli, H. Papp: Diffusion of aromatic guest molecules in zeolite NaX studied by pulsed field gradient NMR, *Microporous and Mesoporous Materials* **120**, 98 - 103 (2009)

S. S. Arzumanov, A. A. Gabrienko, D. Freude, A. G. Stepanov: *In situ* high temperature MAS NMR study of the mechanisms of catalysis. Ethane aromatization on Zn-modified zeolite BEA, *Solid State Nuclear Magnetic Resonance* **35**, 113 - 119 (2009)

E. E. Romanova, F. Grinberg, A. Pampel, J. Kärger, D. Freude: Diffusion studies in confined nematic liquid crystals by MAS PFG NMR, *Journal of Magnetic Resonance* **196**, 110 - 114 (2009)

D. V. Savchenko, E. N. Kalabukhova, V. S. Kiselev, J. Hoentsch, A. Pöppl: Spin-coupling and hyperfine interactions of the nitrogen donors in 6H-SiC, *Phys. Status Solidi* **246**, No. 8, 1908 - 1914 (2009)

J. Banys, M. Kinka, G. Völkel, W. Böhlmann, A. Pöppl: Dielectric response of water confined in metal-organic frameworks, *Appl Phys* **96**, 537 - 541 (2009)

V. Nagarajan, B. Müller, O. Storcheva, K. Köhler, A. Pöppl: Structure and bonding of $[\text{V}^{\text{I}}\text{VO}(\text{acac})_2]$ on the surface of AlF_3 as studied by pulsed electron nuclear double resonance and hyperfine sublevel correlation spectroscopy, *Physical Chemistry Chemical Physics* **11**, 6849 - 6854 (2009)

H. Busse, G. Thörmer, N. Garnov, J. Haase, T. Kahn, M. Moche: MR image-based technique for wireless 3D position tracking of intravascular catheters: experimental evaluation at 1.5 T, *RSNA* 2009

Talks

H. F. Busse, G. Thörmer, N. Garnov, J. Haase, T. K. Kahn, M. Moche: MR image-based technique for wireless 3D position tracking of intravascular catheters: experimental evaluation at 1.5 T, *RSNA* 2009

H. Busse, G. Thörmer, N. Garnov, J. Haase, T. Kahn, M. Moche: Feasibility of wireless 3D position tracking of an intravascular model catheter using an MR image-based localization technique, *ESMRMB* (October 2009)

G. Thörmer, M. Moche, N. Garnov, J. Haase, T. Kahn, H. Busse: Experimentelle Evaluierung eines Verfahrens zur kontinuierlichen 3D-Lokalisation intravaskulärer Katheter in einem Gefäßphantom, *Experimentelle Radiologie Workshop Mainz-Kiel* (Feb. 2009); 90. Deutscher Röntgenkongress Berlin (Mai 2009)

H. Busse, G. Thörmer, N. Garnov, M. Moche, J. Haase, T. Kahn: Absolute Genauigkeit und Geschwindigkeit einer morphologischen Bildanalyse zur 3D-Verfolgung MR-sichtbarer Marker: Ergebnisse aus Experiment und Simulation, 90. Deutscher Röntgenkongress, Berlin (Mai 2009)

- B. Meier: *Local properties via nuclear magnetic resonance*, Cambridge (January 2009)
- M. Moche, D. Zajonz, T.-O. Petersen, J. Fuchs, G. Thörmer, N. Garnov, T. Kahn, H. Busse: *Preliminary clinical experience with a navigation system for biospies in a diagnostic 1.5 T closed-bore MR scanner*, ISMRM 17th Scientific Meeting & Exhibition 2009
- M. Bertmer: *Multinuclear solid-state NMR and EPR of magnetic metal-organic frameworks (MOFs)*, 51st Rocky Mountain Conference on analytical Chemistry, 20. July 2009, Snowmass, Colorado, USA
- M. Bertmer: *Solid-state NMR and EPR of magnetic coordination polymers based on $\text{Cu}_3(\text{BTC})_2$ and MIL-53*, 31st Discussion meeting magnetic resonance in chemistry and materials research, 23.09.2009, Dresden
- M. Bertmer: *Magnetic Resonance spectroscopy of $\text{Cu}_3(\text{BTC})_2$ and MIL-53 based materials*, Kick-off meeting porous metal-organic frameworks, DFG priority program 1362, 02.10.2009, Dresden
- J. Haase: *Spatial inhomogenities in single crystal $\text{HgBa}_2\text{CuO}_4$ from ^{63}Cu NMR*, Second Bilateral Estonian-German Workshop, Cottbus, 21.05.2009
- J. Haase: *Inhomogenities of charge and spin of the hole-doped cuprates from NMR*, Gordon Godfrey Conference on Spins and Strong Correlations, Sydney, 27.10.2009

Posters

- N. Garnov, G. Thörmer, M. Moche, T. K. Kahn, H. F. Busse: *Inductively coupled radio-frequency coils as MR-visible fiducial markers for 3 T MRI*, RSNA 2009
- M. Bertmer, A. Pöppl, M. Hartmann: *Multinuclear Solid-State NMR on Metal-Organic Framework Materials (MOFs)*, 50th Experimental NMR Conference, Pacific Grove, California, USA, March 29 - April 3.
- M. Bertmer, A. Jäger, G. E. Schaumann, J. Schwarz: *Studies on Aging Processes in Soil Organic Matter using NMR-spectroscopy*, European Geosciences Union General Assembly, Vienna, Austria, April 19 - 24.
- J. Schwarz, A. Jäger, M. Bertmer, A. Schlichting, P. Leinweber, G. E. Schaumann, *Physicochemical aging mechanisms in soil organic matter assessed by NMR and DSC*, European Geosciences Union General Assembly, Vienna, Austria, April 19 - 24.
- M. Bertmer: *Photo-crosslinking in Single Crystals and in Polymers using [2+2] Photo-dimerizations of α -Trans-Cinnamic Acid*, 50th Experimental NMR Conference, 29.03. - 03.04.2009, Pacific Grove, California, USA
- A. Pöppl: *Cw and Pulsed ESR Spectroscopy of Transition Metal Ions in porous MOF Materials*, 7th European Federation of EPR groups meeting, 06. - 11.11.2009, Antwerpen, Belgium
- G. Thörmer, N. Garnov, J. Haase, T. Kahn, M. Moche, H. Busse: *Evaluation of accuracy and reliability of a morphological image analysis under progressively reduced spatial resolution*, ESMRMB (October 2009)

H. Busse, G. Thörmer, N. Garnov, J. Haase, T. Kahn, M. Moche: *Experimental evaluation of a wireless technique for the tracking of intravascular catheters in an MRI*, International Annual Scientific Meeting (October 2009)

H. Busse, G. Thörmer, S. Leidich, N. Garnov, J. Haase, T. Kahn, M. Moche: *Design of small MR-visible markers for intravascular catheters: Performance and localization technique*, International Annual Scientific Meeting (October 2009)

G. Thörmer, N. Garnov, J. Haase, T. Kahn, M. Moche, H. Busse: *Accuracy and speed of a morphological image analysis in detecting small MR-visible markers: Experimental and simulation results*, International Annual Scientific Meeting (October 2009)

N. Garnov, G. Thörmer, M. Moche, J. Haase, T. K. Kahn, H. F. Busse: *Verfahren zur Erkennung der 3D-Position und räumlichen Ausrichtung von MR-sichtbaren Markern bei der interventionellen MR-Bildgebung*, 90. Deutscher Röntgenkongress Berlin (Mai 2009)

M. Jurkutat, D. Rybicki, G. V. M. Williams, J. Haase: *^{63}Cu NMR study of electron doped high temperature superconductor $\text{Pr}_{1.85}\text{Ce}_{0.15}\text{CuO}_4$ with co-doped Ni*, 2nd Bilateral Estonian-German Workshop, Cottbus (May 2009)

B. Meier, N. Georgieva, J. Haase, M. Braun, M. Bartkowiak, T. Herrmannsdörfer, J. Wosnitza: *NMR in pulsed magnetic fields*, 2nd Bilateral Estonian-German Workshop, Cottbus (May 2009)

T. Meißner, J. Haase, S. K. Goh, D. Rybicki: *Nuclear Magnetic Resonance in an Anvil Pressure Cell*, 2nd Bilateral Estonian-German Workshop, Cottbus (May 2009)

T. Meißner, J. Haase, G. Williams, C. U. Jung: *^{17}O NMR on the infinite layer compound $\text{Sr}_{0.9}\text{La}_{0.1}\text{CuO}_2$* , 2nd Bilateral Estonian-German Workshop, Cottbus (May 2009)

D. Rybicki, J. Haase, M. Greven, G. Yu: *^{63}Cu NMR Study of High Temperature Superconductor: $\text{HgBa}_2\text{CuO}_4$* , 2nd Bilateral Estonian-German Workshop, Cottbus (May 2009)

6.13 Graduations

Doctorate

- Pavel Sedykh
Nuclear Magnetic Resonance investigations of size effects in ferroelectrics and metals
2009

Diploma

- Benno Meier
High-field NMR of high-temperature superconductors
09.02.2009

- Thomas Meißner
Ein neuartiger Ansatz zur Beobachtung von Kernmagnetresonanz unter hohem Druck
30.09.2009
- Gregor Thörmer
MRT-Visualisierung von Kathetern mit Hilfe induktiv gekoppelter Mikrospulen
2009
- Alexander Jäger
Festkörper-NMR-Untersuchungen zur Dynamik und Bindungsstärke von Wasser in Böden und Modellsubstanzen
06.07.2009

Master

- M. Sc. Michael Jurkutat
 ^{63}Cu NMR Study of electron-doped High Temperature Superconductor $\text{Pr}_{1.85}\text{Ce}_{0.15}\text{CuO}_4$ with co-doped Ni
12.02.2009

6.14 Guests

- Joon Taek Park, Prof.
Korea Basic Science Institute, Republic of Korea
12. - 14.11.2009
- Oc Hee Han, PhD
Korea Basic Science Institute, Republic of Korea
12. - 14.11.2009
- Hwanuk Kim, PhD
Korea Basic Science Institute, Republic of Korea
12. - 14.11.2009
- O. P. Sushkov, Prof.
School of Physics University of New South Wales, Australia
06. - 08.07.2009
- Girsh Blumberg, Prof.
Rutgers, The State University of New Jersey, Department of Physics and Astronomy, USA
22. - 23.06.2009
- YuYe Tong, Prof.
Georgetown University, Department of Chemistry, USA
06. - 09.06.2009
- G.V.M Williams, PhD
The MacDiarmid Institute for advanced materials and nanotechnology, Industrial Research Limited, New Zealand
17.07. -10.08.2009

- Uma Maheswari Venkatesan, PhD
Graz University of Technology, Institut of Physical and theoretical Chemistry, Austria
06.06. - 27.06.2009
- Swee K. Goh, PhD
Trinity College, Quantum Matter Group, Cavendish Laboratory, UK
26.04. - 02.05.2009
- Dmitry Yurievich Podorozhkin
St. Petersburg State University, Institute of Physics, Petrodvorets, Russia
03.05 - 02.06.2009
- Mikhail Andreevich Vovk
St. Petersburg State University, Institute of Physics, Petrodvorets, Russia
19.04. - 18.05.2009

7

Nuclear Solid State Physics

7.1 Introduction

Our research is focused on two main fields: materials sciences (analysis and modification) and life sciences. The latter one includes quantitative microscopy of elemental distributions in biological samples (mainly for neuroscience), the targeted irradiation of living cells with counted single ions for low dose radiobiology. For material analysis we use the standard ion beam analytical methods with the broad as well as the focussed beam, for which we successfully introduced channeling techniques on the micrometer scale. We could also extend the capabilities for 3D-density and elemental analysis by introducing the limited angle tomography for the scanning microbeam.

The high energy proton or helium-ion beam is also used to modify the physical properties of solids (resists, semiconductors and carbon based materials) by ion irradiation. We create high aspect ratio and free standing microstructures in positive and negative resists and in several types of semiconductors. A new ion beam based biotechnological method allows to create areas of confined cell growth for patterned cell cultures. In carbon based materials we are able to change the electronic properties, which is highly interesting for the study of intrinsic ferromagnetism in these systems.

Our working horse is the high-energy ion-nanoprobe LIPSION with specifications which are unique in Germany and belongs to the best systems worldwide. A careful re-adjustment of the ion optical system led to a major improvement which opened up new high current applications that are usually not feasible on focussed microbeams. Over the last ten years, since the first beam in 1998, we have developed to one of the leading high-energy ion-nanobeam laboratories in the world. This was recognized by the international community by awarding us to host the next international conference on nuclear microprobe technology and applications ICNMTA in 2010.

We have also a longterm expertise in perturbed angular correlation of γ -rays (TD-PAC). This method is used to determine the nuclear quadrupole interactions of materials like TiO_2 bulk and TiO_2 nano-particles and nano-wires. TD-PAC is especially suited to assess in-vitro the solubility of these nano-particles in body fluids without separation of the particles and solution. This information is absolutely necessary to determine probable health risks after incorporation of nano-particles.

Our research was financially supported by the European Commission, the Deutsche Forschungsgemeinschaft, and the Federal German Excellence Initiative which we gratefully acknowledge. We also acknowledge the fruitful cooperation with our academic

and industrial partners.

Tilman Butz

7.2 Trace element mapping in Parkinsonian brain by quantitative ion beam microscopy

N. Barapatre, M. Morawski*, T. Arendt*, T. Reinert, T. Butz

*Paul-Flechsig Institute of Brain Research

The Parkinson's disease (PD) is characterised by the severe loss of dopaminergic neurons in the *substantia nigra* (SN) of the brain. These neurons also possess a brown-black pigment called neuromelanin (NM), which chelates and accumulates metal ions. The role of neuromelanin in the regulation of trace metal ions has come under scrutiny, since an overload of iron in the SN of Parkinsonian brain has been reported in many studies [1]. Ion beam analysis methods such as micro-PIXE and RBS suit best in quantifying *in situ* the trace element content [2]. The unstained sections encompassing the SN of three idiopathic PD patients and three non-demented controls were analysed (Tab. 7.1). Particularly, the trace element content bound to NM and in the extra-cellular region was quantified. 10 pigmented cells were measured from each case. Since the degree of pigmentation varies from cell to cell the trace element content bound to NM was normalised to the NM indicator, sulphur. Also, 5 measurements were done in the extracellular region in each case. Surprisingly, no significant difference was found in the iron content either bound to NM or in the extracellular region when the mean of three Parkinsonian cases was compared against the mean of three controls. The calcium content was about 40% lower, whereas the potassium content was around five times higher in the PD affected cases. The elemental content in the extracellular region showed a similar trend. The trace elements copper and zinc were unaltered [3].

Table 7.1: Comparison of the elemental content in neuromelanin and in the extracellular region for three controls and three Parkinsonian cases. Data are mean values \pm SEM.

	Element	Control (10^{-3})	Parkinson's disease (10^{-3})
Neuromelanin	K/S*	9 ± 1	50 ± 5
	Ca/S*	67 ± 5	42 ± 5
	Fe/S	104 ± 4	98 ± 6
Extracellular region		(mmol/l)	(mmol/l)
	K*	1.24 ± 0.15	4.79 ± 0.69
	Ca*	4.08 ± 0.38	2.79 ± 0.52
	Fe	11.00 ± 2.10	7.70 ± 1.40

* Significance $p < 0.05$ (student's *t*-test)

- [1] M. Götz et al.: Ann. N.Y. Acad. Sci. **1012**, 193 (2004)
 [2] T. Reinert et al.: Nucl. Instrum. Meth. B **249**, 734 (2006)
 [3] N. Barapatre et al.: Nucl. Instrum. Meth. B (2010) In press

7.3 Combined STIM- and PIXE-Tomography

M. Rothermel, T. Andrea, T. Butz

At the nanoprobe LIPSION ion micro-tomography can be used to determine the three-dimensional distribution information of a sample's mass density and elemental composition. For ion micro-tomography the two analytical techniques scanning transmission ion microscopy tomography (STIM-T) and particle induced X-ray emission tomography (PIXE-T) are combined. The required data are collected in two consecutive series of measurements, during which the sample is rotated by $180^\circ/360^\circ$ in small steps. Because all ions have to traverse the sample, the upper limit of the sample size is given by the range of the ions in the material. The tomogram is obtained using the discrete image space reconstruction algorithm (DISRA) by A. Sakellariou [1]. This algorithm iteratively (Fig. 7.1) corrects a sketchy initial tomogram estimated from the experimental reconstruction - obtained by backprojection of filtered projections (BFP) - and an a-priori elemental composition. The necessary correction factors are calculated comparing the reconstruction of the experimental data with the reconstruction of simulated data. For the simulated data sets of STIM projections and PIXE maps are computed from the tomogram. These data sets are proceeded with the BFP algorithm to get simulated reconstruction data. Using the DISRA for ion micro-tomography, one can benefit from the high resolution of STIM-T by transferring it to the elemental distribution given by PIXE-T. We tested the algorithm on a phantom (Fig. 7.2).

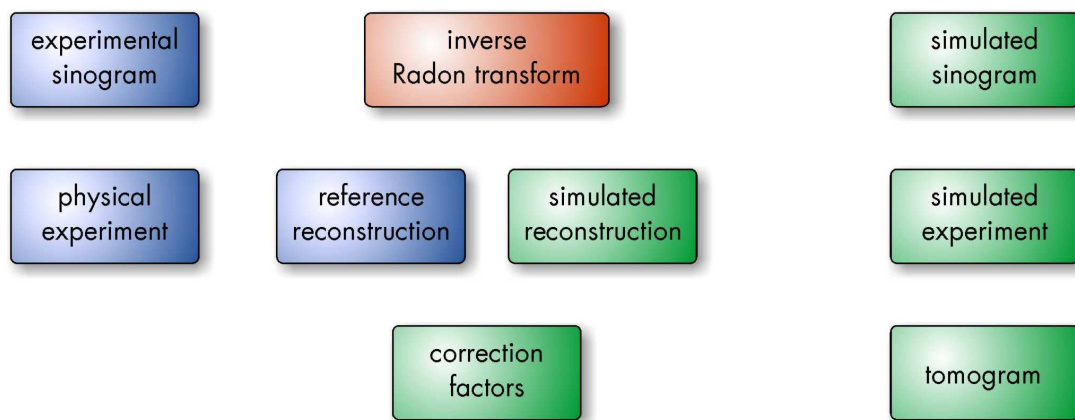


Figure 7.1: Flowchart of the iterative correction algorithm.

[1] A. Sakellariou et al.: Meas. Sci. Technol. 8, 746 (1997)

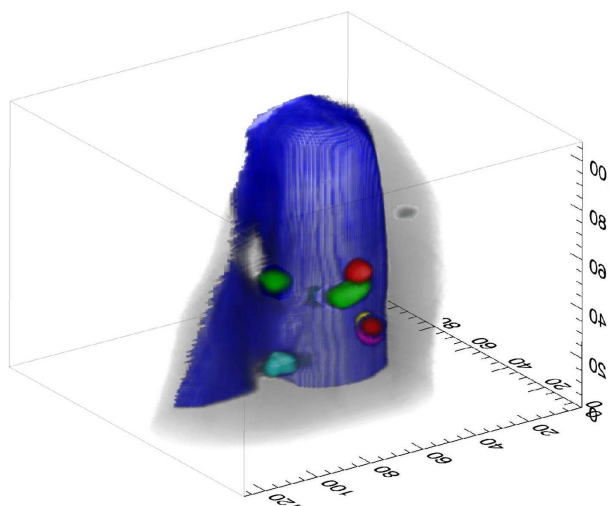


Figure 7.2: Tomogram of the phantom: Various oxide grains glued on a ZnO-wire. Blue: Zn, yellow: Si, magenta: K, cyan: Mn, red: Fe, green: Co, and glue (grey, translucent).

7.4 Characterization and elemental analysis of nano- and microdimensional structures using PIXE and RBS

Ch. Meinecke, C. Czekalla*, J. Vogt, A. Rahm, T. Butz

*Semiconductor Physics

Due to the current research in materials science, like in semiconductor physics, the production of micro- and nanostructures raises more interest for basic researchers. The aim is to control the electronic, magnetic and optical properties by variation of the elemental composition and feature size. During the last few years we developed an elemental characterization of different micro- and nanostructures using ion beam analysis with an expected spatial resolution of 100 nm, which is unique in the world. New analytical experiments using focused high energy ion beams can reveal, apart from stoichiometry and morphology, also the lattice structure of the micro- and nanostructures. The application of ion channeling like channeling-RBS and channeling-STIM to these new nanostructures, reveals lattice distortions. This project characterizes sub-micrometer structures of different shapes and compositions (heterostructures, coated structures, homogeneous doped structures etc.) to learn more about growth procedures, electronic and magnetic properties, elemental distributions of multilayered microstructures and crystal quality using focused high energy ions.

7.5 Spatially resolved characterisation of electronic properties of solar cells using the IBICC technique

A.M. Jakob, R. Thies, D. Spemann, J. Barzola-Quiquia*, T. Reinert, J. Vogt, T. Butz

*Department of Superconductivity and Magnetism

In this study, electronic properties of silicon solar cells were investigated using ion beam induced charge collection IBICC analysis. In order to achieve these measurements a new in-vacuum measuring setup based on an AMPTEK A250 charge sensitive preamplifier was developed to keep the noise level low.

Quantitative information of minority carrier diffusion lengths and mean minority carrier capture cross sections of lattice defects generated by high energy protons were obtained for polycrystalline silicon solar cells. Since lateral IBICC measurements could not be performed on these samples angular-resolved IBICC was used to quantify the electronic diffusion lengths. For this purpose, the experimental data were fitted using a simulation based on the Ramo-Shockley-Gunn theorem and the assumption of an abrupt pn-junction. In order to determine the mean minority carrier capture cross section of proton-induced lattice defects, the loss of charge collection efficiency (CCE) was plotted vs. the accumulated ion dose. It could be demonstrated, that a simple model based on charge carrier diffusion and Shockley-Read-Hall recombination is able to fit the CCE loss well. However, this model is not capable to differentiate between various defect types.

Furthermore, spatially and energetically highly resolved IBICC-maps of grain boundaries were recorded (Fig. 7.3). A comparison with PIXE-maps shows that there is no correlation observable between CCE variations at grain boundaries and metallic impurities within the PIXE detection limits of a few ppm. On the contrary, there is an evident correlation to the morphology of the sample's surface as was observed by comparing IBICC-maps with SEM-micrographs.

Local CCE fluctuations are dominated by the interaction of charge carrier diffusion processes and the sample surface morphology. Neither recombination mechanisms on impurities nor on grain boundaries are significant for local CCE variations on the p-type alkaline-texturized silicon solar cells investigated here.

Moreover IBICC-maps of polycrystalline CIGS thin film solar cells on flexible polyimide substrate foils were obtained (Fig. 7.4(a),(b)) The correlation between CCE and sample topography strongly indicates that larger grains of the CIGS absorber show a better carrier collection than smaller ones. This can be understood when taking into account the increasing number of grain boundaries along the charge carrier drift trajectories with decreasing grain size.

Several samples also show stripes of reduced charge collection, which seem to be induced by mechanical cracks within the CIGS layer probably due to thermal stresses during the production process and mechanical stresses when rolling up the foils, respectively (Fig. 7.4(c)).

7.6 Defect production by single ions traversing multigraphene

R. Feder, A. Arndt, J. Barzola-Quiquia*, P. Esquinazi*, T. Butz

*Department of Superconductivity and Magnetism

In a cooperation between the groups of Nuclear Solid State Physics and Superconductivity and Magnetism the electric and magnetic properties of multigraphene layers

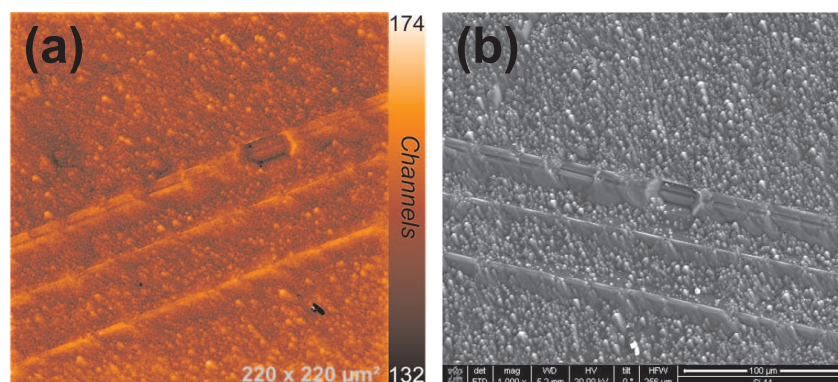


Figure 7.3: (a) IBICC-map of a p-type alkaline-texturized silicon solar cell (1800 keV He⁺ ions); (b) SEM-micrograph of the same region. Correlations between the sample's topology and local CCE variations are clearly visible.

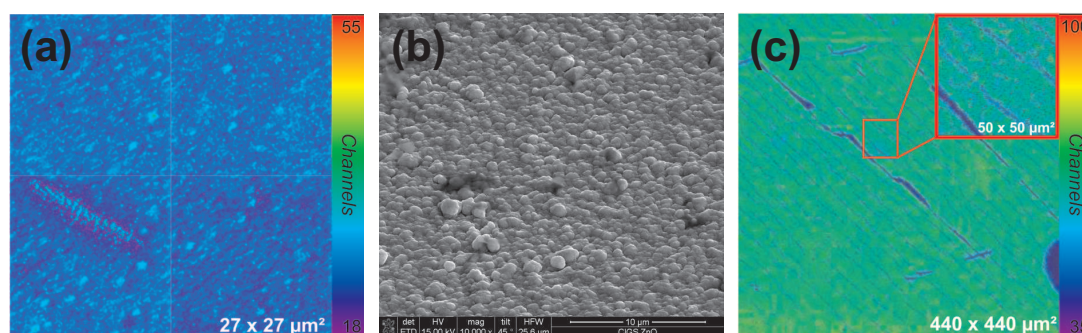


Figure 7.4: (a) IBICC-map of a CIGS solar cell (1800 keV He⁺ ions); (b) SEM-micrograph of a completely processed CIGS solar cell (another region); (c) IBICC-map of a CIGS solar cell (1800 keV He⁺ ions). Stripes of lower CCE are visible.

during ion irradiation are studied. Former experiments have shown that during the irradiation with 2.25 MeV protons the electric resistance of the samples decreases due to the produced defects. Furthermore, after the minimum of the resistance a relaxation behavior was found. After the irradiation, the samples exhibit an increase of resistance and a reduction of the magneto-resistance effect. This effect is correlated with the ion-induced ferromagnetic order within the graphene system.

The setup used in former studies, constructed by Dipl.-Phys. Alexander Arndt, is modified to enable measurements under vacuum conditions and sample cooling. The new setup will allow a more precise measuring of the dependence of these effects to the used fluences and sample temperatures. The envisaged sample preparation on Si₃N₄-windows should also allow the application of this technique as a detector or counter for the ion beam current during other measurements.

The project is founded within the ESF-Nachwuchsforschergruppe “funktionale multiskalige Strukturen” and is a part of the Graduate School Leipzig, School of Natural Sciences – Building with Molecules and Nano-objects (BuildMoNa).

7.7 Micro-fluidic target chamber machined by proton beam writing for the in-situ analysis of gas absorption in synthetic crystals

R. Feder, F. Menzel, T. Butz, F. Hibbe*, C. Chmelik*

*Department of Interface Physics

Many synthetic crystals used for chemical and industrial applications have special internal structures, e.g. nano-pores, which allow to separate different gases and fluids. Ion beam analytical methods can be used to study the gas diffusion and absorption in these materials in-situ and to visualize their inner surfaces which affect these processes. For this purpose, a small target chamber was constructed in PMMA (polymethylmethacrylate) using proton beam writing (PBW)(Fig. 7.5(a)). This micro-fluidic structure enables the establishment of a defined atmosphere around a crystal and allows a simultaneous ion beam analysis. In order to confine the gas from the high vacuum in the measurement chamber Si_3N_4 -windows ($2 \times 2 \text{ mm}^2$) of 200 nm thickness were thermally bonded to the PMMA block ($15 \times 15 \times 2 \text{ mm}^3$) yielding a closed target chamber with the possibility to accomplish PIXE and RBS measurements. In addition, two capillaries (diameter 200 μm) were connected to the chamber for gas inlet and evacuation. First tests showed that the construction is leak-proof and allows to establish a defined atmosphere. After that, the Argon gas diffusion into Zn(tbip)-crystals was studied (Fig. 7.5(b)). These measurements have shown unexpectedly high nickel concentrations in the host crystal which reduces the Argon density in these areas after absorption, because the Ni atoms decrease the pore size by replacing Zn-atoms in the Zn(tbip)-lattice.

It could be demonstrated that gas diffusion and absorption in organic crystals can be studied in-situ with high lateral resolution using ion beam analysis in a dedicated target chamber machined by PBW.

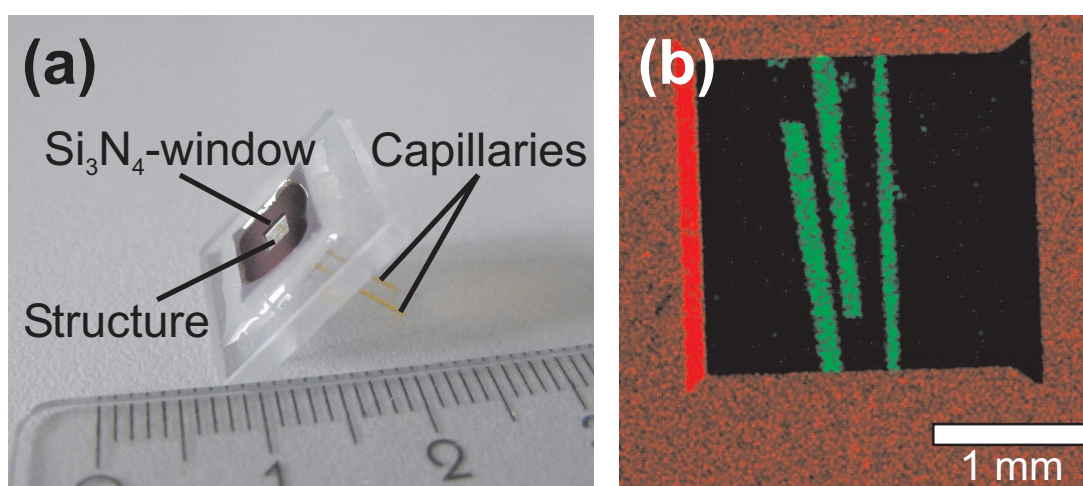


Figure 7.5: a) Target chamber with Si_3N_4 -window covering the micro-fluidic structure and the crystal. (b) PIXE-map showing three Zn(tbip)-crystals (Zn, bright) and the Si-frame (Si, dark) of the window.

7.8 Creation of 3D microsculptures in PMMA by multiple angle proton irradiation

T. Andrea, M. Rothermel, T. Reinert, T. Koal, T. Butz

In recent years the technique of proton beam writing has established itself as a versatile method for the creation of microstructures in resist materials. While these structures can be almost arbitrary in two dimensions, the creation of genuine 3D structures remains a challenge. At the LIPSION accelerator facility a new approach has been developed which combines aspects of ion beam tomography, so far solely an analysis method, with proton beam writing. Key element is the targeted irradiation from multiple angles in order to obtain a much broader range of 3D microstructures than has hitherto been possible. PMMA columns with a diameter of ca. 90 μm (slightly less than the ion range) were produced in order to serve as raw material. Prior to irradiation they were placed in an upright position on top of a rotational axis. A 2.25 MeV proton beam was used to write patterns corresponding to the silhouettes of the desired structures from two or more directions. In a subsequent step of chemical etching irradiated portions were dissolved, leaving behind the finished 3D sculpture. Various objects have been created. For the demonstration of the method a 90 μm high model of the Eiffel tower has been sculpted by irradiation from two angles. Using irradiation from three angles a 40 μm wide screw with right-handed thread could be crafted which might find applications in micromachining (Fig. 7.6). In addition, cage structures with a pore size of ca. 20 μm were written with the intention to use them as scaffolds for the growth of biological cells. For the characterization of these structures STIM-T (scanning transmission ion micro-tomography) is the ideal method, since it provides the 3D information necessary to detect possible flaws.

7.9 Proton beam writing on different types of semiconductor systems

F. Menzel, D. Spemann, W.-M. Schulz *, T. Butz

*Institut für Halbleiteroptik und Funktionelle Grenzflächen, Universität Stuttgart, Stuttgart

The technique of proton beam writing (PBW) applicable for the fabrication of micro- and nanodimensional structures was developed further especially for the structuring of semiconducting materials. Therefore, first experiments concerning the investigation of electrochemical etching behaviour of semiconductor heterostructures were carried out. The heterostructures, consisting of layer systems of different III-V-semiconductors with embedded quantum dots, were grown using MOVPE at the university of Stuttgart. Furthermore, ZnO layers irradiated with protons were electrochemically etched in order to test whether this material can be structured by PBW. The goal of these investigations is the creation of structures with lateral dimensions $<1 \mu\text{m}$ as well as structure heights of some micrometers in these material systems for a direct fabrication of functional microoptical units. However, the first attempts of structuring by ion beam irradiation and subsequent electrochemical etching show that the irradiated as well as

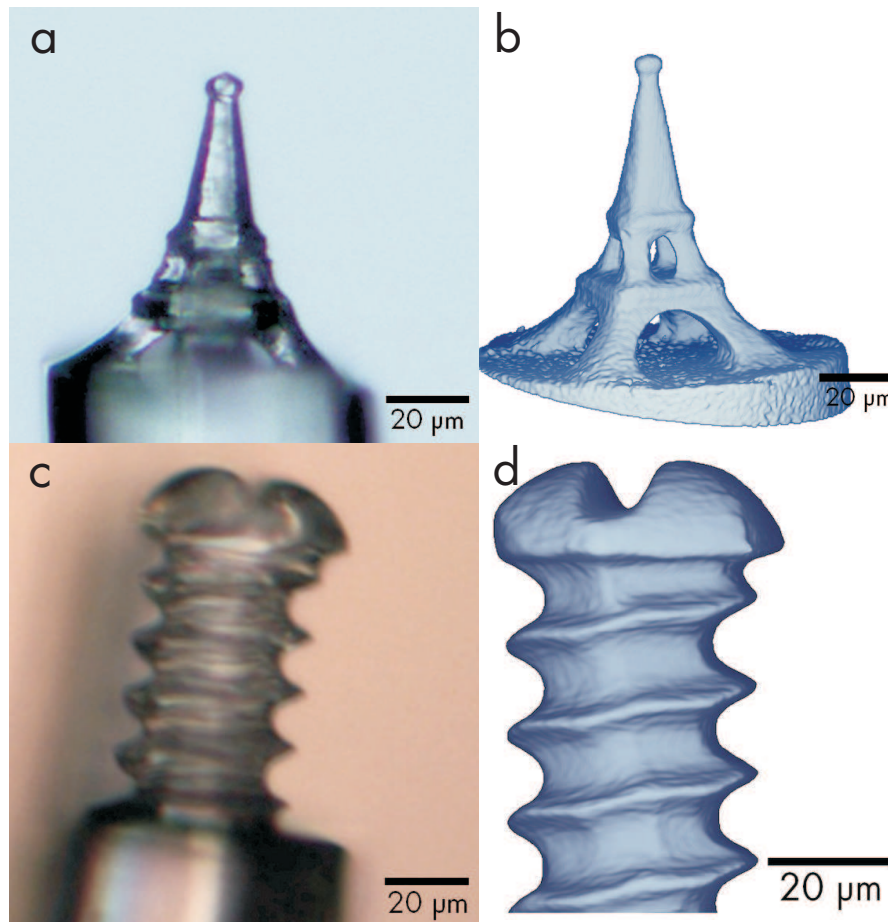


Figure 7.6: Optical micrograph (a) and STIM tomogram (b) of a PMMA model of the Eiffel tower as well as an optical micrograph (c) and STIM tomogram (d) of a PMMA microscrew.

the unirradiated material will be removed during the etch process. Therefore, further experiments using different irradiation and etch parameters have to be carried out.

7.10 Neuronal Networks on structured Petri-dishes

W. Larisch, T. Koal, T. Butz

The development of structured Agar patterns for single cells, especially neurons forming stable networks is of great interest for the study of electrophysiological processes [?]. Therefore, the technique of Proton Beam Writing is used to structure Agar gel layers directly. These layers consist of polysaccharides which are fully biocompatible and do not influence cell growth. The Agar gel has a smooth surface and is electrically neutral and therefore inhibits receptor binding and cell adhesion [? ?]. The Agar layers were irradiated with a focused 2.25 MeV proton beam with a beam spot size of 1 μm . Recent experiments show that a fluence of approximately 0.2 pC/ μm^2 already suffices to convert the polysaccharides in the irradiated areas to oligosaccharides which are water soluble and leave those irradiated areas free of Agar after rinsing. Further experiments in order to study the fluence dependence of Agar in more detail are under way.

First “simple structures” like the logo of the University of Leipzig (see Fig. 7.7) were already created and seeded with cells, e.g. fibroblasts and EA.hy 926.

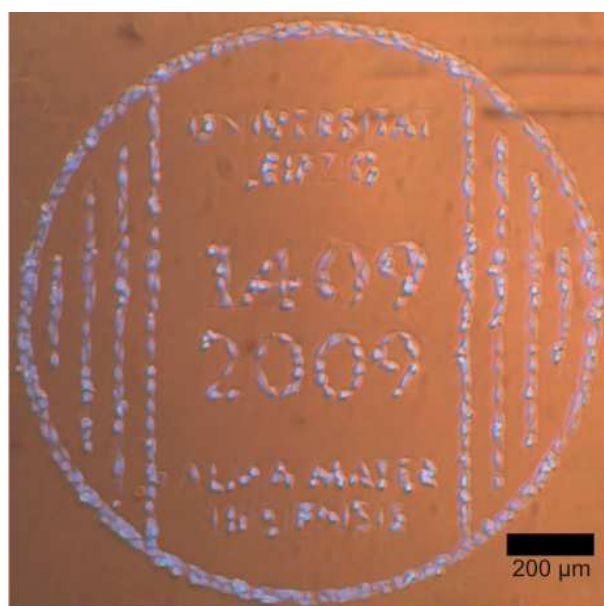


Figure 7.7: Logo of the University of Leipzig, seeded with EA.hy 926 cells and stained with DAPI (4',6-Diamidin-2'-phenylindoldihydrochlorid)

Unfortunately, the adherence of the currently used neuronal cell line PC-12 is not satisfactory. This problem is in the focus of our current research.

In order to be sure that neuronal cells are building stable networks with synapses we plan to mark the neurons with fluorescence dyes, especially for the synapses and then readout with a fluorescence microscope. If this succeeds we will be able to monitor synaptic activity as well.

This technique will help to monitor the development of such networks under chemical and mechanical influences.

[1] P. Fromherz: *Physica E* **16**, 24 (2003)

[2] S. Rohr et al.: *Pflug. Arch. Eur. J. Phy.* **446**, 125 (2003)

[3] A. Rago et al.: *Cytotechnology* **56**, 81 (2008)

7.11 Low dose targeted cell bombardment with counted ions at LIPSION

T. Koal, W. Larisch, T. Reinert, T. Butz

For the study of low-dose radiobiological effects (e.g. Bystander effect - deviation from the linear no threshold dose response model) [1], [2] targeted single cell irradiation with counted single ions is required. For this purpose, a reliable recognition software of cell nuclei/compartments without the use of staining and UV-light with its possible detrimental biological influence and a high-precision irradiation platform were developed [3] at the high energy ion-nanoprobe LIPSION. For single cell irradiation an

external beam was produced using an exit nozzle with a $2 \times 2 \text{ mm}^2$ Si_3N_4 exit window of 200 nm thickness. With this setup a lateral resolution of 500 nm can be achieved in air using a low current mode. Prior to irradiation the cells are imaged using dark field optical microscopy. The images are then processed by the CELLCOGNITION software – an in-house development – which determines the position of nuclei and cell compartments with an accuracy of $1.5 \mu\text{m}$. The positions to be irradiated can be selected and transferred to the irradiation platform. Due to the horizontal beam the Petri dishes have to be positioned vertically for cell irradiation. Therefore, the experimental procedure comprises medium removal and medium refilling. The irradiation is performed with ~ 5000 ions/s which allows to treat up to 2000 cells in less than 2 minutes including Petri dish handling. The experimental setup and procedures used guarantee a targeting precision of $1.5\text{--}2 \mu\text{m}$ (Fig. 7.8). This allows the single ion bombardement of the nucleus of single living cells and to study non-targeted effects, e.g. Bystander effects.

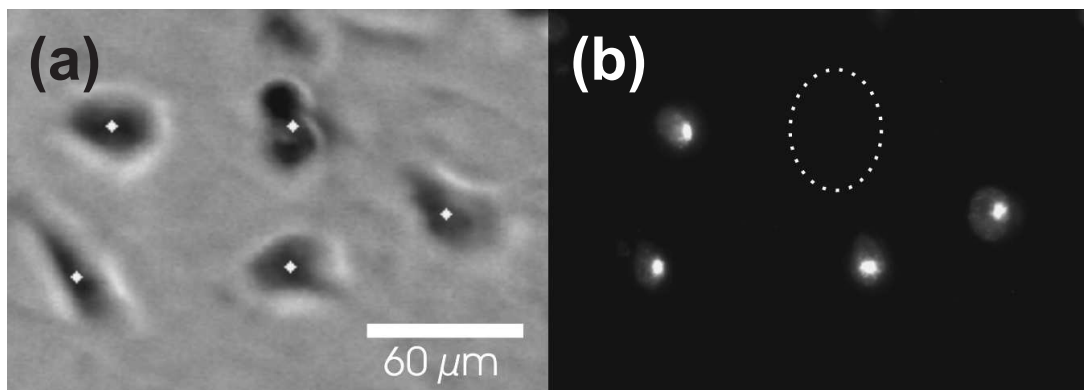


Figure 7.8: (a) Cell nuclei (white crosses) detected by Cellcognition software (no staining required). (b) Nuclei after irradiation (with 200 protons with 2.25 MeV) stained with γH2AX . The missing cell was washed away during the staining procedure.

- [1] K. M. Prise et al.: *Mutat. Res.* **597**, 1 (2006)
- [2] J.B. Little: *Mutat. Res.* **597**, 113 (2006)
- [3] T. Koal et al.: *J. Radiat. Res.* **50**, 108 (2009)

7.12 Study of ZnO-thin film scintillators for use as an ion transmission detector

D. Mehlhorn, T. Reinert, H. Hochmuth*, M. Lorenz*, T. Butz

*Department of Semiconductor Physics

For the use of a thin ZnO-layer as an ion transmission detector a $1 \mu\text{m}$ thick ZnO-layer was formed by Pulsed Laser Deposition and a pressure of $0.016\text{--}0.02$ mbar on a Si_3N_4 -window. During the experiment helium ions were bombarded by an accelerator with an energy of 1.8 MeV on the ZnO-layer. The number of helium ions bombarded on the ZnO-layer were counted by a PIN-diode and the produced photons were measured by

a Multi Pixel Photon Counter (MPPC) (Fig. 7.9). Helium ions and produced photons were compared to each other. After the analysis the determined efficiency was 2.5 % and it could be proved that a 1 μm thick ZnO-layer was not efficient enough for using it as ion transmission detector.

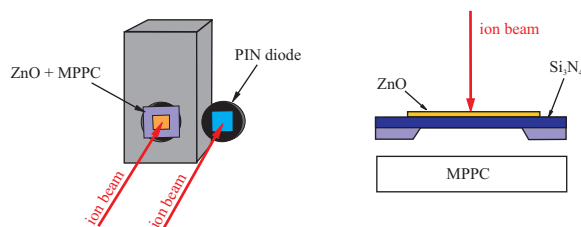


Figure 7.9: Experimental setup for the investigation of the photon emission of a ZnO-thin film scintillator bombarded with ions (left) and detailed side view of the setup (right).

7.13 Study of the nuclear reaction $^{11}\text{B}(p, \alpha)^8\text{Be}$

D. Mehlhorn, T. Reinert, T. Butz

Preliminary investigations were made of the nuclear reaction $^{11}\text{B}(p, \alpha)^8\text{Be}$. The number of the produced α -particles was counted by a detector. For that, a boron solution with a concentration of 1 g/l was mixed with agar powder and put on a 2.5 μm thick Mylar-foil. This sample was bombarded with hydrogen molecules with an energy of 1350 keV. When hitting the sample the bond of the molecules were broken, corresponding then to an energy of 675 keV for each proton, which is equal to the resonance energy for the nuclear reaction $^{11}\text{B}(p, \alpha)^8\text{Be}$. Because of this reason the produced α -particles on the surface of the sample could be detected without loss of energy. With this measurement device the energy spectrum and number of detected particles were obtained (Fig. 7.10), and by the knowledge of the number of the produced α -particles and their associated energy, it can be calculated how much the ion dose of the proton beam for radiotherapy can be lowered this nuclear reaction. It could be shown that the proton dose could only be lowered by an insignificant amount when the boron concentration was 1 $\mu\text{g}/\text{cm}^2$.

7.14 Characterization of TiO_2 nanomaterials by TDPAC

Sh. Ghoshal, L.S. Chang, T. Butz

Various TiO_2 nanomaterials (particles, wires, tubes) were impregnated with a 4 M HCl solution containing carrier-free ^{44}Ti ($t_{1/2} = 60 \text{ y}$). After drying the label was diffused into the nanomaterials at 180 $^\circ\text{C}$ for two hours. This temperature is enough to diffuse the label a few lattice spacings. We performed Time Differential Perturbed Angular Correlation (TDPAC) measurements on the daughter ^{44}Sc and obtained two discrete signals for the nuclear quadrupole interaction in all cases. The prominent one resembles the value obtained for bulk anatase or rutile or $\text{TiO}_2(\text{B})$ whereas the minority fraction

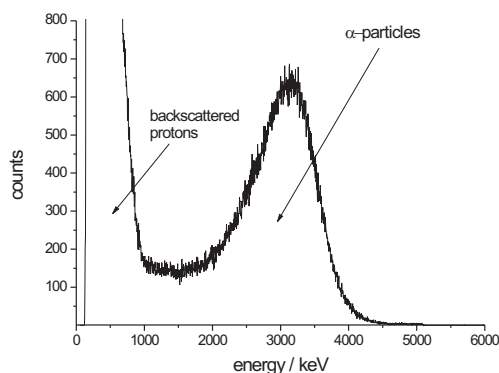


Figure 7.10: Energy spectrum of detected α -particles

is ascribed to the probe atoms close to the surface with an assumed OH-termination (Fig. 7.11). Stable suspensions with ^{44}Ti -labelled nanoparticles were produced. The measured re-orientation correlation time via TDPAC agrees with the particle size as determined by HRTEM.

7.15 Funding

CELLION: Studies of cellular response to targeted single ions using nanotechnology
Prof. Dr. T. Butz
EU-Project:MRTN-CT-2003-503923 2.

Leipzig School of Natural Sciences - Building with Molecules and Nano-objects (Build-Mona)
Prof. Dr. T. Butz
GSC 185/1

DFG Graduiertenkolleg Interdisciplinary Approaches in Cellular Neurosciences (Inter-Neuro)
Prof. Dr. T. Butz
GRK 1097

Non-Targeted Effects of ionising Radiation – NOTE
Prof. Dr. T. Butz
EU Integrated Project FI6R-036465

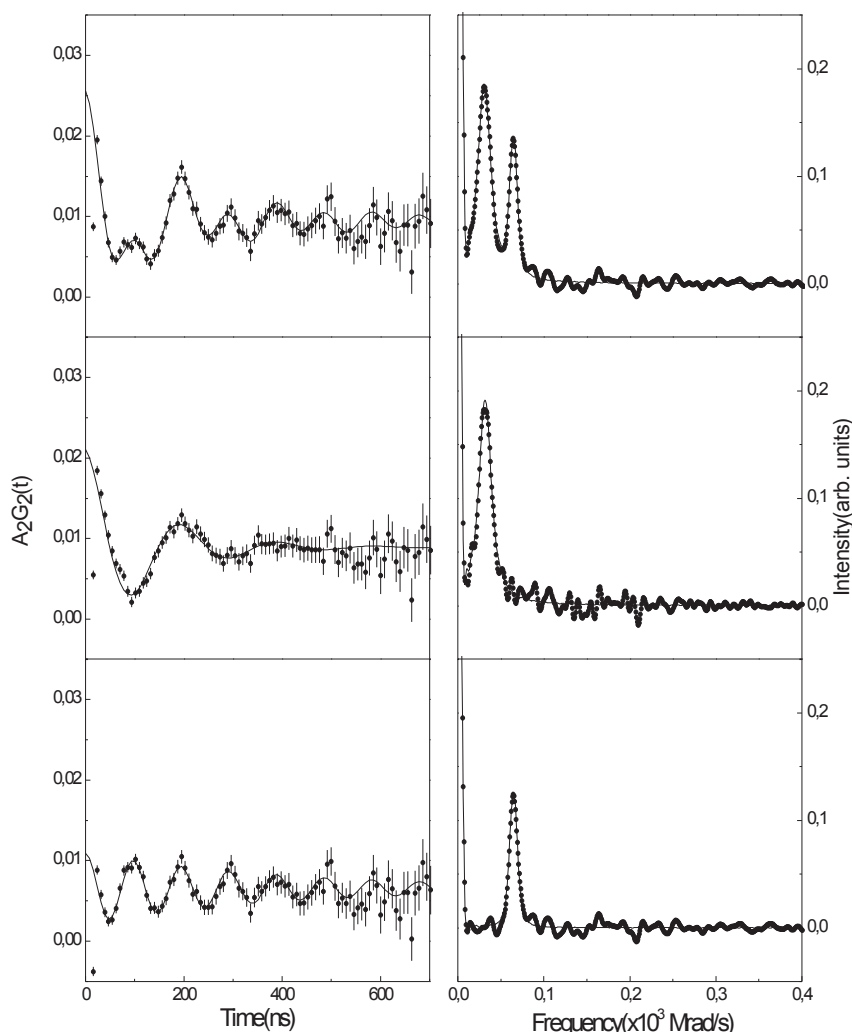


Figure 7.11: Time spectra (left) and cosine-transforms (right) for $\text{TiO}_2(\text{B})$ nanowires; top: total spectrum; middle: slow component (volume signal of $\text{TiO}_2(\text{B})$); bottom: fast component (surface signal).

7.16 Organizational Duties

T. Butz

- Vertrauensdozent der Studienstiftung des deutschen Volkes
- Sprecher der Ortsgruppe Leipzig des deutschen Hochschulverbandes
- Co-tutor for students of Tautenburg (astrophysics), LMU München (astrophysics), DESY/Zeuthen (particle physics)
- external Expert Scientific Committee on Consumer Products, DG Sanco, Brüssel
- Reviewer: DFG, Studienstiftung des deutschen Volkes
- Referee: J. Phys.-Condens. Mat., Phys. Rev. B, Angew. Chem. Int. Edit., Phys. Rev. Lett., J. Alloy. Compd., Alexander von Humboldt Foundation, Nucl. Instrum. Meth. B, Ann. Nucl. Energy, Particle and Fibre Toxicology, University of Barcelona (Agency

for Assessing and Marketing Research Results)

N. Barapatre

- Referee: Nucl. Instrum. Meth. B

M. Rothermel

- Referee: Nucl. Instrum. Meth. B

D. Spemann

- Referee: Nucl. Instrum. Meth. B, J. Nucl. Mater.

7.17 External Cooperations

Academic

- Université de Bordeaux I
CENBG, Prof. Ph. Moretto
- CERN, Genf
ISOLDE Collaboration
- Institute of Physics, Kraków
Dr. Z. Stachura
- IOM Leipzig
Dr. K. Zimmer, Dr. J. Gerlach
- KVL, Kopenhagen
Dr. L. Hemmingsen
- MPI für Demografische Forschung, Rostock
A. Fabig
- National University of Singapore
Center for Ion Beam Applications, Prof. F. Watt, Dr. T. Osipowicz
- Universität Leipzig, Medizinische Fakultät
Paul-Flechsig-Institut, Prof. T. Arendt, Dr. M. Morawski
- Universität Leipzig, Medizinische Fakultät
Institut für Rechtsmedizin, Dr. M. Weber, S. Wernecke
- Universität Leipzig, Medizinische Fakultät
Institut für Laboratoriumsmedizin, Kl. Chemie und Mol. Diagnostik, Prof. J. Thiery,
Dr. D. Teupser
- Universität Leipzig, Medizinische Fakultät
Institut für Medizinische Physik und Biophysik, Prof. E. Donath
- The University of Melbourne
Microanalytical Research Centre, Prof. D. Jamieson
- TU Wien
Prof. K. Schwarz, Prof. P. Blaha

- Universität Hannover
Arbeitskreis Prof. P. Behrens
- Universität Hannover
Arbeitskreis Prof. C. Vogt
- Universitätskliniken Leipzig
Prof. Dr. G. Hildebrandt
- Martin-Luther-University Halle-Wittenberg
Dr. A. Guittoum, Prof. R. Krause-Rehberg
- MPI of Microstructure Physics, Halle (Saale)
Dr. O. Moutanabbir

Industry

- Solarion GmbH
- Roth & Rau AG
- Dechema
Dr. E. Zschau, Self-employed expert in materials research

7.18 Publications

Journals

M. Brandt, H. von Wenckstern, C. Meinecke, T. Butz, H. Hochmuth, M. Lorenz, M. Grundmann: *Dopant activation in homoepitaxial MgZnO:P thin films*, J. Vac. Sci. Technol. B **27**, 1604 (2009)

doi:10.1116/1.3086657

S. Gruhl, F. Witte, J. Vogt, C. Vogt: *Determination of concentration gradients in bone tissue generated by a biologically degradable magnesium implant*, J. Anal. Atom. Spectrom. **24**, 181 (2009)

doi:10.1039/b813734j

J. Barzola-Quiquia, P. Esquinazi, M. Rothermel, D. Spemann, T. Butz: *Magnetic order in proton irradiated graphite: Curie temperatures and magnetoresistance effects*, J. Nucl. Mater. **389**, 336 (2009)

doi:10.1016/j.jnucmat.2009.02.024

T. Butz, S.K. Das, Y. Manzhur: *A Comparative Time Differential Perturbed Angular Correlation Study of the Nuclear Quadrupole Interaction in $\text{HfF}_4 \cdot \text{HF} \cdot 2\text{H}_2\text{O}$ Using $^{180\text{m}}\text{Hf}$ and $^{181}\text{Hf}(\beta^-)^{181}\text{Ta}$ as Nuclear Probes: Is Ta an Innocent Spy?*, Z. Naturforsch. A **64**, 103 (2009)

T. Andrea, M. Rothermel, T. Butz, T. Reinert: *The improved STIM tomography set-up at LIPSION: Three-dimensional reconstruction of biological samples*, Nucl. Instrum. Meth. B **267**, 2098 (2009)

doi:10.1016/j.nimb.2009.03.085

F. Menzel, D. Spemann, J. Lenzner, W. Böhlmann, G. Zimmermann, T. Butz: *Fabrication of microstructures in III-V semiconductors by proton beam writing*, Nucl. Instrum. Meth. B **267**, 2321 (2009)

doi:10.1016/j.nimb.2009.03.023

M. Rothermel, T. Butz, T. Reinert: *Rearranging a nanoprobe: Line foci, grid shadow patterns and performance tests*, Nucl. Instrum. Meth. B **267**, 2017 (2009)

doi:10.1016/j.nimb.2009.03.039

M. Khalid, M. Ziese, A. Setzer, P. Esquinazi, M. Lorenz, H. Hochmuth, M. Grundmann, D. Spemann, T. Butz, G. Brauer, W. Anwand, G. Fischer, W.A. Adeagbo, W. Hergert, and A. Ernst: *Defect-induced magnetic order in pure ZnO films*, Phys. Rev. B **80**, 035331 (2009)

doi:10.1103/PhysRevB.80.035331

S. K. Das, S. V. Thakare, and T. Butz: *The nuclear quadrupole interaction at ^{111}Cd and ^{181}Ta sites in anatase and rutile TiO_2 : a TDPAC study*, J. Phys. Chem. Solids **70**, 778 (2009)

doi:10.1016/j.jpcs.2009.03.008

A. Arndt, D. Spoddig, P. Esquinazi, J. Barzola-Quiquia, S. Dusari, and T. Butz: *Electric carrier concentration in graphite: Dependence of electrical resistivity and magnetoresistance on defect concentration*, Phys. Rev. B **80**, 195402 (2009)

doi:10.1103/PhysRevB.80.195402

T. Butz: *Ion Microscopy and Tomography in Medical Research*, Z. Med. Phys. **19**, 221 (2009)

doi:10.1016/j.zemedi.2009.09.005

R. Dargel, F. Heinemeyer, M. Köntges, J. Vogt, and C. Vogt: *Detection of trace impurities in $\text{Cu}(\text{In,Ga})\text{Se}_2$ thin film solar cells by LA-ICP-MS*, Microchim. Acta **165**, 265 (2009)

doi:10.1007/s00604-008-0131-1

S. Gruhl, F. Witte, J. Vogt, and C. Vogt: *Determination of concentration gradients in bone tissue generated by the degradation of a biologically degradable magnesium implant*, J. Anal. Atom. Spectrom. **24**, 181 (2009)

doi:10.1039/b813734j

T. Koal, T. Butz, and T. Reinert: *High throughput targeted cell irradiation with single ions for low dose radiobiological experiments at LIPSION*, J. Radiat. Res. **50**, A108 (2009)

Books

T. Butz: *Fouriertransformation für Fußgänger*, 6. Aufl. (Vieweg+Teubner, Wiesbaden 2009)

C. Vogt, K. Bechstein, S. Gruhl, M. Lange, H. Drücker, F. Witte, J. Vogt: *Investigation of the degradation of biodegradable Mg implant alloys in vitro and in vivo by analytical methods*, in *Magnesium*, ed. by K.U. Kainer (Wiley-VCH, Weinheim 2009) p 1162

in press

P. Esquinazi, J. Barzola-Quiquia, D. Spemann, M. Rothermel, H. Ohldag, N. García, A. Setzer, T. Butz: *Magnetic order in Graphite: Experimental evidence, intrinsic and extrinsic difficulties*, J. Magn. Magn. Mater. **322**, 1156 (2010)

doi:10.1016/j.jmmm.2009.06.038

M. Dubman, T. Shiroka, H. Luetkens, M. Rothermel, F.J. Litterst, E. Morenzoni, A. Suter, D. Spemann, P. Esquinazi, A. Setzer, T. Butz: *Low-energy μ SR and SQUID evidence of magnetism in highly oriented pyrolytic graphite*, J. Magn. Magn. Mater. **322**, 1128 (2010)

doi:10.1016/j.jmmm.2009.04.023

D. Spemann, V. Gottschalch: *Boron lattice site location in (BGa)As and (BGa)P thin films studied using RBS and NRA with a channeled He⁺ ion beam*, Nucl. Instrum. Meth. B **268**, 2069 (2010)

doi:10.1016/j.nimb.2010.02.028

T. Andrea, M. Rothermel, R. Werner, T. Butz, T. Reinert: *Limited angle STIM and PIXE tomography of single cells*, Nucl. Instrum. Meth. B **268**, 1884 (2010)

doi:10.1016/j.nimb.2010.02.049

N. Barapatre, M. Morawski, T. Butz, T. Reinert: *Trace element mapping in Parkinsonian brain by quantitative ion beam microscopy*, Nucl. Instrum. Meth. B **268**, 2156 (2010)

doi:10.1016/j.nimb.2010.02.039

M. Rothermel, T. Reinert, T. Andrea, T. Butz: *First results on ion micro-tomography at LIPSION*, Nucl. Instrum. Meth. B, **268**, 2001 (2010)

doi:10.1016/j.nimb.2010.02.117

Talks

T. Butz: *Wissen und Wissenslücken zum Thema Hautpenetration von Nanopartikeln*, Umweltbundesamt, Berlin (29. January 2009)

J. Barzola-Quiquia, P. Esquinazi, D. Spemann, T. Butz: *Anisotropic magnetoresistance (AMR) of magnetic graphite*, Frühjahrstagung der DPG, Dresden (22.–27. March 2009)

T. Butz: *Dermal penetration of nanoparticles: what we know and what we don't*, Cosmetic Science Conference, München (22. – 23. April 2009)

T. Butz: *Wissen und Wissenslücken zum Thema Hautpenetration von Nanopartikeln*, 34. Jahrestagung der VDSI-Fachgruppe Hochschulen und wissenschaftliche Einrichtungen, Leipzig (18. – 25. May 2009)

T. Koal, T. Butz: *From cell detection to cell irradiation - Status report on LIPSION facility*, 3. NOTE annual meeting, Rome, Italy (28. June – 1. July 2009)

T. Butz: *Is there dermal penetration of nanoparticles?*, Centrum für Angewandte Nanotechnologie GmbH, Hamburg (3. July 2009)

T. Butz: *Ionenmikroskopie und -tomography in den Material- und Lebenswissenschaften*, Universität Stuttgart (9. July 2009)

T. Butz: *Fabrication of patterned petri-dishes using high-energy ion beams*, China-German Bilateral Symposium on Bioelectronics and Biomaterials, Najing, China (21.–26. August 2009)

T. Andrea, M. Rothermel, T. Reinert, T. Butz: *Limited-angle tomography of single cells using STIM and PIXE*, 19. Int. Conf. on Ion Beam Analysis, Cambridge, UK (7.–11. September 2009)

T. Butz: *Tomography using ion beams*, 19. Int. Conf. on Ion Beam Analysis, Cambridge, UK (7.–11. September 2009)

F. Menzel: *Erzeugung 3-dimensionaler in Resist- und Halbleitermaterialien mittels Protonenstrahlschreiben*, Abschlusskolloquium der FOR 522, Oppurg (28. September 2009)

T. Butz: *Perturbed Angular Correlation*, Workshop on Digital Signal Processing in Nuclear Science, FZ Dresden, Rossendorf (29. September 2009)

T. Butz: *Dermal penetration of nanoparticles in sunscreens: what we know and what we don't*, MPCIC Congress, Warsaw, Poland (24. November 2009)

Posters

M. Rothermel, T. Reinert, T. Andrea, T. Butz: *First results on ion micro-tomography at LIPSION*, 2. Scientific Symposium of the Graduate School BuildMoNa, Leipzig (2.–3. April 2009)

M. Rothermel, T. Reinert, T. Andrea, T. Butz: *First results on combined STIM and PIXE micro-tomography at LIPSION*, 19. Int. Conf. on Ion Beam Analysis, Cambridge, UK, (7.–11. September 2009)

N. Barapatre, M. Morawski, T. Butz, T. Reinert: *Trace element mapping in Parkinsonian brain by quantitative ion beam microscopy*, 19. Int. Conf. on Ion Beam Analysis, Cambridge, UK, (7.–11. September 2009)

M. Khalid, M. Ziese, A. Setzer, P. Esquinazi, H. Hochmuth, M. Lorenz, M. Grundmann, D. Spemann, T. Butz: *Searching for Intrinsic Magnetic Order in Pure ZnO Thin Films*, Frühjahrstagung der DPG, Dresden (22.–27. March 2009)

M. Ziese, A. Setzer, P. Esquinazi, D. Spemann, A. Poepl: *Ferromagnetic Signals in Nominally Non-magnetic Oxide Single Crystals*, Frühjahrstagung der DPG, Dresden (22.–27. March 2009)

D. Spemann, V. Gottschalch: *Boron lattice site location in (BGa)As and (BGa)P thin films studied using RBS and NRA with a channeled He⁺ ion beam*, 19. Int. Conf. on Ion Beam Analysis, Cambridge, UK (07.–11. September 2009)

T. Koal, T. Butz: *From cell detection to cell irradiation - Status report on LIPSION facility*, 3. NOTE annual meeting, Rome, Italy (28. June – 1. July 2009)

7.19 Graduations

Doctorate

- Anja Fiedler
Eisen und Eisenproteine in Neuronen mit perineuronalem Netz
Januar 2009
- Frank Menzel
Erzeugung mikro- und nanodimensionaler Strukturen in Resist- und Halbleitermaterialien mittels Protonenstrahlschreiben
Juni 2009

Diploma

- Alexander Arndt
Modifikation der Transporteigenschaften kohlenstoffbasierter Systeme durch Ionenbeschuss
April 2009
- Niklas Liebing
Channeling Contrast Microscopy - Einführung der Messmethode an der Ionennanoprobe LIPSION
Januar 2009
- Uwe Scholz
Herstellung von Mikrostrukturen in Silizium durch Protonenstrahlschreiben für die Anwendung als phononische Kristalle und akustische Modenkoverter
April 2009
- Ronald Werner
Confined cell growth in structured Petri dishes fabricated by proton beam writing (in agar) and major energy resolution improvements in detectors
September 2009
- René Feder
Protonenstrahlschreiben für Mikrofluidik- und Gasabsorptionsanwendungen
Juli 2009

Bachelor

- Ronja Thies
Quantitative elemental mapping of solar cells by ion microscopy
August 2009

7.20 Guests

-
- Dr. Shamik Ghoshal
Bhabha Atomic Research Centre, Mumbai, India
16. February – 15. May 2009

8

Semiconductor Physics

8.1 Introduction

This year we have succeeded in fabricating high-performance, fully transparent oxide-based thin film transistors. The key is a transparent Schottky gate contact to ZnO and (Mg,Zn)O. Also we could demonstrate ZnO-based MESFETs on glass as well as basic logic elements such as inverters and NOR gates based on MESFETs. Progress was also achieved in various other areas such as (Mg,Zn)O/ZnO quantum wells (large Stark effect), ZnO-based microcavities and controlled doping of ZnO nanowires. Also the identification of pre-breakdown sites as due to bulk defects in pc-Si solar cells was achieved. We hope you find something of interest in our short reports.

We are very grateful to our funding agencies which are acknowledged individually in the short notes. The support by the State of Saxony via the ESF-Nachwuchsforschergruppe "Funktionale multiskalige Strukturen" that started in May 2009 deserves a special mentioning. The work of our students and researchers together with our academic and industrial partners near and far was fruitful and enjoyable and thus it is with pleasure that the semiconductor physics group presents its progress report.

Marius Grundmann

8.2 ZnO-based metal-semiconductor field-effect transistors on glass substrates

M. Lorenz, H. Frenzel, A. Lajn, H. von Wenckstern, G. Biehne, H. Hochmuth, M. Grundmann

ZnO metal-semiconductor field-effect transistors (MESFET) were fabricated by pulsed-laser deposition (PLD) and reactive dc-sputtering on glass and a-plane sapphire substrates. Compared to ZnO thin films on crystalline substrates, the growth on amorphous substrates leads to a higher density of structural defects. Nevertheless MESFET on glass substrates have superior electric properties than silicon-based metal-insulator-semiconductor field-effect transistors (MISFET) commonly used in liquid crystal displays.

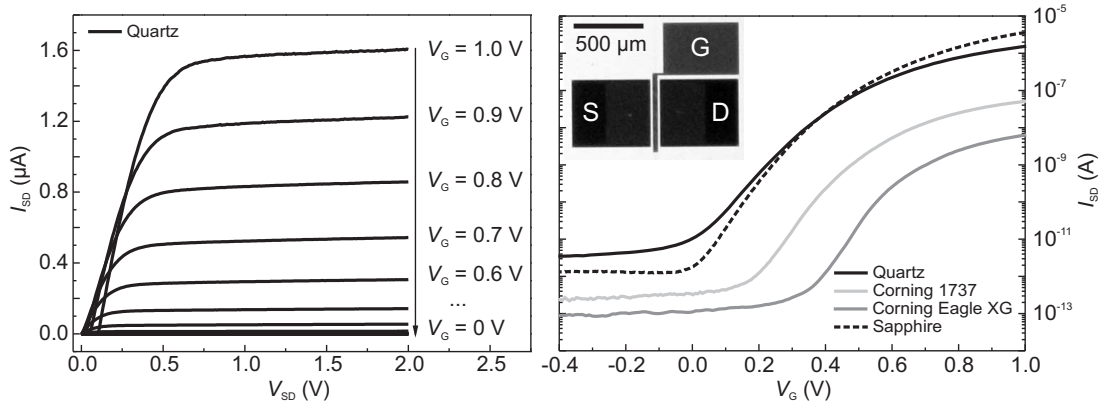


Figure 8.1: (a) Output characteristics of a MESFET on quartz glass and (b) transfer characteristics of MESFETs on different substrates, $V_{SD} = 2$ V. The inset shows a photograph of the MESFET structure with Source (S), Gate (G) and Drain (D) electrode.

ZnO thin films were grown on three different glass substrates: Quartz glass, Corning 1737 and Corning Eagle XG. The Corning glasses are used for consumer TFT production and consist of alkaline earth boro-aluminosilicates. For Eagle XG no heavy metals are used during the fabrication process. Oxygen partial pressure for PLD growth was kept at 3×10^{-4} mbar for thin films on glass and 0.002 mbar for ZnO on a-sapphire. The growth temperature was about 675°C . The reference sample on sapphire was grown using a nominally undoped ZnO PLD target since the diffusion of Al from the substrate generates a homogeneous doping level. This is not the case for the thin films on glass, therefore, PLD targets containing 0.01 wt-% Al_2O_3 were used to obtain a similar doping level. X-ray diffraction spectroscopy revealed a growth of ZnO along the c-axis on sapphire with a full width half maximum (FWHM) of the ω -scan of 0.95° . The amorphous structure of the glass substrates lead to higher FWHM of 2.74° , 3.6° and 2.81° of the ZnO films on quartz, 1737 and Eagle XG respectively, although growth direction is also along the c-axis.

The MESFET were processed by means of standard photolithography. After etching the ZnO mesas as channel, the source and drain contacts were deposited by dc-sputtering of Au and the Ag-Schottky gate contacts (SC) in an oxygen/argon atmosphere. Subsequently an Au capping layer on top of the SC was sputtered to form an equipotential surface. X-ray photoelectron spectroscopy reveals a partial oxidation of the Ag during the reactive dc-sputtering process, which results in a higher Schottky barrier than for the pure metal [1]. The electric properties of the SC were derived by fitting the forward- IV characteristic considering thermionic emission only. Table 8.1 lists these properties along with important electrical parameters of the MESFET deduced from the transfer characteristics (Fig. 8.1(b)).

With the chosen PLD ablation parameters and a channel thickness of approximately 25 nm the MESFET are normally-off, thus no current will flow between the ohmic source and drain contact for gate voltages $V_G \leq 0$ V. For transistors on Corning glasses a shift to higher gate voltages is observed which is caused by a net doping density $N_D - N_A$ consequentially leading to a higher extension of the space charge region. The lower net doping density is likely caused by diffusion of atoms being acceptors in ZnO (e.g. Li, Na, ...) from the Corning glass substrates [2].

Figure 8.1(a) shows exemplarily the output characteristic of a MESFET on quartz

Table 8.1: Channel thickness and measured electrical parameter of the MESFET and the corresponding Schottky gate contact.

Substrate	d_{ZnO} (nm)	$N_{\text{D}}-N_{\text{A}}$ (10^{17}cm^{-3})	V_{on} (mV)	μ_{ch} (cm^2/Vs)	Maximum slope (mV/dec)	on/off (10^5)	ϕ_{B} (eV)	η
Quartz	30	5.7	0	1.30	125	4.7	0.89	1.7
1737	25	1.8	170	0.22	101	2.3	0.91	1.7
Eagle XG	24	1.3	340	0.04	104	0.8	0.94	1.7
Sapphire	15	1.1	0	25.0	77	26.9	0.95	1.7

glass substrate. Clear and almost constant saturation is observed for source-drain voltages between 0 and 2 V. For gate voltages between 0.8 and 1 V, a shift of the characteristics occurs for $V_{\text{SD}} \rightarrow 0$ V due to the influence of gate currents.

From the transfer characteristics the channel mobility of the transistors was derived [3] using the maximum transconductance and the channel's width to length ratio $W/L = 10.75$. The higher on-current and the steeper slope of the transistors on sapphire are indicators for the much higher channel mobility, which is more than one decade higher than the mobility of the MESFET on quartz glass substrate. It further decreases for transistors on the Corning glasses. This is obviously caused by the lower on-current due to the shift of the turn-on voltage and higher currents over the gate electrode. Furthermore the amorphous structure of the glass leads to a significantly different morphology of the ZnO thin films compared to that on crystalline substrates resulting in the observed reduction of the channel mobility [2].

- [1] A. Lajn et al., J. Vac. Sci. Technol. B **27**, 1769 (2009)
- [2] H. Frenzel et al., Appl. Phys. Lett. **95**, 153503 (2009)
- [3] H. Frenzel et al., Appl. Phys. Lett. **92**, 192108 (2008)

8.3 High-gain integrated inverters based on ZnO MES-FET technology

F. Schein, H. Frenzel, A. Lajn, H. von Wenckstern, M. Grundmann

Integrated circuits (ICs) were fabricated by using ZnO-based Schottky diodes and metal-semiconductor field effect transistors (MESFETs) [1]. Primarily we focused on inverter circuitry but additionally a NOR-gate has been realized successfully.

The semiconductor thin films were grown by pulsed-laser deposition (PLD) on $10 \times 10 \text{ mm}^2$ *a*-plane sapphire substrates in an oxygen background pressure of 0.02 mbar and a growth temperature of 675 °C using a ZnO target mixed with 0.25 % MgO. Subsequently, the samples were photolithographically processed: first, mesa structures were wet chemical etched into the thin film to define channels for the MESFETs and the semiconductor part of the Schottky diodes, respectively. Second, a reactively dc-sputtering process of Ag in an Ar/O₂ atmosphere forms the transistor gates and Schottky diodes. Third, ohmic Au contacts and interconnects were non-reactively sputtered in an Ar atmosphere.

For our inverters we adapted the so-called Schottky diode FET logic (SDFL) design approach, known from GaAs-MESFET technology [2]. Figure 8.2a shows the circuitry, consisting of the inverter part with load transistor (Q_L) and switching transistor (Q_S), as well as of the level shifter (LS) with two Schottky diodes (D_1, D_2) and the pull-down transistor (Q_{PD}), serving as current supply for the diodes. By adding the additional diode D_3 to the circuit, a logic NOR-gate has been implemented. The gate's width and length was $210 \mu\text{m}$ and $20 \mu\text{m}$ for Q_S and Q_L whereas the width of Q_{PD} was $105 \mu\text{m}$. The LS is necessary for ensuring compatibility issues. A voltage drop at D_1 and D_2 shifts the inverter characteristic towards higher input voltages, such that one can find a pair of values ($V_{in}|V_{out}$) suitable as high or low input/output, respectively.

The voltage transfer characteristics (VTCs) are shown in Fig. 8.2b for the inverter part only (without LS), with one diode and with two diodes using Q_{PD} operating at $V_{SS} = -1 \text{ V}$. We observe clear inverting behavior, i. e. $V_{out} = V_{DD}$ for low V_{in} as in ideal case and $V_{out} \approx 0$ for high V_{in} . Without the LS, the switching voltage V_S is 0.2 V and too close to zero, i. e. a subsequent inverter with the same VTC could misinterpret an input low level $V_{in} \approx V_S$ as input high level. The LS shifts the VTC by 0.61 V for one diode and by 1.35 V for two diodes, according to the voltage drop produced by the ZnO Schottky diodes. Thus, the two-diode SDFL inverter ($0 \text{ V}|2 \text{ V}$) and ($2 \text{ V}|0 \text{ V}$) ensures safe operation without compatibility problems.

The steepness of the VTC is represented by the peak gain magnitude $\text{pgm} = \max|\partial V_{out}/\partial V_{in}|$ and should be as high as possible. The two voltages fulfilling the relationship $|\partial V_{out}/\partial V_{in}| = 1$ are called input low and high levels, V_{IL} and V_{IH} , respectively. The voltage range between them is denoted as uncertainty level $V_{uc} = V_{IH} - V_{IL}$ and should be as small as possible. V_{uc} and pgm are two important figures of merit for inverters. Our inverters exhibit high pgm up to 197 at $V_{DD} = 3 \text{ V}$. This gain value exceeds other semiconductor oxide based ICs using metal-insulator field-effect transistors as comparisons in ref. [3, 4] reveal.

V_{uc} is in the range of $0.12 - 0.17 \text{ V}$ and is similar to the well established GaAs MESFET technology ($V_{uc} \approx 0.1 \text{ V}$) [5]. Furthermore we calculated the static power dissipation P_D of the inverters and normalized it with the switching transistor's gate area. We obtained $P_D = 111 \text{ pW}/\mu\text{m}^2$ for low-output and $P_D = 46 \text{ pW}/\mu\text{m}^2$ for high-output, respectively. These values are low compared to other reported MESFET-based inverters (GaAs: $34 - 45 \mu\text{W}/\mu\text{m}^2$, AlGaIn/GaN: $444 \mu\text{W}/\mu\text{m}^2$) [4]. The measured NOR-function with clear distinguishably logic levels is shown in the inset of Fig. 8.2b. The output is only logic '1' if both input levels V_{in} and V_{in}' are logic '0'.

Thus, it is possible to create a complete ZnO-based logic consisting of NOR-gates and inverters.

- [1] H. Frenzel et al.: Appl. Phys. Lett. **92**, 192108 (2008), DOI:10.1063/1.2926684.
- [2] R. C. Eden et al.: IEEE J. Solid-St. Circ. **13**, 419 (1978).
- [3] M. Grundmann et al.: M. Grundmann et al.: Phys. Status Solidi A **207**, 1437 (2010)
- [4] H. Frenzel et al.: Appl. Phys. Lett. **96**, 113502 (2010), DOI:10.1063/1.3339876.
- [5] A. S. Sedra and K. C. Smith: *Microelectronic Circuits*, 5th Ed. (Oxford University Press, New York, Oxford 2004).

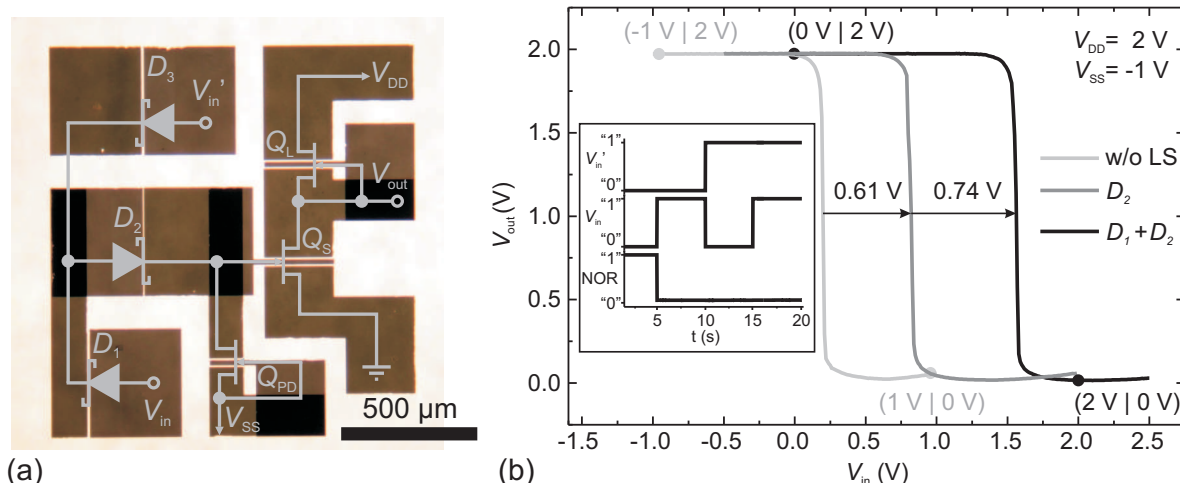


Figure 8.2: (a) Circuit of the SDFL inverter with underlying optical microscopic image of the device. The dark areas are overlaps of two contact layers for interconnections and shortcircuits. (b) Voltage transfer characteristic for the SDFL inverter without level shifter (LS), with one diode (D_2) and with two diodes ($D_1 + D_2$). The operating points for inverter with LS and without LS are marked with dots and labeled with $(V_{in}|V_{out})$. Inset: Measured NOR-function of the SDFL inverter using D_3 as additional input V_{in}' .

8.4 Transparent rectifying contacts and their application in transparent electronics

A. Lajn, H. Frenzel, H. von Wenckstern, M. Grundmann

We report on the fabrication of fully transparent diodes, field-effect transistors and inverters utilizing a new concept employing transparent rectifying contacts (TRC) for transparent electronics based on zinc oxide. The TRC consist of a combination of a reactively dc-sputtered Ag_xO or PtO_y layer and a transparent and highly conducting capping layer; the total thickness is only 100 nm. With that an average transmission of 70 % and 60 % in the visible spectral range was achieved for the complete device structure on a ZnO thin film with Ag_xO and PtO_y , respectively (Fig. 8.3 a)). The so formed Schottky-like diodes exhibit maximum effective barrier heights of 0.87 eV, ideality factors as low as 1.47 and rectification ratios of up to 5×10^6 . Using such kind of contacts as gate contacts in transparent metal-semiconductor field-effect transistors (TMESFET), on/off-ratios of 10^6 and channel mobilities of up to $11.9 \text{ cm}^2/\text{Vs}$, which are only slightly lower than for opaque MESFETs [1, 2], were achieved (Fig. 8.3 a)). With that, our devices meet the requirements for the use in transparent displays formulated by Wager [3]. Moreover the TMESFETs require small voltage sweeps of only 2.7 V for switching between on and off-state. This is due to the absence of a voltage drop at a gate insulator, as it occurs in metal-insulator-semiconductor-FETs. Furthermore, with 120 mV/dec, the subthreshold slope of the TMESFETs already approaches the thermodynamic limit of 60 mV/dec. These advantages of MESFET were successfully transferred to integrated inverters, which have a maximum gain $g = \frac{\partial V_{out}}{\partial V_{in}}$ of 200 at a supply voltage V_{DD} of 4 V and a low uncertainty level of 0.3 V (Fig. 8.3 a)). Their performance is superior among the transparent inverters reported so far (e.g. [4]) and

clears the way to fully transparent logic integrated circuits.

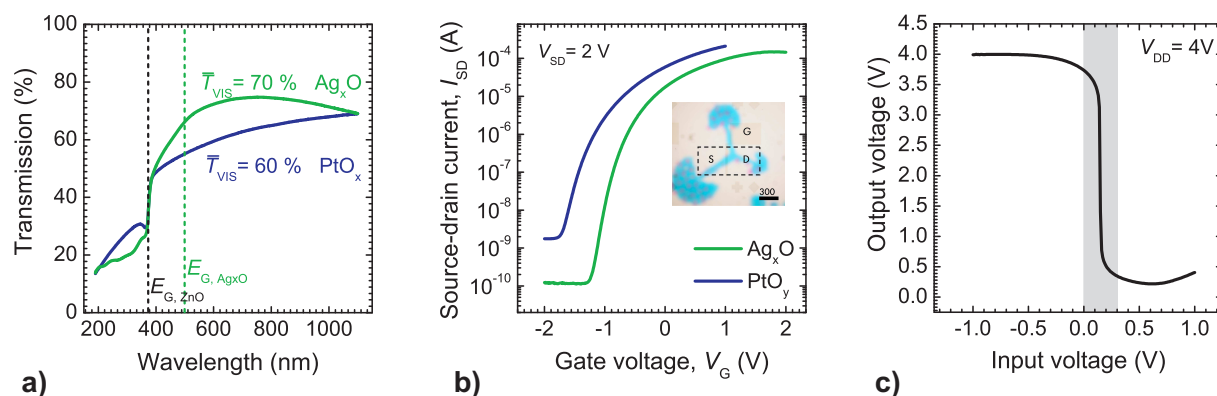


Figure 8.3: a) Transmission spectra of the transparent gate contacts on ZnO thin film on sapphire substrate. The dashed lines indicate the fundamental absorption edges of ZnO and Ag_xO . b) Transfer characteristic of the TMESFETs. The inset depicts an optical microscopic image of a TMESFET structure; the dashed line indicates the channel mesa. c) Output characteristic of a TMESFET-based inverter. The grey highlighted area depicts the uncertainty level.

- [1] H. Frenzel, et al., Appl. Phys. Lett., **92**, 192108 (2008)
- [2] H. Frenzel, et al., Appl. Phys. Lett., **95**, 153503 (2009)
- [3] J. F. Wager, Science, **300**, 1245 (2003)
- [4] J. H. Na, et al., Appl. Phys. Lett., **93**, 213505 (2008)

8.5 Growth and transport properties of ZnO- and ZnO:P-microwires

C.P. Dietrich, M. Brandt, M. Lange, H. von Wenckstern, M. Grundmann

Currently, there is a high interest in fabricating small-sized devices such as LEDs or lasers emitting in the UV. The wurtzite semiconductor ZnO is a promising candidate for such applications due to its band gap of about 3.3 eV at room temperature (RT) and its large exciton binding energy allowing the observation of exciton-related recombinations at RT and above. However, ZnO is a native *n*-type semiconductor. Nevertheless, several indications exist that stable *p*-type conductivity can be achieved by the incorporation of phosphorus atoms into the ZnO host crystal [1].

Micrometer-sized rods were grown by a chemical vapor-phase transport (CVT) process driven by carbothermal reduction. In this process the reducing character of carbon (oxidized to carbondi- or monoxide) is used to generate vapor-phase elements, i.e. Zn(g) and P(g). Performing the growth at ambient air conditions leads to the formation of ZnO- and ZnO:P-microwires showing perfectly shaped low-index facets of the wurtzite lattice structure.

In order to characterize the microwires electrically, they were placed on silicon substrates with an insulating SiO_2 layer and were contacted electron-beam-assisted with Pt-contacts to Au connections predefined on the substrates [2]. Hall bar geometry was

used for temperature-dependent Hall effect measurements. The contact I - U characteristics are ohmic (not shown here) with contact resistances ranging from $10\text{ k}\Omega$ to $1\text{ M}\Omega$.

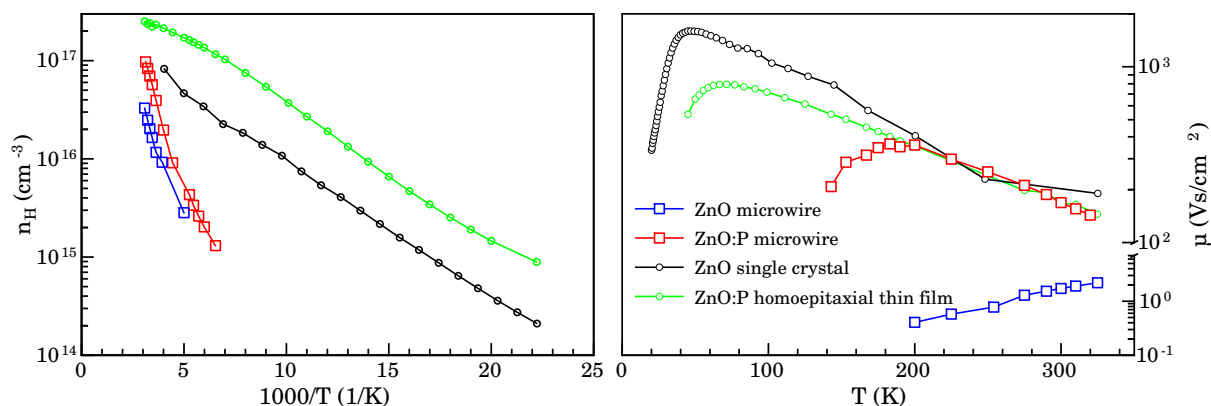


Figure 8.4: Temperature-dependent charge carrier concentration n_H and mobility μ derived from Hall effect measurements

Fig. 8.4 shows the temperature-dependent carrier concentration and mobility (derived from Hall effect measurements) of ZnO- and ZnO:P-microwires compared to bulk and thin film data. All investigated samples clearly show n -type conductivity; the most important scattering mechanism is scattering at ionized impurities. The phosphorus-doped ZnO-microwires show an increased mobility compared to the undoped wire. This is most likely caused by the incorporation of phosphorus as donor on Zn lattice site [3] resulting in higher free electron concentrations and a shorter screening length compared to the undoped wire. Nevertheless, the maximal Hall mobility occurs at higher temperatures and is lower than for the bulk ZnO crystal and the homoepitaxial ZnO:P thin film. In accordance with the high thermal activation energy of the dominant donor in the wire we attribute this behavior to higher compensation.

- [1] B.Q.Cao, M. Lorenz, M. Brandt, H. von Wenckstern, J. Lenzner, G. Biehne, M. Grundmann, *phys.stat.sol.(RRL)* **2**, 37-39 (2008)
- [2] G. Zimmermann, M. Lange, B. Cao, M. Lorenz, M. Grundmann, *phys. stat. sol. (RRL)* **4**, 82 (2010)
- [3] A. Allenic et al., *Adv. Mater.* **19**, 3333 (2007)

8.6 Resistivity control in ZnO nanowires by Al doping

G. Zimmermann, M. Lange, B.Q. Cao*, M. Lorenz, M. Grundmann

*present address: School of Materials Science and Engineering,
University of Jinan, Shandong, P.R. China

The conductivity of nominally-undoped and aluminum-doped ZnO nanowires has been investigated. Both were grown in a low-vacuum PLD chamber, the latter using a target with 0.01 wt. % Al_2O_3 . The incorporation of aluminum into the ZnO nanowires

is confirmed by energy-dispersive X-ray spectroscopy (EDX) and yields an Al content of ~ 0.6 at. %. This shows that the transfer factor from target to sample is significantly larger than the value of 1.6 encountered in PLD growth of ZnO thin films.

In order to access the electrical properties of single ZnO(:Al) nanowires, they were transferred onto a Si/SiO_x substrate with predefined macroscopic contact pads. The ohmic connections between nanowires and contact pads were defined using electron-beam lithography (EBL) and deposited by evaporation of a Ti/Au double layer (see Fig. 8.5a).

The resistivities ρ of both ZnO nanowire types was determined from I - V measurements paying special attention to the tapered morphology of the nanowires under test. In Fig. 8.5 these resistivities are compared. From the graph it is obvious, that ρ has no clear dependencies either on the length of the contacted nanowires or on their average diameter and that the resistivities are homogeneous in the given size regime [1]. The decrease in ρ by more than two orders of magnitude upon Al doping with the given concentration shows furthermore, that this is an efficient way to tune the electrical properties, e.g., for applications as nanoscale transparent conductive oxide.

Transmission line measurements on some of the NWs revealed contact resistances R_C in the order of 1–5 M Ω for undoped and 20–30 k Ω for Al-doped nanowires. For ZnO nanowires $2R_C$ contributes less than 10% to the total resistance, but for ZnO:Al nanowires it this fraction can reach 80%. Therefore, the data for ρ given in Fig. 8.5b are upper bounds and the difference in resistivities between ZnO and ZnO:Al NWs is about a further half an order of magnitude larger.

[1] G. Zimmermann et al.: phys. stat. sol. RRL 4, 82 (2010), doi:10.1002/pssr.201004015

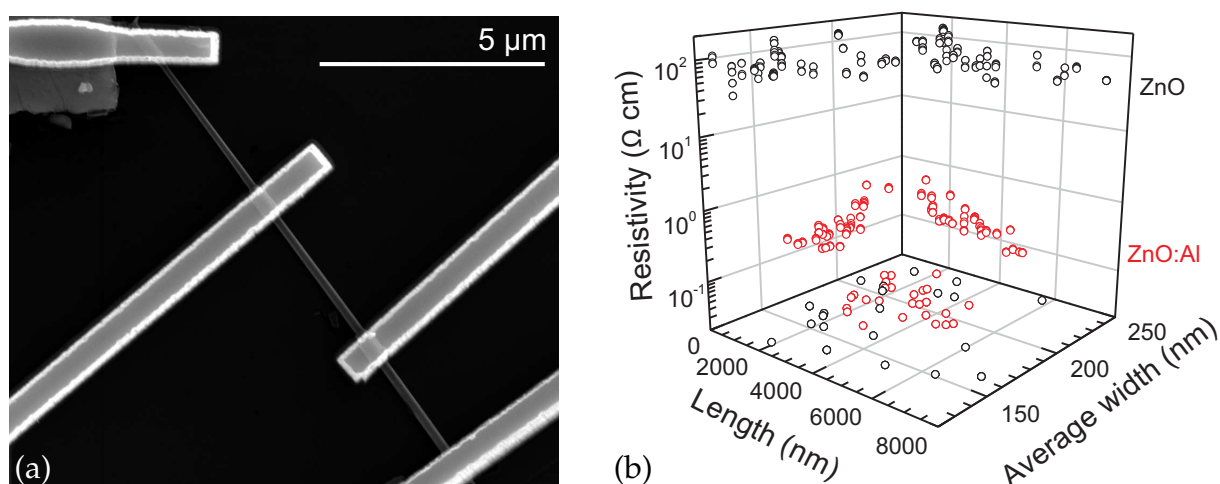


Figure 8.5: SEM micrograph of an EBL-contacted ZnO nanowire (a). The resistivities ρ at 300 K for nominally-undoped (black symbols) and Al-doped (red symbols) ZnO nanowires are shown in (b). While the error in length and diameter is smaller than the symbols, some of the data points are slightly smeared out in the vertical, displaying the effect of multiple consecutive measurements on the corresponding nanowire devices.

8.7 Donor-acceptor pair recombination in non-stoichiometric ZnO thin films

C.P. Dietrich, M. Lange, H. von Wenckstern, G. Benndorf, M. Grundmann

The present work focuses on the stoichiometry-dependent photoluminescence (PL) properties of nominally undoped ZnO thin films. The investigated ZnO thin films were grown by pulsed-laser deposition (PLD) on (11 $\bar{2}$ 0)-oriented sapphire substrates at different oxygen background pressures $p(\text{O}_2)$ in the range from 8×10^{-2} to 2×10^{-3} mbar.

Changing the oxygen background pressure modifies the deposition properties in the highly non-equilibrium process of PLD. At high background pressures lighter species ablated from the polycrystalline ZnO target will be increasingly scattered with higher scattering angle causing a substantially lowered adsorption rate of oxygen atoms compared to Zn atoms on the substrate resulting in a zinc-rich stoichiometry. Lowering the oxygen background pressure enhances the desorption probability of oxygen atoms from the substrate. Therefore, the II/VI-composition ratio of the thin films can be adjusted by the adequate choice of the oxygen background pressure.

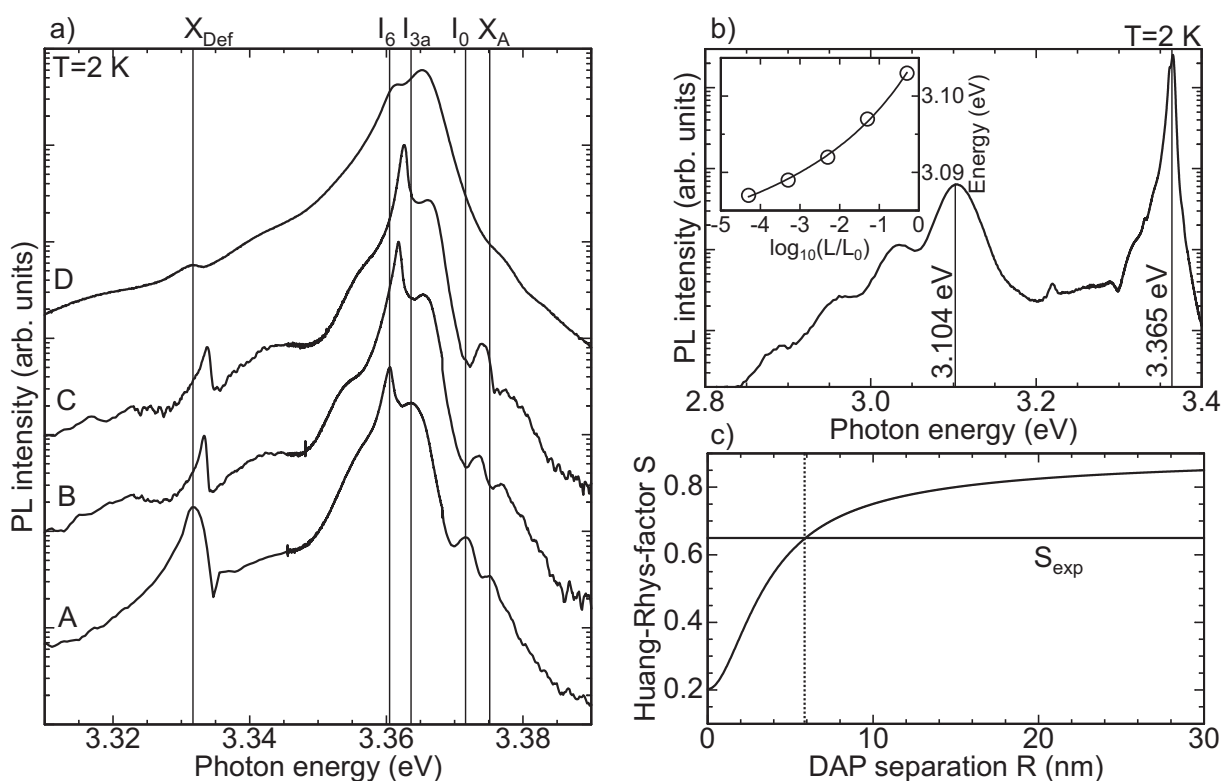


Figure 8.6: a) Low temperature PL-spectra of samples A, B, C and D. b) PL spectrum of sample D at $T = 2$ K in a wider spectral range. The inset shows the spectral position of the DAP maximum in dependence on the excitation power. c) Huang-Rhys parameter S calculated within the quantum defect model using impurity binding energies $E_D = 40$ meV and $E_A = 320$ meV. The horizontal line represents the experimentally determined Huang-Rhys factor S_{exp} .

Photoluminescence spectra of ZnO thin films grown at 8×10^{-2} (A), 4×10^{-2} (B), 2×10^{-2} (C) and 2×10^{-3} mbar (D) are shown in Fig. 8.6a for 2 K. In comparison to A, the spectra B and C show a similar lineshape, however, the spectral features are shifted

towards higher energy with decreasing $p(\text{O}_2)$. For D a redshift is observed again. This can be explained by the modification of bonding lengths in the crystal due to the growth pressure-induced stoichiometry change of the lattice constant. X-ray diffraction patterns (not shown here) exhibit sharp (0002) and (0004) reflexes and prove the high c -axis orientation of the thin films. The reduction of $p(\text{O}_2)$ leads to an increase of the c -lattice constant and a coinciding increased distance between Zn and O atoms affecting the bandgap of the material. Compared to an unstrained ZnO bulk crystal, we conclude that only sample A was grown stoichiometrically.

The luminescence of sample D (Fig. 8.6b) is dominated by the transition of Zn_i -bound excitons with exciton localization energy of 10.9 meV in agreement with the thermal activation energy of the exciton-impurity complex. The corresponding donor binding energy is $E_D(I_{3a}) = 40.2$ meV according to Hayne's rule for ZnO [1]. Furthermore, a broad violet band is visible at 3.104 eV followed by three phonon replicas with a separation of 72 meV.

The spectral position of the violet band depends on the excitation density (inset of Fig. 8.6b). Typically, DAP recombinations redshift with decreasing excitation density due to a change of the mean distance R between donors and acceptors involved, thus leading to a decreased Coulomb interaction. Hence, we attribute the violet band at 3.104 eV to a DAP recombination. The DAP-energy $E_{\text{DAP}}(R)$ for the limiting case of infinitely separated impurities is $E_{\text{DAP}}(\infty) = 3.077$ eV at 2 K (fitted by a $1/R$ -function). With that the Coulomb energy is 27 meV for the excitation density used to record the spectrum of Fig. 8.6b.

An Arrhenius fit of the integrated intensity reveals a thermal activation energy of (40.2 ± 1.5) meV for the DAP recombination which is in excellent agreement to the calculated binding energy of the Zn_i -donor complex and proofs its participation in the DAP recombination. The resulting acceptor binding energy is $E_A = 320$ meV. The most probable and suitable acceptor complex is the zinc vacancy (only assuming intrinsic defects) having a low formation energy and binding energies in the range 260 - 390 meV [2].

The strong intensity of the phonon sidebands is typical for DAP recombinations and indicates a strong electron-LO-phonon interaction. The Huang-Rhys-factor S quantifies the electron-phonon-coupling strength and is determined by a Poisson distribution $I_n = \frac{S^n}{n!} I_0$ with n being the number of phonons involved. For the DAP recombination we find $S_{\text{exp}} = 0.65$ at 2 K (Fig. 8.6c). An analytical model to describe the electron-LO-phonon interaction is the quantum defect model [3] which takes different chemical origins of impurities into account. It is used to describe the dependence of the Huang-Rhys-factor S on the DAP separation distance R . An experimental value $S_{\text{exp}} = 0.65$ would herein mean a separation distance of about $R = 6$ nm and a Coulomb energy of $E_{\text{Cou}} = 30$ meV at 2 K which is in good agreement to our excitation-dependent PL measurements.

- [1] B. K. Meyer, J. Sann, S. Lautenschläger, M. R. Wagner, and A. Hoffmann, Phys. Rev. B **76**, 184120 (2007).
- [2] C.P. Dietrich, M. Lange, G. Benndorf, H. von Wenckstern, and M. Grundmann, Solid State Commun. **150**, 379 (2010).
- [3] A.L. Gurskii and S.V. Voitkov, Solid State Commun. **112**, 339 (1999).

8.8 Lineshape theory of photoluminescence from semiconductor alloys

C.P. Dietrich, M. Grundmann

Semiconductor alloys are important materials used for band gap engineering in heterostructures for applications in electronics and photonics. We investigate $\text{Mg}_x\text{Zn}_{1-x}\text{O}$ and discuss $\text{Al}_y\text{Ga}_{1-y}\text{N}$ alloys in which excitons are stable close to or above room temperature due to their large exciton binding energy E_X . The recombination spectra of semiconductor alloys are mostly inhomogeneously broadened and only one recombination peak is observed for all temperatures masking the near-band edge finestructure. We establish here a theory for the recombination lineshape for semiconductor alloys in the presence of two recombination channels: impurity donor bound excitons and free excitons.

The alloy recombination peak energy typically shows a characteristic temperature de-

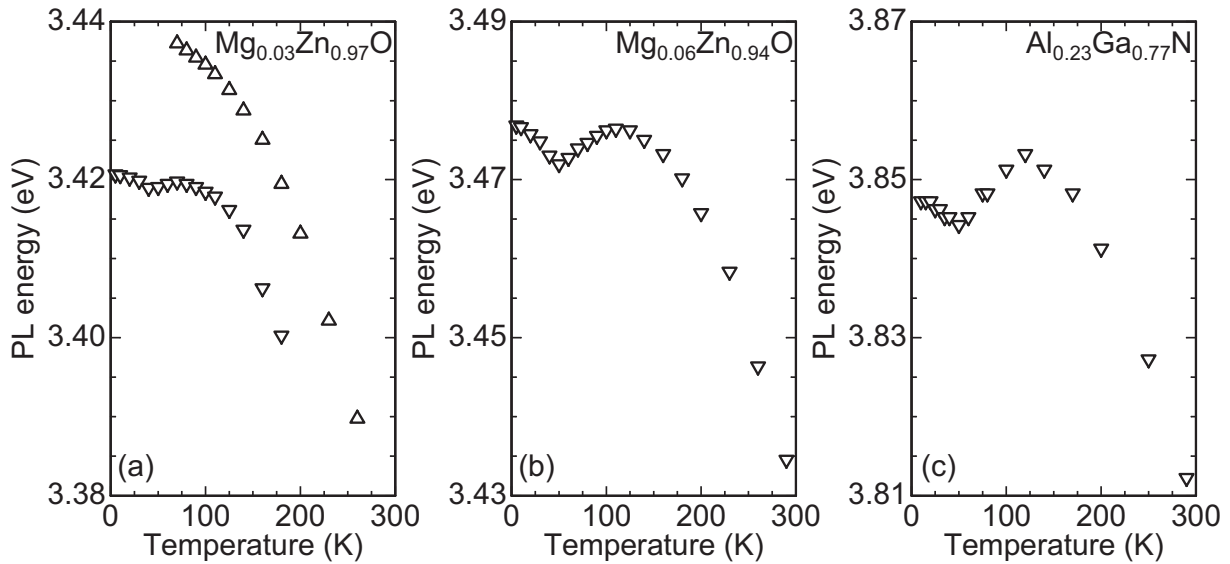


Figure 8.7: Temperature dependence of the energy position of photoluminescence recombination peaks in $\text{Mg}_x\text{Zn}_{1-x}\text{O}$ alloys and $\text{Al}_y\text{Ga}_{1-y}\text{N}$. The energy position is given relative to the maximum position of the low temperature recombination spectrum. For $x = 0.03$, recombination from donor bound and free excitons can be observed spectrally separated. For $x = 0.06$ and $y = 0.23$, only a single recombination peak is observed.

pendence. With increasing temperature it first shifts to lower energies, then to higher energies, and then again to lower energies. This so-called S-shape temperature dependence is shown for $\text{Mg}_{0.06}\text{Zn}_{0.94}\text{O}$ and $\text{Al}_{0.23}\text{Ga}_{0.77}\text{N}$ alloys in Fig.8.7. The shift to lower energies at high temperatures is easily explained with the band gap shrinkage $E_g(T)$ and is modeled with two phonon energies[1]. The initial redshift $S = \gamma(T)kT$ of the alloy recombination peak at low temperatures is believed to be due to activation of exciton transport within the alloy disorder potential and can be derived by

$$\gamma \exp \gamma = \beta(\gamma_0 - \gamma) \exp(-\tilde{E}/kT) \quad (8.1)$$

\tilde{E} being the mean barrier for exciton transport, β being the ratio of carrier recombination and carrier transport time and $\gamma_0 = (\sigma/kT)^2$ with σ being the standard deviation of

Gaussian broadening. In [2] we showed that the initial redshift is also accompanied by the exciton delocalization from shallow defects such as impurities and structural defects with increasing temperature. An energetic shift of Q is expected with Q being the exciton localization energy[3, 4].

A major point of our model is the correct modeling of the population of states for donor-bound and free excitons. Here, we derive the population numbers of free and bound excitons and introduce a temperature-dependent ratio of degeneracies of the involved excitonic levels C' [1]. This reads as

$$\frac{n_2}{n_1 + n_2} = \left[1 + C' \frac{N_D}{N_D^0} \exp\left(-\frac{E'}{kT}\right) \right]^{-1} \quad (8.2)$$

with n_1 and n_2 being the density of free and bound excitons, respectively, N_D being the concentration of donors and N_D^0 being the concentration of neutral donors. Further, the temperature-dependent width of donor bound and free exciton recombination could be modeled by assuming phonon scattering to be responsible for the broadening at higher temperatures.

In summary, Fig. 2 shows the successful modeling of temperature-dependent energy position, spectral width and spectral intensity for the semiconductor alloy $\text{Mg}_{0.06}\text{Zn}_{0.94}\text{O}$.

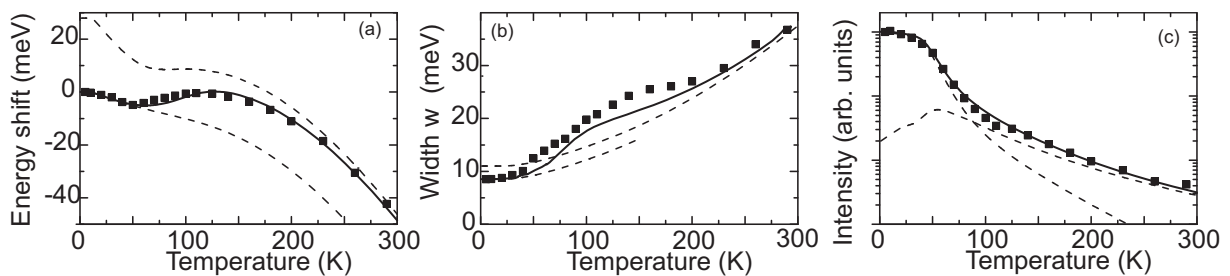


Figure 8.8: Temperature dependence of the energy position (a), intensity (b) and spectral width (c) of photoluminescence recombination peak in $\text{Mg}_{0.06}\text{Zn}_{0.94}\text{O}$ alloy. The solid line represents the lineshape fit after [1]. The dashed lines show the individual contributions of donor bound and free excitons.

- [1] M. Grundmann and C.P. Dietrich, *J. Appl. Phys.* **106**, 123521 (2009).
- [2] A. Müller, M. Stölzel, C.P. Dietrich, G. Benndorf, M. Lorenz and M. Grundmann, *J. Appl. Phys.* **107**, 013704 (2010).
- [3] C.P. Dietrich, A. Müller, M. Stölzel, M. Lange, G. Benndorf and M. Grundmann, *Mater. Res. Soc. Symp. Proc.* **1201**, H03-08 (2010).
- [4] C.P. Dietrich, M. Lange, G. Benndorf, J. Lenzner, M. Lorenz and M. Grundmann, *New J. Phys* **12**, 033030 (2010).

8.9 Identification of a donor related recombination channel in ZnO thin films

M. Brandt, H. von Wenckstern, G. Benndorf, M. Lange, C. P. Dietrich, C. Kranert, C. Sturm, R. Schmidt–Grund, H. Hochmuth, M. Lorenz, M. Grundmann, M. R. Wagner*, M. Alic*, C. Nenstiel*, A. Hoffmann*

*Institute of Solid State Physics, TU Berlin, Hardenbergstr. 36, 10623 Berlin, Germany

The near band edge recombination spectrum of ZnO single crystals and thin films is typically dominated by transitions due to free and bound excitons. A remarkable number of bound exciton transitions has been reported [1]. Furthermore excited states of bound exciton transitions can be observed in high-quality samples and additionally recombination of excitons bound to the defect in an ionized state and recombinations involving holes from deeper valence band (B excitons) were reported [1, 2].

We report on the observation of a neutral donor bound excitonic (D^0X) recombination in ZnO thin films grown on a MgO or heavily aluminum doped ZnO buffer layer which is not present in ZnO thin films directly grown on sapphire [3]. The films investigated were grown by pulsed laser deposition on *a*-plane sapphire substrates. Sample A contains an approximately 160 nm thick highly aluminum doped ZnO layer; the aluminum concentration was around 1 wt.%. Sample B contains a roughly 10 nm thick MgO buffer layer. On top of the respective buffer layers a $\approx 1\mu\text{m}$ thick nominally undoped ZnO layer was deposited. Sample C was grown without a buffer layer.

The films were investigated by Raman spectroscopy, photoluminescence spectroscopy (PL) and photoluminescence excitation spectroscopy (PLE).

The relative strain of the ZnO layers in sample A and B with respect to sample C was calculated from the Raman measurements. Values of -1.3×10^{-3} and -2.2×10^{-3} with respect to sample C were obtained for samples A and B, respectively.

The photoluminescence spectra of the films A and B showed a redshift of 1.4 meV and 1.9 meV, respectively. Following Ref. [4] the strain induced shift of the band gap with respect to sample C was calculated to be -1.0 meV and -1.7 meV for samples A and B respectively, and is in good agreement with the experimental values.

A prominent line at 3.3465 eV was observed for samples A and B, only, and labeled I_{12} line. Also, an additional feature appears at 3.283 eV, exclusively in samples showing the I_{12} line. We attribute this transition to be a 2s two-electron satellite transition (TES) of the I_{12} line, as its intensity scales with that of the I_{12} line, and it is found close to the theoretically predicted spectral position of the 2s TES [1, 3]. It is therefore concluded, that the I_{12} line corresponds to a D^0X transition.

The results of the photoluminescence excitation experiment are depicted in Fig. 8.9. The excitation channels of I_6 and I_{12} are shown. Both show resonant excitation channels via the free A and B excitons. Two excitation channels are seen for both recombination lines, located 6.2 meV and 4.9 meV above the I_6 and 6 meV and 5.1 meV above the I_{12} recombination line. We concluded that these excitation channels stem from the excitation of the bound B exciton ($\Delta E \approx 4.9$ meV) and most likely a rotator state of the bound B exciton ($\Delta E \approx 6.1$ meV). For the I_6 line a resonant excitation was found at the position of the I_0 line, consistent with the attribution of that peak to an (D^+X) transition of the Al_{Zn} defect. For the I_{12} line, an excitation channel is present at 3.3545 eV. Following

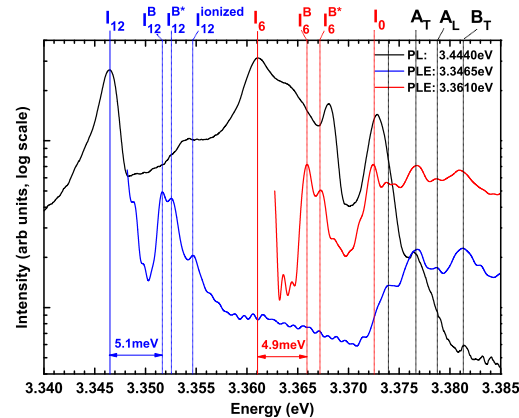


Figure 8.9: PL and PLE spectra obtained from sample A, detection was carried out at the I_{12} and I_6 peak position.

Ref. [2] and assuming I_{12} being a (D^0X) recombination line, a binding energy of 90.8 meV was calculated, resulting in an expected position of the corresponding (D^+X) transition at 3.3535 eV, identical with the excitation channel. We therefore conclude that the feature observed at 3.3545 eV is the (D^+X) transition corresponding to I_{12} .

The I_{12} line corresponds to the recombination of an exciton bound to a neutral donor with an activation energy of ≈ 90 meV. A donor with a similar thermal activation energy of about 100 meV was indeed reported in ZnO thin films grown on Al doped buffer layers[5].

- [1] B. K. Meyer et al: phys. stat. sol. (b) **241**, 231 (2004).
- [2] B. K. Meyer et al.: Phys. Rev. B **76**, 184120 (2007).
- [3] M. Brandt et al.: Phys. Rev. B **81**, 073306 (2010).
- [4] M. R. Wagner et al.: Phys. Rev. B **79**, 035307 (2009).
- [5] F. D. Auret et al.: J. Phys. **100**, 042038 (2008).

8.10 Temperature-dependent properties of nearly ideal ZnO Schottky diodes

H. von Wenckstern, M. Allen*, S.M. Durbin*, M. Grundmann

*The MacDiarmid Institute for Advanced Materials and Nanotechnology, University of Canterbury, Christchurch 8140, New Zealand

The current-voltage characteristic of a low-ideality-factor ZnO Schottky diode was investigated between room temperature and 423 K. The diodes consist of a semi-insulating ($n = 10^{14} \text{ cm}^{-3}$) hydrothermally grown high-quality ZnO single crystal and circular silver oxide Schottky contacts. The Ohmic contact surrounds the Schottky contact; the diode is a planar geometry device. Both contact types were realized on the Zn-polar face of the ZnO single crystal.

The current-voltage characteristics measured in atmospheric conditions are depicted in Fig. 8.10a) for temperatures between 25 and 150°C. The forward current shows

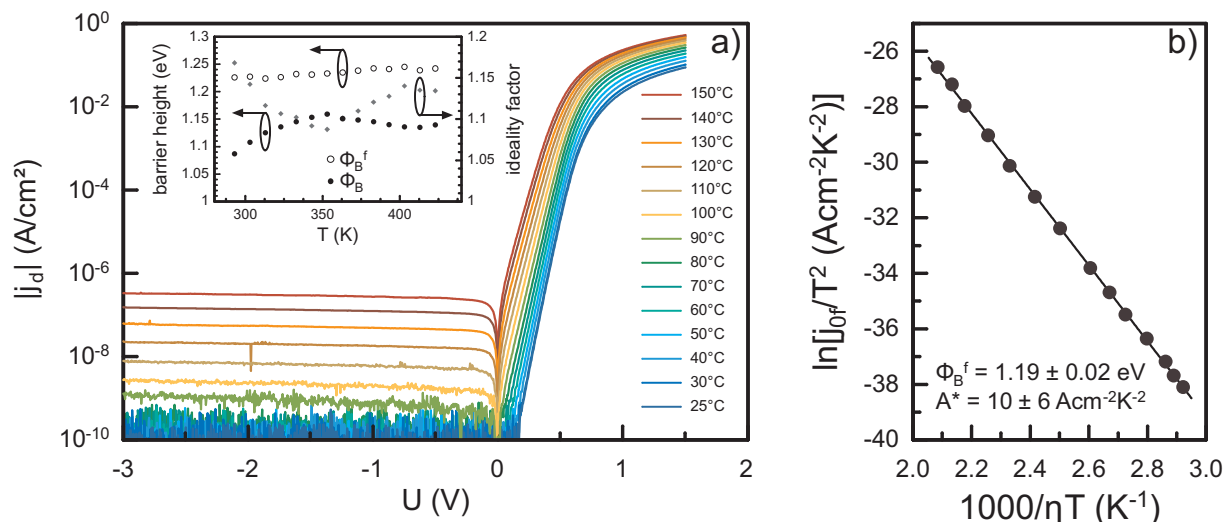


Figure 8.10: a) $I - V$ characteristics of planar silver oxide Schottky diode on the Zn-polar face of a hydrothermal ZnO bulk single crystal measured in atmospheric conditions. The inset shows the variation of the effective barrier height Φ_B , the flat-band barrier height Φ_B^f and the ideality factor η with temperature. b) Modified Richardson plot $\ln(j_{of}/T^2)$ versus $1000/\eta T$. The straight line is a linear fit to determine A^* and Φ_B^f .

exponential behavior over many orders of magnitude indicating that thermionic emission (TE) is the dominant transport process. Further evidence that TE is dominant is obtained from the analysis of the reverse current which can be accurately modeled considering image force lowering as only cause of the voltage dependence of the reverse current. For TE the effective barrier height Φ_B and the ideality factor η are obtained from a fit of the forward current. From the ideality factor and the effective barrier height the so-called flat-band barrier height Φ_B^f , a quantity that eliminates the influence of most non-ideal behavior, can be calculated. The inset of Fig. 8.10a) shows the variation of the Φ_B , Φ_B^f and η with temperature. We have used the ideality factor and the flat-band saturation current j_{of} (calculated from the flat-band barrier height) to construct a modified Richardson plot from which the effective Richardson constant A^* can be determined [1]. The value of 10 ± 6 Acm⁻²K⁻² is very close to the theoretical value of 32 Acm⁻²K⁻² and two orders of magnitude higher than previously reported values substantiating the nearly ideal properties of the investigated diodes.

- [1] Martin W. Allen, Steven M. Durbin, Xiaojun Weng, Joan M. Redwing, K. Sarpatwari, Suzanne E. Mohny, Holger von Wenckstern, and Marius Grundmann, IEEE Transaction on Electron Devices **56**, 2160-2164 (2009).

8.11 Dielectric passivation of ZnO-based Schottky Diodes

H. von Wenckstern, S. Müller, H. Hochmuth, M. Lorenz, M. Grundmann

Surface conduction of ZnO is a long-known phenomenon. Electron accumulation layers can be created on a clean Zn-polar surface by heat treatment at temperatures around

370 K [1]. The formation of an electron accumulation layer depends besides temperature on the ambient. Measurements of the electric properties of ZnO single crystals at elevated temperatures in ambient air reveal the semiconducting, bulk properties of the single crystal whereas measurements at the same temperatures but in vacuum are dominated by a quasi-metallic near surface layer [2]. Recently, we have demonstrated the influence of vacuum-activated surface conduction on the performance of ZnO-based Schottky diodes and pointed out the necessity to passivate the ZnO surface, which is markedly important for the realization of stable devices integrating ZnO nanowires [3]. Here, we show how such vacuum-activated surface conduction, lowering the rectification of ZnO Schottky diodes, can efficiently be suppressed by dielectric passivation [4].

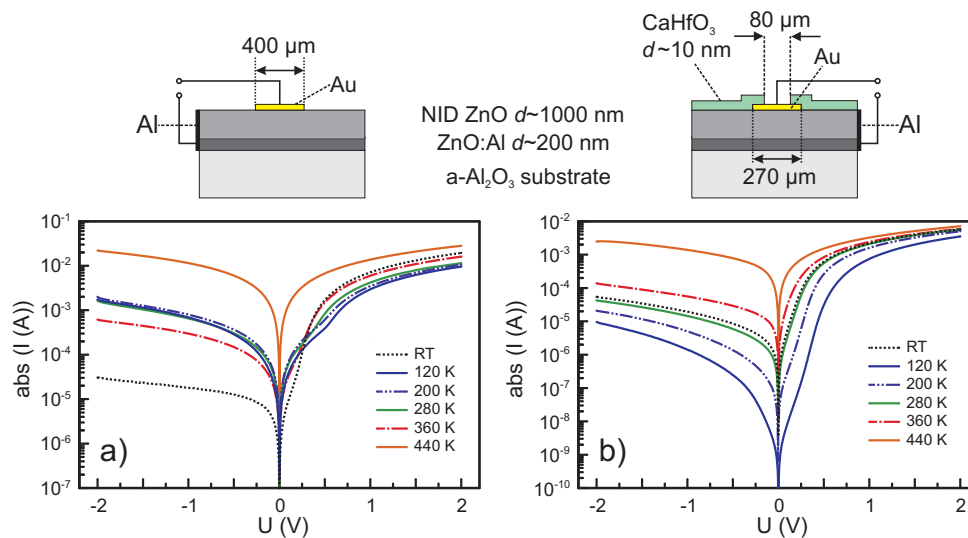


Figure 8.11: Schematic representation and $I - V$ characteristic at RT and in ambient air and at 10^{-4} mbar for selected temperatures of a) an unpassivated and b) a passivated Au/ZnO Schottky barrier diode.

Two ZnO thin films were grown by pulsed-laser deposition on *a*-plane sapphire substrates at 650°C at an oxygen background pressure of 0.016 mbar. First, a metallic conducting ZnO:Al layer having a nominal thickness of 200 nm was deposited. This layer serves as an Ohmic back-contact for the Schottky diodes on the insulating substrate [5]. Then a 1-μm-thick nominally undoped ZnO layer was grown. Circular Au Schottky diodes were deposited through a shadow mask using reactive DC sputtering. On one of the samples a CaHfO₃ layer was grown by PLD at room temperature (RT) and an oxygen pressure of 0.002 mbar for dielectric passivation; the center part of these contacts was not covered by the dielectric for bonding purpose. A schematic representation of the unpassivated and the passivated diodes is shown in fig. 1. Figure 1 further depicts current-voltage ($I - V$) characteristics of both diodes measured at RT in air and in the temperature range from 100 K to 450 K at a pressure of about 10^{-4} mbar. For the unpassivated diode (fig. 1 a) an unexpected behavior is observed: for each measurement performed at reduced pressure the reverse current is significantly higher than that acquired at RT in ambient air contradicting thermionic emission theory. The behavior is caused by a decrease of the diode's parallel resistance due to the creation of a vacuum-activated surface conduction path. A dielectric passivation effectively suppressed its formation which is evident from fig. 1 b). Here, the diode's reverse current

increases expectedly with increasing temperature. With that we have demonstrated a route to prevent vacuum-activated surface conduction of ZnO which is particularly important for structures with high surface-to-volume ratio such as micro- and nano-wires. Further, reliable ZnO-based outer space applications are possible through our approach of dielectric passivation.

- [1] G. Heiland and P. Kunstmann, *Surf. Sci.* **13**, 72 (1969).
- [2] O. Schmidt, A. Geis, P. Kiesel, C.G.V. de Walle, N.M. Johnson, A. Bakin, A. Waag, and G.H. Döhler, *Superlattices Microstruct.* **39**, 8 (2006).
- [3] M.W. Allen, S.M. Durbin, X. Weng, J.M. Redwing, S.E. Mohny, K. Sarpatwari, H. von Wenckstern and M. Grundmann, *IEEE Trans. Electron. Dev.* **56**, 2160 (2009).
- [4] H. von Wenckstern, S. Müller, G. Biehne, H. Hochmuth, M. Lorenz and M. Grundmann, *J. Electron. Mater.* **39**, 559 (2010).
- [5] H. von Wenckstern, G. Biehne, R.A. Rahman, H. Hochmuth, M. Lorenz and M. Grundmann, *Appl. Phys. Lett.* **88**, 092102 (2006).

8.12 Investigation of structural and electronic properties of $\text{Mg}_x\text{Zn}_{1-x}\text{O}$ thin films

K. Brachwitz, H. von Wenckstern, M. Schmidt, F. Schmidt, C.P. Dietrich, M. Stölzel, M. Lorenz, M. Grundmann

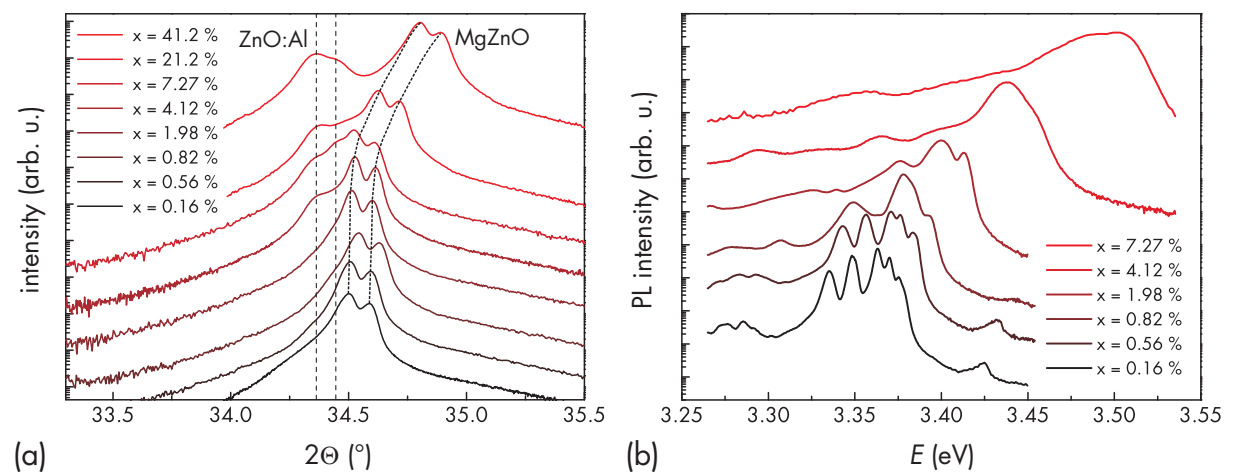


Figure 8.12: (a) $2\theta - \omega$ scan of the (0002)-reflex and (b) near band-edge PL-spectra of $\text{Mg}_x\text{Zn}_{1-x}\text{O}$ PLD thin films. The dashed lines of a) indicate the position of the reflex for the ZnO:Al and the $\text{Mg}_x\text{Zn}_{1-x}\text{O}$ layer, respectively, for the Cu $K_{\alpha 1}$ and the $K_{\alpha 2}$ transition.

$\text{Mg}_x\text{Zn}_{1-x}\text{O}$ thin films ($x=0\% - 40\%$) were grown by pulsed-laser deposition (PLD) and investigated by electrical methods like current-voltage (IV) and capacitance-voltage (CV) measurements. Defects in the samples were investigated by deep level transient spectroscopy (DLTS) and Laplace DLTS. Furthermore optical and structural properties were characterized by photoluminescence measurements (PL) and X-ray diffraction (XRD).

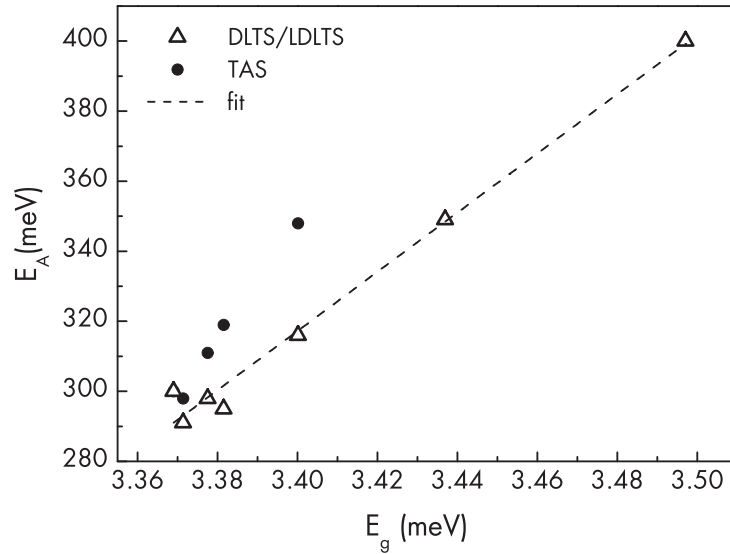


Figure 8.13: Activation energy of the E3 defect level in MgZnO versus band gap energy and linear regression of LDLTS/DLTS data.

Fig. 8.12 (a) shows the $2\theta - \omega$ scan of the (0002)-reflexes of ZnO:Al and $\text{Mg}_x\text{Zn}_{1-x}\text{O}$ for different Mg contents. The investigated $\text{Mg}_x\text{Zn}_{1-x}\text{O}$ thin films crystallize in wurtzite structure and the c-lattice constant decreases with increasing Mg content. After annealing the ZnO:Al (0002)-reflex diminishes and the MgZnO (0002)-reflex shifts to lower angles (not shown), indicating an interdiffusion of the ZnO:Al- and the $\text{Mg}_x\text{Zn}_{1-x}\text{O}$ -layer. For the thin film with $x = 40\%$ phase separation was found after annealing at 900°C . By means of PL measurements the recombination of donor-bound excitons was investigated for the different Mg contents (Fig. 8.12 (b)). For the lowest Mg content of $x = 0.16\%$ the near band-edge emission is similar to that of nominally undoped ZnO grown on a ZnO:Al buffer, however, it is shifted towards higher energies due to the increased band gap. For higher Mg-contents alloy broadening causes the individual recombination lines to overlap increasingly, such that the recombination lines cannot be resolved individually for $x \geq 0.82\%$. From the location of the PL maxima we deduced the band gap energy and from that the Mg content.

To investigate the MgZnO thin films by space-charge layer spectroscopy, high quality Schottky contacts are necessary. These contacts were realized by reactive DC-sputtering of palladium [1]. An Al-doped ZnO-layer was used as highly conductive ohmic back contact. Shallow and deep defects have been studied in the MgZnO thin films. The observed shallow defects are similar to known defects in ZnO [2]. The deep defect E3 was studied by DLTS and Laplace DLTS measurements. LDLTS is capable to separate defect states with similar emission rates, like the E3 and the E3' defect in ZnO [3]. Hence it was used to determine the thermal activation energy and the capture cross-section of the E3 defect state in dependence on x . We found that E3 activation energy increases with increasing x [4]. Assuming that the E3 defect level energy with respect to the vacuum energy level is independent of x , the ratio of conduction band shift to band gap increase was estimated to be 0.84. The E3' defect level vanishes for $x > 0.56\%$. Therefore it is not suitable to determine the conduction band shift.

- [1] A. Lajn *et al.*, J. Vac. Sci. Technol. B **27**, 1769 (2009)
- [2] F.D.Auret *et al.*, J. Phys. Conf. Ser. **100**, 042004 (2007)
- [3] F.D.Auret *et al.*, Phys. B **401**, 378 (2007)
- [4] H. von Wenckstern *et al.*, J. Electron. Mater. **39**, 584 (2010)

8.13 Defects in nitrogen-implanted ZnO thin film

M. Schmidt, M. Ellguth, F. Schmidt, H. von Wenckstern, R. Pickenhain, M. Grundmann, G. Brauer*, W. Skorupa*

*Forschungszentrum Dresden-Rossendorf, PF510119 D-01314 Dresden, Germany

Despite the enormous efforts made in the last thirty years, p - doping of the wide band gap semiconductor zinc oxide (ZnO) is still a challenge. Nitrogen on oxygen lattice site (N_O) is often dealt as the most promising acceptor. Several groups gave experimental proofs that p - type conducting ZnO can be achieved by nitrogen doping [1–3] but up to now the reproducibility and stability of the p - type conduction as well as the control of the hole concentration are poor. The binding energy of the nitrogen related acceptor was estimated to 165 meV [4], 177 meV [5], and 195 meV [6], respectively, from donor -acceptor-pair transitions observed in low temperature photoluminescence spectra. From temperature-dependent Hall effect measurements a thermal activation energy of about 100 meV was deduced [1]. Contrary to that, Lyons, Janotti, and van de Walle [7] recently published first principle calculations showing, that nitrogen is a deep acceptor and should therefore not lead to p - type ZnO. Another first principles investigation on complexes of N_O with intrinsic defects by Lee *et al.* revealed, that each of the five considered nitrogen related complexes is a donor [8]. In order to shed some more light into the properties of nitrogen and related defects we set out to provide experimental data on defects generated by the implantation of nitrogen ions into ZnO thin films [9].

Four ZnO thin films grown pulsed laser deposition were investigated: a nitrogen implanted and, in order to minimize implantation damage, thermally annealed sample, an as grown reference, a merely annealed reference, and an oxygen implanted and thermally annealed sample. The oxygen implanted sample was chosen, since mass and ionic radius of oxygen and nitrogen are almost equal and therefore a similar lattice damage caused by the ion implantation can be expected. In preparation of the capacitance spectroscopic methods used for the defect studies, Pd Schottky contacts were evaporated onto the samples. The structure of the samples is schematically depicted in figure 8.14 (a1,a2).

The net doping concentration of the samples was determined by capacitance - voltage spectroscopy. In the as- grown sample it amounts to approx. 10^{16} cm^{-3} , while it was increased by a factor of four in the merely annealed sample and a factor of twelve in the oxygen implanted and annealed one. Contrary to that a highly compensated region which correlates well with the calculated [10] implantation profile was found in the nitrogen implanted sample. Defects in the upper third of the ZnO band gap were investigated by deep level transient spectroscopy (DLTS). While the commonly observed E3 trap [11] was present in every sample, an up to now undescribed trap TN1

[9] was found solely in the nitrogen implanted sample (figure 8.14 (d)). From Arrhenius analysis its thermal activation energy was determined to 580 ± 20 meV and the apparent capture cross-section amounts to approx. 2×10^{-15} cm².

Due to their low thermal electron emission rates at experimentally accessible temperatures and the absence of holes, the investigation of midgap states and hole traps is more involved. Optical emission of trapped charge carriers from these levels was observed by photocapacitance, photocurrent, and optical deep level transient spectroscopy. Only in the nitrogen implanted sample two hole traps in high concentration were observed by these measurements (figure 8.14 (c)). Their electronic states are approx. 60 meV and 100 meV above the valence band edge, respectively.

From our investigations it is evident, that nitrogen in ZnO can form acceptor states approx. 100 meV above the valence band, which is in good agreement with previously published experimental data [1, 4, 5], and does not support the calculations of Lyons *et al.* [7]. Furthermore the formation of the TN1 trap approx. 580 meV below the conduction band edge supports the results of Lee *et al.* [8] on the formation of donor-like defect complexes including nitrogen. For future ZnO-based devices this might be bad news. If TN1 is a recombination center, the efficiency of light emitting diodes and lasers might be drastically decreased by such defects.

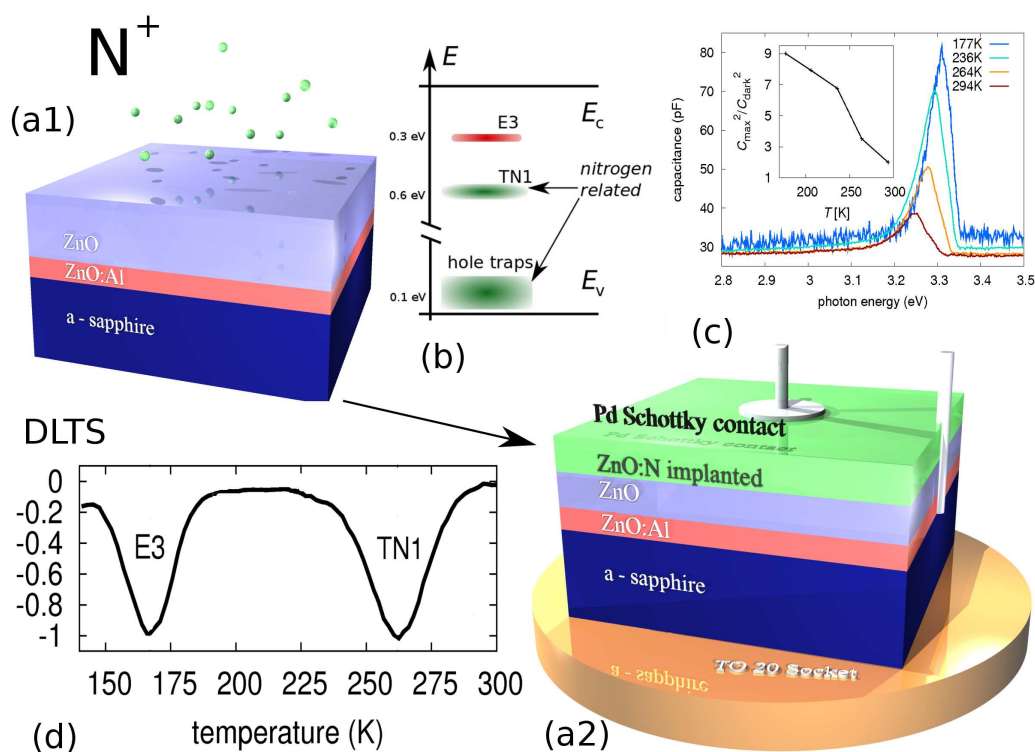


Figure 8.14: Schematics of the nitrogen implanted and thermally annealed sample (a1,a2). Scaled diagram of the energetic position of deep levels (b) as obtained from photocurrent, photocapacitance (c) and DLTS (d).

[1] A. Tsukazaki *et al.*, *Nat. Mater.* **4**, 42 – 46 (2005)

[2] H. v. Wenckstern *et al.*, *Appl. Phys. Lett.* **89**, 092122 (2006)

[3] Q.L. Gu *et al.*, *Appl. Phys. Lett.* **92**, 222109 (2008)

- [4] A. Zeuner et al., Phys. Stat. Sol. (b) **234**, R7 – R9 (2002)
- [5] G. Xiong et al., Jour. Appl. Phys. **97**, 043528 (2005)
- [6] K. Thonke et al., Physica B **308 – 310**, 945 (2001)
- [7] J.L. Lyons et al., Appl. Phys. Lett. **95**, 252105 (2009)
- [8] E.C. Lee et al., Phys. Rev. B **64**, 085120 (2001)
- [9] M. Schmidt et al., phys. stat. sol. (b) **247**, 1220 (2010)
- [10] www.srim.org
- [11] F.D. Auret, Superlatt. Microstruct. **39**, 17 (2006)

8.14 Space-charge regions in ZnO-based metal-semiconductor-metal photodetectors

Z. P. Zhang, L. Behnke*, C. Czekalla†, M. Schmidt, G. Biehne, H. Hochmuth, H. von Wenckstern, M. Grundmann

*present address: Max-Planck-Institut für Mikrostrukturphysik, Halle, Germany

†present address: AIXTRON AG, Herzogenrath, Germany

The extension of the space-charge region (SCR) and lateral homogeneity of the Schottky barrier potential of reactively sputtered, interdigital, Pd-capped PdO_y/ZnO Schottky contacts (SCs) have been studied by current-voltage (*IV*) and light beam induced current (LBIC) measurements on high-quality ZnO-based metal-semiconductor-metal photodetectors (MSM-PDs) [1]. We probed the generated photocurrent between the electrodes for varying external biases using the LBIC method, which enabled us to characterize the shape of the SCR and the lateral homogeneity of the carrier generation in the samples. Further, the photon energy selectivity and bandwidth of visible-blind MSM-PDs based on Mg_{x₁}Zn_{1-x₁}O/Mg_{x₂}Zn_{1-x₂}O-heterostructures ($x_1 < x_2$) was demonstrated by using spectrally resolved photocurrent measurements.

The MSM-PDs were fabricated on nominally undoped ($N_D \sim 10^{16} \text{ cm}^{-3}$) ZnO thin films grown by pulsed-laser deposition on a-plane sapphire substrates. The growth temperature and oxygen background pressure were 650°C and 0.016 mbar, respectively. The thickness of the films is about 2 μm. The interdigital PdO_y-electrodes were realized by photolithography and reactive dc sputtering of Pd in an argon/oxygen-atmosphere. Subsequently, a metallic Pd capping layer was sputtered in pure argon.

Fig. 8.15 (a) and (b) show LBIC maps recorded using an external voltage $V_{\text{ext}} = \pm 2 \text{ V}$. Fig. 8.15 (c) and (d) depict LBIC line scans for biases ranging from $V_{\text{ext}} = -4.0 \text{ V}$ to 4.0 V along the center part (dashed line) of (a) and (b).

The lateral extension of the SCR and lateral variations of the photosensitivity were determined. From the comparison of Fig. 8.15 (a) and (b) it clear that the photocurrent is generated in the vicinity of the negatively biased contact fingers. For negatively biased contacts the extension and the maximal electric field of the SCR increase resulting in a drastically increased photocurrent in comparison to the unbiased case. This unbiased case and the bias voltage dependence of photocurrent is depicted in the LBIC line scans of Fig. 8.15 (c) and (d). For zero bias the photocurrent generation is very similar for all seven electrodes that the MSM structure consists of. If an external voltage is applied the

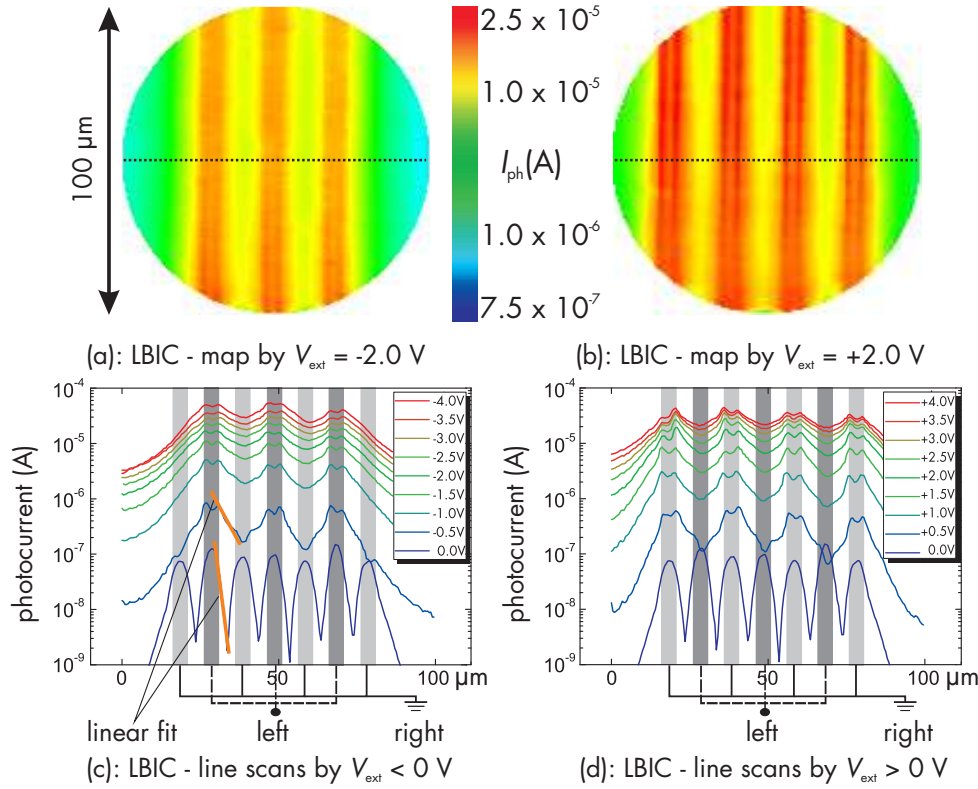


Figure 8.15: LBIC maps acquired using a bias of (a) -2 V and (b) 2 V and LBIC line scans for biases ranging from -4 V to 0 V (c) and from 0 V to 4 V (d). The orange lines indicate exponential fits by means of equ. 8.3. The line scans were recorded as indicated by the dashed lines indicated in (a) and (b).

photocurrent is predominately generated close to the negatively biased contact fingers as explained above. The decrease of the photocurrent I_{Ph} in dependence on the distance from an electrode shows exponential behavior

$$I_{\text{Ph}}(\Delta x) = I_{\text{Ph,max}}(V_{\text{ext}}) \exp(-\Delta x/L_T). \quad (8.3)$$

The orange lines in Fig. 8.15 (c) indicate fits to the data yielding the *characteristic transport length* L_T that increases with increasing reverse bias.

[1] H. von Wenckstern et al.: Mater. Res. Soc. Symp. Proc. Vol. 1201, H04-02 (2010)

8.15 Space-charge regions in ZnO-based Schottky diodes and metal-semiconductor field-effect transistors

Z. P. Zhang, M. Lorenz, C. Czekalla*, M. Schmidt, H. Frenzel, A. Lajn, H. Hochmuth, H. von Wenckstern, M. Grundmann

*present address: AIXTRON AG, Herzogenrath, Germany

Spatial variations of photocurrent generation and Schottky barrier potential of reactively sputtered PdO_y/ZnO Schottky contacts (SCs) have been investigated by light

beam induced current (LBIC) measurements on the μm -scale. These rectifying contacts were employed in photodiodes and further as gate of ZnO-based metal-semiconductor field-effect transistors (MESFETs). The spatial dependence of the generated photocurrent was studied using the LBIC method; it depends on the lateral extension of the space charge region (SCR), fluctuations of the Schottky barrier potential and externally applied electric fields. The ZnO thin films used for the Schottky diodes were grown

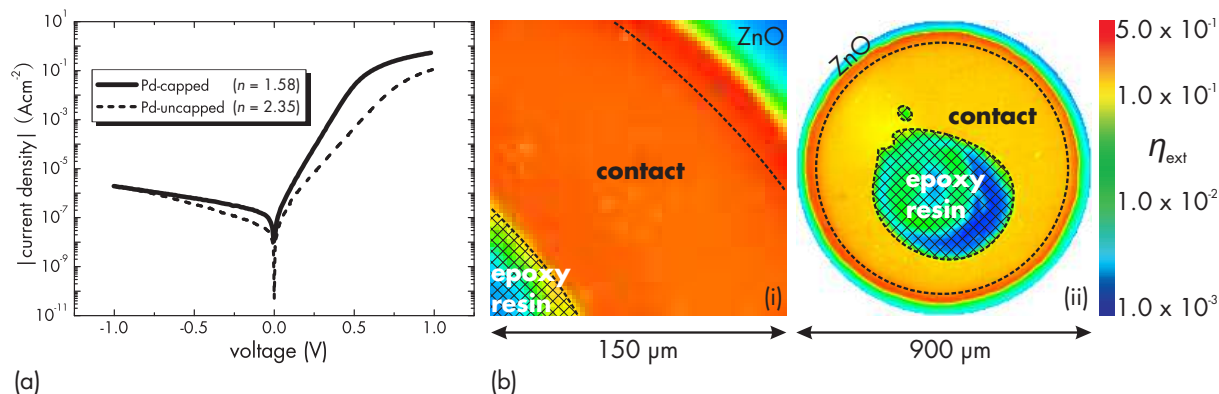


Figure 8.16: (a) IV -characteristic of the current density and (b) LBIC maps of the external quantum efficiency η_{ext} of an uncapped (i) and a capped (ii) reactively sputtered PdO_y/ZnO SC.

by pulsed-laser deposition (PLD) on a-plane sapphire. In case of the MESFET we used quartz glass as substrate.

The reactive sputtering of Ag, Pd or Pt results in partial oxidation of the deposited material. Therefore, a metallic capping layer is necessary to provide an equipotential surface [1]. We compared the properties of capped and uncapped PdO_y/ZnO SCs by means of current-voltage (IV)- and LBIC-measurements. Figure 8.16 depicts the IV -characteristic and the spatially resolved external quantum efficiency of an uncapped and a capped PdO_y/ZnO SC.

The IV -characteristic is improved for the capped PdO_y/ZnO SC, the ideality factor is with 1.6 much lower than that of 2.35 of the uncapped diode. This is obvious from the steeper slope for forward bias.

The LBIC maps of an uncapped and capped PdO_y/ZnO SC are depicted in Fig. 8.16 (b). A HeCd laser (325 nm) was used for excitation (100 kW/cm²). Its spot size is 1 μm^2 and determines the spatial resolution of the setup. The conductivity of the PdO_y-layer of the uncapped SC is sufficient to collect the photocurrent, also from the contact edges in contrast to uncapped Ag_xO/ZnO SCs exhibiting strong fluctuations of photocurrent signal among the contact area [1]. For the capped PdO_y/ZnO SC the photocurrent decreases from the contact edge towards the center following the increase in thickness of the Pd capping layer.

A normally-on ZnO-based MESFET on glass substrate with Pd-capped PdO_y gate contact (see the transfer characteristic in Fig. 8.17 (a)) has been investigated by LBIC. Compared to the SC in Fig. 8.16 (a) it has smaller rectification due to a lower barrier height.

LBIC line scans between the source and drain contact are shown for a *closed* (gate voltage of $V_G = -1.0$ V) and *open* ($V_G = 1.0$ V) channel for varying source-drain voltages V_D in Fig. 8.17 (b), respectively. The photocurrent is one order of magnitude

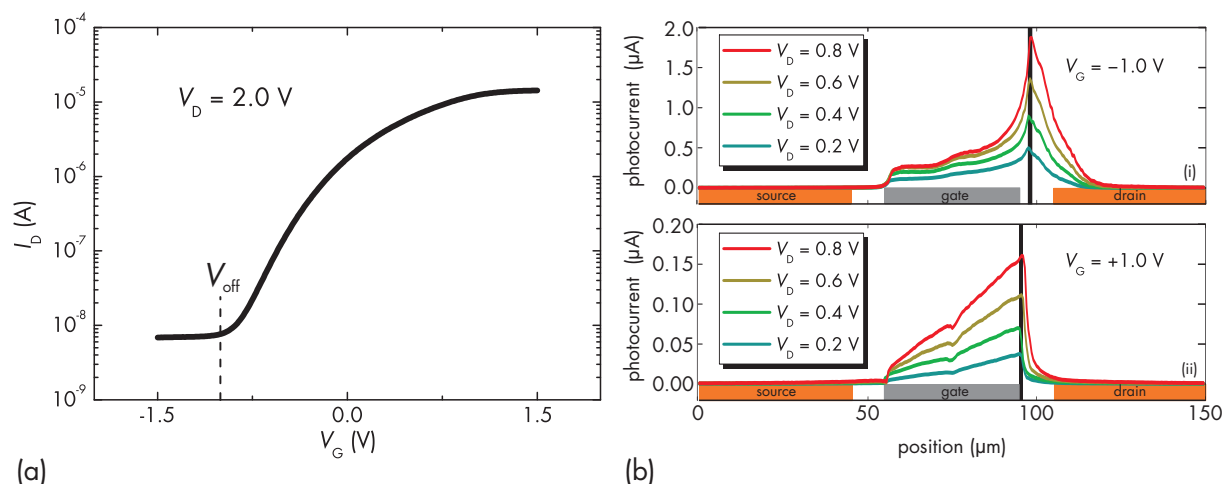


Figure 8.17: (a) Transfer of a MESFET with a Pd-capped PdO_y/ZnO SC as gate. (b) LBIC line scans along the channel with (i) $V_G = -1.0$ V and (ii) $V_G = 1.0$ V for different V_D . The thick lines represent positions of maximal photocurrent.

larger for closed channel conditions, for which the device acts as a phototransistor. For open channel condition the device behaves like a photoconductor. The position of maximum photocurrent for constant $V_G = -1.0$ V shifts expectedly towards the drain for higher V_D , whereas it is in principle independent of V_D for an open channel [2]. This behavior reflects once more that the device acts as photoconductor under open channel conditions, otherwise typical properties of a phototransistor are observed.

[1] A. Lajn et al.: J. Vac. Sci. Technol. B. **27**, 1769 (2009).

[2] H. von Wenckstern et al.: Mater. Res. Soc. Symp. Proc. Vol. 1201, H04-02 (2010).

8.16 Correlation of pre-breakdown sites and bulk defects in multicrystalline silicon solar cells

H. von Wenckstern*, D. Lausch*[†], K. Petter[†], M. Grundmann*,

*Universität Leipzig Institut für Experimentelle Physik II, Halbleiterphysik,
Linnéstraße 5, 04103 Leipzig, Germany

[†]Q-Cells SE, Process Development - Silicon Materials, OT Thalheim,
Guardianstraße 16, Bitterfeld-Wolfen, Germany

The photovoltaic (PV) market grew tremendously within the last years. Multicrystalline silicon (mc-Si) has the highest share at it, even though the share of thin film PV technology is rapidly increasing. One of the hot topics in current mc-Si solar cell research is their pre-breakdown limiting the number of cells to be used in a string of a PV module. Pre-breakdown in mc-Si solar cells occurs locally. Different origins and mechanisms of pre-breakdown exist and for some of them electroluminescence (EL) can be observed under reverse bias at the site of pre-breakdown. This fact has been used to classify different types of pre-breakdown according to their breakdown voltage. The process resulting in the highest heat dissipation shows a hard breakdown occurring for

reverse voltages of about 12.5 V. It was speculated that electric field enhancement at etch pits, which are introduced in the vicinity of extended defects by the commonly used acidic texturing, is the prime cause of local breakdown [1]. We showed that the position of pre-breakdown is independent of the texturing of the solar cells [2].

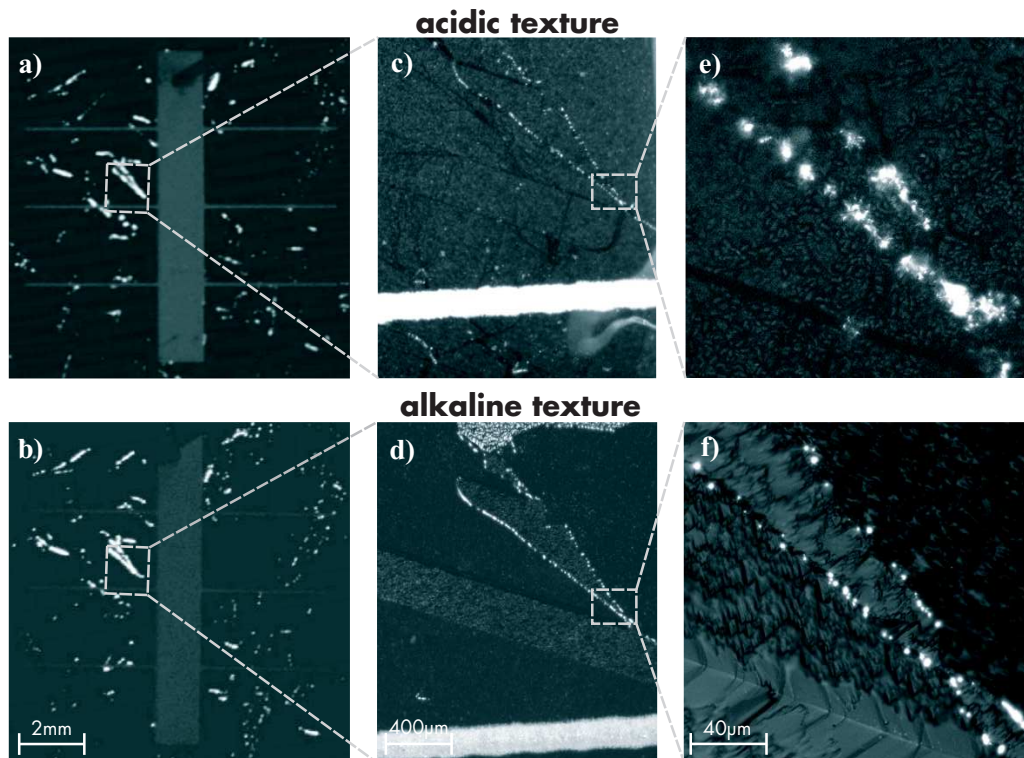


Figure 8.18: μ -ReBEL images of an acidic (a,c,e) ($U = -13$ V) and an alkaline (b,d,f) ($U = -17$ V) texturised solar cell processed from a neighboring wafer for different magnifications. Areas in grey boxes are depicted with higher magnification right beside the respective picture.

We analyzed silicon solar cells fabricated by the same commercial process, except for the texturing. For the process we used neighboring (in relation to the block from which they were cut) boron doped mc-Si wafers. The usage of neighboring wafers ensures that the position of extended bulk defects such as dislocations or grain boundaries is similar. Slight differences are caused by the unavoidable kerf loss of about $200 \mu\text{m}$ during the sawing process and the wafer thickness of $200 \mu\text{m}$. Figure 8.18 depicts spectrally integrated, spatially resolved EL images of reverse-biased neighboring but differently texturised solar cells in three different magnifications (μ -ReBEL). Especially the images of higher magnification show that positions of high EL intensity (corresponding to positions of local breakdown) are located at grain boundaries and in principle coincide for the different texturing. Small difference are due to the kerf loss and wafer thickness as discussed above. This is a striking evidence that the texturing does not determine the positions of pre-breakdown since those were the same for the acidic and the alkaline texturing. It is the defect structure of the bulk that causes local breakdown. However, the texturing influences the voltage of pre-breakdown which is higher for alkaline texturised solar cells.

In summary we have demonstrated that spectrally integrated measurements of EL with high spatial resolution (μ -ReBEL) provides a powerful method to study positions

of pre-breakdown of mc-Si solar cells. It was used to show that, in contrast to current literature, the positions of pre-breakdown are determined by the defect structure of the bulk; field-enhancement at etch pits probably causes lower pre-breakdown voltages for the acidic texturised solar cells but is not causing local breakdown by itself.

- [1] J. Bauer, J.-M. Wagner, A. Lotnyk, H. Blumtritt, B. Lim, J. Schmidt and O. Breitenstein, *phys. stat. sol. (RRL)* **3**, 40, (2009).
 [2] D. Lausch, K. Petter, H. von Wenckstern and M. Grundmann, *phys. stat. sol. (RRL)* **3**, 70 (2009).

8.17 Influence of the incorporation of sodium on electrical properties of flexible Cu(In,Ga)Se₂ solar cells

S. Puttnins*[†], F. Daume*[†], H. Zachmann[†], A. Rahm[†], M. Grundmann*

*Universität Leipzig Institut für Experimentelle Physik II, Halbleiterphysik,
 Linnéstraße 5, 04103 Leipzig, Germany

[†]Solarion AG, Ostende 5, 04288 Leipzig, Germany

Thin film solar cells based on Cu(In,Ga)Se₂ (CIGSe) absorbers can be deposited on flexible substrates such as metal or plastic foils hence making new innovative applications and a fabrication in continuous roll-to-roll production lines feasible.

We investigated the influence of sodium on the electrical properties of flexible CIGSe solar cells on polyimide foil produced at Solarion AG. Efficiencies up to 14.1 % (with anti reflection coating) were demonstrated for Solarion cells containing sodium. Since Solarion AG uses sodium free flexible substrates the extrinsic incorporation of sodium into the CIGSe solar cells is indispensable to achieve high efficiencies. Despite its significance there is no comprehensive understanding of how sodium exactly influences the electrical and structural properties of CIGSe yet.

For higher sodium content capacitance spectroscopy shows an increased net doping concentration along with a decreased width of the space charge region; open circuit voltage (V_{OC}) and fillfactor increase while the short circuit current decreases [1].

IV curves of thin film solar cells sometimes show a roll over effect, i.e. a change of curvature and a (partial) current saturation for voltages above V_{OC} . The dependency of this effect on the sodium content is shown in fig 8.19. Fig 8.19a depicts the fraction of cells showing a roll over at standard test conditions (STC, AM 1.5, 25°C) versus the temperature T_{Na} of the sodium evaporator (with higher evaporation temperature more sodium is supplied and deposited during the deposition of the CIGSe absorber). The occurrence probability of the roll over effect decreases with higher sodium content, for evaporation source temperatures above 750 °C no roll over effect was measured at STC.

In figures 8.19b-8.19d the temperature dependence of the roll over effect is shown. With decreasing temperature the influence of the roll over effect increases. This means that the current saturation starts at lower currents and the slope of the partial saturation is lower (in terms of equivalent circuits the roll over shunt resistance is higher).

Samples with low sodium content (fig 8.19b) show the roll over effect at room temperature, samples with medium sodium content show the roll over effect for temperatures lower than about 200 K (fig 8.19c) and for samples with high sodium content

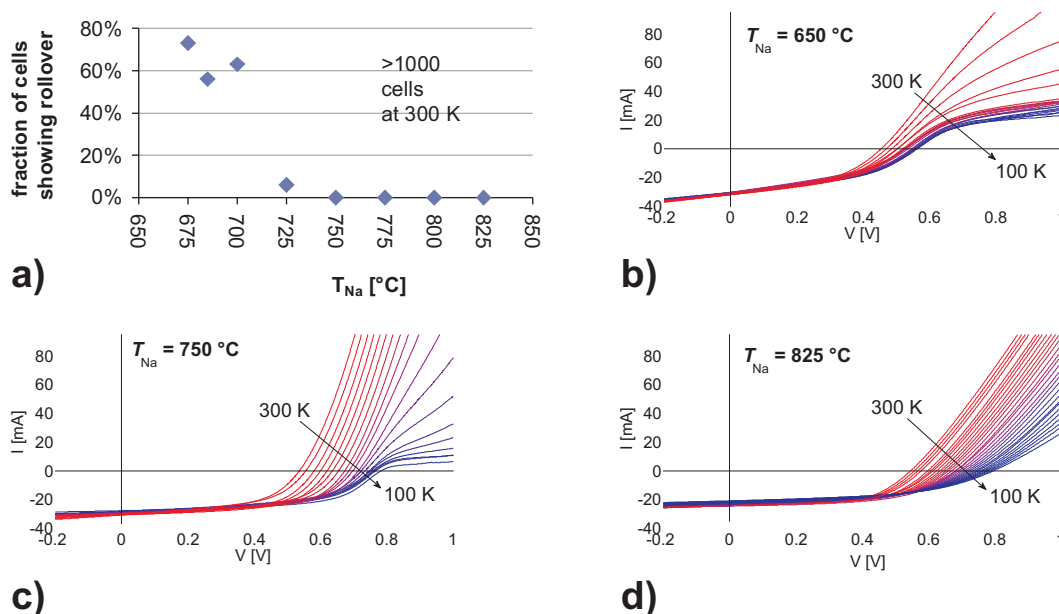


Figure 8.19: Influence of temperature and sodium content on the roll over effect.

no roll over effect was measured in the investigated temperature range of 300 K to 100 K (fig 8.19d). With decreasing temperature the influence of the roll over effect on the IV curve increases and with increasing sodium content this influence starts at lower temperatures.

This dependency can be reproduced by numerical simulations in SCAPS [2] by assuming a second diode oppositely wired and serially connected to the pn-junction. The model is based on the assumption of a non-ohmic back contact and an increase of net doping concentration with higher sodium content. The latter was shown in our capacitance spectroscopy measurements.

- [1] H. Zachmann, S. Puttnins, F. Daume, A. Rahm, K. Otte, R. Caballero, C. A. Kaufmann, T. Eisenbarth and H.-W. Schock "Incorporation of Na in low-temperature deposition of CIGS flexible solar cells" MRS Fall Meeting Boston (Symposium Q), in press.
- [2] M. Burgelman, P. Nollet and S. Degraeve, "Modelling polycrystalline semiconductor solar cells", *Thin Solid Films*, 361-362, 527-532 (2000).

8.18 Polarization behaviour of the exciton-polariton emission in ZnO-based microresonators

C. Sturm, H. Hilmer, R. Schmidt-Grund, M. Grundmann

The strong light-matter coupling (exciton-polaritons) in microresonators is of special interest due to the possibility to form a Bose-Einstein condensate (BEC) at elevated temperatures [1]. ZnO-based microresonators are promising candidates for the realization of a BEC above room temperature because they reveal the strong coupling regime up

to 410 K [2]. We report on properties of the polariton population which knowledge is essential in order to reach a massive occupation of the ground state.

The exciton-polaritons were observed by photoluminescence measurements in a ZnO-based resonator in the temperature range (10–290) K. The microresonator consists of a wedge-shaped $\lambda/2$ -ZnO cavity embedded between two Bragg reflectors (BR) made of 10.5 layer pairs of yttria stabilized zirconia and Al_2O_3 each (c.f. Sec. 8.19). The detuning Δ of the resonator, i.e. the energetic separation between the cavity and electronic modes, was changed on the one hand by temperature variation of the exciton energy and on the other hand by variation of the cavity mode energy, due to the wedge-shaped cavity, by varying the lateral position on the sample.

The dispersion behavior of the lower polariton branch at a temperature of 10 K is shown in Fig. 8.20a for $\Delta \approx -70$ meV. Due to the polarization dependence of the uncoupled cavity mode we observe a large energy splitting of about 6 meV for the emission polarized perpendicular (s) and parallel (p) to the plane of detection. Besides the different dispersion of the LPB for the two polarizations we found a different polariton occupation behavior. In contrast to the s-polarization, the p-polarization shows a strong bottleneck effect which reflects a large polariton population. With increasing Δ this bottleneck effect gets smaller and vanishes at large positive Δ (Fig. 8.20c). Furthermore the difference between the two polarizations vanishes. These two effects can be explained by the fact that with increasing Δ the photonic fraction on the LPB decreases whereas the excitonic one increases which leads to an enhancement of the polariton-polariton scattering rate (Fig. 8.20d). By increasing the temperature we observe a similar effect which indicates that the scattering rate of hot polaritons into their ground state is enhanced by temperature, in agreement with theoretical predictions [3]. From these results we conclude that positive detuning and elevated temperatures should be preferred in order to achieve a strong occupation of exciton-polaritons at the ground state.

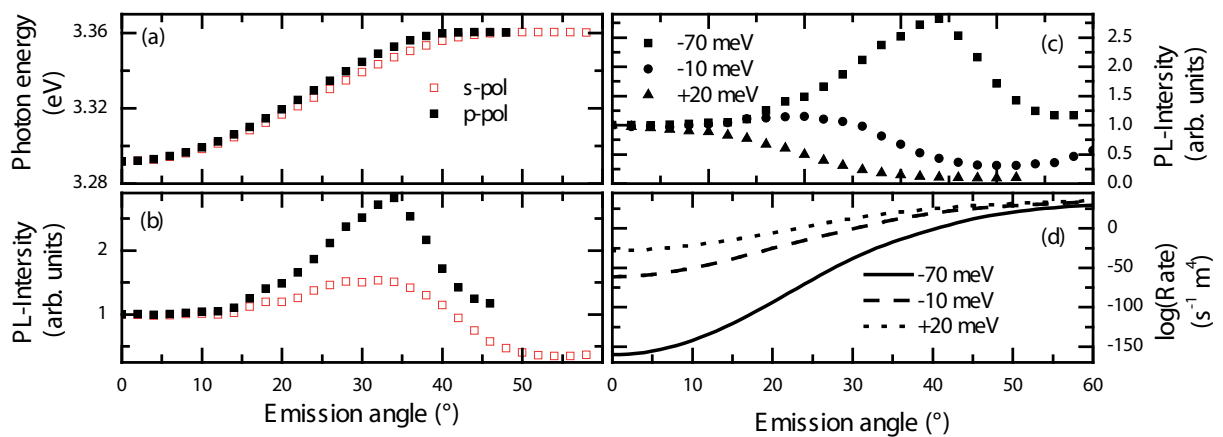


Figure 8.20: (a) Dispersion of the LPB at a temperature of 10 K and $\Delta = -70$ meV for the two polarizations. (b) The corresponding behaviour of the photoluminescence intensity. (c) Photoluminescence intensity of the p-polarized emission for different Δ . (d) The calculated scattering rate into the LPB according the approach by Porras *et al.*[4]

[1] J. Kasprzak *et al.*: Nature **443**, 409 (2006).

[2] C. Sturm *et al.*: New. J. Phys. **11**, 073044 (2009).

[3] F. Tassone and Y. Yamamoto: Phys. Rev. B **59**, 10830 (1999).

[4] D. Porras et al.: Phys. Rev. B **66**, 08304 (1999).

8.19 Growth of ZnO-cavities for planar microresonators

H. Hilmer, C. Sturm, R. Schmidt-Grund, J. Zúñiga-Pérez, H. Hochmuth, M. Cornejo*, F. Frost*, M. Grundmann

*Leibniz-Institut für Oberflächenmodifizierung e. V., Permoserstr. 15, 04318 Leipzig

We report on the growth of planar microresonators by pulsed laser deposition (PLD), which consist of two all-oxide Bragg reflectors (BR), made of yttria stabilized zirconia (YSZ) and alumina (Al_2O_3), surrounding a ZnO-cavity as active medium. The substrate temperature during growth was chosen to be about 650 °C and oxygen pressures in the range of 0.002 mbar to 0.02 mbar were applied. The cavity layer was grown at about 150 °C leading to an rms roughness of 1.8 nm, then covered with (YSZ) and subsequently annealed. This cavity was designed as a wedge-shaped layer in order to be able to study the exciton-photon coupling in dependence on the detuning by varying the spot position on the sample (c.f. Sec. 8.18) [1]. Still, the surface roughness and inhomogeneities of the cavity layer have to be improved. For this purpose, two different strategies have been pursued:

On the one hand, the cavity has been deposited by means of molecular beam epitaxy (MBE) [2], a high-quality growth technique, on PLD-grown BR on Si substrates. These samples show intensive and narrow photoluminescence as is indicated by the spectra in Fig. 8.21a. However the sample surface is rougher ($R_q = 9.2$ nm) compared to PLD grown cavities (Fig. 8.21d and e), which is not very promising for application in microresonators.

On the other hand rough PLD-grown cavity layers, grown at 650 °C have been polished by ion beam (IB) bombardment with Ar^+ -ions [3]. Doing so, it is possible to considerably reduce the rms roughness from 8.2 nm for the virgin sample down to only 1.5 nm after the ion beam smoothing (Fig. 8.21f). Figure 8.21b shows the PL spectra of the untreated sample, where clearly the free exciton emission is visible, but which is dominated by the donor bound exciton emission. After the IB treatment (Fig. 8.21c), the free exciton vanishes, but the donor bound exciton emission is increased by a factor of 2-3; the reason for that puzzling fact may be the increase of the density of defects in the layer but has to be further investigated.

[1] C. Sturm et al.: New. J. Phys. **11**, 073044 (2009).

[2] F. Médard et al.: Phys. Rev. B **79**, 125 302 (2009).

[3] F. Frost et al.: J. Phys.: Condens. Matter **21**, 224 026 (2009).

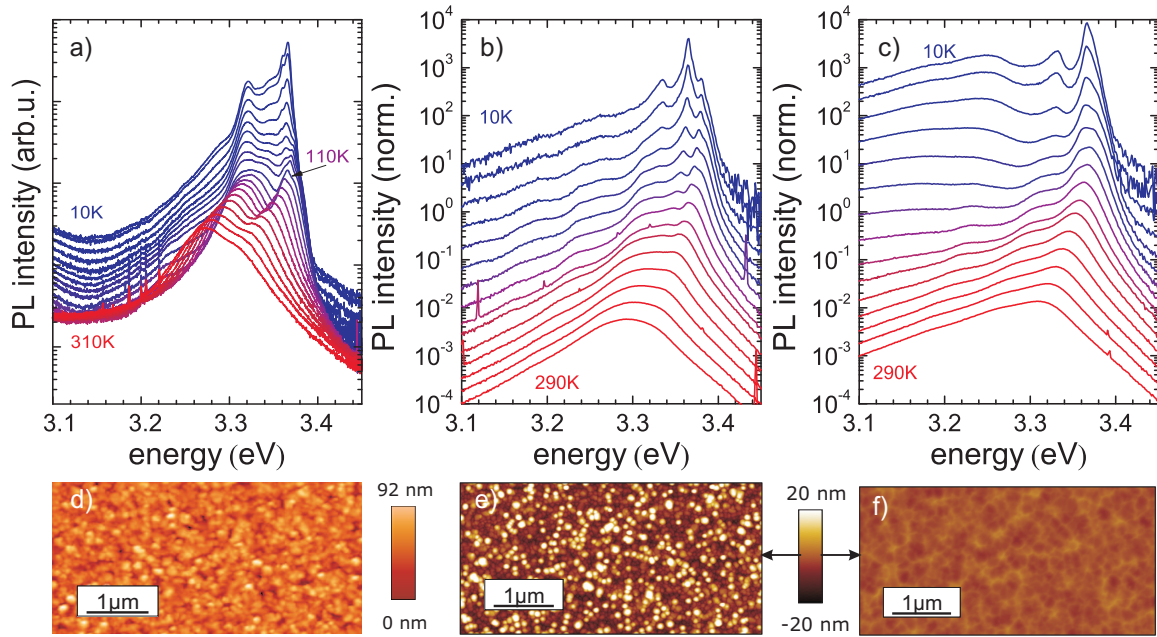


Figure 8.21: Photoluminescence spectra of ZnO-cavities grown on dielectric BR by MBE (a), by PLD (b) and by PLD with consequent ion beam smoothing (c) and their corresponding AFM images (d–f).

8.20 2D and 3D confined ZnO-nanopillar resonators

R. Schmidt-Grund, H. Hilmer, A. Meißner, J. Zúñiga-Pérez, C. Sturm, M. Lange, and M. Grundmann

We report on photonic-wire (PWR) and -dot (PDR) resonators consisting of self-organized grown ZnO nanopillars as cavity which are conformally coated with high reflective Bragg reflector (BR) shells as mirrors. The electromagnetic field is confined to a very small volume in such optical nanopillar resonators. This leads, compared to conventional planar microresonators, to a very high coupling strength to an electronic excitation and, depending on the dimensionality of the confinement and the size of the system, to a multitude of resonator modes. We could confirm this prediction by means of angularly and spatially resolved photoluminescence and reflectivity measurements.

The low area density arranged ZnO-nanopillars with diameters in the range (50–700) nm and with a length in the range of (5–10) μm [1] and the BR materials [2] have been fabricated by using three-step pulsed laser deposition in the high- and low-pressure regime, respectively. The ZnO-pillar cavities, which act simultaneously as active medium, are coated with concentric cylindrical shell BR consisting of 10.5 pairs of the materials YSZ (yttria stabilized zirconia) and Al_2O_3 [2].

The BR shells now provide an efficient confinement of the electromagnetic wave propagating perpendicularly to the pillar axis. For long pillars, the waves which propagate in the direction of the wire axis are not confined and therefore these resonators are two-dimensional confined PWR. From the thickness (Fig. 8.22a,b) and temperature (Fig. 8.22c,d) evolution of the observed resonator modes we have found very strong hints for the resonators to be in the regime of strong light-matter coupling (cavity exciton-polaritons) and we can estimate a coupling strength of about 80 meV [2], which

exceeds that found for the best developed planar counterparts considerably [3], reflecting the enhancement of the exciton-polariton coupling strength due to the reduction of the mode volume in such PWR. For pillars whose length is below approximately $5\ \mu\text{m}$, the coating of the end-faces comes into play and the confinement is three-dimensional, so called PDR, which we could confirm from the mode dispersion which is flat for this case and, compared to the PWR, the considerably enhanced amount of modes observable (Fig. 8.23). By mode analysis, the strong coupling regime for the 3D confined modes could not be clearly confirmed.

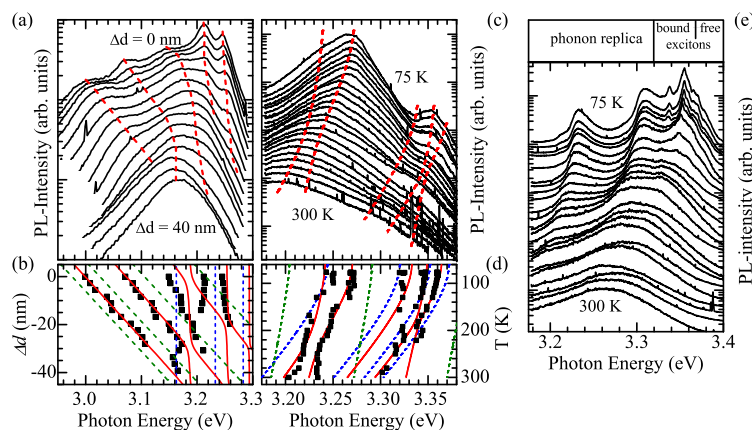


Figure 8.22: (a-d): PL spectra of PWRs as a function of (a) the thickness Δd at 300 K and (c) the temperature. The most prominent resonator modes are indicated by red lines. In (b) and (d), these modes are plotted as symbols along with the calculated exciton-polariton branches (red lines) and the uncoupled cavity (green) and excitonic (blue) modes. (e): PL spectra as a function of the temperature of a non-coated ZnO-nanopillar.

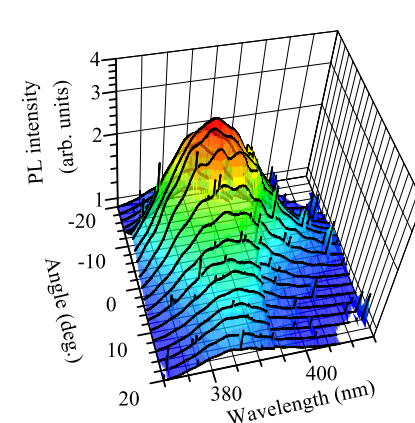


Figure 8.23: PL spectra of a PDR as a function of the emission angle (dispersion) at 300 K. The peaks indicate 3D confined resonator modes.

[1] B.Q. Cao et al.: *Nanotech.* **20**, 305701 (2009).

[2] R. Schmidt-Grund et al.: *phys. stat. sol. b* **247**, 1351 (2010).

[3] C. Sturm et al.: *New J. Phys.* **11**, 073044 (2009).

8.21 Growth and characterization of MgZnO nanowires

M. Lange, C.P. Dietrich, C. Czekalla, J. Zúñiga-Pérez, M. Lorenz, M. Grundmann

For optoelectronic ZnO based nanowire heterostructure (NW-HS) devices, bandgap engineering of ZnO is necessary. Alloys of ZnO with Mg or Cd are in focus, as they allow an increase or decrease of the bandgap. $\text{Mg}_x\text{Zn}_{1-x}\text{O}$ nanowires (NW) can be used to realize NW-HS being the core structure and inner barrier, which can be coated with ZnO quantum wells and $\text{Mg}_x\text{Zn}_{1-x}\text{O}$ outer barriers. A low area density of the NWs on the substrate is necessary to obtain a controlled and uniform coating.

Freestanding $\text{Mg}_x\text{Zn}_{1-x}\text{O}$ NWs with a hexagonal cross section and a pyramidal base have been grown by high-pressure pulsed laser deposition. Lengths up to $10\ \mu\text{m}$ were

achieved with diameters ranging from 50 nm to several 100 nm. A variation of the NW density was possible due to the use of a ZnO template-layer. For low Mg-contents the NWs show a high-quality morphology comparable to ZnO NWs, but NWs with more Mg incorporated show less optimal morphology (Fig. 8.24B,C). In order to characterize the luminescence properties and determine the composition, cathodoluminescence measurements were performed at temperatures of ~ 10 K (Fig. 8.24A,D). Different peaks in the spectra can be attributed to $\text{Mg}_x\text{Zn}_{1-x}\text{O}$, as they are energetically above the ZnO luminescence. From the position of the luminescence maximum, the alloy composition was calculated [1]. Apparently the Mg content in the film is different compared to that of the NW.

The luminescence spectra of the NWs exhibit emission in two spectral ranges which implies the presence of regions with different alloy compositions in the NWs; one with low content up to 10% and another with up to $\sim 20\%$ (Fig. 8.24A,D). In general, NWs with a lower distance to the target show higher Mg-contents for both alloy compositions (see Fig. 8.24E). The use of $\text{Mg}_x\text{Zn}_{1-x}\text{O}$ NW-cores for NW-HS is at the moment not yet possible due to the presence of several alloy compositions and the low quantum confinement that can be obtained using the lowest Mg composition.

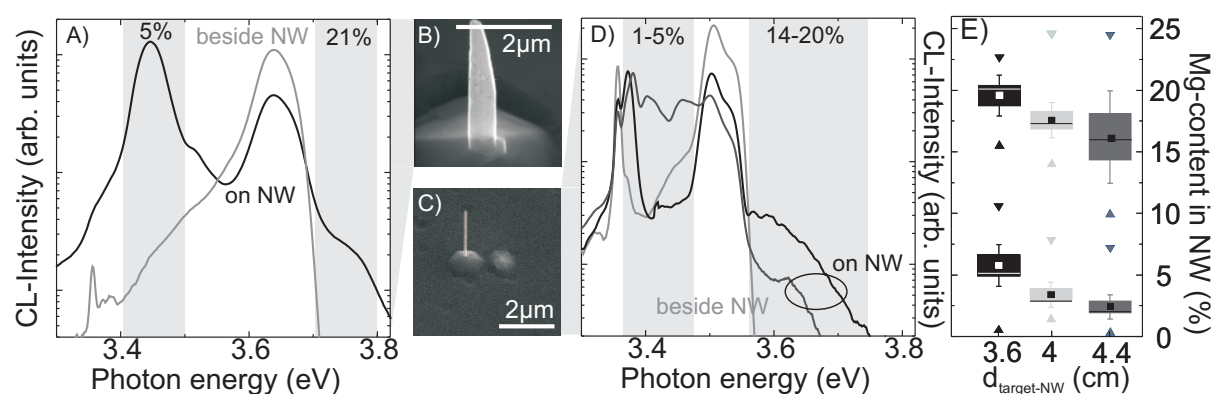


Figure 8.24: Cathodoluminescence spectra for two NWs grown under different conditions and measured at $T \sim 10$ K in (A,D) with respective scanning electron microscopy images in (B,C). The values in the highlighted bars give the composition. In (E) the statistics of the Mg-content as function of the distance between target and NW is plotted.

[1] A. Müller et al.: Solid State Commun. 148, 570 (2008)

8.22 Trap saturation in ZnO microwires observed by time-resolved photoluminescence

A. Müller, G. Benndorf, M. Grundmann

Time-resolved photoluminescence (TRPL) measurements have been performed on ZnO microwires (diameter ≈ 50 μm) grown by carbo-thermal evaporation. Due to the nearly strain-free growth process, the microwires exhibit a low defect concentration, leading to a very good crystalline quality.

As excitation source served a pulsed, frequency tripled titanium:sapphire laser ($\lambda_0 = 270 \text{ nm}$). At highest excitation, the resulting energy density of a single pulse is $10 \mu\text{J}/\text{cm}^2$, thus generating an initial carrier density of $n_{\text{exc}} = 3 \times 10^{18} \text{ cm}^{-3}$ (not taking into account reflection and scattering losses). Although this is well below the Mott density in ZnO ($1.7 \times 10^{20} \text{ cm}^{-3}$), strong nonlinear effects can be observed.

While for the lowest excitation intensity a nearly monoexponential luminescence decay was observed, a strongly nonexponential decay is visible for higher excitation powers (Fig. 8.25). The decay strongly slows down for increasing excitation intensities. At high excitation powers, the luminescence decay accelerates at large times after the excitation pulse. The observed behavior can be understood taking into account a saturated nonradiative center (density $n_{\text{tr}} \approx 1/3 n_{\text{exc}}$) with a fast capture ($\tau_{\text{cap},0} = 1.7 \text{ ns}$) and slow decay time ($\tau_{\text{nr}} \approx 300 \text{ ns}$). The luminescence decay can be numerically modeled by the following differential equation system

$$dn_{\text{exc}}/dt = -(\tau_{\text{rad}}^{-1} + \tau_{\text{cap}}^{-1}(t))n_{\text{exc}} \quad (8.4)$$

$$\tau_{\text{cap}}^{-1}(t) = \tau_{\text{cap},0}^{-1}(1 - n_{\text{tr},1}/n_{\text{tr}}) \quad (8.5)$$

$$dn_{\text{tr},1}/dt = n_{\text{exc}}/\tau_{\text{cap}}(t) - n_{\text{tr},1}/\tau_{\text{nr}}, \quad (8.6)$$

where $\tau_{\text{rad}} = 30 \text{ ns}$ is the radiative decay time and $n_{\text{tr},1}$ is the density of the occupied trap states. For high excitation powers, the τ_{cap} first increases as $n_{\text{tr},1} \approx n_{\text{tr}}$, leading to the slow luminescence decay, and then decreases again as the saturation drops down, resulting in the accelerated decay.

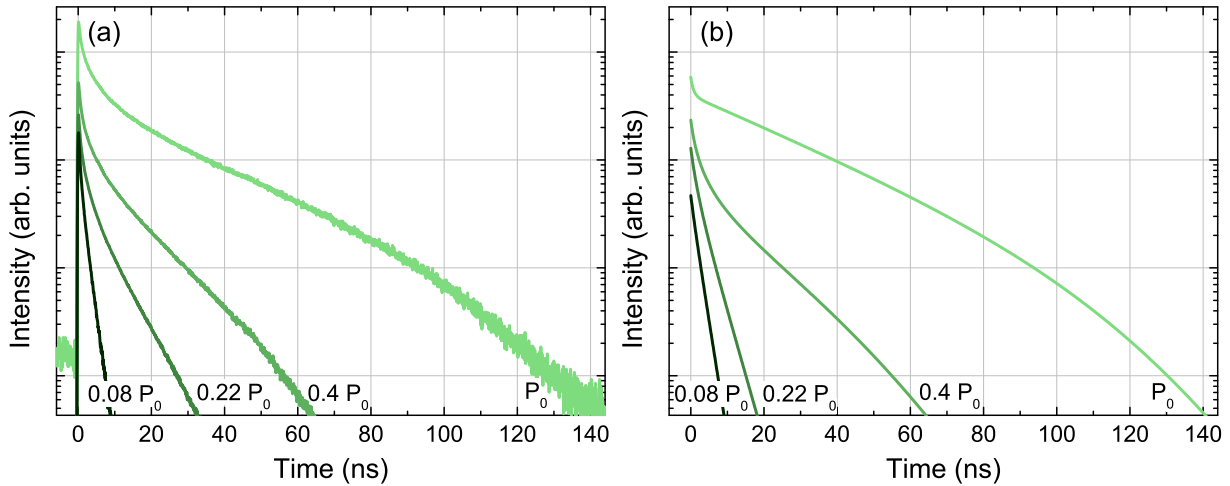


Figure 8.25: (a) Measured transients at the spectral emission maxima ($\lambda \approx 380 \text{ nm}$) of a bunch of ZnO microwires in dependence on excitation power. In (b), the modeled transients using the differential equations 8.4-8.6 are shown.

8.23 Lattice constants of PLD-grown $\text{Mg}_x\text{Zn}_{1-x}\text{O}$ thin films

C.P. Dietrich, H. Hochmuth, M. Grundmann

$\text{Mg}_x\text{Zn}_{1-x}\text{O}$ thin films were grown by pulsed-laser deposition (PLD) on $(11\bar{2}0)$ -oriented sapphire substrates and investigated using X-ray diffraction (XRD). The oxygen partial

pressure ($3 \times 10^{-4} - 1 \times 10^{-1}$ mbar) as well as the target composition (ZnO:MgO ratio between 1000:1 and 50:1) was varied in order to achieve Mg-contents $0 \leq x \leq 0.09$ and to alter the stoichiometry in the films. All thin films show the wurtzite structure c -axis perpendicular to the sample surface. The lattice parameters c in growth direction were precisely determined from the symmetric [0002]- and [0004]-Bragg reflexes using Braggs law and the correction function D3 according to Ref. [1]. The in-plane lattice constants a were derived from asymmetric [10 $\bar{1}$ 4]-reflexes without any correction.

For Mg-contents $x < 0.05$ the lattice parameter c increases with decreasing oxygen partial pressure, but decreases for $x > 0.05$ (Fig. 8.26a) and vice versa for the lattice constant a (Fig. 8.26b). In other words, the slope of the linear x -dependence of the lattice constants for the samples grown each with same target decreases (increases) for c (a). This finding can be explained as follows: The growth process, for constant target composition, is determined by the ionic radii and weights of the species as well as the growth pressure. High pressures cause an increase of the scattering angle for lighter species resulting in a lowered adsorption of these species on the substrate. Since oxygen has the lowest ionic weight but largest radius, its amount in the film determines the values of a and c primarily. Zinc and magnesium have similar radii but different weights, i.e. $M(\text{Zn}^{2+}) > M(\text{Mg}^{2+})$, thus high pressures always cause zinc-rich conditions and therefore low values of the c -axis length. As a second consequence, low pressure allows a more efficient incorporation of Mg ions into the crystal than high pressure which leads to a larger x variation as a function of the pressure for higher Mg content in the target (Fig. 8.26). Since the pressure-induced change of the lattice parameters is finite for finite pressure intervals, the composition-induced change is much larger the more Mg is involved and dominates above $x = 0.05$.

In summary, the lattice parameters for low Mg-contents are sensible functions of the amount of oxygen in the films which is influenced by the pressure in the growth chamber, whereas for higher Mg-contents the parameters a and c are more determined by the amount of MgO in the target.

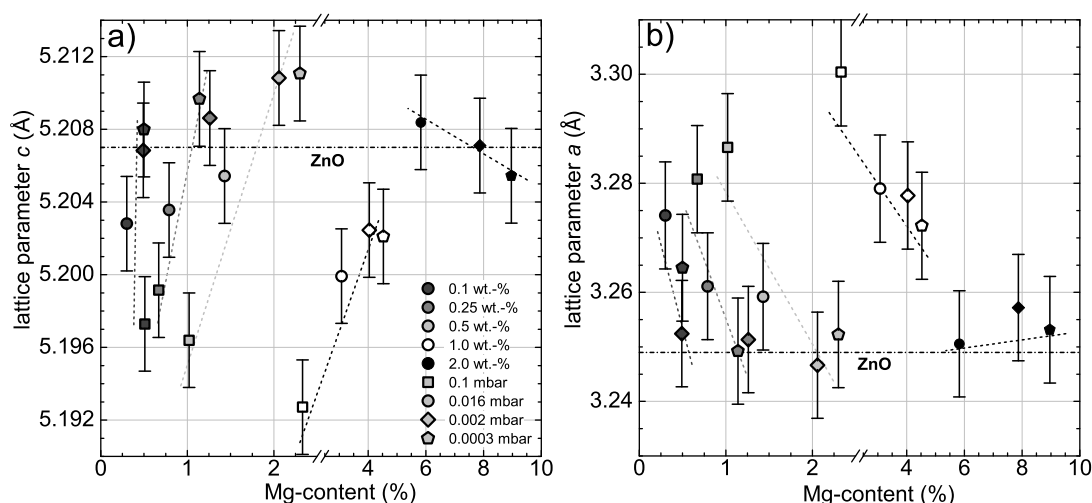


Figure 8.26: Lattice parameters c (a) and a (b) vs. Mg-content x for different oxygen partial pressures and target compositions. The dashed-dotted line represents the lattice values for bulk ZnO with $c = 5.207$ Å and $a = 3.249$ Å.

- [1] L. Spiess, R. Schwarzer, H. Behnken, and G. Teichert, *Moderne Röntgenbeugung*, 1. Auflage (Vieweg+Teubner Verlag, 2005).

8.24 Refractive index tensor of ZnO bulk and microwire single crystals

R. Schmidt-Grund, C. Czekalla, P. Kühne, C. Sturm, M. Grundmann

We present comparative spectroscopic ellipsometry (SE) investigations on high-quality ZnO bulk single crystals and photonic-mode-structure (whispering-gallery-modes, WGM) studies by means of spatially resolved photoluminescence (PL) measurements of ZnO single crystal microwires. By applying such complementary methods we can overcome the uncertainties in the determination of the bulk refractive index introduced by surface properties. The physical effects used are (a) the electromagnetic field reflection used by SE at large scale planar single crystals which is strongly influenced by the surface near region and (b) the whispering-gallery-mode (WGM) formation by total internal reflection in confined micro-structures whose propagation is mainly determined by the wire bulk. As for (a) the inversion of the experimentally data requires the consideration of a layer-stack model including unknown surface properties, in (b) the energetic position of WGMs yields directly (by knowing the geometrical dimensions of the structure) the refractive index of the material. The problem here is the assignment of the correct mode order and a typically restricted spectral range where WGMs can be observed.

We use (1) large scale $[1\bar{1}00]$ oriented ZnO bulk samples and (2) carbo-thermal grown hexagonally shaped ZnO microwires with diameters in the range of $(1 - 10) \mu\text{m}$. Real structure investigations yield the samples (1) and (2) to be high-quality single crystals with equal lattice constants. The geometrical dimensions of the micro-structures have been determined by means of scanning electron microscopy.

The following strategy was applied in order to obtain the refractive index dispersion: First, the samples (1) have been investigated by SE in the spectral range $(0.75 - 5.0) \text{ eV}$ for orientations of the light beam parallel and perpendicular to the optical axis. Second, the energetic mode positions of TE and TM WGMs, which have been extracted from spectra of the PL of the samples (2) by using the so called green as well as the excitonic emission of ZnO in the spectral range of $(2.8 - 3.3) \text{ eV}$, was analyzed by a plane wave model using the first guess refractive index from the first step in order to obtain the correct mode numbers of the observed WGMs. Then, the refractive index was refined numerically and finally used as an input for the analysis of the SE data. This final SE analysis yields that the above mentioned surface near region has to be taken into account (Fig. 8.27). We have found, assuming an simplified model, that in a surface near region of about 20 nm depth the lifetime of the electronic excitations is considerably influenced which is expressed in up to two times larger broadening parameters. We ascribe this finding to the influence of electronic surface states, but mechanical or structural damages of the surface cannot be excluded. Please note, by neglecting this layer one obtains wrong dielectric functions and therefore wrong energy (with an error of up to 15 meV), broadening, and amplitude parameters of the band-gap related electronic excitations.

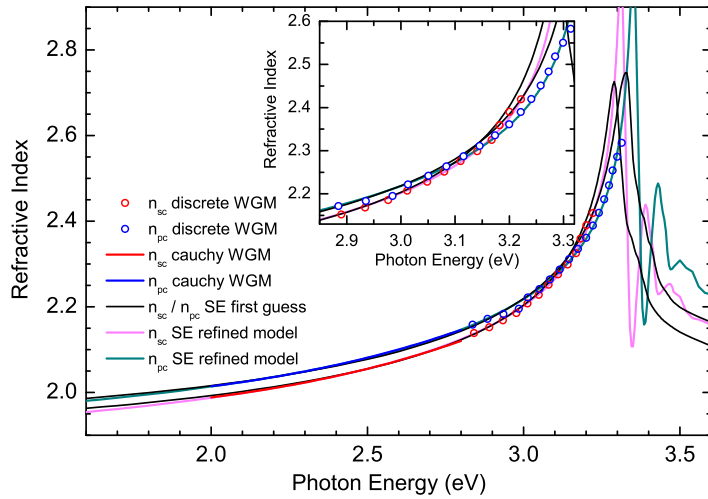


Figure 8.27: Spectra of the ZnO single crystal refractive index obtained from the WGM structures (symbols: discrete data, blue and red lines: cauchy function approximation) of the micro-wires and obtained by means of SE (black lines: first guess model, cyan and violet: refined model) from the bulk single crystal. The pronounced structures above 3.2 eV are caused in the band-gap related electronic excitations. The inset shows an enlarged section energetically close below the lowest excitonic excitation.

8.25 Low-temperature dielectric tensor of a -plane $\text{Mg}_x\text{Zn}_{1-x}\text{O}$ thin films

D. Schumacher, R. Schmidt-Grund, P. Kühne*, H. Hilmer, C. Sturm, H. Hochmuth, M. Lorenz, M. Grundmann

*now at Department of Electrical Engineering, University of Nebraska-Lincoln, USA

There is a long-standing debate whether the valence band (VB) ordering in wurtzite ZnO is the usual Γ_9 - Γ_7 - Γ_7 one or the so called negative spin-orbit coupling order Γ_7 - Γ_9 - Γ_7 . In order to get more insight in the VB-ordering, we determined the quasi-cubic (QC) parameters, i.e. the spin-orbit interaction (Δ_{so}) and the crystal-field splitting (Δ_{cf}) energies from the spectra of the dielectric functions of $\text{Mg}_x\text{Zn}_{1-x}\text{O}$ thin films and discussed their evolution as a function of temperature and Mg-content x in the films.

The a -plane $\text{Mg}_x\text{Zn}_{1-x}\text{O}$ thin films with thicknesses of (220–520) nm were deposited by pulsed laser deposition on r -oriented sapphire substrate and passivated by an 60 nm YSZ cap layer. The experimental data were obtained by means of spectroscopic ellipsometry in the temperature range between 10 K and 470 K and at energies from 1 eV to 4.5 eV. In order to prevent the accumulation of ice and residual gases on the sample surface, all measurements were performed under UHV conditions ($p < 10^{-9}$ mbar).

The independent components of the dielectric tensor parallel ε_{\parallel} and perpendicular ε_{\perp} to the crystal axis were found by layer stack model analysis. The parameterized dielectric function is based on Adachi's model [1] including exciton-phonon-complexes [2]. We derived the near bandgap band-to-band transition energies, amplitudes and broadening parameters (Fig. 8.28). The QC model [3], which gives expressions for the energy differences of the split-off bands, leads to a strength ratio of the corresponding squared p -matrix elements between the p -like valence and s -like conduction bands in terms of Δ_{so} and Δ_{cf} . During the data analysis the oscillator strength parameters of all electronic contributions to the model dielectric function were constrained to satisfy this ratio assuming the validity of the QC model for ZnO.

With increasing temperature Δ_{so} is expected to decrease caused by volume expansion, while Δ_{cf} should be nearly temperature independent for unstrained films. In

wurtzite $\text{Mg}_x\text{Zn}_{1-x}\text{O}$, a decrease for both, Δ_{so} and Δ_{cf} , is expected [4]. We found that the temperature evolution (Fig. 8.28b) as well as the evolution with increasing Mg-content x (not shown here) of the QC parameters for Γ_7 - Γ_9 - Γ_7 ordering is closer to what would be expected from theory [4].

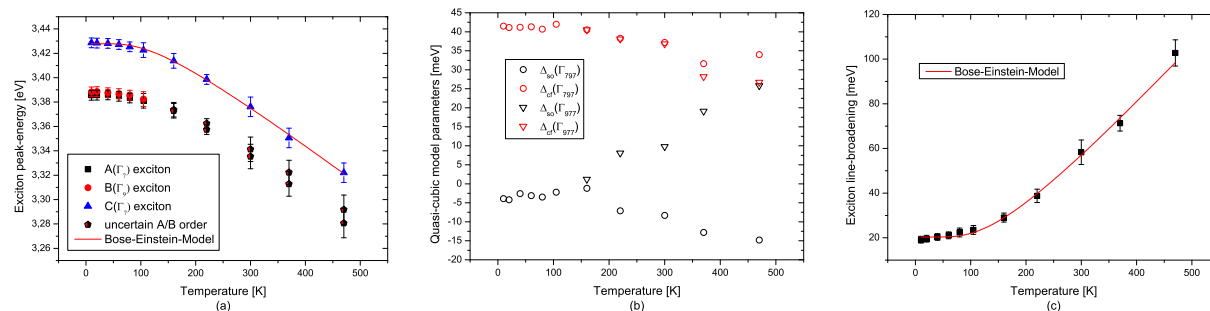


Figure 8.28: Selected parameters of the ZnO thin film model-dielectric function: (a) exciton peak-energies, (b) related quasi-cubic parameters for the Γ_9 - Γ_7 - Γ_7 and the Γ_7 - Γ_9 - Γ_7 ordering, (c) exciton line-broadening.

- [1] H. Yoshikawa, S. Adachi: Jpn. J. Appl. Phys., **36**, 6237 (1997)
- [2] W.Y. Liang, A.D. Yoffe: Appl. Phys. Lett., **20**, 59 (1969)
- [3] J. J. Hopfield, J. Phys. Chem. Solids, **15**, 97 (1959)
- [4] P. Carrier, S. H. Wei: Phys. Rev. B, **70**, 035212 (2004)

8.26 Observation of the quantum confined Stark effect in ZnO/MgZnO quantum wells

M. Stölzel, A. Müller, M. Brandt, J. Kupper, G. Benndorf, M. Grundmann

ZnO and MgZnO are polar semiconductors with different spontaneous electrical polarizations. Therefore, for quantum wells (QWs) based on these materials the presence of the quantum confined Stark effect (QCSE) is expected. The QCSE leads to a redshift of the QW emission energy even beneath the bulk values of ZnO and an increase in the exciton lifetime due to the decreased overlap of the electron and hole wave-functions (Fig. 8.29a) with increasing well width. Up to now, no significant influence of the QCSE could be found in QW samples grown by pulsed laser deposition (PLD) [1, 2].

Therefore we have optimized the PLD process parameters. By lowering of the laser fluence down to 1.8 J/cm^2 it was possible to grow QWs with abrupt interfaces which are a necessity for the QCSE. The samples were deposited on a-sapphire and ZnO substrates and have been investigated by power dependent and time resolved photoluminescence (PL) spectroscopy.

We observed a systematic redshift of the QW emission energy with increasing well width of up to 200 meV beneath the emission of the free exciton in bulk ZnO. The dynamics of the QW luminescence (not shown here) shows clear non-exponential behavior and could be described by a stretched exponential decay function. In doing so, a average decay time is obtained. A comparison to MBE grown samples with very

high quality QW interfaces is given in Fig. 8.29b showing longer decay times for a given redshift in the PLD grown QWs. Additionally the PL spectra show a blueshift of the QW emission maximum (Fig. 8.29c) with increasing excitation power due to the screening of the electric field at high exciton densities.

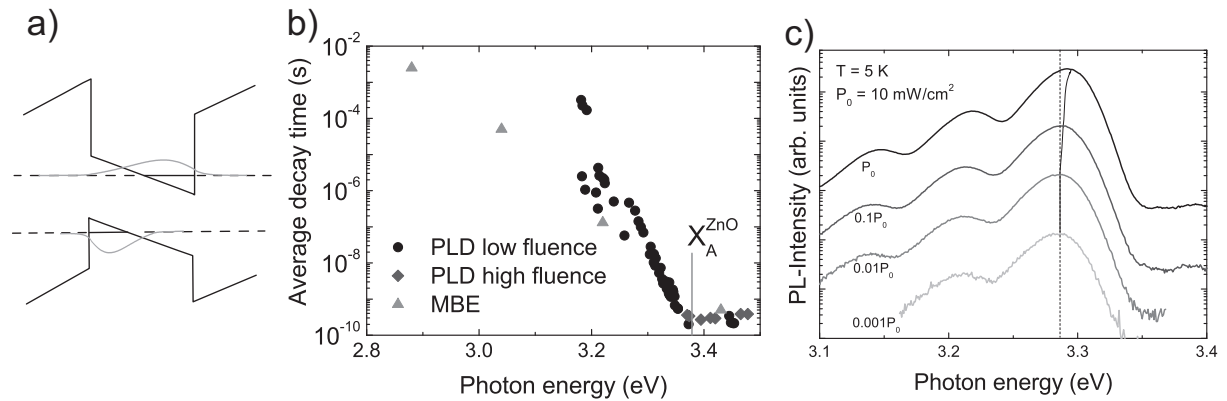


Figure 8.29: a) Potential profile for a QW with internal electric field, b) dependence of the decay time on the QW emission energy in samples grown by PLD with low laser fluence compared to samples grown by PLD with high laser fluence and MBE as taken from Ref. [3] and c) photoluminescence spectra depending on the excitation power of a QW grown with PLD with low laser fluence.

[1] S. Heitsch et al.: MRS proceedings, 0957-K07-23, (2006)

[2] P. Misra et al.: Superlattices Microstruct. **42**, 212 (2007)

[3] C. Morhain et al.: Phys. Rev. B **72**, 241305(R)

8.27 Dielectric function of BaTiO₃ thin films in IR and VUV range

T. Böntgen, S. Schöche, R. Schmidt-Grund, C. Sturm, M. Brandt, H. Hochmuth, M. Lorenz, M. Grundmann

We present the dielectric function (DF) of BaTiO₃ (BTO) thin films in the IR and VUV spectral range, which complement our previous studies in the VIS-NUV spectral range [1]. The (001)-oriented films with thicknesses of 45 nm and 654 nm were grown by pulsed laser deposition on (100)-SrTiO₃(STO) substrates.

Spectra of the DF have been obtained by model analysis of spectroscopic ellipsometry (SE) data and show clear deviations between the thinner and the thicker film, especially in the vicinity of the fundamental band-edge and in the spectral range of higher band-to-band transitions. This is in accordance with the previously found dependence of the optical response of BTO films on the thickness which was ascribed to the relaxation of thicker films compared to the pseudomorphically grown and therefore strained thin films [1]. IR-SE was carried out to gain information on the phonon modes of the BTO films. The observed phonon modes of the films show a shift to higher energies when compared to single crystal values (Tab. 8.2) in concordance with

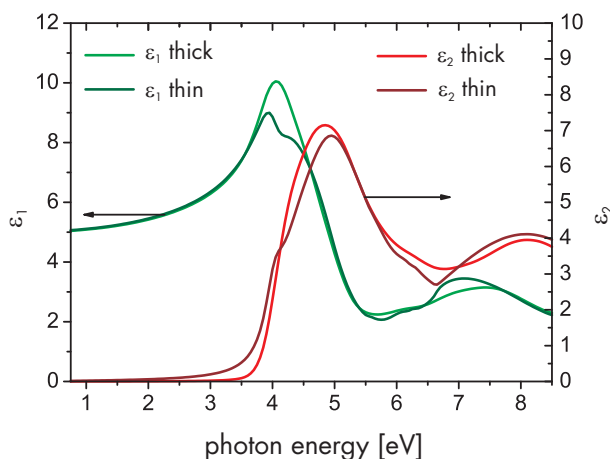


Figure 8.30: Dielectric function for two BTO films with thicknesses of 45 nm and 654 nm.

the assumption that the thin films are strained due to the pseudomorphical growth on the STO substrate.

In conclusion the additional studies of the BTO DF in the VUV and IR range complete the picture that was developed in earlier studies [1] and strengthen these results. Furthermore, the knowledge of the BTO DF in this extended spectral range improves the parametric model for the DF of BTO thin films.

Table 8.2: Measured phonon mode frequencies.

phonon mode	single crystal [cm^{-1}]	thin film [cm^{-1}]
TO	488	488
LO	640	675
TO	641	678
LO	707	734

[1] S. Schöche et al.: *Structural and Optical Properties of BaTiO₃ Thin Films*, in *The Physics Institutes of Universität Leipzig, Report 2008*, M Grundmann (Ed.), p 181.

8.28 Phonon modes of BaTiO₃ thin films

C. Kranert, C. Sturm, T. Böntgen, S. Schöche, R. Schmidt-Grund, H. Hochmuth, M. Grundmann

Due to its ferroelectric properties, BaTiO₃ (BTO) is an interesting material for many applications, e.g. thin film capacitors or non-volatile memory. Furthermore, in combination with pyroelectric materials, coupling effects between the polarizations of these two materials are expected which can be used in devices such as optical switchers. In this work we present the behavior of the phonon modes of BTO thin films whose knowledge are essential to understand those of a coupled system.

We have investigated BTO thin films with film thicknesses of (90–900) nm on SrTiO₃ (STO) substrates as well as ZnO-BTO-heterostructures on *a*-plane sapphire substrates,

all grown by pulsed laser deposition. The phonon modes were obtained by infrared spectroscopic ellipsometry, which is sensitive to the in-plane modes (E -symmetry) as well as by Raman spectroscopy, which for our configuration is sensitive to the out-of-plane modes (A_1 -symmetry). The latter one was carried out using a HeCd-laser with a wavelength of 325 nm in order to excite the system in the spectral range of high absorption and therefore avoid the Raman signal from the substrate. For the BTO films we observe that the E -modes vary slightly with the film thickness, while the phonon modes with A_1 -symmetry shift towards the bulk values with increasing film thickness (Fig. 8.31). This is in good agreement with X-Ray diffraction (XRD) measurements which yield that the in-plane lattice constant is almost fully relaxed while the c -lattice constant relaxes towards the bulk value with increasing thickness.

Annealing of the BTO film at 1100°C causes the relaxation of the film as stated by XRD. Analogously the phonon modes also approached bulk values without reaching them. The line shape of the peaks became much sharper which indicates an enhancement of the crystal quality. This allows the observation of the temperature dependence of the $A_1(\text{TO}_2)$ -mode up to room temperature, contrary to the as-grown samples, where the broadening of this feature is too large (Fig. 8.32). The $A_1(\text{TO}_3)$ -mode shows an opposite temperature dependence before and after annealing. The reason for this finding is not understood yet and requires further investigation.

For the BTO films of the heterostructures, the spectral position and broadening of the phonon modes are in between those of the annealed and as-grown samples. The temperature dependence is the same as for the annealed sample, but with smaller shifts. That leads to the conclusion that BTO grows mostly relaxed on ZnO in accordance with XRD measurements.

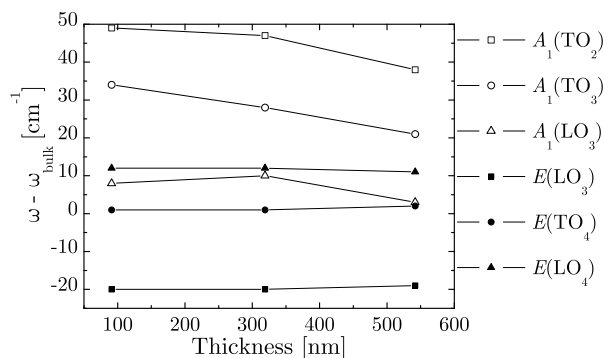


Figure 8.31: Phonon energies of BTO films relative to the bulk values in dependence on the film thickness at room temperature.

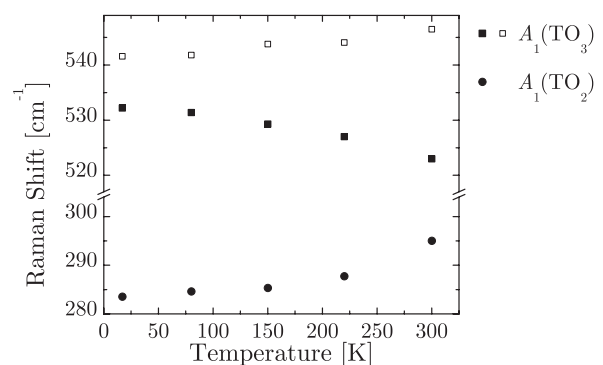


Figure 8.32: Temperature dependence of the phonon energies, solid symbols illustrate the annealed film, open symbols the as-grown one.

8.29 Optical properties of BaTiO₃/ZnO heterostructures under the effect of an electric bias

T. Böntgen, K. Brachwitz, S. Schöche, R. Schmidt-Grund, C. Sturm, M. Brandt, H. Hochmuth, M. Lorenz, and M. Grundmann

Based on its switchable ferroelectric polarization, BaTiO₃ (BTO) has become an integral part of semiconductor physics and technology due to its role as a gate electrode in non-volatile memories [1] or its potential to be used in polarization coupled heterostructures [2]. Of special interest here is the coupling to the spontaneous polarization of ZnO in BTO/ZnO heterostructures. By applying an electrical bias to switch the polarization of the ferroelectric BTO layer in such a structure we could observe a remanent change in the optical properties of the ZnO layer.

The BTO/ZnO heterostructures were grown by pulsed laser deposition on a-sapphire substrates. First, a ZnO:Al layer (thickness $t \sim 100$ nm) was grown as conductive ohmic back contact. Then the ZnO layer ($t \sim 200$ nm) and the BTO layer ($t \sim 200$ nm) were deposited. Finally a 15 nm thick Pt contact was sputtered using reactive DC-sputtering. X-Ray diffraction patterns reveal high quality single phase (100)-ZnO as well as high quality BTO films (Fig. 8.33). By changing the growth properties the crystal orientation of the BTO layer can either be (001) or (111).

By applying an electrical bias, electro-optical ellipsometry measurements were carried out. These show a change of the optical properties of the heterostructures under the effect of the electric field in the vicinity of the excitonic polarizability of ZnO (Fig. 8.34). Moreover a persistent change of the optical properties after removing the bias was measured. This change is attributed to the ferroelectric polarization of the BTO film which causes an electrical field and therefore induces a change of the band gap energy of ZnO. To confirm this hypothesis the same measurements were carried out on pure ZnO and BTO layers. No change was observed for the BTO layer while the ZnO layer shows an effect similar to the heterostructure but does not exhibit a persistent change (Fig. 8.34).

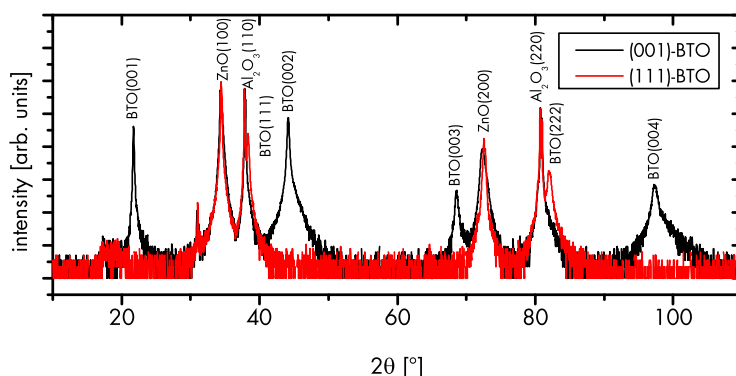


Figure 8.33: 2θ - ω scan of BTO/ZnO heterostructures on a-sapphire. Black and red curves show a heterostructure with (001)- and (111)-BTO, respectively.

[1] M. Brandt et al.: J. Vac. Sci. Technol. B 27, 1789 (2009)

[2] V.M. Voora et al.: J. Electr. Mat. 37, 1029 (2008)

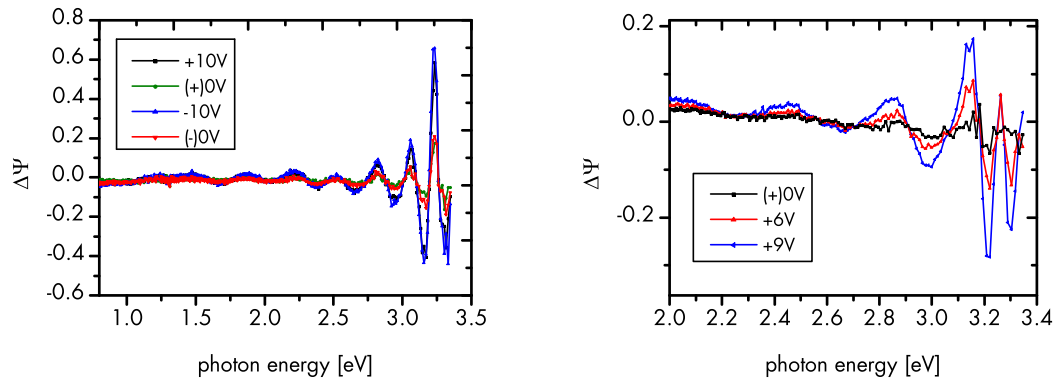


Figure 8.34: Ellipsometry difference data between a reference scan and scans with various bias conditions (left: BTO/ZnO heterostructure, right: pure ZnO structure). A persistent change (curve with 0 V) is only visible for the BTO/ZnO structure. The + and - for the 0 V curves indicates the bias history.

8.30 Teaching

M. Grundmann

As a teacher you always learn something yourself. I share three aspects that have been new to me last semester in the mechanics lecture (Experimental Physics I).

8.30.1 Mathematical pendulum with finite amplitude

The formula $T(\phi_0) \approx T_0 / \sqrt{\cos(\phi_0/2)}$ ($T_0 = 2\pi \sqrt{l/g}$) is a good and practical approximation to the oscillation period of the mathematical pendulum with finite amplitude ϕ_0 . It is better than 1% for $\phi_0 \leq \pi/2$ [1]. Up to second order, this formula gives the same result, $T = T_0 (1 + \phi_0^2/16)$, as the exact solution involving an elliptical integral.

8.30.2 Collapse of the Tacoma Narrows bridge

The collapse of the Tacoma Narrows bridge in 1940 due to high winds is often attributed to forced harmonic oscillation and a resonance catastrophe. Actually, the collapse is due to the exponentially increasing amplitude of a torsional motion (aerodynamic flutter) [2].

8.30.3 Explaining the Rubens flame tube

The Rubens flame tube [3] is a beautiful demonstration experiment for a standing sound wave in a long tube. The sound is coupled at one end through a membrane; the other end of the tube is fixed. Combustible gas streams into the pipe and the sound field modulates (at resonance periodically) the height of little flames reaching out of a linear array of holes at the top of the tube (Fig. 8.35). From the spatial period of the flame pattern ($\lambda/2$), the sound velocity in the gas can (roughly) be determined.

Many explanations of the effect found in textbooks and on the internet are wrong. What actually happens is the following: At the fixed end of the tube the gas velocity



Figure 8.35: Rubens flame tube with fixed end on the left.

has a node and the pressure has an antinode. At first surprisingly, this results in a *lower* flame height although the pressure maxima are located there. However, one should not forget that also the pressure minima are located there! At the pressure node, the flame is *higher* than without sound field. The pressure is time dependent and the time-averaged pressure at each point of the tube is equal. However, following Bernoulli's law, the gas flow out of each hole is proportional to the square root of the pressure difference between inside and outside: The flame height is proportional to the time average of the gas flow out of the holes, causing the observed effect as detailed in [4].

I like to thank A. Märcker for assisting in experiments and taking the above photograph of the Rubens tube.

- [1] R.B. Kidd, S.L. Fogg, *Physics Teacher* 40, 81 (2002)
- [2] B.J. Feldmann, *Physics Teacher* 41, 92 (2003)
- [3] H. Rubens, O. Krigar-Menzel, *Flammenröhre für akustische Beobachtungen*, *Annalen d. Physik* 322, 149 (1905)
- [4] G.W. Ficken, F.C. Stephenson, *Physics Teacher* 17, 306 (1979)

8.31 Funding

One-dimensional heterostructures and nanowire arrays

Prof. Dr. M. Grundmann, PD Dr. M. Lorenz, Dipl.-Phys. C. Czekalla, Dipl.-Phys. G. Zimmermann

DFG GR 1011/11-1 within DFG Forschergruppe FOR 522 *Architecture of nano- and microdimensional building blocks*

Lateral optical confinement of microresonators

Prof. Dr. B. Rheinländer, Dr. V. Gottschalch, Dr. Rüdiger Schmidt-Grund, Dr. Karsten Goede, Dipl.-Phys. C. Dietrich

DFG RH 28/4-1 within DFG Forschergruppe FOR 522 *Architecture of nano- and microdimensional building blocks*

Transferability of the codoping concept to ternary ZnO:(Cd,Mg)

Prof. Dr. M. Grundmann, Dr. H. v. Wenckstern

DFG GR 1011/10-3 within DFG-Schwerpunktprogramm 1136 *Substitutionseffekte in ionischen Festkörpern*

Leipzig School of Natural Sciences - Building with Molecules and Nano-objects (Build-MoNa)

Prof. Dr. M. Grundmann
DFG GSC 185/1

Nanophotonic and nanoelectronic Devices from Oxide Semiconductors (NANDOS)

Prof. Dr. M. Grundmann, PD Dr. M. Lorenz, Dipl.-Phys. G. Zimmermann
EU STReP Contract No. 016424

Polarisationswechselwirkung in Laser-MBE Wurtzit-Perowskit-Heterostrukturen

PD Dr. M. Lorenz

SFB 762/1-2008, TP A2 within SFB 762 *Funktionalität Oxidischer Grenzflächen*

Optische Untersuchungen zur dielektrischen Funktion und Ihrer Dynamik an oxidischen Heterostrukturen

Prof. Dr. M. Grundmann, Prof. Dr. H. Gräner (Martin-Luther-Universität Halle-Wittenberg), Dipl.-Phys. M. Brandt, Dipl.-Phys. P. Kühne

SFB 762/1-2008, TP B03 within SFB 762 *Funktionalität Oxidischer Grenzflächen*

Lateraler Transport in oxidischen Feldeffekt-Strukturen

Prof. Dr. M. Grundmann, Prof. Dr. J. Christen (Otto-von-Guericke-Universität Magdeburg), Dipl.-Phys. H. Frenzel

SFB 762/1-2008, TP B04 within SFB 762 *Funktionalität Oxidischer Grenzflächen*

Spinabhängiges Tunneln in oxidischen Heterostrukturen

Prof. Dr. M. Grundmann, Prof. Dr. I. Mertig (Martin-Luther-Universität Halle-Wittenberg), Dipl.-Phys. M. Ellguth, Dipl.-Phys. S. Schöche

SFB 762/1-2008, TP B06 within SFB 762 *Funktionalität Oxidischer Grenzflächen*

Bose-Einstein-Kondensation von Exziton-Polaritonen bei Raumtemperatur

Prof. Dr. M. Grundmann, Dr. R. Schmidt-Grund, Dipl.-Phys. C. Sturm

DFG GR 1011/20-1

Herstellung und Charakterisierung von UV-Mikrokavitäten

Dipl.-Phys. H. Hilmer

Landesinnovationsstipendium des Freistaates Sachsen im Rahmen des Europäischen Sozialfonds

Herstellung und Charakterisierung von transparenten Feldeffekttransistoren

Dipl.-Phys. A. Lajn

Landesinnovationsstipendium des Freistaates Sachsen im Rahmen des Europäischen Sozialfonds

Herstellung und charakterisierung von Quantendraht-Heterostrukturen

Dipl.-Phys. M. Lange

Landesinnovationsstipendium des Freistaates Sachsen im Rahmen des Europäischen Sozialfonds

Magnetische Tunnelkontakte

Dipl.-Phys. J. Zippel

Landesinnovationsstipendium des Freistaates Sachsen im Rahmen des Europäischen Sozialfonds

Funktionalisierte Nanosäulen

Prof. Dr. M. Grundmann, Dr. H. v. Wenckstern, Dipl.-Phys. C. Dietrich, Dipl.-Phys. M. Stölzel

ESF-Nachwuchsforschergruppe *Funktionale multiskalige Strukturen* des Freistaates Sachsen im Rahmen des Europäischen Sozialfonds

8.32 Organizational Duties

M. Grundmann

- Direktor des Instituts für Experimentelle Physik II
- Coordinator of the European Network of Excellence on "Self-Assembled semiconductor Nanostructures for new Devices in photonics and Electronics" (SANDiE, <http://www.sandie.org>)
- Sprecher der DFG Forschergruppe "Architektur von nano- und mikrodimensionalen Strukturelementen" (FOR522), <http://www.uni-leipzig.de/~for522>
- Stellvertretender Sprecher der Graduiertenschule "Leipzig School of Natural Sciences - Building with Molecules and Nano-objects" (BuildMoNa), <http://www.buildmona.de>
- Stellvertretender Sprecher des Sonderforschungsbereiches zur "Funktionalität Oxidischer Grenzflächen" (SFB762), <http://www.physik.uni-halle.de/sfb762>
- Sprecher der Fächerübergreifenden Arbeitsgemeinschaft Halbleiterforschung Leipzig (FAHL), <http://www.uni-leipzig.de/~fahl>
- Mitglied des Beirats Ionenstrahlzentrum, FZR, Dresden-Rossendorf
- Project Reviewer: Deutsche Forschungsgemeinschaft (DFG), Alexander von Humboldt-Stiftung (AvH), Schweizerischer Nationalfonds zur Förderung der wissenschaftlichen Forschung (FNSNF), Fonds zur Förderung der Wissenschaften (FWF)
- Referee: Appl. Phys. Lett., Electr. Lett., J. Appl. Phys., Nature, Physica E, Phys. Rev. B., Phys. Rev. Lett., Phys. Stat. Sol, Science

M. Lorenz

- Project Reviewer: Department of Energy, Office of Basic Energy Sciences (DOE-BES) U.S.A, National Research Foundation of South Africa, United States–Israel Binational Science Foundation (BSF)
- Referee: Advanced Materials, Applied Physics Letters, IEEE Transactions on Electron Devices, Journal of Crystal Growth, Journal of Physical Chemistry, Journal of Physics D, Journal of Applied Physics, Journal of Vacuum Sciences and Technology A and B, Materials Chemistry and Physics, Materials Research Bulletin, Nanotechnology, Physica E, Physica Status Solidi (a) and RRL, Semiconductor Science and Technology, Thin Solid Films

H. v. Wenckstern

- Referee: Appl. Phys. Lett., J. Appl. Phys., Thin Solid Films, Solid State Electron., Phys. Stat. Sol., Superlatt. Microstruct., J. Electron. Mater., Turk. J. Phys., J. Mater. Sci., Mater. Electron., J. Vac. Sci. Technol., Mater. Sci. Eng. B, J. Nanosci. Nanotechnol., Microelectron. Eng., J. Phys. D, J. Cryst. Growth, Surf. Sci.

R. Schmidt-Grund

- Referee: J. Appl. Phys, Phys. Stat. Sol. b, J. Alloy Comp.

8.33 External Cooperations

Academic

- Leibniz-Institut für Oberflächenmodifizierung e. V., Leipzig, Germany
Prof. Dr. B. Rauschenbach, Prof. Dr. T. Höche, Dr. J. Gerlach
- Universität Leipzig, Fakultät für Biowissenschaften, Pharmazie und Psychologie
Prof. Dr. A. Beck-Sickinger
- Universität Leipzig, Fakultät für Chemie und Mineralogie, Germany
Dr. V Gottschalch, Prof. Dr. H. Krautscheid, Prof. Dr. K. Bente, Prof. Dr. R. Denecke
- Universität Halle-Wittenberg, Germany
Prof. Dr. I. Mertig, Prof. Dr. W. Widdra, Prof. Dr. H. Graener
- Max-Planck-Institut für Mikrostrukturphysik, Hall/Saale, Germany
Prof. Dr. U. Gösele†, Dr. O. Breitenstein, Dr. A. Ernst, Dr. P. Werner, Prof. Dr. D. Hesse
- Forschungszentrum Dresden-Rossendorf, Germany
Prof. Dr. M. Helm
- Technische Universität Berlin, Germany
Prof. Dr. D. Bimberg, Dr. A. Hoffmann
- University of Aveiro
Prof. N. A. Sobolev
- Universität Gießen, Germany
Prof. Dr. B. Meyer, Dr. D. Hofmann, Prof. Dr. J. Janek
- Universität Magdeburg, Germany
Prof. Dr. A. Krost, Dr. A. Dadgar, Prof. Dr. J. Christen
- Universität Ulm, Germany
Prof. Dr. F. Scholz, Prof. Dr. K. Thonke
- Universität Bonn, Germany
Prof. Dr. W. Mader
- Universität Hannover, Germany
Prof. Dr. M. Binnewies
- Göteborg University, Sweden
Prof. Dr. M. Willander

- NCSR "Demokritos", Institute of Materials Science, Greece
Prof. Dr. A. Travlos
- Université Joseph Fourier, Grenoble, France
Prof. Dr. D. Le Si Dang
- University of Pretoria, South Africa
Prof. F. D. Auret
- University of Canterbury, Christchurch, New Zealand
Prof. Dr. S. Durbin
- University of Nebraska, Lincoln, USA
Prof. Dr. M. Schubert
- Centre de Recherche sur l' Hétéro-Epitaxie et ses Applications (CNRS-CRHEA),
Valbonn, France
Dr. J. Zúñiga-Pérez

Industry

- Solarion AG, Leipzig Germany
Dr. Alexander Braun, Dr. Andreas Rahm
- OSRAM Opto-Semiconductors GmbH, Regensburg, Germany
Dr. V. Härle, Dr. S. Lutgen
- Freiburger Compound Materials GmbH, Freiberg, Germany
Dr. G. Leibiger
- Q-Cells SE, Thalheim, Germany
Dr. K. Petter

8.34 Publications

Journals

M. W. Allen, S. M. Durbin, X. Weng, J. M. Redwing, K. Sarpatwari, S. E. Mohny, H. von Wenckstern, Marius Grundmann: *Temperature-Dependent Properties of Nearly Ideal ZnO Schottky Diodes*, IEEE Transaction on Electron Devices **56**, 2160-2164 (2009)

A.O. Ankiewicz, W. Gehlhoff, J.S. Martins, A.S. Pereira, S. Pereira, A. Hoffmann, E.M. Kaidashev, A. Rahm, M. Lorenz, M. Grundmann, M.C. Carmo, T. Trindade, N.A. Sobolev: *Magnetic and structural properties of transition metal doped zinc-oxide nanostructures*, phys. stat. sol. (b) **246**, 766 (2009)

R. Bakowskie, H. von Wenckstern, D. Lausch, M. Müller, K. Petter, M. Grundmann, *Thermal admittance spectroscopy of multicrystalline silicon wafers and solar cells*, Proc. 24th European Photovoltaic Solar Energy Conference, 2DV.1.30 (2009)

M. Binnewies, S. Locmelis, B. Meyer, A. Polity, D. M. Hofmann, H. von Wenckstern, *Gas phase synthesis of ionic solid solutions-crystalline bulk materials and thin films*, Prog. Sol. Stat. Chem. **37**, 57-69 (2009)

- M. Brandt, H. von Wenckstern, C. Meinecke, T. Butz, H. Hochmuth, M. Lorenz, M. Grundmann: *Dopant activation in homoepitaxial MgZnO:P thin films*, *J. Vac. Sci. Technol.* **27**, 1604-1608, (2009)
- M. Brandt, H. von Wenckstern, G. Benndorf, H. Hochmuth, M. Lorenz, M. Grundmann: *Formation of a two-dimensional electron gas in zno/mgzno single heterostructures and quantum wells*, *Thin Solid Films* **518**, 1048 - 1052, (2009)
- M. Brandt, H. Frenzel, H. Hochmuth, M. Lorenz, M. Grundmann, J. Schubert: *Ferroelectric thin film field-effect transistors based on ZnO/BaTiO₃ heterostructures*, *J. Vac. Sci. Technol.* **27**, 1789-1793, (2009)
- B.Q. Cao, J. Zúñiga-Pérez, N. Boukos, C. Czekalla, H. Hilmer, J. Lenzner, A. Travlos, M. Lorenz, M. Grundmann: *Homogeneous core/shell ZnO/MgZnO quantum well heterostructures on vertical ZnO nanowires* *Nanotechnology* **20**, 305701 (2009)
- C. Czekalla, C. Sturm, R. Schmidt-Grund, B. Cao, J. Zúñiga-Pérez, M. Lorenz, M. Grundmann: *Optical characterization of zinc oxide microlasers and microwire core-shell heterostructures*, *J. Vac. Sci. Technol. B* **27**, 1780 (2009)
- H. Frenzel, A. Lajn, M. Brandt, H. von Wenckstern, G. Biehne, H. Hochmuth, M. Grundmann: *ZnO-based metal-semiconductor field-effect transistors with Ag-, Pt-, Pd-, and Au-Schottky gates*, *Thin Solid Films* **518**, 1119 (2009)
- H. Frenzel, M. Lorenz jr., A. Lajn, H. v. Wenckstern, G. Biehne, H. Hochmuth, and M. Grundmann, *ZnO-based metal-semiconductor field-effect transistors on glass substrates*, *Appl. Phys. Lett.* **95**, 153503 (2009)
- M. Grundmann, C.P. Dietrich: *Lineshape Theory of Photoluminescence from Semiconductor Alloys*, *J. Appl. Phys.* **106**, 123521 (2009)
- M. Khalid, M. Ziese, A. Setzer, P. Esquinazi, M. Lorenz, H. Hochmuth, M. Grundmann, D. Spemann, T. Butz, G. Brauer, W. Anwand, G. Fischer, W.A. Adeagbo, W. Hergert, A. Ernst: *Defect-induced magnetic order in pure ZnO films*, *Phys. Rev. B* **80**, 035551 (2009)
- A. Lajn, H. von Wenckstern, Z. Zhang, C. Czekalla, G. Biehne, J. Lenzner, H. Hochmuth, M. Lorenz, M. Grundmann, S. Künzel, C. Vogt, R. Deneke: *Properties of reactively sputtered Ag, Au, Pd, and Pt Schottky contacts on n-type ZnO* *J. Vac. Sci. Technol. B* **27**, 1769 (2009)
- A. Lajn, H. von Wenckstern, G. Benndorf, C. P. Dietrich, M. Brandt, G. Biehne, H. Hochmuth, M. Lorenz, and M. Grundmann: *Shallow Donors and Compensation in Homoepitaxial ZnO Thin Films* *J. Electron. Mater.* **39**, 595 (2009)
- M. Lange, J. Zippel, G. Benndorf, C. Czekalla, H. Hochmuth, M. Lorenz, M. Grundmann: *Temperature dependence of localization effects of excitons in ZnO/CdZnO/ZnO double heterostructures*, *J. Vac. Sci. Technol. B* **27**, 1741 (2009)
- Dominik Lausch, Kai Petter, Holger von Wenckstern, Marius Grundmann: *Correlation of pre-breakdown sites and bulk defects in multicrystalline silicon solar cells*, *phys. stat. sol. RRL* **3**, 70 (2009)

D. Lausch, K. Petter, R. Bakowskie, H. von Wenckstern, M. Grundmann, *Correlation of pre-breakdown sites and bulk defects in multicrystalline silicon solar cells*, Proc. 24th European Photovoltaic Solar Energy Conference, 2DV.1.17 (2009).

M. Lorenz, B. Cao, G. Zimmermann, G. Biehne, C. Czekalla, H. Frenzel, M. Brandt, H. von Wenckstern, M. Grundmann: *Stable p-type ZnO:P nanowire / n-type ZnO:Ga film junctions, reproducibly grown by two-step pulsed laser deposition*, J. Vac. Sci. Technol. B **27**, 1693 (2009)

M. Lorenz, M. Brandt, G. Wagner, H. Hochmuth, G. Zimmermann, H. von Wenckstern, M. Grundmann: *MgZnO:P homoepitaxy by pulsed laser deposition: pseudomorphic layer-by-layer growth and high electron mobility*, Proc. SPIE 7217, 72170N (2009)

M. Schmidt, M. Ellguth, C. Czekalla, H. v. Wenckstern, R. Pickenhain, M. Grundmann, G. Brauer, W. Skorupa, M. Helm, Q. Gu, C. Chung Ling: *Defects in zinc-implanted ZnO thin films*, J. Vac. Sci. Technol. B **27** (2009)

C. Sturm, H. Hilmer, R. Schmidt-Grund, M. Grundmann: *Observation of strong exciton-photon coupling at temperatures up to 410 K*, New J. Phys. **11**, 073044 (2009)

C. Sturm, H. Hilmer, R. Schmidt-Grund, C. Czekalla, J. Sellmann, J. Lenzner, M. Lorenz, M. Grundmann: *Strong Exciton-Photon Coupling in ZnO based Resonators*, J. Vac. Sci. Technol. B **27**, 1726 (2009)

V.M. Voora, T. Hofman, M. Schubert, M. Brandt, M. Lorenz, M. Grundmann, N. Ashkenov: *Resistive hysteresis and interface charge coupling in BaTiO₃-ZnO heterostructures*, Appl. Phys. Lett. **94**, 142904 (2009)

M. Voora, T. Hofmann, M. Brandt, M. Lorenz, N. Ashkenov, M. Grundmann, M. Schubert: *Electrical properties of ZnO-BaTiO₃-ZnO heterostructures with asymmetric interface charge distribution*, Appl. Phys. Lett. **95**, 082902 (2009)

H. von Wenckstern, H. Schmidt, M. Brandt, A. Lajn, R. Pickenhain, M. Lorenz, M. Grundmann, D.M. Hofmann, A. Polity, B.K. Meyer, H. Saal, M. Binnewies, A. Börger, K.-D. Becker, V.A. Tikhomirov, K. Jug: *Anionic and cationic substitution in ZnO*, Prog. Sol. Stat. Chem. **37**, 153-172 (2009)

M. Willander, O. Nur, Q.X. Zhao, L.L. Yang, M. Lorenz, B.Q. Cao, J. Zúñiga-Pérez, C. Czekalla, G. Zimmermann, M. Grundmann, A. Bakin, A. Behrends, M. Al-Suleiman, A. Al-Shaer, A. Che Mofor, B. Postels, A. Waag, N. Boukos, A. Travlos, J. Guinard, D. Le Si Dang: *Zinc Oxide Nanorods Based Photonic Devices: Recent Progress in Growth, Light Emitting Diodes and Lasers*, Nanotechnology **20**, 332001 (2009)

Q.Y. Xu, S. Zhou, D. Markó, K. Potzger, J. Fassbender, M. Vinnichenko, M. Helm, H. Hochmuth, M. Lorenz, M. Grundmann, H. Schmidt: *Paramagnetism in Co-doped ZnO films*, J. Phys. D: Appl. Phys. **42**, 085001 (2009)

S.Q. Zhou, K. Potzger, Q.Y. Xu, G. Talut, M. Lorenz, W. Skorupa, M. Helm, J. Fassbender, M. Grundmann, H. Schmidt: *Ferromagnetic transition metal implanted ZnO: A diluted magnetic semiconductor?*, Vacuum **83**, S13-S19 (2009)

J. Zippel, J. Lenzner, G. Benndorf, M. Lange, H. Hochmuth, M. Lorenz, M. Grundmann: *Electronic coupling in $Mg_xZn_{1-x}O/ZnO$ double quantum wells*, J. Vac. Sci. Technol. B **27**, 1735 (2009)

Books

R. Schmidt-Grund, A. Hinkel, H. Hilmer, J. Zúñiga-Pérez, Ch. Sturm, B. Rheinländer, M. Grundmann: *ZnO nano-pillar resonators with coaxial Bragg reflectors*, in: *Semiconductor Nanowires - Growth, Size-Dependent Properties, and Applications*, edited by Ali Javey, Mater. Res. Soc. Symp. Proc. Volume 1178E (MRS, Warrendale, PA, 2009) p 1178-AA10-13

Talks

K. Brachwitz, H. von Wenckstern, H. Hochmuth, G. Biehne, C. Dietrich, M. Brandt, M. Grundmann: *Electrical properties of ZnMgO thin films grown by pulsed-laser deposition*, 73rd Spring Meeting of the German Physical Society, Dresden, 22.–27. March 2009

S. Chouthe, C. Sturm, G. Seifert, R. Schmidt-Grund, M. Grundmann, H. Graener: *Femtosecond Pump-Probe Spectroscopy of ZnO Thin Films*, 73rd Spring Meeting of the German Physical Society, Dresden, 22.–27. March 2009

C. Czekalla, R. Schmidt-Grund, C. Sturm, J. Lenzner, M. Lange, M. Lorenz, M. Grundmann: *Whispering Gallery Mode Lasing in Zinc Oxide Microwires*, EMRS Spring Meeting 2009, Strasbourg, France, 8.–12. June 2009

C. Czekalla, C. Sturm, R. Schmidt-Grund, J. Zúñiga-Pérez, M. Lorenz, M. Grundmann: *Optical characterization of zinc oxide microwire lasers*, 73rd Spring Meeting of the German Physical Society, Dresden, 22.–27. March 2009

C.P. Dietrich, G. Benndorf, J. Lenzner, M. Grundmann: *Identification of excitonic recombination transitions in MgZnO thin films grown by pulsed laser deposition*, 73rd Spring Meeting of the German Physical Society, Dresden, 22.–27. March 2009

C.P. Dietrich, A. Müller, M. Stölzel, G. Benndorf, J. Lenzner, M. Lorenz, M. Grundmann: *Effect of Donor-bound and Free Excitons on Luminescence of MgZnO Thin Films*, MRS Fall Meeting 2009 Boston, USA, 30. November – 4. December 2009

M. Ellguth, M. Schmidt, H. von Wenckstern, R. Pickenhain, M. Grundmann: *Investigation of ZnO electronic properties by optical deep level transient spectroscopy*, 73rd Spring Meeting of the German Physical Society, Dresden, 22.–27. March 2009

M. Ellguth, M. Schmidt, H. von Wenckstern, R. Pickenhain, M. Grundmann: *Characterisation of point defects in ZnO thin films by Optical Deep Level Transient Spectroscopy*, 25th Internat. Conference on Defects in Semiconductors

H. Frenzel, M. Lorenz, F. Schein, H. von Wenckstern, A. Lajn, H. Hochmuth, G. Biehne, and M. Grundmann, *Design and characterization of ZnO-based MESFET devices*, Electronic Materials Conference, University Park, Pennsylvania (2009)

M. Grundmann: *MESFETs based on ZnO*, EMRS 2009, Straßburg, Symposium F, 9.6.2009, invited

M. Grundmann: *ZnO-based devices and technology: Nanoscale building blocks, transparent electronics and photonics*, CeNS Kolloquium, München, 19.6.2009

M. Grundmann: *ZnO-based transparent MESFET devices*, MRS 2009 Fall Meeting, Boston, Symposium H "ZnO and Related Materials", H1.1, 30.11.2009, invited

H. Hilmer, C. Sturm, R. Schmidt-Grund, M. Grundmann: *Strong Exciton-Photon Coupling in ZnO-based Microresonators*, MRS Fall Meeting 2009, Boston, USA, 30. November – 4. December 2009

H. Hilmer, C. Sturm, R. Schmidt-Grund, J. Sellmann, H. Hochmuth, M. Lorenz, B. Rheinländer, and M. Grundmann: *Ellipsometry on ZnO-based Microresonators*, 5th Workshop Ellipsometry, Zweibrücken, Germany, 2.–4. March 2009

A. Hinkel, R. Schmidt-Grund, H. Hilmer, Zúñiga-Pérez, C. Sturm, C. Czekalla, M. Lorenz, M. Grundmann: *Optical Modes in ZnO Nano-Pillar Resonators*, 73rd Spring Meeting of the German Physical Society, Dresden, 22.–27. March 2009

P. Kühne, R. Schmidt-Grund, C. Sturm, M. Brandt, M. Grundmann: *Temperature dependent dielectric function of nonpolar ZnO*, 73rd Spring Meeting of the German Physical Society, Dresden, 22.–27. March 2009

M. Lange, J. Zippel, G. Benndorf, C. Czekalla, H. Hochmuth, M. Lorenz, M. Grundmann: *Investigations of ZnO/ZnCdO double heterostructures grown by pulsed laser deposition*, 73rd Spring Meeting of the German Physical Society, Dresden, 22.–27. March 2009

A. Lajn, H. v. Wenckstern, G. Biehne, H. Hochmuth, M. Lorenz, M. Grundmann, S. Wickert, C. Vogt, R. Denecke: *Properties of reactively sputtered Ag, Au, Pd, and Pt Schottky contacts on n-type ZnO*, 73rd Spring Meeting of the German Physical Society, Dresden, 22.–27. March 2009

A. Lajn, H. v. Wenckstern, M. Brandt, C. Dietrich, G. Benndorf, M. Lorenz, G. Biehne, H. Hochmuth, M. Grundmann: *Electrical properties of homoepitaxial ZnO thin films*, 73rd Spring Meeting of the German Physical Society, Dresden, 22.–27. March 2009

A. Lajn, H. v. Wenckstern, M. Brandt, C. Dietrich, G. Benndorf, M. Lorenz, G. Biehne, H. Hochmuth, M. Grundmann: *Electrical properties of homoepitaxial ZnO thin films*, 14th International Conference on II-VI compounds, Saint-Petersburg, Russia, August 2009

A. Lajn, H. v. Wenckstern, M. Brandt, C. Dietrich, G. Benndorf, M. Lorenz, G. Biehne, H. Hochmuth, M. Grundmann: *Electrical properties of homoepitaxial ZnO thin films*, 51st Electronic Materials Conference, University Park, Pennsylvania, USA, June 2009

M. Lorenz, H. Frenzel, G. Biehne, H. Hochmuth, M. Grundmann: *Design and characterization of ZnO-based MESFETs on glass substrates*, 73rd Spring Meeting of the German Physical Society, Dresden, 22.–27. March 2009

A. Müller, M. Stölzel, G. Benndorf, M. Grundmann: *Exciton Recombination Dynamics in MgZnO Thin Films*, 73rd Spring Meeting of the German Physical Society, Dresden, 22.–27. March 2009

A. Müller, M. Stölzel, S. Heitsch, G. Benndorf, J. Zippel, M. Lorenz, M. Grundmann: *Time-Resolved Photoluminescence on ZnO-Based Single and Double Quantum Wells*, MRS Fall Meeting 2009, Boston, MA, USA, 30. November – 04. December 2009

F. Schein, H. Frenzel, A. Lajn, G. Biehne, H. Hochmuth, M. Lorenz, M. Grundmann: *Discrete Inverter Structures based on Zinc Oxide*, 73rd Spring Meeting of the German Physical Society, Dresden, 22.–27. March 2009

M. Schmidt, M. Ellguth, T. Lüder, F. Schmidt, R. Pickenhain, M. Grundmann, G. Brauer, W. Skorupa: *Deep levels in nitrogen implanted ZnO*, 73rd Spring Meeting of the German Physical Society, Dresden, 22.–27. March 2009

R. Schmidt-Grund, C. Sturm, H. Hilmer, A. Hinkel, J. Zúñiga-Pérez, M. Grundmann: *Exciton-polaritons in one- and two-dimensional confined ZnO resonators*, 11th International Conference on Optics of Excitons in Confined Systems (OECS 11), Madrid, Spain, 7.–11. September 2009

R. Schmidt-Grund, A. Hinkel, H. Hilmer, J. Zúñiga-Pérez, C. Sturm, C. Czekalla, G. Zimmermann, J. Lenzner, M. Lorenz, M. Grundmann: *ZnO nano-pillar resonators with coaxial Bragg-Reflectors*, MRS Spring Meeting 2009, San Francisco, USA, 13.–17. April 2009

S. Schöche, R. Schmidt-Grund, C. Sturm, H. Hochmuth, M. Brandt, M. Lorenz, M. Grundmann: *Optische und strukturelle Untersuchung an Bariumtitanat-Dünnschichten*, 73rd Spring Meeting of the German Physical Society, Dresden, 22.–27. March 2009

M. Stölzel, A. Müller, J. Zippel, G. Benndorf, H. Hochmuth, M. Lorenz, M. Grundmann: *Time-resolved photoluminescence on ZnO based quantum well structures*, 73rd Spring Meeting of the German Physical Society, Dresden, 22.–27. March 2009

C. Sturm, H. Hilmer, R. Schmidt-Grund, C. Czekalla, J. Lenzner, H. Hochmuth, B. Rheinländer, M. Grundmann: *Strong Exciton-Photon Coupling up to 410 K*, 9th International Conference on Physics of Light-Matter Coupling in Nanostructures (PLMCN9), Lecce, Italy, 16.–20. April 2009

C. Sturm, H. Hilmer, R. Schmidt-Grund, C. Czekalla, M. Lorenz, M. Grundmann: *Formation of Exciton-Polaritons up to 410 K in ZnO based planar resonators*, 73rd Spring Meeting of the German Physical Society, Dresden, 22.–27. March 2009

H. von Wenckstern, K. Brachwitz, M. Schmidt, F. Schmidt, S. Müller, Ch. Dietrich, J. Zippel, M. Ellguth, G. Biehne, M. Lorenz and M. Grundmann: *Electrical characterization of defect levels in Mg_xZn_{1-x}O PLD thin films*, Electronic materials conference, University Park, Pennsylvania (2009)

H. von Wenckstern, S. Müller, M. Schmidt, M. Brandt, A. Lajn, F. Schmidt, G. Biehne, M. Lorenz and M. Grundmann: *Stability of Schottky barriers on ZnO PLD thin films beyond 400 K*, Electronic materials conference, University Park, Pennsylvania (2009)

H. von Wenckstern: *ZnO-based devices*, 1st PhD Workshop of SFB 762, Wittenberg (2009)

H. von Wenckstern: *Anionic and Cationic substitution in ZnO*, Abschlusstreffen des SPP1136, Eisenach (2009)

H. von Wenckstern, M. Brandt, M. Bonholzer, M. Lange, R. Heinhold, K. Brachwitz, F. Schmidt, M. Lorenz, M. Grundmann: *Properties of $Mg_xZn_{1-x}O:P$ thin films grown on (000-1) ZnO*, MRS Fall Meeting, Boston (2009)

H. von Wenckstern, K. Brachwitz, M. Schmidt, F. Schmidt, S. Müller, Ch. Dietrich, J. Zippel, M. Ellguth, G. Biehne, M. Lorenz, M. Grundmann: *Schottky barrier contacts on $Mg_xZn_{1-x}O$ thin films*, MRS Fall Meeting, Boston (2009).

J. Zippel, G. Benndorf, H. Hochmuth, M. Lorenz, M. Grundmann: *Cathodoluminescence on ZnO/MgZnO Double Quantum Wells*, 73rd Spring Meeting of the German Physical Society, Dresden, 22.–27. March 2009

Posters

S. Chouthe, S. Acharya, C. Sturm, G. Seifert, R. Schmidt-Grund, M. Grundmann, H. Graener: *Charge Carriers Dynamics of ZnO and ZnO-BaTiO₃ thin films*, 11th International Conference on Optics of Excitons in Confined Systems (OECS 11), Madrid, Spain, 7.–11. September 2009

H. Hilmer, C. Sturm, R. Schmidt-Grund, J. Zúñiga-Pérez, J. Sellmann, A. Hinkel, C. Czekalla, J. Lenzner, G. Zimmermann, H. Hochmuth, M. Lorenz, B. Rheinländer, M. Grundmann: *PLD-growth of ZnO-based planar and cylindrical microresonators*, 73rd Spring Meeting of the German Physical Society, Dresden, 22.–27. March 2009

P. Kühne, R. Schmidt-Grund, C. Sturm, M. Brandt, M. Grundmann: *Temperature dependent dielectric function of ZnO*, 5th Workshop Ellipsometry, Zweibrücken, Germany, 2.–4. March 2009

A.Lajn, H. Frenzel, M. Lorenz, F. Schein, H. v. Wenckstern, M. Grundmann: *Transparente Elektronik*, Presentation on the occasion of the visit of the Minister-President of saxony, November 2009

M. Lange, C. Czekalla, J. Zúñiga-Pérez, G. Zimmermann, M. Lorenz, M. Grundmann: *Growth and characterization of MgZnO nanowires*, 2nd Scientific Symposium of the Graduate School BuildMoNa, Leipzig, 2./3. March 2009

M. Lange, C. Czekalla, J. Zúñiga-Pérez, M. Lorenz, M. Grundmann: *Growth and characterization of MgZnO nanowires*, WEH Physics School: Nanoscaled Oxides-Big Opportunities in Small Structures, Bad Honnef, 2.–8. August 2009

M. Lange, C. P. Dietrich, C. Czekalla, M. Lorenz, M. Grundmann: *Luminescence properties of ZnO/ZnCdO double heterostructures*, MRS Fall Meeting 2009, Boston, USA, 30. November – 2. December 2009

A. Müller, M. Stölzel, G. Benndorf, Ch. Dietrich, M. Grundmann: *Origin of the Near-Band-Edge Luminescence in MgZnO*, 2. Scientific Symposium of BuildMoNa, Leipzig, Germany, 02./03. April 2009

S. Puttnins, H. Zachmann, A. Rahm, M. Grundmann: *Novel Determination Method for Solar Cell Series Resistance and Shunt Resistance Considering Voltage Dependent Carrier Collection*, MRS Fall Meeting Boston, Symposium Q, 30. November – 4. December 2009

M. Schmidt, M. Ellguth, T. Lüder, H. v. Wenckstern, R. Pickenhain, M. Grundmann, G. Brauer, W. Skorupa: *Investigation of defects in nitrogen implanted n - type ZnO by capacitance spectroscopy with simultaneous optical excitation*, 25th Internat. Conference on Defects in Semiconductors

S. Schöche, R. Schmidt-Grund, C. Sturm, M. Brandt, H. Hochmuth, M. Lorenz, M. Grundmann: *Optical and structural investigations on BaTiO₃-thin films*, 5th Workshop Ellipsometry, Zweibrücken, Germany, 2.–4. March 2009

C. Sturm, H. Hilmer, R. Schmidt-Grund, M. Grundmann: *Polarization Behaviour of the Exciton-polariton Emission in ZnO Based Microresonators*, MRS Fall Meeting 2009, Boston, USA, 30. November – 4. December 2009

H. Zachmann, S. Puttnins, F. Daume, A. Rahm, K. Otte, R. Caballero(3), C. A. Kaufmann, T. Eisenbarth, Hans-Werner Schock: *Incorporation of Na in low-temperature deposition of CIGS flexible solar cells*, MRS Fall Meeting Boston, Symposium Q, 30. November – 4. December 2009

Zh. Zhang, C. Czekalla, M. Schmidt, A. Lajn, H. Hochmuth, H. v. Wenckstern, M. Grundmann: *Ortsaufgelöste Photostromuntersuchungen an Zinkoxid Schottky-Kontakten*, 73rd Spring Meeting of the German Physical Society, Dresden, 22.–27. March 2009

Zh. Zhang, M. Lorenz, L. Behnke, C. Czekalla, H. Frenzel, M. Schmidt, G. Biehne, H. Hochmuth, H. v. Wenckstern, M. Grundmann: *Space-charge regions in ZnO-based metal-semiconductor field-effect transistors and metal-semiconductor-metal photodetectors*, MRS Fall Meeting, Boston, USA, 30. November – 04. December 2009

8.35 Graduations

Doctorate

- Jens Bauer
Metallorganische Gasphasenepitaxie von GaAs und InAs Nanodrahtstrukturen über den 'vapor-liquid-solid' Mechanismus
June 2009
- Christian Czekalla
Ortsaufgelöste Lumineszenz von Zinkoxid-Mikronadeln
December 2009

Diploma

- Ronny Bakowski (in collaboration with Q-Cells)
Elektrische Charakterisierung von Defekten in multikristallinem Silizium für photo-voltische Anwendungen
March 2009
- Lucie Behnke
Eigenschaften von ZnO und MgZnO MSM Photodetektoren
September 2009
- Kerstin Brachwitz
Untersuchung der strukturellen und elektronischen Eigenschaften von Magnesium-zinkoxid
October 2009
- Felix Daume
Die elektrische Charakterisierung des Absorbers Cu(In, Ga)Se₂ von flexiblen Solarzellen
December 2009
- Christof Peter Dietrich
Strukturelle und optische Eigenschaften von Magnesiumzinkoxid-Dünnschichten
March 2009
- Andreas Kraus
Untersuchungen zur Löcherinjektion in n-ZnO/p-Substrat-Heterostrukturen
September 2009
- Philipp Kühne
Tiefenellipsometrie: Aufbau und Erprobung eines Messplatzes und Messungen an ZnO
May 2009
- Thomas Lange (in collaboration with Solarion AG)
Analyse der Quanteneffizienz flexibler Dünnschichtsolarzellen auf Cu(In,Ga)Se₂ Basis
September 2009
- Niklas Liebing
Channeling Contrast Microscopy
March 2009
- Michael Lorenz
Herstellung und Charakterisierung von ZnO-basierten Metall-Halbleiter- Feldefekt-transistoren auf Glassubstraten
August 2009
- Thomas Lüder
Untersuchungen zur Stickstoff-Implantation in Zinkoxid
January 2009
- Matthias Müller (in collaboration with Q-Cells)
Modellierung und Verifizierung des Jahreswirkungsgrades von Solarzellen
March 2009

- Charlotte Pfau (in collaboration with Forschungszentrum Dresden-Rossendorf)
Dephasierung und Intersubbandrelaxation in InGaAs/AlAsSb-Halbleiter-Quantensstrukturen
January 2009
- Stefan Puttnins (in collaboration with Solarion AG)
Kennlinienanalyse und Simulation von flexiblen CIGSe Dünnschichtszellen
October 2009
- Friedrich Leonhard Schein
Design, Aufbau und Charakterisierung von integrierten Schaltungen basierend auf Zinkoxid
December 2009
- Stefan Schöche
Kristallstruktur und dielektrische Funktion von Bariumtitanat-Einkristallen und -Dünnschichten
October 2009
- Dieter Stender
Spektroskopie der Photoleitung an Magnesium-Zinkoxid-Dünnschichten im mittleren Infrarot
October 2009
- Marko Stölzel
Zeitaufgelöste Photolumineszenz an ZnO-Strukturen
May 2009
- Zhipeng Zhang
Untersuchungen an Raumladungszonen in Zinkoxid-Schottky-Kontakten
August 2009

Master

- Nuchjarim Yensoung
Investigation of Insulating Oxide Layers and Related MIS Diodes
February 2009
- Moritz Steffler
Interfacing Neurons with Transparent Semiconductors
August 2009

Bachelor

- Uta Allenstein
Elektrische Charakterisierung von ionenimplantiertem ZnO
October 2009
- Michael Bonholzer
MgZnO:P-Dünnschichten: Herstellung, Charakterisierung und Aktivierung von Akzeptoren
October 2009

- Martin Glaser
Polarisationsaufgelöste Lumineszenz-Untersuchungen an ZnO-Mikronadeln
September 2009
- Christoph Grüner
Untersuchung des PLD-Laserplasmas mittels optischer Emissionsspektroskopie
October 2009
- Lars Heerklotz
Diffusion von Metallen in Zinkoxid
December 2009
- Oliver Kramer
Schottky-Kontakte auf MgZnO
October 2009
- Marcus Müller
Elektrische Charakterisierung von Störstellen in kommerziellem Silizium (umg-Si)
December 2009
- Peter Schwinkendorf
Untersuchungen an ferroelektrischen Feldeffekttransistoren auf Zinkoxid/Bariumtitanat-Basis
October 2009
- Thies (in collaboration with Q-Cells)
Quantitative elemental mapping of solar cells by ion microscopy
August 2009

8.36 Guests

- Prof. Dr. Mathias Schubert
Department of Electrical Engineering & Center for Materials Research and Analysis,
University of Nebraska, Lincoln, USA
03. August - 28. August 2009
- V. Manikyala Rao Voora
Department of Electrical Engineering & Center for Materials Research and Analysis,
University of Nebraska, Lincoln, USA
27. July - 31. August 2009

9

Solid State Optics and Acoustics

9.1 Introduction

The research is concentrating on the study of transport properties of elementary excitations in condensed matter of the Bosonic type (Bosonic quasi particles). Concerning the conventional description this relates mainly to acoustic and optic waves. Special interest is currently given to the influence of anisotropy but also of inhomogeneity to the dynamics of mechanical excitations. Furthermore novel schemes and first principle modeling is developed for the study and in support of applications concerning nonlinear interaction of acoustic excitations.

Applications concentrate on the enhancement and application of high resolution monitoring in space and time. The respective technologies include scanning Bosonic confocal microscopy for which even a combined instrument for optical and acoustical excitations has been developed. Three dimensional microscopic imaging is also pursued with support of novel technologies including microscopic holographic imaging and microscopic tomography. With relation to temporal resolution the developments pursued in 7th European framework for "Aircraft Integrated Structural Health Assessment (AISHA II) include refinements of electronic schemes capable of pico-second resolution. Concerning microscopic applications fuel cell membranes are characterized in the Project MultiPlat of the 7th European framework. Furthermore bio-medical applications involve non-invasive high resolution acoustic imaging of living mesenchymal stem cells for substantial fractions of the life cycle, acoustic monitoring of cell constructs by optical and acoustic methods, and monitoring of the muscle dynamics of exercising athletes. The transport properties of transverse acoustic waves in fluids and soft matter are studied to determine rheological properties.

The development of monitoring technologies is supported in international co-operations including combined developments with institutions in Bangladesh, India and the USA, in European projects of the 7th Framework, and in international and national projects in cooperation with industry including also projects (MagnaCode im Vorhabensbereich ForMat, NEMO Netzwerk MONIFER) of the Bundesministerium für Bildung und Forschung (BMBF).

9.2 Cartilage tissue engineering by collagen scaffold associated mesenchymal stem cells in a novel bioreactor

E. vonderBurg, M. vonButtlar, W. Grill

9.2.1 Objectives

Non-invasive monitoring is an important element of regenerative medicine because implants and components of implants should be 100% quality-checked with non-invasive and therefore also marker-free methods. This can be accomplished by ultrasound monitoring and rheological measurements during culturing.

9.2.2 Material and Methods

For this purpose a novel bioreactor with computer controlled mechanical activation and integrated non-invasive online monitoring has been constructed for the in situ determination of ultrasonic and rheological parameters (Figure 9.1). The system has been employed for the production of collagen scaffolds seeded with mesenchymal stem cells (MSC's). The principle of tissue engineering in a bioreactor is described here [1].



Figure 9.1: Bioreactor with integrated non-invasive monitoring for the in situ measurement of ultrasonic and rheological parameters

During the cultivation period of about two weeks the scaffold is periodically compressed by two movable pistons for improved differentiation of the MSC's [2][3]. Furthermore the periodic compression beneficially ensures the supply with nutrition even inside the sample. During the physiological stimuli, rheological properties are measured by means of highly sensitive load cells. In addition measurements of the speed of sound in the sample with frequencies up to 16 MHz and in the culture media are performed continuously (Figure 9.2). Therefore piezoceramic transducers are attached to the pistons and emit and detect ultrasonic waves, travelling through the pistons, the sample and the culture medium. The time-of-flight (TOF) of the ultrasonic signals is determined in real time with the aid of chirped excitation and correlation procedures with a resolution of at least 10 ps. The implemented ultrasonic measurement scheme allows beside the speed of sound measurements the detection of the distance between the pistons with a resolution better than 100 nm. The monitoring delivers information on rigidity, fluid dynamics and velocity of sound in the sample and in the culture media. The hermetically sealed Bioreactor with its life support system provides an biocompatible environment for MSC's for long time cultivation.

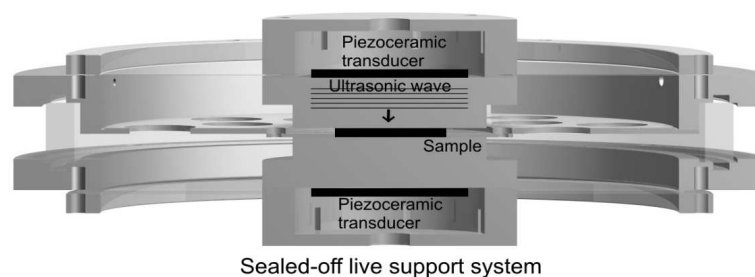


Figure 9.2: Bioreactor with implemented ultrasonic measurement scheme.

9.2.3 Results and Conclusions

Rheological measurements are performed by monitoring the relaxation process of the scaffold following a defined compression with the load cells (measurement of pressure) and with the ultrasonic detection scheme (measurement of the creeping of pistons). The piston is therefore held in the position of maximal contraction for 12 seconds. The scaffold cannot hold the pressure and releases fluid, allowing the pressure to drop. Figure 9.3 shows a relaxation curves which can be reproduced precisely by the stated adjusted model. A single exponential Model will not suffice. We identify the three parts of the model as the effect of solid fraction (parameter γ_0), the relative fast deformation of the collagen matrix ($\tau_1=0,35$ s) and the relative slow squeeze out of the fluid ($\tau_2=3,16$ s). The effect of the solid fraction (parameter γ_0) correlates with the rigidity of the sample and is therefore an indicator of the extracellular matrix which was building up by the MSCs.

The development of the parameter γ_0 over the cultivation period (2 weeks) is displayed in Figure 9.4. We can identify the desired increase in rigidity γ_0 in the first

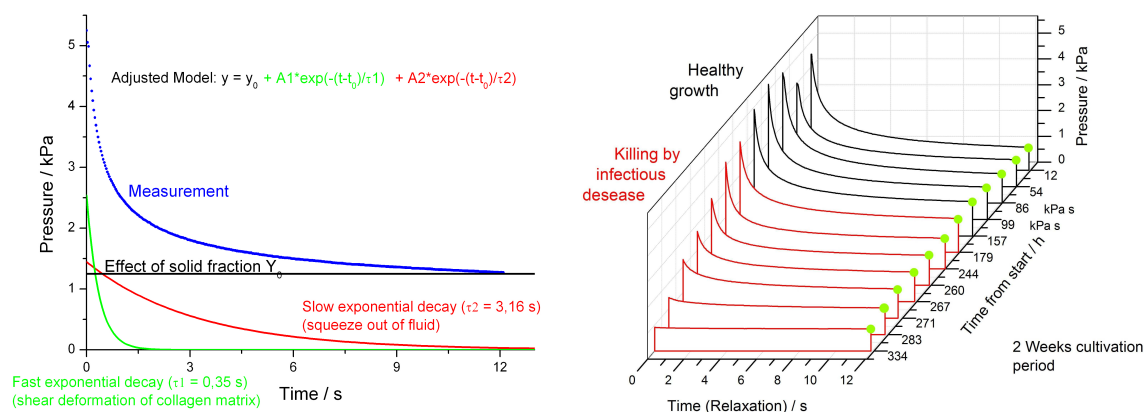


Figure 9.3: Measurement of the relaxation process following compression of a collagen scaffold with human MSC's (left). Development of the relaxation curve of figure to the left over the cultivation period. The parameter Y_0 (Effect of solid fraction) is marked by the green points (right).

week. In the second week deterioration is observed. The origin is obviously a contamination introduced by the exchange of culture medium at 99 hours. This unfortunate event serves here the purpose to demonstrate the capability of the non-invasive monitoring scheme for the detection of shortcomings in the culturing process. The combined

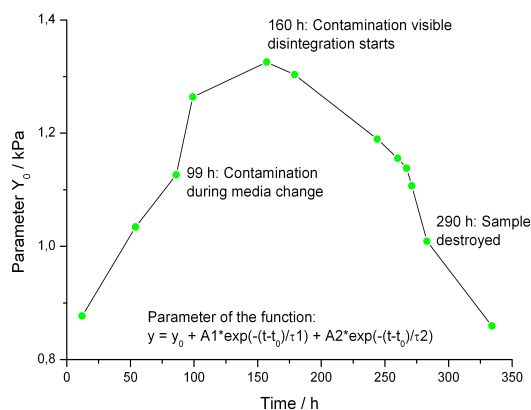


Figure 9.4: Development of the parameter Y_0 over the cultivation period (2 weeks).

acoustical and rheological monitoring inside the bioreactor allows to identify different developmental stages of the cell constructs. The measurements inside the bioreactor characterize the growth process of neo-cartilage and allow the online adjustments of process parameters for optimized culturing.

- [1] I. Martin, D. Wendt, and M. Heberer: *The role of bioreactors in tissue engineering* Trends Biotechnol **22(2)** 80-6 (2004)
- [2] D.L. Butler, S.A. Goldstein, and F. Guilak: *Functional tissue engineering: the role of biomechanics* J Biomech Eng **122(6)** 570-5 (2000)
- [3] C.Y. Huang, K.L. Hagar, L.E. Frost, Y. Sun, and H.S. Cheung: *Effects of cyclic compressive loading on chondrogenesis of rabbit bone-marrow derived mesenchymal stem cells* Stem Cells **22(3)** 313-23 (2004)

9.3 Non invasive high resolution acoustic monitoring of mesenchymal stem cells

M. von Buttlar, W. Grill

In this project living stem cells are observed with scanning acoustic microscopy. The instrument works at an ultrasound frequency of 1.2 GHz and has magnitude and phase contrast [3]. The goal of the project is to observe adherent ovine stem cells non-invasively for extended periods of time. Advances in the imaging of biological cells were made by improved signal and image processing [1]. The system consists of a combinatory inverted optical laser scanning microscope and a scanning acoustic microscope with access to the sample from above with facilities for live-cell imaging [2]. The observation chamber has a pre-mixed gas atmosphere and a constant temperature of 37° Celsius. The captured magnitude data serves as the texture and the phase information is used as the height map assuming constant sound velocity inside the cells. Figure 9.5 shows one frame of a time-lapsed movie of ovine mesenchymal stem cells. The movie was processed for 3D-view with red cyan glasses. This view shows an excerpt from the imaged area of $306\mu\text{m} \times 225\mu\text{m}$. Image acquisition took 40 seconds. A condensed cell is visible on the right side whereas the cells on the left side are spread out on the substrate.

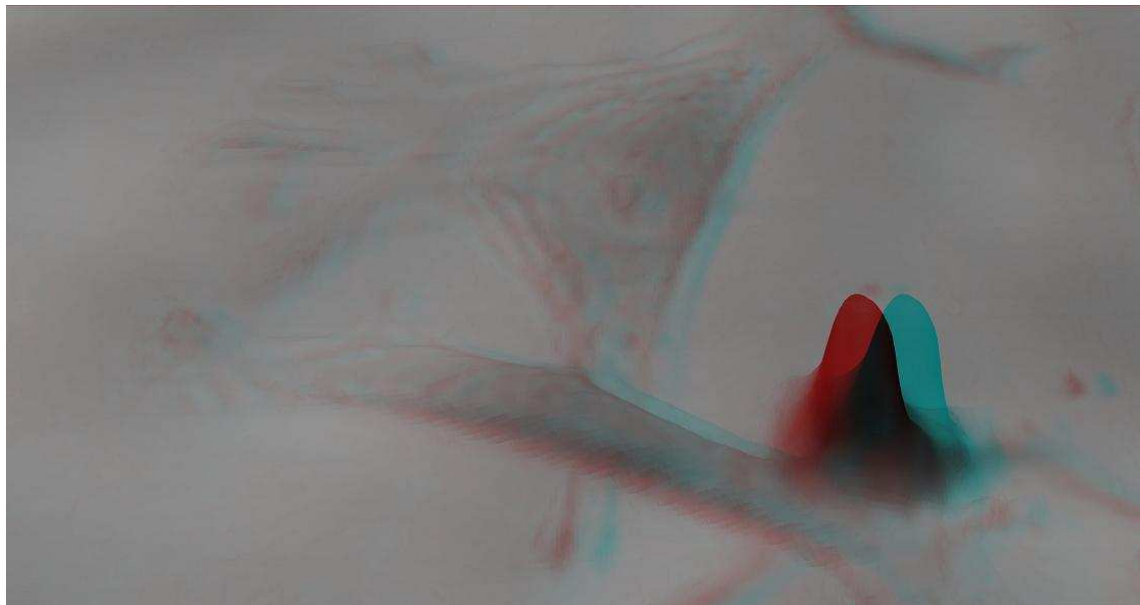


Figure 9.5: Pseudo 3D view of ovine mesenchymal stem cells created from acoustic images in magnitude and phase contrast

- [1] M. von Buttlar and Esam Ahmed Mohamed and W. Grill: *Signal processing for time-lapse cell imaging with vector-contrast scanning acoustic microscopy*, Acoustical Imaging: Volume 30 ,editors Joie P. Jones and Hua Lee, Springer; 1st Edition. edition, in press
- [2] A. Kamanyi, W. Ngwa, T. Betz and R. Wannemacher and W. Grill: *Combined phase-sensitive acoustic microscopy and confocal laser scanning microscopy*, Ultrasonics **44**, e1295 (2006)

- [3] W. Grill, K. Hillmann, T. J. Kim, O. Lenkeit, J. Ndop, M. Schubert: *Scanning acoustic microscopy with vector contrast*, *Physica B* **263**, 553 (1999)

9.4 Ultra-high resolution thin film delineation using reflection phase-sensitive acoustic microscopy

E.T. AhmedMohamed, A. Kamanyi, M. vonButtlar, R. Wannemacher*, K. Hillmann[†], W. Ngwa[‡], W. Grill

*IMDEA, Ciudad Universitaria de Cantoblanco, Madrid, Spain

[†]SAP Deutschland AG & Co. KG, Albert-Einstein-Allee 3, D-64625 Bensheim, Germany

[‡]Department of Physics, University of Central Florida, Orlando, Florida, FL 32816, USA

Phase-sensitive acoustic microscopy has long been known as a high-resolution non-contacting height profiling tool [1]. If the acoustic magnitude and phase data gained from the acoustic images are plotted such that the phase data corresponds to the angular coordinate and the magnitude data corresponds to the radial part, that will result in a single polar curve with the data points distributed spatially depending on the variation of the thickness of the material. The signature of the deposited object can be fitted based on a model that simulates propagation of sound in the coupling fluid, the sample and the substrate resulting in the determination of sample properties with a resolution of less than 1% [2]. After optimum adjustment of the model parameters, the thickness corresponding to each measured value of the reflectivity (the spatially distributed points in the polar plot) can inversely be mapped. The method allows topographical mapping of thin films with a height resolution beyond the diffraction limit of optical confocal microscopy [3]. The method was applied for a thin film of chitosan deposited on glass, and imaged in reflection at 1.2 GHz focusing on the glass-substrate. The variation of the complex reflected signal with the variable local thickness $V(d)$ is given by [4]:

$$V(d) = \int P^2\left(\frac{r}{f_0}\right) R\left(\frac{r}{f_0}, d\right) e^{-i2kd} \sqrt{1 - \left(\frac{r}{f_0}\right)^2} \frac{r}{\sqrt{1 - \left(\frac{r}{f_0}\right)^2}} dr, \quad (9.1)$$

where $P(r/f_0)$ is the pupil function, that describes the transmission through the spherical surface of the lens, $r/f_0 = k_r/k$, where k_r is the lateral component of the wave vector \mathbf{k} in the coupling fluid and the variables r and f_0 are geometrical parameters of the lens.

$R(r/f_0, d)$ is the thickness-dependent reflection coefficient of the studied layer which is calculated as the infinite sum of a geometrical progression that is built from the reflection from the top of the layer and multiple contributions from the transmission through the surface of the layer, reflection from the sample-substrate interface and transmission back into the coupling fluid within a wedge-shaped sample.

$$R(\theta, d) = r_{12}(\theta) + \frac{[1 - r_{12}^2(\theta)] r_{23}(\theta_1) e^{2ik_2 d}}{1 + r_{12}(\theta_1) r_{23}(\theta_1) e^{2ik_2 d}}, \quad (9.2)$$

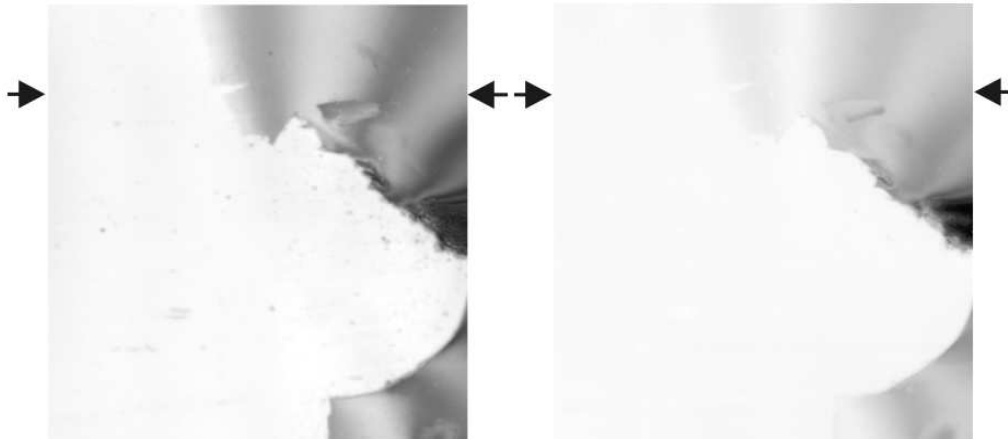


Figure 9.6: Images in magnitude contrast (Left, black representing zero signal) and phase contrast (right, full gray scale of the image representing 2π) of a chitosan layer of variable thickness on a glass substrate. The data has been evaluated for the area above the line between the arrows. The size of the images is $140\mu\text{m}\times 140\mu\text{m}$.

where, $r_{12}(\theta)$ is the reflection coefficient corresponding to the coupling fluid-sample interface, $r_{23}(\theta)$ is the reflection coefficient corresponding to the sample-substrate-interface, and d is the local thickness.

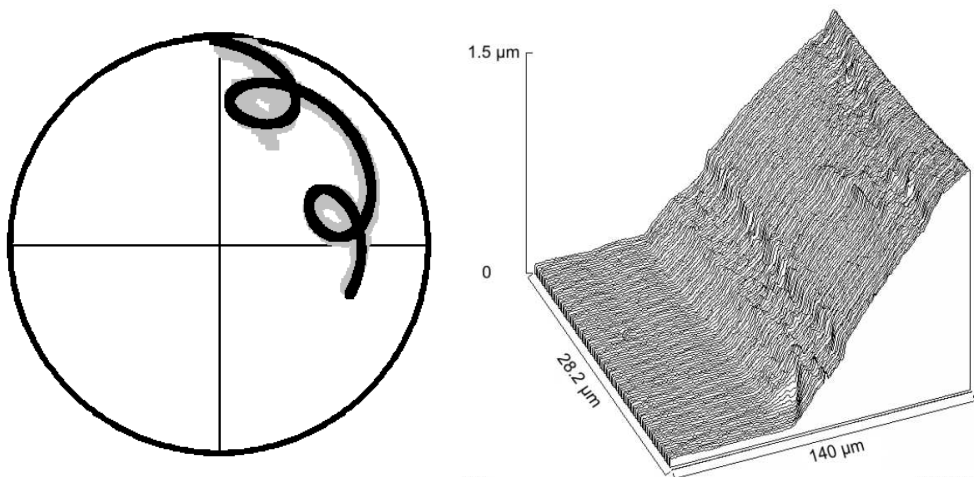


Figure 9.7: Polar diagram of the magnitude and phase of the reflected signal for data taken from the area above the line between the arrows (left). The experimental values are in gray and the fit of the experimental data is the black solid line. Existence of a residual layer of $0.06\mu\text{m}$ was assumed. Waterfall representation of the height (right), as calculated by the model for each point in the marked area in the images in 9.6

The model calculations simulate the reflection from a thin film that has a thickness varying from a minimum value d_{min} to a maximum value d_{max} in n_z steps of thickness intervals ds such that:

$$d_s = \frac{d_{max} - d_{min}}{n_z - 1}. \quad (9.3)$$

The software is fed with trial input values for the parameters of the sample (density, attenuation and speed of longitudinal sound wave) iteratively, until the best agreement between the calculated and measured data is achieved. The thickness corresponding to a calculated value of the complex reflection coefficient is ascribed to the nearest measured point in the polar plot, such that the distance between the measured and calculated points, in the polar graph, t as calculated by (Equation 9.4) assumes a minimum.

$$t = \sqrt{(X_c - X_m)^2 + (Y_c - Y_m)^2}, \quad (9.4)$$

where, X_m, Y_m are the Cartesian coordinates of the measured value and X_c, Y_c corresponds to the coordinates of the nearest calculated value. The height profile was calculated for the area (140 μm by 28.2 μm) above the arrows in the images in figure 1. The mapped height profile is represented by a color scale (figure 9.7 right). A waterfall representation of the data of figure 9.7(left) is shown in figure 9.7(right).

The systematic error was evaluated from the deviation of calculated height values from an assumed and fitted linear rise (figure 9.8(left)) to be 33 nm. For parts of the line where the systematic error defined in this way vanishes, the deviations from optimum linear fit is attributed to statistical errors, which were about 2.6 nm for the data taken a long a line of about 5 μm . This indicates that the resolution for height mapping as provided by the current method is higher than could be achieved by most of the available optical confocal microscopic techniques.

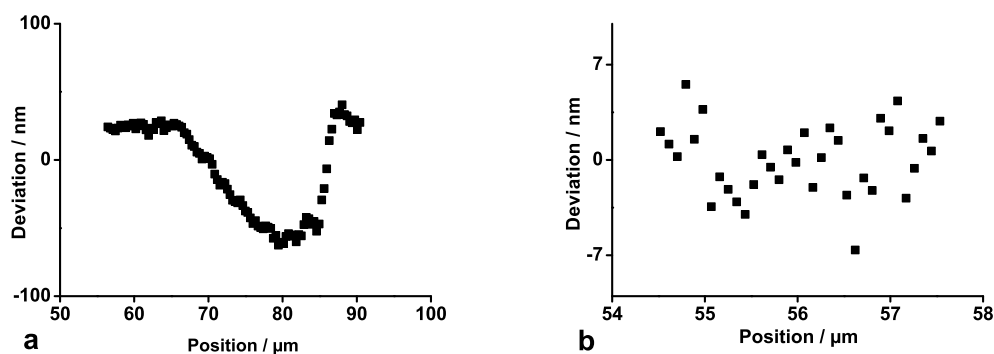


Figure 9.8: Estimation of the systematic (left) and statistical (right) errors.

- [1] K. Liang, S.D. Bennett, B. Khuri-Yakub, Phys. Lett. **41** (1982)
- [2] E. T Ahmed Mohamed A. Kamanyi, M. von Buttlar, R. Wannemacher, K. Hillmann, W. Ngwa, W. Grill, Proc. SPIE **6935**, 69351Z (2008)
- [3] E. T Ahmed Mohamed A. Kamanyi, M. von Buttlar, R. Wannemacher, K. Hillmann, W. Ngwa, W. Grill. Proc. Acoustical Imaging **30**, (2010)
- [4] P. Reinholdtsen, C-H. Chou, B. Khuri-Yakub. IEEE Ultrasonic symposium (1987)

9.5 Characterization of elastomers with transverse sonic waves

E. vonderBurg, W. Grill

The production of certain elastomer-products suffers from a lack of control notably during vulcanization of the rubber. Some products like membrane materials have to be delivered with a specific degree of vulcanization and are therefore critical concerning slight changes in the composition and in the relevant parameters during production (mainly temperature and time of vulcanization). There are no standard instruments available for an on-line and non-destructive measurement of the elastic parameters of rubber in the production process. Most of the quality control is done by static or quasistatic measurements on samples which are extracted from the products. Due to the fact that sonic waves rely on the mechanical properties of the materials in which they propagate, they should be well suited for this task. There have been some attempts to investigate rubber, particularly the degree of vulcanization, with sound waves or vibrations e.g. [1][2].

We have performed measurements of the dependency between the degree of vulcanization and the velocity of longitudinal sound. The measurements employed the short-pulse-transit method described in [3] which is similar to the well established pulse-echo method but performed double ended in transition. In Figure 9.9 results are presented. Despite the high resolution of the measurement, it is obvious that there exists no significant dependence of the velocity of longitudinal waves (varying typically less than 1 %) on the degree of vulcanization. Propagation of shear waves over

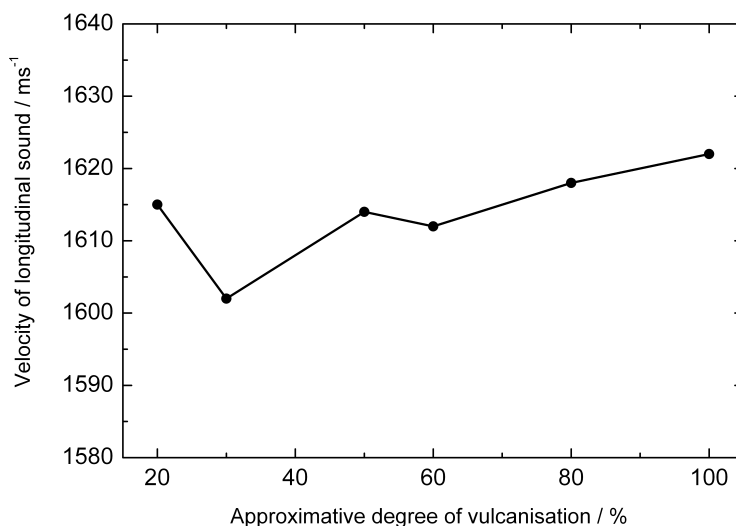


Figure 9.9: Measurement of the velocity of longitudinal sound in 6 elastomer samples. All samples are based on the same natural-rubber-mixture with sulphur as vulcanizer and differ only by their degree of vulcanization.

the distance of several wavelengths has not been achieved before. This may be due to the relatively high and frequency dependent damping of the elastomers for transversal

waves. In addition common, single crystalline transducers for shear waves have parasitic longitudinal resonances leading to the excitation of longitudinal waves. These compressional waves can propagate nearly without damping in comparison to the shear waves and govern the detectable signals. We achieved to measure the shear wave velocity in macroscopic elastomer samples (length of our sample is up to 1 m) and in particular during vulcanization with propagating shear waves over long distances (up to 0,5 m). Necessary therefore was a newly developed system for the dynamic measurement of the shear modulus of elastomers which is based on the construction of compound transducers capable to excite and detect shear waves in rubber (Figure 9.10)

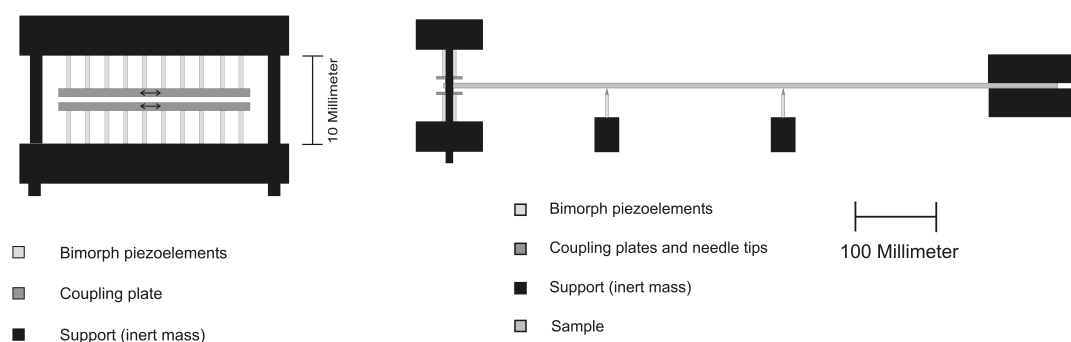


Figure 9.10: Compound transducer (left) . Main parts of the experimental set-up (right).

The sample is clamped at its end between the two coupling plates. The compound transducer holds one end of the sample avoiding unwanted reflections from a free end of the sample. The movement of the coupling plates and the clamped part of the sample is indicated in the figure. The amplitude of the oscillations ranges between 100 nm and 1 μm . In case of a wide sample stripe (width much larger than the wavelength), this leads to pure shear waves, only relying on the shear modulus. For the polarization chosen in the plane of the sample plate the propagation is independent of the thickness of the sample. Figure 9.10 (right) shows the major parts of the experimental set-up. It consists of one compound transducer serving as transmitter and two specially designed receivers for the shear waves at different positions. At the far end of the sample the support consists of a clamp covered with rubber in order to avoid reflections. The set-up is installed in a box to suppress audible noise. Every element of it is mounted on separate acoustically damped supports to avoid cross-talk from the excitation.

Figure 9.11 shows the results for 4 samples with different peroxide content obtained at 2.1 kHz. There is a clear dependency between the degree of vulcanization (content of peroxide) and the velocity of the shear waves. The shear waves are in all cases very slow. In Figure 9.12 the velocities of the shear waves in the frequency range between 600 Hz and 1.9 kHz for three samples were measured. The three samples differ in their degree of vulcanization. Sample cc got the highest degree of vulcanization and aa the lowest. All samples show strong dispersions of the shear waves which can be expected for elastomers over a broad frequency range [4]. For the characterization of the vulcanization of rubber the experimental set-up was modified in a way that the sample could be exposed to infrared radiation. The temperature has been measured with a sensor

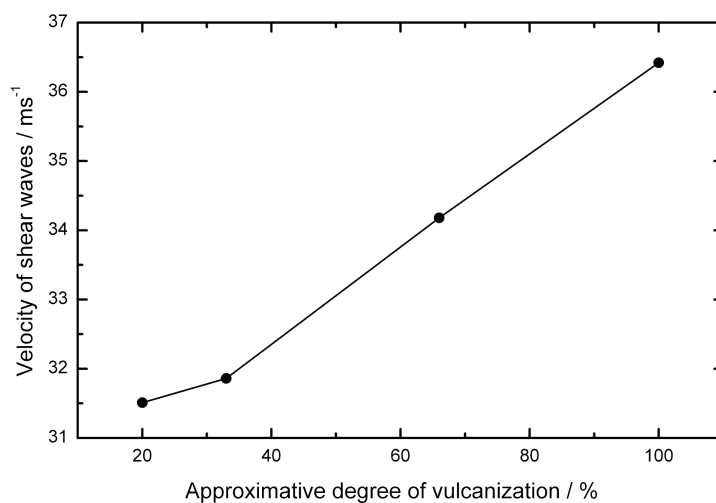


Figure 9.11: Dependence of the velocity of shear waves on the degree of vulcanization for four elastomer samples at 2.1 kHz.

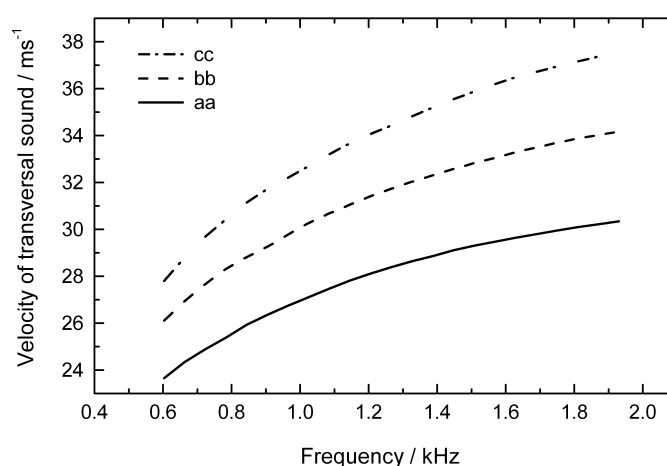


Figure 9.12: Dependence of the velocity of shear waves on the frequency in three different samples. The three samples differ in their degree of vulcanization. Sample cc got the highest degree of vulcanization and aa the lowest.

directly attached to the surface of the sample. Figure 9.13 shows the time dependence of the temperature and velocity of the shear wave for a natural rubber sample with a fabric layer. In the beginning of the heating period the velocity drops sharply due to the softening of the material (decrease of the shear modulus). After 5 minutes the velocity increases even though the temperature is still rising which indicates that the vulcanization process is already ongoing. After cooling of the sample the velocity is still rising. The effect of increasing shear wave velocity following the heating-period

can have two reasons: increase in shear modulus or decrease in density. According to our knowledge the density does not alter significantly during vulcanization so that the main effect should arise from the increase of the shear modulus. It has to be considered that in comparison to measurements with longitudinal waves the velocity of transversal polarized waves is much more sensitive for the degree of vulcanization in a relative soft elastomer. The formulas for the velocity of the longitudinal and transversal polarized

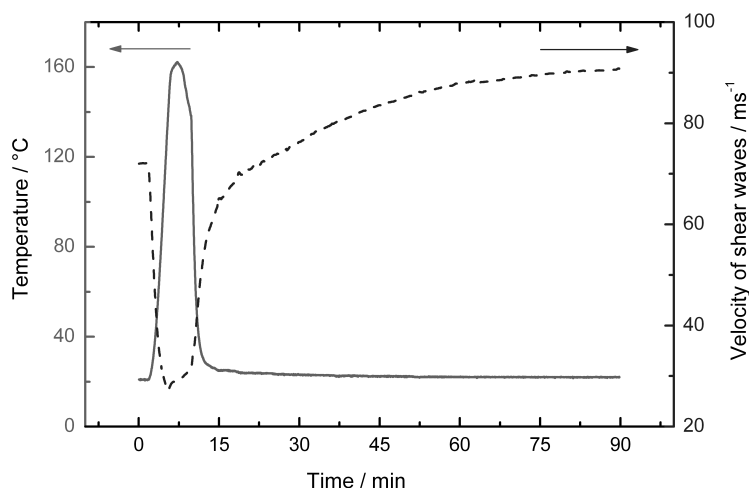


Figure 9.13: Velocity of shear waves with a frequency of 1500 Hz before, during and after heating.

waves follow $v_l = \sqrt{\frac{K + \frac{4}{3}G}{\rho}}$, $v_t = \sqrt{\frac{G}{\rho}}$,

with the shear modulus G , the bulk modulus K and the density ρ . In our elastomers the typical bulk modulus amounts to 2.9 GPa while the shear modulus varies around 1.4 MPa. According to our own measurements the bulk modulus doesn't change significantly due to the vulcanization. The change in the velocity of longitudinal polarized sound during vulcanization originates primarily from the increase of the shear modulus.

During vulcanization chemical crosslinking builds up in elastomers and affects the shear modulus. According to the formulas the effect of vulcanization on the velocity of longitudinal polarized sound can be 100 to 1000 times smaller compared with the effect of vulcanization on the velocity of transversal polarized sound in relative soft elastomers.

- [1] M. Sinha, B. Erman, J. E. Mark, T. H. Ridgway, H. E. Jackson: *Pulse propagation in end-linked poly(dimethylsiloxane) networks* *Macromolecules* **36** 6127 (2003)
- [2] K. G. Häusler, P. Hauptmann, E. Schröder, R. Säuberlich, P. Wagnitz: *Zur Netzwerkcharakterisierung mittels Ultraschall* *Plaste und Kautschuk* **9** 485 (1983)
- [3] T. J. Kim, W. Grill: *Determination of the Velocity of Ultrasound by Short Pulse Switched Sinusoidal Excitation and Phase-Sensitive Detection by a Computer-Controlled Pulse-Echo System* *Ultrasonics* **36** 233 (1998)
- [4] J. D. Ferry: *Viscoelastic Properties of Polymers* John Wiley & Sons, Inc. USA (1980)

9.6 High speed ultrasonic monitoring of joint kinematics of athletes trained for high performance sport

M. Zakir Hossain, W. Grill

9.6.1 Introduction

Muscle dynamics and joint kinematics are monitored and quantified with a novel ultrasonic detection scheme [1]. Based on the measurement of the transit time of longitudinally polarized ultrasound propagating across the observed muscle, the geometric variation of the muscle for isometric and isotonic contraction have been detected. This allows quantification of numerous performance parameters including stress, endurance, energy expenditure, coordination, rhythm ability, optimum repetition, maximum power, reaction time. The achieved temporal and spatial resolutions are 0.01 ms and 0.02 mm respectively

9.6.2 Methods and results

Flexion of the knee joint was restricted by an ultrasonic force sensor to quantify gastrocnemius muscle force and muscle dynamics as well for maximum isometric tetanus. Action was initiated by a sound beep at zero time. Inflection points and conventional fitting are employed to quantify the performance variables depicted in the graphs. Isotonic actions for half-squads (60 rep/min) and elbow motion (120 rep/min) are initiated by rhythmic sound beep and light blink of a metronome. Individual maximum action speed is monitored and quantified in elbow joint dynamics. Comparative analysis of single and multiple action with different stimulus are depicted in respective graphs. By FFT on joint actions data the frequency components of the joint dynamics are derived. Pressing force of the surrounding elastic band allow us to monitor the inertial effect.

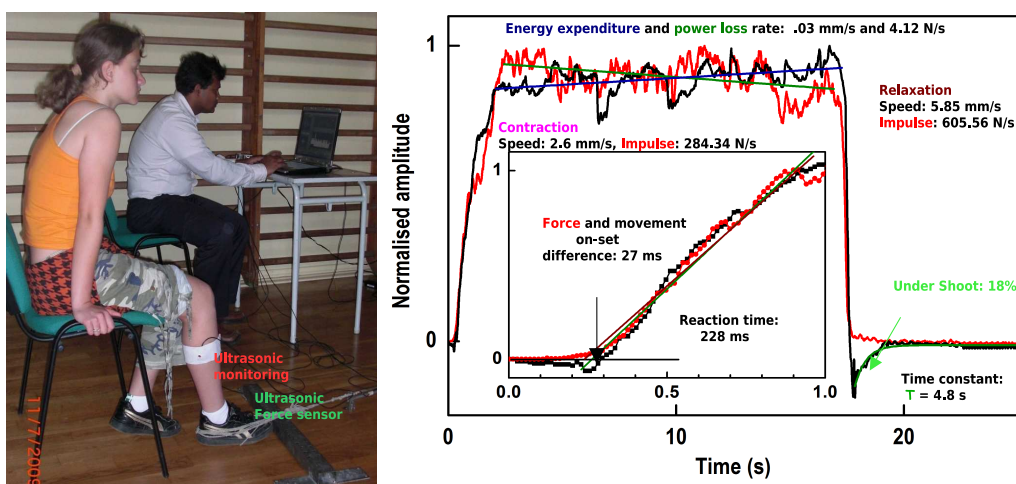


Figure 9.14: Online monitoring set-ups (left). Monitored muscle force and lateral expansion due to all-out isometric tetanus (right). Inset graph shows first one second data.

Synchronously monitored muscle dynamics and force are shown in figure 9.14. The analysis of first one second data (figure 9.14 (right), inset graph) depict the movement reaction time of 228 ms. The muscle force on-set is of 27ms earlier that the on-set of muscle movement. Contraction speed and impulse, relaxation speed and impulse due to the isometric tetanus are found to be: 2.6 mm/s and 284.34 N/s; 5.85mm/s and 605 N/s respectively. Figure 9.15 (right), depicted the characteristic curves for the knee joint

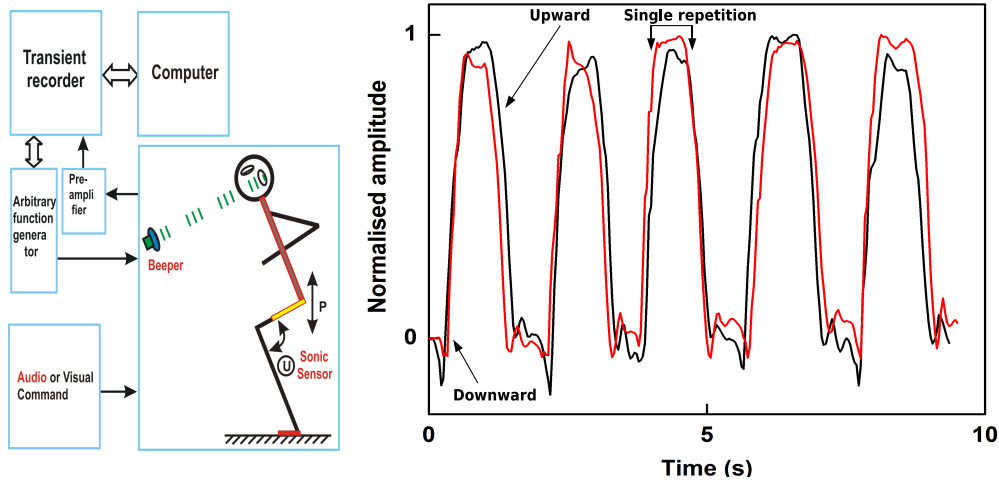


Figure 9.15: Block diagram for joint action monitoring and graphical view of knee joint dynamic data for half-squads.

dynamic data for selected five half squads with sound and light signal initiations. The action was started from standing position. One of the selected actions is analyzed to quantify the knee joint kinematics for single action. Quantitative results are shown in figure 3. Undershoot in the curve depicted the inertial effect due to sudden upward motion in each repetition. Up and down-ward velocity is more for the light initiation. The retarded motion is shown at the top part of the graph which occur due to the adjustment factor of the neuromuscular coordination with the initiated rhythm. The derivative of a single action are performed for the further interpretations of results. From the kinematic analysis of a single action of half squads (figure 9.16 left) it is found

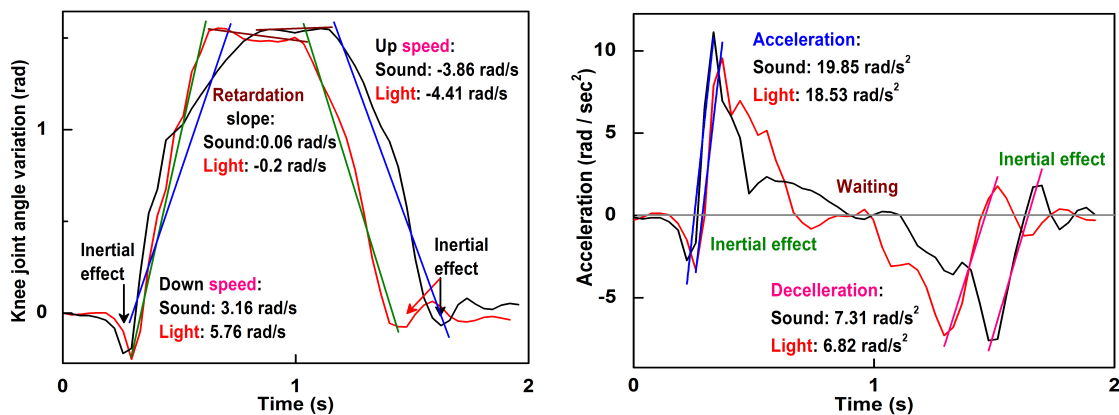


Figure 9.16: Block diagram for joint action monitoring and graphical view of knee joint dynamic data for half-squads.

that up and down speed for sound initiation: -3.86 rad/s and 3.16 rad/s and for light initiation: -4.41 rad/s and 5.76 rad/s respectively. The retardation slope 0.06 rad/s for the sound and -0.2 rad/s for the light initiation. The derivative of this single action data e.g the acceleration of this action (figure 3, right) was found to be: 19.85 rad/s^2 for sound and 18.53 rad/s^2 for light and the deceleration was: 7.31 rad/s^2 with sound and 6.82 rad/s^2 with light initiation. The graphical representation of the elbow joint action data recorded with the initiation of sound, light and maximum possible rhythm (figure 4, right). Average ROM was about 130.23° for sound. The maximum Range of Motion (ROM) was found to be: 144.46° , 129.45° for light and 143.75° for maximum movement speed. FFT on selected data derived the action frequency, which are 0.95 Hz , 0.91 Hz and 1.47 Hz for sound, light and maximum possible initiations respectively. Maximum observable frequency up to 7.54 for sound 5.93 Hz for light and 10.16 Hz for maximum initiation respectively. The variation in phases were within 4 degrees. FFT of half squad data depict that the highest action frequency for sound initiation

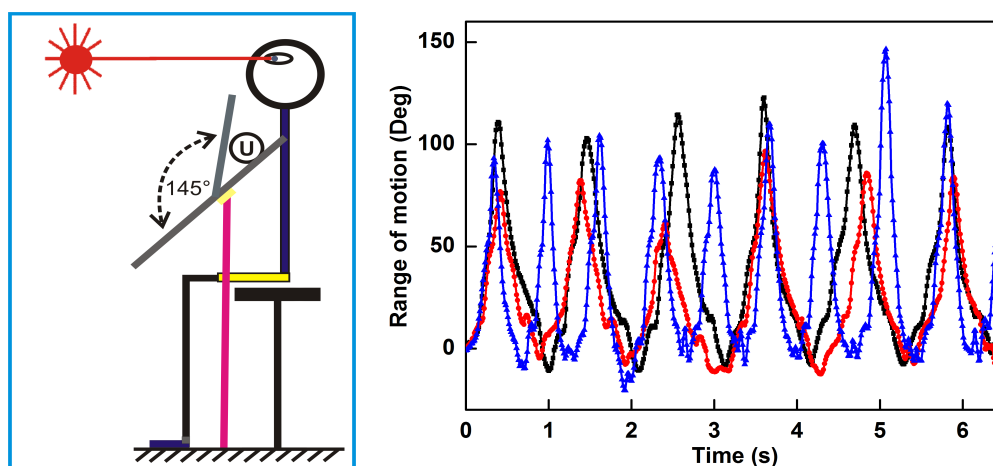


Figure 9.17: Set-up for elbow joint action monitoring and graphical view of the data for 6.5s. Black: sound, red: light and blue: maximum movement speed.

0.59 Hz , for light initiation 0.58 Hz (figure 9.18, right). The maximum observable frequency 4.85 Hz and 4.90 Hz for sound and light initiation respectively. The variation in phases were within 3 degrees. Different techniques and types of sensors are used to monitor joint kinematics [2]. The developed detection scheme is non-invasive, easily accessible and cost effective. The achieved spatial and temporal resolution proves its applicability in monitoring all possible mammalian motion. Small data streams and long time monitoring are provided. Quantitative findings ensure its applicability in on-line monitoring of range of motion, number of repetition, movement speed, maximum possible repetition, rhythm ability, endurance, contraction speed, relaxation speed, energy depletion rate, et cetera. Stride-length, stride-frequency, ground contact time, toe-off time, supporting phase, flying phase of running, jumping and walking are also amiable with this system.

- [1] M. Zakir Hossain, W. Grill: *High speed ultrasonic detection scheme for sports performance monitoring* Proceedings of ISBS 2009, Limerick, Ireland, SO7-3:268-903 (2009)

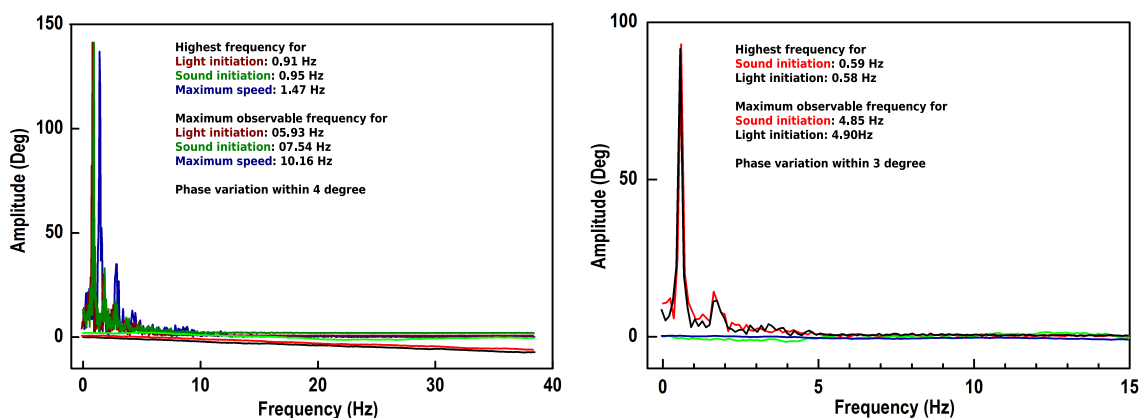


Figure 9.18: Set-up for elbow joint action monitoring and graphical view of the data for 6.5s. Black: sound, red: light and blue: maximum movement speed.

- [2] R.E. Mayagoitia et al.: *Accelerometer and rate gyroscope measurement of kinematics: an inexpensive alternative to optical motion analysis systems*, J Biomech 35(4)537-42 (2002)

9.7 Stress detection with guided acoustic ultrasonic waves by non-linear elastic and geometric effects

K.S. Tarar, R. Meier, U. Amjad, W. Grill

9.7.1 Introduction

Stress detection by ultrasonic bulk waves for applications involving the detection of the load in bolts dates back, concerning respective patents [1], to 1976 and suitable instrumentation and transducers are available on a commercial basis. Applications involving standing waves are long introduced since string instruments are tuned by this effect. From a guided wave perspective, the standing wave phenomenon can be regarded as the superposition of two traveling waves propagating in opposite directions along the structure. Hence, it is possible to exploit the properties of propagating waves rather than standing waves for load measurement based on guided waves. This has been suggested by Damjanovic and Weaver [2]. They used a laser interferometer to measure the wave number of a propagating flexural mode in a rail excited by an electromagnetic shaker at a frequency of around 200 Hz. The authors show that this frequency provides adequate load estimation accuracy, although they do not explicitly examine the possibility of operating at higher frequencies. At 200 Hz, the flexural mode in question is a simple bending mode throughout the whole cross section of the rail, and the rail must therefore still be released from a number of sleepers. Hence there remains interest in investigating whether any modes at higher frequencies have any load dependence and also have mode shapes that do not significantly involve motion of the rail foot.

It has been observed, that the velocity of guided acoustic waves in long slender components has a rather high sensitivity to absolute load. The consequences of this phenomenon (at relatively low frequencies) are well known since it is the physical basis of stringed musical instruments. This effect has been directly exploited to estimate the tension in hanger cables in suspension bridges [3], and the load in a beam.

9.7.2 Stress dependence of the time-of-flight of transversal and longitudinal polarized acoustic waves in strings and rods

It is, unfortunately, well introduced by oversimplifying argumentation, that due to the fact that under stress the extension of a rod is increasing, an increase in the time-of-flight of acoustic waves traveling in the direction of the extension is to be expected. To illustrate the actually to be expected stress dependence it is suitable to consider basic models, well introduced by the literature. This is demonstrated here for a microscopic model, the linear chain, generally employed for lattice dynamics, and for the continuum model approach applied to isotropic media. The properties of waves, in the examples given here guided acoustic waves or from a quantum mechanical point of view phonons in one dimensional atomic chain, can be demonstrated by the dispersion relation, equating the dependence of (circular) frequency ω on wave number k (k-vector) respectively in the microscopic model the dependence of quantum energy on the also quantized (linear) momentum. In this scheme the phase velocity for a wave (excitation) of a given k -vector is derived from the quotient and the group velocity from the respective gradient (in lower dimensions: derivative) of the dispersion relation at position k . In the microscopic approach a linear chain is treated, consisting of mass free ideal springs with spring constant Ct . These springs are idealized according to Hooke's. The idealized springs connect point masses with mass m positioned in a linear arrangement (linear chain) at distance a (figure 9.19). For simplification it is assumed that the forces act along the springs instantaneously (the speed of light as limit velocity would such need to be infinite). For acoustic waves, traveling at only about $1/100\,000$ of the speed of light, this assumption leads only to small, even though in some cases not negligible deviations. The well known Lenard-Jones potential used

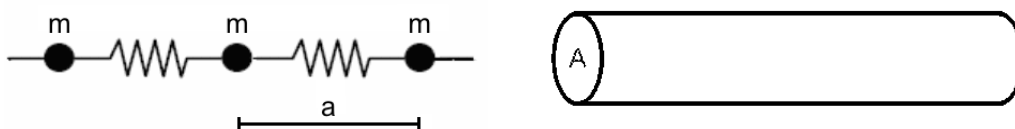


Figure 9.19: Linear chain (left) and isotropic homogeneous rod with cross sectional area A (right).

for modeling of inter-atomic forces can serve here to demonstrate the main features as observed in experiments for longitudinal polarized bulk acoustic waves, for which the

linear chain model is a simplifying example. This will lead to a reduced spring constant under dilatation and an increased one for compression. As a result the time-of-flight of acoustic waves traveling along the direction of the applied stress will increase for dilatational stress, as normally observed for longitudinally polarized bulk waves.

As a choice from basic models guided acoustic waves traveling on rods assuming the validity of a continuum model¹⁰ are well suited for this purpose. In this approximation the involved masses are introduced as (mass) densities ρ together with respective volumes. The elastic properties of rod shaped materials relevant for guided waves of the lowest branch for the axial-radial mode are expressed by Young's modulus E . Independent of the cross section the velocity of the axial-radial mode in the long

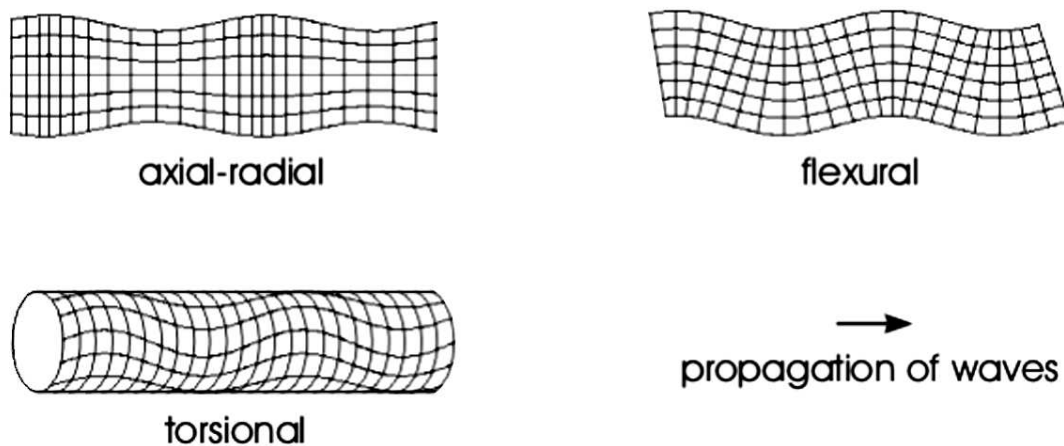


Figure 9.20: Deformation for the lowest branch of the different modes for guided acoustic waves traveling axially in a rod.

wavelength limit is independent of the actual sizes of the rod with vanishing dispersion and can therefore be expressed equally for phase and group velocity in that limit by:

$$v = \sqrt{E/\rho} \quad (9.5)$$

In this model, the velocity depends exclusively on E and ρ . The range of the Poisson ratio of stable materials is -1 to 0.5 with typical values for metallic alloys in the range of 0.2 to 0.3 . Depending on the actual Poisson ratio, the density will be reduced if the solid rod is elongated by stress. This will lead to an increase of the velocity since the density will exhibit a relative decrease if the volume increases.

For any practically relevant Poisson ratio between 0 and 0.5 it is evident that dt_{of}/t_{of} has the same sign as dl/l since for small enough variation (higher order terms neglected) the following holds:

$$dt_{of}/t_{of} = dl/l + (v - 1/2)dl/l = dl/l = (v + 1/2)dl/l. \quad (9.6)$$

Propagating transverse vibrations traveling on a linear chain can exist even in the absence of bending stiffness and are usually described by stretching phonons. If a

bending force constant f is present on the chain, the dispersion relation¹³ for transverse polarized acoustic waves is represented by

$$\omega = 2\sqrt{f/m}[1 - \cos(ka)] \quad (9.7)$$

and for $k \rightarrow 0$

$$\omega = a^2 k^2 \sqrt{f/m}. \quad (9.8)$$

he group velocity for transverse polarized acoustic waves traveling under the presence of a bending force (but not including stretching forces) is given by

$$\omega = 2a^2 k \sqrt{f/m}. \quad (9.9)$$

Group and phase velocities are zero for $k = 0$ corresponding to $\lambda \rightarrow \infty$ since restoring lateral forces approach zero. The group velocity is also zero at the boundary of the Brillouin zone $k = \pi/a$ where standing waves are established. This case is nevertheless not of relevance for the applications treated here.

If the idealized chain is (longitudinally) soft, then under respective stress an elongation will occur that needs a further refined treatment beyond the scope of this paper. The basic features concerning the dispersion relations for the microscopic approach discussed here are presented in figure 9.21. Whereas the longitudinal phonon branches have in both demonstrated cases the shape well known from lattice dynamics, the stretching mode exhibits an unusual relation with rising group velocity for diminishing wave length. This can easily be understood by the relative softening of a bar supported at two positions at (axial) distance d and a central load with respect to this support. The bar will turn soft under lateral loads (forces) if d increases.

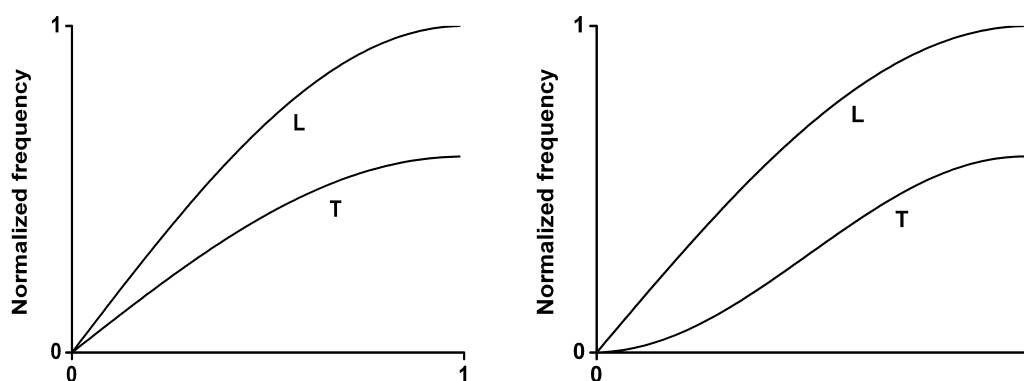


Figure 9.21: The graphs display the typical features of the dispersion relations for longitudinal and transversal polarized acoustic waves (phonons) traveling on a chain (left) as with similar results also known from lattice dynamics, and for stretching phonons (right) as derived in the literature [4].

9.7.3 Experimental results

The experimental set-up used for the experiments is similar to the one published earlier [5]. Observations are performed in transmission along the axis of a probe that can be put under variable stress by external axial forces. The results for a threaded copper rod (M10 with a length of the stressed zone of about 185 mm) are displayed in figure 9.22 (left) for longitudinal polarized bulk acoustic waves at a frequency of 8 MHz and guided axial-radial acoustic waves at 250 kHz. The time-of-flight of the longitudinal polarized bulk mode increases linearly while the time-of-flight of the guided mode decreases linearly with applied force. Whereas the first observation is well established and relates to the influence of the higher order elastic constants relating to anharmonicity and deviation from Hooke's law, the reduction of the time-of-flight indicates that the effect to be expected from vibrating strings or stretching modes influences the result and even dominates the influence of anharmonicity. Even though a symmetric Lamb mode is involved, the restoring forces due to lateral stress will act on the surface near layers and such contribute to the here observed increase of the velocity of guided waves, which even overcomes the influence of elongation and anharmonicity. Since anharmonicity

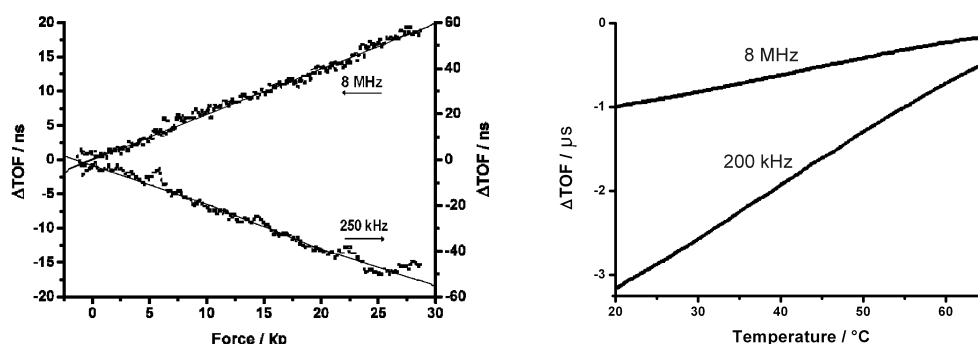


Figure 9.22: (left) Variation of the time-of-flight in a copper rod for longitudinal bulk (upper line) and axial-radial guided (lower line) acoustic waves as a function of the stress introduced by an applied force.(right) The dependence of the observed variation of the time-of-flight (Δ TOF) on temperature for transport in a copper rod for the longitudinal polarized bulk acoustic mode at 8 MHz and the axial-radial guided mode at 200 kHz

is also the origin of thermal expansion, the temperature dependencies concerning the TOF have been studied (figure 9.22 (right)). For both modes the time-of-flight increases linearly with temperature. This demonstrates that in this case, where external stress is absent, the influence on both modes is similarly caused by softening of the material properties introduced by thermal expansion, as to be expected from the potentials relevant for the binding on atomic scales in the material (figure 9.20). The guided mode exhibits an even stronger dependence (steeper slope) than the bulk mode, further indicating the separate and even opposing influence of geometric stiffening as observed under stress and the softening influence of anharmonicity observed in the absence of external stress for variable temperature.

9.7.4 Conclusions

The results of microscopic and macroscopic modeling for the stress dependence of propagating acoustic modes in isotropic solids are compared to experimental observation. The observed stress dependence, which exhibits an anomalous effect for the guided axial-radial mode if compared to the well known behavior of bulk modes, demonstrate the expected opposing influence of geometric stiffening by external forces and anharmonic softening under extension by external forces. Thermal expansion on the other hand leads for bulk and guided modes to softening and an increase of the time-of-flight. The observed effects open a wide range of novel applications for stress detection including schemes for compensation of thermal effects which are currently under implementation for structural health monitoring of aircraft structures.

- [1] D.A.Pagano: *Method for tightening a bolt to exert a predetermined tension force by monitoring bolt elongation while the bolt is being installed* US Patent 3969810 (1976)
- [2] S.E. Chen and S. Petro: *Nondestructive bridge cable tension assessment using laser vibrometry* Exp. Tech. 29(2) 29 (2005)
- [3] T. Livingston, J.G. Beliveau, and D.R. Huston: *Estimation of axial load in prismatic members using flexural vibrations* J. Sound Vib. 179 5 899 (1995)
- [4] G. Hartwig: *Polymer properties at room and cryogenic temperatures* Springer (1994)
- [5] K.S. Tarar, R. Meier, E. Twerdowski, R. Wannemacher, and W. Grill: *A differential method for the determination of the time-of-flight for ultrasound under pulsed wide band excitation including chirped signals* SPIE 693519-8 (2008)

9.8 Surface acoustic wave generation and detection by Coulomb excitation

M. Pluta, U. Amjad, A. Habib*, W. Grill

*Department of Solid State Physics, University of Siegen, ENC, D-57072, Siegen, Germany

Described technique is restricted to the crystals exhibiting the piezoelectric effect. The main purpose of this work is to utilize the inherent piezoelectric properties of the sample for transforming electrical signals into acoustic waves and vice versa.

A simplified experimental scheme of the full-transient, two channel acquisition is presented in 9.23. A similar experimental set-up for the point contact excitation and detection of surface acoustic waves has been reported previously [1]. An excitation burst with a carrier frequency of 89.9 MHz and duration of 220 ns (approximately, 20 oscillations) was cut by an electronic switch from a continuous sinusoidal signal (CW) generated by a stabilized oscillator and used to drive the probe for excitation of the acoustic waves on the crystal. The electronic switch is controlled by a pulse delay generator. The electric burst signal is supplied to a sending point like electrode, where it is converted by the piezo-effect into ultrasound propagating through a piezoelectric

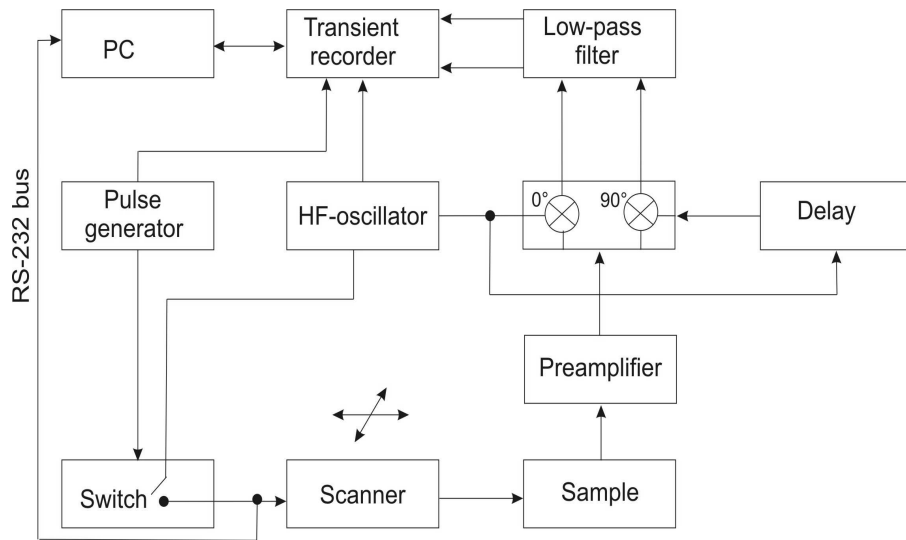


Figure 9.23: Schematic drawing of the signal generation, detection and processing for the point contact excitation and detection. Scanner moves the sending electrode 9.24 in two dimensions

sample of interest 9.24. On the same side of the sample the ultrasonic oscillations are converted back into an electric signal by a receiving tip.

Two motor-driven translation stages are used to position the excitation probe in two dimensions at the surface of the sample. The scanning tips are manufactured from 50 μm gold wire that gets in contact with the sample and 200 μm bronze supporting wire. The scanning contact is used for excitation and on the other hand a fixed probe, made of the same components, is used for the signal detection 9.24. The scanner moves the probe across the sample surface, while the transferred electric signal transient is registered and averaged for each position. The typical scan area are $4 \times 4 \text{ mm}^2$. An advantage of the

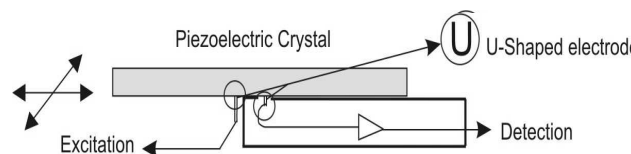


Figure 9.24: Schematic diagram for piezoelectric excitation and detection of ultrasound.

above mentioned technique is, that a three-dimensional set of complex numbers can be acquired involving only a two-dimensional mechanical scan. That allows holographic registration of the surface acoustic waves including signals resulting from skimming surface waves. The respective analysis is entirely performed by post-experimental processing of the acquired three-dimensional complex valued data set 9.25

Fourier spectrum of the 2D quadrature detection measurements performed at the half space $x > 0$ is presented in 9.26. In the figure positions of maxima are related to the reciprocals of the respective wavelengths. By sampling in space with step of

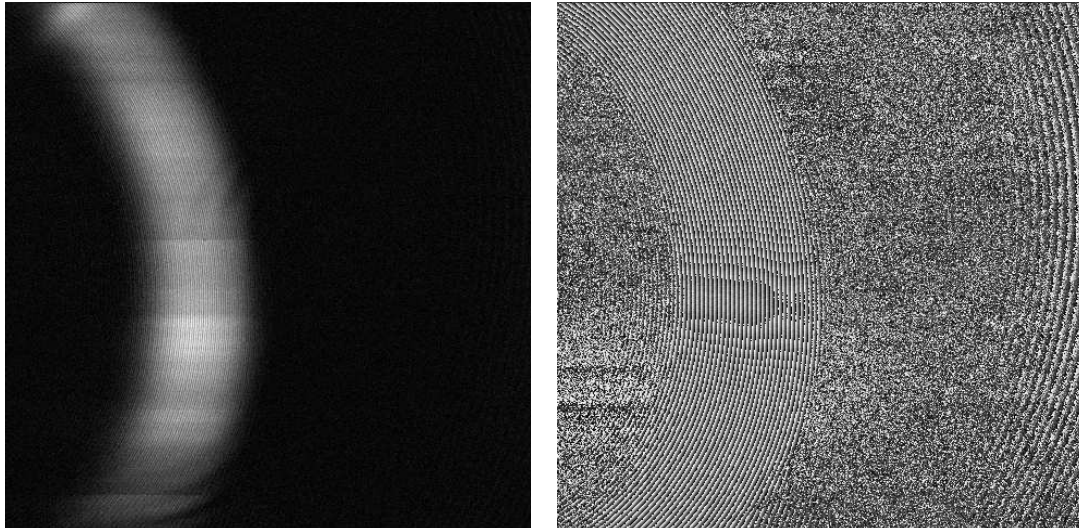


Figure 9.25: Scanned wave field. The magnitude (left) and the phase with full gray scale span equal to 2π (right) of the surface acoustic wave. Scan area of $4 \times 4 \text{ mm}^2$

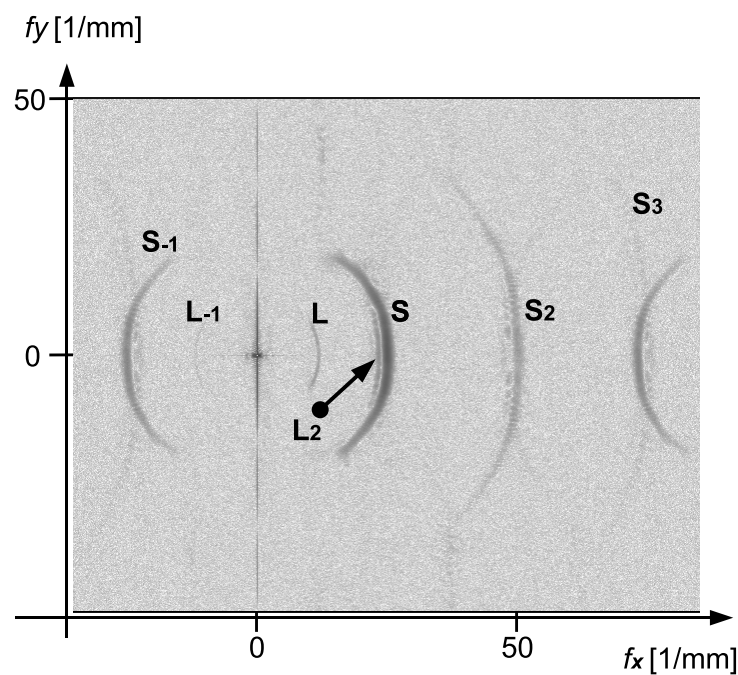


Figure 9.26: Two dimensional Fourier spectrum of the registered complex valued field presented in negative logarithmic scale (maxima are dark). L is the spectrum of the longitudinal wave, L_2 is the second order spectrum of longitudinal wave, L_{-1} is the weak -1^{st} order spectrum of the longitudinal wave. Symbols S, S_2 and S_3 denote the respective orders of spectra of the slower surface wave. S_{-1} is the relatively strong -1^{st} order spectrum of the surface wave. Due to the aliasing effect some spectra for higher and negative order harmonics overlap.

Table 9.1: Spatial frequencies, wavelengths and calculated velocities read from the 2D Fourier spectrum of the wave field.

	f_x [1/mm]	λ [μm]	c [km/s]
L	12.1	82.6	7.42
L_2	23.8	83.8	7.54
L_{-1}	-12.3	81.2	7.3
S	25.6	39.1	3.51
S_2	51.2	39.1	3.51
S_3	76.7	39.1	3.51
S_{-1}	-25.6	39.1	3.51

$\Delta x = 0.01\text{mm}$, the Nyquist spatial frequency is 50 1/mm. While sampling of the wave field fulfills that criteria (we were collecting about four points per the shortest wave cycle), it is not fulfilled for higher harmonics, but position of those harmonics brings additional information on the observed velocities (see table 9.1).

The results obtained in this paper demonstrate the potential of holographic imaging by means of electrostatic point contact excitation and detection for the study of the electro-mechanical properties of piezoelectric materials. The method of excitation and detection is simple and versatile. It allows for variation of the frequency of the surface acoustic waves over a wide range since neither mechanical nor electrical resonances are involved in the coupling scheme. The values of the skimming longitudinal wave and SAW velocity obtained from the measurements are in good agreement with those presented in literature [2].

- [1] A. Habib, E. Twerdowski, M. von Buttlar, M. Pluta, M. Schmachtl, R. Wannemacher and W. Grill : *Acoustic holography of piezoelectric materials by Coulomb excitation* Proc. SPIE **6177** 61771A (2006)
- [2] SG. Joshi, BD. Zaitsev, IE. Kuznetsova, AA. Teplykh, A. Pasachhe, *Characteristics of fundamental acoustic wave modes in thin piezoelectric plates* Ultrasonics **44** 787-791, (2006)

9.9 Funding

Mesoscale Acoustics on Soft Matter Systems

W. Grill

GR 566/11-2

Development of a Miniaturized Advanced Diagnostic Technology Demonstrator 'DIAMOND' - Technology Study Phase 2

W. Grill, R. Wannemacher

European Space Organization ESA/ESTEC

Ultrasound Diagnostics of Directional Solidification

W. Grill, R. Wannemacher

European Space Organization ESA/ESTEC

In-vivo Ultrasonic Holographic Imaging (within the Translational Centre for Regenerative Medicine (TRM Leipzig))

E. Twerdowski, R. Wannemacher, W. Grill
BMBF AZA 0845 IMONIT 1040AB 50810213

Multiparametric Monitoring and Steering of Mesenchymal Stem Cell derived Cartilage Formation in 3D Production Systems (MS CartPro)

Development of a 2D bioreactor with integrated phase-sensitive acoustic microscopy combined with confocal laser microscopy (AP2.2)

Integration of a multi-parameter online monitoring system in a 3D bioreactor (AP2.3)

W. Grill, E. v d. Burg, M. v. Buttler
BMBF FKZ 0313836, MS CartPro

Aircraft Integrated Structural Health Assessment II (AISHA II)

W. Grill, U. Amjad, K.S. Tarar, M. Pluta, M. Zakir Hossain,
EU Seventh Framework Programme (FP7) Grant Agreement No. 212912

Magnetische Barcodes zur Überwachung von Biologiestikprozessen (ForMaT)

W. Grill, A. Abdelrahman, K. Hahn
BMBF 03FO3221

Biomimetic Ultrathin Structures as a Multipurpose Platform for Nanotechnology-Based Products (MultiPlat)

W. Grill, R. Wannemacher
EU Seventh Framework Programme (FP7) Grant Agreement No. 228943

9.10 Organizational Duties

Wolfgang Grill

- Adjunct Professor and Member of the Graduate School, The University of Georgia, Athens, GA, USA

9.11 External Cooperations

Academic

- University of the Witwatersrand, Johannesburg, South Africa
Prof. Dr. A. Every
- Wroclaw Institute of Technology, Wroclaw, Poland
Dr. M. Pluta
Dr. hab. T. Gudra
- University of Arizona, Tucson, Arizona, USA
Prof. Dr. T. Kundu

- University of Central Florida, Orlando, Florida, USA
Prof. Dr. W. Luo
Dr. W. Ngwa
- Stanford University, Stanford, California, USA
Dr. K. Vodopyanov
- Johann Wolfgang Goethe-Universität Frankfurt
Prof. Dr. J. Bereiter-Hahn
- Bernard Nocht Institute for Tropical Medicine, Hamburg
Dr. T.W. Gilberg

International Organizations

- European Space Organization ESA/ESTEC

Industry

- Schott GLAS, Mainz, Germany
- Kayser-Threde GmbH
- EPCOS AG, Surface Acoustic Wave Components, Munich, Germany
- ContiTech Holding GmbH, Hannover, Germany

9.12 Publications

Journals

U. Amjad, K. Hahn, T.G. Tang, W. Grill: *Non-inertial ultra-wideband acoustic transducers* Health Monitoring of Structural and Biological Systems 2009, Proc. SPIE **7295**26(2009)

E.v.d. Burg, W. Grill: *Characterization of elastomers with transverse sonic waves* Polymer Testing **29** 281-287 (2010) (online published 2009)

K. S. Tarar, R. Meier, U. Amjad, W. Grill: *Stress detection with guided acoustic ultrasonic waves by non-linear elastic and geometric effects* Health Monitoring of Structural and Biological Systems 2009, Proc. SPIE, **7295 (1)** 8 (2009)

M. Zakir Hossain, H Voigt, W. Grill: *Monitoring of variations in the speed of sound in contracting and relaxing muscle* Health Monitoring of Structural and Biological Systems 2009, Proc. SPIE **7295-16**(2009)

in press

M. von Buttler, E. Ahmed Mohamed and W. Grill: Signal processing for time – lapse cell imaging with vector-contrast scanning acoustic microscopy *Acoustical Imaging*, **30**, (Eds. J. P. Jones, H. Lee), (2010)

E. Ahmed Mohamed, A. Kamanyi, M. von Buttlar, R. Wannemacher, K. Hillmann, W. Ngwa and W. Grill: *Ultra-high resolution thin film thickness delineation using reflection phase-sensitive acoustic microscopy* *Acoustical Imaging*, **30**, (Eds. J. P. Jones, H. Lee), (2010)

K. S. Tarar, U. Amjad, and W. Grill: *Lumped circuit mechanical models and lattice dynamics approach to the dependence of the time-of-flight of bulk and guided acoustical modes on elongation* in press *Proc. SPIE 7650* (2010)

M. Zakir Hossain and Wolfgang Grill: *Synchronous monitoring of muscle dynamics and muscle force for maximum isometric tetanus* in press *Proc. SPIE 7650* (2010)

A. Habib, U. Amjad, M. Pluta, U. Pietsch and W. Grill: *Surface acoustic wave generation and detection by Coulomb excitation* in press *Proc. SPIE 7650* (2010)

Talks

E.v.d. Burg, M.v. Buttlar, and W. Grill: *Cartilage Tissue Engineering by Collagen Scaffold Associated Mesenchymal Stem Cells in a Novel Bioreactor: Ultrasound Imaging and Monitoring from Single Stem Cells to Implants* *World Conference on Regenerative Medicine*, October 31st, Leipzig (2009)

E. v. d. Burg, M. v. Buttlar, and W. Grill: *Non-invasive acoustical imaging of mesenchymal stem cells* *Sächsischer Biotechnologietag*, Leipzig (2009)

M Zakir Hossain, Wolfgang Grill: *High speed ultrasonic detection scheme for sports performance monitoring* *27th International Conference of Biomechanics in Sports, ISBS2009 proceedings*, (2009)

Posters

E. v. D. Burg, M. von Buttlar, W. Grill: *Bioreactor with integrated monitoring and mechanical stimulation for cartilage tissue engineering by collagen scaffold associated Mesenchymal Stem Cells* *Sächsischer Biotechnologietag*, Leipzig (2009)

M. von Buttlar, E. Ahmed Mohamed, A. Abdelrahman, A. Kamanyi, W. Grill: *Non-invasive acoustical imaging of mesenchymal stem cells* *Sächsischer Biotechnologietag*, Leipzig (2009)

9.13 Graduations

Diploma

- Katrin Hahn
Strukturierte piezoelektrische Transducer zur modenselektiven Erzeugung und Detektion geführter Ultraschallwellen
10.6.2009

Master

- Angeline Kasina
Application of high frequency ultrasonic phase measurements in the detection of infrared radiation
2. 2. 2009
- The Gia Tang
Investigation of ultrasonic transport with time reversed generation
17. 4. 2009

9.14 Guests

- Prof. Dr. Albert Kamanyi
Animal Physiology and Phytopharmacology Laboratory, Faculty of Science, University of Dschang, Dschang, Cameroon
15. 2. 2009 - 15. 5. 2009
- Amit Shelke
Department of Civil Engineering and Engineering Mechanics,
University of Arizona , Tucson , Arizona, US,
18. 5. 2009 - 18. 7. 2009

10

Superconductivity and Magnetism

10.1 Introduction

The Division of Superconductivity and Magnetism focuses its research on the study of magnetic ordering and superconductivity in a range of materials, especially carbon-based systems and magnetic oxides.

Prof. Pablo Esquinazi

10.2 Defect-induced magnetic order in pure ZnO films

M. Khalid, M. Ziese, A. Setzer, P. Esquinazi, M. Lorenz, H. Hochmuth, M. Grundmann, D. Spemann, T. Butz, G. Brauer^{*}, W. Anwand^{*}, G. Fischer[†], W.A. Adeagbo[†], W. Hergert[†], A. Ernst[‡]

^{*}Forschungszentrum Dresden-Rossendorf, 01314 Dresden, Germany

[†]Institute of Physics, Martin Luther University Halle-Wittenberg, 06120 Halle, Germany

[‡]Max Planck Institute of Microstructure Physics, 06120 Halle, Germany

The magnetic properties of pure ZnO thin films grown under N₂ pressure on a-, c-, and r-plane Al₂O₃ substrates by pulsed-laser deposition were studied. The substrate temperature and the N₂ pressure were varied from room temperature to 570°C and from 0.007 to 1.0 mbar, respectively. The magnetic properties of first the bare substrates and then the ZnO films fabricated on these were investigated by SQUID magnetometry. ZnO films grown on c- and a-plane Al₂O₃ substrates did not show significant ferromagnetism. However, ZnO films grown on r-plane Al₂O₃ showed reproducible ferromagnetism at 300 K when grown at 300–400°C and 0.1–1.0 mbar N₂ pressure. The magnetization is shown as a function of the N₂ pressure in Fig. 10.1. Positron annihilation spectroscopy measurements as well as density-functional theory calculations suggest that the ferromagnetism in ZnO films is related to Zn vacancies.

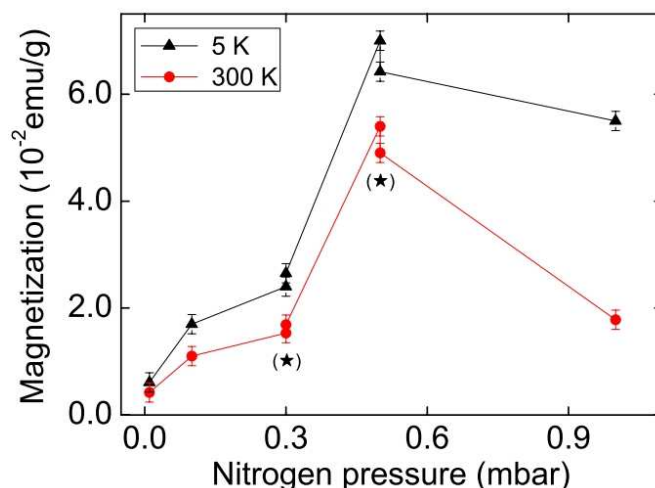


Figure 10.1: ZnO films grown under N₂ pressure: The saturation magnetization of ZnO films grown at 400°C on r-plane sapphire vs. N₂ partial pressure at 5 and 300 K. The points marked with a ★ are from four independently fabricated samples.

10.3 Ferroelectric switching in multiferroic magnetite thin films

M. Ziese, P. Esquinazi, M. Alexe*, D. Hesse*, U. Gösele¹, K. Yamauchi[†], T. Fukushima[†], S. Picozzi[†]

*Max Planck Institute of Microstructure Physics, 06120 Halle, Germany

[†]Consiglio Nazionale delle Ricerche, CNR-INFM, CASTI Regional Lab., 67100 L'Aquila, Italy

The ferrimagnetic and ferroelectric properties of magnetite films grown either by pulsed laser deposition (PLD) or magnetron sputtering onto Nb-doped SrTiO₃ substrates were studied. Film thickness was about 100 nm. The films were clearly ferrimagnetic with a Verwey temperature around 115 K. Below about 40 K a spontaneous electric polarization appears. The onset temperature of this polarization varies somewhat for the PLD-made and the sputtered films. In this low temperature regime magnetite films are clearly multiferroic. Fig. 10.2 shows (a) the polarization hysteresis loop as well as the switching current of a magnetite film at 4.2 K; in (b) the saturation polarization is presented as a function of temperature. A weak coupling between ferrimagnetic magnetization and ferroelectric polarization was detected in measurements of the magnetodielectric effect, see Fig. 10.2(c); this shows clear magnetic hysteresis and depends on the orientation of the magnetic field.

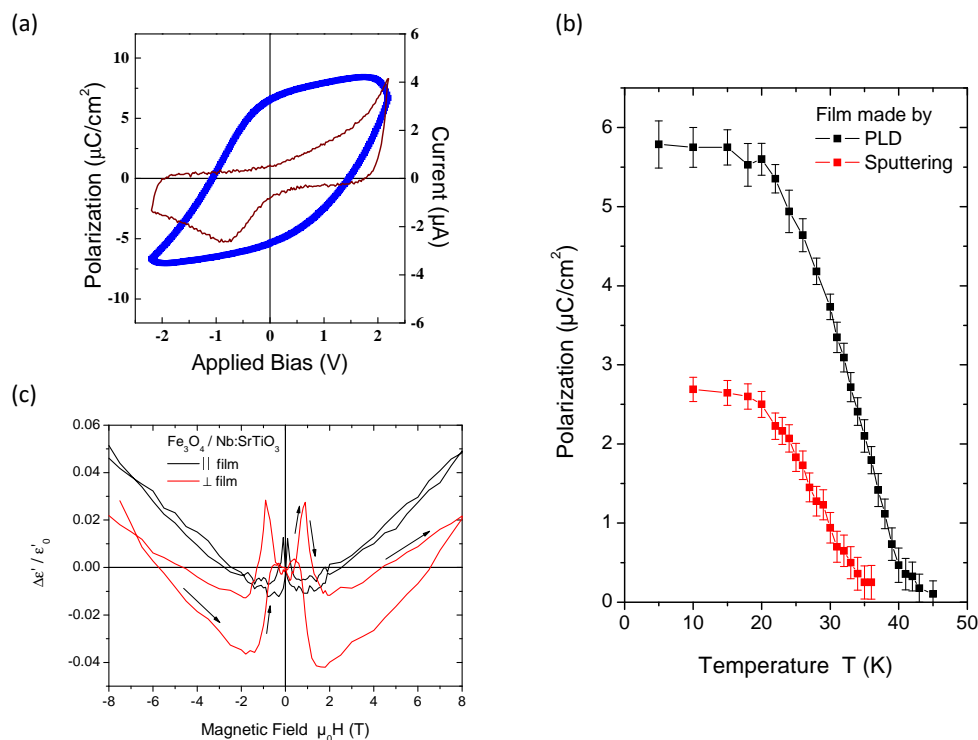


Figure 10.2: (a) Electric polarization hysteresis loop and switching current of a PLD-made magnetite film as a function of applied bias voltage at 4.2 K. (b) Saturation polarization measured for a PLD-made and a sputtered magnetite film as a function of temperature. (c) Magnetodielectric effect of a 100 nm thick PLD-made magnetite film at 10 K for two principal orientations of the magnetic field.

10.4 Magneto- and electroresistance of $\text{La}_{0.7}\text{Ca}_{0.3}\text{MnO}_3/\text{Nb}:\text{SrTiO}_3$ junctions

M. Ziese, Y.F. Chen*

*University of Electronic Science and Technology, Chengdu 610054, China

The magnetotransport properties of junctions between $\text{La}_{0.7}\text{Ca}_{0.3}\text{MnO}_3$ and Nb-doped SrTiO_3 were studied. These junctions have the character of ferromagnetic Schottky-type junctions with the Nb-doped SrTiO_3 being the metal and the manganite being the semiconductor component. Current-voltage characteristics show nonlinear behaviour with slight asymmetry and weak magnetoresistance. The junction character, however, leads to large electroresistance. This type of junctions is of interest, since it allows for the construction of devices with electric field controlled magnetoresistance and magnetic field controlled electroresistance.

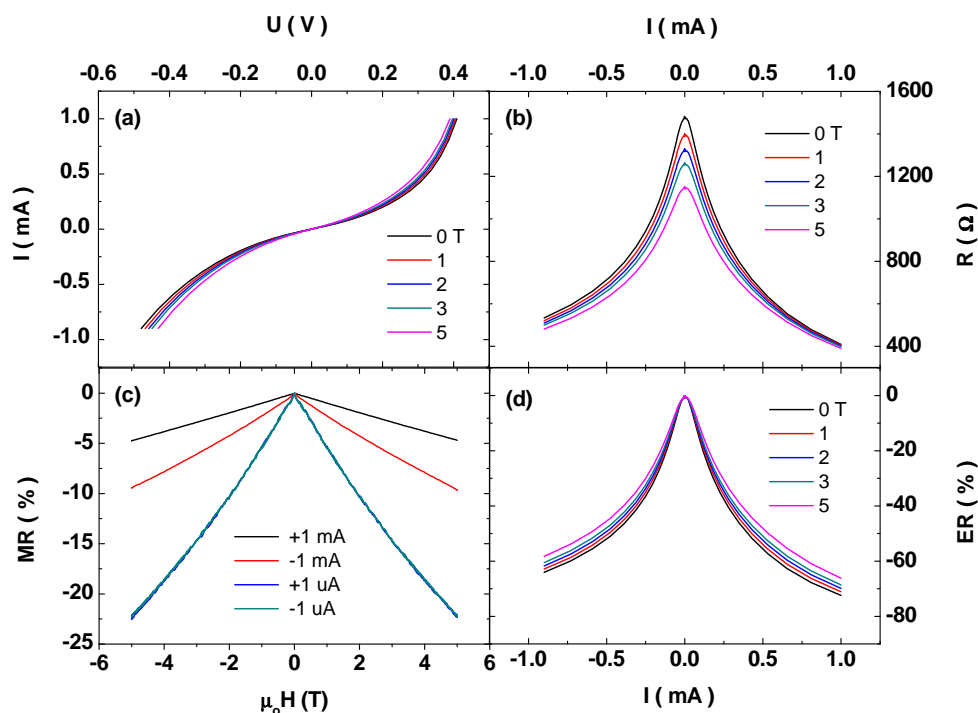


Figure 10.3: Magnetotransport behavior of a $\text{La}_{0.7}\text{Sr}_{0.3}\text{MnO}_3/\text{Nb}(1.0\%):\text{SrTiO}_3$ junction at 180 K: (a) I - V characteristics, (b) bias-current dependence of junction resistance under various magnetic fields, (c) bias-current and magnetic field dependence of magnetoresistance, and (d) bias-current dependence of electroresistance under various magnetic fields.

10.5 Funding

Study of intrinsic and extrinsic phenomena in the electrical transport properties of multi-graphene

Prof. P. Esquinazi
DFG ES 86/16-1

Defect-induced Magnetism in Oxides

Prof. P. Esquinazi and Dr. M. Ziese
DFG SFB762 B1

Spin-dependent Transport and Exchange-Biasing in multiferroic Heterostructures

Dr. M. Ziese and Prof. P. Esquinazi
DFG SFB 762 B5

Magnetotransport in graphite nano-constrictions

Prof. P. Esquinazi
DAAD

Defect induced magnetic order in ZnO and TiO₂ thin films

Prof. P. Esquinazi
DAAD

Measurements of the mean free path and of the transport anisotropy in multigraphene

Prof. P. Esquinazi

DFG und SMWK

Exchange biasing in manganite bilayers

Prof. P. Esquinazi

SMWK 4-7531.50-04-0361-09/1

10.6 Organizational Duties

P. Esquinazi

- Project Reviewer: Deutsche Forschungsgemeinschaft (DFG), National Science Foundation (USA), German-Israeli Foundation
- Referee: Phys. Rev. Lett, Phys. Rev. B., Physica C, Phys. Lett. A, phys. stat. sol., J. Low Temp. Phys., Carbon, J. Chem. Phys., Eur. J. Phys. B, J. Magn. Magn. Mater.

M. Ziese

- Project Reviewer: European Science Foundation
- Referee: APS Outstanding Referee, Phys. Rev. Lett., Phys. Rev. B., J. Phys.: Condens. Matter, J. Phys. D: Appl. Phys., phys. stat. sol., J. Magn. Magn. Mater., Eur. J. Phys. B, Thin Solid Films

10.7 External Cooperations

Academic

- State University of Campinas, Campinas, Brazil
Prof. Dr. Yakov Kopelevich
- Umea University, Sweden
Dr. Tatiana Makarova
- Universidad Autónoma de Madrid, Spain
Prof. Dr. Miguel Angel Ramos
- Universidad Autónoma de Madrid, Spain
Prof. Dr. Sebastian Vieira
- Institute for Metal Physics of National Academy of Sciences of Ukraine, Kiev, Ukraine
Prof. Dr. V. M. Pan
- Max-Planck-Institut für Metallforschung
Dr. E. H. Brandt
- University of Ioannina, Greece, Ioannina, Greece
Prof. I. Panagiotopoulos,
- Institute for Materials Science, National Center of Scientific Research “Demokritos”, Athens, Greece
Dr. Nikos Moutis
- IFW Dresden
Dr. Kathrin Dörr

- University of Sheffield, UK
Prof. G. Gehring
- University of the Negev, Beer Sheva, Israel
Dr. Alex Shames
- Max-Plank Institute of Microstructure Physics, Halle, Germany
Dr. Ionela Vrejoiu
- Max-Plank Institute of Microstructure Physics, Halle, Germany
Prof. Dietrich Hesse

10.8 Publications

Journals

- J. Barzola-Quiquia, S. Schulze and P. Esquinazi:
Transport properties and atomic structure of ion-beam-deposited W/Pd and Pt nanostructures
Nanotechnology **20**, 165704 (2009)
- S. Dusari, J. Barzola-Quiquia, P. Esquinazi and S. P. Heluani:
Changes in the electrical transport of ZnO under visible light
Solid State Commun. **150**, 22 (2009)
- P. Rödiger, P. Esquinazi and N. García:
Andreev Oscillations in Normal-Superconducting-Normal Nanostructures
J. Supercond. Nov. Magn. **22**, 331 (2009)
- N. García and P. Esquinazi:
Mean field superconductivity approach in two dimensions
J. Supercond. Nov. Magn. **22**, 439 (2009)
- J. Barzola-Quiquia, P. Esquinazi, M. Rothermel, D. Spemann and T. Butz:
Magnetic order in proton irradiated graphite: Curie temperatures and magnetoresistance effect
J. Nuclear Mater. **389**, 336 (2009)
- A. Arndt, D. Spoddig, P. Esquinazi, J. Barzola-Quiquia, S. Dusari and T. Butz:
Electric carrier concentration in graphite: Dependence of electrical resistivity and magnetoresistance on defect concentration
Phys. Rev. B **80**, 195402 (2009)
- M. Khalid, M. Ziese, A. Setzer, P. Esquinazi, M. Lorenz, H. Hochmuth, M. Grundmann, D. Spemann, T. Butz, G. Brauer, W. Anwand, G. Fischer, W. A. Adeagbo, W. Hergert and A. Ernst:
Defect-induced magnetic order in pure ZnO films
Phys. Rev. B **80**, 035331 (2009)

M. Alexe, M. Ziese, D. Hesse, P. Esquinazi, K. Yamauchi, T. Fukushima, S. Picozzi and U. Gösele:

Ferroelectric switching in multiferroic magnetite thin films
Adv. Mater. **21**, 1 (2009)

X. S. Gao, L. F. Liu, B. Birajdar, M. Ziese, W. Lee, M. Alexe and D. Hesse:
High-Density Periodically Ordered Magnetic Cobalt Ferrite Nanodot Arrays by Template-Assisted Pulsed Laser Deposition
Adv. Func. Mater. **19**, 3450 (2009)

A. J. Behan, A. Mokhtari, H. J. Blythe, M. Ziese, M. Fox and G. A. Gehring:
Magnetoresistance of magnetically doped ZnO films
J. Phys.: Condens. Matter **21**, 346001 (2009)

Y. F. Chen and M. Ziese:
Magneto- and electroresistance of LaSrMnO/Nb:SrTiO junctions
J. Appl. Phys. **105**, 07C918 (2009)

Y. F. Chen and M. Ziese:
Magnetic and Magnetotransport Properties of Magnetite/Co-Ferrite/Magnetite Trilayers
Acta Physica Polonica A **115**, 284 (2009)

in press

X. Gao, B. J. Rodriguez, L. Liu, B. Birajdar, D. Pantel, M. Ziese, M. Alexe and D. Hesse:
Microstructure and Properties of Well-Ordered Multiferroic Pb(Zr,Ti)O₃/CoFe₂O₄ Nanocomposites
ACS Nano **4**, 1099 (2010)

M. Ziese, I. Vrejoiu, E. Pippel, P. Esquinazi, D. Hesse, C. Etz, J. Henk, A. Ernst, I. V. Maznichenko, W. Hergert and I. Mertig:
Tailoring Magnetic Interlayer Coupling in La_{0.7}Sr_{0.3}MnO₃/SrRuO₃ Superlattices
Phys. Rev. Lett. **104**, 167203 (2010)

Talks

P. Esquinazi:
Too many to be listed.

Posters

M. Ziese, I. Vrejoiu, J. Barzola-Quiquia, P. Esquinazi, E. Pippel and D. Hesse:
Artificial antiferromagnetic state in La_{0.7}Ca_{0.3}MnO₃/SrRuO₃ multilayers
ICMFS 2009, Berlin, Germany

M. Ziese, I. Vrejoiu, P. Esquinazi, E. Pippel and D. Hesse:
Artificial antiferromagnetic state in La_{0.7}Sr_{0.3}MnO₃/SrRuO₃ multilayers
ICM 2009, Karlsruhe, Germany

M. Khalid, M. Ziese, A. Setzer, P. Esquinazi, H. Hochmuth, M. Lorenz, M. Grundmann, D. Spemann and T. Butz:
Ferromagnetic order in nitrogen doped ZnO films
ICM 2009, Karlsruhe, Germany

10.9 Graduations

Bachelor

- Niko Klingner
Transportmessungen an Multiwall Carbon Nanotubes
02.10.2009
- Thomas Scheike
Supraleitende Eigenschaften von gemahlenden MgB_2 -Graphit Mischungen
08.09.2009
- Ralf Wunderlich
Herstellung und Untersuchung von orthorhombischen $HoMnO_3$ -Schichten auf $SrTiO_3$
24.09.2009

10.10 Guests

- Prof. Dr. Nicolas García (Chair of Leibniz)
CSIC Madrid, Spain
01.01. - 30.03.2009, 12.10. - 19.10.2009
- Dr. Soumik Mukhopadhyay
Saha Institute of Nuclear Physics, Kolkata, India
13.05. - 20.05.2009
- Federico Golmar
University Buenos Aires, Argentina
15.05. - 15.06.2009
- Carlos Ivan Zandalazini
Centro Láser de Ciencias Moleculares, Dpto. De Fisicoquímica, Córdoba, Argentina
18.06. - 28.12.2009
- Kemal Yaylali
Istanbul Technical University, Istanbul, Turkey
30.06. - 31.08.2009
- Arber Murturi
Yildiz Technical University, Istanbul, Turkey
30.07. - 30.09.2009
- Niels Spannenberg
University of Twente, NL
13.07. - 26.07.2009

- Claudio Chilotte
Ciudad Universitaria, Buenos Aires, Argentina
01.09. - 30.11.2009
- Prof. Dr. Victoria Bekeris
University Buenos Aires, Argentina
25.09. - 09.10.2009
- Dr. Hendrik Ohldag
Stanford Synchrotron Radiation Laboratory, Stanford University, USA
12.10. - 14.10.2009
- Prof. Dr. Klaus Leifer
Institute of Electron Microscopy and Nano Engineering, Uppsala University, Sweden
26.10. - 28.10.2009
- Dr. Manuel Villafuerte
Universidad Nacional de Tucumán, Argentina
22.11. - 13.12.2009

III

Institute for Theoretical Physics

11

Computational Quantum Field Theory

11.1 Introduction

The Computational Physics Group performs basic research into classical and quantum statistical physics with special emphasis on phase transitions and critical phenomena. In the centre of interest are the physics of spin glasses, diluted magnets and other materials with quenched, random disorder, soft condensed matter physics with focus on fluctuating paths and interfaces, biologically motivated problems such as protein folding, aggregation and adhesion as well as related properties of semiflexible polymers, and the intriguing physics of low-dimensional quantum spin systems. Investigations of a geometrical approach to the statistical physics of topological defects with applications to superconductors and superfluids and research into fluctuating geometries with applications to quantum gravity (e.g., dynamical triangulations) are conducted within a European Research Training Network (RTN) collaboration of 13 teams, and within an Institute Partnership of the Humboldt Foundation the statistical mechanics of complex networks is studied in collaboration with our partner university in Krakow, Poland.

The methodology is a combination of analytical and numerical techniques. The numerical tools are currently mainly Monte Carlo computer simulations and high-temperature series expansions. The computational approach to theoretical physics is expected to gain more and more importance with the future advances of computer technology, and is likely to become the third cornerstone of physics besides experiment and analytical theory. Already now it can help to bridge the gap between experiments and the often necessarily approximate calculations of analytical work. To achieve the desired high efficiency of the numerical studies we develop new algorithms, and to guarantee the flexibility required by basic research all computer codes are implemented by ourselves. The technical tools are Fortran, C, and C++ programs running under Unix or Linux operating systems and computer algebra using Maple or Mathematica. The software is developed and tested at the Institute on a cluster of PCs and workstations, where also most of the numerical analyses are performed. Large-scale simulations requiring vast amounts of computer time are carried out at the Institute on quite powerful compute servers, at the parallel computers of the University computing center, and, upon successful grant application at the national supercomputing centres in Jülich and München on IBM and Hitachi parallel supercomputers. This hierarchy of various

platforms gives good training opportunities for the students and offers promising job perspectives in many different fields for their future career.

Within the University, our research activities are closely integrated into the Graduate School “BuildMoNa”: Leipzig School of Natural Sciences – *Building with Molecules and Nano-objects* funded by the German Research Foundation (DFG) within the German Excellence Initiative and the international DFH-UFA Graduate School *Statistical Physics of Complex Systems* with Nancy Université, France, supported by the Deutsch-Französische Hochschule. The two Graduate Schools are both “Classes” of the Research Academy Leipzig (RAL), providing the organizational frame for hosting visiting students, offering language courses and for many other practical matters. At the post-graduate level our research projects are embedded into the “Sächsische DFG-Forschergruppe” FOR877 *From Local Constraints to Macroscopic Transport*, the International Max Planck Research School (IMPRS) *Mathematics in the Sciences* and into two of the top level research areas (“Profilbildende Forschungsbereiche (PbF)”) and the Centre for Theoretical Sciences (NTZ) of the University. In particular the latter structures are instrumental for our cooperations with research groups in experimental physics and biochemistry.

On an international scale, our research projects are carried out in a wide net of collaborations funded by the German Academic Exchange Service (DAAD), the Alexander-von-Humboldt Foundation through an Institute Partnership with the Jagellonian University in Krakow, Poland, as well as their Fellowship Programme, and the European Commission through the Research Training Network “ENRAGE”: *Random Geometry and Random Matrices: From Quantum Gravity to Econophysics*. From 17.–22. May 2009 an International Network Conference under the title *ENRAGEing Perspectives – Random Geometry and Random Matrices: From Quantum Gravity to Econophysics* has been organized by us at the Max-Planck-Institut für Physik komplexer Systeme in Dresden (<http://www.mpipks-dresden.mpg.de/~enrage09/>). Since 2008 our group is annually hosting the Humboldt Research Prize Winner Professor Bernd A. Berg from Florida State University, Tallahassee, USA, for a few months. Further close contacts and collaborations are established with research groups in Armenia, Austria, China, France, Great Britain, Israel, Italy, Japan, Poland, Russia, Spain, Sweden, Taiwan, Turkey, Ukraine, and the United States. These contacts are refreshed and furthered through topical Workshops and Tutorials and our International Workshop series *CompPhys: New Developments in Computational Physics*, taking annually place at the end of November just before the first advent weekend.

A special event in 2009 was the 34th Conference of the Middle European Cooperation in Statistical Physics *MECO34* with about 120 participants, which we organized together with Prof. S. Trimper (Martin-Luther-Universität Halle-Wittenberg) here in Leipzig in our main department building Linnéstraße 5 from 30. March – 01. April 2009 (<http://www.physik.uni-leipzig.de/~meco34/>).

Wolfhard Janke

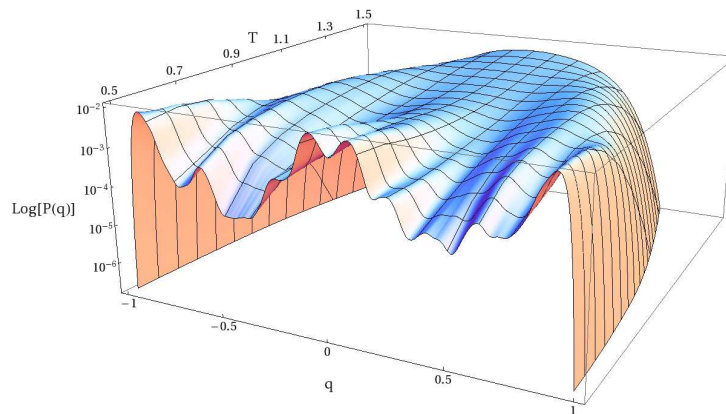


Figure 11.1: The logarithm of the canonical distribution $P(q)$ of the spin-glass overlap parameter q for the 3D Edwards-Anderson model on a moderately large 8^3 lattice as a function of the temperature T for a typical disorder realisation, illustrating how the rugged free-energy landscape develops for low temperatures.

11.2 Edwards-Anderson Ising Spin Glass Model

A. Nußbaumer, E. Bittner, W. Janke

One of the most challenging problems in the statistical physics of disordered systems is the nature of the low-temperature phase of finite-dimensional spin-glass systems. There is a still on-going debate over which of the most prominent theses in the field, Parisi's replica symmetry-breaking theory or the phenomenological droplet scaling picture of Fisher and Huse, describes the nature of the spin-glass phase correctly (for some reviews see Refs. [1–3]). There exist even views according to which neither of the two scenarios alone can capture the intriguing physics of spin glasses completely.

Due to the complexity of the problem, advances in analytical considerations are very limited and also computer simulations are at the verge of what can be achieved presently. The origin of the numerical problems is that, like in the thermodynamic limit of the (infinite-range) mean-field spin glass, the frozen phase of a finite system shows a complicated corrugated structure. As a consequence of the disorder and frustration characterising spin glasses in general, there is a rugged free-energy landscape with probable regions separated by rare event-states [4]. Consequently, conventional Monte Carlo simulations tend to get stuck in local free-energy valleys.

In this project we try to overcome this kind of problem by using a novel update algorithm which combines the parallel tempering method [5] with the multioverlap Monte Carlo algorithm [6]. Extensive large-scale simulations on our local computer cluster as well as on the "JUROPA" capability computer of the Jülich Supercomputing Centre have been performed mainly for the (short-range) Edwards-Anderson Ising spin-glass model [7] and, for comparison and gauging of the analysis methods, also for the Sherrington-Kirkpatrick mean-field limit [8].

The typical outcome for a randomly chosen disorder realisation is shown in Fig. 11.1. To get "physical" results, several thousand different realisations must be averaged, making the vast amount of computer time needed (many CPU years) understandable. A preliminary discussion of our results can be found in Ref. [9].

- [1] A.P. Young (ed.): *Spin Glasses and Random Fields* (World Scientific, Singapore 1997)
- [2] K.H. Fischer, J.A. Hertz: *Spin Glasses* (Cambridge University Press, Cambridge (England) 1991)
- [3] K. Binder, A.P. Young: *Rev. Mod. Phys.* **58**, 801 (1986)
- [4] W. Janke (ed.): *Rugged Free Energy Landscapes: Common Computational Approaches to Spin Glasses, Structural Glasses and Biological Macromolecules*, *Lect. Notes Phys.* **736** (Springer, Berlin 2008)
- [5] K. Hukushima, K. Nemoto: *J. Phys. Soc. Jpn.* **65**, 1604 (1996)
- [6] B.A. Berg, W. Janke: *Phys. Rev. Lett.* **80**, 4771 (1998)
- [7] S.F. Edwards, P.W. Anderson: *J. Phys. F: Metal Phys.* **5**, 965 (1975)
- [8] D. Sherrington, S. Kirkpatrick: *Phys. Rev. Lett.* **35**, 1792 (1975)
- [9] E. Bittner et al.: in *NIC Symposium 2008*, ed. by G. Münster et al., *NIC Series Vol. 39* (John von Neumann Institute for Computing, Jülich 2008) p 229

11.3 Stretching Polymers in Crowded Environments

V. Blavatska*, W. Janke

*Institute for Condensed Matter Physics, National Academy of Sciences of Ukraine, Lviv, Ukraine

Long flexible macromolecules in good solvent possess configurational statistics which is perfectly captured by the model of self-avoiding random walks (SAW) on a regular lattice [1]. This corresponds to the *regime of polymer coils* which holds when the temperature T is above the so-called Θ -temperature. In this regime, the mean end-to-end distance of an N -step chain scales as $R_N \sim N^{\nu_{\text{SAW}}}$, where ν_{SAW} is a universal exponent which depends on the dimension d only. When lowering the temperature, the effect of monomer-monomer attraction grows and the polymer radius shrinks. At $T = T_\Theta$ the effective repulsion due to the volume exclusion constraint is exactly balanced by attractive interactions. At this particular temperature, a crossover occurs from high temperature SAW behaviour to Θ -statistics with another critical exponent ν_Θ . The properties of polymers in the vicinity of the Θ -point can be modeled by *self-attracting SAWs* (SASAWs), where a nearest-neighbour attraction between non-covalently bound monomers is included [2]. Below the Θ -temperature, the entropic effects, which make the polymer chain swell, are overcome by interaction energy and a collapse to the *globule regime* characterized by a size exponent $\nu_c = 1/d$ occurs. The coil-globule transition is of second order, in the sense that the density of an infinite globule is zero at $T = T_\Theta$ and increases continuously when T is lowered further; more precisely, it is a tricritical point with the upper critical dimension $d_c = 3$.

New challenges have been raised recently when studying protein folding in the natural cellular environment [3]. Real biological cells can be described as a very crowded environment built of various biochemical species, which occupy a large fraction of the total volume; the "volume exclusion" arises due to the steric repulsion between molecules. In the language of lattice models, the crowded environment with structural obstacles can be considered as a disordered lattice, where some amount of randomly

chosen sites contains defects. Of particular interest is the case, when the concentration p of lattice sites allowed for the SAWs equals the critical concentration p_c and the lattice becomes percolative. Under these conditions, the critical exponents for SAWs take different values [4–6] and the interesting phenomenon of multifractality can be observed [7, 8].

The recent progress in experimental techniques employing optical tweezers, atomic force microscopy and soft microneedles makes it possible to monitor the behaviour of various polymers under tension and stress. In particular, applying a force on an isolated protein, the mechanism of force-driven phase transitions was studied. Of special interest in biophysics is the stretching of a collapsed polymer, i.e., of a polymer in a poor solvent below the Θ -temperature. Unfolding proteins in this way could give important information on their spontaneous folding pathways.

The aim of the present study is to apply state-of-the-art computer simulations based on the pruned-enriched Rosenbluth method (PERM) to analyze the properties of SASAWs on site-diluted lattices at the percolation threshold under applied external stretching force in space dimensions $d = 2$ and 3 . We estimate the shift of the Θ -temperature of the globule-coil transition under the influence of stretching and analyze the effect of applied force on the phase transitions between collapsed, extended and stretched phases [9].

- [1] P.-G. de Gennes: *Scaling Concepts in Polymer Physics* (Cornell University Press, Ithaca and London 1979)
- [2] C. Vanderzande: *Lattice Models of Polymers* (Cambridge University Press, Cambridge (England) 1998)
- [3] A. Horwich: *Nature* **431**, 520 (2004)
- [4] V. Blavatska, W. Janke: *Europhys. Lett.* **82**, 66006 (2008)
- [5] V. Blavatska, W. Janke: in *Proceedings of the International Conference Path Integrals – New Trends and Perspectives*, ed. by W. Janke, A. Pelster (World Scientific, Singapore 2008) p 585
- [6] V. Blavatska, W. Janke: *J. Phys. A* **42**, 015001 (2009)
- [7] V. Blavatska, W. Janke: *Phys. Rev. Lett.* **101**, 125701 (2008)
- [8] V. Blavatska, W. Janke: in *Computer Simulations in Condensed Matter Physics XXII*, ed. by D.P. Landau et al., *Physics Procedia* **3**, 1431 (2010)
- [9] V. Blavatska, W. Janke: *Phys. Rev. E* **80**, 051805 (2009)

11.4 Worm Algorithm Applied to Critical Loop Gases

W. Janke, T. Neuhaus*, A.M.J. Schakel

*Jülich Supercomputing Centre, Forschungszentrum Jülich, Germany

The loop gas approach to lattice field theory provides an alternative, geometrical description in terms of fluctuating loops. It derives from the strong-coupling expansion in relativistic quantum field theories formulated on a spacetime lattice, representing the hopping of particles from one lattice site to the next. The standard approach, which is rooted in the functional integral approach to field quantization, involves estimating

observables (expressed in terms of the fields) by sampling a representative set of field configurations. New configurations are typically generated by means of a Monte Carlo technique which uses importance sampling, with each field configuration weighted according to the probability that it occurs. In contrast, the approach based on the strong-coupling, or hopping expansion, which is closely connected to Feynman's spacetime approach to quantum theory [1], involves linelike objects. Physical observables are in this geometrical approach no longer estimated by sampling an ensemble of field configurations, but by sampling a grand canonical ensemble of (mostly closed) world lines, known as a *loop gas*, instead. The weight of a given world-line configuration is typically determined by the total length of the paths, the number of intersections, and the number of loops contained in the tangle. In statistical physics, the strong-coupling expansion is known as the high-temperature series expansion [2]. Lattice field theories studied in this context are typically spin models, such as the $O(N)$ spin model, whose representation in terms of high-temperature (HT) graphs is known as a *loop model*.

About a decade ago, Prokof'ev and Svistunov [3] have introduced a Monte Carlo update algorithm that, although based on local updates, does away with critical slowing down almost completely. The so-called *worm algorithm* generates loop configurations through the motion of the end points of an *open* world line – the “head” and “tail” of a “worm”. A loop is generated in this scheme when the head bites the tail, or through a “back bite” where the head erases a piece (bond) of its own body and thereby leaves behind a detached loop and a shortened open chain.

Besides this outstanding technical advantage, the worm algorithm has the additional advantage in the context of statistical physics that the complete set of standard critical exponents can be determined at a stroke. This set is known to split into two, namely the thermal and the magnetic exponents. While the thermal exponents, such as the specific heat exponent α , pertain to closed paths, the magnetic exponents, such as the magnetic susceptibility exponent γ , pertain to open paths in the geometrical approach. By the nature of the worm algorithm, which features an open path between loop updates, data for both sectors are generated on the fly in this scheme. More specifically, the open paths directly sample the spin-spin, or two-point, correlation function.

In this project, which extends previous work by two of us on the subject [4, 5], we describe estimators of physical observables that naturally arise in a loop gas and that allow determining the standard critical exponents. Our approach amalgamates concepts from percolation theory – the paradigm of a geometrical phase transition – and the theory of self-avoiding random walks. We relate this geometrical approach to phase transitions in terms of fluctuating paths to the more familiar field theory approach by considering the $O(N)$ symmetric ϕ^4 theory. To support our arguments we performed Monte Carlo “worm” simulations for the two-dimensional $O(1)$ loop model on a honeycomb lattice [6]. This model serves as a prototype with its various exact results providing a yardstick for our numerical results and also for the feasibility of our approach.

- [1] R.P. Feynman: Rev. Mod. Phys. **20**, 367 (1948)
- [2] H.E. Stanley: *Introduction to Phase Transitions and Critical Phenomena* (Oxford University Press, New York 1971)
- [3] N. Prokof'ev, B. Svistunov: Phys. Rev. Lett. **87**, 160601 (2001)
- [4] W. Janke, A.M.J. Schakel: Nucl. Phys. B [FS] **700**, 385 (2004)

- [5] W. Janke, A.M.J. Schakel: Phys. Rev. Lett. **95**, 135702 (2005)
[6] W. Janke et al.: Nucl. Phys. B **829**, 573 (2010) [arXiv:0910.5231]

11.5 Partially Asymmetric Exclusion Processes

R.A. Blythe^{*}, W. Janke, D.A. Johnston[†], R. Kenna[‡]

^{*}SUPA, School of Physics and Astronomy, University of Edinburgh, UK

[†]Department of Mathematics and the Maxwell Institute for Mathematical Sciences,
Heriot-Watt University, Edinburgh, UK

[‡]Applied Mathematics Research Centre, Coventry University, UK

Although the asymmetric exclusion process (ASEP) has been reinvented in various different guises over the years [1], it is only relatively recently that exact solutions have been available. The solution of the ASEP with open boundary conditions in [2] using a matrix-product ansatz was a landmark in the study of driven diffusive systems and this was extended in [3, 4] to the partially asymmetric exclusion process (PASEP), in which backward hops are also admitted. As discussed in a recent review of the matrix product approach to solving for the steady state of nonequilibrium Markov processes [1], there are a range of different methods for analysing the thermodynamic phase behaviour of the simplest versions of the ASEP. By contrast, more general models – collectively known as the partially asymmetric exclusion process (PASEP) – that admit particles to hop in both directions in the bulk, and even more generally to enter and exit at both left and right boundaries (cf. Fig. 11.2), have so far been studied only through a diagonalisation of the matrices appearing in the formalism [3, 4]. In this project, we extended a technique that previously admitted an extremely quick derivation of the ASEP phase behaviour under various updating schemes [5, 6] to these more general models.

The idea is to consider the behaviour of a “grand-canonical partition function” for the model. More precisely, we examine the generating function of the normalization of the nonequilibrium steady-state distribution over an ensemble of different lattice lengths whose mean is controlled by a fugacity. The thermodynamic phase behaviour can then be read off from the singularities of this generating function. Whilst obtaining this generating function is straightforward for the ASEP [5, 6], a convenient closed form for the PASEP had remained elusive.

Here we demonstrate that a representation of the generating function that allows the thermodynamic phase behaviour to be determined with relative ease takes the form of an infinite continued fraction [7]. This we arrive at through an interpretation of the PASEP normalization as the (equilibrium) partition function of lattice paths. We show how to analyse the singularities embedded in the continued fraction representation. We find that the analysis is intimately related to an approach based on finite-dimensional matrix representations [8, 9], exact along special lines in the phase diagram, and that the continued fraction shows how these particular solutions and the general solution are related. We further show that the continued-fraction approach extends to the most general version of the PASEP and that one can access both currents and correlation

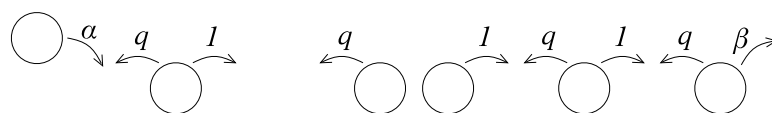


Figure 11.2: Typical particle configuration and allowed moves in the PASEP model.

lengths through it. Finally, we return to the lattice path picture to elucidate the equilibrium counterpart of a nonequilibrium phase transition identified in [4] that occurs when the bias on bulk hop rates opposes that imposed by the boundary conditions.

- [1] R.A. Blythe, M.R. Evans: *J. Phys. A: Math. Theor.* **40**, R333 (2004)
- [2] B. Derrida et al.: *J. Phys. A: Math. Gen.* **26**, 1493 (1993)
- [3] T. Sasamoto: *J. Phys. A: Math. Gen.* **32**, 7109 (1999)
- [4] R.A. Blythe et al.: *Phys. A: Math. Gen.* **33**, 2313 (2000)
- [5] R.A. Blythe et al.: *J. Stat. Mech.: Theor. Exp.* P06001 (2004)
- [6] R.A. Blythe et al.: *J. Stat. Mech.: Theor. Exp.* P10007 (2004)
- [7] R.A. Blythe et al.: *J. Phys. A: Math. Theor.* **42**, 325 002 (2009)
- [8] K. Mallick, S. Sandow: *J. Phys. A: Math. Gen.* **30**, 4513 (1997)
- [9] F.H. Jafarpour: *J. Phys. A: Math. Gen.* **33**, 1797 (2000)

11.6 Pair-Factorized Steady States in Stochastic Mass-Transport Models

B. Waclaw, J. Sopik*, W. Janke, H. Meyer-Ortmanns*

*School of Engineering and Science, Jacobs University, Bremen, Germany

A variety of stochastic processes out-of-equilibrium is summarized under the name of stochastic mass transport models, with stochastic transport of some conserved quantity, called “mass”. Examples for such processes are traffic flow, ranging from the intracellular to the macroscopic level, force propagation in granular media, aggregation and fragmentation of clusters, and others [1]. We have studied mass transport models which lead to steady states that factorize over the links of arbitrary connected graphs, so-called pair-factorized steady states [2–4].

For systems in one and two dimensions we derive the phase structure from these states, in particular the transition from a liquid phase to a phase with a condensate. Condensation amounts to spontaneous symmetry breaking in these systems where the dynamical rules are symmetric. In one dimension we derive the critical mass density of the transition, analytically predict the shape of the condensate, its scaling with the system size, its fluctuations and the single-site mass distribution. The shape of the condensate is not universal, but can be tuned from an extended to a localized one via the competition of local and ultralocal interactions that are implemented in the hopping rates (cf. Fig. 11.3). The scaling shows features familiar from first- and second-order phase transitions. The system of anisotropic hopping that we considered in two dimensions can be dimensionally reduced to an effective zero-range process in one

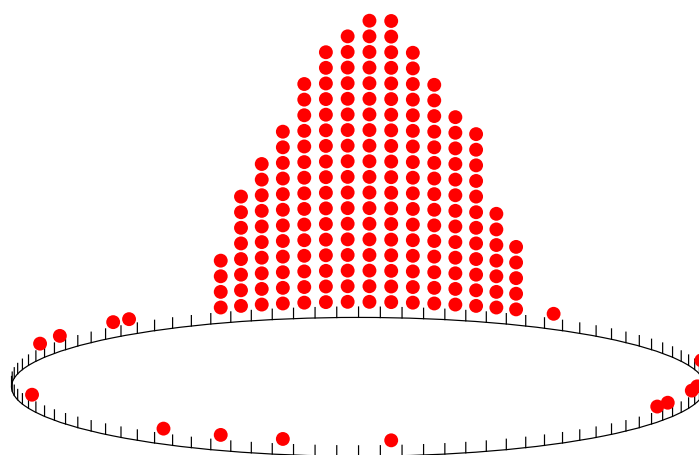


Figure 11.3: Schematic illustration of a condensate of bell shape on a ring.

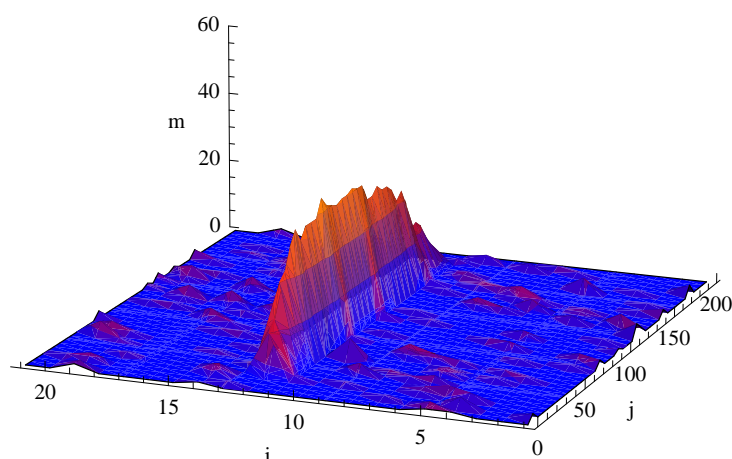


Figure 11.4: Condensate localized in x -direction and extended in y -direction for $\rho_1 < \rho < \rho_2$.

dimension. Here we predict two transitions, in particular in a certain density range the formation of a condensate that is extended in one direction and localized in the other direction, see Fig. 11.4. We also discuss possible extensions on arbitrary graphs [5].

This work is partially supported by an Institute Partnership grant “Krakow-Leipzig” (<http://www.physik.uni-leipzig.de/~wacław/AvH>) of the Alexander von Humboldt Foundation, the EU Network “ENRAGE”, and the Deutsche Forschungsgemeinschaft.

- [1] M.R. Evans et al.: Phys. Rev. Lett. **97**, 010602 (2006)
- [2] B. Waclaw et al.: J. Phys. A: Math. Theor. **42**, 315003 (2009)
- [3] B. Waclaw et al.: Phys. Rev. Lett. **103**, 080602 (2009)
- [4] B. Waclaw et al.: J. Stat. Mech. P10021 (2009)
- [5] B. Waclaw et al.: in Proceedings of the *XI Latin American Workshop on Nonlinear Phenomena: LAWNP'09*, Búzios, Brazil, to appear in J. Phys.: Conf. Ser. (in press)

11.7 Ground-States and Thermodynamics of Tubelike Flexible Polymers

T. Vogel, T. Neuhaus*, M. Bachmann†, W. Janke

*Jülich Supercomputing Centre (JSC), Forschungszentrum Jülich, Germany

†Present address: IFF-2 and IAS-2, Forschungszentrum Jülich, Germany

The thickness of tubelike flexible polymers is controlled by a single parameter, the global radius of curvature, which depends on three-body interactions [1]. It is well known that the resulting geometrical constraint tends to enhance secondary structure formation. By means of computer simulations we studied the thermodynamical behaviour of such a tube model for simple homopolymers as well as for an exemplified hydrophobic-polar heteropolymer [2, 3].

After focusing on ground states of homopolymers and their properties in a preceding step [4], we identified dominant structural pseudophases at finite temperatures, i.e., specific-heat landscapes depending on the thickness parameter ρ and temperature T , representing the conformational phase diagram. Independently of the polymer length, we find four major structural phases. These include helices (α), sheetlike planar structures (β), bended rings (γ) and sprawled random coils (δ). The resulting phase diagram in the ρ - T plane is shown in Fig. 11.5 for a 10mer and a 13mer. The different secondary structure phases can thus be assigned to different ranges of the tube thickness. The thickness parameter is therefore suitable for a classification of the structural behaviour of classes of polymers.

Furthermore, we introduced the AB tube model for hydrophobic-polar heteropolymers and obtained results for a specific sequence of monomers, which has extensively been studied before without thickness [5]. We showed that a specific monomer sequence can stabilize the general secondary structures. We find, for example, a very pronounced and stable region of β -sheet structures. We further showed that the additional introduction of a bending stiffness plays a subordinate role. This observation is important to relate our general conclusions to existing results for special systems. We could in particular reproduce simulational results published within the past years for polymer models without explicit thickness as limiting case of our study [3].

[1] O. Gonzalez, J. Maddocks: Proc. Natl. Acad. Sci. USA **96**, 4769 (1999)

[2] T. Vogel et al.: Europhys. Lett. **85**, 10003 (2009)

[3] T. Vogel et al.: Phys. Rev. E **80**, 011802 (2009)

[4] T. Vogel et al.: Eur. Phys. J. E **30**, 7 (2009)

[5] M. Bachmann et al.: Phys. Rev. E **71**, 031906 (2005), and references therein

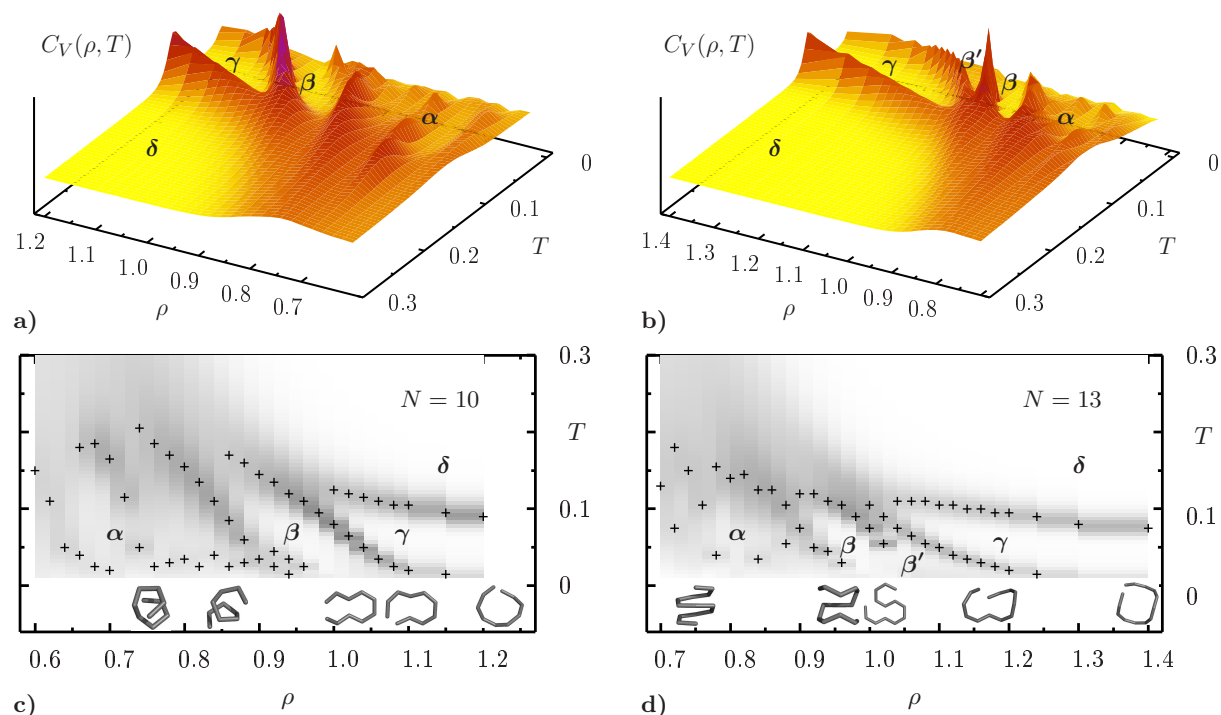


Figure 11.5: Phase diagrams of the homopolymers with $N = 10$ (left) and $N = 13$ (right). The labels α , β , γ , and δ indicate the different pseudophases at finite temperature. The panels **a)** and **b)** show the perspective view of the specific-heat landscape, and in **c)** and **d)**, the top-views are plotted with marked peak positions for various parameters ρ . The specific-heat values are encoded in gray scale. The conformations depicted in the insets in **c)** and **d)** correspond to the ground states obtained in Ref. [4].

11.8 Dominance of Finite-Size Effects in Nucleation Processes

S. Schnabel, T. Vogel, M. Bachmann*, W. Janke

*Present address: IFF-2 and IAS-2, Forschungszentrum Jülich, Germany

Thermodynamic phase transitions are typically analyzed in the thermodynamic limit, i.e., for an idealized infinite system size. This approach is reasonable for inherently large systems, where finite-size effects vanish with increasing system size. However, there are many physical systems where the thermodynamic limit is a nonsensical idealization. A typical scenario is the nucleation of a system and prominent examples for such processes are atomic cluster formation, the freezing of polymers, the aggregation of polymers, and the folding of proteins.

This project is devoted to numerical investigations of the freezing or crystallization transition of single elastic polymers [1, 2]. In the model that we employed the bond length is adaptive in a way that highly symmetric conformations can form in the crystalline phase. In our high-performance Monte Carlo simulations employing generalized ensemble methods we found for all different chain lengths low-energy conformations with basic icosahedral symmetries. The formation of such “discretized spherical” shapes is not surprising. A small system that has to reduce surface contacts

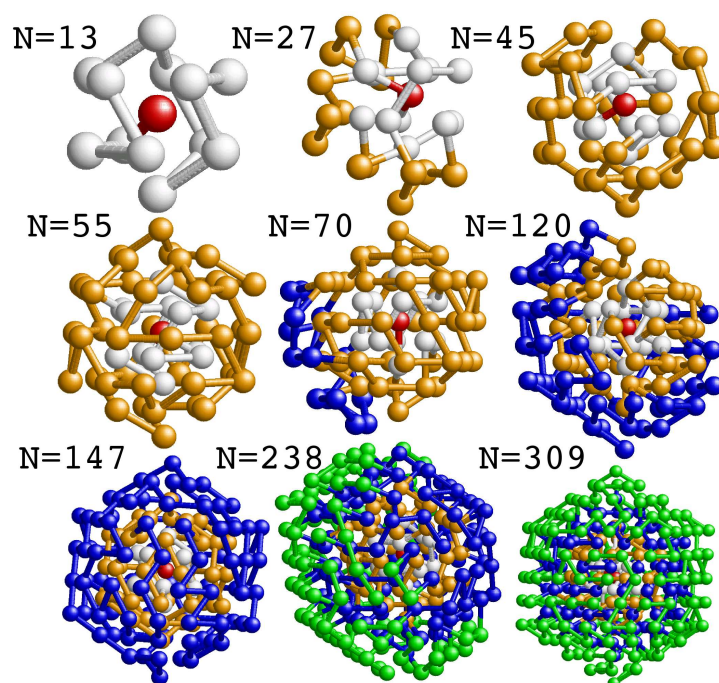


Figure 11.6: Icosahedral or icosahedral-like ground-state state conformations of elastic polymers for different system sizes [2]. Equally colored monomers belong to the same shell.

with its environment and requires stable structures prefers an icosahedral shape. A prominent example are virus capsids enclosing the viral genetic material.

In our study, we also verified the expectation that the thermodynamic crystallization behaviour is different for all system sizes. We identified a nontrivial systematic chain-length dependence that is associated with the type of growth of the nucleus [1, 2]. However, a conventional scaling behaviour has not been found – it simply does not exist. This is also known from atomic clusters [3]. A particularly sharp transition signal from fluctuating quantities, such as the specific heat, is obtained for “magic” chain lengths $N = 13, 55, 147, 309, \dots$, in which cases almost perfect icosahedra can form (see Fig. 11.6). These shapes are particularly stable and typically represent the core cells in the structure formation of longer chains.

The formation of optimally discretized spherical shapes is required for systems that have to optimize the contact surface to a less attractive environment (for example, a “poor” solvent). The residence of a monomer at this interface is energetically disfavored compared to a position in the interior. In small systems, however, all possible structures, including the most compact ones, have an insufficient surface-to-volume ratio, i.e., a large fraction of particles or monomers reside in the surface layer. Yet for the “magic” 309mer, more monomers are located on the surface (162) than in the bulk (147). Thus, all nucleation processes, even for much larger systems, are still influenced by surface effects. For this reason, quantitative analyses of “first-order-like” nucleation transitions require a treatment different from standard scaling approaches.

[1] S. Schnabel et al.: Chem. Phys. Lett. **476**, 201 (2009)

[2] S. Schnabel et al.: J. Chem. Phys. **131**, 124904 (2009)

[3] J.P.K. Doye, F. Calvo: J. Chem. Phys. **116**, 8307 (2002)

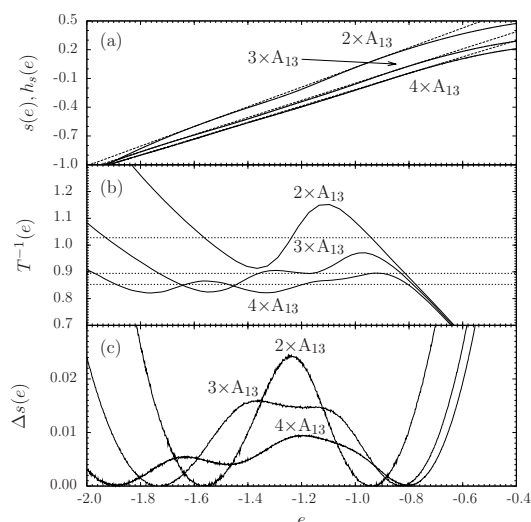


Figure 11.7: (a) Microcanonical entropy per monomer $s(e)$ and the Gibbs constructions $h_s(e)$ (dashed lines) as functions of the energy per monomer $e = E/N$, (b) reciprocal caloric temperatures $T^{-1}(e)$ and Maxwell constructions, and (c) relative surface entropies per monomer Δs_{surf} .

11.9 Microcanonical Analysis of Macromolecule Aggregation

C. Junghans^{*}, M. Bachmann[†], W. Janke

^{*}Max-Planck-Institut für Polymerforschung, Mainz, Germany

[†]Present address: IFF-2 and IAS-2, Forschungszentrum Jülich, Germany

The aggregation of macromolecules may be considered as a special case of the nucleation transition. In biosystems, the formation of peptide plaque can have disastrous consequences. An example is the aggregation of $A\beta$ peptides in the human brain which is associated to the neurodegenerative Alzheimer's disease.

To analyze the aggregation of a few polymers, we proposed in Ref. [1] an approach based on microcanonical statistics. The central quantity in the microcanonical approach is the density of states $g(E)$ which can intuitively be understood as the degeneracy of the energetic states of the system. Then, the microcanonical entropy can be introduced by $S(E) = k_B \ln g(E)$ [2, 3]. In Fig. 11.7(a), it is plotted for systems of two ($2 \times A_{13}$), three ($3 \times A_{13}$), and four polymer chains with 13 monomers ($4 \times A_{13}$). All these entropy curves exhibit a particularly interesting feature: In a certain energy region, they possess *convex monotony* [4]. Consequently, at a certain temperature, the canonical probability density distribution $p(E) \sim g(E) \exp(-E/k_B T_{\text{agg}})$ is bimodal with two peaks of equal height at two energies E_{agg} and E_{frag} that can be associated to phases, where aggregates or fragments dominate, respectively [2]. A minimum at the energy E_{sep} separates the two coexisting phases at the transition temperature T_{agg} . Hence, we conclude that the convex region of the entropy corresponds to the phase separation of the first-order-like aggregation transition. This behaviour is common to all nucleation processes. However, it is a finite-size effect and will vanish in the thermodynamic limit (provided, its definition makes sense at all) [1, 4, 5].

Thus, it is useful to construct the Gibbs hull of the entropy curves in the transition region by connecting the two points $S(E_{\text{agg}})$ and $S(E_{\text{frag}})$, where the entropy changes its monotony [see Fig. 11.7(a)]. Since the temperature is defined via $T^{-1}(E) = \partial S(E)/\partial E$, the slope of the Gibbs tangent $H_S(E)$ is identical with the reciprocal aggregation transition temperature T_{agg}^{-1} . Figure 11.7(b) shows another characteristic feature. The caloric temperature curves $T^{-1}(E)$ bend back in the transition region, i.e., additional energy pumped into the system during the fragmentation process leads to a decrease of the temperature: The melting aggregate becomes first *colder* during the fragmentation transition. This is due to the large entropy deviation from the “expected” Gibbs hull $\Delta S(E)$ plotted in Fig. 11.7(c). The maximum at the separation energy is called “surface entropy” and corresponds to the entropic reduction due to monomer rearrangements at the surface of the aggregate during the melting process. Entropy reduction costs energy. That is why the caloric temperature decreases with increasing energy. In Fig. 11.7(b) we also see that the backbending region becomes flatter with increasing system size (number of chains) and converges to the Maxwell lines, i.e., to the slopes of the Gibbs hulls.

By closer inspection of Fig. 11.7(b), we find for the systems a *hiercharchical sub-structure* caused by the surface effects. The frequency of oscillations of the curves, increasing with system size, reveals that the aggregation transition is actually a composition of different subprocesses, each of which is an individual phase-separation process. The amplitude of these oscillations decreases with system size showing that these subprocesses have a smaller surface-entropic barrier [4].

- [1] C. Junghans et al.: Phys. Rev. Lett. **97**, 218103 (2006)
- [2] W. Janke: Nucl. Phys. B (Proc. Suppl.) **63A-C**, 631 (1998)
- [3] D.H.E. Gross: *Microcanonical Thermodynamics* (World Scientific, Singapore 2001)
- [4] C. Junghans et al.: Europhys. Lett. **87**, 40002 (2009)
- [5] C. Junghans et al.: J. Chem. Phys. **128**, 085103 (2008)

11.10 Microcanonical Analyses of Polymer Adsorption Transitions

M. Möddel, M. Bachmann*, W. Janke

*Present address: IFF-2 and IAS-2, Forschungszentrum Jülich, Germany

After we recently derived the complete phase structure of a single polymer near an attractive substrate of varying adsorption strength combining the information of the canonical expectations values of various structural and energetical quantities obtained in multicanonical computer simulations [1], we focused last year on the detailed properties of the adsorption transition using a microcanonical approach [2].

The model applied is a simple bead-stick model with 12-6 Lennard-Jones (LJ) interaction between nonbonded monomers, a bending stiffness and an attraction to a flat substrate at $z = 0$ whose strength is proportional to a parameter ϵ_s . The bond lengths between adjacent monomers are fixed and normalized to unity. For an illustration of

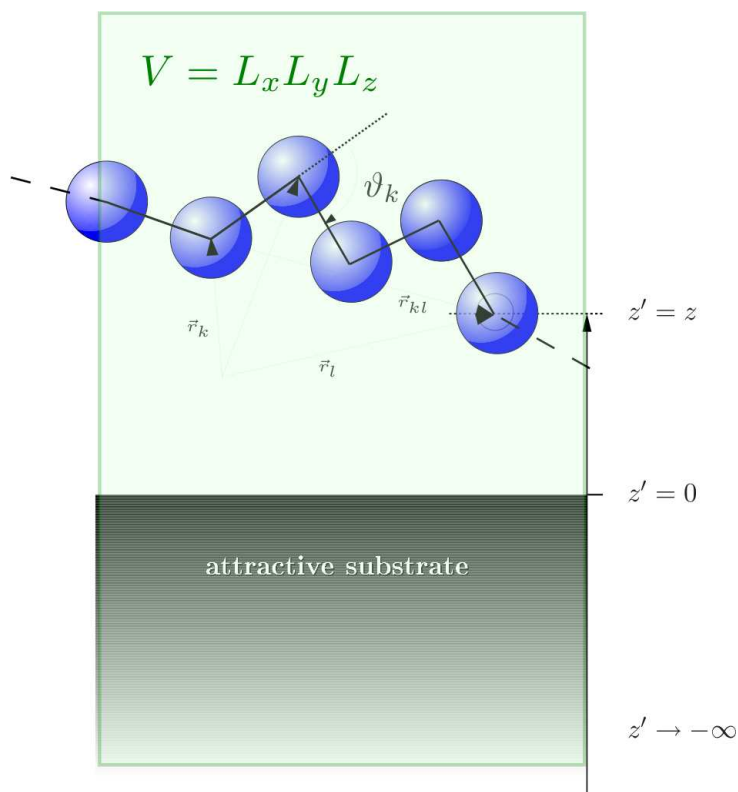


Figure 11.8: The model of the polymer as a Lennard-Jones chain interacting with an attractive substrate at $z = 0$. The distance between two adjacent monomers is fixed to unity. The bending angle at the $(k+1)$ th monomer is denoted by ϑ_k and the vector between the k th and l th monomer by \vec{r}_{kl} . Each monomer k has a distance to the substrate z_k .

the considered system and the nomenclature, see Fig. 11.8. Altogether, the Hamiltonian of the system reads as

$$E = 4 \sum_{i=1}^{N-2} \sum_{j=i+2}^N (r_{ij}^{-12} - r_{ij}^{-6}) + \frac{1}{4} \sum_{i=1}^{N-2} (1 - \cos \vartheta_i) + \epsilon_s \sum_{i=1}^N \left(\frac{2}{15} z_i^{-9} - z_i^{-3} \right). \quad (11.1)$$

The densities of states necessary for our data analyses were obtained by extensive multicanonical Monte Carlo computer simulations over many orders of magnitude. We used microcanonical analyses because for short chains and strong surface attraction, the microcanonical entropy turns out to be a convex function of energy in the transition regime, see Fig. 11.9. This indicates that surface-entropic effects are relevant. Albeit known to be a continuous transition in the thermodynamic limit of infinitely long chains, the adsorption transition of polymers with finite length thus exhibits a clear signature of a first-order-like transition, with coexisting phases of adsorbed and desorbed conformations. Another remarkable consequence of the convexity of the microcanonical entropy is that the transition is accompanied by a decrease of the microcanonical temperature with increasing energy. Since this is a characteristic physical effect it should not be ignored in analyses of cooperative macrostate transitions in finite systems.

[1] M. Möddel et al.: J. Phys. Chem. B **113**, 3314 (2009)

[2] M. Möddel et al.: e-print arXiv:1002.2000 (cond-mat.stat-mech)

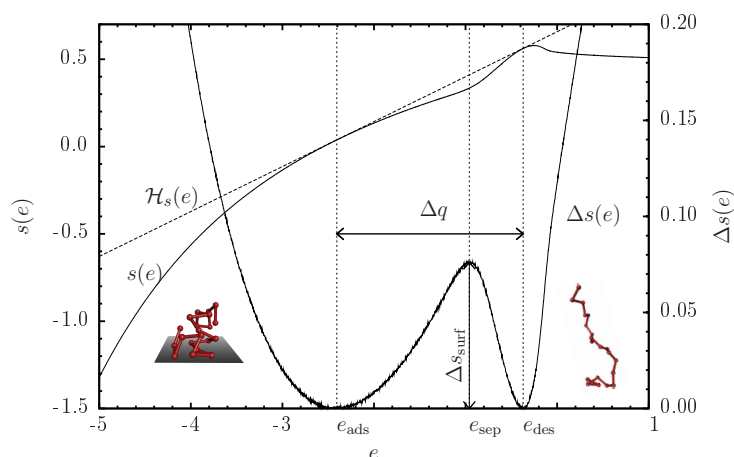


Figure 11.9: Microcanonical entropy $s(e)$ (up to an unimportant constant) for a 20mer at $\epsilon_s = 5$, the Gibbs hull $\mathcal{H}_s(e)$, and their difference $\Delta s(e)$ as functions of the energy per monomer e . The convex adsorption regime is bounded by the energies e_{ads} and e_{des} of the coexisting phases of adsorbed and desorbed conformations at the adsorption temperature T_{ads} , defined via the slope of $\mathcal{H}_s(e)$ [2]. Δs_{surf} denotes the surface entropy per monomer and Δq the latent heat of the first-order-like transition.

11.11 Peptide Adhesion to Semiconductor Substrates: Simulations and Experiments

M. Bachmann^{*}, K. Goede[†], A.G. Beck-Sickinger[‡], M. Grundmann[†], A. Irbäck[§], W. Janke

^{*}Present address: IFF-2 and IAS-2, Forschungszentrum Jülich, Germany

[†]Semiconductor Physics Group, Institut für Experimentelle Physik II

[‡]Institut für Biochemie

[§]Computational Biology & Biological Physics Division, Lunds Universitet, Lund, Sweden

In the past few years, the interest in hybrid interfaces formed by “soft” molecular matter and “hard” solid substrates has rapidly grown as such systems promise to be relatively easily accessible candidates for novel biosensors or electronic devices. The enormous progress in high-resolution microscopy and in biochemical engineering of macromolecules is the major prerequisite for studies of hybrid systems and potential applications [1]. One particularly important problem is the self-assembly and adhesion of polymers, proteins, or protein-like synthetic peptides to solid materials such as, e.g., metals [2] and semiconductors [3–5]. Peptide and substrate-specific binding affinity is particularly relevant in pattern recognition processes [6]. Basic theoretical considerations of simplified polymer–substrate and protein–substrate models have predicted complex pseudophase diagrams [7, 8].

In bacteriophage display experiments, only a few peptides out of a library of 10^9 investigated sequences with 12 amino acid residues were found to possess a particularly strong propensity to adhere to (100) gallium-arsenide (GaAs) surfaces [3]. The sequence-specificity of adsorption strength is a remarkable property, but the question remains how it is related to the individual molecular structure of the peptides. We expect that *relevant* mutations of sites in the amino-acid sequence can cause a change of the binding affinity. Indeed, one key aspect of our study is to provide evidence that

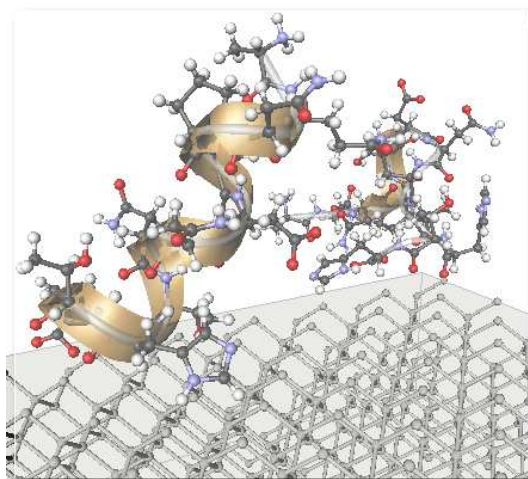


Figure 11.10: The binding properties of a peptide adsorbing at a substrate are influenced by the strongly geometry-dependent, heterogeneous electronic properties of molecule and substrate. The resulting high specificity of adsorption requires a careful force-field parametrization in semiclassical models. The image shows a snapshot from a simulation of two synthetic helical peptides interacting with a de-oxidized silicon (100) surface.

proline is a potential candidate for switching the adsorption propensities to cleaned (100) silicon (Si) substrates.

In this project, we show by means of experimental and computational analyses that the adsorption properties of mutated synthetic peptides at semiconductors exhibit a clear sequence-dependent adhesion specificity. Our simulations of a novel hybrid peptide-substrate model reveal the correspondence between proline mutation and binding affinity to a clean silicon substrate, for a snapshot of typical configurations see Fig. 11.10. After synthesizing the theoretically suggested amino-acid sequences with different binding behaviour, we could confirm the relevance of the selective mutations upon adhesion in our subsequent atomic force microscopy experiments [9].

- [1] M. Sarikaya et al.: *Nature Mat.* **2**, 577 (2003)
- [2] S. Brown: *Nature Biotechnol.* **15**, 269 (1997)
- [3] S.R. Whaley et al.: *Nature* **405**, 665 (2000)
- [4] K. Goede et al.: *Nano Lett.* **4**, 2115 (2004)
- [5] K. Goede et al.: *Langmuir* **22**, 8104 (2006)
- [6] T. Bogner et al.: *Phys. Rev. Lett.* **93**, 268108 (2004)
- [7] M. Bachmann, W. Janke: *Phys. Rev. Lett.* **95**, 058102 (2005); *Phys. Rev. E* **73**, 041802 (2006)
- [8] M. Bachmann, W. Janke: *Phys. Rev. E* **73**, 020901(R) (2006)
- [9] M. Bachmann et al.: *Microscopic Mechanism of Specific Peptide Adhesion to Semiconductor Substrates*, Leipzig preprint, submitted

11.12 Free-Energy Barrier at Droplet Condensation

A. Nußbaumer, E. Bittner, W. Janke

The precise mechanism for the formation of the first large droplet in condensing systems is one of the fundamental problems in statistical physics. Early analytical studies date back to the 1960s. Over the years this problem has been taken up several times and further advanced both analytically and numerically. Our own simulational study is guided by mathematical considerations of Biskup *et al.* [1, 2], which are based on an equilibrium framework and result in largely model independent scaling predictions for the condensation process in the infinite-volume limit.

In rather elaborate Monte Carlo simulations of the 2D Ising lattice gas model we could verify that the behaviour of droplets which live on a square lattice is compatible with these predictions already for moderately large system sizes [3]. Moreover, recently we have shown that the underlying lattice structure and interaction range are largely irrelevant provided that properly scaled variables are used [4].

Having established the insensitivity of the droplet condensation mechanism to microscopic details, we next turned to exploratory analyses of the coexistence region where the system is either in the condensed phase with a single large droplet that has adsorbed a fraction $\lambda = 2/3$ of the particles (respectively of the excess magnetisation) or in the evaporated phase with many small bubbles ($\lambda = 0$). In Fig. 11.11 the probability distribution of λ is shown which clearly demonstrates the expected two-phase signal. The minimum between the two peaks corresponds to a free-energy barrier. More precisely, according to the theory [5], the ratio of the minimum to the maximum should decrease with system size L as $\exp(-\beta\Delta F) \approx \exp(-cL^{2/3})$ with $c = 0.1522$ at $T = 1/\beta = 1.5$. If we allow for an additional power-like prefactor $\propto L^\kappa$, a least-squares fit through the data points for $L \geq 90$ yields $c = 0.211 \pm 0.003$ with a goodness-of-fit parameter $Q = 0.22$. Even though this estimate is quite far off the expectation, if we fix $c = 0.1522$ and consider the data for $L \geq 170$, we obtain a perfectly compatible fit with a goodness of $Q = 0.16$. For the larger lattice sizes the two fits are hardly distinguishable which makes it so difficult to estimate the parameter c reliably [5].

Alternatively, by measuring the (integrated) autocorrelation time τ_{int} in simulations with the magnetisation fixed directly at the evaporation/condensation point, we also find a compatible asymptotic scaling behaviour, $\tau_{\text{int}} \approx \exp(cL^{2/3})$, with $c = 0.124 \pm 0.008$, but the parameter c is again difficult to estimate reliably with the present data set [5]. Presumably much larger lattices are needed to arrive at a firm estimate.

Note that in multimagnetical simulations with a flat magnetisation distribution, this free-energy barrier is not directly visible when monitoring the magnetisation alone. Rather, it appears as a “hidden” obstacle in an “orthogonal” direction of phase space. However, it is still clearly reflected by a slowing down of the performance of the simulations, which makes it important to understand the scaling properties of this barrier also from a purely algorithmic point of view.

- [1] M. Biskup *et al.*: *Europhys. Lett.* **60**, 21 (2002)
- [2] M. Biskup *et al.*: *Comm. Math. Phys.* **242**, 137 (2003)
- [3] A. Nußbaumer *et al.*: *Europhys. Lett.* **75**, 716 (2006)
- [4] A. Nußbaumer *et al.*: *Phys. Rev. E* **77**, 041109 (2008)

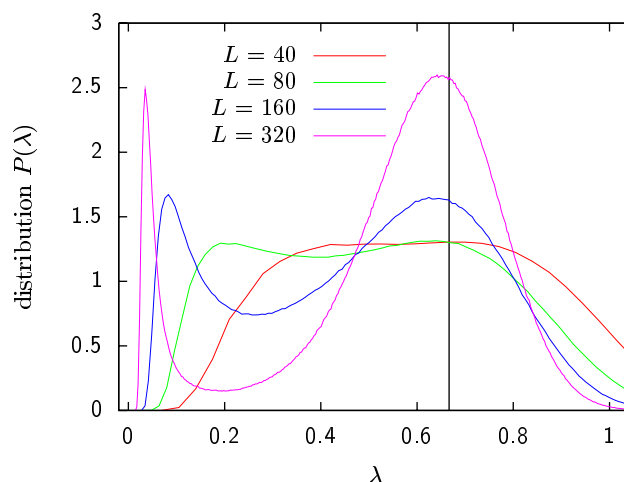


Figure 11.11: Probability distribution of the fraction λ close to the evaporation/condensation transition on 2D square lattices at $T = 1.5$, exhibiting a clear two-phase signal. The minimum between the two peaks corresponds to the free-energy barrier.

- [5] A. Nußbaumer et al.: *Free-Energy Barrier at Droplet Condensation*, Prog. Theor. Phys. Suppl. (in press)

11.13 Quantum Critical Points for Mixed Heisenberg Spin Chains

R. Bischof, W. Janke

The main focus of this project is on quantum critical phenomena and low-temperature properties of various versions of the 1D antiferromagnetic quantum Heisenberg model, which is one of the most fundamental models of quantum magnetism and is related to high-temperature superconductors. The low-temperature properties of quantum spin chains depend significantly on the size of spins involved. Uniform chains of half-odd integer spins have no energy gap between the ground state and first excited states (i.e., they are quantum critical), whereas chains with integer spins do show an excitation gap. Above that, spin chains can be driven to and away from criticality by tuning appropriate parameters (such as bond alternation, exchange anisotropy, next-nearest-neighbour interaction, spin-phonon coupling, etc.). While there exists a wide literature about quantum critical phenomena in uniform spin chains, mixed chains have yet rarely been considered.

By means of quantum Monte Carlo (QMC) simulations based on the continuous imaginary time loop algorithm [1, 2] and quantum reweighting methods [3] we have first investigated the uniform $S = 1/2$ Heisenberg spin chain with bond alternation and alternating quantum chains of mixed spins, consisting of two different kinds of spin, $S_a = 1/2$ and $S_b = 1$, that appear alternatingly in pairs (“model A”). For comparison, we recently also started investigations of the cases $S_a = 1/2$ and $S_b = 3/2$ (“model B”) as well as $S_a = 1$ and $S_b = 3/2$ (“model C”).

If the coupling-constant ratio $\alpha = J'/J$ is varied at fixed anisotropy parameter Δ (multiplying the z-component of the spin-spin scalar product), one observes a second-order phase transition at zero temperature. For the simple Heisenberg model symmetric in spin space ($\Delta = 0$) one has $\alpha_c = 1$ and the critical exponent of the correlation length takes the value $\nu = 2/3$. Due to the self duality of the Heisenberg spin chain, $\alpha_c = 1$ is valid for all $0 \leq \Delta \leq 1$, but ν varies continuously from $2/3$ to 1 for $\Delta = 0$. Mixed spin chains do not exhibit self duality and hence also the critical coupling α_c varies with Δ . One of our goals was therefore a precise determination of the phase diagrams in the $\alpha - \Delta$ parameter space. While most data have already been generated, the final analysis will still take some time. In general the scaling behaviour of the correlation length ξ is complicated by multiplicative logarithmic corrections which, in the simplest case, take the form $\xi \sim \alpha^{-2/3} |\ln \alpha|^{1/2}$. Such a behaviour is difficult to analyze numerically and often results in the determination of effective exponents which include or imitate the logarithmic correction term.

The twist order parameter is well suited to signal quantum phase transitions between different valence bond configurations in various 1D quantum spin systems. At non-zero temperature we have found the formation of a plateau in the twist order parameter around the (zero temperature) quantum critical point [4]. We have investigated the possibility that this plateau is related to the quantum critical region that fans out from the quantum critical point. However, up to the present accuracy of our simulations the data does not yet support this conjecture [4]. Alternative one may also consider a disorder parameter for which we have developed a suitable generalization to mixed spin chains. This new observable is currently tested numerically.

[1] B.B. Beard, U.J. Wiese: Phys. Rev. Lett. **77**, 5130 (1996)

[2] H.G. Evertz: Adv. Phys. **52**, 1 (2003)

[3] M. Troyer et al.: Braz. J. Phys. **34**, 377 (2004)

[4] R. Bischof, W. Janke: in Proceedings of the International Conference *Path Integrals – New Trends and Perspectives*, ed. by W. Janke, A. Pelster (World Scientific, Singapore 2008) p 514

11.14 Critical Behaviour of Quantum Compass and Plaquette Orbital Models

S. Wenzel, W. Janke, A. Läuchli*

*Max Planck Institute for the Physics of Complex Systems (MPI PKS), Dresden, Germany

This project deals with a new type of quantum spin models that is currently getting into focus of condensed matter physics. These are systems which look very similar to an ordinary Heisenberg model but lack some of the couplings which are present there. Examples are the famous Kitaev model [1] which has prompted enormous efforts because of a potential realization as a topological quantum computer. In this line of research also a related model, the so-called compass model, was investigated in the literature in connection to interesting physics ranging from orbital order in transition

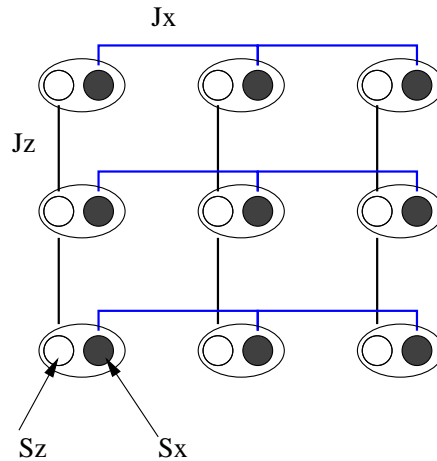


Figure 11.12: Visualization of the quantum compass model. The different components of the spin interact differently and only along specific directions.

metal compounds to topologically protected qubits [2, 3]. The compass model is defined in two dimensions by the following Hamiltonian

$$\mathcal{H} = (1/4) \sum_i \left(J_x \sigma_i^x \sigma_{i+e_x}^x + J_z \sigma_i^z \sigma_{i+e_z}^z \right), \quad (11.2)$$

where σ are the usual Pauli operators, J_x, J_y coupling constants and e_z a unit vector in z direction (cp. Fig. 11.12). Although this is a simple looking Hamiltonian it is rather hard to study. It was actually shown to possess rich physics ranging from highly degenerate ground states, quantum phase transitions to an exciting thermal phase transition. A recent Letter [4] furthermore proposes that directional order in the quantum compass model is rather stable against dilution, which is not the case for the classical model.

To investigate these questions in more detail, we have performed a comprehensive study of the two-dimensional (2D) compass model on square lattices for classical and quantum spin degrees of freedom using classical and quantum Monte Carlo methods [5]. We employed state-of-the-art implementations using Metropolis, stochastic series expansion (SSE) and parallel tempering (PT) techniques to obtain the critical ordering temperatures and critical exponents. In a pre-investigation we reconsidered the classical compass model where we study and contrast the finite-size scaling (FSS) behaviour of ordinary periodic boundary conditions against annealed boundary conditions. We found that periodic boundary conditions suffer from extreme finite-size effects, which might be caused by closed loop excitations on the torus, so that one needs to go to very large lattice sizes to see the asymptotic scaling behaviour. Our numerical results are at odds with recent literature on the subject which we can trace back to neglecting these strong finite-size effects on periodic lattices. Our analysis showed, however, that one arrives at quite different conclusions when these effects are properly taken into account [5, 6]. Our findings for the quantum model might have an impact on previous conclusions concerning the dilution effects on the compass model because a precise estimate of the critical temperature T_c enters crucially into this analysis [6].

In the search for other fundamental spin models and to gain further insights into the field around the underlying Kitaev model, we have proposed a different, topolo-

gical modification of the compass model and studied its intriguing physics [7]. Our main result for this “plaquette orbital model” is the establishment of an interesting (topological) order that can be described by a crystallization and modulation of local energy contributions but which lacks conventional magnetic order. We show that our new model falls into the Ising universality class and that it possesses well behaved FSS properties in contrast to the compass model. As a bi-product we can then argue that quantum spins make these orbital models stiff against all kinds of disturbances – geometrical variations and impurities – in contrast to classical fields [6, 7].

The precision of our results for the quantum model was still rather low compared to many other systems of statistical physics. In this respect it was therefore a challenging project to devise and analyze special boundary conditions for the quantum model with improved FSS behaviour compared to periodic boundary conditions. To this end we re-considered recently the directional-ordering transition in the two-dimensional classical and quantum compass model on the square lattice, obtaining several improvements [8]. First, an improved algorithm is proposed which builds on the Wolff cluster algorithm in one-dimensional subspaces of the configuration space. This improvement allows us now to study much larger classical systems up to $L = 512$. Based on the new algorithm we give evidence for the presence of strongly anomalous scaling for periodic boundary conditions which is much worse than anticipated before. Second, we propose and study alternative boundary conditions for the compass model which do not make use of extended configuration spaces of the annealed boundary schemes and show that they completely remove the problem with finite-size scaling. In particular we apply these boundary conditions to the quantum problem and present a considerably improved estimate for the critical temperature which should be of interest for future studies on the compass model. The origin of the anomalous scaling is also discussed.

Work supported by the Studienstiftung des deutschen Volkes and the Leipzig Graduate School *BuildMoNa*.

- [1] A. Kitaev: *Ann. Phys.* **321**, 2 (2006)
- [2] K.I. Kugel, D.I. Khomskii: *Sov. Phys. Usp.* **25**, 231 (1982)
- [3] B. Douçot et al.: *Phys. Rev. B* **71**, 024505 (2005)
- [4] T. Tanaka, S. Ishihara: *Phys. Rev. Lett* **98**, 256402 (2007)
- [5] S. Wenzel, W. Janke: *Phys. Rev. B* **78**, 064402 (2008); see also “Publisher’s Note” in *Phys. Rev. B* **78**, 099902(E) (2008) [Fig. 1 selected for *Phys. Rev. B* “Kaleidoscope” August 2008]
- [6] S. Wenzel: *Monte Carlo Investigations of Low-Dimensional Classical and Quantum Spin Systems: Unconventional Criticality and Orbital Ordering*, PhD thesis, Universität Leipzig (2009)
- [7] S. Wenzel, W. Janke: *Phys. Rev. B* **80**, 054403 (2009) [Fig. 2(c) selected for *Phys. Rev. B* “Kaleidoscope” August 2009]
- [8] S. Wenzel et al.: *Phys. Rev. E* **81**, 066702 (2010) [arXiv:1002.3508]

11.15 Universal Amplitude Ratios for the Potts Model

B. Berche^{*}, P. Butera[†], W. Janke, L. Shchur[‡]

^{*}Laboratoire de Physique des Matériaux, Nancy Université, France

[†]Istituto Nazionale di Fisica Nucleare, Milano, Italy

[‡]Landau Institute for Theoretical Physics, Chernogolovka, Russia

At a second-order phase transition not only critical exponents are universal but also certain amplitude ratios, i.e., they do not depend on the details of the considered statistical system. A typical example is provided by the scaling relation for the magnetic susceptibility χ which in the vicinity of the critical temperature T_c behaves according to $\chi \sim \Gamma_{\pm}|T/T_c - 1|^{-\gamma}$, where γ is the critical exponent and Γ_+ and Γ_- denote the critical amplitudes in the high- and low-temperature phase, respectively. The ratio Γ_+/Γ_- is then such a universal amplitude ratio.

Values for Γ_+/Γ_- could recently be predicted analytically for the two-dimensional q -state Potts model with $q = 2, 3$ and 4 states [1, 2]. This is one of simplest models which exhibit a phase transition. It is solved exactly at the critical point for any number of spin components q and it is known that for $q \leq 4$ it has a continuous phase transition whereas for $q > 4$ the phase transition is of first order. The model has a great theoretical interest as new theories may be tested in this model. At the same time, these models may have some practical interest as they may be realized in an adsorbate lattice placed onto a clean crystalline surface. The full classification of such systems with continuous transitions is known theoretically and there exist experiments in which some of them realize the 3-state and 4-state Potts models, so that the critical exponents can be experimentally estimated.

While for $q = 2$ and 3 the prediction for the amplitude ratios could subsequently be confirmed with numerical techniques (Monte Carlo simulations and high-temperature series expansions) [3], the situation for $q = 4$ remained controversial. The origin for the disagreement can probably be traced back to relatively strong logarithmic corrections of the leading scaling behaviour [4]. It is a common belief that the $q = 4$ Potts and the Baxter-Wu model (a model with three-spin interaction on a triangular lattice) [5] belong to the same universality class. Still, at the same time, the critical behaviour of the Baxter-Wu model is *not* modified by logarithmic corrections. Our extensive numerical analysis shows that critical amplitude ratios are very close for both models and, therefore, gives support to the hypothesis that the critical behaviour of both systems is governed by the same renormalization group fixed point.

[1] G. Delfino, J.L. Cardy: Nucl. Phys. B [FS] **519**, 551 (1998)

[2] G. Delfino et al.: Nucl. Phys. B **565**, 521 (2000)

[3] L.N. Shchur et al.: Nucl. Phys. B **620**, 579 (2002)

[4] B. Berche et al.: Comp. Phys. Comm. **180**, 493 (2009)

[5] R.J. Baxter, F.Y. Wu: Phys. Rev. Lett. **31**, 1294 (1973); Aust. J. Phys. **27**, 357 (1974)

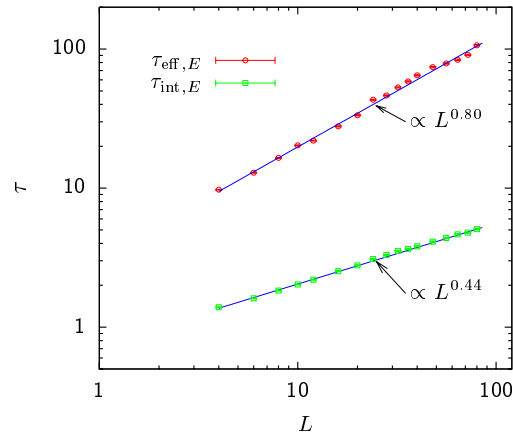


Figure 11.13: Autocorrelation times τ_{int} and τ_{eff} for the energy of the 3D Ising model, where $\tau_{\text{eff}} = N_{\text{rep}} \tau_{\text{int}}$ and N_{rep} is the number of replica of the parallel tempering algorithm.

11.16 Parallel Tempering Cluster Algorithm

E. Bittner, W. Janke

While much attention has been paid in the past to simulations of first-order phase transitions and systems with rugged free-energy landscapes in generalized ensembles (umbrella, multicanonical, Wang-Landau, parallel/simulated tempering sampling) [1], the merits of this non-Boltzmann sampling approach also for simulation studies of critical phenomena have been pointed out only recently. In finite-size scaling analyses of Monte Carlo simulations of second-order phase transitions one often needs an extended temperature range around the critical point. In Ref. [2], Berg and one of the authors combined multibondic sampling [3] with the Wang-Landau recursion [4] to cover the complete desired “critical” temperature range in a single simulation for each lattice size, where the “desired” range derives from a careful finite-size scaling (FSS) analysis of all relevant observables. Since the individual reweighting ranges of the involved observables may be quite disparate, this scaling analysis is the second important ingredient of the method.

Here we combine the parallel-tempering algorithm [5] with cluster updates [6] and an improved adaptive routine to find the range of interest [7]. To assess the performance of our method, we measured the integrated autocorrelation time $\tau_{\text{int}}(T_i, L)$ for each temperature and system size. We found that the maximal integrated autocorrelation times $\tau_{\text{int}}(L) = \max_{i=1, N_{\text{rep}}} \tau_{\text{int}}(T_i, L)$ for the energy, squared magnetization and the first structure factor scale only weakly $\propto L^z$ with the system size L , e.g., $z = 0.44(1)$ for the energy of the 3D Ising model. To make a fair comparison with other methods, we also take the computational effort into account and include the number of replica N_{rep} of the parallel tempering algorithm into the definition of an effective autocorrelation time according to $\tau_{\text{eff}} = N_{\text{rep}} \tau_{\text{int}} \propto L^{z_{\text{eff}}}$, yielding for the energy an exponent $z_{\text{eff}} = 0.80(1)$, i.e., $N_{\text{rep}} \propto L^{0.36}$, cf. Fig. 11.13.

As a result, we gain two further orders of magnitude in the performance for 2D and 3D Ising models in comparison with the recently proposed Wang-Landau recursion for cluster algorithms based on the multibondic algorithm, which is already a great improvement over the standard multicanonical variant [8, 9].

- [1] W. Janke (Ed.): *Rugged Free Energy Landscapes: Common Computational Approaches to Spin Glasses, Structural Glasses and Biological Macromolecules*, Lect. Notes Phys. **736** (Springer, Berlin 2008)
- [2] B.A. Berg, W. Janke: Phys. Rev. Lett. **98**, 040602 (2007)
- [3] W. Janke, S. Kappler: Phys. Rev. Lett. **74**, 212 (1995)
- [4] F. Wang, D.P. Landau: Phys. Rev. Lett. **86**, 2050 (2001)
- [5] K. Hukushima, K. Nemoto: J. Phys. Soc. Jpn. **65**, 1604 (1996)
- [6] R.H. Swendsen, J.-S. Wang: Phys. Rev. Lett. **58**, 86 (1987)
- [7] E. Bittner et al.: Phys. Rev. Lett. **101**, 130603 (2008)
- [8] E. Bittner, W. Janke: PoS (LAT2009) 042
- [9] E. Bittner, W. Janke: *Parallel Tempering Cluster Algorithm for Computer Simulations of Critical Phenomena*, Leipzig preprint, submitted

11.17 Error Estimation and Reduction with Cross Correlations

M. Weigel*, W. Janke

*Institut für Physik, Johannes Gutenberg-Universität Mainz, Germany

Monte Carlo simulations, and in particular Markov chain based methods, have matured over the last decades into a highly versatile and powerful toolbox for studies of systems in statistical and condensed-matter physics, ranging from classical spin models over soft-matter problems to quantum systems. Their competitiveness with other approaches such as, e.g., field-theoretic expansions for the study of critical phenomena, is largely based on the development and refinement of a number of advanced simulation techniques such as cluster algorithms and generalized-ensemble methods.

Equally important to the generation of simulation data, however, is their correct and optimal analysis. In this field, a number of important advances over the techniques used in the early days have been achieved as well. These include, e.g., the finite-size scaling (FSS) approach, turning the limitation of simulational methods to finite system sizes into a systematic tool for accessing the thermodynamic limit, reweighting techniques, lifting the limitation of numerical techniques to the study of single points in parameter space to allow for continuous functions of estimates to be studied, as well as advanced statistical tools for error estimation such as the jackknife and other resampling schemes of data analysis [1].

Of these techniques, the statistical data analysis appears to have received the least attention. Hence, while FSS analyses, even including correction terms, are quite standard in computer simulation studies, a proper analysis and reduction of statistical errors and bias appears to be much less common. More specifically, data generated by a Monte Carlo (MC) simulation are subject to two types of correlation phenomena, namely (a) autocorrelations or temporal correlations for the case of Markov chain MC (MCMC) simulations, which are directly related to the Markovian nature of the underlying stochastic process and lead to an effective reduction of the number of independently sampled events, and (b) cross correlations between different estimates extracted from the same set of original time series data coming about by the origin of estimates in

the same statistical data pool. The former can be most conveniently taken into account by a determination of the relevant autocorrelation times and a blocking or binning transformation resulting in an effectively uncorrelated auxiliary time series [2, 3]. Such analyses are by now standard at least in seriously conducted simulational studies.

On the contrary, the effects of cross correlations have been mostly neglected to date (see, however, Refs. [4–6]), but are only systematically being discussed following our recent suggestion [7, 8]. In this project, we investigate how such cross correlations lead to systematically wrong estimates of statistical errors of averaged or otherwise combined quantities when a naive analysis is employed, and how a statistically correct analysis can be easily achieved within the framework of the jackknife resampling method. Furthermore, one can even take benefit from the presence of such correlation effects for significantly reducing the variance of estimates without substantial additional effort. We demonstrate the practical relevance of these considerations for a finite-size scaling study of the Ising model in two and three dimensions and report in some cases improvement factors up to 10 in simulation time [9].

- [1] B. Efron, R.J. Tibshirani: *An Introduction to the Bootstrap* (Chapman and Hall, Boca Raton 1998)
- [2] H. Flyvbjerg, H.G. Petersen: *J. Chem. Phys.* **91**, 461 (1989)
- [3] W. Janke: *Lect. Notes Phys.* **739**, 79 (2008)
- [4] H.G. Ballesteros et al.: *Phys. Lett. B* **387**, 125 (1996)
- [5] W. Janke, T. Sauer: *J. Chem. Phys.* **107**, 5821 (1997)
- [6] M. Weigel, W. Janke: *Phys. Rev. B* **62**, 6343 (2000)
- [7] M. Weigel, W. Janke: *Phys. Rev. Lett.* **102**, 100601 (2009)
- [8] L.A. Fernández, V. Martín-Mayor: *Phys. Rev. E* **79**, 051109 (2009)
- [9] M. Weigel, W. Janke: *Phys. Rev. E* **81**, 066701 (2010) [arXiv:1002.4517]

11.18 Funding

Excellence Initiative, Graduate School “BuildMoNa”: Leipzig School of Natural Sciences – Building with Molecules and Nano-objects

W. Janke (Principal Investigator)

Deutsche Forschungsgemeinschaft (DFG)

Forschergruppe 877: From Local Constraints to Macroscopic Transport

W. Janke (Principal Investigator)

Deutsche Forschungsgemeinschaft (DFG)

Research Training Network (RTN) “ENRAGE”: Random Geometry and Random Matrices: From Quantum Gravity to Econophysics

W. Janke (Principal Investigator)

EU, Grant No. MRTN-CT-2004-005616

Statistical Mechanics of Complex Networks

W. Janke (with Z. Burda, Krakau)

Alexander von Humboldt Foundation, “Institutspartnerschaft” with the Jagiellonian University, Krakow, Poland, Grant No. 3.4-Fokoop-DEU/1117877

Statistical Physics of Complex Systems

W. Janke (with B. Berche, Nancy)

Deutsch-Französische Hochschule, "Deutsch-Französisches Doktorandenkollegium (DFDK)" with "Co-tutelle de Thèse", jointly with Nancy Université, France, Grant No. CDFA-02-07

Θ-Polymers in Porous Media Under Applied Force

W. Janke

Alexander von Humboldt Foundation, Host of Humboldt Fellowship for Dr. Viktoria Blavatska, Lviv, Ukraine, Grant No. 3.3-UKR/11207567 STP-2

Host of Alexander von Humboldt Research Prize Winner Bernd A. Berg (Florida State University, Tallahassee, USA)

W. Janke

Alexander von Humboldt Foundation

Dynamik und Statik von Spingläsern

W. Janke

Deutsche Forschungsgemeinschaft (DFG), Grant No. JA483/22-1

Phasenübergänge in Systemen mit einschränkender Geometrie

W. Janke

Deutsche Forschungsgemeinschaft (DFG), Grant Nos. JA483/23-1 and 2

Investigation of Thermodynamic Properties of Lattice and Off-Lattice Models for Proteins and Polymers

M. Bachmann and W. Janke

Deutsche Forschungsgemeinschaft (DFG), Grant Nos. JA483/24-1 and 2

Molecular Conformation Mechanics of Proteins and Polymers

W. Janke

Deutsche Forschungsgemeinschaft (DFG), Grant No. JA483/24-3

Mass Transport Models on Networks

W. Janke (twin project with H. Meyer-Ortmanns, Jacobs University Bremen)

Deutsche Forschungsgemeinschaft (DFG), Grant No. JA483/27-1

Monte Carlo Simulationen der Statik und Dynamik von Spingläsern

E. Bittner and W. Janke

NIC Jülich (computer time grant for "JUROPA"), Grant No. hlz10

Statistical Mechanics of Protein and Polymer Structure Formation Processes

M. Bachmann and W. Janke

NIC Jülich (computer time grant for "JUROPA"), Grant No. hlz11

Quantum Monte Carlo Simulations of Quantum Spin Models

W. Janke

NIC Jülich (computer time grant for "JUROPA"), Grant No. hlz12

Grant for support of the Conference *MECO34*, 29. March – 01. April 2009
 W. Janke (Organizer, together with S. Trimper, Universität Halle)
 Deutsche Forschungsgemeinschaft (DFG), Grant No. JA 483/26-1

Grant for support of the Conference *MECO34*, 29. March – 01. April 2009
 W. Janke (Organizer, together with S. Trimper, Universität Halle)
 SMWK, Grant No. 4-7531.50-05-09/4

Grant for support of students participating in the Conference *MECO34*, 29. March – 01. April 2009
 W. Janke (Organizer, together with S. Trimper, Universität Halle)
 Wilhelm und Else Heraeus-Stiftung

Grant for full support of 75 participants of the *International Conference ENRAGEing Perspectives – Random Geometry and Random Matrices: From Quantum Gravity to Econophysics*, 17.–22. May 2009
 W. Janke (Organizer)
 Max-Planck-Institut für Physik komplexer Systeme, Dresden

Grant for support of the Workshop *Simulations on GPU*, 11.-12. June 2009
 W. Janke (Organizer, together with M. Bordag, Abt. QFG)
 Deutsche Forschungsgemeinschaft (DFG), Grant No. BO1112/17-1

Quanten Monte Carlo Simulationen von (ungeordneten) Quantenspinsystemen
 R. Bischof
 Landesgraduiertenstipendium

Dimerized Heisenberg Models
 S. Wenzel
 Studienstiftung des deutschen Volkes

11.19 Organizational Duties

Michael Bachmann

- Referee for Physical Review Letters, Journal of the American Chemical Society, IEEE/ACM Transactions on Computational Biology and Bioinformatics, Physical Review A, Physical Review E, Journal of Physics A, European Journal of Physics D, Biophysical Reviews and Letters, Computer Physics Communications, Journal of Computational Chemistry, Macromolecules, PhysChemChemPhys
- External Reviewer for Engineering and Physical Sciences Research Council (EPSRC), Great Britain; National Science Foundation (NSF), USA

Elmar Bittner

- Scientific Secretary of the 34th Conference of the Middle European Cooperation in Statistical Physics *MECO34*, Universität Leipzig, 29. March – 01. April 2009
- Scientific Secretary of the Workshop *Simulations on GPU*, ITP, Universität Leipzig, 11.–12. June 2009

- Co-organizer of the contribution *Fußball-Fieber wissenschaftlich betrachtet*, Wissenschaftsmesse *Studieren in Mitteldeutschland* (with W. Janke, A. Nußbaumer), Neue Messe Leipzig, 5. September 2009
- Scientific Secretary of the Workshop *CompPhys09 – 10th International NTZ-Workshop on New Developments in Computational Physics*, ITP, Universität Leipzig, 26.–29. November 2009
- Scientific Secretary of the Workshop *CompPhys10 – 11th International NTZ-Workshop on New Developments in Computational Physics*, ITP, Universität Leipzig, 25.–27. November 2010
- Referee for Physical Review Letters, Physical Review E, Journal of Physics A, European Journal of Physics B, Computer Physics Communications

Wolfhard Janke

- Director, Naturwissenschaftlich-Theoretisches Zentrum (NTZ), Universität Leipzig
- Chairperson of the Programme Committee “Scientific Computing” of Forschungszentrum Jülich
- Member of the Scientific-Technical-Council of the Supervisory Board (“Aufsichtsrat”) of the Forschungszentrum Jülich GmbH
- External Member of the Jagiellonian University Graduate School *International Ph.D. Studies in Physics of Complex Systems*, Krakow, Poland
- Specialist Editor, Computer Physics Communications (CPC), Elsevier, Amsterdam, The Netherlands
- Editor “Computational Sciences”, Lecture Notes of Physics, Springer, Berlin, Heidelberg, Germany
- Editor “Computational Physics”, Central European Journal of Physics, Krakow, Poland
- Member of Editorial Board, *Condens. Matter Phys.*, Lviv, Ukraine
- Permanent Member of the “International Advisory Board”, *Conference of the Middle European Cooperation in Statistical Physics (MECO)*
- Organizer of the *Symposium der Sächsischen Forschergruppe FOR877* (with K. Kroy, Abt. TKM), Fakultät für Physik und Geowissenschaften, Universität Leipzig, 27. January 2009
- Organizer of the 34th Conference of the Middle European Cooperation in Statistical Physics *MECO34* (with S. Trimper, Martin-Luther-Universität Halle-Wittenberg), Universität Leipzig, 29. March – 01. April 2009
- Organizer of the International Conference *ENRAGEing Perspectives – Random Geometry and Random Matrices: From Quantum Gravity to Econophysics*, Max-Planck-Institut für Physik komplexer Systeme in Dresden, 17.–22. May 2009
- Organizer of the contribution of the DFH-UFA German-French Graduate College *Physics of Complex Systems* at the International Science Fair *Research*, FU Berlin, 28. May 2009
- Organizer of the Workshop *Simulations on GPU* (with M. Bordag, Abt. QFG), ITP, Universität Leipzig, 11.–12. June 2009
- Organizer of the Workshop and Tutorial *Modeling and Simulating Macromolecules*, ITP, Universität Leipzig, 9.–10. July 2009
- Co-organizer of the contribution *Fußball-Fieber wissenschaftlich betrachtet*, Wissenschaftsmesse *Studieren in Mitteldeutschland* (with E. Bittner, A. Nußbaumer), Neue

Messe Leipzig, 5. September 2009

- Organizer of the Workshop *CompPhys09 – 10th International NTZ-Workshop on New Developments in Computational Physics*, ITP, Universität Leipzig, 26.–29. November 2009
- Member of International Organization Committee of the 10th International Conference *Path Integrals* (with L.S. Schulman (USA), M. Gutzwiller (USA), A. Inomata (USA), J.R. Klauder (USA), D. Fujikawa (Japan) und Chooky Lee (South Korea)), Washington DC, USA, 11.–16. July 2010
- Organizer of the Workshop *CompPhys10 – 11th International NTZ-Workshop on New Developments in Computational Physics*, ITP, Universität Leipzig, 25.–27. November 2010
- External Reviewer for Humboldt-Stiftung; Deutsche Forschungsgemeinschaft; Studienstiftung des deutschen Volkes; the Jeffress Memorial Trust, Bank of America, Virginia, USA; “Fond zur Förderung der wissenschaftlichen Forschung (FWF)”, Österreich; “The Royal Society”, Great Britain; The “Engineering and Physical Sciences Research Council (EPSRC)”, Great Britain; The University of Warwick, England, Great Britain; Coventry University, England, Great Britain; CECAM, Lyon, France; National Science Foundation (NSF), USA; Israel Science Foundation, Israel
- Referee for Physical Review Letters, Physical Review B, Physical Review E, Journal of Chemical Physics, Europhysics Letters, Physics Letters A, Physics Letters B, The European Physical Journal B, Physica A, Proceedings of the Royal Physical Society, Journal of Physics A, Computer Physics Communications, JSTAT, New Journal of Physics, International Journal of Modern Physics C

Andreas Nußbaumer

- Scientific Secretary of the 34th Conference of the Middle European Cooperation in Statistical Physics *MECO34*, Universität Leipzig, 29. March – 01. April 2009
- Co-organizer of the contribution *Fußball-Fieber wissenschaftlich betrachtet*, Wissenschaftsmesse *Studieren in Mitteldeutschland* (with E. Bittner, W. Janke), Neue Messe Leipzig, 5. September 2009

11.20 External Cooperations

Academic

- EU RTN “ENRAGE” – *Random Geometry and Random Matrices: From Quantum Gravity to Econophysics*
Research Training Network of 13 teams throughout Europe
- Dept. of Physics, Florida State University, Tallahassee, USA
Prof. Dr. Bernd A. Berg
- CEA/Saclay, Service de Physique Théorique, France
Dr. Alain Billoire
- Laboratoire de Physique des Matériaux (UMR CNRS No 7556), Nancy Université, France
Prof. Dr. Bertrand Berche, Dr. Christophe Chatelain, Dr. Olivier Collet, Prof. Dr. Malte Henkel, Dr. Dragi Karevski

- Groupe de Physique des Matériaux (UMR CNRS No 6634), Université de Rouen, France
Dr. Pierre-Emmanuel Berche
- Department of Mathematics and the Maxwell Institute for Mathematical Sciences, Heriot-Watt University, Edinburgh, Scotland, UK
Prof. Dr. Desmond A. Johnston
- SUPA, School of Physics and Astronomy, University of Edinburgh, Scotland, UK
Dr. Richard A. Blythe, Prof. Dr. Martin Evans
- Applied Mathematics Research Centre, Coventry University, England, UK
Dr. Ralph Kenna, PD Dr. Christian von Ferber
- Applied Mathematics, Universitat Pompeu Fabra, Barcelona, Spain
Dr. Ramon Villanova
- Engineering of Physics, Ankara University, Turkey
Prof. Dr. Handan Arkin (Olgar)
- Dept. of Physics, Hacettepe University, Ankara, Turkey
Prof. Dr. Tarik Çelik, Gökhan Gökoğlu
- Institute for Condensed Matter Physics, National Academy of Sciences, Lviv, Ukraine
Dr. Viktoria Blavatska, Prof. Dr. Yuriy Holovatch
- Complex Systems Division, Department of Theoretical Physics, Lund University, Lund, Sweden
Prof. Dr. Anders Irbäck, Simon Mitternacht
- Dept. of Physics, Michigan Technological University, Houghton, USA
Prof. Dr. Ulrich H.E. Hansmann
- Jülich Supercomputing Centre (JSC), Forschungszentrum Jülich
Prof. Dr. Peter Grassberger, PD Dr. Thomas Neuhaus
- Institut für Physik, Universität Mainz
Prof. Dr. Kurt Binder, Dr. Hsiao-Ping Hsu, Dr. Martin Weigel
- Atominstytut, TU Wien, Austria
Prof. Dr. Harald Markum, Dr. Rainer Pullirsch
- Istituto Nazionale di Fisica Nucleare, Sezione di Milano-Bicocca, Milano, Italy
Prof. Dr. Pablo Butera
- Banaras Hindu University, Varanasi, India
Prof. Dr. Sanjay Kumar
- Brunel Univ. of West London, England, UK
Dr. Gernot Akemann
- Inst. für Theoretische Physik, FU Berlin
Prof. Dr. Hagen Kleinert
- IAC-1, Universität Stuttgart
Prof. Dr. Rudolf Hilfer, Anjan Prasad Gantapara
- Inst. für Theoretische Physik, Universität Duisburg-Essen
PD Dr. Axel Pelster

- Inst. für Theoretische Physik, Universität Bielefeld
Prof. Dr. Friderike Schmid
- Jacobs Universität Bremen
Prof. Dr. Hildegard Meyer-Ortmanns
- Institute of Physics, Jagiellonian University, Kraków, Poland
Prof. Dr. Piotr Białas, Dr. Leszek Bogacz, Prof. Dr. Zdzisław Burda
- Landau Institute for Theoretical Physics, Chernogolovka, Russia
Prof. Dr. Lev N. Shchur
- Yerevan Physics Institute, Yerevan, Armenia
Prof. Dr. David B. Saakian
- Zhejiang Institute of Modern Physics, Zhejiang University, Hangzhou, P.R. China
Prof. Dr. He-Ping Ying, Prof. Dr. Bo Zheng

11.21 Publications

Journals

- G. Akemann, E. Bittner, M.J. Philips, L. Shifrin: *A Wigner Surmise for Hermitian and Non-Hermitian Chiral Random Matrices*, Phys. Rev. E **80**, 065201(R)-1–4 (2009)
- B. Berche, P. Butera, W. Janke, L. Shchur: *Universal Ratios of Critical Amplitudes in the Potts Model Universality Class*, Comp. Phys. Comm. **180**, 493–496 (2009)
- E. Bittner, A. Nußbaumer, W. Janke: *Anisotropy of the Interface Tension of the Three-Dimensional Ising Model*, Nucl. Phys. B **820**, 694–706 (2009)
- E. Bittner, A. Nußbaumer, W. Janke: *Tune the Autocorrelation Time and Unleash the Full Power of the Parallel Tempering Algorithm*, PoS (LAT2009) 027-1–7 (2009)
- E. Bittner, A. Nußbaumer, W. Janke, M. Weigel: *Football Fever: Goal Distributions and Non-Gaussian Statistics*, Eur. Phys. J. B **67**, 459–471 (2009) [discussed in Nature News Feature article *Goal Beget Goals*, Nature **441**, 793 (2006)]
- V. Blavatska, W. Janke: *Walking on Fractals: Diffusion and Self-Avoiding Walks on Percolation Clusters*, J. Phys. A: Math. Theor. **42**, 015001-1–18 (2009)
- V. Blavatska, W. Janke: *Polymers in Crowded Environment Under Stretching Force: Globule-Coil Transitions*, Phys. Rev. E **80**, 051805-1–10 (2009)
- R.A. Blythe, W. Janke, D.A. Johnston, R. Kenna: *Continued Fractions and the Partially Asymmetric Exclusion Process*, J. Phys. A: Math. Theor. **42**, 325002-1–21 (2009)
- M. Hasenbusch: *The Kosterlitz-Thouless Transition in Thin Films: A Monte Carlo Study of Three-Dimensional Lattice Models*, J. Stat. Mech.: Theor. Exp. P02005-1–34 (2009)
- M. Hasenbusch, F. Parisen Toldin, A. Pelissetto, E. Vicari: *Critical and Multicritical Behavior of the $\pm J$ Ising Model in Two and Three Dimensions*, J. Phys.: Conf. Ser. **145**, 012055-1–4 (2009)

- W. Janke, E. Bittner: *Replica-Exchange Cluster Algorithm*, PoS (LAT2009) 042-1-7 (2009)
- W. Janke, E. Bittner, A. Nußbaumer, M. Weigel: *Football Fever: Self-Affirmation Model for Goal Distributions*, *Condens. Matter Phys.* **12**, 739-752 (2009)
- W. Janke, T. Neuhaus, A.M.J. Schakel: *Critical Loop Gases and the Worm Algorithm*, *Nucl. Phys. B* **829**, 573-599 (2010)
- C. Junghans, M. Bachmann, W. Janke: *Statistical Mechanics of Aggregation and Crystallization for Semiflexible Polymers*, *Europhys. Lett.* **87**, 40002-1-5 (2009)
- M. Möddel, M. Bachmann, W. Janke: *Conformational Mechanics of Polymer Adsorption Transitions at Attractive Substrates*, *J. Phys. Chem. B* **113**, 3314-3323 (2009)
- S. Schnabel, M. Bachmann, W. Janke: *Elastic Lennard-Jones Polymers meet Clusters – Differences and Similarities*, *J. Chem. Phys.* **131**, 124904-1-9 (2009)
- S. Schnabel, T. Vogel, M. Bachmann, W. Janke: *Surface Effects in the Crystallization Process of Elastic Flexible Polymers*, *Chem. Phys. Lett.* **476**, 201-204 (2009)
- T. Vogel, T. Neuhaus, M. Bachmann, W. Janke: *Thickness-Dependent Secondary Structure Formation of Tubelike Polymers*, *Europhys. Lett.* **85**, 10003-1-5 (2009)
- T. Vogel, T. Neuhaus, M. Bachmann, W. Janke: *Thermodynamics of Tubelike Flexible Polymers*, *Phys. Rev. E* **80**, 011802-1-8 (2009)
- T. Vogel, T. Neuhaus, M. Bachmann, W. Janke: *Ground-State Properties of Tubelike Flexible Polymers*, *Eur. Phys. J. E* **30**, 7-18 (2009)
- B. Waclaw, J. Sopik, W. Janke, H. Meyer-Ortmanns: *Pair-Factorized Steady States on Arbitrary Graphs*, *J. Phys. A: Math. Theor.* **42**, 315003-1-8 (2009) [Selected by the Editors for the special IoP Select collection (July 2009)]
- B. Waclaw, J. Sopik, W. Janke, H. Meyer-Ortmanns: *Tuning the Shape of the Condensate in Spontaneous Symmetry Breaking*, *Phys. Rev. Lett.* **103**, 080602-1-4 (2009)
- B. Waclaw, J. Sopik, W. Janke, H. Meyer-Ortmanns: *Mass Condensation in One Dimension with Pair-Factorized Steady States*, *J. Stat. Mech.: Theor. Exp.* P10021-1-29 (2009)
- S. Wenzel, W. Janke: *Comprehensive Quantum Monte Carlo Study of the Quantum Critical Points in Planar Dimerized/Quadrumerized Heisenberg Models*, *Phys. Rev. B* **79**, 014410-1-11 (2009)
- S. Wenzel, W. Janke: *Finite-Temperature Néel Ordering of Fluctuations in a Plaquette Orbital Model*, *Phys. Rev. B* **80**, 054403-1-6 (2009) [Fig. 2(c) selected for *Phys. Rev. B* “Kaleidoscope” August 2009]
- M. Weigel, W. Janke: *Cross Correlations in Scaling Analyses of Phase Transitions*, *Phys. Rev. Lett.* **102**, 100601-1-4 (2009) [selected for *Phys. Rev. Lett. Highlights Synopsis* of April 13, 2009, by Yonko Millev]

Books

V. Blavatska, W. Janke: *Fractals Meet Fractals: Self-Avoiding Random Walks on Percolation Clusters*, in *Computer Simulations in Condensed Matter Physics XXII*, ed. by D.P. Landau, S.P. Lewis, H.-B. Schüttler, *Physics Procedia* **3**, 1431–1435 (2010)

in press

B.A. Berg, W. Janke: *Wang-Landau Multibondic Cluster Approach to Simulations of Second-Order Transitions*, in *Computer Simulations in Condensed Matter Physics XX*, ed. by D.P. Landau, S.P. Lewis, H.-B. Schüttler (Springer, Heidelberg 2010) (in press)

A. Nußbaumer, E. Bittner, W. Janke: *Free-Energy Barrier at Droplet Condensation*, *Prog. Theor. Phys. Suppl.* (in press)

A. Nußbaumer, E. Bittner, T. Neuhaus, W. Janke: *Universality of the Evaporation/Condensation Transition*, in *Computer Simulations in Condensed Matter Physics XX*, ed. by D.P. Landau, S.P. Lewis, H.-B. Schüttler (Springer, Heidelberg 2010) (in press)

B. Waclaw, J. Sopik, W. Janke, H. Meyer-Ortmanns: *Mass Condensation on Networks*, in *XI Latin American Workshop on Nonlinear Phenomena – LAWNP'09*, Búzios, Brazil, *J. Phys.: Conf. Ser.* (in press)

Talks

M. Bachmann: *Conformational Mechanics of Molecular Structure Formation Processes*, Seminar talk, Universität zu Köln, 20. January 2009

M. Bachmann: *Conformational Mechanics of Molecular Structure Formation Processes*, invited talk, 22nd Annual Workshop on *Recent Developments in Computer Simulation Studies in Condensed Matter Physics*, Athens, Georgia, USA, 23.–27. February 2009

M. Bachmann: *Modeling and Simulation of Peptide Adsorption at Silicon Substrates*, invited talk, SimBioMa Workshop *Challenges in Modelling the Interface between Biomolecules and Inorganic Surfaces*, Schloss Waldthausen, Mainz, 18.–20. March 2009

M. Bachmann: *Modeling and Simulation of Macromolecule Adsorption to Substrates* Workshop *ProSurf – Protein Surface Interaction*, Sestri Levante, Italy, 04.–06. July 2009

M. Bachmann: *Challenges in Computational Biology*, NTZ Colloquium talk, Universität Leipzig, 09. July 2009

M. Bachmann: *Modeling and Simulation of Macromolecule Adsorption to Substrates*, invited talk, Symposium *Simulation of Molecules and Nanotubes*, Technion, Haifa, Israel, 13. October 2009

M. Bachmann: *Challenges in Computational Biology*, Colloquium talk, Forschungszentrum Jülich, 06. November 2009

M. Bachmann, G. Schröder: Presentation of the *Computational Biology Cluster Jülich*, Workshop *Theoretical Biology*, Universität zu Köln, 09. December 2009

R. Bischof: *QMC of Spin Chains: Order Parameter, Improved Estimators, Reweighting*, Workshop *Simulations on GPU*, Universität Leipzig, 11.–12. June 2009

E. Bittner: *Droplet Condensation at First-Order Phase Transitions*, invited talk, Conference *ENRAGEing Perspectives – Random Geometry and Random Matrices: From Quantum Gravity to Econophysics*, MPI PKS, Dresden, 18.–22. May 2009

E. Bittner: *Make Life Simple: Unleash the Full power of the Parallel Tempering Algorithm*, *The XXVII International Symposium on Lattice Field Theory – Lattice 2009*, Peking University, Beijing, China, 26.–31. July 2009

E. Bittner: *Football Fever: Goal Distributions and Non-Gaussian Statistics*, invited talk, *Österreichische Statistiktage 2009*, WU Wien, Wien, Österreich, 21.–23. September 2009

W. Janke: *Fractals Meet Fractals – Random Walks on Percolation Clusters*, *SFG FOR877 Symposium*, Universität Leipzig, 27. January 2009

W. Janke: *Fractals Meet Fractals – Self-Avoiding Random Walks on Percolation Clusters*, 22th Annual Workshop on *Recent Developments in Computer Simulation Studies in Condensed Matter Physics*, University of Georgia, Athens, USA, 23.–27. February 2009

W. Janke: *Aggregation and Crystallization of Semiflexible Polymers*, invited talk, *SimBioMa Workshop Challenges in Modelling the Interface Between Biomolecules and Inorganic Surfaces*, Schloss Waldthausen, Mainz, 18.–20. March 2009

W. Janke: *Computational Statistical Physics*, invited talk (“Hauptvortrag”), Focused Session *50 years DY: Trends in Dynamics and Statistical Physics*, DPG Frühjahrstagung 2009, TU Dresden, 23.–27. March 2009

W. Janke: *Fractals Meet Fractals – Self-Avoiding Random Walks on Percolation Clusters*, invited talk, *Atelier Nancy Statistical Physics and Low Dimensional Systems 2009*, Nancy Université, France, 13.–15. May 2009

W. Janke: *Monte Carlo Sampling of Rare Event States*, invited talk, *Mainz Materials Simulation Days*, Max-Planck-Institut für Polymerforschung, Mainz, 03.–05. June 2009

W. Janke: *Football Fever: Self-Affirmation Model for Goal Distributions*, invited plenary talk, 3rd Conference on *Statistical Physics: Modern Trends and Applications – Stat Phys 09*, Lviv, Ukraine, 23.–25. June 2009

W. Janke: *Universal Aspects of the Condensation/Evaporation Transition of Ising Droplets*, invited talk, Workshop on *Frontiers in Nonequilibrium Physics*, Kyoto, Japan, 21. July – 21. August 2009

W. Janke: *Modeling and Simulating Macromolecules*, *Physikalisches Kolloquium*, Universität Duisburg-Essen, 11. November 2009

M. Möddel: *Polymer Adsorption Transitions at Attractive Substrates Analysed from a Canonical and a Microcanonical Perspective*, Spring Meeting of the German Physical Society, TU Dresden, 23.–27. March 2009

M. Möddel: *The Adsorption Transition of a Single Coarse-Grained Polymer in the Microcanonical Ensemble*, Workshop and Tutorial Modeling and Simulating Macromolecules, ITP, Universität Leipzig, 09.–10. July 2009

M. Möddel: *Systematic Microcanonical Analyses of Polymer Adsorption Transitions*, 2nd BuildMoNa Workshop for Doctoral Candidates, Neukirchen/Pleiße, 08.–09. October 2009

M. Möddel: *Systematic Microcanonical Analyses of Polymer Adsorption Transitions*, 10th International NTZ-Workshop on New Developments in Computational Physics – CompPhys09, Universität Leipzig, 26.–29. November 2009

S. Schnabel: *Solid-Solid Transitions of Flexible Polymers*, Saxonian Theory Seminar, Chemistry Department, Universität Leipzig, 26.–27. February 2009

S. Schnabel: *Solid-Solid Transitions of Flexible Polymers*, Spring Meeting of the German Physical Society, TU Dresden, 23.–27. March 2009

S. Schnabel: *Tieftemperaturverhalten minimalistischer Polymermodelle*, PhD Defense talk, ITP, Universität Leipzig, 28. Oktober 2009

S. Schöbl: *Semiflexible Polymers in Random Disorder*, Seminar talk, DFH-UFA guest stay, Nancy Université, France, 14. September 2009

S. Schöbl: *Effect of Disorder on Equilibrium Conformations of Semiflexible Polymers*, 2nd BuildMoNa Workshop for Doctoral Candidates, Neukirchen/Pleiße, 08.–09. October 2009

T. Vogel: *Secondary Structure Formation of Tubelike Polymers*, Saxonian Theory Seminar, Chemistry Department, Universität Leipzig, 26.–27. February 2009

T. Vogel: *Thickness-Dependent Secondary Structure Formation of Tubelike Polymers*, Spring Meeting of the German Physical Society, TU Dresden, 23.–27. March 2009

T. Vogel: *Secondary Structure Formation of Tubelike Polymers*, Seminar talk, Universidad Complutense de Madrid, Spain, 15. April 2009

T. Vogel: *Structural Behavior of Polymers from Monte Carlo Studies of Coarse-Grained Models*, invited talk, Symposium Simulation of Molecules and Nanotubes, Technion, Haifa, Israel, 13. October 2009

T. Vogel: *Structural Behavior of Polymers from Monte Carlo Studies of Coarse-Grained Models*, PhD Defense talk, ITP, Universität Leipzig, 13. November 2009

B. Waclaw: *Condensation in Mass Transport Models with Factorized Steady States*, Seminar talk, Universität Freiburg, 04. March 2009

B. Waclaw: *Condensation in 1D Systems with Pair-Factorized Steady States*, Spring Meeting of the German Physical Society, TU Dresden, 23.–27. March 2009

B. Waclaw: *Localization in Maximal-Entropy Random Walk*, TKM Seminar, ITP, Universität Leipzig, 29. April 2009

B. Waclaw: *Localization in Maximal-Entropy Random Walk*, Seminar talk, Physics Department, Humboldt Universität zu Berlin, 06. May 2009

B. Waclaw: *Condensation in Pair-Factorized Steady States*, Conference *ENRAGEing Perspectives – Random Geometry and Random Matrices: From Quantum Gravity to Econophysics*, MPI PKS, Dresden, 18.–22. May 2009

S. Wenzel: *Quantum Phase Transitions in Systems of Coupled Spin Dimers*, Spring Meeting of the German Physical Society, TU Dresden, 23.–27. March 2009

S. Wenzel: *Evidence for an Unconventional Universality Class From a Two-Dimensional Dimerized Quantum Heisenberg Model*, 34th Conference of the Middle European Cooperation in Statistical Physics *MECO34*, Universität Leipzig, 29. March – 01. April 2009

S. Wenzel: *Monte Carlo Investigations of Low-Dimensional Classical and Quantum Spin Systems: Unconventional Criticality and Orbital Ordering*, PhD Defense talk, ITP, Universität Leipzig, 22. April 2009

S. Wenzel: *The Compass Model with Screw-Periodic Boundary Conditions*, Seminar talk, Ecole Polytechnique Fédéral de Lausanne (EPFL), Switzerland, 09. December 2009

M. Wiedenmann: *Evaporation/Condensation Transition of 3D Ising Droplets*, 2nd *BuildMoNa* Workshop for Doctoral Candidates, Neukirchen/Pleisse, 08.–09. October 2009

Posters

M. Aust, E. Bittner, W. Janke: *Free Energy Inherent Structures in Spin Glass Models*, Spring Meeting of the German Physical Society, TU Dresden, 23.–27. March 2009

M. Aust, E. Bittner, W. Janke: *Free Energy Inherent Structures in Spin Glass Models*, 34th Conference of the Middle European Cooperation in Statistical Physics *MECO34*, Universität Leipzig, 29. March – 01. April 2009

R. Bischof, W. Janke: *Plateau Formation in the Twist Parameter of the Bond Alternating Antiferromagnetic $S=1/2$ Heisenberg Spin Chain*, Spring Meeting of the German Physical Society, TU Dresden, 23.–27. March 2009

R. Bischof, W. Janke: *Formation of a Plateau in the Twist Parameter of the Bond Alternating Antiferromagnetic $S=1/2$ Heisenberg Spin Chain*, 34th Conference of the Middle European Cooperation in Statistical Physics *MECO34*, Universität Leipzig, 29. March – 01. April 2009

R. Bischof, W. Janke: *Phase Diagram of a Mixed Quantum Spin Chain with Bond Alternation and Exchange-Anisotropy*, 10th International NTZ-Workshop on *New Developments in Computational Physics – CompPhys09*, Universität Leipzig, 26.–29. November 2009

E. Bittner, A. Nußbaumer, W. Janke: *Anisotropy of the Interface Tensions of the Three-Dimensional Ising Model*, Spring Meeting of the German Physical Society, TU Dresden, 23.–27. March 2009

E. Bittner, A. Nußbaumer, W. Janke: *Anisotropy of the Interface Tensions of the Three-Dimensional Ising Model*, 34th Conference of the Middle European Cooperation in Statistical Physics *MECO34*, Universität Leipzig, 29. March – 01. April 2009

E. Bittner, A. Nußbaumer, W. Janke, M. Weigel: *Fußballfieber*, Wissenschaftsmesse *Studieren in Mitteldeutschland*, Neue Messe Leipzig, 05. September 2009

E. Bittner, A. Nußbaumer, W. Janke: *Anisotropy of the Interface Tensions of the Three-Dimensional Ising Model*, 10th International NTZ-Workshop on *New Developments in Computational Physics – CompPhys09*, Universität Leipzig, 26.–29. November 2009

W. Janke, E. Bittner: *Replica-Exchange Cluster Algorithm*, *The XXVII International Symposium on Lattice Field Theory – Lattice 2009*, Peking University, Beijing, China, 26.–31. July 2009

M. Weigel, W. Janke: *Cross Correlations in Scaling Analyses of Phase Transitions*, 34th Conference of the Middle European Cooperation in Statistical Physics *MECO34*, Universität Leipzig, 29. March – 01. April 2009

S. Karalus, W. Janke, M. Bachmann: *Cutting the Energy Range in Multicanonical Monte Carlo Simulations*, 10th International NTZ-Workshop on *New Developments in Computational Physics – CompPhys09*, Universität Leipzig, 26.–29. November 2009

M. Möddel, M. Bachmann, W. Janke: *Conformational Mechanics of Polymer Adsorption Transitions at Attractive Substrates*, Workshop *BioStruct09*, Florence, Italy, 16.–18. February 2009

M. Möddel, M. Bachmann, W. Janke: *Conformational Mechanics of Polymer Adsorption Transitions at Attractive Substrates*, SimBioMa Workshop *Challenges in Modelling the Interface Between Biomolecules and Inorganic Surfaces*, Schloss Waldthausen, Mainz, 18.–20. March 2009

M. Möddel, M. Bachmann, W. Janke: *Conformational Mechanics of Polymer Adsorption Transitions at Attractive Substrates*, 34th Conference of the Middle European Cooperation in Statistical Physics *MECO34*, Universität Leipzig, 29. March – 01. April 2009

M. Möddel, M. Bachmann, W. Janke: *Conformational Mechanics of Polymer Adsorption Transitions at Attractive Substrates*, 2nd Scientific Symposium of the Graduate School *BuildMoNa*, Universität Leipzig, 02.–03. April 2009

M. Möddel, M. Bachmann, W. Janke: *Conformational Mechanics of Polymer Adsorption Transitions at Attractive Substrates*, Workshop *Statistical Physics and Low Dimensional Systems 2009*, Nancy, France, 13.–14. May 2009

M. Möddel, M. Bachmann, W. Janke: *Conformational Mechanics of Polymer Adsorption Transitions at Attractive Substrates*, Workshop *ProSurf – Protein Surface Interaction*, Sestri Levante, Italy, 04.–06. July 2009

M. Möddel, W. Janke, M. Bachmann: *Systematic Microcanonical Analyses of Polymer Adsorption Transitions*, Jülich Soft Matter Days 2009, Bonn, 10.–13. November 2009

H. Nagel, P. Białas, B. Waclaw, W. Janke: *Monte Carlo Generation of Equilibrated Graphs*, Spring Meeting of the German Physical Society, TU Dresden, 23.–27. March 2009

H. Nagel, P. Białas, B. Waclaw, W. Janke: *Monte Carlo Generation of Equilibrated Graphs*, 34th Conference of the Middle European Cooperation in Statistical Physics MECO34, Universität Leipzig, 29. March – 01. April 2009

A. Nußbaumer, E. Bittner, W. Janke: *A Nearly Local Observable for a Global Quantity*, 34th Conference of the Middle European Cooperation in Statistical Physics MECO34, Universität Leipzig, 29. March – 01. April 2009

A. Nußbaumer, E. Bittner, W. Janke: *A Nearly Local Observable for a Global Quantity*, Conference *ENRAGEing Perspectives – Random Geometry and Random Matrices: From Quantum Gravity to Econophysics*, MPI PKS Dresden, 18.–22. May 2009

S. Schnabel, M. Bachmann, W. Janke: *Solid-Solid Transitions of Flexible Polymers*, 34th Conference of the Middle European Cooperation in Statistical Physics MECO34, Universität Leipzig, 29. March – 01. April 2009

S. Schnabel, M. Bachmann, W. Janke: *Solid-Solid Transitions of a Flexible Elastic Off-Lattice Polymer Model*, 2nd Scientific Symposium of the Graduate School BuildMoNa, Universität Leipzig, 02.–03. April 2009

S. Schöbl, K. Kroy, W. Janke: *Effect of Disorder on Equilibrium Conformations of Semiflexible Polymers*, Spring Meeting of the German Physical Society, TU Dresden, 23.–27. March 2009

S. Schöbl, K. Kroy, W. Janke: *Effect of Disorder on Equilibrium Conformations of Semiflexible Polymers*, 34th Conference of the Middle European Cooperation in Statistical Physics MECO34, Universität Leipzig, 29. March – 01. April 2009

S. Schöbl, K. Kroy, W. Janke: *Effect of Disorder on Equilibrium Conformations of Semiflexible Polymers*, 2nd Scientific Symposium of the Graduate School BuildMoNa, Universität Leipzig, 02.–03. April 2009

T. Vogel, T. Neuhaus, M. Bachmann, W. Janke: *Thickness-Dependent Secondary Structure Formation of Tubelike Polymers*, 34th Conference of the Middle European Cooperation in Statistical Physics MECO34, Universität Leipzig, 29. March – 01. April 2009

T. Vogel, T. Neuhaus, M. Bachmann, W. Janke: *Thermodynamics of Tubelike Flexible Polymers*, Jülich Soft Matter Days 2009, Bonn, 10.–13. November 2009

S. Wenzel, W. Janke: *Monte Carlo Simulations on the 2D Compass Model*, School on Modern Theories of Correlated Electron Systems, Les Houches, France, 11.–29. May 2009

M. Wiedenmann, A. Nußbaumer, E. Bittner, W. Janke: *Monte Carlo Study of the Evaporation/Condensation Transition of Ising Droplets*, 34th Conference of the Middle European Cooperation in Statistical Physics *MECO34*, Universität Leipzig, 29. March – 01. April 2009

M. Wiedenmann, A. Nußbaumer, E. Bittner, W. Janke: *Monte Carlo Study of the Evaporation/Condensation Transition of Ising Droplets*, 2nd Scientific Symposium of the Graduate School *BuildMoNa*, Universität Leipzig, 02.–03. April 2009

M. Wiedenmann, A. Nußbaumer, E. Bittner, W. Janke: *Monte Carlo Study of the Evaporation/Condensation Transition of Ising Droplets*, 10th International NTZ-Workshop on *New Developments in Computational Physics – CompPhys09*, Universität Leipzig, 26.–29. November 2009

11.22 Graduations

Doctorate

- Sandro Wenzel
Monte Carlo Investigations of Low-Dimensional Classical and Quantum Spin Systems: Unconventional Criticality and Orbital Ordering
22. April 2009
- Stefan Schnabel
Tieftemperaturverhalten minimalistischer Polymermodelle
28. Oktober 2009
- Thomas Vogel
Structural Behaviour of Polymers from Monte Carlo Studies of Coarse-Grained Models
13. November 2009

11.23 Guests

- Prof. Dr. Günter Ahlers
University of California at Santa Barbara, USA
Stochastically Driven Large-Scale Circulation in Turbulent Rayleigh-Benard Convection
29. March – 02. April 2009
- Prof. Dr. Hagen Kleinert
Institut für Theoretische Physik, FU Berlin
Multivalued Fields
29. March – 02. April 2009
- Prof. Dr. David P. Landau
University of Georgia, Athens, USA
Monte Carlo Simulations of Systems with Complex Energy Landscapes
29. March – 05. April 2009

- Prof. Dr. Hartmut Löwen
Institut für Theoretische Physik II, Universität Düsseldorf
Colloidal Suspensions Subjected to External Fields
29. March – 02. April 2009
- Prof. Dr. Georg Maret
Dept. of Physics, Universität Konstanz
Melting and Glass Transition of a 2D Colloidal Model System
29. March – 02. April 2009
- Prof. Dr. Sidney Redner
Dept. of Physics, Boston University, USA
Dynamical Approach for Solving Complex Networks
29. March – 02. April 2009
- Prof. Dr. Matthias Troyer
Theoretische Physik, ETH Zürich, Switzerland
Continuous Time QMC Solvers for Quantum Impurity Problems
29. March – 02. April 2009
- Prof. Dr. Royce K. P. Zia
Virginia Tech, Blacksburg, USA
*Non-Equilibrium Statistical Mechanics: A Growing Frontier of “Pure and Applied”
Theoretical Physics*
29. March – 02. April 2009
- Prof. Dr. Bertrand Berche
Statistical Physics Group, IJL, Nancy Université, France
Gauge Field Theory Approach to Spin Transport in 2D Electron Gas
29. March – 02. April 2009
- Prof. Dr. Thomas Nattermann
Institut für Theoretische Physik, Universität zu Köln
Localized States and Interaction Induced Delocalization in Bose Gases with Quenched Disorder
29. March – 02. April 2009
- Prof. Dr. Handan Arkin (Olgar)
Physics Engineering, Ankara University, Turkey
Study of the Conformational Changes of Hydrophobic-Polar Polymer Chain near a Hydrophobic Chain
29. March – 02. April 2009
- Prof. Dr. Malte Henkel
Nancy Université, France
Non-Equilibrium Kinetics and Ageing in Non-Glauberian Ising Models
29. March – 02. April 2009
- Prof. Dr. Ferenc Iglói
Institute of Theoretical Physics, Research Institute for Solid State Physics and Optics, Budapest, Hungary
Entanglement Entropy of Quantum Spin Chains
29. March – 02. April 2009

- Prof. Dr. Bernd A. Berg
Florida State University, Tallahassee, USA
Research Prize Winner of the Alexander von Humboldt Foundation
01. May – 31. July 2009
- Dr. Viktoria Blavatska
Institute for Condensed Matter Physics, Lviv, Ukraine
Humboldt Fellow/FOR877 guest
01. May – 31. July 2009
- Marcin Zagorski
Jagellonian University, Krakow, Poland
22.–31. May 2009
- Prof. Dr. Stefan Boettcher
Emory University, Atlanta, USA
Heuristische Bestimmung und die Auswertung von Ising Spin-Glas-Grundzuständen
5.–6. November 2009
- Prof. Dr. Nobuyasu Ito
Department of Applied Physics, Graduate School of Engineering, The University of Tokyo, Japan
Simulation Study on Nonequilibrium Transport Phenomena
26.–30. November 2009
- Jean-Charles Walter
Université Henri Poincaré, Nancy, France
Numerical Investigation of the Aging of the Fully-Frustrated XY Model
25.–29. November 2009
- Prof. Dr. Victor Martín-Mayor
Departamento de Física Teórica I, Universidad Complutense de Madrid, Spain
Large-Scale Equilibrium Simulation of the 3D Edwards-Anderson Model
25.–29. November 2009
- PD Dr. Stefan Wessel
Institut für Theoretische Physik III, Universität Stuttgart
Optimized Broad-Histogram Ensembles for the Simulation of Quantum Systems
25.–29. November 2009
- Dr. Viktoria Blavatska
Institute for Condensed Matter Physics, Lviv, Ukraine
Polymers in Crowded Environment Under Stretching Force: Globule-Coil Transitions
25. November – 02. December 2009

12

Molecular Dynamics / Computer Simulation

12.1 Introduction

Using methods of statistical physics and computer simulations we investigate classical many-particle systems interacting with interfaces. One aim of the research in our group is to build up a bridge between theoretical and experimental physics. By means of analytical theories of statistical physics and computer simulations (Molecular dynamics, Monte Carlo procedures, percolation theories) using modern workstations and supercomputers we examine subjects for which high interest exists in basic research and industry as well. The examinations involve transport properties (diffusion of guest molecules) in zeolites and the structural and phase behaviour of complex fluids on bulk conditions and in molecular confinements.

Especially we are interested to understand

- the diffusion behaviour of guest molecules in zeolites in dependence on thermodynamic parameters, steric conditions, intermolecular potentials and the concentration of the guest molecules,
- structure and phase equilibria of complex (aqueous) fluids in interfacial systems (e.g. pores, thin films, model membranes) in dependence on geometric and thermodynamic conditions,
- and the migration of molecules in (random) porous media by the use of percolation theories.

in microscopic detail and to compare the results with experimental data.

The use of a network of PC's and workstations (Unix, Linux, Windows), the preparation and application of programs (Fortran, C, C⁺⁺), and the interesting objects (zeolites, membranes) give excellent possibilities for future careers of undergraduates, graduate students and postdocs. Our research is part of several national and international programs (DFG - Schwerpunktprogramme SPP1155 und SPP1362, an International Research Graduate Training program (IRTG 1056), a joint research project DFG/TRF-Thailand, a joint research project DAAD/TRF-Thailand and joint research projects with UOIT Oshawa and SHARCNET, Canada) and includes a close collaboration with the Institute of Experimental Physics I (Physics of Interfaces and Biomembranes) of Leipzig

University and many institutions in Germany and other countries. Details are given in the list of external cooperations.

H.L.Vörtler and S. Fritzsche

12.2 Analytical Treatment and Computer Simulations of the influence of the crystal surface on the exchange of guest molecules between zeolite nanocrystals and the surrounding gas phase

S. Fritzsche*, O. Saengsawang*, M. Knauth*, S. Vasenkov†

*Abteilung MDC

†University of Florida, Gainesville, USA

In the framework of the DFG priority program SPP 1155 we investigated the surface effects influencing the dynamics of adsorption of guest molecules into porous crystals. A new treatment of the interplay between diffusion within zeolite crystals and through mesopores surrounding these crystals has been successfully developed [1]. Such arrangements play an important rule in currently developed hierarchically ordered porous materials. In cooperation with Prof. F. Keil Hamburg the diffusion of methanol in the zeolite NaX has been studied [2]. This was part of an investigation of surface effects for this system which is still in progress.

[1] M. Knauth and S. Vasenkov and J. Kärger and S. Fritzsche,, *Chem. Phys. Lett.* **479**(2009) 95–99

[2] T. Nanok and O. Saengsawang and S. Vasenkov and F. J. Keil and S. Fritzsche, *Molecular Dynamics Simulation Study of the Concentration Dependence of the Self-Diffusivity of Methanol in NaX Zeolite*, *diffusion-.org* **11**(2009) 33:1–2

12.3 Diffusion and Rotation of Water in the Zeolite Chabazite

S. Fritzsche*, R. Channajaree*, P. A. Bopp† J. Kärger‡,

*Abteilung MDC

†University Bordeaux, France

‡Institut für Experimentelle Physik I, Abteilung GFP

The diffusion of water in the zeolite chabazite was investigated basing on own earlier work [1] and new methods. in a project in the framework of the International Research Training Group (IRTG) "Diffusion in Porous Materials". Particularly the nonmonotonic dependence of the self diffusion coefficient upon the concentration of water molecules is of high interest. This investigation is challenging because the water molecule moves between different cations are rare events and hence the diffusion coefficients are very

small. Our methods are now being complemented by so called boost potential MD a highly efficient method for the treatment of rare events that is based on analytical Transition State Theory.

Rotational diffusion was now also included into this research and could be treated successfully [2].

- [1] S. Jost, P. Biswas, A. Schüring, J. Kärgler, P. A. Bopp, R. Haberlandt, Siegfried Fritzsche, *J. Phys. Chem. C*, **111**, 14707 (2007)
- [2] R. Chanajareea, P. A. Bopp, S. Fritzsche, J. Kärgler, *Water in Chabazite revisited: Self Diffusion and Rotational Relaxation*, Poster at the Diffusion Fundamentals III, Conference, Athens, 2009, Abstracts

12.4 How Do Guest Molecules Enter Zeolite Pores? Quantum Chemical Calculations and Classical MD Simulations

S. Fritzsche*, S. Thompho*, S. Hannongbua[†], T. Remsungnen[‡], P. A. Bopp[§], O. Saengsawang*

*Abteilung MDC

[†]Chulalongkorn University, Bangkok, Thailand

[‡]Khon Khaen University, Khon Khaen, Thailand

[§]University Bordeaux, France

Within this common project of the German DFG and the NRCT (Thailand) surface effects caused by the presence of silanol groups have been studied. The effects turned out to be significant [1]. Moreover the commonly used Crank model for the penetration of particles through the surface into the zeolite and the underlying concept of the surface permeability could be critically revisited within this paper.

The molecular interaction parameters for this study have partially been developed in our group by quantum chemical calculations [1].

- [1] S. Thompho, R. Channajaree, T. Remsungnen, S. Hannongbua, P. A. Bopp, S. Fritzsche, *J. Phys. Chem A*, **113**, 2004 (2009).

12.5 Investigation of the rotation and diffusion of pentane in the zeolite ZK5

S. Fritzsche*, O. Saengsawang* A. Schüring*, P. Magusin[†] M.-O. Coppens[‡] A. Dammers[‡] D. Newsome[‡]

*Abteilung MDC

[†]Eindhoven University, The Netherlands

[‡]Delft University, The Netherlands

Earlier investigations [1] for the system pentane/ZK5 have been continued. The very

slow diffusion of pentane molecules in the zeolite ZK5 has now been studied using a new method, called HTCE, that was a recently developed in our group [2]

This method is based on Transition State Theory. It could be successfully applied to the present problem.

- [1] O. Saengsawang, A. Schüring, T. Remsungnen, A. Loisuangsinn, S. Hannongbua, P. C. M. M. Magusin and S. Fritzsche, *J. Phys. Chem. C* **112**, 5922 (2008)
- [2] A. Schüring, S. M. Auerbach and S. Fritzsche, *A simple method for sampling partition function ratios*, *Chem. Phys. Lett.* **450** (2007) 164–169
- [3] O. Saengsawang, A. Schüring, T. Remsungnen, S. Hannongbua, D. A. Newsome, A. J. Dammers, M. O. Coppens, S. Fritzsche, *Diffusion of n-Pentane in the Zeolite ZK5 Studied by High-Temperature Configuration-Space Exploration*, *Chem. Phys.* **368** (2010) 121–125

12.6 Diffusion of Guest Molecules in Metal Organic Frameworks

S. Fritzsche^{*}, K. Seehamart^{*}, S. Hannongbua[†], T. Remsungnen[‡], J. Kärger[§], C. Chmelik[§]

^{*}Abteilung MDC

[†]Chulalongkorn University, Bangkok, Thailand

[‡]Khon Khaen University, Khon Khaen, Thailand

[§]Institut für Experimentelle Physik I, Abteilung GFP

The promising new nanoporous materials called Metal Organic Frameworks (MOF's) are investigated within the framework of the SPP1362 in a common DFG project with experimental groups (Prof. Kärger, Leipzig, Prof. Caro, Hannover, Dr. Wiebcke, Hannover) and NRCT (Thailand, Prof. Hannongbua and other groups).

A breakthrough could be reached when our common examinations with Prof. Krishna (Amsterdam), published in [2] and [1] could show, that the lattice flexibility of the MOF Zntbip did not only influence the size of the self diffusion coefficient of ethane in Zntbip but, lead to a qualitatively different concentration dependence of this self diffusion coefficient. The effect is caused mainly by the change of the lattice structure of the highly flexible MOF and could be explained in [3].

This is particularly important because most simulations about MOF are still being done by simplifying the system by use of a rigid framework.

- [1] K. Seehamart, T. Nanok, R. Krishna, J.M. van Baten, T. Remsungnen, S. Fritzsche, *Microporous and Mesoporous Materials*, <http://dx.doi.org/10.1016/j.micromeso.2009.01.020>
- [2] K. Seehamart and T. Nanok and R. Krishna and J. M. van Baten and T. Remsungnen and S. Fritzsche, *A Molecular Dynamics investigation of the influence of structural flexibility on self-diffusion of ethane in Zn(tbip)*, *Microporous and Mesoporous Materials* **125**(2009)97–100
- [3] K. Seehamart, T. Nanok, J. Kärger, C. Chmelik, R. Krishna, S. Fritzsche, *Investigating the Reasons for the Significant Influence of Lattice Flexibility on Self-Diffusivity of Ethane in Zn(tbip)*, *Microporous and Mesoporous Materials* **130** (2010) 92

12.7 Phase equilibria and critical behaviour of molecular fluids in bulk systems and under geometrical restrictions

H.L. Vörtler, I. Nezbeda *, S. Kalisch

*Czech. Acad. Sci., Prague and Jan Evangelista Purkinje University, Usti n. L., Czech Republic

This long-term research of real (molecular) fluids deals with a hierarchic ansatz of the potential energy with respect to the range of the intermolecular forces. The total potential of a real fluid is composed of a short ranged molecular model that describes the structure and thermodynamics basically correct and a long-ranged perturbation term. Virtual parameter variation techniques are used to simulate chemical potentials and thermodynamic pressures. From chemical potential isotherms phase equilibria are estimated by thermodynamic integration. Critical data are found by scaling laws (Wegner expansion). This approach is applicable to both bulk and confined fluids.

While we studied in previous parts of the project mainly homogeneous bulk fluids (square-well fluids, primitive models of water) we focus now on the influence of geometric restrictions to phase equilibria and critical properties. Particularly, we deal with the shift of critical data under confinement. In the case of square-well fluids we found a simple analytic relation [1] that describes quantitatively nearly all existing simulation data [2, 3] for the decrease of the critical temperature with increasing geometrical restrictions (i.e. decreasing pore size).

Quite recently it was found by grand canonical MC [4] that in very narrow slit-like pores some deviations from our simple analytic expression seem to exist: particularly, the two-dimensional value of the critical temperature is preserved up to a slit width of 1.5 particle diameter. This behaviour we confirmed with our virtual parameter variation methodology [5, 6]. The properties of the critical pressure and density under the confinement were found to be much more complicated and require further studies.

The long-term goal of this research is to contribute to a statistical-mechanical theory of phase equilibria of inhomogeneous fluids with applications to nanoporous materials and biointerfaces.

- [1] H.L. Vörtler, Collect. Czech. Chem. Commun. **73**, 518 (2008)
- [2] H.L. Vörtler, W.R. Smith, J. Chem. Phys. **112**, 5168 (2000)
- [3] J.K. Singh and S.K. Kwak, J. Chem. Phys. **126**, 024702 (2007).
- [4] S. Jana, J.K. Singh and S.K. Kwak, J. Chem. Phys. **130**, 2147072 (2009).
- [5] H. L. Vörtler, *Monte Carlo Simulation of Chemical Potentials and Phase Equilibria of Bulk and Confined Fluids*, Liquid Matter Workshop, Tabor (Czech Republic), October 22, 2009
- [6] S. Kalisch, Diploma Thesis, *Monte Carlo simulation and theory of geometrically confined hard core fluids in the transition range from three to two dimensions*, University Leipzig, 2010

12.8 Simulation of fluid phase equilibria in very narrow slit-like pores: Transition range to two dimensions

H.L. Vörtler, W. R. Smith^{*}, S. Kalisch

^{*}University of Ontario Institute of Technology Oshawa, Ontario, Canada

We continue the studies of phase equilibria of fluid systems confined to very narrow slit-like pores in the transition range to monomolecular layers. Systematically, we perform MC simulations of isotherms of the chemical potential and of phase equilibria in the subcritical vapour-liquid coexistence range under canonical conditions applying virtual parameter variations.[1, 2] We focus on square-well fluids confined to hard pores with widths between one and two molecular diameters. In the special case of hard spheres first results for the excess chemical potentials versus density are shown in the figure.

Excess chemical potential vs. slit width (hard spheres)

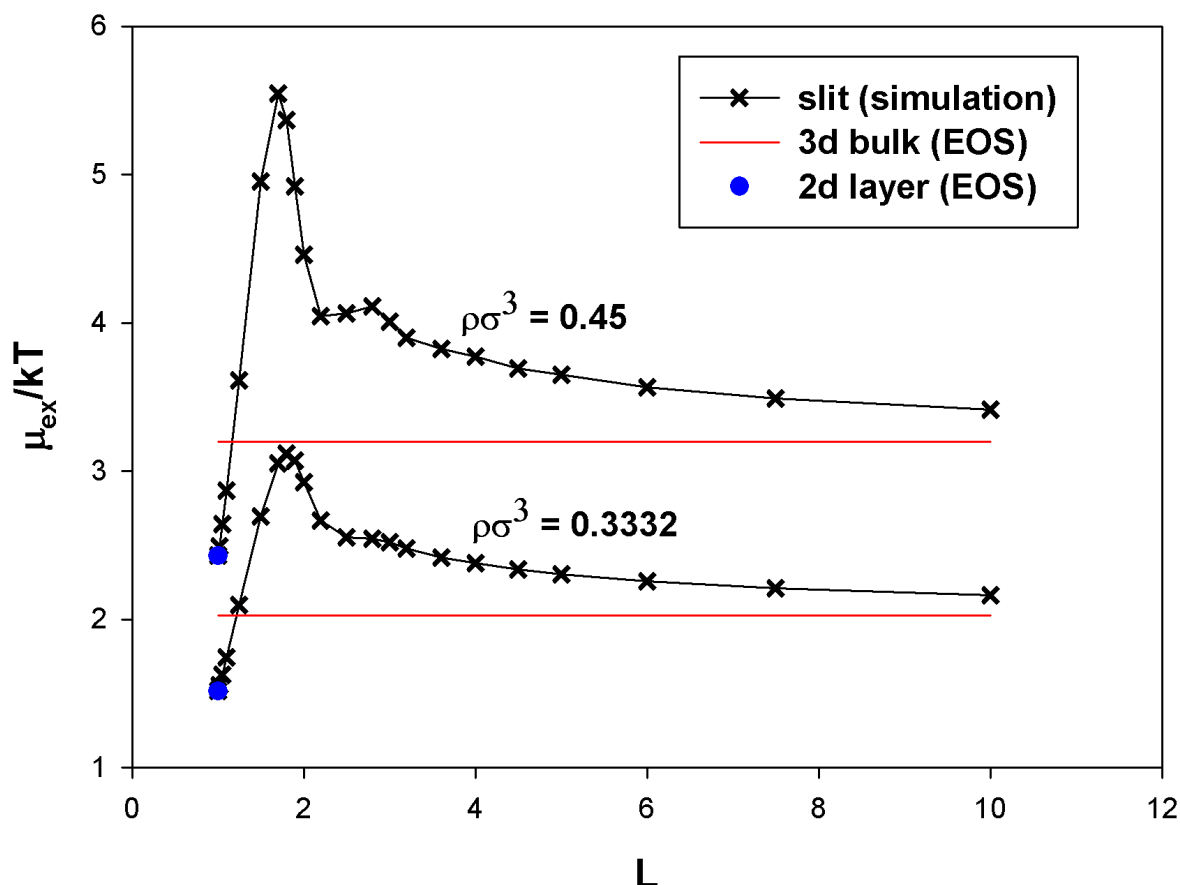


Fig.: Excess chemical potential in very narrow slits.

We observe a significant increase of the excess chemical potential before for wider slits the expected decay of the excess chemical potential takes place. This behaviour is quite analog to that of the spreading pressure discussed in a previous part of this project

[3]. The results may serve as reference data for a theoretical estimation of fluid phase equilibrium data in thin films and monolayers.

The research was supported by research fund of University of Ontario Institute of Technology (research stay 2009 of H.L. Vörtler in Oshawa) and by the facilities of SHARCNET computer network (Ontario, Canada).

[1] H.L. Vörtler, K. Schäfer, W.R. Smith, *J. Phys. Chem. B* **112**, 4656 (2008)

[2] H.L. Vörtler, W.R. Smith, *J. Chem. Phys.* **112**, 5168 (2000)

[3] H. L. Vörtler, *Molecular-level Simulation of Chemical Potentials and Phase Equilibria of Bulk and Confined Fluids*, Science Colloquium Series, University of Ontario Institute of Technology, Oshawa (Ontario, Canada), March 6, 2009

12.9 Funding

Analytical Treatment and Computer Simulations of the influence of the crystal surface on the exchange of guest molecules between zeolite nanocrystals and the surrounding gas phase

S. Fritzsche, S. Vasenkov, T. Nanok, O. Saengsawang,
SPP1155, DFG-code FR1486/2-3

Diffusion of Water in the Zeolite Chabazite

S. Fritzsche, R. Channajaree,
DFG: IRTG 1056

Investigation of the rotation and diffusion of pentane in the zeolite ZK5

S. Fritzsche, O. Saengsawang,
DFG: IRTG 1056

How do guest molecules enter zeolite pores? Quantum Chemical calculations and classical MD simulations

S. Fritzsche, S. Thompho
DFG-code FR1486/1-4

Diffusion of Guest Molecules in Metal Organic Frameworks

K. Seehamart

funded by a stipend of the University of Technology Isan (RMUTI), Kon Khaen, Thailand,

S. Fritzsche,
SPP1362, DFG-code FR1486/5-1

Simulation of phase equilibria in two- and three-dimensional Fluids

W.R. Smith, H.L. Vörtler

Research fund of University of Ontario Institute of Technology (research stay of H.L. Vörtler in Oshawa) and SHARCNET computer network (Ontario, Canada)

12.10 Organizational Duties

H.L. Vörtler

- Speaker of the MDC group
- Reviewer for projects (Czech Science Foundation)
- Referee for journals (J.Chem. Phys, Physica A, Chem. Phys. Lett, J. Molec. Liquids, Chem. Phys)

S. Fritzsche

- Project leader of one project in the International Research Training Group, IRTG 1056
- Project leader of one project in the SPP1155, DFG-code FR1486/2-2
- Project leader of one project in the SPP1362, DFG-code FR1486/5-1
- Project leader of a German/Thai research project, DFG-code FR1486/1-4
- Referee for journals (Chem. Phys. Lett., Microporous and Mesoporous Materials, Journal of Molecular Graphics and Modelling)

12.11 External Cooperations

Academic

- Chulalongkorn University, Bangkok, Thailand
Prof. Dr. S. Hannongbua
- Khon Khaen University, Khon Khaen, Thailand
Dr. T. Remsungnen
- University Bordeaux, France
Prof. Dr. P. A. Bopp
- Eindhoven University, Eindhoven, The Netherlands
Prof. Dr. P. Magusin
- Technical University, Delft, The Netherlands
Prof. Dr. M.-O. Coppens, Dr. A. Dammers, Dr. D. Newsome
- Leibniz University Hannover
Prof. Dr. J. Caro, Dr. M. Wiebcke
- Van't Hoff Institute for Molecular Sciences, University of Amsterdam, The Netherlands
Prof. R. Krishna
- University of Ontario Institute of Technology ,Oshawa (Ontario, Canada)
Prof. W. R. Smith
- Czech. Acad. Sci., Prague and Jan Evangelista Purkinje University, Usti n. L., (Czech Republic)
Prof. I. Nezbeda

12.12 Publications

Journals

- A. Schüring and J. Gulín-González and S. Vasenkov and S. Fritzsche, *Quantification of the Mass-Transfer Coefficient of the External Surface of Zeolite Crystals by Molecular Dynamics Simulations and Analytical Treatment*, *Microporous and Mesoporous Materials* **125**(2009)107–111
- S. Thompho and R. Chanajaree and T. Remsungnen and S. Hannongbua and P. A. Bopp and S. Fritzsche, *The Permeation of Methane Molecules through Silicalite-1 Surfaces*, *J. Phys. Chem. A* **113**(2009)2004–2014
- K. Seehamart and T. Nanok and R. Krishna and J. M. van Baten and T. Remsungnen and S. Fritzsche, *A Molecular Dynamics investigation of the influence of structural flexibility on self-diffusion of ethane in Zn(tbip)*, *Microporous and Mesoporous Materials* **125**(2009)97–100
- T. Nanok and O. Saengsawang and S. Vasenkov and F. J. Keil and S. Fritzsche, *Molecular Dynamics Simulation Study of the Concentration Dependence of the Self-Diffusivity of Methanol in NaX Zeolite*, *diffusion-.org* **11**(2009) 33:1–2
- R. Chanajaree and Ph. A. Bopp and S. Fritzsche and J. Kärger, *Water in Chabazite Revisited: Self Diffusion and Rotational Relaxation*, *diffusion-.org* **11**(2009) 21:1–2
- T. Nanok and S. Vasenkov and F. J. Keil and S. Fritzsche, *Molecular Dynamics simulation study of the concentration dependence of the self-diffusivity of methanol in NaX zeolite*, *Microporous and Mesoporous Materials* (2009), <http://dx.doi.org/10.1016/j.micromeso.2009.07.011>
- A. Schüring and J. Gulin-Gonzalez and S. Vasenkov and S. Fritzsche, *Quantification of the Mass-Transfer Coefficient of the External Surface of Zeolite Crystals by Molecular Dynamics Simulations and Analytical Treatment*, *Microporous and Mesoporous Materials* **125**(2009) 107–111
- M. Knauth and S. Vasenkov and J. Kärger and S. Fritzsche, *Molecular dynamics study of sorbate diffusion in a simple porous membrane containing microporous nanocrystals and mesopores*, *Chem. Phys. Lett.* **479**(2009) 95–99
- K. Seehamart and T. Nanok and J. Kärger and C. Chmelik and R. Krishna and S. Fritzsche, *Examining the Reason of the Observed Influence of the Lattice Flexibility on the Diffusion of Ethane in Zn(tbip)*, *diffusion-.org* **11**(2009) 38:1–2
- O. Saengsawang, A. Schüring, T. Remsungnen, S. Hannongbua, D. A. Newsome, A. J. Dammers, M. O. Coppens, S. Fritzsche, *Diffusion of n-Pentane in the Zeolite ZK5 Studied by High-Temperature Configuration-Space Exploration*, *Chem. Phys.* **368** (2010) 121–125
- K. Seehamart, T. Nanok, J. Kärger, C. Chmelik, R. Krishna, S. Fritzsche, *Investigating the Reasons for the Significant Influence of Lattice Flexibility on Self-Diffusivity of Ethane in Zn(tbip)*, *Microporous and Mesoporous Materials* **130** (2010) 92

Talks

T. Nanok, S. Vasenkov, S. Fritzsche, *Molecular Dynamics Simulation Study of Methanol Diffusion in NaX Zeolite*, Talk at the Workshop of SPP1155, Hamburg, March 2009

H. L. Vörtler, *Molecular-level Simulation of Chemical Potentials and Phase Equilibria of Bulk and Confined Fluids*, Science Colloquium Series, University of Ontario Institute of Technology, Oshawa (Ontario, Canada), March 6, 2009

H. L. Vörtler, *Monte Carlo Simulation of Chemical Potentials and Phase Equilibria of Bulk and Confined Fluids*, Liquid Matter Workshop, Tabor (Czech Republic), October 22, 2009

Posters

T. Nanok, O. Saengsawang, S. Vasenkov, F. J. Keil, S. Fritzsche, *Molecular Dynamics Simulation Study of the Concentration Dependence of the Self-Diffusivity of Methanol in NaX Zeolite*, Poster at the Diffusion Fundamentals III, Conference, Athens, 2009, Abstracts

R. Chanajareea, P. A. Bopp, S. Fritzsche, J. Kärger, *Water in Chabazite revisited: Self Diffusion and Rotational Relaxation*, Poster at the Diffusion Fundamentals III, Conference, Athens, 2009, Abstracts

K. Seehamart, T. Nanok, J. Kärger, C. Chmelik, R. Krishna, S. Fritzsche, *Examining the reason of the observed influence of the lattice flexibility on the diffusion of ethane in Zn(tbip)*, Poster at the Diffusion Fundamentals III, Conference, Athens, 2009, Abstracts

12.13 Graduations

Diploma

- M. Knauth, *Diffusion in Zeolithkristall and Mesopore*, Diploma thesis, University of Leipzig, 2009

12.14 Guests

- Dr. T. Remsungnen
Khon Khaen University, Thailand
30.09.-26.11.2009
- Dr. M. Tafipolsky
Anorganic Chemistry II, Organometallics and Materials Chemistry Ruhr-University Bochum, 26.10.-27.10.2009
- Prof. Dr. S. Hannongbua,
Chulalongkorn University, Bangkok, 10.12.-14.12.2009
- Dr. M. Wiebcke,
Leibniz University Hannover, Institute for Anorganic Chemistry, 16.12.2009

13

Quantum Field Theory and Gravity

13.1 Geometry Dependence of the Casimir Force

M. Bordag

The vacuum of quantum fields shows a response to changes in external conditions with measurable consequences. The most prominent manifestation is the Casimir effect. It belongs to the few number of macroscopic quantum effects and it is of big importance in nanometer sizes systems. At present, the dependence of the Casimir forces on geometry is in the focus of actual research using a new representation in terms of a functional determinant. It was possible, for the first time, to obtain corrections beyond the *Proximity Force Approximation*. In the electromagnetic case these corrections were found to have an unexpected logarithmic behavior [1].

- [1] M. Bordag and V. Nikolaev. First analytic correction to the Casimir effect beyond PFA for the electromagnetic field in sphere-plane geometry. *Phys.Rev.D*, to be published, 2010. ArXiv: 0911.0146

13.2 Casimir effect and real media

M. Bordag B. Geyer G.L. Klimchitskaya* V.M. Mostepanenko[†] U. Mohideen[‡]

*U St. Petersburg

[†]U Moscow

[‡]U California, Riverside

The vacuum of quantum fields shows a response to changes in external conditions with measurable consequences. The investigation of the electromagnetic vacuum in the presence of real media is of actual interest in view of current experiments as well as nanoscopic electro-mechanical devices. In recent experiments using atomic force microscopy the Casimir effect had been measured with high accuracy. This required a detailed investigation of the influence of real experimental structures on the corresponding force.

Since the year 2000, the behavior of the thermal correction to the Casimir force between real metals has been hotly debated. As was shown by several groups, the Lifshitz theory, which provides the theoretical foundation for calculations of both the van der Waals and Casimir forces, leads to different results depending on the model of metal conductivity used. To resolve these controversies, the theoretical considerations based on the principles of thermodynamics and new experimental tests were invoked. Additional, the study has to be extended to the case of dielectrics and semiconductors.

Previous common work on that subject has been reviewed in the recent monography “Advances in the Casimir Effect” [1]. In addition, the invited review article “The Casimir force between real materials: experiment and theory” [2] appeared in 2010.

In 2009 the following has been obtained:

- The *thermal Casimir effect in rectangular boxes*, starting from the general expression for the Casimir free energy in the framework of Matsubara quantum field theory at nonzero temperature, has been considered. Using the method of zeta function regularization, a finite expression for the Casimir free energy associated with a closed volume V was obtained going to zero when the characteristic dimensions of this volume go to infinity. This is achieved by subtracting the free energy of the black body radiation and two other geometrical contributions of quantum origin.

- The application of the Lifshitz theory and its modifications to *systems with mobile charge carriers* has been analyzed on the basis of first principles of quantum statistical physics and electrodynamics.

(i) One modification, taking into account the penetration of the static component of the fluctuating electric field into a conductor to a depth of the Debye-Hückel radius, has been shown to be thermodynamically inconsistent, i.e., violates the third law of thermodynamics (the Nernst heat theorem) for wide classes of different materials including semiconductors with the concentration of charge carriers n below the critical value, semimetals of dielectric type and solids with ionic conductivity. The theoretical predictions following from this modification of the Lifshitz theory were compared with the measurement data of the experiment on the optically modulated Casimir forces performed in 2007. It was shown that this theoretical approach is excluded by the experimental data at a 70% confidence level. These results were published in Refs. [3, 4].

(ii) Another modification, recently proposed in the literature, obtains the modified reflection coefficients by using the Boltzmann transport equation which takes into account the drift and diffusion currents. We showed that also this modification violates the Nernst heat theorem for the same classes of dielectric materials. We have compared the theoretical predictions following from the proposed modification of the reflection coefficients with the measurement data of two recent experiments (the optical modulation experiment and the experiment using a micromechanical torsional oscillator) and found that the theoretical predictions are excluded by the data at 70% and at 99.9% confidence level, respectively. The failure of both modifications of the Lifshitz theory was explained by the violation of the thermal equilibrium which is the basic applicability condition of this theory. The obtained results were published in Refs. [5, 6].

(iii) We also started an analysis of the application conditions of the fluctuation-dissipation theorem and the investigation of conceptual differences between fluctuating and ex-

ternal electromagnetic fields. It was shown that in the presence of free charge carriers the concept of frequency-dependent dielectric permittivity is not as well defined as for insulators and requires additional regularization. This means that the application of the fluctuation-dissipation theorem with such kind of response functions, as commonly done in the literature, cannot be considered as either exact or rigorous. Partial results related to this part of work have been published in Refs. [7–9].

- The *influence of the magnetic properties* of plate material and of atoms and molecules on the Casimir and Casimir-Polder force was investigated. Specifically, the Lifshitz-type formulas for the free energy and Casimir-Polder force between an atom possessing a permanent magnetic moment and a plate made of different materials were derived. It was shown that the inclusion of the atomic magnetic moment can lead to both decrease and increase in the magnitude of the Casimir-Polder force depending on the material of the plate.

(i) Especially, the influence of magnetic properties on the thermal Casimir interaction was investigated for the configuration of two parallel magnetodielectric plates described by the frequency dependent dielectric permittivity $\varepsilon(\omega)$ and magnetic permeability $\mu(\omega)$. On the basis of the Lifshitz theory, it was shown that for diamagnets and for paramagnets in the broad sense (with exception of ferromagnets) the magnetic properties do not influence the magnitude of the Casimir free energy and force. The computations of the Casimir free energy and pressure were performed for the configurations of two plates made of ferromagnetic metals (Co and Fe), for one plate made of ferromagnetic metal and the other of nonmagnetic metal (Au), for two ferromagnetic dielectric plates (on the basis of polystyrene), and for a ferromagnetic dielectric plate near a nonmagnetic metal plate. The dielectric permittivity of metals was described using both the Drude and the plasma model. In all cases considered, the respective analytical results in the asymptotic limit of large separations between the plates were obtained. It was shown that the results of numerical computations agree with the analytic results. The obtained results were published in Ref. [10].

(ii) Special attention was paid to the possibility of the Casimir repulsion between the two plates in vacuum due to their magnetic properties. It was shown that the model of magnetic materials with frequency independent ε and μ used in the literature to obtain such a repulsion is inadequate. Thereby, the Casimir repulsion due to magnetic properties arises in the configuration of two dissimilar plates one of which is made of ferromagnetic dielectric and the other one of nonmagnetic metal described by the plasma model. The analytic conditions on $\varepsilon(0)$ and $\mu(0)$ leading to Casimir repulsion were found. In order to check whether the magnetic properties really influence the Casimir interaction and to independently verify the applicability of the Drude and plasma model approaches, several experiments on the measurement of the thermal Casimir force between magnetodielectric bodies have been proposed. The obtained results were submitted for publication [11].

- We have calculated the *lateral Casimir force* in the experimental configuration created by U. Mohideen at the University of California, Riverside. The used test bodies were a plate and a sphere covered with aligned longitudinal corrugations of a sinusoidal shape with the amplitudes $A_1 = 85.4$ nm (on the plate) and $A_2 = 13.7$ nm (on the sphere). The period of corrugations $\Lambda = 574.7$ nm was more than two times smaller than in a previous measurement performed in 2002 in order to achieve the nonadditive regime

where new interesting physical effects were expected. The calculations of the maximum values of the lateral Casimir force as functions of separation were performed (a) by using the proximity force approximation and (b) in the framework of the scattering approach based on the first principles of quantum field theory. In both cases real material properties of Au coatings on the test bodies were described by means of the plasma model. The comparison of both sets of theoretical results with the measurement data demonstrated excellent agreement between the data and computational results using the scattering approach. The use of rather large corrugation amplitudes has also allowed a first experimental demonstration of an asymmetry in the phase dependences of the lateral Casimir force, as predicted by us in 2002. The phase dependences calculated were found to be in excellent agreement with the experimental data. The obtained results open new prospective opportunities in nanotechnology because they give the possibility to actuate lateral transitions in micromachines by means of electromagnetic zero-point fluctuations. They were published as the Rapid Communication [12].

- [1] M. Bordag, G.L. Klimchitskaya, U. Mohideen, V.M. Mostepanenko, *Advances in the Casimir Effect*, Oxford University Press, Oxford, 2009
- [2] G.L. Klimchitskaya, U. Mohideen, and V.M. Mostepanenko, *Rev. Mod. Phys.*, **81** (2010) 1827–1885
- [3] B. Geyer, G.L. Klimchitskaya, U. Mohideen, V.M. Mostepanenko, *Phys. Rev. Lett.* **102** (2009) 189301
- [4] G.L. Klimchitskaya, E.V. Blagov, and V.M. Mostepanenko, *Int. J. Mod. Phys. A* **24** (2009) 1777
- [5] R.S. Decca, E. Fischbach, B. Geyer, G.L. Klimchitskaya, D.E. Krause, D. López, U. Mohideen, V.M. Mostepanenko, *Phys. Rev. Lett.* **102** (2009) 189303
- [6] V.M. Mostepanenko, R.S. Decca, E. Fischbach, B. Geyer, G.L. Klimchitskaya, D.E. Krause, D. López, U. Mohideen, *Int. J. Mod. Phys. A* **24** (2009) 1721
- [7] G.L. Klimchitskaya, *J. Phys.: Conf. Ser.* **161** (2009) 012002
- [8] B. Geyer, *J. Phys.: Conf. Ser.* **161** (2009) 012013
- [9] M. Bordag, B. Geyer, G.L. Klimchitskaya, V.M. Mostepanenko, *J. Phys. A: Math. Theor.* **43** (2010) 015402
- [10] G. Bimonte, G.L. Klimchitskaya, V.M. Mostepanenko, *Phys. Rev. A* **79** (2009) 042906
- [11] B. Geyer, G.L. Klimchitskaya, V.M. Mostepanenko, *Phys. Rev. B*, submitted.
- [12] H.-C. Chiu, G.L. Klimchitskaya, V.N. Marachevsky, V.M. Mostepanenko, U. Mohideen, *Phys. Rev. B* **80** (2009) 121402(R)-1-4

13.3 Structure of the gauge orbit space and study of gauge theoretical models

G. Rudolph Sz. Charzynski* H. Grundling† A. Hertsch J. Huebschmann‡ P. Jarvis§, J. Kijowski* M. Schmidt

*U Warsaw

†U Sydney

‡U Lille

§U Hobart

The investigation of gauge theories in the Hamiltonian approach on finite lattices with emphasis on the role of nongeneric strata was continued. This includes, in particular, stratified Kähler quantization for gauge groups $SU(2)$ and $SU(3)$ [1, 2] and the study of the question how the stratification may be encoded on the level of the algebra of observables [3]. A part of these problems was studied in collaboration with J. Huebschmann.

Based on [4], the investigations of specific models of quantum lattice gauge theory in terms of gauge invariant quantities concerning the structure of the algebra of observables and its representations were continued.

A. Hertsch completed the classification of the orbit types of the action of the group of local gauge transformations on the space of connections for arbitrary compact gauge group [5].

- [1] J. Huebschmann, G. Rudolph, M. Schmidt, *Commun. Math. Phys.* **286**, Nr. 2 (2009) 459–494
- [2] J. Boehnke, *The Costratified Structure of an $SU(3)$ -Lattice Gauge Model*, diploma thesis, University of Leipzig, 2008
- [3] G. Rudolph, M. Schmidt, *J. Math. Phys.* **50** (2009) 052102
- [4] J. Kijowski, G. Rudolph, C. Śliwa, *Annales H. Poincaré* **4** (2003) 1137.
J. Kijowski, G. Rudolph, *J. Math. Phys.* **46** (2005) 032303; *Rep. Math. Phys.* **55** (2005) 199-210
P. Jarvis, J. Kijowski, G. Rudolph, *J. Phys. A* **38** (2005) 5359
- [5] A. Hertsch, *On the Gauge Orbit Stratification for Theories with Classical Compact Gauge Group*, PhD thesis, University of Leipzig, 2009
A. Hertsch, G. Rudolph, M. Schmidt, hep-th arxiv:0812.0228

13.4 Quantum field theory on non-commutative geometries, quantum field theory and cosmology, generally covariant quantum field theory

R. Verch P. Marecki M. Borris T. Ludwig J. Schlemmer F. Lindner A. Knospe B. Eltzner A. Degner

One of the questions of recent interest is if there is a general framework for quantum field theory on non-commutative spacetimes. This question is analysed in collaboration with M. Borris. On one hand, an approach to Lorentzian non-commutative geometry in the spirit of spectral geometry is being established. On the other hand, the quantization of such structures is shown to lead to simple examples of quantum field theories on non-commutative spacetimes for concrete non-commutative spacetime models. The research on these topics is in progress. The relation between the Euclidean and Lorentzian approach to non-commutative quantum field theory is investigated with T. Ludwig. In collaboration with C.J. Fewster it is investigated how to specify that quantum field theories are the same on all spacetimes, which is an extension of the framework of

generally covariant quantum field theory.

The definition and analysis of states which can be viewed as local thermal equilibrium states in quantum field theory will be extended to quantum fields in curved spacetime, with a view on application in cosmological situations. Current research work with J. Schlemmer analyzes the question of existence of thermal equilibrium states. Further work with F. Lindner investigates the stability of local thermal equilibrium with respect to variations of the spacetime metric. Solutions to the semiclassical Friedman equations in local thermal equilibrium states are studied with A. Knospe, the results indicate that quantum corrections lead to an increase in temperature in scenarios of early cosmology compared to the classical results. The consistency of quantization of metric fluctuations in the semiclassical Friedman scenario is studied in collaboration with B. Eltzner. This work has prospective connections to non-commutative spacetimes. With A. Degner we investigated and calculated quantum particle creation in cosmological spacetimes in states of low energy.

A special class of spacetimes are certain types of rotating spacetimes. Several issues in setting up quantum field theories on such spacetimes, and the possibility of local detection of spacetime rotation by quantum effects, are studied by P. Marecki.

13.5 Funding

Structure of the gluon polarization tensor in a color magnetic field background at finite temperature

M. Bordag

DFG BO 1112/16-1

Spectral Zeta Functions and Heat Kernel Technique in Quantum Field Theory with Nonstandard Boundary Condition

M. Bordag

Heisenberg-Landau programme

New Trends and Applications of the Casimir Effect (CASIMIR)

Research Networking Program der ESF (European Research Foundation)

M. Bordag – Member of the Steering Committee

Improved study of the Casimir force between real metals and its application to constraints for testing extra-dimensional physics

B. Geyer

DFG: GE 696/09-1

Gauge Orbit Space Stratification

A. Hertsch

IMPRS fellowship at MPI MIS

Non-commutative quantum field theory

M. Borris, T. Ludwig

IMPRS fellowship

Local thermodynamic equilibrium in cosmological spacetimes

J. Schlemmer, B. Eltzner

IMPRS fellowship at MPI MIS

Fluid analog models for classical and quantum field theory in curved spacetimes

P. Marecki

DFG

24th LQP Workshop "Foundations and Constructive Aspects of QFT", ITP, University of Leipzig, June 26-27, 2009

Ev. Studienwerk Villigst, RAL, PbF2

DPG School on Mathematical Physics, Physikzentrum Bad Honnef, 13-18 Sep 2009

DPG, Heraeus foundation

13.6 Organizational Duties

Priv.-Doz. Dr. Michael Bordag

- Referee: J. Phys. A, Phys. Rev. D, J. Math. Phys.
- Chair of the International Organizing Committee of the Conference on Quantum Field Theory under the Influence of External Conditions (QFEXT09), Oklahoma, 21.-25.9.2009
- Member of the Steering Committee of the ESF Research Networking Program *New Trends and Applications of the Casimir Effect (CASIMIR)*

Prof. Dr. Bodo Geyer

- Vertrauensdozent der Gesellschaft Dt. Naturforscher und Ärzte (GDNÄ)
- Referee: DFG, DAAD, Humboldt Foundation

Prof. Dr. G. Rudolph

- Referee: Class. Quant. Grav., J. Math. Phys., J. Geom. Phys., J. Phys. A, Rep. Math. Phys., Commun. Math. Phys.

Dr. Matthias Schmidt

- Referee: J. Phys. A, Int. J. Mod. Phys. A, Class. Quant. Grav., Gen. Relativity Gravitation

Prof. em. Dr. Armin Uhlmann

- Board member: Rep. Math. Phys., Open Systems and Information Dynamics

Prof. Dr. Rainer Verch

- Dean of Studies, Faculty of Physics and Geosciences, University of Leipzig
- Director of the Institute for Theoretical Physics, University of Leipzig
- Associate Editor, Journal of General Relativity and Gravitation
- Book Series Editor, Fundamental Theories of Physics (Springer)
- Chairman of the Board for the Theoretical and Mathematical Physics Section, Deutsche Physikalische Gesellschaft (DPG) (until 04/2009)
- IMPRS Board Member

- Referee for the Alexander von Humboldt Foundation
- Referee for AERES (France)
- Referee for Studienstiftung des Deutschen Volkes
- Referee: Commun. Math. Phys., J. Math. Phys., Rev. Math. Phys., Class. Quantum Grav., Gen. Rel. Grav.
- Organizer, 24th LQP Workshop “Foundations and Constructive Aspects of QFT”, ITP, University of Leipzig, June 26-27, 2009
- Organizer, DPG School on Mathematical Physics, Physikzentrum Bad Honnef, 13-18 Sep 2009

13.7 External Cooperations

Academic

- II. Inst. f. Theoretische Physik, Universität Hamburg
Prof. Dr. K. Fredenhagen
- Mathematisches Institut, Universität Göttingen
Prof. Dr. D. Bahns
- Mathematisches Institut, Universität Münster
Prof. Dr. R. Wulkenhaar
- AEI-MPI Golm,
Dr. N. Szpak
- Fachbereich Physik, Universität Ulm
Dr. E. Kajari
- Institute of Theoretical Physics, Brandenburg Technical University, Cottbus
Prof. Dr. Dieter Robaschik
- DESY-Institute of High Energy Physics, Zeuthen
Dr. Johannes Blümlein
- Mathematics Department, Universität Hamburg
Dr. Ch. Fleischhack
- National University, Dnepropetrovsk
Prof. V. Skalozub
- St. Petersburg University
Prof. Yu.V. Novozhilov
- VIK Dubna
Dr. V. Nesterenko, Dr. I. Pirozhenko
- Dept. of Physics, North-West Polytechnical University St. Petersburg
Prof. Dr. Galina L. Klimchitskaya
- Noncommercial Partnership “Scientific Instruments” of Ministry of Industry, Sciences and Technologies, Moscow
Prof. Dr. Vladimir M. Mostepanenko

- Polish Academy of Sciences, Center for Theoretical Physics, Warsaw
Prof. Dr. J. Kijowski
Dr. Sz. Charzynski
- Polish Academy of Sciences, Mathematics Institute and University of Warsaw
Prof. Dr. P. Hajac
- Université des Sciences et Technologies de Lille
Prof. Dr. J. Huebschmann
- Department of Mathematics, University of York, England
Dr. C.J. Fewster
- School of Mathematics, Cardiff University, Wales
Dr. S. Hollands
- Dipartimento di Science, Università di Trento, Italy
Prof. Dr. V. Moretti
- Lawrence Livermore National Laboratory, USA
Prof. G. Chapline
- High Energy Theory Group, Brookhaven National Laboratory, Upton, NY,
Dr. Oliver Witzel
- University of Tasmania, Hobart
Prof. Dr. P. Jarvis
- University of Newcastle (Australia)
Prof. Dr. W. Szymanski
- University of New South Wales, Sydney
Prof. H. Grundling

13.8 Publications

Journals

J. Blümlein, D. Robaschik, B. Geyer

Target mass and finite t corrections to diffractive deeply inelastic scattering
Eur. Phys. J. C **61** (2009) 279

M. Bordag

Ultraviolet divergences, repulsive forces and a spherical plasma shell
J. Phys. Conf. Ser. **161** (2009) 012018

M. Bordag, I.V. Fialkovsky, D.M. Gitman, D.V. Vassilevich

Casimir interaction between a perfect conductor and graphene described by the Dirac model

Phys. Rev. B **80** (2009) 245406

M. Bordag and V. Nikolaev

Beyond Proximity Force Approximation in the Casimir effect
Int. J. Mod. Phys. A **24** (2009) 1743–1747

M. Bordag, V. Nikolaev

The vacuum energy for two cylinders with one increasing in size

J. Phys. A: Math. Gen. **42** (2009) 415203

R.S. Decca, E. Fischbach, B. Geyer, G.L. Klimchitskaya, D.E. Krause, D. López, U. Mohideen, V.M. Mostepanenko

Comment on "Contribution of drifting carriers to the Casimir-Lifshitz and Casimir-Polder interactions with semiconductor materials"

Phys. Rev. Lett. **102** (2009) 189303

B. Geyer

On thermal Casimir force between real metals

J. Phys.: Conf. Ser. **161** (2009) 012013

B. Geyer, G.L. Klimchitskaya, U. Mohideen, V.M. Mostepanenko

Comment on "Thermal Lifshitz force between an atom and a conductor with a small density of carriers"

Phys. Rev. Lett. **102** (2009) 189301

J. Huebschmann, G. Rudolph, M. Schmidt

A gauge model for quantum mechanics on a stratified space

Commun. Math. Phys. **286**, Nr. 2 (2009) 459–494

P. Marecki

On the wave equation in spacetimes of Gödel type

in: Gödel Type Spacetimes: History and New Developments, ed. M. Scherfner and M. Plaue, 2009

V.M. Mostepanenko, R.S. Decca, B. Geyer, E. Fischbach, G.L. Klimchitskaya, D.E. Krause, D. López, U. Mohideen

Why the screening effects do not influence the Casimir force

Int. J. Mod. Phys. A **24** (2009) 1721–1742

G. Rudolph, M. Schmidt

On the algebra of quantum observables for a certain gauge model

J. Math. Phys. **50** (2009) 052102

in press

M. Bordag, B. Geyer, G.L. Klimchitskaya, V.M. Mostepanenko

On the definition of dielectric permittivity for media with temporal dispersion in the presence of free charge carriers

J. Phys. A **43** (2010) 015402; arXiv:0911.3231.

M. Bordag, B. Geyer, G.L. Klimchitskaya, V.M. Mostepanenko

On the definition of dielectric permittivity for media with temporal dispersion in the presence of free charge carriers

J. Phys. A **43** (2010) 015402, arXiv:0911.3231 [quant-ph]

M. Bordag and V. Nikolaev

First analytic correction beyond PFA for the electromagnetic field in sphere-plane geometry

Phys. Rev. D, to appear, 2010; arXiv: 0911.0146

G.L. Klimchitskaya, B. Geyer, V.M. Mostepanenko

Thermal Casimir Force between Magnetic Materials

Proc. Int. Workshop "Quantum Field Theory under external conditions" (QFEXT09), Norman, OK, September 21-25, 2009

Books

M. Bordag, G.L. Klimchitskaya, U. Mohideen, V.M. Mostepanenko

Advances in the Casimir Effect

International Series of Monographs on Physics 145, Oxford University Press, 2009

B. Geyer, P. M. Lavrov

Covariant quantizations of gauge theories

Tomsk State Pedagogical University Press, Tomsk 2009

Talks

M. Bordag

Vacuum energy: old and new approaches (inv. T)

NPQCD, Dnepropetrovsk, May 3–6, 2009

M. Bordag

Vacuum energy in quantum field theory: status, problems and recent advances (inv. T)

4th International Sakharov Conference on Physics, Moscow, May 18–23, 2009

M. Bordag

Casimir force at small separation (inv. T)

Quantum Field Theory under the Influence of External Conditions, Oklahoma, September 21–25, 2009

A. Degner, R. Verch

Cosmological Particle Creation in States of Low Energy

DPG-Tagung, München, March 9-13, 2009

A. Degner, R. Verch

Cosmological Particle Creation in States of Low Energy

23th Workshop "Foundations and Costructive Aspects of QFT", G'ottingen, January 30–31, 2009

B. Geyer

Some remarkable steps in the history of (theoretical) physics during 600 years of Leipzig University (inv T)

Workshop on Local Quantum Physics (LPQ24), Leipzig, June 26–27, 2009

G.L. Klimchitskaya, B. Geyer, V.M. Mostepanenko
Thermal Casimir Force between Magnetic Materials
Int. Workshop Quantum Field Theory under external conditions (QFEXT09), Norman,
OK, September 21–25, 2009

G. Rudolph
G-manifolds, Hamiltonian systems and symmetries
Three lectures at the IMPRS, MIS, Leipzig, Januar 2009

G. Rudolph
Lattice gauge theory: singular reduction and quantization
Institute for Theoretical Physics, Polish Academy of Sciences, March 2009

G. Rudolph
Aspects of singular Marsden-Weinstein reduction
Institute of Mathematics, Polish Academy of Sciences, March 2009

G. Rudolph
Singular reduction and quantization of lattice gauge models
Institute of Mathematics, University of New South Wales, Sydney, May 2009

G. Rudolph
A model of singular reduction and quantization
School of Mathematics and Physics, University of Tasmania, Hobart, June 2009

G. Rudolph
Hamiltonian systems with symmetries
Four lectures at the School of Mathematics and Physics, University of Tasmania, Hobart,
June 2009

G. Rudolph
On singular reduction, quantization and the observable algebra for gauge models
XVIth International Congress on Mathematical Physics, Prag, August 3–8, 2009

R. Verch
Quantum Field Theory on Lorentzian Non-Commutative Spacetimes and Non-Commu-
tative Potential Scattering
Conference "Algebraic and Combinatorial Structures of QFT", Cargèse, Corsica, March
29–April 4, 2009

R. Verch
A Guided Tour to Concepts and Developments in QFT in Curved Spacetime
Conference "Algebraic Quantum Field Theory – The First 50 Years", G'ottingen, July
29–31, 2009

13.9 Graduations

Doctorate

- Alexander Hertsch
On the Gauge Orbit Stratification for Theories with Classical Compact Gauge Group
June 3, 2009

Diploma

- Falk Lindner
Lokales thermales Gleichgewicht mit zeitlich variierendem Hintergrund
October 6, 2009
- Juliane Stanja
Lokal thermales Gleichgewicht des freien quantisierten elektromagnetischen Feldes auf gekrümmten Raumzeiten
September 28, 2009
- Konrad Zimmermann
Quantum Theory of a lattice gauge model
April 7, 2009

Bachelor

- Steve Linke
Die kosmologische Konstante
September 25, 2009
- Sven Prüfer
From Maxwell's Equations to Yang-Mills Theory
August 17, 2009
- Matthias Rampke
Rotating Spacetimes
August 27, 2009
- Christopher Weber
Wormholes and Time Machines
July 3, 2009

13.10 Guests

- Dr. V. Demchik and Dr. A. Strelchenko
University of Dnepropetrovsk
June 6–26, 2009
- Prof. Dr. H. Grundling
University of New South Wales, Sydney
July 10–13, 2009
- Prof. Dr. Galina L. Klimchitskaya
Dept. of Physics, North-West Polytechnical University St. Petersburg
July 09–September 24, 2009

- Prof. Dr. Vladimir M. Mostepanenko
Noncommercial Partnership “Scientific Instruments” of Ministry of Industry, Sciences
and Technologies, Moscow
July 09–September 24, 2009
- Prof. V. Skalozub
University of Dnepropetrovsk
January 11–February 8, 2009
- Dr. Oliver Witzel
High Energy Theory Group, Brookhaven National Laboratory, Upton, NY 11973,
USA
November 16–20, 2009

14

Theory of Condensed Matter

14.1 Introduction

Major research topics in our group include nonequilibrium phenomena and pattern formation in systems of various nature, e.g. in soft condensed matter and in biological systems. Modern analytic methods of statistical physics and computer simulations complement and stimulate each other. Cooperations with mathematicians, theoretical and experimental physicists, biologists and medical researchers in Germany, Europe and around the world are well established. Specifically we are interested in the following problems.

Noise induced phenomena (Behn). Noise induced non-equilibrium phase transitions are studied in coupled arrays of stochastically driven nonlinear systems. Furthermore, stability and statistical characteristics of stochastic nonlinear systems with time delay are investigated.

Mathematical modeling of the immune system (Behn). Using methods of nonlinear dynamics and statistical physics, we study the architecture and the random evolution of the idiotypic network of the B-cell subsystem and describe the regulation of balance of the Th1/Th2-cell subsystem including regulatory T-cells, its relation to allergy and the hyposensitization therapy (cooperation with G. Metzner, Clinical Immunology).

Non-equilibrium dynamics in soft-condensed-matter systems (Kroy). The systems under investigation range from desert dunes spontaneously developing as a generic consequence of aeolian sand transport, through non-equilibrium gels of adhesive colloids and proteins, the viscoelastic mechanics of the cytoskeleton, to the non-equilibrium dynamics of single DNA molecules under strong external fields. (Related experimental work is currently in progress at EXP1: PWM, PAF.) A common feature is the presence of strong fluctuations and stochastic dynamics on the micro-scale. The emergence of macroscopic structure and (non-linear) deterministic macroscopic dynamics is to be understood. The applied methods range from analytical studies of stochastic integro-differential equations through liquid-state theories, mode-coupling theory, effective hydrodynamic equations, phenomenological modeling, to numerical simulations.

14.2 Stochastic Phenomena in Systems with Many Degrees of Freedom

U. Behn, F. Anselmi, S. Gütter, M. Höll, N. Kühn

Arrays of spatially coupled nonlinear dynamical systems driven by multiplicative Gaussian white noise show close analogies to phase transitions in equilibrium [1]. Concepts developed to describe equilibrium phase transitions such as symmetry or ergodicity breaking, order parameter, critical behaviour, critical exponents etc. can be transferred to noise induced nonequilibrium phase transitions, see e.g. [2].

For multiplicative noise, essential characteristics of phase transitions can be found already in finite arrays. In the limit of strong coupling there is a clear separation of time scales which allows to eliminate the fast degrees of freedom of the relative coordinates. The slow center of mass coordinate exhibits a critical behaviour. Analytical results for probability distribution and expectation value are confirmed by simulations [3].

We applied the concept of center of mass and relative coordinates, cf. Fig. 14.1, also to finite systems with additive noise. For large but finite coupling the relative coordinates are symmetrically distributed with small variance. We developed a self-consistent mean field theory to determine the probability distributions of both center of mass and relative coordinates. The mean field results agree very well with simulations [4].

Also for systems with multiplicative noise we use mean field theory to describe the corrections to the analytically solvable cases considering inverse coupling strength and/or inverse system size as small parameters.

We have continued the numerical simulations to investigate stability and statistical properties of stochastic systems with delayed time argument and explored systematically the parameter space near the stability threshold and the Ornstein-Uhlenbeck limit (collaboration with L. Wetzol, MPI PKS).

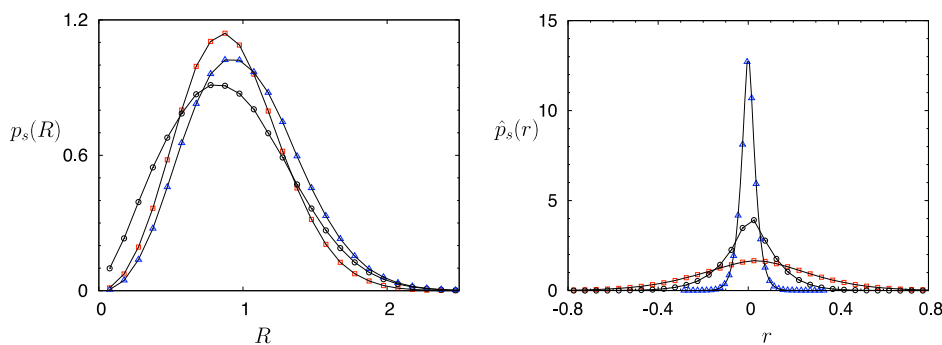


Figure 14.1: Stationary probability densities for center of mass (*left*) and relative coordinates (*right*) for two coupled Stratonovich models. We show simulation results for increasing coupling strength $D = 1$ (squares), 10 (circles), and 100 (triangles), control parameter $a = 1$, and noise strength $\sigma = 1$. The distribution of relative coordinates is centered around zero and becomes sharp with increasing coupling strength. From [3].

- [1] F. Sagués, J. García-Ojalvo, J.M. Sancho, *Rev. Mod. Phys.* **79**, 829 (2007)
- [2] T. Birner et al.: *Phys. Rev. E* **65**, 046110 (2002)
- [3] F. Senf et al.: *New J. Phys.* **11**, 063010 (2009), 18 pp
- [4] F. Anselmi: Diplomarbeit, Universität Leipzig, 2010

14.3 Mathematical Modeling of the Immune System

U. Behn, F. Groß, D. Kröber, A. Kühn, H. Schmidtchen, H. Seder, B. Werner, S. Willner

The paradigm of idiotypic networks, developed about 3 decades ago by Jerne [1], finds today a renewed interest mainly from the side of system biology and from clinical research; for a recent review see [2].

B-cells express receptors (antibodies) of a given idiootype; crosslinking these receptors by complementary structures (antigen or antibodies) stimulates the lymphocyte to proliferate. Unstimulated B-cells die. Thus a macroscopically large, though finite, functional network of lymphocytes, the idiotypic network emerges. The dynamics is driven by the influx of new idiotypes randomly produced in the bone marrow and by the population dynamics of the lymphocytes themselves.

In our minimalistic model [3] idiotypes are represented by bitstrings. The model evolves to a highly organized dynamical architecture where groups of nodes with distinct statistical characteristics can be identified. We can analytically compute size and connectivity of these groups and calculate in a modular mean field theory mean occupation and mean life time of the nodes [4].

We further developed the modular mean field theory and included correlations within and between core and peripheral groups of the 12-group architecture which improves the agreement with simulations (A. Kühn).

To describe more realistic biological features we extended the model allowing for weighted links. We included antigens in our model and found a bistable situation where the antigen induces an internal image which persists after the antigen is defeated, cf. Fig. 14.2. In a second exposition to the antigen the network responds faster and more efficient. We further found that in the presence of a long lasting self-antigen the architecture of the network organizes in such a way that the idiotypes complementary to self are only weakly occupied. This is a first hint that our model can describe self-tolerance [5].

T-helper lymphocytes have subtypes which differ in their spectrum of secreted cytokines. These cytokines have autocrine effects on the own subtype and cross-suppressive effects on the other subtype and regulate the type of immunoglobulines secreted by B-lymphocytes. In allergy, the balance of Th1- and Th2-cells is perturbed: the response to allergen is Th2-dominated. Recent clinical studies show that during specific immunotherapy the concentration of Tregs is increasing [8, 9]. We extended our previous model [6] to include these regulatory T-cells [10]. If successful, the periodic injections of allergen in the maintenance phase of the therapy drive the system towards a stable fixed point where a high population of Tregs dominates both Th2- and Th1-cells, similar to experimental findings [10]. It would be interesting to include other novel Th-subtypes such as Th17 which is found to play a role, e.g., in allergic asthma (collaboration with G. Metzner, Institute of Clinical Immunology).

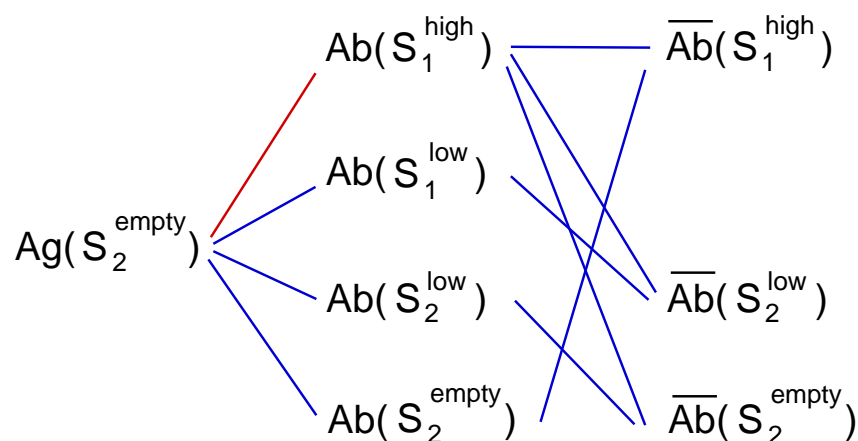


Figure 14.2: Internal image of antigen Ag . For a certain parameter region Ag induces on the base graph $G_{12}^{(3)}$ a splitting of the medium occupied group S_1 into subgroups $S_1^{\text{high/low}}$ and of the empty group S_2 into $S_2^{\text{low/empty}}$. We show these groups and the one-mismatch links (*blue*). Ag is perfectly complementary (*red* link) to $Ab(S_1^{\text{high}})$. The one-mismatch complementary antibody $\overline{Ab}(S_1^{\text{high}})$ is a highly occupied internal image of Ag and persists when Ag is already defeated.

- [1] N.K. Jerne: Ann. Inst. Pasteur Immunol. **125C**, 373 (1974)
- [2] U. Behn: Immunol. Rev. **216** 142 (2007)
- [3] M. Brede, U. Behn: Phys. Rev. E **67**, 031920 (2003)
- [4] H. Schmidtchen, U. Behn: in *Mathematical Modeling of Biological Systems*, Volume II. ed. by A. Deutsch et al. (Birkhäuser, Boston 2008) p157; H. Schmidtchen et al., in preparation
- [5] B. Werner: Diplomarbeit, Universität Leipzig, 2010.
- [6] J. Richter et al.: J. Theor. Med. **4**, 119 (2002)
- [7] R. Vogel, U. Behn: in *Mathematical Modeling of Biological Systems*, Volume II. ed. by A. Deutsch et al. (Birkhäuser, Boston 2008) p145
- [8] M. Larché et al.: Nature Reviews Immunology **6**, 761 (2006)
- [9] E. Mamessier et al.: Clin. Exp. Allergy **36**, 704 (2006)
- [10] F. Groß et al.: *Mathematical Modelling of Allergy and Specific Immunotherapy: Th1-Th2-Treg Interactions*, arXiv:1003.1053, submitted for publication (2010)

14.4 Tube Width Fluctuations in F-Actin solutions

J. Glaser, D. Chakraborty, K. Kroy

In collaboration with the experimental research group of Prof. Merkel, Jülich, the equilibrium properties of entangled networks of the cytoskeletal polymer F-actin (Fig.14.3, *left*) on intermediate time scales have been investigated *in-vitro*. The Brownian motion of the topologically entangled actin filaments is slowed down on large length scales due to the cage effect - the average conformations of the polymers are effectively “quenched” and the polymer is trapped in a narrow tube.

Like for other porous materials, such as packings of colloids and granular matter, it is possible to characterize the heterogeneities of the solution in terms of the distribution of void spaces. In a recent paper [1] we successfully showed that the different measured tube diameters can be explained by a non-Gaussian distribution with broad tails (Fig.14.3, *right*). The experimental measurements are explained by a segment fluid model (Fig.14.3, *center*), which represents a systematic generalization of the established mean-field theory for stiff polymers. The model makes an explicit connection between the slow, frozen degrees of freedom of the solution and those of a dense fluid of effective quasi-particles.

The results promise to contribute to a better understanding of the broad distribution of elastic properties of living cells. This, on the other hand, could hold the key to the explanation of the slow, glassy dynamics of the cytoskeleton [2], for which the work group has recently developed the phenomenological model of a “glassy wormlike chain” [3], which has been impressively validated by dynamic light scattering on F-actin [4] solutions and by rheological data of living cells [5].

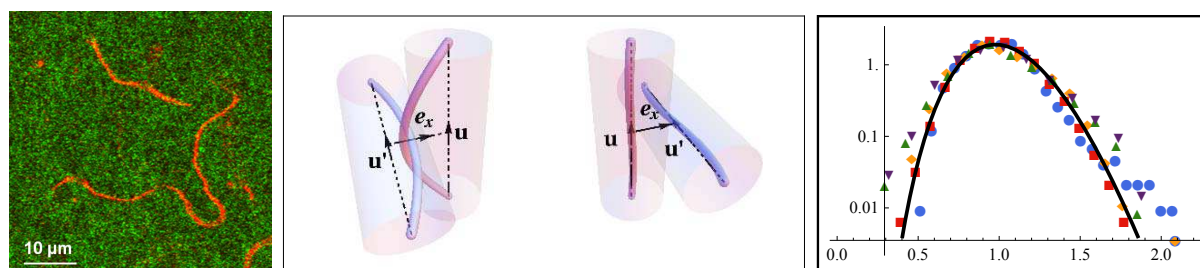


Figure 14.3: *Left:* Fluorescent microscopy image of a F-actin solution labeled with two different colors. *Center:* Two different topologically equivalent configurations of two entangled filaments in their confinement tubes have to be considered separately. *Right:* Skewed leptokurtic tube radius distributions for different actin concentrations (symbols) and comparison to the self-consistent analytic theory.

- [1] J. Glaser, D. Chakraborty, K. Kroy, I. Lauter, M. Degawa, N. Kirchgeßner, B. Hoffman, R. Merkel, and M. Giesen: *Tube width fluctuations in f-actin solutions*, arXiv:0910.5864, Phys. Rev. Lett., in press
- [2] C. Semmrich, T. Storz, J. Glaser, R. Merkel, A. R. Bausch, and K. Kroy: Proc. Natl. Acad. Sci. USA, **104**(52), 20199 (2007)
- [3] K. Kroy and J. Glaser. New J. Phys., **9**, 416 (2007)
- [4] J. Glaser, C. Hubert, and K. Kroy: *Dynamics of sticky polymer solutions* in *Proceedings of the 9th International Conference Path Integrals – New Trends and Perspectives*, ed. by W. Janke and A. Pelster (World Scientific, 2008)
- [5] K. Kroy and J. Glaser: AIP Conf. Proc., **1151**, 52 (2009)

14.5 The conformations of a stiff polymer in random media

M. Hennes, K. Kroy

Stiff polymers play a crucial role in many biophysical processes. In the eukaryotic cell, they assemble to a dense meshwork, the cytoskeleton, which confers the cell its unique mechanical properties. In this crowded environment the conformations and dynamic properties of the biopolymers are strongly influenced by the surrounding macromolecules. The theoretical description of the resulting complicated many body problem is usually provided by a mean-field ansatz, like the tube model or the glassy wormlike chain [1].

Little attention has been paid so far to the effect of a quenched random environment on a stiff filament. Therefore, we investigated the influence of quenched random forces and quenched random potentials on the conformations of a semiflexible chain in the weakly bending rod limit within the context of a diploma thesis.

[1] K. Kroy, J. Glaser: *New J. Phys.*, **9**, 416 (2007).

14.6 Glassy dynamics in pectin networks

M. Hennes, R. R. Vincent*, M. A. K. Williams[†], K. Kroy

*Adolphe Merkle Institute (AMI), University of Fribourg, Switzerland

[†]IFS, Massey University, New Zealand

Semiflexible polymers are ubiquitous in nature. F-Actin for example, a main constituent of the cytoskeleton, has been extensively studied over the last twenty years. There is by now a thorough understanding of the properties of single filaments: the so called wormlike chain model (WLC) has emerged as a paradigmatic description of the nontrivial physics of semiflexible polymers.

Less is known about the complex behavior of networks of semiflexible chains. Usual theoretical approaches reduce the many body problem to a an effective single chain problem. In the tube model for example, the network surrounding one single test chain is modelled by an effective harmonic potential: the chain is assumed to be confined to a tube. Macroscopic network properties like the shear modulus are then deduced from the behavior of the test polymer.

The glassy wormlike chain (GWLC), a recently proposed extension of the original WLC model [1], can also be considered as such an effective model. There, the presence of surrounding chains is taken into account by a stretching of the relaxation times of modes of large wavelength of a test chain. This approach is very generic and might in principle be extended to any polymer model which presents fractal dynamics.

An interesting system where these theoretical predictions can be tested are pectin networks. Indeed, recent microrheological experiments performed on this plant cell wall biopolymer demonstrated that depending on sample preparation, either flexible or semiflexible network behavior emerged [2]. The aim of the present project is thus to

study the applicability of a phenomenological glassy extension of existing relaxation models (Rouse chain, WLC) in order to understand the results gained by the study of gelling pectin samples.

- [1] K. Kroy, J. Glaser: *New J. Phys.*, **9**, 416 (2007)
- [2] R. R. Vincent, A. Cucheval, Y. Hemar and M. A. K. Williams: *Eur. Phys. J. E*, **28**, 79 (2009)

14.7 Force transmission through the cytoskeleton

S. Sturm, K. Kroy

Stiff and semiflexible polymers such as filamentous actin or microtubules form a major building block of biological tissue. While a systematic analytical theory of their non-equilibrium mechanics under the influence of external forces has been put forward in recent years [1, 2], such approaches are usually tailored to single-molecule experiments and thus neglect the presence of a surrounding polymer network. A simple modification of the weakly bending rod model called the “Glassy Wormlike Chain”[3] has been found successful in the description of experimental data on actin solutions and cells. The aforementioned theories of force propagation in stiff and semiflexible polymers have thus been extended to the Glassy Wormlike Chain model to obtain an analytical description of the quick non-equilibrium response of the cytoskeleton to external forces.

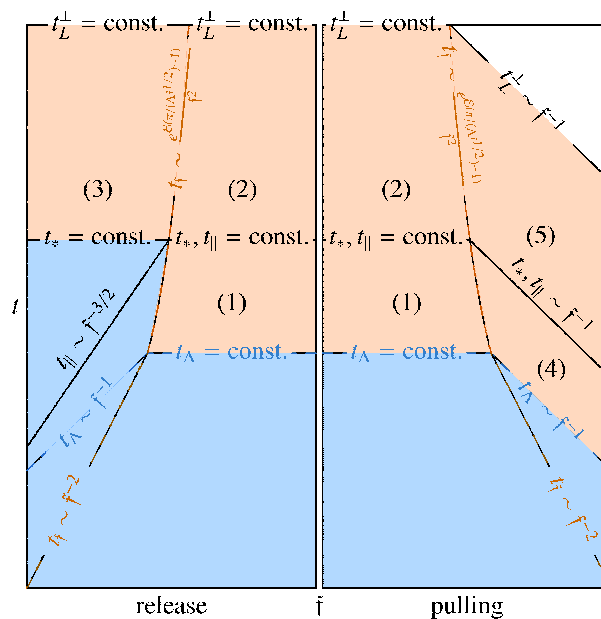


Figure 14.4: Dynamical phase diagram for ‘pulling’ and ‘release’ scenarios as shown in ref. [2], with GWLC modifications. Blue shaded areas indicate plain Wormlike Chain dynamics, orange areas show new intermediate asymptotes arising from the GWLC model.

- [1] O. Hallatschek, E. Frey, K. Kroy: *Phys. Rev. Lett.* **94**, 077804 (2005)
- [2] O. Hallatschek, E. Frey, K. Kroy: *Phys. Rev. E* **75**, 031906 (2007)
- [3] K. Kroy, J. Glaser: *New J. Phys.* **9**, 416 (2007)

14.8 Inelastic mechanics of sticky biopolymer networks

L. Wolff, P. Fernandez*, K. Kroy

*Lehrstuhl für Zellbiophysik, TU München, James-Franck-Str. 1, Garching

For a long time, cells and *in vitro* reconstituted biopolymer networks have been considered as viscoelastic bodies. This point of view has, however, been challenged by recent experimental findings characterizing cells and biopolymer networks as glassy fragile and inelastic objects. We developed a minimal phenomenological model by combining the Glassy Wormlike Chain (GWLC) with an inelastic bond-kinetics scheme to account for these observations [1]. At the heart of our approach lies the assumption that the interactions of a test polymer segment with the background network can be summarized into an effective interaction potential. This potential then governs (via the GWLC) the relaxation of the single-polymer modes of the test polymer, as well as (via the bond kinetics) the mean fraction of closed bonds. The number of parameters introduced by this approach is strongly constrained by consistency requirements, relating GWLC parameters to the parameters of the bond kinetics. The interplay of the GWLC and the bond-kinetics responses leads to a rich variety of non-trivial responses. Depending on the amplitude of external stimulus, our model shows stiffening or passive remodelling effects such as fluidization or visco-elastic shakedown, both in accordance with experimental findings for reconstituted networks and cells. Therefore, our model paves the way to a better understanding of many surprising mechanical features of cells and biopolymer networks. A particularly promising direction for future research is the introduction of an additional slip rate into the bond kinetics, which would allow to study experiments with residual plastic strain.

[1] L. Wolff, P. Fernandez, and K. Kroy: *New J. Phys.* **12**, 053024 (2010)

14.9 Hot Brownian Motion

D. Rings, M. Selmke*, R. Radünz*, F. Cichos*, K. Kroy

*Molekulare Nanophotonik, Institut für Experimentalphysik I

Brownian motion is abundant throughout the microscopic and mesoscopic world. It is the erratic motion of suspended particles that are large enough to admit some hydrodynamic coarse-graining, yet small enough to exhibit substantial thermal fluctuations. Since Einstein's seminal work, there is a good understanding of this process under conditions of thermal equilibrium. We derive the generalized Markovian description for the non-equilibrium Brownian motion of a heated particle in a simple solvent with a temperature-dependent viscosity. Our analytical results for the generalized fluctuation-dissipation and Stokes-Einstein relations compare favorably with measurements of laser-heated gold nano-particles and provide a practical rational basis for emerging photothermal technologies [2]. Of special interest is a new technique called Photothermal Correlation Spectroscopy (PhoCS) for the measurement of particle dynamics, which is sensitive to single metal nano-particles down to a radius of 2.5 nm [1]. Due

to the photostability of gold nano-particles, the method promises broad applications especially in the field of high throughput biological screening.

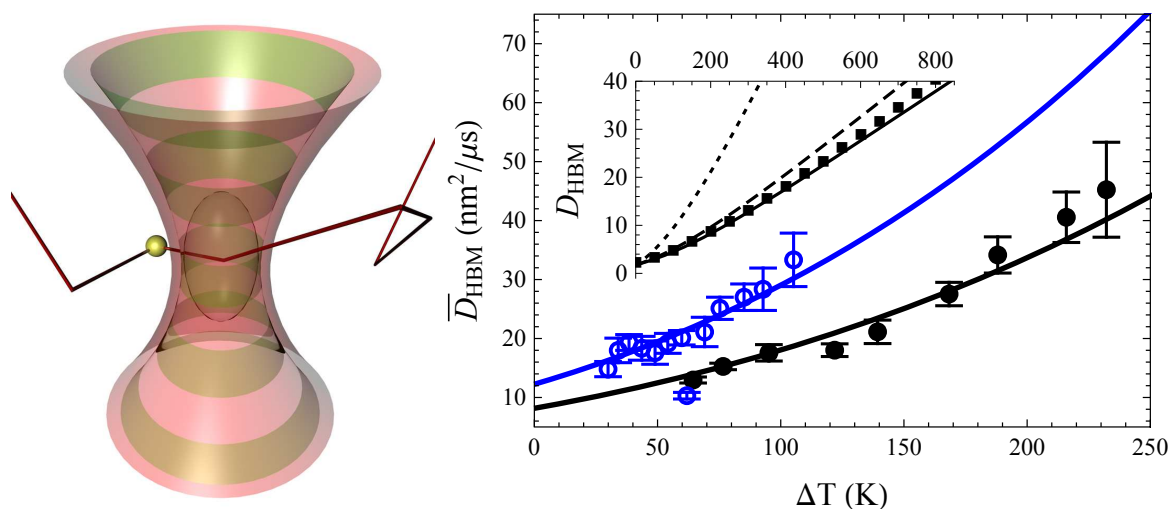


Figure 14.5: (Left) PhoCS detection scheme with overlapping foci of the heating (green) and the detection (red) laser. (Right) The effective diffusion coefficient $\bar{D}_{\text{HBM}}(\Delta T)$ of hot gold nano-particles traversing a laser focus in water: experimental data (open/closed symbols for $R = 40/60$ nm) versus analytical predictions from our model (solid lines). *Inset:* $D_{\text{HBM}}(\Delta T)$ according to numerical predictions (squares), analytical solutions of our model at two levels of sophistication, and the naive suggestion to identify the HBM parameters with the conditions at the particle surface (dotted).

- [1] R. Radünz, D. Rings, K. Kroy, F. Cichos: J. Phys. Chem. A **113**(9), 1674-1677 (2009), doi:10.1021/jp810466y
 [2] D. Rings, R. Schachoff, M. Selmke, F. Cichos, K. Kroy: arXiv:1003.4596

14.10 Funding

Sächsische Forschergruppe

J. Glaser

DFG FOR 877 (P3)

The Leipzig Graduate School "Building with Molecules and Nano-objects"

S. Sturm, L. Wolff

IMPRS Mathematics in the Sciences

H. Schmidtchen

14.11 Organizational Duties

U. Behn

- Speaker of the Condensed Matter Theory Group
- Vertrauensdozent für die Nobelpreisträgertagungen in Lindau

- Bibliotheksbeauftragter of the Faculty
- Member of PbF2
- Scientific Member of the International Max Planck Research School "Mathematics in the Sciences"
- Referee: New J. Phys., Phys. Rev. E, J. Math. Phys.
- Reviewer: Santa Fe Institute

K. Kroy

- Vice Director of the Institute for Theoretical Physics
- Organization of faculty- & physics colloquia
- Organization of "Die mitteldeutsche Physikcombo"
- Member of the graduation committee
- Member of the committee for information & communication technology
- Study counselor for physics
- Member of PbF1 and PbF2
- Scientific Member of the International Max Planck Research School "Mathematics in the Sciences"
- PI in FG877 and The Leipzig Graduate School "Building with Molecules and Nano-objects"
- Referee: Nature Phys., Proc. Natl. Acad. Sci. USA, Phys. Rev. Lett., Europhys. Lett., New J. Phys., Phys. Rev. E, J. Phys.: Condensed Matter, Eur. Phys. J. E, Soft Matter, PLoS ONE, Chem. Phys. Chem., Phys. Chem. Chem. Phys., EarthSurface
- Reviewer: DFG, NSF, ERC, FWF, ISF

14.12 External Cooperations

Academic

- Max-Planck-Institute for Dynamics and Self-Organization Göttingen
Dr. O. Hallatschek
- FZ Jülich
Prof. R. Merkel, Dr. M. Degawa
- TU Munich
Prof. A. Bausch, Dr. P. Fernandez
- LMU Munich
Prof. E. Frey
- Massey University, New Zealand
Prof. M. Williams, Dr. R. Vincent
- Harvard School of Public Health, Boston, USA
Prof. J. Fredberg
- University of Cambridge
Dr. P. Benetatos
- Molekulare Nanophotonik, Institut für Experimentalphysik I
Prof. F. Cichos

- Otto-von-Guericke-Universität Magdeburg
Prof. Dr. J. Richter
- Joint Institute for Nuclear Research, Dubna, Russia
Prof. Dr. N.M. Plakida
- Ernst-Moritz-Arndt-Universität Greifswald
Prof. Dr. H. Fehske
- Institut für Klinische Immunologie
Prof. Dr. G. Metzner
- Philipps-Universität Marburg
Prof. Dr. G. Germano, Dr. E. Martin
- Max-Planck-Institut für Evolutionsbiologie, Plön
Dipl.-Phys. P. Altrock
- Leibniz-Institut für Atmosphärenphysik, Kühlungsborn
Dipl.-Phys. F. Senf
- Max-Planck-Institut für Physik komplexer Systeme, Dresden
Dipl.-Phys. L. Wetzel
- Physik Weicher Materie, Institut für Experimentalphysik I
Prof. Dr. A. Käs, Dipl.-Math. M. Knorr
- European School of Molecular Medicine, Milan, Italy
Dipl.-Phys. F. Groß

14.13 Publications

Scientific Journals

P. Fernandez, S. Grosser, K. Kroy: *A unit-cell approach to the nonlinear rheology of biopolymer solutions*, *Soft Matter* **5** 2047–2056 (2009)

I. Juhász Junger, D. Ihle, J. Richter: *Thermodynamics of layered Heisenberg magnets with arbitrary spin*, *Phys. Rev. B* **80**, 064425 (2009), 9pp

K. Kroy and J. Glaser: *Rheological Redundancy - from Polymers to Living Cells*, in: *Advanced Materials and Nanotechnology: Proceedings of the International Conference (AMN-4)*, *AIP Conf. Proc.* **1151**, ed. by S. C. Hendy and I. W. M. Brown, (American Institute of Physics, 2009), pp. 52–55

B. Obermayer, W. Möbius, O. Hallatschek, E. Frey, K. Kroy: *Freely relaxing polymers remember how they were straightened*, *Phys. Rev. E* **79**, 021804 (2009)

R. Radünz, D. Rings, K. Kroy, F. Cichos: *Hot Brownian Particles and Photothermal Correlation Spectroscopy*, *J. Phys. Chem. A* **113**(9), 1674-1677 (2009)

J. Richter, M. Härtel, D. Ihle, S.-L. Drechsler: *Thermodynamics of the frustrated ferromagnetic spin-1/2 Heisenberg chain*, *J. Phys. Conference Series* **145**, 012064 (2009), 4pp

F. Senf, P.M. Altrock, U. Behn: *Nonequilibrium phase transitions in finite arrays of globally coupled Stratonovich models: Strong coupling limit*, New J. Phys. **11**, 063010 (2009), 18 pp. Erratum: New J. Phys. **11**, 089801 (2009), 1 p.

A. A. Vladimirov, D. Ihle, N.M. Plakida: *Dynamic spin susceptibility in the t - J model*, Phys. Rev. B **80**, 104425 (2009) 12pp

L. Wolff, K. Kroy: *Mechanical stability: A construction principle for cells*, in: *Diffusion Fundamentals* **11**, 56 (2009)

under review

F. Groß, G. Metzner, U. Behn: *Mathematical Modelling of Allergy and Specific Immunotherapy: Th1-Th2-Treg Interactions*, arXiv:1003.1053, submitted to J. Theor. Biol.

in press

J. Glaser, D. Chakraborty, K. Kroy, I. Lauter, M. Degawa, N. Kirchgeßner, B. Hoffman, R. Merkel, and M. Giesen: *Tube width fluctuations in f -actin solutions*, arXiv:0910.5864, Phys. Rev. Lett., in press

L. Wolff, P. Fernandez, and K. Kroy: New J. Phys. **12**, 053024 (2010)

Talks

U. Behn, M. Krieger, J. Emmerich, C. Brettschneider, L. Wetzel: *Statistical Characteristics of Delayed Stochastic Systems at Marginal Stability*, Workshop Delayed Complex Systems, MPI PKS, Dresden, Germany 5.-9. October 2009

J. Glaser: *A liquid state theory for biopolymers*, 73. Annual Meeting of the German Physical Society, Dresden, 22.-27. March 2009

J. Glaser: *Brownian Dynamics of Stiff Polymers*, Workshop 'Simulations on GPU', Institute for Theoretical Physics Leipzig, 11.-12. June 2009

M. Hennes: *The conformations of stiff polymers in random media*, Workshop and Tutorial: Modeling and Simulating Macromolecules, Leipzig, 09.-10. July 2009

M. Knorr, D. Koch, T. Fuhs, T. Betz, U. Behn, J.A. Käs: *Stochastic Lamellipodium Dynamics*, DPG Spring Meeting, Dresden, Germany 22.-27. March 2009

K. Kroy: *Rheological Redundancy and Universality – From Polymers to Living Cells*, Advanced Materials and Nanotechnology 4, Dunedin (New Zealand), 08.-12. February 2009

K. Kroy: *On Growth and Form of Desert Dunes*, Massey University, Palmerston North, New Zealand, 13. February 2009

K. Kroy: *Hot Brownian Motion*, Victoria University, Wellington (New Zealand), 13. February 2009

K. Kroy: *Die Physik der Wanderdünen - warum ist die Wüste nicht flach?*, Institut für Oberflächenmodifizierung, Leipzig, 16. April 2009

K. Kroy: *Rheological Redundancy and Universality - From Polymers to Living Cells*, Diffusion Fundamentals III, Athens (Greece), 23.-26. August 2009

K. Kroy: *Nonlinear Cell Mechanics is Plastic Mechanics*, Physics of Cells (EMBO), Primosten (Croatia), 08.-13. September 2009

K. Kroy: *From Polymers to Living Cells*, LMU Munich, 11.-14. October 2009

K. Kroy: *Rheologische Redundanz - vom Polymer zur lebenden Zelle*, Karlsruher Institut für Technologie, 19. November 2009

K. Kroy: *Are We Built of Glass - The Strange Mechanics of Living Cells*, Montpellier (France), 16. December 2009

D. Rings: *Hot Brownian motion*, Meeting of the Saxonian 73. Annual Meeting of the German Physical Society, Dresden, 22.-27. March 2009

D. Rings: *Kaustiken - Das Spiel von Licht und Staub*, 9. Leipziger Promotionsvorträge, Leipziger Initiative für Promovierende, 19. November 2009

S. Sturm: *Nonequilibrium GWLC dynamics*, Workshop for Doctoral Candidates of the Graduate School BuildMoNa, Neukirchen/Pleiße, 08.-09. October 2009

L. Wolff: *Nonlinear cell mechanics is inelastic mechanics*, Gruppenseminar der Abteilung Statistische und Biologische Physik, Arnold Sommerfeldt Center, LMU Munich, October 2009

L. Wolff: *Nonlinear cell mechanics is inelastic mechanics*, Workshop for Doctoral Candidates of the Graduate School BuildMoNa, Neukirchen/Pleiße, 08.-09. October 2009

Posters

D. Chakraborty: *Finite Size Effects in Persistence in Random Walk*, 34. Conference of the Middle European Cooperation in Statistical Physics, Leipzig, 30. March - 01. April 2009

D. Chakraborty: *Simulating Hot Nano Beads*, Diffusion Fundamentals III, Athens (Greece), 23.-26. August 2009

J. Glaser: *Packing structure and dynamics of stiff polymers*, 2. SFG Symposium, Eibenstein, 11.-13. March 2009

J. Glaser: *A liquid state approach to biopolymers*, 34. Conference of the Middle European Cooperation in Statistical Physics, Leipzig, 30. March - 01. April 2009

J. Glaser: *A liquid state approach to biopolymers*, 2. Scientific Symposium of the Graduate School BuildMoNa, Leipzig, 02.-04. April 2009

J. Glaser: *Tube Geometry and Brownian Dynamics in Semiflexible Polymer Networks*, Diffusion Fundamentals III, Athens (Greece), 23.-26. August 2009

F. Groß , G. Metzner, U. Behn: *Mathematical Modelling of Th1-Th2-Treg Interactions in Allergy and During Specific Immunotherapy*, World Immune Regulation Meeting III, Davos, Switzerland, 22.-25. March 2009

M. Knorr, D. Koch, U. Behn, J.A. Käs: *Stochastic Lamellipodium Dynamics*, Poster, Scientific Symposium of the Graduate School BuildMona, Leipzig, Germany, 2.-3. April 2009

D. Rings: *Hot Brownian Motion*, 2. SFG Symposium, Eibenstock, 11.-13. March 2009

D. Rings: *Hot Brownian Motion*, Diffusion Fundamentals III, Athens (Greece), 23.-26. August 2009

H. Schmidtchen: *Randomly Evolving Idiotypic Networks: A Mean Field Approach*, IMPRS Evaluation Meeting, MPI MIS, Leipzig, Germany 9. January 2009

F. Senf, P.M. Altrock, U. Behn: *Nonequilibrium Phase Transitions in Finite Arrays of Globally Coupled Stratonovich Models: Strong Coupling Limit*, DPG Spring Meeting, Dresden, Germany 22.-27. March 2009

F. Senf, P.M. Altrock, U. Behn: *Globally Coupled Stratonovich Models in the Strong Coupling Limit*, Workshop CompPhys09, Leipzig, Germany 26.-29. November 2009

S. Sturm: *How molecular crowding speeds up mechanotransduction*, 73. Annual Meeting of the German Physical Society, Dresden, 22.-27. March 2009

S. Sturm: *Force propagation through the cytoskeleton* , 2. Scientific Symposium of the Graduate School BuildMoNa, Leipzig, 02.-04. April 2009

L. Wolff: *Fluctuations and slow glassy dynamics in biopolymer networks*, 73. Annual Meeting of the German Physical Society, Dresden, 22.-27. March 2009

L. Wolff: *Nonlinear cell mechanics*, 435. WE Heraeus Seminar 'Physics of cell function', Bad Honnef, June 2009

L. Wolff: *Nonlinear cell mechanics*, 3. European Meeting on Cell Mechanics, Bad Honnef, October 2009

14.14 Graduations

Diploma

- Marcel Hennes
Weakly bending polymers in a random environment
March 2009

14.15 Awards

BuildMoNa award for outstanding scientific results (2009), 2nd prize,

Jens Glaser

Leipzig School of Natural Sciences "Building with molecules and nano-objects"

Presentation award at the Workshop for Doctoral Candidates of the Graduate School
BuildMoNa, Neukirchen/Pleiße, 08.-09. October 2009, 3rd prize,

Sebastian Sturm

Leipzig School of Natural Sciences "Building with molecules and nano-objects"

14.16 Guests

- D. Chakraborty (DFG FOR 877)
Indian Ass. for the Cultivation of Science
26.02.-02.05.2009 and 14.08.-31.12.2009

Author Index

A

Adeagbo, W.A.	241
Adhikari, S.	42
Ahmed Mohamed, E.T.	218
Alexe, M.	242
Alireza, P.L.	122
Allen, M.	168
Alvarado, J.	111
Amecke, N.	40
Amirjalayer, S.	83
Amjad, U.	228, 233
Andrea, T.	137, 142
Anselmi, F.	320
Anwand, W.	241
Arendt, T.	136
Arndt, A.	139

B

Bachmann, M.	262, 263, 265, 266, 268
Barapatre, N.	136
Barzola-Quiquia, J.	138, 139
Bathe, M.	111
Beck-Sickinger, A.G.	268
Behn, U.	320, 321
Behnke, L.	175
Benndorf, G.	163, 186, 191
Berche, B.	275
Bertmer, M.	123, 124
Biehne, G.	155, 175
Binder, T.	76
Biniwale, B.	84
Bischof, R.	271

Bittner, E.	255, 270, 276
Blavatska, V.	256
Blythe, R.A.	259
Bordag, M.	305
Borris, M.	309
Brachwitz, K.	171, 195
Brandt, M.	160, 191, 192, 195
Brauer, G.	173, 241
Braun, M.	36, 37
Bregulla, A.	37
Brunner, C.A.	107
Bräuer, P.	81
Burg, E.v.d.	221
Butera, P.	275
Butz, T.	136–139, 141–146, 241
Bux, H.	77, 78
Böntgen, T.	192, 193, 195
Böttcher, R.	125

C

Cao, B.Q.	161
Caro, J.	77, 78
Chakraborty, D.	322
Chang, L.S.	146
Charzynski, Sz.	308
Chen, Y.F.	243
Chmelik, C.	76–79, 141
Cichos, F.	36–38, 40–42, 326
Cornejo, M.	183
Czekalla, C.	138, 175, 176, 185, 189

D

Daume, F.	180
----------------	-----

- Degner, A. 309
 Diedrich, U. 109
 Dietrich, C.P. .. 160, 163, 165, 171, 185, 187
 Dominguez-Espinosa, G. 65
 Drechsler, A. 65
 Durbin, S.M. 168
 Dvoyashkin, M. 89
- E**
-
- Ebert, S. 104
 Ehrlicher, A. 107
 Ellguth, M. 173
 Elmahdy, M.M. 65, 66
 Eltzner, B. 309
 Ene, R. 60
 Enke, D. 79
 Ernst, A. 241
 Esquinazi, P. 139, 241, 242
- F**
-
- Feder, R. 139, 141
 Fernandez, P. 326
 Fischer, G. 241
 Fonseca, I. 123
 Frenzel, H. 155, 157, 159, 176
 Frey, E. 111
 Fritsch, A. 104
 Fritzsche, S. 78
 Frost, F. 183
 Fuhs, T. 107
 Fukushima, T. 242
- G**
-
- Galvosas, P. 79, 85
 Gapke, J. 80
 Gentry, B. 111
 Geyer, B. 305
 Ghoshal, Sh. 146
 Glaser, J. 322
 Gobin, O. 79
 Goede, K. 268
 Goh, S.K. 122
 Gratz, M. 83, 85
 Greven, M. 122
- Grill, W. .. 214, 217, 218, 221, 225, 228, 233
 Groß, F. 321
 Grundling, H. 308
 Grundmann, M. 155, 157, 159–
 161, 163, 165, 168, 169, 171, 173,
 175, 176, 178, 180, 181, 183–187,
 189–193, 195, 196, 241, 268
 Gul-E-Noor, F. 124
 Gutberlet, T. 109
 Gutsche, C. 65, 66
 Gyger, M. 104
 Gögler, M. 107
 Gösele, U. 242
 Gütter, S. 320
- H**
-
- Haase, J. 121, 122
 Habib, A. 233
 Heber, A. 40
 Heinke, L. 77
 Hennes, M. 324
 Hergert, W. 241
 Hertel, S. 83
 Hertsch, A. 308
 Hertäg, L. 78
 Hesse, D. 242
 Heussinger, C. 111
 Hibbe, F. 77, 141
 Hillmann, K. 218
 Hilmer, H. 181, 183, 184, 190
 Hochmuth, H. 145, 155, 169, 175, 176, 183,
 187, 190, 192, 193, 195, 241
 Hoentsch, J. 123
 Horch, C. 86
 Huber, F. 111
 Huebschmann, J. 308
 Höll, M. 320
- I**
-
- Iacob, C. 54, 55, 57–59
 Irbäck, A. 268
- J**
-
- Jakob, A.M. 138

- Janke, W. 255–257, 259, 260, 262, 263, 265,
266, 268, 270–272, 275–277
- Jarvis, P. 308
- Jentys, A. 79
- Jobic, H. 79, 84
- Johnston, D.A. 259
- Junghans, C. 265
- Lercher, J. 79
- Lindner, F. 309
- Lorenz, M. . . . 145, 155, 161, 169, 171, 176,
185, 190, 192, 195, 241
- Ludwig, T. 309
- Läuchli, A. 272

K

- Kalies, G. 80, 81
- Kamanyi, A. 218
- Kenna, R. 259
- Khalid, M. 241
- Kiessling, T. 104
- Kijowski, J. 308
- Klimchitskaya, G.L. 305
- Knospe, A. 309
- Koal, T. 142–144
- Koch, D. 107
- Kondrashova, D. 90
- Kossack, W. 64
- Kranert, C. 193
- Krause, C. 59
- Krause, C.B. 79
- Kremer, F. 49–52, 54, 55, 57–60, 62–66, 68,
69
- Krishna, R. 78
- Kropat, G. 38
- Kroy, K. 36, 322, 324–326
- Kröber, D. 321
- Krüger, P. 109
- Kullmann, J. 79
- Kupper, J. 191
- Kärger, J. 76–79, 87, 89
- Käs, J.A. 104, 107–109, 111
- Kühn, A. 321
- Kühn, N. 320
- Kühne, P. 189, 190

L

- Lajn, A. 155, 157, 159, 176
- Lange, M. 160, 161, 163, 184, 185
- Langhammer, H.T. 125
- Larisch, W. 143, 144
- Lausch, D. 178

M

- Mapesa, E.U. 49, 50, 52
- Marecki, P. 309
- Mehlhorn, D. 145, 146
- Meier, R. 228
- Meinecke, Ch. 138
- Meißner, A. 184
- Meissner, T. 122
- Menzel, F. 141, 142
- Meyer-Ortmanns, H. 260
- Mohideen, U. 305
- Morawski, M. 136
- Mostepanenko, V.M. 305
- Möddel, M. 266
- Müller, A. 186, 191
- Müller, S. 169
- Müller, T. 125

N

- Naumov, S. 79, 87
- Neuhaus, T. 257, 262
- Ngwa, W. 218
- Nnetu, D. 104
- Nußbaumer, A. 255, 270

P

- Papadopoulos, P. 60, 62–64, 68
- Pawlizak, S. 108
- Petter, K. 178
- Pickenhain, R. 173
- Picozzi, S. 242
- Pluta, M. 233
- Pumpa, M. 41
- Pusch, A.-K. 84
- Puttnins, S. 180
- Pöppl, A. 123

R

-
- Radünz, R. 326
 Rahm, A. 138, 180
 Reinert, T. 136, 138, 142, 144–146
 Rings, D. 36, 326
 Rockmann, R. 80
 Rothermel, M. 137, 142
 Rudolph, G. 308
 Rybicki, D. 122
- S**
-
- Sangoro, J.R. 54, 55, 57–59
 Schachoff, R. 36
 Schakel, A.M.J. 257
 Schein, F. 157
 Schlayer, S. 85, 86
 Schlayer, St. 84
 Schlemmer, J. 309
 Schmid, R. 83
 Schmidt, F. 171, 173
 Schmidt, M. 171, 173, 175, 176, 308
 Schmidt, W. 76
 Schmidt-Grund, R. 181, 183, 184, 189, 190,
 192, 193, 195
 Schmidtchen, H. 321
 Schnabel, S. 263
 Schnauss, J. 111
 Schubert, T. 54
 Schulz, W.-M. 142
 Schumacher, D. 190
 Schöche, S. 192, 193, 195
 Seder, H. 321
 Selmke, M. 36, 37, 42, 326
 Semenov, I. 68
 Serghei, A. 49–52
 Setzer, A. 241
 Shchur, L. 275
 Skorupa, W. 173
 Slichter, C.P. 121
 Sopik, J. 260
 Spemann, D. 138, 142, 241
 Stallmach, F. 83–86
 Stamm, M. 65
 Stange, R. 104
 Stangner, T. 66
 Stober, G. 68
- Strehle, D. 111
 Sturm, C. 181, 183, 184, 189, 190, 192, 193,
 195
 Sturm, S. 325
 Stölzel, M. 171, 191
 Synytska, A. 65
 Szombathely, M.v. 81
- T**
-
- Tarar, K.S. 228
 Theodorou, D. 84
 Thies, R. 138
 Titze, T. 79
 Tress, M. 49–52
 Tuma, D. 80
 Turkey, G. 55
- U**
-
- Ueberschär, O. 65, 69
 Uhlmann, P. 65
- V**
-
- Valiullin, R. 87, 89, 90
 Verch, R. 309
 Vogel, T. 262, 263
 Vogt, J. 138
 von Wenckstern, H. 159, 171
 von Buttlar, M. 214, 218
 von der Burg, E. 214
- W**
-
- Waclaw, B. 260
 Wagner, R. 38
 Wannemacher, R. 218
 Wehring, M. 83, 85
 Weigel, M. 277
 Wenzel, S. 272
 Werner, B. 321
 Wetzlar, F. 104
 Williams, G.V.M. 121
 Willner, S. 321
 Wolff, L. 326
- Y**

Yamauchi, K. 242

Z

Zachmann, H. 180
Zhang, Z. P. 175, 176
Ziese, M. 241–243
Zimmermann, G. 161
Zink, M. 104
Zúñiga-Pérez, J. 183–185



600 JAHRE

UNIVERSITÄT LEIPZIG



MECO34

34th Conference of the Middle European Cooperation
in Statistical Physics

30 March - 01 April 2009, Universität Leipzig, Germany

Main Topics:

Soft-matter physics
Magnetic systems
Complex systems and networks
Non-equilibrium systems
Interdisciplinary applications

Organizers:

Wolfhard Janke (Leipzig)
Steffen Trimper (Halle)

Invited Speakers:

Günter Ahlers	UC Santa Barbara, USA
Hagen Kleinert	FU Berlin, Germany
David P. Landau	Univ. of Georgia, USA
Hartmut Löwen	Düsseldorf, Germany
Georg Maret	Konstanz, Germany
Zoltán Rácz	Budapest, Hungary
Sidney Redner	Boston Univ., USA
Matthias Troyer	ETH Zürich, Switzerland
Royce Zia	Virginia Tech, USA

<http://www.physik.uni-leipzig.de/~meco34>
meco34@itp.uni-leipzig.de



Deutsche
Forschungsgemeinschaft
DFG

Freistaat Sachsen
Staatsministerium für Wissenschaft und Kunst

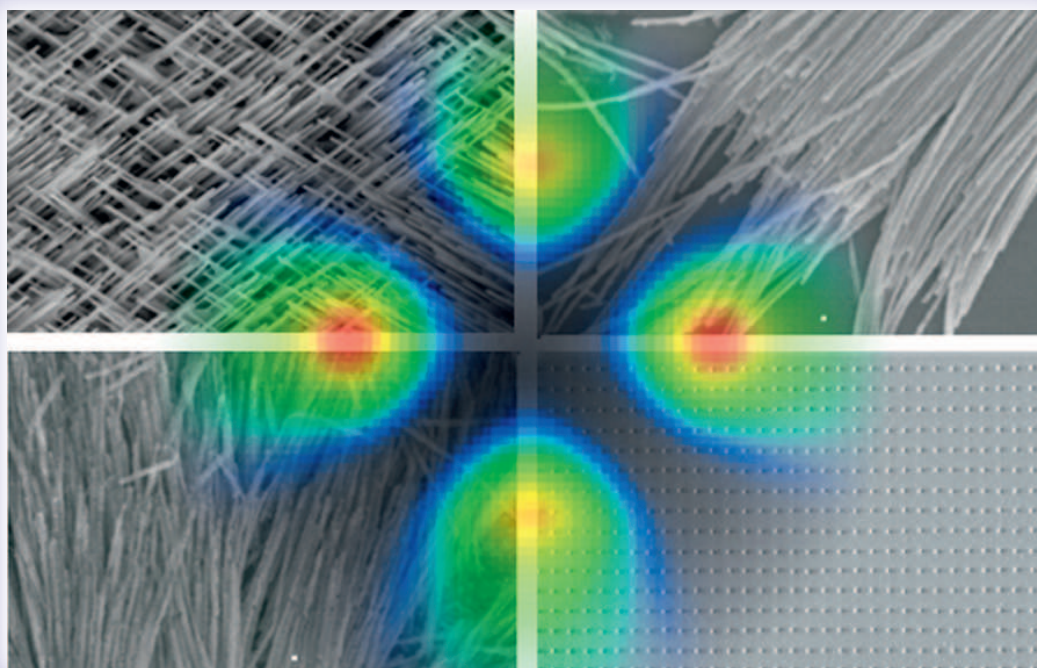


Université
franco-allemande
Deutsch-Französische
Hochschule

EPJ
The European
Physical Journal

basic solid state physics

**Architecture of Nano- and Microdimensional
Building Blocks**



Guest Editor: Marius Grundmann

247 • 6 • June 2010

 **WILEY-VCH**

ISSN 0370-1972 Phys. Status Solidi B
247, No. 6 (June), 1249–1572 (2010)

SPECIAL SECTION
(pp. 1257–1392)